DEVELOPMENT AND UTILIZATION OF NOVEL IMAGE PROCESSING TECHNIQUES TO CHARACTERIZE THE CHOROID IN ASIANS

PREETI GUPTA

(Masters in Optometry)

A THESIS SUBMITTED

FOR THE DEGREE OF DOCTOR OF PHILOSOPHY

DEPARTMENT OF OPHTHALMOLOGY

NATIONAL UNIVERSITY OF SINGAPORE

2016

DECLARATION

I hereby declare that the thesis is my original work and it has been written by me in its entirety. I have duly acknowledged all the sources of information which have been used in the thesis.

This thesis has also not been submitted for any degree in any university previously.

Preeti Gupta 29/12/2016.

Preeti Gupta
December 2016

THESIS SUPERVISORS AND COMMITTEE

Thesis Supervisors:

Ching-Yu Cheng, Ph.D., M.D., A/Professor, Department of Ophthalmology, Yong Loo Lin School of Medicine, National University of Singapore; and Ophthalmology & Visual Sciences Academic Clinical Program, Duke-NUS Medical School (Main)

Wong Tien Yin, Ph.D., M.D., Professor, Department of Ophthalmology, Yong Loo Lin School of Medicine, National University of Singapore; and Ophthalmology & Visual Sciences Academic Clinical Program, Duke-NUS Medical School (Co-supervisor)

Cheung Carol, Ph.D., Assistant Professor, Department of Ophthalmology, Yong Loo Lin School of Medicine, National University of Singapore; and Ophthalmology & Visual Sciences Academic Clinical Program, Duke-NUS Medical School (Co-supervisor)

Thesis Advisory Committee (TAC):

Cheung Chui Ming Gemmy, PhD., M.D., Adjunct Associate Professor, Department of Ophthalmology, Yong Loo Lin School of Medicine, National University of Singapore. (Chairman)

Lamoureux L. Ecosse, PhD., Professor, Office of Clinical Sciences| Duke-NUS Medical School, Dep. Dir. AMRI (Academic Medical Research Institute). (Member)

ACKNOWLEDGEMENTS

My heartfelt thanks go to my principal supervisor, A/Prof Ching-Yu Cheng who provided superb support, mentorship and guidance from the beginning to the end of my PhD. I also thank him for motivating me to continue striving for excellence. I would also like to extend my gratitude to my co-supervisors, Prof Wong Tien Yin and Dr Carol Cheung for their valuable comments, assistance and critical review of my work. I am truly indebted to Prof Wong for providing me with the opportunity to undertake this journey. Carol is a mentor and friend who has always found the time for insightful and detailed discussions, and advice. Thank you Carol. I attribute this dissertation and all the publications to the encouragement and effort of my supervisors, without which it is impossible for me to finish this dissertation and publish research papers.

I am grateful to Prof Ecosse and Dr Gemmy Cheung for agreeing to be the chairman of my Thesis Committee and giving me valuable ideas and suggestions. Thank you Dr Baskar Monisha, Ryan and Queenie for your encouragement, advice and the numerous exciting discussions. To my team mates, Yih Chung, Jacqueline and Gowtham, thank you for providing the much needed constructive feedback. I extend my gratitude to all the members of the Singapore Epidemiology of Eye Disease Study. My friends and colleagues in Singapore Eye Research Institute, particularly Binu Thapa and Wei Hong for walking with me in this journey, all the while providing the much needed support. You guys are awesome!!

Finally, I am grateful to my family for their love, continual encouragement, support and prayers throughout. I dedicate this thesis to my husband, Ajay and daughter, Yashi, for their daily sacrifices and support that enabled me to pursue my goals.

TABLE OF CONTENTS

CHAPTER 5

ENHANCEMENT OF CHOROID-SCLERAL INTERFACE VISIBILITY USING THE SEMI-AUTOMATED TECHNIQUE OF ADAPTIVE COMPENSATION

CHAPTER 6

FULLY AUTOMATED CHOROIDAL IMAGE PROCESSING TECHNIQUE TO OVERCOME THE LIMITATIONS OF SEMI-AUTOMATED TECHNIQUE

CHAPTER 7

DISTRIBUTION AND DETERMINANTS OF CHOROIDAL THICKNESS AND VOLUME USING AUTOMATED CHOROIDAL IMAGE PROCESSING TECHNIQUE IN A MULTI-ETHNIC POPULATION IN SINGAPORE

CHAPTER 10

CHARACTERIZATION OF CHOROID IN DIABETES AND DIABETIC RETINOPATHY

SUMMARY

The choroid contributes blood supply to the outer retina including photoreceptors and is therefore associated with the pathogenesis of a number of major retinal diseases, such as high myopia, age-related macular degeneration (AMD), and diabetic retinopathy (DR). To elucidate the mechanisms how the choroid may affect chorioretinal diseases, an easy, objective and quantitative analysis of the choroid is required. The field of choroidal imaging has been greatly transformed with the introduction of enhanced depth imaging (EDI) technique of spectral domain optical coherence tomography (SD-OCT). However, despite these new techniques, it has not been easy to characterize and image the choroid. Among various reasons, one was that the junction between the choroid and sclera called "choroid-scleral interface" (CSI) was still not adequately visible. Anatomically, CSI forms the posterior boundary of the choroid; a well-defined CSI is therefore a critical landmark for accurate quantification of the choroid such as choroidal thickness (CT), the distance between the retinal pigmented epithelium (RPE) and CSI.

We hypothesize that poor visibility of CSI will lead increased variability in CT measurements (**Chapter 4**). To test this hypothesis we conducted a pilot study in 179 healthy eyes from a population-based study with the aim to assess (i) percentage visibility of CSI in EDI OCT images and (ii) variability in CT measurement in images with differently visible CSI. We found that only 60% of EDI images had well-defined CSI and that the variability in CT measurement was higher in the images with poorly defined CSI (ICC: 0.97 for images with well-defined CSI vs. ICC: 0.51 for images with poorly defined CSI). Thereby confirming that visibility of CSI was critical for accurate determination of CT.

The measurement of CT was performed manually at few points around foveal centre, therefore subject to intra- and inter-operator biases and this does not adequately reflect the profile of entire choroid. Thus, there was a need for novel image processing techniques which can enhance the CSI, objectively and accurately define the CSI as well as measure CT and choroidal volume. In Aim 1 of this dissertation we first overcame the primary challenge of poor CSI visibility by enhancing the visualization of CSI by a novel technique of "adaptive compensation" (**Chapter 5**). In our enhanced images the contrast between choroid and sclera was significantly increased and CT measurements were more reliable (ICC: 0.93 to 0.97) than the non-enhanced images (ICC: 0.90 to 0.93). However, our technique was semi-automated as it required manual input to mark the CSI and measure CT, thus subject to measurement errors. To overcome this problem we used a fully automated choroidal segmentation technique which can objectively and accurately define CSI and measure CT and volume (**Chapters 6 and 7**). We compared our automated technique with the reference standard manual technique and found good agreement (ICC: 0.90 to 0.96) between the 2 techniques. Thus, our automated choroidal image processing technique was valid and comparable to existing manual CT measurement technique (**Chapter 6).**

There is currently limited population-based data on CT in Asians. It is unknown whether there exists any ethnic variation in CT among Asians; neither is it known if there are differences in systemic and ocular risk factors of CT among the different ethnic groups (e.g., Malays versus Indians) in Asians. We addressed these gaps in knowledge through a multi-ethnic population-based study in Singapore. In Aim 2 of this project, we performed a population-based evaluation of the distribution and determinants of most commonly used macular and peripapillary choroidal traits

such as CT and volume using our novel fully automated choroidal segmentation technique (**Chapter 7**). After adjusting for the differences in population specific characteristics, we found slight difference in macular CT (mean difference [MD] 12 µm), macular choroidal volume (MD 0.02 mm^3) and peripapillary CT (MD ~32 µm, p <0.001) among ethnic Malays and Indians. Both macular and peripapillary choroid was asymmetrically distributed (macular: thickest subfoveally and thinnest nasally; peripapillary: thickest superiorly and thinnest inferiorly) in the 2 ethnic groups, but, there was no difference in topographical profile of either macular and peripapillary choroid. Factors such as age, gender and axial length were the major determinants of CT and volume among both ethnic groups and should be taken into account when interpreting EDI OCT based CT measurements in clinical settings. Furthermore, two-third (~66%) of the subfoveal choroid was found to be vascular in healthy eyes (**Chapter 8**).

Lastly, detailed morphological and vascular analyses of the choroid would further help to better understand the role of choroid in eye diseases such as high myopia, DR and AMD. We found significant alterations in choroidal attributes such as CT, volume, morphology and vasculature in the above diseases (**Chapters 9, 10 and 11**). In high myopia there was marked reduction in CT, volume and vasculature but no change in morphological features such as curvature of CSI and inflection points compared to emmetropes (**Chapter 9**). Conversely, persons with diabetes with DR showed significant increase in thickness, volume and vasculature, and decrease in inflection points compared to no DR (**Chapter 10**). Nevertheless, in AMD there was no significant difference in any of the above choroidal traits compared to PCV (**Chapter 11**).

In summary, in this Thesis, I developed and utilized novel image techniques (semi- and fully-automated) to perform detailed characterization of the morphological and vascular attributes of the choroid in normal and diseased eyes in Asians. Results will be useful in further understanding the role and contribution of choroidal measures in the pathogenesis of major retinal diseases.

LIST OF TABLES

Chapter 8

Chapter 9

Chapter 10

Chapter 11

LIST OF FIGURES

Chapter 1

Chapter 3

Chapter 4

Chapter 5

Chapter 6

Chapter 8

Chapter 9

Chapter 11

LIST OF ABBREVIATIONS

EDI……	Enhanced depth imaging
SD-OCT……	Spectral domain optical coherence tomography
CSI……	Choroidal scleral interface
RPE……...	Retinal pigmented epithelium
CT…….	Choroidal thickness
ICC……...	Intra-class correlation coefficient
MD…….....	Mean deviation
DR…….	Diabetic retinopathy
AMD…….	Age-related macular degeneration
FAZ……...	Foveal avascular zone
ONH…….	Optic nerve head
ICGA……....	Indocyanine green angiography
PCV……..	Polypoidal choroidal vasculopathy
CSCR……	Central serous chorio-retinopathy
FFA……...	Fundus fluorescein angiography
TD-OCT……	Time domain optical coherence tomography
SEED……	Singapore Epidemiology of Eye Disease
SiMES……...	Singapore Malay Eye Study
SINDI……	Singapore Indian Eye Study
SCES…….	Singapore Chinese Eye Study
SAF……	Singapore Armed Forces
SERI……..	Singapore Eye Research Institute
SNEC…….	Singapore National Eye Center
RNFL…….	Retinal nerve fiber layer thickness
LSO……	Line scanning ophthalmoscope
Log MAR……...	Log of minimum angle of resolution
SE……...	Spherical equivalent
D…….	Diopters
ETDRS……	Early Treatment Diabetic Retinopathy Study
VA……...	Visual acuity
AL……	Axial length
ACD……	Anterior chamber depth
CCT…….	Central corneal thickness
IOP……..	Intraocular pressure
BMI…….	Body Mass Index
BP……	Blood pressure
OPP…….	Ocular perfusion pressure
MAP……	Mean arterial pressure
HDL……	High-density lipoprotein
LDL…….	Low-density lipoprotein
HbA1c …….	Haemoglobin
NPDR……...	Non proliferative diabetic retinopathy
PDR……..	Proliferative diabetic retinopathy
CSME……...	Clinically significant macular edema
VTDR……	Vision threatening diabetic retinopathy
ISGEO……...	International Society of Geography and Epidemiology of Ophthalmology

PACG……	Primary angle closure glaucoma
POAG……...	Primary open angle glaucoma
LOCS……	Lens Opacity Classification System
Kw……	Weighted Kappa
SD……	Standard deviation
CI…….	Confidence interval
LOA…….	Limits of agreement
PPCT……	Peripapillary choroidal thickness
CVI……..	Choroidal vascularity index
TCA…….	Total choroidal area
LA……	Luminal area
SA……	Stromal area
SFCT……	Sub foveal choroidal thickness
COV…….	Coefficient of variation
CS…….	Contrast sensitivity
NVG…….	Night vision goggles
PPA……..	Peripapillary atrophy
ANOVA……...	Analysis of variance
BCVA……...	Best corrected visual acuity
VA…….	Vascular area

LIST OF PUBLICATIONS

Publications directly related to the thesis

1. **Gupta P,** Sidhartha E, Girard MJ, et al. A simplified method to measure choroidal thickness using adaptive compensation in enhanced depth imaging optical coherence tomography. *PLoS One.* 2014;9(5):e96661.

2. **Gupta P**, Saw S, Cheung CY, et al. Choroidal thickness and high myopia: a case-control study of young Chinese men in Singapore. *Acta Ophthalmol.* 2015;93(7):585-592.

3. **Gupta P**, Jing T, Marziliano P, et al. Peripapillary choroidal thickness assessed using automated choroidal segmentation software in an Asian population. *Br J Ophthalmol.* 2015;99(7):920-926.

4. **Gupta P**, Cheung CY, Saw SM, et al. Peripapillary Choroidal Thickness in Young Asians with High Myopia. *Invest Ophthalmol Vis Sci.* 2015;56(3):1475-1481.

5. **Gupta P**, Jing T, Marziliano P, et al. Distribution and determinants of choroidal thickness and volume using automated segmentation software in a population-based study. *Am J Ophthalmol.* 2015;159(2):293-301.

6. **Gupta P**, Cheung CY, Baskaran M, et al. Relationship between Peripapillary Choroid and Retinal Nerve Fiber Layer Thickness in a Population-based Sample of Non-Glaucomatous Eyes. *Am J Ophthalmol.* 2016 Jan;161:4-11.e1-2. doi: 10.1016/j.ajo.2015.09.018. Epub 2015 Sep 24.

7. **Gupta P,** Cheng CY, Cheung CM, et al. Relationship of ocular and systemic factors to the visibility of Choroid-scleral interface using Spectral domain optical coherence tomography. *Acta Ophthalmol.* 2016;94(2):e142-149.

8. **Gupta P**, Cheung CY, Saw SM, et al.Choroidal thickness does not predict visual acuity in young, high myopes. *Acta Ophthalmol.* 2016 May 19. doi: 10.1111/aos.13084. [Epub ahead of print]

9. Agrawal R,* **Gupta P,*** Tan KA, et al. Choroidal vascularity index as a measure of vascular status of the choroid: Measurements in healthy eyes from a population-based study. *Scientific Reports*. 2016 Feb 12;6:21090. doi: 10.1038/srep21090.
   *Joint first author

10. Tan KA,* **Gupta P,***Chhablani J, et al. State of Science: Choroidal thickness and systemic health. *Survey of Ophthalmol*. 2016 Mar 12. pii: S0039-6257(15)30010-2. doi: 10.1016/j.survophthal.2016.02.007. [Epub ahead of print]
    *Joint first author

11. **Gupta P,** Cheung CY. Refining the Definition of the Choroidal-Scleral Interface. *Acta Ophthalmol.* 2016 May 27. doi: 10.1111/aos.13101. [Epub ahead of print]

12. **Gupta P**, Ting, DW, Thakku SG, et al. "Detailed Characterization of Choroidal Morphological and Vascular Features in Age-Related Macular Degeneration and Polypoidal Choroidal Vasculopathy." *Retina* 2016

13. **Gupta P**, Thakku SG, Sabanayagam C, et al. "Characterization of Choroidal Morphology and Vasculature in Diabetes and Diabetic Retinopathy." *British Journal of Ophthalmology* 2016

14. **Gupta, P**, Thakku SG, Saw SM, et al. "Detailed Phenotyping and Characterization of Choroidal Morphological and Vascular Features in Young Men with High Myopia using Spectral Domain Optical Coherence Tomography." *American Journal of Ophthalmology* 2016 (under review).

CHAPTER I

REVIEW OF LITERATURE

1.1 THE CHOROID AND ITS COMPOSITION

1.1.1 Anatomical Location

The choroid is the posterior part of the eyeball, which is sandwiched between the retina and the sclera. Anatomically, the choroid extends from the margins of the optic nerve to the pars plana, where it continues anteriorly, becoming the ciliary body.[1] Histologic investigations demonstrate that it is 0.22 mm thick posteriorly and 0.10 to 0.15 mm thick anteriorly.[2]

1.1.2 Composition

The choroid is predominantly composed of blood vessels surrounded by stromal tissue comprising of connective tissue, melanocytes, nerves and extracellular fluid.[3] Being a highly vascularized tissue accounting for ~ 85% of the ocular blood flow,[4] most of the choroidal space is taken by vessels differentiated in three vascular layers. From internal to external, with increasing vessel luminal diameter, the innermost layer is the choriocapillaris, the middle is Sattler's layer with medium vessels, and the outer is Haller's layer, with large vessels[1,3,5] (**Figure 1.1**).

Choriocapillaris: The choriocapillaris is a highly anastomosed network of capillaries, forming a thin sheet opposed to Bruch's membrane (**Figure 1.1**).[6] It is 10 µm thick at the fovea, thinning to ~ 7 µm in the periphery. The capillaries arise from the arterioles in the Sattler's layer, each of which give rise to a hexagonal-shaped domain of a single layer of capillaries, giving a patch-like structure of the choriocapillaris.[7] The fenestrated choriocapillaris are highly permeable to proteins, contributing to the high oncotic pressure in the extravascular stroma, which fosters the movement of fluids

from the retina to the choroid.[8] On the other hand, in the retina, the capillaries are continuous type (the walls have no fenestrations), constituting the blood-ocular barrier, and are impermeable to even small molecules such as glucose and amino acid which require a special transport system to move them across the endothelium. The choroidal circulation is crucial in supplying nutrients as well as oxygen because choriocapillaris are fenestrated (with large pores) and have high permeability. The molecules pass through the fenestrations into extracellular matrix, creating a high glucose concentration there, thereby facilitating transport across the RPE to the retina.[3] The choriocapillaris supplies oxygen and nutrients to Bruch's membrane and the outer third of the retina, except in the macula, where it supplies the entire retina. It is slightly flattened under Bruch's membrane, providing a large surface area for metabolic exchange, whereas the external floor (scleral surface) of the capillaries is gently undulating.

Choroidal Vascular Layers: The vascular region of the choroid consists of the outer Haller's layer of large blood vessels and the inner Sattler's layers of medium and small arteries and arterioles that feed the capillary network, and veins.[6, 7] The stroma (extravascular tissue) contains collagen and elastic fibers, fibroblasts, non-vascular smooth muscle cells and numerous very large melanocytes that are closely opposed to the blood vessels.

The blood supply to the choroid comes from the short posterior ciliary arteries which are branches of ophthalmic artery.[3] Blood from the choroid drains into the 4-6 vortex veins which drain into the ophthalmic veins and eventually exit the eye via the cavernous sinus.

Supra-choroid: The interface between choroid and sclera is called the suprachoroid. This transition zone composed of thin interconnected lamellar fibers that bind the

choroid and sclera together,[9] is a potential space and measures 30 μm in thickness. Anteriorly, the suprachoroid is continuous with the supraciliary space and posteriorly, it extends to the optic nerve. Externally, it is limited by the lamina fusca, the melanocytic layer lining the inner sclera.

1.2 FUNCTIONS OF THE CHOROID

1.2.1 Primary Function: Vascular Support

Being one of the most vascular tissue of the human body, such that about 85% of the blood flow in the eye circulates through the choroidal vessels, its principal function is to provide the metabolic support. Choroid nourishes the following structures/regions in the eye:

Outer Retina: Choroid plays a vital role in nourishing outer third of the retina.[3, 10] In the retina, the capillaries are the continuous type (the walls have no fenestrations), constituting the blood-ocular barrier, and are impermeable to even glucose and amino acids, therefore they require special transport system to move them across the endothelium. Given the fenestrated nature of capillaries of the choroid, the choroidal circulation is crucial in supplying nutrients as well as oxygen, creating a very high glucose concentration, thereby facilitating transport across the retinal pigmented epithelium (RPE) to the retina.[11] Thus, while retinal vasculature nourishes the inner retinal layers, choroid is responsible for the vascular support of outer third of the retina including RPE and photoreceptors.[3, 10]

Foveal Avascular Zone: In particular, in foveal avascular zone (FAZ), which contains metabolically active photoreceptors and is responsible for central vision, there is no retinal vascular supply and the choroid is the only source of metabolic

exchange for the avascular fovea. This area is therefore most vulnerable to changes in the normal structure or physiology of the choroid.

Optic Nerve Head: In addition to RPE and photoreceptors, choroid also supplies blood to optic nerve, including the optic disc.[12, 13] Although the circulation of the posterior ciliary artery is the main source of blood supply to the optic nerve head (ONH), the choroid as an important vascular bed affect the peripapillary region as the pre-laminar portion of the ONH is primarily nourished by the peripapillary choroid.[12-14] According to the vascular theory of glaucoma, ischaemia occurs in the prelaminar area of the ONH[15, 16] and given that the blood supply of this region is derived from the branches within the peripapillary choroid,[14] peripapillary choroid might therefore play a significant role in the pathogenesis of glaucoma.

1.2.2 Other Functions

Apart from the traditional function of providing vascular support, other functions of the choroid include:

Thermoregulation of the Retina via Heat Dissipation[17]: The high metabolism of the outer retina generates heat and the choroidal blood flow acts as a heat sink.[18, 19]

Emmetropization: Choroid participates in refractive adjustment by changes in its thickness which moves the retina forward and back, bringing the photoreceptors into the plane of focus.[20] The choroid increases its thickness in response to myopic defocus (where image is formed in front of the retina) pushing the retina towards the image plane and thus compensating for the imposed refractive error whereas choroid thins in response to hyperopic defocus (where image is focused behind the retina) pushing the retina backwards.[21, 22] 1 mm change in the thickness of the choroid can

account for +15 D to -15D of defocus which could possibly be due to expansion of the lacunae.

Modulation of Intra-ocular Pressure: The choroid also plays an important role in the drainage of the aqueous humour from the anterior chamber, via the uveo-scleral pathway which is responsible for 35% of the drainage in humans.[23]

1.3 CHOROIDAL BLOOD FLOW

Since choroid is an important vascular bed with metabolic support as its prime function, knowledge of choroidal blood flow/circulation is essential. The choroid is supplied by the posterior ciliary arteries, branching from the ophthalmic artery[24, 25] whereas the drainage of choroidal circulation is mainly through vortex veins.[24]

1.3.1 Choroidal Circulation is NOT Autoregulated

An important feature of choroidal circulation which makes it substantially different from retinal circulation is "autoregulation". Autoregulation is an adaptive compensatory mechanism to adjust blood flow according to the local needs of the tissue supplied. Almost every tissue in the body including retina has some form of autoregulation i.e. fluctuations in perfusion pressure do not cause proportional changes in blood flow because of compensatory dilation or constriction of the vessels locally. In contrast, the choroid does not exhibit any autoregulation,[26-28] as choroidal circulation is characterized by high choroidal blood flow (higher than any other tissues) and low oxygen extraction ratio which precludes the need for it.

1.3.2 Choroidal Blood Flow and Eye Diseases

Because the choroidal blood flow constitutes 85% of the ocular blood flow[4] and is the major source of oxygen and nutrients for not only the choroid but also the outer retina, including RPE and metabolically active photoreceptors,[3, 8, 10] impaired choroidal circulation would cause functional damage to the retina specifically in the avascular foveal zone eventually leading to vision loss. Therefore normal choroidal circulation is critical for not only the normal function of the choroid but also the retina.

Reduced choroidal blood flow is shown to be associated with photoreceptors dysfunction and death eventually causing vision loss.[29] Impaired choroidal blood flow has also been found to be associated with pathogenesis of various ocular diseases such as diabetic retinopathy,[30-32] age related macular degeneration[33] and high myopia.[34, 35] In addition, since the peripapillary choroid supplies blood to the ONH,[10, 14, 24, 27] altered choroidal circulation is hypothesised to be related to pathogenesis of conditions like glaucoma.[14, 36, 37] Therefore, determination of the choroidal blood flow is crucial for understanding the pathogenesis and progression of many vision threatening eye diseases.

1.3.3 Limitations of Current Blood Flow Assessment Methods

Various choroidal blood flow evaluation techniques such as pulsatile choroidal blood flow,[38] indocyanine green angiography (ICGA),[39] laser speckle flowgraphy[40] and laser Doppler flowmetry[41] have been used to evaluate choroidal blood flow in-vivo. But all these techniques provide an indirect estimation of the choroidal blood flow. With the limitation of none of the existing techniques capable of measuring absolute blood flow rate, and therefore unable to reliably quantifying choroidal hemodynamics, necessitate the need for a reliable alternative to examine

changes in the choroid, which may help clinicians assisting in risk-profiling for various diseases where choroid is implicated in the pathophysiology.

1.4 CHOROIDAL THICKNESS AS AN INDEX TO EVALUATE CHOROIDAL HEALTH

The choroid because of its vital roles plays an integral part in the functioning of the eye.[29] However, in order to sustain proper functioning of the choroid, its normal structure has to be maintained. We speculate that any changes in the structure of the choroid such as its thickness, volume or any alterations in its other morphological and vascular characteristics would lead to disturbances in the normal physiological functions of the choroid which in turn would reduce perfusion to the outer retina, which may have impact on visual function. For example, studies have shown that abnormality in the choroid such as its thinning can lead to compromised circulation, which can lead to photoreceptor dysfunction and death with resultant vision loss.[29, 42] A structurally and functionally normal choroid is therefore essential for functioning of the retina as a whole. However, this doctoral thesis concentrates on the structural aspect of the choroid.

The emergence of new imaging technology, in particular optical coherence tomography (OCT)[43] has now made it possible to visualize not only the cross-sectional images of the choroid with substantially enhanced imaging sensitivity[44] but also can perform quantitative measurements of parameters such as its thickness.[44, 45] It was not until relatively recently (2008) that OCT has been employed to characterize the choroid by quantifying its thickness, which is measured as a perpendicular distance between the RPE and the choroid scleral interface (CSI). Since then

"choroidal thickness" (CT) is emerging as a new index to quantitatively characterize the choroid in-vivo.

1.4.1 Choroidal Thickness and Eye Diseases

Numerous studies have now measured CT in normal[46-50] and different disease states.[51-56] These studies have reported variations in the thickness of the choroid in different diseases, with choroidal thinning in age related macular degeneration (AMD),[33, 57] diabetic retinopathy (DR),[58-61] and high myopia related chorio-retinal atrophy,[52, 54, 62-64] whereas thickening in polypoidal choroidal vasculopathy (PCV)[53, 65] and central serous chorioretinopathy (CSCR).[55, 66] Given the role of choroidal vasculature in the blood supply of anterior optic nerve head,[13, 24] CT is also associated with pathologies like glaucoma. Glaucoma eyes were found to have thinner peripapillary choroid.[36, 67, 68] These observations of variations in the thickness of the choroid suggest that CT could be a potential marker in the evaluation of ocular diseases as well as signal their progression and provide insights into their prognosis.

Studies have suggested CT could be an important surrogate marker for the differential diagnosis of diseases with similar presentation. For example, AMD and PCV are often difficult to differentiate since they share many clinical features. Measuring the thickness of choroid may help to differentiate between these two conditions as studies have revealed significant thinning of the choroid in AMD[33, 57] and marked thickening in PCV.[53, 65] However recent studies have demonstrated significant overlap in CT between PCV and exudative AMD, indicating that CT alone is not sufficient to differentiate between the two conditions and a more detailed investigation of the choroid in terms of its morphometric and vascular features is essential to better understand the role of choroid in typical AMD and PCV.

1.4.2 Choroidal Thickness and Systemic Diseases

Due to vascular nature of the choroid, potentially any disease affecting vasculature or blood supply could also affect the choroidal health. CT is altered in many systemic diseases such as diabetes mellitus,[58-61] hypertension[69] and hypercholesterolemia.[70] There are reports on significant increase in CT in subjects with hypertension.[69] Likewise choroid is considered as a potential site for the occurrence of atherosclerotic changes[71] which occur in presence of hypercholesterolemia. Thickness of the choroid is shown to be significantly higher in subjects with hypercholesterolemia.[70] Interestingly, although various studies have reported CT in patients with diabetes mellitus, the results have been equally contrasting, with some suggesting CT is increased,[59] and some decreased[58] and other no difference.[72] Even though, the general consensus is that diabetes mellitus as a systemic disease causes a decrease in CT, further investigations are warranted to confirm these findings.

In summary, CT could be considered as a significant marker to assess both ocular and systemic health status. Measurements of CT would enable new directions to study normal and pathological processes within the choroid.

1.5 CHOROIDAL IMAGING METHODS

Imaging of the choroid along with quantitative assessment of its thickness is gaining increasing importance for the diagnosis, management and follow-up of diseases where choroid is implicated in the pathophysiology. The current choroidal imaging methods include the following:

Histological Analysis: Most anatomical information regarding the choroid has been gained through histological analysis.[73, 74] However, in the fixation of the tissues

during the histological process, there is shrinkage of the choroid, making it difficult to study the changes in vascular tone of the choroid. Therefore, the validity of in-vitro studies is compromised.

Angiography: Presently, angiographies, in particular ICGA[75] and to a lesser extent fundus fluorescein angiography (FFA) are the current standards in clinical settings to evaluate the functional aspects such as detecting vascular abnormalities of the choroid.[76, 77] FFA (absorption peak between 465 and 490 nm) is limited by light absorption and scattering by the pigment in the RPE and the choroid as well as the blood vessels in the choroid (up to 5% of light is absorbed), decreasing the light transmittance and hence visualization of the choroid. Furthermore, fluorescein extravasates rapidly from choriocapillaris preventing delineation of the choroidal anatomy.

On the other hand, ICGA with absorption peak between 790 and 805 nm penetrates the pigmentation of the eye better (only 38% is absorbed by the RPE and the choroid) and is less likely to leak from the normal choroidal vessels.[78] Nevertheless, both FFA and ICGA do not provide cross-sectional anatomical information of the choroid and poorly identify the depth of vascular pathology. In addition, these imaging techniques are invasive, time-consuming and have limitations of low resolution and inability for reliable quantitative assessment.[79, 80]

B-scan Ultrasonography: B-scan ultrasonography is another imaging modality which is used especially in the presence of opaque media. However, a problem with ultrasonography is that the exact location of the image obtained is not known, thereby providing limited repeatability. In addition its low image resolution makes the detection of small changes in the choroid difficult.[81]

Laser Doppler Flowmetry: Laser Doppler flowmetry[41] is a non-invasive technique for the measurement of local choroidal blood flow and its regulation. However, the assessment of blood flow in this technique is limited to the foveal region (because it is free of retinal vessels), resulting in the Doppler signal arising predominantly from the choriocapillaris.[41] Therefore this technique evaluates only a limited area of the posterior pole that may or may not be representative of the flow in other regions of the choroid. It is further constrained by its inability to provide reliable quantitative assessment.

Although, the above techniques are useful for determining vessel abnormalities or changes in the choroidal blood flow, quantitative assessment of the choroid such as its thickness measurement has been very challenging with these techniques as they do not provide three-dimensional anatomical information about the RPE or the choroidal layers.

1.6 OPTICAL COHERENCE TOMOGRAPHY FOR CHOROIDAL IMAGING

It was the introduction of OCT, an optical imaging technique based upon interferometry,[43, 82] that has revolutionized the imaging of the posterior segment of the eye including the choroid.[44] OCT enables visualization of detailed in-vivo structures non-invasively and provides high-quality, cross-sectional images with greater resolution and reliability.[83] Furthermore, it can perform quantitative measurements of different structures in the eye.[84] However, not all OCT devices are adequate to visualize the choroid.

The first commercially available OCT devices used time domain modality (TD-OCT) and were designed to visualize retina at 10 μm resolution. The more recent commercial OCT's, which are based on the spectral domain detection (SD-OCT)

technology allow for even higher scanning speeds (~ 20,000 to 40,000 A-scans/sec), higher scan density and image resolution (axial resolution 5 μm and transverse resolution 15 μm) further improving visualization of the deeper structures in the eye.[83] The current commercially available SD-OCT devices uses light wavelengths in the 800-870 nm range, which is appropriate for achieving highly detailed images of the retina. However, due to scattering and absorption of the melanin in this range,[85] it is difficult to visualize structures that lay beneath this layer, such as the choroid and choriocapillaris.

1.6.1 Limitations of Conventional OCT in Imaging the Choroid

Even though, the above features make conventional OCT an important diagnostic tool for disease documentation, disease progression and therapeutic outcomes, imaging of the choroid with SD-OCT is not adequate to visualize the entire choroidal structures. Mainly, because of difficulty in signal penetration beyond the heavily pigmented RPE, decreased maximal dynamic range inherent in SD-OCT, wavelength dependent light scattering, and signal loss in image path.[44] More importantly, it is decreasing sensitivity and resolution with increasing displacement from the zero-delay line or the line of peak sensitivity.[86] Zero-delay line is a reference point set by the software where the image captured is optimal and theoretically, structures that are closer to the zero delay line have higher signals than structures that are farther from zero delay line (**Figure 1.2**).

However, in conventional SD-OCT, the zero-delay line is placed at posterior vitreous,[44, 45] maximizing the sensitivity from the retina and vitreoretinal interface. In this way, the retinal image is improved but it leaves the outer choroid farther from the zero delay line with subsequent diminished signal and therefore a poor quality of choroidal image (**Figure 1.3, panel A**).[87]

1.6.2 Technological Advances in OCT Technique of Choroidal Imaging

Research to improve understanding of functional aspects of the choroid, and identification of choroidal changes as potential markers for the onset and progression of many ocular diseases has provided the catalyst to develop improved imaging techniques to allow better visualization of the choroidal structures. One such successful attempt is a novel modification to the standard technique of SD-OCT, termed **"enhanced depth imaging" (EDI)** which allows cross-sectional imaging of the choroid[44] including the sclera, with substantially enhanced imaging sensitivity.

Principle of Enhanced Depth Imaging: In EDI technique the instrument is moved closer to the eye to image deeper layers, the inverted image is displaced such that the choroid is shown facing up (i.e. closer to zero-delay) while the inner retina is facing down.[44] Since the zero-delay line is placed further posteriorly, usually at CSI instead of vitreoretinal interface, it maximize the sensitivity on the outer limit of the choroid thereby giving better visualization of the choroid than retina (**Figure 1.3, panel B**). EDI-OCT has revolutionized choroid studies as it was not until relatively recently (2008) that the measurement of CT became possible through EDI technique of SD-OCT.

Other advantages of SD-OCT: Apart from providing enhanced visualization of the choroid, by setting it adjacent to the zero delay line, SD-OCT also have other additional advantages such as:

1) Multiple Image Averaging (an average of maximum 100 B-Scans): is another important technique to visualize the choroid by using multiple scans obtained from the same retinal locations that are subsequently averaged together by the OCT

software. This reduces the speckle and increases signal-to-noise ratio, thereby enhancing the continuity and sharpness of the underlying structures.

2) Eye Tracking: minimizes artefacts caused by eye drift and micro-saccades to ensure that all the images to be averaged are taken from the same retinal location, thereby increasing signal by reducing the motion artefact. Given the topographical variation in the thickness of the choroid this feature is of great importance.

3) High-speed Scanning and Low Speckle Noise: can further produce high-quality choroidal images with the EDI mode in Spectralis SD-OCT.

Thus, because of the above technological amelioration, it is conceived that SD-OCT (Spectralis) with EDI mode can provide more reliable and accurate assessment of CT compared to conventional OCT.

1.7 CHALLENGES IN CHOROIDAL IMAGING DESPITE EDI TECHNIQUE

The field of choroidal imaging is greatly transformed with the advent of the technique of EDI-OCT and since then numerous studies have measured CT in normal[45, 47, 48, 50] and different disease states.[33, 52, 54-56] However, despite this technique it is not a trivial task to image the choroid as it is still not adequately visible for reliable determination of CT. The EDI technique of SD-OCT and current CT assessment technique lacks some of the critical aspects which are discussed in next chapter and forms the basis of this doctoral work.

1.8 REFERENCES

1. Kaufman PL, Alm A. Anatomy of the ocular circulation. Adler's Physiology of the Eye, 10th ed. St. Louis: Elsevier Health Sciences, 2002.

2. Ryan SJ. Retina, 4th ed. Philadelphia, PA: Elsevier Mosby, 2006.

3. Nickla DL, Wallman J. The multifunctional choroid. Prog Retin Eye Res 2010;29(2):144-68.

4. De Moraes CG, Reis AS, Cavalcante AF, et al. Choroidal expansion during the water drinking test. Graefes Arch Clin Exp Ophthalmol 2009;247(3):385-9.

5. Zhang HR. Scanning electron-microscopic study of corrosion casts on retinal and choroidal angioarchitecture in man and animals. Prog Retin Eye Res1994;13(1):243-70.

6. Remington LA. Clinical Anatomy of the Visual System, 2nd ed: Elsevier, 2005.

7. Forrester JV, Dick AD, McMenamin PG, Lee WR. The Eye. Basic Sciences in Practice. Edinburgh: Saunders, 2002.

8. Bill A, Sperber G, Ujiie K. Physiology of the choroidal vascular bed. Int Ophthalmol 1983;6(2):101-7.

9. Tasman W, Jaeger AE. Choroid and suprachoroid. Duane's Foundation of Clinical Ophthalmology. Philadelphia J. B. Lippincott, 1991; v. 1.

10. Linsenmeier RA, Padnick-Silver L. Metabolic dependence of photoreceptors on the choroid in the normal and detached retina. Invest Ophthalmol Vis Sci 2000;41(10):3117-23.

11. Bill A, Tornquist P, Alm A. Permeability of the intraocular blood vessels. Trans Ophthalmol Soc U K 1980;100(3):332-6.

12. Hayreh SS. The blood supply of the optic nerve head and the evaluation of it - myth and reality. Prog Retin Eye Res 2001;20(5):563-93.

13. Hayreh SS. The 1994 Von Sallman Lecture. The optic nerve head circulation in health and disease. Exp Eye Res 1995;61(3):259-72.

14. Hayreh SS. Blood supply of the optic nerve head and its role in optic atrophy, glaucoma, and oedema of the optic disc. Br J Ophthalmol 1969;53(11):721-48.

15. Duijm HF, van den Berg TJ, Greve EL. Choroidal haemodynamics in glaucoma. Br J Ophthalmol 1997;81(9):735-42.

16. Grunwald JE, Piltz J, Hariprasad SM, DuPont J. Optic nerve and choroidal circulation in glaucoma. Invest Ophthalmol Vis Sci 1998;39(12):2329-36.

17. Parver LM. Temperature modulating action of choroidal blood flow. Eye (Lond) 1991;5 (Pt 2):181-5.

18. Parver LM, Auker C, Carpenter DO. Choroidal blood flow as a heat dissipating mechanism in the macula. Am J Ophthalmol 1980;89(5):641-6.

19. Parver LM, Auker CR, Carpenter DO. The stabilizing effect of the choroidal circulation on the temperature environment of the macula. Retina 1982;2(2):117-20.

20. Walls GL. The Vertebrate Eye and its Adaptive Radiations. Michigan: Bloomfield Hills, 1942.

21. Wallman J, Wildsoet C, Xu A, et al. Moving the retina: choroidal modulation of refractive state. Vision Res 1995;35(1):37-50.

22. Wildsoet C, Wallman J. Choroidal and scleral mechanisms of compensation for spectacle lenses in chicks. Vision Res 1995;35(9):1175-94.

23. Alm A, Nilsson SF. Uveoscleral outflow--a review. Exp Eye Res 2009;88(4):760-8.

24. Flammer J, Orgul S, Costa VP, et al. The impact of ocular blood flow in glaucoma. Prog Retin Eye Res 2002;21(4):359-93.

25. Oyster CW. The Human Eye: Structure and Function, 1st ed: Sunderland: Sinauer Associates Inc., 1999.

26. Delaey C, Van De Voorde J. Regulatory mechanisms in the retinal and choroidal circulation. Ophthalmic Res 2000;32(6):249-56.

27. Riva CE, Titze P, Hero M, Petrig BL. Effect of acute decreases of perfusion pressure on choroidal blood flow in humans. Invest Ophthalmol Vis Sci 1997;38(9):1752-60.

28. Riva CE, Titze P, Hero M, et al. Choroidal blood flow during isometric exercises. Invest Ophthalmol Vis Sci 1997;38(11):2338-43.

29. Cao J, McLeod S, Merges CA, Lutty GA. Choriocapillaris degeneration and related pathologic changes in human diabetic eyes. Arch Ophthalmol 1998;116(5):589-97.

30. Nagaoka T, Kitaya N, Sugawara R, et al. Alteration of choroidal circulation in the foveal region in patients with type 2 diabetes. Br J Ophthalmol 2004;88(8):1060-3.

31. Langham ME, Grebe R, Hopkins S, et al. Choroidal blood flow in diabetic retinopathy. Exp Eye Res 1991;52(2):167-73.

32. Geyer O, Neudorfer M, Snir T, et al. Pulsatile ocular blood flow in diabetic retinopathy. Acta Ophthalmol Scand 1999;77(5):522-5.

33. Koizumi H, Yamagishi T, Yamazaki T, et al. Subfoveal choroidal thickness in typical age-related macular degeneration and polypoidal choroidal vasculopathy. Graefes Arch Clin Exp Ophthalmol 2011;249(8):1123-8.

34. Akyol N, Kukner AS, Ozdemir T, Esmerligil S. Choroidal and retinal blood flow changes in degenerative myopia. Can J Ophthalmol 1996;31(3):113-9.

35. Moriyama M, Ohno-Matsui K, Futagami S, et al. Morphology and long-term changes of choroidal vascular structure in highly myopic eyes with and without posterior staphyloma. Ophthalmology 2007;114(9):1755-62.

36. Yin ZQ, Vaegan, Millar TJ, et al. Widespread choroidal insufficiency in primary open-angle glaucoma. J Glaucoma 1997;6(1):23-32.

37. Spraul CW, Lang GE, Lang GK, Grossniklaus HE. Morphometric changes of the choriocapillaris and the choroidal vasculature in eyes with advanced glaucomatous changes. Vision Res 2002;42(7):923-32.

38. Lovasik JV, Gagnon M, Kergoat H. A novel noninvasive videographic method for quantifying changes in the chromaticity of the optic nerve head with changes in the intraocular pressure, pulsatile choroidal blood flow and visual neural function in humans. Surv Ophthalmol 1994;38 Suppl:S35-51.

39. Flower RW. Extraction of choriocapillaris hemodynamic data from ICG fluorescence angiograms. Invest Ophthalmol Vis Sci 1993;34(9):2720-9.

40. Isono H, Kishi S, Kimura Y, et al. Observation of choroidal circulation using index of erythrocytic velocity. Arch Ophthalmol 2003;121(2):225-31.

41. Riva CE, Cranstoun SD, Grunwald JE, Petrig BL. Choroidal blood flow in the foveal region of the human ocular fundus. Invest Ophthalmol Vis Sci 1994;35(13):4273-81.

42. Hidayat AA, Fine BS. Diabetic choroidopathy. Light and electron microscopic observations of seven cases. Ophthalmology 1985;92(4):512-22.

43. Huang D, Swanson EA, Lin CP, et al. Optical coherence tomography. Science 1991;254(5035):1178-81.

44. Spaide RF, Koizumi H, Pozzoni MC. Enhanced depth imaging spectral-domain optical coherence tomography. Am J Ophthalmol 2008;146(4):496-500.

45. Margolis R, Spaide RF. A pilot study of enhanced depth imaging optical coherence tomography of the choroid in normal eyes. Am J Ophthalmol 2009;147(5):811-5.

46. Gupta P, Jing T, Marziliano P, et al. Peripapillary choroidal thickness assessed using automated choroidal segmentation software in an Asian population. Br J Ophthalmol 2015;99(7):920-6.

47. Gupta P, Jing T, Marziliano P, et al. Distribution and determinants of choroidal thickness and volume using automated segmentation software in a population-based study. Am J Ophthalmol 2015;159(2):293-301.

48. Fujiwara A, Shiragami C, Shirakata Y, et al. Enhanced depth imaging spectral-domain optical coherence tomography of subfoveal choroidal thickness in normal Japanese eyes. Jpn J Ophthalmol 2012;56(3):230-5.

49. Wei WB, Xu L, Jonas JB, et al. Subfoveal choroidal thickness: the Beijing Eye Study. Ophthalmology 2013;120(1):175-80.

50. Manjunath V, Taha M, Fujimoto JG, Duker JS. Choroidal thickness in normal eyes measured using Cirrus HD optical coherence tomography. Am J Ophthalmol 2010;150(3):325-9.

51. Gupta P, Cheung CY, Saw SM, et al. Peripapillary Choroidal Thickness in Young Asians with High Myopia. Invest Ophthalmol Vis Sci 2015;56(3)1475-81.

52. Gupta P, Saw S, Cheung CY, et al. Choroidal thickness and high myopia: a case-control study of young Chinese men in Singapore. Acta Ophthalmol 2015;93(7):585-92.

53. Chung SE, Kang SW, Lee JH, Kim YT. Choroidal thickness in polypoidal choroidal vasculopathy and exudative age-related macular degeneration. Ophthalmology 2011;118(5):840-5.

54. Fujiwara T, Imamura Y, Margolis R, et al. Enhanced depth imaging optical coherence tomography of the choroid in highly myopic eyes. Am J Ophthalmol 2009;148(3):445-50.

55. Imamura Y, Fujiwara T, Margolis R, Spaide RF. Enhanced depth imaging optical coherence tomography of the choroid in central serous chorioretinopathy. Retina 2009;29(10):1469-73.

56. Fong AH, Li KK, Wong D. Choroidal evaluation using enhanced depth imaging spectral-domain optical coherence tomography in Vogt-Koyanagi-Harada disease. Retina 2011;31(3):502-9.

57. Grossniklaus HE, Green WR. Choroidal neovascularization. Am J Ophthalmol 2004;137(3):496-503.

58. Querques G, Lattanzio R, Querques L, et al. Enhanced depth imaging optical coherence tomography in type 2 diabetes. Invest Ophthalmol Vis Sci 2012;53(10):6017-24.

59. Xu J, Xu L, Du KF, et al. Subfoveal choroidal thickness in diabetes and diabetic retinopathy. Ophthalmology 2013;120(10):2023-8.

60. Kim JT, Lee DH, Joe SG, et al. Changes in choroidal thickness in relation to the severity of retinopathy and macular edema in type 2 diabetic patients. Invest Ophthalmol Vis Sci 2013;54(5):3378-84.

61. Regatieri CV, Branchini L, Carmody J, et al. Choroidal thickness in patients with diabetic retinopathy analyzed by spectral-domain optical coherence tomography. Retina 2012;32(3):563-8.

62. Ikuno Y, Tano Y. Retinal and choroidal biometry in highly myopic eyes with spectral-domain optical coherence tomography. Invest Ophthalmol Vis Sci 2009;50(8):3876-80.

63. Fitzgerald ME, Wildsoet CF, Reiner A. Temporal relationship of choroidal blood flow and thickness changes during recovery from form deprivation myopia in chicks. Exp Eye Res 2002;74(5):561-70.

64. Cheung CM, Loh BK, Li X, et al. Choroidal thickness and risk characteristics of eyes with myopic choroidal neovascularization. Acta Ophthalmol 2013;91(7):e580-1.

65. Gomi F, Tano Y. Polypoidal choroidal vasculopathy and treatments. Curr Opin Ophthalmol 2008;19(3):208-12.

66. Gupta B, Mohamed MD. Photodynamic therapy for variant central serous chorioretinopathy: efficacy and side effects. Ophthalmologica 2011;225(4):207-10.

67. Hirooka K, Tenkumo K, Fujiwara A, et al. Evaluation of peripapillary choroidal thickness in patients with normal-tension glaucoma. BMC Ophthalmol 2012;12:29.

68. Roberts KF, Artes PH, O'Leary N, et al. Peripapillary choroidal thickness in healthy controls and patients with focal, diffuse, and sclerotic glaucomatous optic disc damage. Arch Ophthalmol 2012;130(8):980-6.

69. Ahn SJ, Woo SJ, Park KH. Retinal and choroidal changes with severe hypertension and their association with visual outcome. Invest Ophthalmol Vis Sci 2014;55(12):7775-85.

70. Wong IY, Wong RL, Zhao P, Lai WW. Choroidal thickness in relation to hypercholesterolemia on enhanced depth imaging optical coherence tomography. Retina 2013;33(2):423-8.

71. Salazar JJ, Ramirez AI, de Hoz R, et al. Alterations in the choroid in hypercholesterolemic rabbits: reversibility after normalization of cholesterol levels. Exp Eye Res 2007;84(3):412-22.

72. Vujosevic S, Martini F, Cavarzeran F, et al. Macular and peripapillary choroidal thickness in diabetic patients. Retina 2012;32(9):1781-90.

73. McLeod DS, Lutty GA. High-resolution histologic analysis of the human choroidal vasculature. Invest Ophthalmol Vis Sci 1994;35(11):3799-811.

74. Ramrattan RS, van der Schaft TL, Mooy CM, et al. Morphometric analysis of Bruch's membrane, the choriocapillaris, and the choroid in aging. Invest Ophthalmol Vis Sci 1994;35(6):2857-64.

75. Spaide RF, Yannuzzi LA, Slakter JS, et al. Indocyanine green videoangiography of idiopathic polypoidal choroidal vasculopathy. Retina 1995;15(2):100-10.

76. Yannuzzi LA. Indocyanine green angiography: a perspective on use in the clinical setting. Am J Ophthalmol 2011;151(5):745-51.

77. Stanga PE, Lim JI, Hamilton P. Indocyanine green angiography in chorioretinal diseases: indications and interpretation: an evidence-based update. Ophthalmology 2003;110(1):15-21; quiz 2-3.

78. Cherrick GR, Stein SW, Leevy CM, Davidson CS. Indocyanine green: observations on its physical properties, plasma decay, and hepatic extraction. J Clin Invest 1960;39:592-600.

79. Guyer DR, Puliafito CA, Mones JM, et al. Digital indocyanine-green angiography in chorioretinal disorders. Ophthalmology 1992;99(2):287-91.

80. Coleman DJ, Lizzi FL. In vivo choroidal thickness measurement. Am J Ophthalmol 1979;88(3 Pt 1):369-75.

81. Malhotra A, Minja FJ, Crum A, Burrowes D. Ocular anatomy and cross-sectional imaging of the eye. Semin Ultrasound CT MR 2011;32(1):2-13.

82. Hee MR, Puliafito CA, Wong C, et al. Quantitative assessment of macular edema with optical coherence tomography. Arch Ophthalmol 1995;113(8):1019-29.

83. Wojtkowski M, Srinivasan V, Fujimoto JG, et al. Three-dimensional retinal imaging with high-speed ultrahigh-resolution optical coherence tomography. Ophthalmology 2005;112(10):1734-46.

84. Spaide RF, Curcio CA. Anatomical correlates to the bands seen in the outer retina by optical coherence tomography: literature review and model. Retina 2011;31(8):1609-19.

85. Wolbarsht ML, Walsh AW, George G. Melanin, a unique biological absorber. Appl Opt 1981;20(13):2184-6.

86. Mrejen S, Spaide RF. Optical coherence tomography: imaging of the choroid and beyond. Surv Ophthalmol 2013;58(5):387-429.

87. Wu L, Alpizar-Alvarez N. Choroidal imaging by spectral domain-optical coherence tomography. Taiwan Journal of Ophthalmology;3(1):3-13.

CHAPTER I FIGURES

Figure 1.1 Illustration of the typical features observed in histological images of the choroid (Adapted from: Nickla DL, Wallman J. The multifunctional choroid. Prog Retin Eye Res. 2010; 29: 144-168).

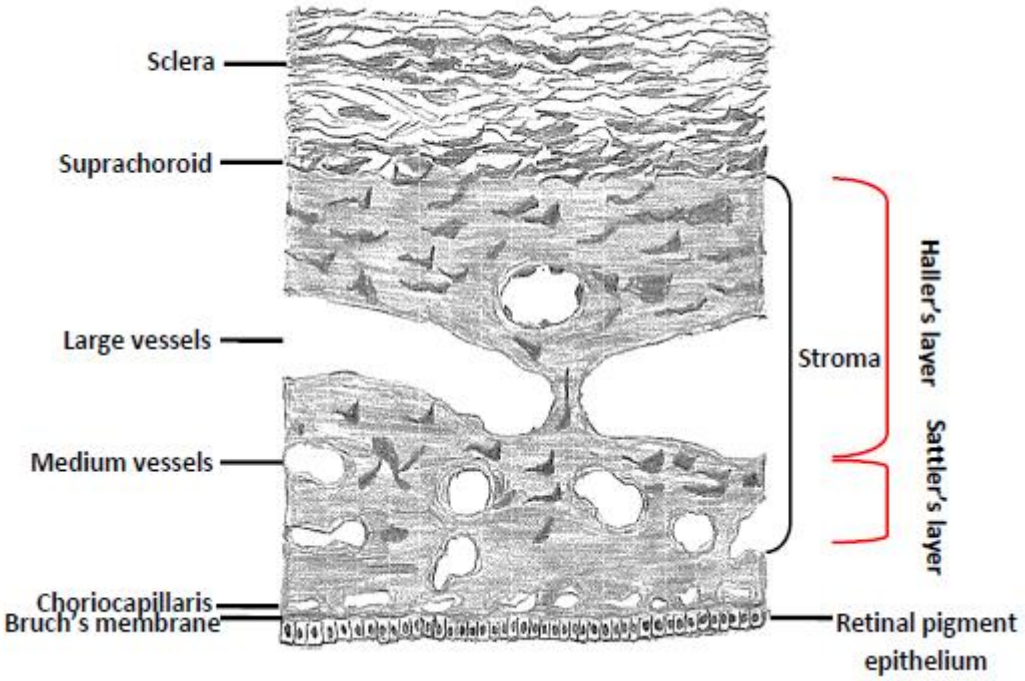

Figure 1.2 Illustration of zero delay line in conventional spectral domain optical coherence tomography (SD-OCT) vs. enhanced depth imaging (EDI) SD-OCT. **(A)** In a conventionally acquired OCT image the peak sensitivity is located at the posterior vitreous and the sensitivity curve is flipped on its side and overlaid on the SD-OCT. **(B)** In EDI-OCT, when instrument is pushed closer to the eye to invert the image, the peak sensitivity curve is moved to the inner sclera (Adapted from Spaide RF, Koizumi H, Pozzoni MC. Enhanced depth imaging spectral-domain optical coherence tomography. Am J Ophthalmol. 2008;146:496-500).

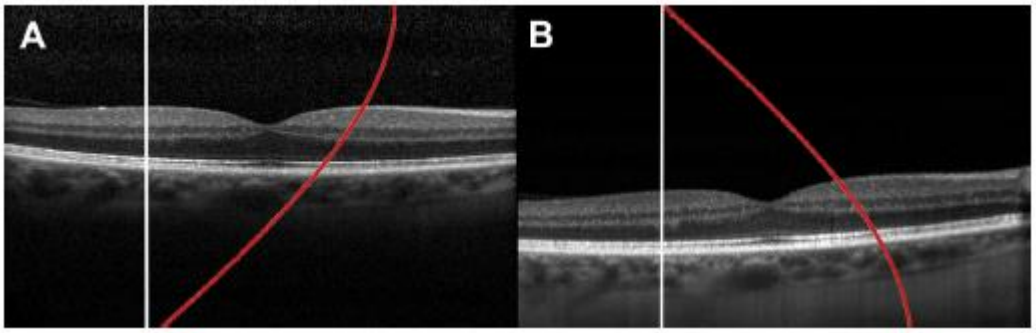

.

Figure 1.3 Optical coherence tomography image demonstrating enhanced depth imaging on Spectralis (Heidelberg Engineering). **(A)** Image was acquired with the inner retina adjacent to the zero delay. Note that the choroid–sclera junction is not distinct (white arrowheads) and there is low signal from the choroid but high signal from the inner retina. **(B)** Image was acquired with the choroid adjacent to the zero delay by advancing the instrument toward the patient. Note that the choroid–sclera junction is distinct and that there is reduced signal from the inner retina but increased signal from the choroid (Adapted from Regatieri CV, Branchini L, Fujimoto JG, Duker JS. Choroidal imaging using spectral-domain optical coherence tomography. Retina 2012;32:865-76).

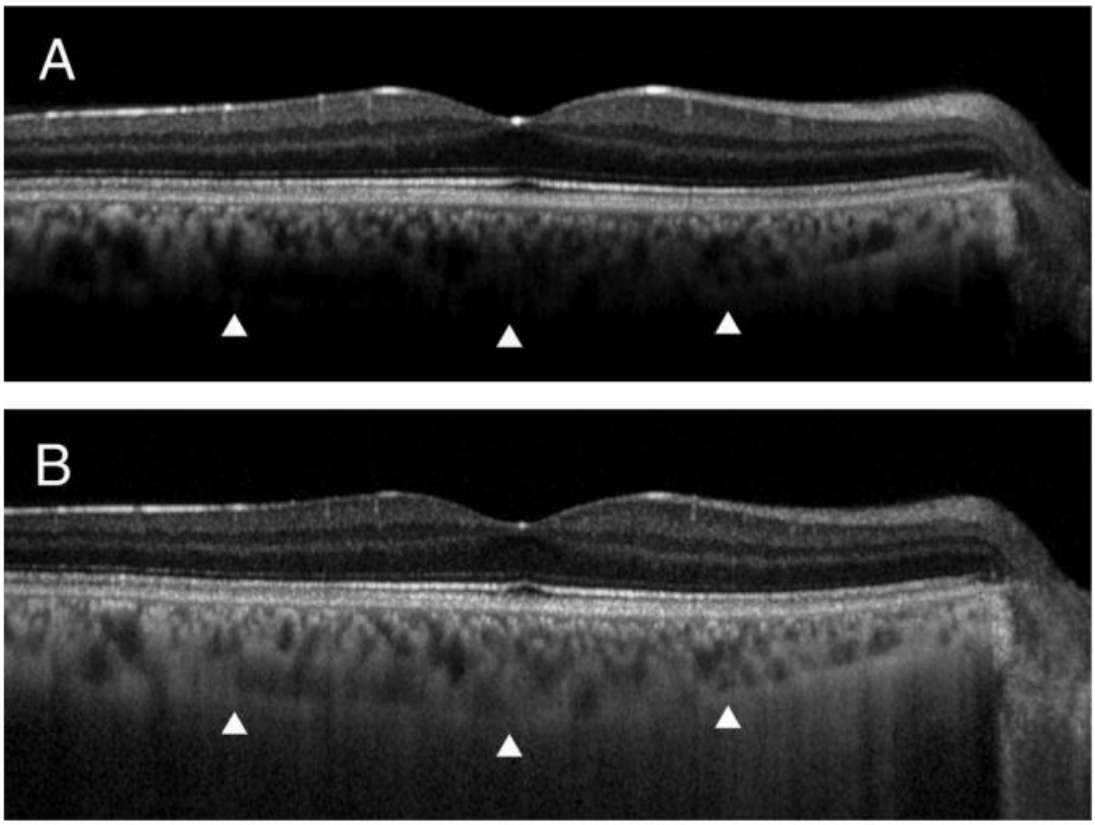

CHAPTER II

RATIONALE AND THESIS OVERVIEW

2.1 STATEMENT OF THE PROBLEM AND RATIONALE

The emergence of EDI technique of SD-OCT has made it possible to visualize cross-sectional images of the choroid with enhanced sensitivity and also to perform quantitative measurements of choroidal parameters such as CT.[1] However, current CT assessment technique lacks objectivity or the resolution/information needed to accurately measure CT. Hence, there is a need for development of novel choroidal image processing techniques to objectively and accurately quantify various choroidal parameters including CT which is essential in distinguishing clinically significant change of CT and assisting in risk-profiling for various posterior segment diseases.

2.2 UNMET CLINICAL NEEDS IN CHOROIDAL THICKNESS MEASUREMENT

The currently available techniques to measure CT and other choroidal features using SD-OCT with EDI techniques **lack** the following aspects:

2.2.1 There is Inadequate Visualization of CSI

Despite the technique of EDI, the choroid is still difficult to image thoroughly: first because of its posterior location. Choroid lies behind the pigmented RPE[2] and within the shell of the opaque and rigid sclera, therefore it is less accessible than the retina and thus difficult to visualize. Second, the pigmentation in the RPE and the choroid itself which leads to light scattering and signal attenuation thereby further compromising the visibility of the choroid. Third, the choroid is a vascular layer, presence of blood vessels further impede choroidal imaging by shadowing effects of

the vasculature, thereby decreasing the contrast between the choroid and the sclera. Last, but most important is that unlike retinal layers, wherein the RPE and internal limiting membrane are thin and clearly identifiable,[3] the transition zone between the choroid and sclera called "CSI" has blurred border and is broader making it further difficult to visualize the choroid. Because CSI forms the posterior boundary of the choroid, it is a principal landmark in quantification of CT which is measured as a perpendicular distance between the RPE and CSI. The visibility of CSI is therefore crucial for precise measurement of CT.

However, despite the current technique of EDI, the contrast between the choroid and the sclera is still weak,[4-7] giving CSI a poor visibility. We postulate that poor visibility of CSI will result in increased variability in CT measurements. Therefore, to test our hypothesis we aim to conduct a pilot study to assess the percentage visibility of CSI in EDI-OCT images and the variability in CT measurements in images with differently visible CSI.

2.2.2 There is no Robust Automated Choroidal Segmentation Software

The poor visualization of the CSI is also a hindrance to the development of automated choroidal segmentation software. Presently, none of the commercially available SD-OCT can either define the CSI or measure CT objectively. As a result, current studies segment the CSI and measure the CT manually by using the in-built caliper system provided by the machine.[8-11] Manual measurements are subject to both intra- and inter-operator biases which might lead to large variations and inaccuracies in the measurement of CT. In addition, manual method is also time-and effort-consuming. Thus the above limitations of manual CSI marking and CT measurements

make it impractical for both clinical use and epidemiological research involving large samples.

2.2.3 A Comprehensive Evaluation of the Choroid beyond the Foveal Center is Lacking

Owing to unavailability of automated choroidal segmentation software, current measurements of choroid are not comprehensive enough as the assessment of CT in most of the studies is usually limited to a few points around the foveal centre. However, measurements of a few sampling points are influenced by focal thickening or thinning of the choroid,[12, 13] or by irregularity of the inner chorioscleral border,[14, 15] and thus highly dependent on location of measurements. Since choroid is a complex three-dimensional vascular structure, consisting of a highly anastomosed network of blood vessels,[16] measurement of point thicknesses therefore provides limited information on the actual topographical variation of the choroid at the macula. Because point measurements do not adequately reflect the profile of entire choroid, measuring the choroidal volume may be a better way to study its anatomy. Thus, an objective and comprehensive assessment of choroid, such as CT maps and volumetric analysis, is required but is still unavailable.

We aim to address the above gaps in knowledge in Aims 1a and 1b, wherein, we first addressed the primary challenge of poor CSI visibility by enhancing the visualization of CSI by a novel technique of "adaptive compensation" (Aim 1a). However, our technique of adaptive compensation to enhance the CSI is still a semi-automated technique as it requires manual input to mark the CSI and measure CT, thus subject to measurement errors. We overcome this problem in Aim 1b, wherein we used a fully automated choroidal segmentation technique which can objectively and accurately define the CSI and measure CT as well as addresses the present

concern of non-comprehensive choroidal assessment by computing choroidal volume. However, apart from the above technological challenges in CT measurement, there are other issues (discussed below) which need to be addressed.

2.2.4 Choroidal Thickness, Distribution and Determinants in Asians has not been well studied

There are limited population-based data on CT in Asians.[17] The Beijing Eye Study is the only population-based study on CT. However, their measurement of CT was performed manually and at sub-foveal location only, thus limited by measurement error and non-comprehensive assessment of the choroid. None of the studies so far have performed a comprehensive assessment of the ocular and systemic factors that might influence CT. To date, it is not known whether there exists any ethnic variation in CT among Asians. Neither is it known if there are differences in systemic and ocular risk factors of CT in different ethnic groups in Asians.

2.2.5 There are few studies on the Distribution and Determinants of the Peripapillary Choroid

Furthermore, because peripapillary choroid supplies blood to the anterior optic nerve head,[18, 19] it might be associated with conditions like glaucoma[20-22] and high myopia. Knowledge of the distribution of peripapillary CT in the population may therefore be useful in facilitating the detection of abnormal changes in peripapillary CT and thus help in elucidating the pathophysiology of such eye diseases. Despite this present focus of the current SD-OCT studies is macular CT.

We propose to address these gaps in knowledge in our project through population-based study to evaluate CT and volume among ethnic groups in Singapore. Singapore has three major racial/ethnic groups, Malay, Indian and Chinese, which

provides a unique opportunity to study the effect of ethnic differences on CT in a relatively common geographic and socio-economic environment. In Aim 2 of this project, we propose to perform a population-based evaluation of the distribution and determinants of macular and peripapillary choroidal characteristics such as CT and volume using our novel fully automated choroidal segmentation technique.

2.2.6 The Relationship of Choroidal Features in Major Retinal Diseases require Further Investigations

The choroid has been implicated in the pathogenesis of many sight threatening diseases such as high myopia,[23, 24] DR[25, 26] and AMD.[15] Given that the choroid is a three dimensional vascular structure predominantly composed of blood vessels, a detailed morphological and vascular analysis of the choroid would provide clearer understanding of the role of choroid in these diseases. However, attempts to quantify and define choroidal structural and vascular characteristics in-vivo have been limited. With the rising trend in the prevalence and severity of these diseases in particular in Asia, it is imperative to have baseline measures of various choroidal morphological and vascular features in diseases where choroid is implicated in the pathophysiology.

In Aim 3 of this doctoral work, in addition to CT and volume measurements (which alone may not always reflect specific changes in the choroid), we propose to perform a more detailed analysis of various morphological features like curvature of the CSI, inflection points and distance of the thickest point from the fovea as well as additional architectural features of the stromal and vascular parameters in the choroid of the above eye diseases and their comparison with healthy eyes.

2.3 AIMS AND OBJECTIVES OF THESIS

The overall objective of this thesis is to develop and utilize novel image processing techniques (semi- and fully-automated) to characterize the macular and peripapillary choroid in Asians and to determine the relationship of choroidal features with major retinal diseases including high myopia, DR and AMD. Our novel choroidal imaging techniques will provide the platform for filling the above gaps to fulfil all of the unmet needs. The specific aims are as follows:

Aim 1: To develop and evaluate novel image processing techniques to quantify choroidal characteristics such as CT and choroidal volume using EDI SD-OCT

a. Development and evaluation of novel semi-automated image processing technique to quantify macular choroidal thickness; and its comparison with reference standard manual method
b. Development and evaluation of novel fully automated macular and peripapillary choroidal segmentation technique; and its comparison with reference standard manual method

Hypothesis: New choroidal imaging techniques will provide comparable but more reliable choroidal measurements than existing manual methods.

Aim 2: To determine the distribution and determinants of choroidal characteristics such as thickness, volume and vasculature in a multi-ethnic Asian population

a. Multi-ethnic population-based evaluation of the distribution and determinants of macular and peripapillary CT and macular choroidal volume using the fully automated choroidal segmentation method

b. Evaluation of choroidal vasculature and its determinants in healthy eyes from a population-based study

   Hypothesis: There are differences in the distribution and determinants of choroidal characteristics (thickness, volume and vasculature) among two major Asian ethnic groups.

Aim 3: To characterize choroidal morphological and vascular features in eyes with major retinal diseases

a. Evaluation of choroidal morphological and vascular features in high myopia
b. Evaluation of choroidal morphological and vascular features in diabetic retinopathy
c. Evaluation of choroidal morphological and vascular features in age related macular degeneration

   Hypothesis: Choroidal morphological traits such as curvature of the CSI, inflection points, distance of the thickest point from the fovea and vascular features like luminal area are different in eyes with different retinal diseases.

2.4 THESIS STRUCTURE

This thesis consists of nine chapters: **Chapter 1** reviews the published literature on various choroidal imaging methods and highlight the limitations of current techniques; **Chapter 2** presents statement of the problem and study rationale; **Chapter 3** presents measurement methods, disease definitions and baseline characteristics of the study participants from a multi-ethnic population; **Chapter 4** evaluates the visibility of CSI in EDI-OCT images as well as the variability in CT measurements in images with differently visible CSI; **Chapter 5** describes our

attempts to enhance the visibility of CSI by novel semi-automated technique of "adaptive compensation" to quantify macular CT and its comparison with reference standard manual method; **Chapter 6** describes development and evaluation of novel fully automated macular and peripapillary choroidal segmentation techniques to quantify macular and peripapillary CT and macular choroidal volume and their comparison with reference standard manual method; **Chapter 7** presents multi-ethnic population-based evaluation of the distribution and determinants of macular and peripapillary choroidal characteristics using the fully automated choroidal segmentation technique; **Chapter 8** describes the distribution and determinants of choroidal vasculature in healthy eyes from a population-based study; **Chapter 9** describes characterization of morphological and vascular traits of the choroid in high myopia; **Chapter 10** presents characterization of morphological and vascular features of the choroid in DR; **Chapter 11** describes characterization of morphological and vascular traits of the choroid in AMD; and **Chapter 12** summarizes the key findings, and also discusses the strengths and limitations of this doctoral work. In addition, the significance of the findings and potential directions for future research in this area are also highlighted.

2.5 REFERENCES

1. Spaide RF, Koizumi H, Pozzoni MC. Enhanced depth imaging spectral-domain optical coherence tomography. Am J Ophthalmol 2008;146(4):496-500.

2. Povazay B, Hermann B, Unterhuber A, et al. Three-dimensional optical coherence tomography at 1050 nm versus 800 nm in retinal pathologies: enhanced performance and choroidal penetration in cataract patients. J Biomed Opt 2007;12(4):041211.

3. Hee MR, Puliafito CA, Duker JS, et al. Topography of diabetic macular edema with optical coherence tomography. Ophthalmology 1998;105(2):360-70.

4. Chiu SJ, Li XT, Nicholas P, et al. Automatic segmentation of seven retinal layers in SDOCT images congruent with expert manual segmentation. Opt Express 2010;18(18):19413-28.

5. Duan L, Yamanari M, Yasuno Y. Automated phase retardation oriented segmentation of chorio-scleral interface by polarization sensitive optical coherence tomography. Opt Express 2012;20(3):3353-66.

6. Kajic V, Esmaeelpour M, Povazay B, et al. Automated choroidal segmentation of 1060 nm OCT in healthy and pathologic eyes using a statistical model. Biomed Opt Express 2012;3(1):86-103.

7. Ghorbel I, Rossant F, Bloch I, et al. Automated segmentation of macular layers in OCT images and quantitative evaluation of performances. Pattern Recognition 2011;44(8):1590-603.

8. Imamura Y, Iida T, Maruko I, et al. Enhanced depth imaging optical coherence tomography of the sclera in dome-shaped macula. Am J Ophthalmol 2011;151(2):297-302.

9. Margolis R, Spaide RF. A pilot study of enhanced depth imaging optical coherence tomography of the choroid in normal eyes. Am J Ophthalmol 2009;147(5):811-5.

10. McCourt EA, Cadena BC, Barnett CJ, et al. Measurement of subfoveal choroidal thickness using spectral domain optical coherence tomography. Ophthalmic Surg Lasers Imaging 2010;41 Suppl:S28-33.

11. Rahman W, Chen FK, Yeoh J, et al. Repeatability of manual subfoveal choroidal thickness measurements in healthy subjects using the technique of enhanced depth imaging optical coherence tomography. Invest Ophthalmol Vis Sci 2011;52(5):2267-71.

12. Yasuno Y, Okamoto F, Kawana K, et al. Investigation of multifocal choroiditis with panuveitis by three-dimensional high-penetration optical coherence tomography. J Biophotonics 2009;2(6-7):435-41.

13. Yeoh J, Rahman W, Chen F, et al. Choroidal imaging in inherited retinal disease using the technique of enhanced depth imaging optical coherence tomography. Graefes Arch Clin Exp Ophthalmol 2010;248(12):1719-28.

14. Chung SE, Kang SW, Lee JH, Kim YT. Choroidal thickness in polypoidal choroidal vasculopathy and exudative age-related macular degeneration. Ophthalmology 2011;118(5):840-5.

15. Koizumi H, Yamagishi T, Yamazaki T, et al. Subfoveal choroidal thickness in typical age-related macular degeneration and polypoidal choroidal vasculopathy. Graefes Arch Clin Exp Ophthalmol 2011;249(8):1123-8.

16. Nickla DL, Wallman J. The multifunctional choroid. Prog Retin Eye Res 2010;29(2):144-68.

17. Wei WB, Xu L, Jonas JB, et al. Subfoveal choroidal thickness: the Beijing Eye Study. Ophthalmology 2013;120(1):175-80.

18. Flammer J, Orgul S, Costa VP, et al. The impact of ocular blood flow in glaucoma. Prog Retin Eye Res 2002;21(4):359-93.

19. Hayreh SS. Blood supply of the optic nerve head and its role in optic atrophy, glaucoma, and oedema of the optic disc. Br J Ophthalmol 1969;53(11):721-48.

20. Hirooka K, Tenkumo K, Fujiwara A, et al. Evaluation of peripapillary choroidal thickness in patients with normal-tension glaucoma. BMC Ophthalmol 2012;12:29.

21. Roberts KF, Artes PH, O'Leary N, et al. Peripapillary choroidal thickness in healthy controls and patients with focal, diffuse, and sclerotic glaucomatous optic disc damage. Arch Ophthalmol 2012;130(8):980-6.

22. Yin ZQ, Vaegan, Millar TJ, et al. Widespread choroidal insufficiency in primary open-angle glaucoma. J Glaucoma 1997;6(1):23-32.

23. Fujiwara T, Imamura Y, Margolis R, et al. Enhanced depth imaging optical coherence tomography of the choroid in highly myopic eyes. Am J Ophthalmol 2009;148(3):445-50.

24. Gupta P, Saw S, Cheung CY, et al. Choroidal thickness and high myopia: a case-control study of young Chinese men in Singapore. Acta Ophthalmol 2014.

25. Kim JT, Lee DH, Joe SG, et al. Changes in choroidal thickness in relation to the severity of retinopathy and macular edema in type 2 diabetic patients. Invest Ophthalmol Vis Sci 2013;54(5):3378-84.

26. Querques G, Lattanzio R, Querques L, et al. Enhanced depth imaging optical coherence tomography in type 2 diabetes. Invest Ophthalmol Vis Sci 2012;53(10):6017-24.

CHAPTER III

SUBJECTS AND METHODS

3.1 STUDY POPULATIONS

To achieve the 3 Specific Aims proposed, data from the following studies were used:

- Singapore Epidemiology of Eye Disease (SEED) Study
- Aetiology of Pathological Myopia in NSF Study
- Asian Age-related Macular Degeneration Phenotyping Study

3.1.1 Singapore Epidemiology of Eye Disease (SEED) Study

The analyses of this dissertation included data from the Singapore Epidemiology of Eye Disease (SEED) Study, a population-based, cohort study of eye diseases in three major ethnic groups in Singapore: Malays, Indians, and Chinese adults aged 40 and older residing in south-western Singapore (**Figure 3.1**). The baseline examination[1, 2] was conducted between 2004 and 2011 and a follow-up examination[3] of the participants has been conducted since January 2011, 6 years after the baseline examination and is on-going. Using an age-stratified random sampling strategy, 5,600 Malay names, 6,350 Indian names, and 6,752 Chinese names were selected from the Ministry of Home Affairs. A total of 4,168 Malays, 4,497 Indians, and 4,605 Chinese were deemed eligible to participate. The "ineligible" persons were those who had moved from the residential address, had not lived there in the past six months, or were deceased or terminally ill. A total of 3,280 Malays, 3,400 Indians and 3,353 Chinese participated in the baseline SEED study, giving a response rate of 78.7%, 75.6%, and 72.8% respectively (**Figure 3.1**). In the follow up examination, a total of 1,901 Malays and 2,200 Indians participated, giving a response rate of 72.2%

and 75.6% respectively. The follow up of Chinese participants is on-going and therefore we could not include them in this dissertation. The study adhered to the Declaration of Helsinki, and ethics approval was obtained from the Singapore Eye Research Institute (SERI) Institutional Review Board. All examinations were carried out at SERI. A detailed interviewer-administered questionnaire was used to collect information regarding socioeconomic status (e.g., education, income and housing type) and medical history of eye diseases.

Participants were invited to attend a comprehensive eye and physical exam at the SERI via telephone, by mail, and/or by home visit. A booklet outlining the overall eye study findings and an invitation letter (reply-paid postage) were sent to all baseline participants to elicit a strong spirit of cooperation.

3.1.2 Aetiology of Pathological Myopia in NSF Study

This is a case control study of 718 Singapore Armed Forces (SAF) conscripts with high myopia measurements (defined as spherical equivalent [SE] of more than -6.00 diopter [D]) and a control group of up to 200 emmetropes who were invited to participate in this study at SERI. All participants underwent detailed clinical and ocular examination including retina, optic disc and choroidal architectural parameters, using Heidelberg Spectralis OCT. SAF conscripts were eligible to participate in the study if they do not have any history of anterior ocular diseases, trauma or conditions that affects visual performance i.e. visual acuity (VA) and contrast sensitivity and no refractive surgery done to any of their eyes.

3.1.3 Asian Age-related Macular Degeneration Phenotyping Study

The Asian AMD Phenotyping Study is a prospective, observational clinical study which recruited consecutive AMD patients from the Singapore National Eye

Centre (SNEC) who provided a complete set of data during the baseline visit to phenotype this condition. Each patient was examined according to a standardized protocol.[4] Data collected and risk factors examined were compared against age-matched Asian controls from population studies under the SEED programme, which has a clinical database of persons of Chinese, Malays and Indian ethnicity.

3.2 CHOROIDAL IMAGING

3.2.1 Macular Choroidal Imaging

The choroidal architectural parameters were determined using SD-OCT (Spectralis, Wavelength: 870 nm; Heidelberg Engineering, Heidelberg, Germany) with EDI modality after pupil dilation. OCT raster scans with EDI were acquired in macular region of each subject. Each set of images comprised 7 serial horizontal B-scans (each composed of 1536 A-scans) covering a rectangular region of 30° X 5°centered on the fovea. Distance between consecutive scans was 240 µm. To reduce speckle noise, each B-scan was averaged 100 times during acquisition (**Figure 3.2**). The CT at each location was defined as the distance between the Bruch's membrane (lower boundary of RPE) and the CSI.

3.2.2 Peripapillary Choroidal Imaging

Peripapillary choroid was imaged using EDI mode of Spectralis SD-OCT. The peripapillary region was scanned using a 360°, 3.4 mm diameter circle that was centered on the optic disc (**Figure 3.3**), each comprising 100 averaged scans (using the proprietary automatic averaging and eye tracking features of the device). Scans were centered using an internal fixation and centering was confirmed by a scanning laser ophthalmoscope integrated in the instrument.

For both macular and peripapillary choroidal scans, following Spectralis user manual guidelines subjects' keratometry readings and the most recent refraction were entered into the Software Program to estimate optical magnification and, therefore, to allow for more accurate comparisons across individuals.

3.3 RETINAL IMAGING

3.3.1 Macular Scan

The retinal architectural parameters were determined using SD-OCT (Cirrus, Wavelength: 870 nm; Carl Zeiss Meditec, Inc, Dublin, CA) after pupil dilation. Cirrus SD-OCT has a scan speed of 27,000 axial scans per second and an axial resolution of 5 µm.[5] It was used to acquire 1 macular scan in an area of 6 X 6 mm^2 using the macular cube 200 X 200 scan protocol in each eye after pupil dilation. The built-in software was used to produce retinal thickness maps, which then were averaged over nine retinal subfields in a 6-mm diameter circle centered at the true fovea location, as defined by the Early Treatment Diabetic Retinopathy Study (ETDRS).

3.3.2 Optic Nerve Head Scan

Cirrus SD-OCT also images the ONH and peripapillary retinal nerve fiber layer (RNFL) in an area of 6 X 6 mm^2, and samples 200 X 200 data points in <1.5 seconds. After pupil dilation, ONH and RNFL scan acquisitions were performed for each participant using an optic disc cube 200 X 200 scan protocol, which generates a cube of data in a 6 X 6 mm^2 grid with 200 X 200 axial measurements, following the recommended procedure (Cirrus HD-OCT manual).

3.3.3 Cirrus Image Acquisition Protocol

In brief, the subject's pupil was first centered and focused in an iris viewing camera on acquire screen, and the line scanning ophthalmoscope (LSO) with "auto focus" mode was then used to optimize the view of the retina. The "center" and "enhance" modes were used to optimize the *Z*-offset and scan polarization respectively for the OCT scan to maximize the OCT signal. After each capture, motion artifact was checked with the LSO image with the OCT en face overlaid. Rescanning was performed if a motion artefact (indicated by discontinuity of blood vessels) or saccades were detected. Centration was checked to confirm whether the central subfield aligned to center of fovea correspondingly. In addition, each of the B-scans were scrutinized manually in each eye by trained technicians and checked for segmentation boundaries displayed. Images with motion artefact, centration error, or macular and RNFL or ONH algorithm segmentation failure were excluded from the analysis. All the OCT scans included in the study had signal strength of at least 6, which is considered as acceptable quality. Macular and RNFL thicknesses (average, clock hours, and quadrants), were derived automatically from a single scan using the in-built automated software for segmentation and parameter measurements without manual operator adjustment.

3.4 CLINIC INTERVIEW

A face-to-face detailed interviewer-administered questionnaire was used to collect information on socioeconomic characteristics (e.g. education, occupation, income level and housing type), lifestyle factors such as smoking and alcohol use, medical history (e.g. diabetes, hypertension and hyperlipidaemia) and medication use from participants.

3.5 OTHER OCULAR EXAMINATION

Visual Acuity: Distance presenting VA was measured using a logarithm of the minimum angle of resolution (Log MAR) number chart (Lighthouse International, New York, USA) at a distance of 4 meters, with the participant wearing their current optical correction (spectacles or contact lenses), if any. A number chart was used for participants who were unable to identify the Latin alphabets. If no number could be read at 4 meters, the participant was moved to 3, 2 or 1 meters consecutively and finally VA was assessed as counting fingers, hand movements, perception of light, or no perception of light. Subjective refraction and distance best-corrected VA in Log MAR scores were measured by trained and certified study optometrists. Near vision acuity test was done using the Log MAR near vision chart.

Refraction: The refraction (sphere, cylinder and axis) was measured using an autorefractor machine (Canon RK 5 Auto Ref-Keratometer, Canon Inc. Ltd., Tochigiken, Japan) operated by optometrists or trained technicians. The first five valid readings were used and averaged using vector methods to give a single estimate of refractive error. All five readings should be at most 0.50 D apart in both the spherical and cylinder components.

Ocular Biometry: Ocular biometry was performed using an optical biometry machine (Zeiss IOL Master, version: 3.01.0294). This device is a non-contact optical biometry machine that is non-invasive as opposed to the ultrasound A-scan biometry machine. The axial length (AL), anterior chamber depth (ACD) and corneal curvature radii in the horizontal and vertical meridian will be measured in the right and left eye.

Visual Field Testing: Standardized visual field testing was performed with static automated white-on-white threshold perimetry (SITA Fast 24-2, Humphrey Field

Analyzer II; Carl Zeiss Meditec, Inc., Oberkochen, Germany). A visual field was defined as reliable when fixation losses were less than 20%, and false-positive, false-negative rates were less than 33%. Visual field test was repeated if the test result was unreliable. A glaucomatous visual field defect was defined as the presence of three or more significant ($p<0.05$) non-edge contiguous points with at least one at the $p<0.01$ level on the same side of the horizontal meridian in the pattern deviation plot, and classified as "outside normal limits" on the Glaucoma Hemifield Test, confirmed on 2 consecutive visual field examinations.

Fundus Photography: Fundus photography was performed using a digital non-mydriatic retinal camera (Canon CRDGi with a 20Diopter SLR backing, Canon, Japan). Retinal photographs centered on the optic disc and the macula was taken from both eyes after pupil dilation using eye drops containing 1% tropicamide according to a standardized protocol adapted by all studies affiliated to the SERI.[1, 2]

Slit Lamp Examination: Anterior and posterior segment examinations were performed at the slit-lamp (Haag-Streit model BQ-900; Haag-Streit, Switzerland) using a 78 D lens, which included measurements of vertical dimensions of the optic disc and cup with an eyepiece graticule, etched in 0.1 mm units.

Central Corneal Thickness and Intraocular Pressure: Central corneal thickness (CCT) was measured in each eye with an ultrasound pachymeter (Advent; Mentor O & O Inc, Norwell, Massachusetts). Goldmann applanation tonometry (AT900, Haag-Streit AG International, Switzerland) was used to measure intraocular pressure (IOP) before pupil dilation. One reading was taken from each eye. If the IOP reading was greater than 21mm Hg, a repeat reading was taken, and the second reading was used for analysis.

3.6 SYSTEMIC EVALUATION

Anthropometry: Height was measured in centimeters using a wall-mounted measuring tape. Weight was measured in kilograms using a digital scale (SECA, model 782 2321009; Vogel & Halke, Germany). Body mass index (BMI) was calculated as body weight (in kilograms) divided by body height (in meters) squared.

Blood Pressure and Pulse Rate: Blood pressure was taken with the participant seated and after 5 minutes of rest. Systolic and diastolic blood pressure (BP) and pulse rate were measured with a digital automatic blood pressure monitor (Dinamap model Pro Series DP110X-RW, 100V2; GE Medical Systems Information Technologies, Inc., USA). Blood pressure was measured on two occasions 5 minutes apart. If the blood pressures differed by more than 10 mmHg systolic and 5 mmHg diastolic, a third measurement was made. The blood pressure of the individual was then taken as the mean between the two closest readings.

Mean Ocular Perfusion Pressure: Mean ocular perfusion pressure (OPP) was calculated using the following equation: mean OPP = (2/3 x mean arterial pressure [MAP] – IOP), where MAP = diastolic BP + (1/3 x [systolic BP – diastolic BP]). Systolic and diastolic OPP were calculated using the following equations: systolic OPP = systolic BP – IOP and diastolic OPP = diastolic BP – IOP, respectively.

Biochemistry Tests: Non-fasting venous blood samples were drawn and sent for biochemistry tests, including analysis of total cholesterol, high density lipoprotein cholesterol (HDL), low density lipoprotein cholesterol (LDL), triglycerides, glycosylated haemoglobin (HbA1c), and serum glucose level.

3.7 DEFINITION OF EYE AND SYSTEMIC DISEASES

The clinical definitions of various ocular and systemic conditions are summarized below:

Refractive Error: SE was defined as sphere plus half cylinder. Myopia was defined as a SE of -0.5 D or less, hyperopia as a SE of 0.5D or more, and emmetropia as a SE of between -0.5 and 0.5D. Moderate myopia was defined as a SE of -3.0 D or less. High myopia was defined as SE less than -6.0 D.

Age-Related Macular Degeneration: A digital retinal camera (Canon CR-DGi with a 10-D SLR back; Canon, Tokyo, Japan) was used to obtain color photographs centered at the optic disc and macula of each eye. The photographs were graded for AMD signs based on the Wisconsin Age-Related Maculopathy Grading System.[6]

Diabetic Retinopathy: Signs of DR were graded from fundus photographs using the modified Airlie House classification system and a modification of the ETDRS severity system for DR.[7, 8] Graders assessed the presence/severity of diabetic macular edema, and sign of laser treatment scar. Retinopathy severity was categorized into minimal non-proliferative diabetic retinopathy (NPDR; level 15 through 20), mild NPDR (level 35), moderate NPDR (level 43 through 47), severe NPDR (level 53), and proliferative diabetic retinopathy (PDR, level more than 60). Macular edema was defined by hard exudates in the presence of microaneurysms and blot hemorrhage with one disc diameter from the foveal center or presence of focal photocoagulation scars in the macular areas. Those with macular edema were further divided into cases with clinically significant macular edema (CSME) and without CSME. CSME was defined by macular edema within 550 μm of the foveal center or if focal

photocoagulation scars were present in the macular area. Vision-threatening diabetic retinopathy (VTDR) was defined as the presence of severe NPDR, PDR, or CSME.

Glaucoma Suspect: was defined as having any of the following criteria: (1) IOP>21 mm Hg, (2) vertical cup-to-disc ratio (VCDR) > 0.6 or VCDR asymmetry > 0.2 (3) signs consistent with pseudoexfoliation or pigment dispersion syndrome, (4) narrow angles (posterior trabecular meshwork visible for <180 degrees during static gonioscopy), and (5) peripheral anterior synechiae, (6) other findings consistent with secondary glaucoma, and (7) known history of glaucoma.

Glaucoma: was defined according to the International Society of Geographical and Epidemiological Ophthalmology (ISGEO) criteria based on three categories.[9] In brief, category 1 cases were defined as optic disc abnormality (VCDR/VCDR asymmetry ≥ 97.5 percentile with a corresponding glaucomatous visual field defect. Category 2 cases were defined as having a severely damaged optic disc (VCDR or VCDR asymmetry ≥ 99.5th percentile) in the absence of reliable visual field test results. Category 3 cases were defined for subjects who were blind (corrected visual acuity of <3/60), without visual field or optic disc data and had previous glaucoma surgery or IOP >99.5 percentile.

A narrow anterior chamber angle was diagnosed if the posterior trabecular meshwork was seen for 180° or less of the angle circumference during static gonioscopy. Primary angle-closure glaucoma (PACG) was defined as glaucoma case presented with narrow anterior chamber angles and trabecular obstruction by peripheral iris (such as peripheral anterior synechiae, elevated IOP, iris whirling, "glaukomflecken" lens opacities, or excessive pigment deposition on the trabecular surface). Subjects with glaucoma and an open, normal drainage angle with no

identifiable secondary pathologic processes were defined as primary open angle glaucoma (POAG).

Hypertension: was defined as systolic BP of ≥140 mmHg or diastolic BP≥90 mm Hg at the time of the examination, or a reported history of physician diagnosed hypertension or self-reported history of antihypertensive medication use, or both.

Hyperlipidaemia: was defined as total cholesterol of 6.2 mmol/l or more or use of lipid-lowering drugs.

Diabetes Mellitus: was defined as random glucose ≥11.1 mmol/L or HbA1c≥6.5 mmol/L or subjects' self-reported use of diabetic medication or a reported history of physician-diagnosed diabetes.[10]

3.8 REFERENCES

1. Foong AW, Saw SM, Loo JL, et al. Rationale and methodology for a population-based study of eye diseases in Malay people: The Singapore Malay eye study (SiMES). Ophthalmic Epidemiol 2007;14(1):25-35.

2. Lavanya R, Jeganathan VS, Zheng Y, et al. Methodology of the Singapore Indian Chinese Cohort (SICC) eye study: quantifying ethnic variations in the epidemiology of eye diseases in Asians. Ophthalmic Epidemiol 2009;16(6):325-36.

3. Rosman M, Zheng Y, Wong W, et al. Singapore Malay Eye Study: rationale and methodology of 6-year follow-up study (SiMES-2). Clin Experiment Ophthalmol 2012;40(6):557-68.

4. Cheung CM, Bhargava M, Laude A, et al. Asian age-related macular degeneration phenotyping study: rationale, design and protocol of a prospective cohort study. Clin Experiment Ophthalmol 2012;40(7):727-35.

5. Leung CK, Cheung CY, Weinreb RN, et al. Retinal nerve fiber layer imaging with spectral-domain optical coherence tomography: a variability and diagnostic performance study. Ophthalmology 2009;116(7):1257-63, 63 e1-2.

6. Klein R, Davis MD, Magli YL, et al. The Wisconsin age-related maculopathy grading system. Ophthalmology 1991;98(7):1128-34.

7. Wong TY, Klein R, Islam FM, et al. Diabetic retinopathy in a multi-ethnic cohort in the United States. Am J Ophthalmol 2006;141(3):446-55.

8. Grading diabetic retinopathy from stereoscopic color fundus photographs--an extension of the modified Airlie House classification. ETDRS report number 10. Early Treatment Diabetic Retinopathy Study Research Group. Ophthalmology 1991;98(5 Suppl):786-806.

9. Foster PJ, Buhrmann R, Quigley HA, Johnson GJ. The definition and classification of glaucoma in prevalence surveys. Br J Ophthalmol 2002;86(2):238-42.

10. Association AD. Standards of medical care in diabetes. Diabetes Care 2015;38(supp1):S1 -93.

CHAPETR III FIGURES

Figure 3.1 Study sampling areas in Singapore.

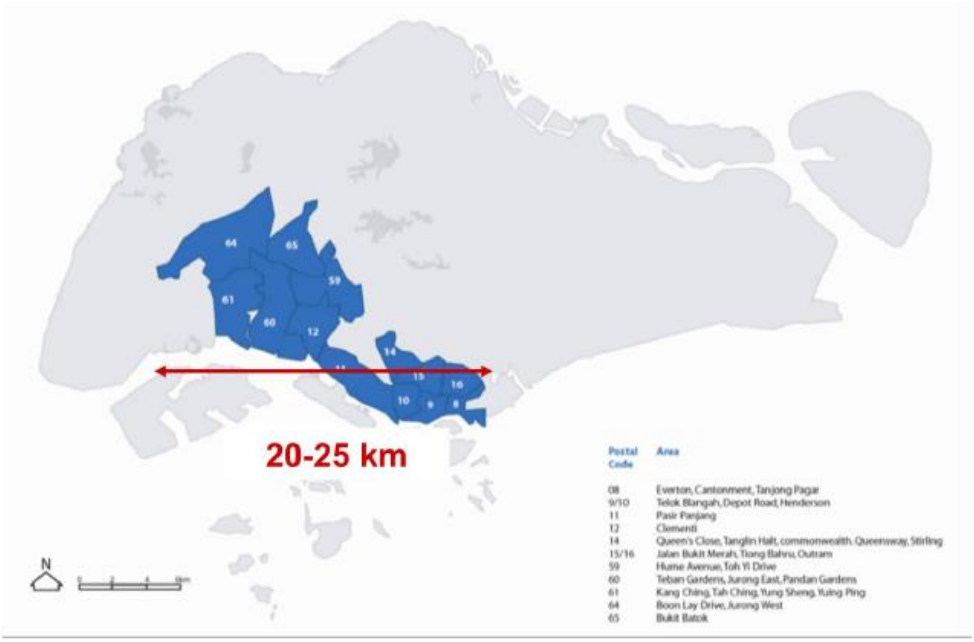

Figure 3.2 An illustration of macular choroid imaged using EDI mode of Spectralis SD-OCT. Each set of images comprised of 7 serial horizontal B-scans (each composed of 1536 A-scans) covering a rectangular region of 30° X 5°centered on the fovea. Distance between consecutive B-scans was 240 µm and each B-scan was averaged 100 times during acquisition.

Figure 3.3 An illustration of peripapillary choroid imaged using EDI mode of Spectralis SD-OCT. The peripapillary region was scanned using a 360°, 3.4 mm diameter circle that was centered on the optic disc, each comprising 100 averaged scans.

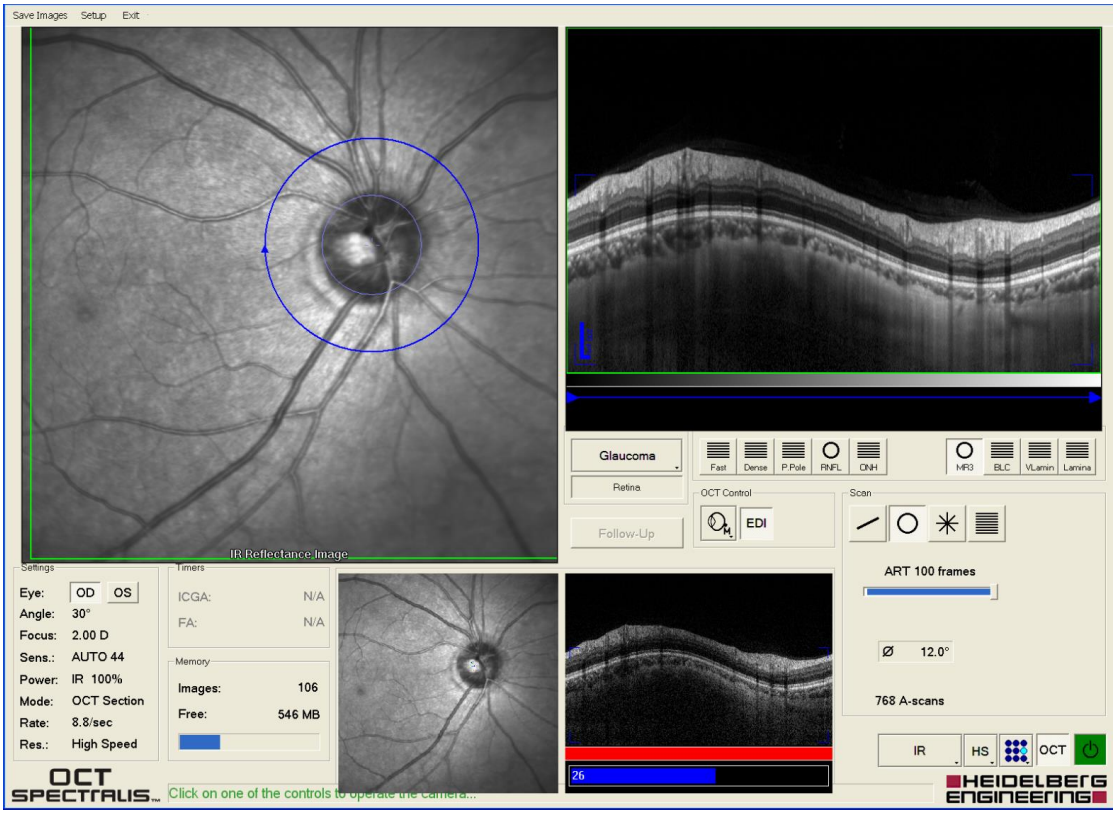

CHAPTER IV

THE VISIBILITY OF CHOROIDAL-SCLERAL INTERFACE

Since CSI forms the posterior boundary of the choroid, it is a principal landmark for quantification of CT which is measured as a perpendicular distance between the RPE and CSI. The visibility of CSI is therefore essential for accurate thickness and volumetric analysis of the choroid. However, despite the current technique of EDI, the contrast between the choroid and the sclera is still weak, giving CSI a poor visibility. We believe/ hypothesize that poor visibility of CSI is the main obstacle to accurate measurement of CT and will result in increased variability in CT measurements. Therefore, to test this hypothesis we conducted a pilot study to assess the percentage visibility of CSI in images obtained by EDI technique of SD-OCT in healthy eyes as well as the variability in CT measurement in images with differently visible CSI. Furthermore we also investigated the effects of a range of ocular and systemic factors on CSI visibility in the population-based sample. Knowledge of the factors influencing the visibility of CSI is crucial for accurate analysis of the thickness and volume of the choroid.

The manuscript relevant to the contents of this chapter has been published in the journal: *Acta Ophthalmologica*

Gupta, P., C. Y. Cheng, C. M. Cheung, H. M. Htoon, Y. Zheng, E. L. Lamoureux, T. Aung, T. Y. Wong and C. Y. Cheung. "Relationship of Ocular and Systemic Factors to the Visibility of Choroidal-Scleral Interface Using Spectral Domain Optical Coherence Tomography." *Acta Ophthalmologica* 2016;94(2):e142-149.

Gupta P., C. Y. Cheung. Refining the Definition of the Choroidal-Scleral Interface. *Acta Ophthalmologica* May 2016 [Epub ahead of print].

4.1 INTRODUCTION

The choroid is a major vascular layer of the eye which provides oxygen and nourishment to the outer layers of the retina including the photoreceptors.[1] Abnormalities in choroidal vasculature (e.g. vascular hyper-permeability, vascular changes and loss, and thinning) are of importance in the pathophysiology of a number of retinal diseases such as AMD,[2, 3] PCV,[4, 5] CSCR[6, 7] and high myopia-related chorioretinal atrophies.[8-10] To elucidate the mechanisms how the choroid may affect chorioretinal diseases, an easy, objective and quantitative analysis of the choroid is required. ICG, and to a lesser extent FA are the current standard to evaluate the choroidal circulation in clinic; however they are invasive and can only provide qualitative assessment of choroid.

Since the introduction of optical coherence tomography based EDI-OCT by Spaide and colleagues,[11] this technique has been used to study changes in CT in many conditions [2, 4, 5, 7-9] as well as other ocular abnormalities.[12] Nonetheless, an accurate estimation of CT with EDI-OCT relies mainly on the visibility of CSI, which anatomically represents the junction between the choroid and the sclera and is a principal landmark for quantitative measurements of choroid. However, unlike retinal layers, the contrast between the choroid and scleral border is weak,[13-16] giving CSI a variable visibility leading to variations and inaccuracy in CT measurements across the clinical studies. There have been no studies which investigate factors which may determine the visibility of the CSI.

The aim of this study was to assess the visibility of CSI in EDI-OCT images in healthy eyes and to determine the effects of a range of ocular and systemic factors on CSI visibility in the population-based sample.

4.2 METHODS

4.2.1 Study Population

Data for this analysis were derived from the SiMES-2, a population-based cohort study of eye diseases in Malay adults aged 46-86 years living in Singapore. Details of the baseline study design, sampling plan, and methodology (SiMES-1), conducted in 2004-6, have been have been described in Chapter III and previously reported elsewhere.[17] For this analysis, we enrolled 176 consecutive participants of the SiMES-2[18] from June 2012 to January 2013. Participants recruited in this phase underwent standardized and detailed ophthalmic examination, including Spectralis EDI SD-OCT.

Normal participants had no history of ocular disease except cataract. Participants were excluded based on the following characteristics: best corrected LogMAR VA >0.3, evidence of macular or vitroretinal diseases, DR, previous retinal or refractive surgery, past history of intraocular surgery, or clinical features compatible with a diagnosis of glaucoma suspect or glaucoma.

A glaucoma suspect[19] was defined as described in Chapter III. Glaucoma was diagnosed and classified using the ISGEO scheme,[20] based on findings from gonioscopy, optic disc characteristics, and visual fields results (see details in Chapter III). The study was approved by the Institutional Review Board of SERI. It followed the tenants of the Declaration of Helsinki and written informed consent was obtained from the subjects.

4.2.2 EDI-OCT Imaging

CT was obtained using a SD-OCT (Spectralis, Heidelberg Engineering, Heidelberg, Germany) with EDI modality as specified in details in Chapter III. All the scans included in the study had signal strength of at least 18, which is considered

as acceptable quality. One of the authors (PG) who was masked to subject characteristics and clinical diagnosis performed the EDI-OCT examination. Only the horizontal section passing through the center of the fovea was selected for analysis.

4.2.3 Image Analysis

Choroidal Thickness Measurement: Using the Spectralis linear measurement tool, a single observer (PG) measured CT perpendicularly from the outer portions of the hyperreflective line, corresponding to the RPE (automatically detected by the instrument), to the hyporeflective line or margin corresponding to the sclerochoroidal interface (drawn manually) at sub-foveal location.

CSI Visibility Grading System: We developed a new grading system to assess visibility of CSI for EDI-OCT images. 2 masked observers evaluated all the OCT scans to locate the CSI on each EDI-OCT image. The CSI was defined as a hypo-reflective line between the large vessel layer of the choroid and the sclera **(Figure 4.1)**. For the grading of CSI visibility, the EDI-OCT images were given a score between 0 and 2. A score of "2" was assigned if the image contained a well-defined CSI. A score of "1" was assigned if the visibility of CSI was between well-defined and poorly defined CSI and a score of "0" was given if the image had poorly defined CSI visibility i.e. no clearly identifiable border between the choroid and sclera was seen. **Figure 4.1** demonstrates examples of well-defined, moderately defined and poorly defined CSI in EDI-OCT images in the SiMES-2 cohort.

Reliability Assessment: We evaluated both the intra and inter-observer reliability in assessing CSI visibility. For intra-observer reliability, 176 Spectralis images were assessed again by the same grader (grader 1 vs. grader 1) after an interval of one

week. Two independent graders (grader 1 vs. grader 2) assessed the inter-observer reliability of CSI visibility in 176 Spectralis images.

In addition, sub-foveal CT at the foveal center was measured twice by the same grader to assess the reliability of CT measurement in each score of CSI visibility (15 images for each score).

4.2.4 Measurement of Ocular Factors

All participants underwent an extensive and standardized examination procedure, which included measurement of VA monocularly using LogMAR number chart (Lighthouse International, New York, USA) at a distance of 4 m. IOP was measured with a Goldmann applanation tonometer (Haag-Streit, Bern, Switzerland) before pupil dilation. The static refraction of each eye was measured using an autorefractor (Canon RK 5 Auto Ref-Keratometer, Canon Inc. Ltd., Tochigiken, Japan). SE refraction was calculated as the sum of the value of the spherical value and half of the cylindrical value. CCT was measured with an ultrasound pachymeter (Advent, Mentor O & O, Norwell, MA) and the mean of five measurements was used in the analysis. AL, corneal curvature and ACD were measured with a non-contact partial coherence laser interferometry (IOLMaster V3.01, Carl Zeiss Meditec AG, Jena, Germany) and the mean of five measurements was used in the analysis. Lens opacity was assessed by trained ophthalmologists using Lens Opacities Classification System (LOCS) III [21] with a Haag-Streit slit-lamp microscope (model BQ-900) in comparison to standard photographic slides for nuclear opalescence, nuclear color, cortical and posterior subcapsular cataract. Retinal thickness of central 1 mm region was obtained from Spectralis OCT after pupil dilation.

4.2.5 Assessment of Demographic, Lifestyle and Systemic Factors

All participants underwent a detailed interview using standardized questionnaires. Information on socio-demographic status, lifestyle risk factors (e.g. smoking, alcohol consumption), medication use and self-reported history of systemic disease were collected. Systolic and diastolic BP were measured using a digital automatic blood pressure monitor (Dinamap model Pro Series DP110X-RW, 100V2; GE Medical Systems Information Technologies, Inc., Milwaukee, WI), after subjects were seated for at least five minutes. BMI was calculated as body weight (in kilograms) divided by body height (in meters) squared. Smoking status was defined as those currently smoking, ex-smokers and non-smokers. The number of packs smoked per week was recorded. Nonfasting venous blood samples were analyzed at the National University Hospital Reference Laboratory for biochemical testing of serum total cholesterol, HDL cholesterol, LDL cholesterol, triglycerides, glycosylated haemoglobin (HbA1c), glucose and creatinine.

4.2.6 Statistical Analyses

Statistical analyses was performed using MedCalc version 12.3 (Medcalc Software, Ostend, Belgium) and SPSS version 20.0 (SPSS, Inc., Chicago, IL, USA).

Intra-inter Grader Reliability Assessment: The intra-inter grader reliability in assessing CSI visibility was measured by weighted Kappa Statistics (K_w).[22] K_w values of 0.81 – 1.00 indicate almost perfect agreement, values of 0.61 – 0.80 indicate good agreement and values of 0.41 to 0.60 indicate moderate agreement. Values of less than 0.40 indicate poor to fair agreement. The reliability of CT measurement in each score of CSI visibility was measured by the absolute agreement model of the intra-class correlation coefficient (ICC). ICC value of 0.81 – 1.00 indicates almost perfect agreement. Values of less than 0.40 indicate poor to fair agreement.

Relationship of Ocular and Systemic Factors with CSI Visibility: Since the dependent variable (CSI visibility scores 0, 1 & 2) is ordinal in nature, we used ordinal regression for our analysis. Univariate and multiple ordinal regression analysis were performed to assess the ocular and systemic factors (independent variables) related to the CSI visibility (dependent variable). For multiple regression analysis, gender and factors which showed significant association in univariate analysis were included. The three groups (CSI visibility score 0, 1 & 2) were not evenly distributed. Thus, the Logit link function could not be used and instead complementary log-log (higher scores more probable) was used. However, this function could only determine the direction of the relationship between each predictor and the ordinal nature of categorical outcome. A p-value of < 0.05 was considered statistically significant. Right eye (n= 161) of each subject was selected for the analysis. However, when images of right eye was not available then left eye (n= 15) was used.

4.3 RESULTS

4.3.1 Participants' Characteristics and Distribution of CSI Visibility Grades

Table 4.1 shows the baseline characteristics and the distribution of CSI visibility grade of the study subjects. A total of 176 eyes from 176 subjects (85 men and 91 women) with a mean±SD (standard deviation) age of 60.44±8.19 years (range, 48-86 years) were included in the study. The CSI was clearly identifiable (score 2) in 59.1% (104/176 eyes), poorly defined (score 0) in 8.5 % (15/176 eyes) and was between clearly and poorly defined (score 1) in 32.4% (57/176 eyes) of our subjects.

4.3.2 Intra- and Inter-grader Reliability Assessment

Table 4.2 shows the intra and inter grader reliability assessment of CSI visibility. Both the intra and inter-observer reliability was moderate to good (Kw =

0.78, 95% CI: 0.70-0.85 and Kw = 0.74, 95% CI: 0.64-0.83 for intra and inter-observer reliability respectively).

The reliability of sub-foveal CT measurement was highest for CSI visibility score 2 (ICC = 0.977, 95% CI, 0.935 to 0.992) followed by score 1 (ICC = 0.734, 95% CI, 0.585 to 0.940) and score 0 (ICC = 0.514, 95% CI, 0.058 to 0.853) respectively. In addition, in our previously published paper,[23] we have reported that both the intra-grader reliability (ICC: 0.87 to 0.94) and inter-grader reliability (ICC: 0.90 to 0.93) for the CT measurement using Spectralis SD-OCT were excellent.

4.3.3 Association of Ocular and Systemic Factors with Visibility of CSI

Among the ocular factors, decreased AL ($p = 0.006$), thicker retinal ($p<0.001$) and choroidal ($p=0.012$) thicknesses were more likely to have lower CSI visibility score. Among other factors, young individuals ($p = 0.003$) and those with diabetes ($p = 0.033$) were associated with lower CSI visibility score. We did not observe any associations between CSI visibility with other factors for example gender, BMI, systolic and diastolic blood pressure, HDL and LDL cholesterol, blood creatinine, triglycerides, serum blood glucose level, HbA1c, smoking status, and hypertension (all $p>0.10$) **(Table 4.3)**. Factors with $p<0.10$ in the univariate analysis were further included into the multivariate analysis. However, because of collinearity between AL and spherical equivalent, only AL was selected and retained in the multivariate analysis.

In the multivariate adjusted model, decreased AL (estimate of ordinal regression = 0.465, $p = 0.003$), thicker retinal thickness (estimate of ordinal regression = -0.030, $p = 0.004$), younger age (estimate of ordinal regression = 0.045, $p = 0.030$) and diabetes (estimate of ordinal regression = -0.746, $p = 0.004$) were significantly and independently associated with lower CSI visibility score (**Table 4.4)**. In this

sample, we found that 10.9% of younger people (age less than 60 years), 12.5% of those with thicker retinal thickness (≥ 280 μm), 11.8% of those with shorter AL (≤ 23 mm) and 11.76% of those with diabetes had poor CSI visibility (grade 0).

4.4 DISCUSSION

In this study, we found that only 60% of subjects had well delineated CSI that allowed good visualization of the choroid, and the CT measurements had higher variability in the images with poor visualization of CSI. Moreover, we demonstrated that the visualization of CSI was poorer in eyes with shorter eye ball, thicker retinal thickness, and in younger persons and persons with diabetes.

Correct identification and knowledge of factors determining CSI visibility is essential for the accuracy and performance of imaging programs that aim to automatically detect this anatomical structure. We found that younger age was associated with poorer identification of choroid scleral junction **(Figure 4.2)**. Previous histologic studies have shown a decrease in vascular density, overall luminal area and diameter of chorio-capillary vessels with increase in age.[24-26] This leads to a decrease in physiological functions of the choroid i.e. the ability of the choroid to provide sufficient levels of oxygen and other metabolites to the RPE and outer retina may decrease[11] contributing to the onset of many diseases in elderly people. There is an increasing trend of data from other older adult studies which states that CT decreases with age.[27,28] Thicker choroid in younger age would undergo more attenuation of incident light resulting in poor visualization of the CSI. Nevertheless, we did not find any significant association between CSI visibility score and CT in the multiple regression model **(Table 4.4)**. Another possible explanation of poorer CSI visibility at

younger age is higher concentration of choroidal melanin pigments in young individuals, which tend to progressively decrease with advancing age.[29]

In addition to age, persons with diabetes had poorer visibility of choroid-scleral junction. There is inconsistency in literature in terms of choroidal blood flow, which is reported to decrease, increase and remain unchanged in patients with diabetes.[30-32] However, many studies have demonstrated significant decrease in choroidal blood flow in diabetic patients, especially those with macular edema.[30, 33] However, in our cohort, none of the diabetic subjects had diabetic macular edema or intraretinal cystic changes. While comparing the retinal thickness in diabetics (259.15 μm) and non-diabetics (262.12 μm), we found no significant difference ($p = 0.402$) in thickness. Thus, the reasons for diabetic people having poor CSI visibility are still unclear. We can only speculate that poor CSI visibility in diabetics might be associated with blood flow changes in choroid, but unfortunately, in our study we did not obtain any information pertaining to blood flow. An alternative explanation could be the hypereflectivity of incident light from the intraretinal fluid which can lead to a shadowing effect of the deeper layers resulting in poorer CSI visibility.[34]

Another reason for diabetic subjects having poor CSI visibility could be the fact that diabetes leads to a faster development of cataract which in turn might be associated with poorer visibility of CSI. However, in a subgroup analysis in diabetic subjects with cataracts, we found no significant association between the presence of cataract and CSI visibility score ($p = 0.074$, chi-square test), indicating that the presence of cataract in diabetic subjects does not affect the visibility of CSI. In our study, we also found that thicker retinal thickness was associated with poorer CSI visibility. It is noted that there were no relationships between CSI visibility with most systemic factors such as BMI, blood pressure, cholesterol, glucose, and smoking.

Among the ocular factors, the visibility of CSI was influenced by AL. CSI was poorly distinct in eyes with shorter AL. Our results are compatible with histologic findings that in eyes with greater AL, the elongation of the eyeball leads to mechanical stretching and thinning of retina.[35, 36] The excessive elongation affects not only the retina but also the choroid and Bruch membrane. There is found to be choroidal thinning in eyes with high myopia[8, 9, 27, 37] due to significant thinning of the choriocapillaris and focal lack of vessels.[38-40] The sclera is also weaker in myopes with a correlation between high myopes and scleral thinning found in human eyes.[41] The choroid adheres to the sclera because of the fixed position of the blood vessels passing through the sclera, and it is likely that the choroid is stretched in myopic eyes.[42] This allows more penetration of light into the deep choroid giving greater resolution and potentially better specification of the posterior choroidal border. In addition, myopic subjects usually have less pigmented RPE which facilitates detection of the scleral interface.

An important factor in standardizing CT measurements is the definition of the choroid-scleral junction. While most EDI-OCT studies, including the landmark Spaide et al. study, define the choroidal-scleral junction as the inner border of the sclera, a recent study by Yiu et al.[43] reported the presence of a hyporeflective band likely corresponding to the suprachoroidal layer (SCL). However, it is often difficult to visualize SCL and in Yiu et al. study, SCL was visible in only 45% of their healthy Caucasian subjects. In contrast, in our cohort of healthy Asian subjects, we could not appreciate the presence of SCL and therefore, like majority of other EDI-OCT studies on CT assessment, we considered inner border of the sclera as posterior boundary of the choroid. A probable reason for invisible SCL in our subjects of Asian descent is

the presence of greater pigmentation in Asian eyes compared to Caucasians, thereby affecting the visibility of SCL.

The strengths of this study include its unselected population based sample, standardized assessment of systemic and ocular factors, and laboratory investigations. Our study had some limitations. Although the location of the CSI on Spectralis images was determined qualitatively as the junction between posterior choroid and sclera, there was no reference standard to confirm where this structure is actually located in the eye. The study population only consisted of subjects of Malay ethnicity and the findings may vary in other racial groups. Further studies in other ethnic populations are thus warranted. Although we performed a 7 line scan but only the horizontal section passing through the center of the fovea was used to evaluate the CSI. It is ideal to assess intra-session repeatability. However, in this study we did not assess intra-session repeatability of the CSI visibility. Knowing that subject pigmentation might influence signal penetration thus affecting the visibility of CSI, it was not considered in our study. However, all our subjects were of Malay ethnicity having more or less similar pigmentation, therefore, there should be no impact of pigmentation on our results. Visualization of the choroidal scleral boundary may vary across different OCT modalities. However, this study only described the visibility of CSI using the Spectralis OCT. Lastly, even though we have explored series of ocular and systemic factors affecting CSI, reflectivity of the choroid might have influenced the visibility of CSI.

4.5 CONCLUSIONS

In summary, we found that only 60% of our images had well delineated CSI and the variability in the measurement of CT was higher in the images with poorly

defined CSI. The factors associated with poorer CSI visibility are younger age, shorter AL, thicker retinal thickness and diabetes. The CSI visibility is critical for accurate determination of CT which can help clinicians evaluate choroioretinal disorders such as age related macular degeneration, central serous chorioretinopathy as well as monitoring the effect of therapeutic interventions.

4.6 REFERENCES

1. Linsenmeier RA, Padnick-Silver L. Metabolic dependence of photoreceptors on the choroid in the normal and detached retina. Invest Ophthalmol Vis Sci 2000;41(10):3117-23.

2. Grossniklaus HE, Green WR. Choroidal neovascularization. Am J Ophthalmol 2004;137(3):496-503.

3. Koizumi H, Yamagishi T, Yamazaki T, et al. Subfoveal choroidal thickness in typical age-related macular degeneration and polypoidal choroidal vasculopathy. Graefes Arch Clin Exp Ophthalmol 2011;249(8):1123-8.

4. Gomi F, Tano Y. Polypoidal choroidal vasculopathy and treatments. Curr Opin Ophthalmol 2008;19(3):208-12.

5. Chung SE, Kang SW, Lee JH, Kim YT. Choroidal thickness in polypoidal choroidal vasculopathy and exudative age-related macular degeneration. Ophthalmology 2011;118(5):840-5.

6. Gupta B, Mohamed MD. Photodynamic therapy for variant central serous chorioretinopathy: efficacy and side effects. Ophthalmologica 2011;225(4):207-10.

7. Imamura Y, Fujiwara T, Margolis R, Spaide RF. Enhanced depth imaging optical coherence tomography of the choroid in central serous chorioretinopathy. Retina 2009;29(10):1469-73.

8. Fujiwara T, Imamura Y, Margolis R, et al. Enhanced depth imaging optical coherence tomography of the choroid in highly myopic eyes. Am J Ophthalmol 2009;148(3):445-50.

9. Ikuno Y, Tano Y. Retinal and choroidal biometry in highly myopic eyes with spectral-domain optical coherence tomography. Invest Ophthalmol Vis Sci 2009;50(8):3876-80.

10. Fitzgerald ME, Wildsoet CF, Reiner A. Temporal relationship of choroidal blood flow and thickness changes during recovery from form deprivation myopia in chicks. Exp Eye Res 2002;74(5):561-70.

11. Spaide RF, Koizumi H, Pozzoni MC. Enhanced depth imaging spectral-domain optical coherence tomography. Am J Ophthalmol 2008;146(4):496-500.

12. Beck M, Schlatter B, Wolf S, Zinkernagel MS. Senile scleral plaques imaged with enhanced depth optical coherence tomography. Acta Ophthalmol 2014.

13. Duan L, Yamanari M, Yasuno Y. Automated phase retardation oriented segmentation of chorio-scleral interface by polarization sensitive optical coherence tomography. Opt Express 2012;20(3):3353-66.

14. Chiu SJ, Li XT, Nicholas P, et al. Automatic segmentation of seven retinal layers in SDOCT images congruent with expert manual segmentation. Opt Express 2010;18(18):19413-28.

15. Ghorbel I, Rossant F, Bloch I, et al. Automated segmentation of macular layers in OCT images and quantitative evaluation of performances. Pattern Recognition 2011;44(8):1590-603.

16. Kajic V, Esmaeelpour M, Povazay B, et al. Automated choroidal segmentation of 1060 nm OCT in healthy and pathologic eyes using a statistical model. Biomed Opt Express 2012;3(1):86-103.

17. Foong AW, Saw SM, Loo JL, et al. Rationale and methodology for a population-based study of eye diseases in Malay people: The Singapore Malay eye study (SiMES). Ophthalmic Epidemiol 2007;14(1):25-35.

18. Rosman M, Zheng Y, Wong W, et al. Singapore Malay Eye Study: rationale and methodology of 6-year follow-up study (SiMES-2). Clin Experiment Ophthalmol 2012;40(6):557-68.

19. Shen SY, Wong TY, Foster PJ, et al. The prevalence and types of glaucoma in malay people: the Singapore Malay eye study. Invest Ophthalmol Vis Sci 2008;49(9):3846-51.

20. Foster PJ, Buhrmann R, Quigley HA, Johnson GJ. The definition and classification of glaucoma in prevalence surveys. Br J Ophthalmol 2002;86(2):238-42.

21. Chylack LT, Jr., Wolfe JK, Singer DM, et al. The Lens Opacities Classification System III. The Longitudinal Study of Cataract Study Group. Arch Ophthalmol 1993;111(6):831-6.

22. Fleiss JL, Cohen J. The Equivalence of Weighted Kappa and the Intraclass Correlation Coefficient as Measures of Reliability. Educational and Psychological Measurement 1973;33(3):613-9.

23. Gupta P, Sidhartha E, Girard MJ, et al. A simplified method to measure choroidal thickness using adaptive compensation in enhanced depth imaging optical coherence tomography. PLoS One 2014;9(5):e96661.

24. Ramrattan RS, van der Schaft TL, Mooy CM, et al. Morphometric analysis of Bruch's membrane, the choriocapillaris, and the choroid in aging. Invest Ophthalmol Vis Sci 1994;35(6):2857-64.

25. Feeney-Burns L, Burns RP, Gao CL. Age-related macular changes in humans over 90 years old. Am J Ophthalmol 1990;109(3):265-78.

26. Sarks SH. Ageing and degeneration in the macular region: a clinico-pathological study. Br J Ophthalmol 1976;60(5):324-41.

27. Margolis R, Spaide RF. A pilot study of enhanced depth imaging optical coherence tomography of the choroid in normal eyes. Am J Ophthalmol 2009;147(5):811-5.

28. Fujiwara A, Shiragami C, Shirakata Y, et al. Enhanced depth imaging spectral-domain optical coherence tomography of subfoveal choroidal thickness in normal Japanese eyes. Jpn J Ophthalmol 2012;56(3):230-5.

29. Weiter JJ, Delori FC, Wing GL, Fitch KA. Retinal pigment epithelial lipofuscin and melanin and choroidal melanin in human eyes. Invest Ophthalmol Vis Sci 1986;27(2):145-52.

30. Langham ME, Grebe R, Hopkins S, et al. Choroidal blood flow in diabetic retinopathy. Exp Eye Res 1991;52(2):167-73.

31. MacKinnon JR, O'Brien C, Swa K, et al. Pulsatile ocular blood flow in untreated diabetic retinopathy. Acta Ophthalmol Scand 1997;75(6):661-4.

32. Schmidt KG, von Ruckmann A, Kemkes-Matthes B, Hammes HP. Ocular pulse amplitude in diabetes mellitus. Br J Ophthalmol 2000;84(11):1282-4.

33. Geyer O, Neudorfer M, Snir T, et al. Pulsatile ocular blood flow in diabetic retinopathy. Acta Ophthalmol Scand 1999;77(5):522-5.

34. Adhi M, Brewer E, Waheed NK, Duker JS. Analysis of Morphological Features and Vascular Layers of Choroid in Diabetic Retinopathy Using Spectral-Domain Optical Coherence Tomography. JAMA Ophthalmol 2013.

35. Lim MC, Hoh ST, Foster PJ, et al. Use of optical coherence tomography to assess variations in macular retinal thickness in myopia. Invest Ophthalmol Vis Sci 2005;46(3):974-8.

36. Lam DS, Leung KS, Mohamed S, et al. Regional variations in the relationship between macular thickness measurements and myopia. Invest Ophthalmol Vis Sci 2007;48(1):376-82.

37. Ikuno Y, Kawaguchi K, Nouchi T, Yasuno Y. Choroidal thickness in healthy Japanese subjects. Invest Ophthalmol Vis Sci 2010;51(4):2173-6.

38. Hirata A, Negi A. Morphological changes of choriocapillaris in experimentally induced chick myopia. Graefes Arch Clin Exp Ophthalmol 1998;236(2):132-7.

39. Grossniklaus HE, Green WR. Pathologic findings in pathologic myopia. Retina 1992;12(2):127-33.

40. Okabe S, Matsuo N, Okamoto S, Kataoka H. Electron microscopic studies on retinochoroidal atrophy in the human eye. Acta Med Okayama 1982;36(1):11-21.

41. Avetisov ES, Savitskaya NF, Vinetskaya MI, Iomdina EN. A study of biochemical and biomechanical qualities of normal and myopic eye sclera in humans of different age groups. Metab Pediatr Syst Ophthalmol 1983;7(4):183-8.

42. Wildsoet CF. Myopia and Nearwork: Butterworth-Heinemann, 1998; 31-90.

43. Yiu G, Pecen P, Sarin N, et al. Characterization of the choroid-scleral junction and suprachoroidal layer in healthy individuals on enhanced-depth imaging optical coherence tomography. JAMA Ophthalmol 2014;132(2):174-81.

CHAPTER IV TABLES

Table 4.1 A summary of subjects' demographics, ocular parameters and systemic factors

	Included (n =176)
Age, yrs	60.44 (8.19)
Gender, % male	48.3
Spherical equivalent, D	0.03 (2.03)
Best corrected visual acuity, logMAR	0.13 (0.10)
Axial length, mm	23.62 (1.07)
Anterior chamber depth, mm	3.22 (.35)
Corneal curvature, mm	7.45 (1.19)
Intraocular pressure, mmHg	14.90 (2.94)
Central corneal thickness, μm	541.15 (35.68)
LOCS III nuclear cataract, %	35 (19.9)
LOCS III cortical, %	56 (38.8)
LOCS III PSC, %	8 (4.5)
Retinal thickness, μm	261.25 (21.17)
Subfoveal choroidal thickness, μm	244.36 (95.31)
OCT signal strength	30.56 (5.08)
Systolic blood pressure, mmHg	137.23 (19.50)
Body mass index, kg/m^2	77.52 (9.84)
Current smoking, %	36 (20.05)
Diabetes Mellitus, %	51 (29.0)
Hypertension, %	74 (42.0)
Visibility Grade	
Grade 0	15 (8.5)
Grade 1	57 (32.4)
Grade 2	104 (59.1)

Data are means (SD), except for gender, cataracts, HbA1c, current smoking, diabetes hypertension and visibility grades which are expressed as number (%).

Table 4.2 Intra- and interobserver reliability assessment of CSI visibility

Inter and intra-grader reliability	Inter-grader				Intra-grader			
	Score 0	Score 1	Score 2	Total	Score 0	Score 1	Score 2	Total
Score 0	12	4	1	17	8	10	0	18
Score 1	5	35	12	52	3	39	13	55
Score 2	1	10	96	107	0	10	93	103
Total	18	49	109	176	11	59	106	176

Gray shades indicate agreement of CSI visibility scores between the graders (intra and inter).

Table 4.3 Univariate analysis between ocular and systemic factors (independent variables) with visibility of choroidal scleral interface (dependent variable)

	Choroid Scleral Interface Visibility			
			95% Confidence Interval	
	Estimate	P-value*	Lower bound	Upper bound
Ocular factors				
Axial length (mm)	0.375	**0.006**	0.106	0.645
Spherical equivalent (D)	-0.143	0.054	-2.88	0.003
Anterior chamber depth (mm)	-0.290	0.383	-0.942	0.362
Central corneal thickness (μm)	0.004	0.229	-0.003	0.011
Corneal curvature (mm)	0.104	0.197	-0.054	0.262
Intraocular pressure (mmHg)	0.021	0.605	-0.059	0.101
LOCS III nuclear cataract (no vs. yes)	-0.683	0.056	-1.382	0.017
LOCS III cortical (no vs. yes)	0.011	0.966	-0.487	0.509
LOCS III PSC (no vs. yes)	0.546	0.261	-0.406	1.498
Retinal thickness (μm)	-0.034	**<0.001**	-0.052	-0.016
Subfoveal choroidal thickness (μm)	-0.003	**0.012**	-0.006	-0.001
OCT signal strength	0.022	0.352	-0.024	0.068
Systemic factors				
Age (yrs)	0.048	**0.003**	0.016	0.080
Diabetes Mellitus (yes vs. no)	-0.524	**0.033**	-1.006	-0.042

Bolded font indicates statistical significance.

*Given the ordinal nature of dependent variable (visibility of CSI), p-values are based on ordinal regression

Table 4.4 Multivariate analysis of ocular and systemic factors (independent variables) with visibility of choroidal scleral interface (dependent variable)

	Choroid Scleral Interface Visibility			
			95% Confidence Interval	
	Estimate	P-value*	Lower bound	Upper Bound
Axial length (mm)	0.465	**0.003**	0.160	0.771
LOCS III nuclear cataract (no vs. yes)	-0.104	0.795	-0.891	0.683
Age (yrs)	0.045	**0.030**	0.004	0.086
Retinal thickness (μm)	-0.030	**0.004**	-0.050	-0.009
Subfoveal choroidal thickness (μm)	-0.002	0.278	-0.005	0.001
Gender (male vs. female)	0.218	0.413	-0.304	0.740
Diabetes Mellitus (yes vs. no)	-0.746	**0.004**	-1.256	-0.236

Bolded font indicates statistical significance.
*Given the ordinal nature of dependent variable (visibility of CSI), p-values are based on ordinal regression; adjusting for age, gender, diabetes, axial length, retinal and choroidal thickness.

CHAPTER IV FIGURES

Figure 4.1 The choroidal-scleral interface (CSI) is indicated by hyper-reflective line shown by arrowheads. **Panel (A)** demonstrates an example of a well-defined CSI, **Panel (B)** shows a moderately defined CSI and **Panel (C)** a poorly defined CSI in EDI-OCT image in the SiMES-2 cohort.

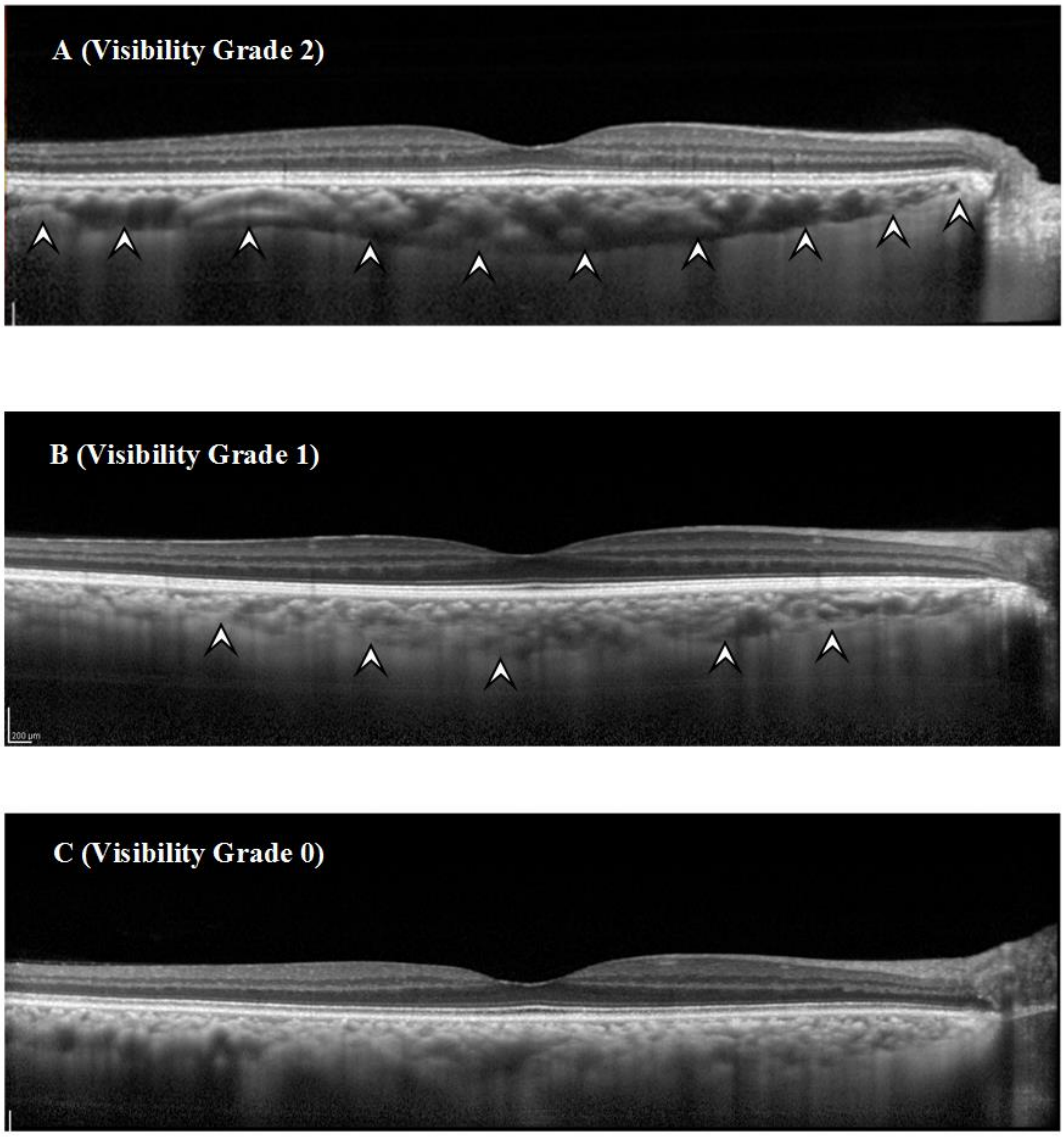

Figure 4.2 Comparison of CSI visibility between EDI-OCT scans in two subjects of different ages. **(A)** A 46-year-old male with poorly demarcated CSI (subfoveal choroidal thickness of 326 µm). **(B)** An 83-year-old man with CSI distinctly visible (subfoveal choroidal thickness of 163 µm).

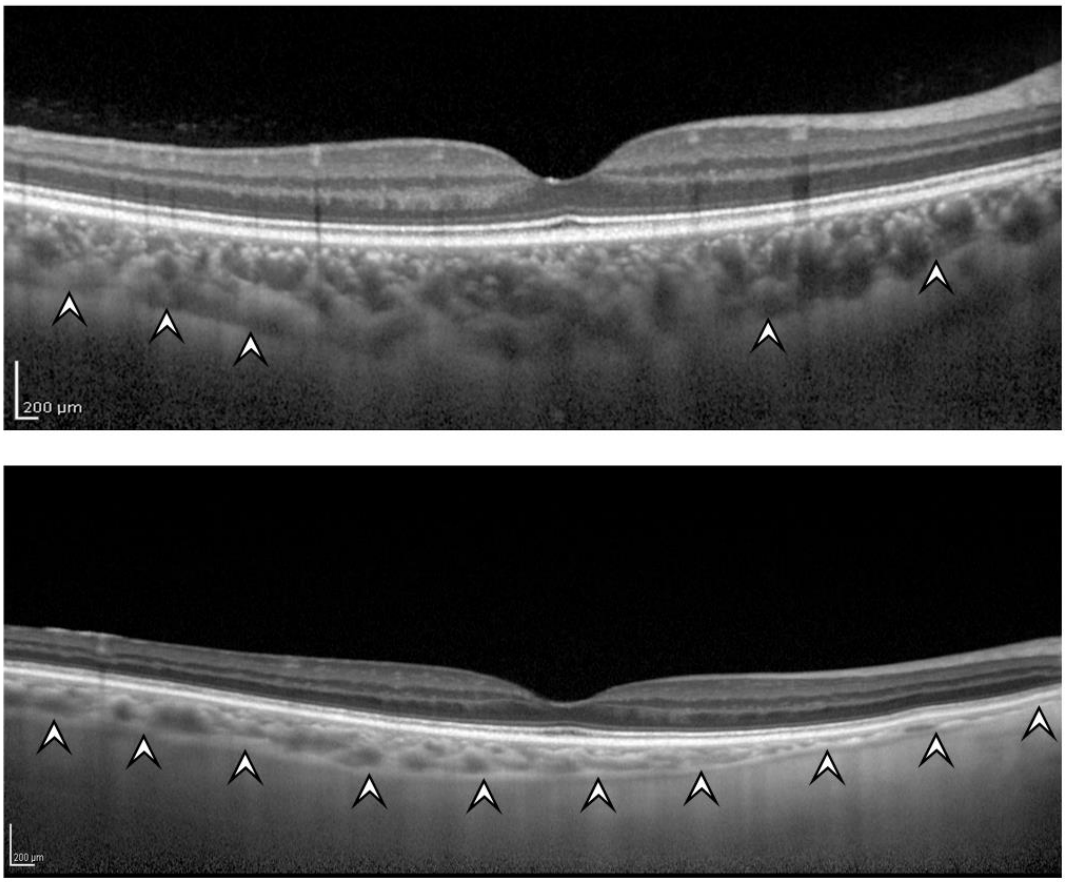

Figure 4.3 Comparison of CSI visibility between EDI-OCT scans in two subjects according to refractive status. **(A)** A 46-year-old male with no refractive error (AL=23.41) and a poorly demarcated CSI (subfoveal choroidal thickness of 275 µm). **(B)** A 46-year-old male with myopia (AL=29.57) with a well-defined CSI (subfoveal choroidal thickness of 165 µm).

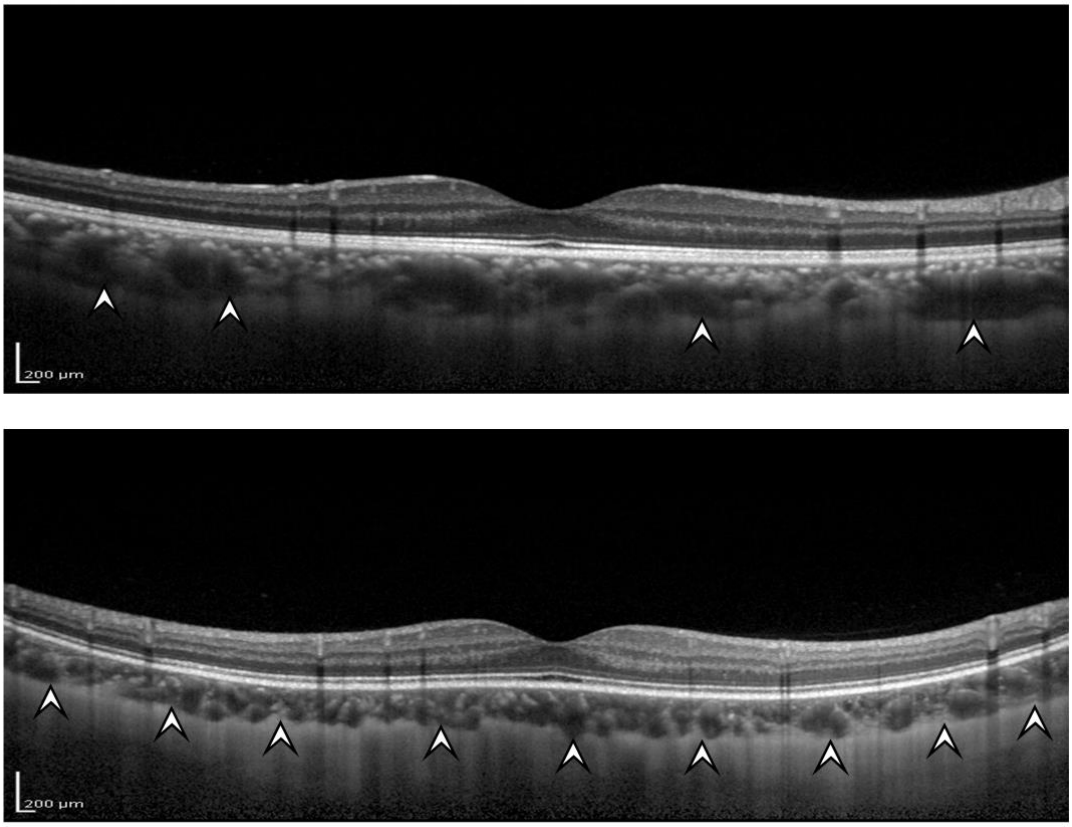

CHAPTER V

ENHANCEMENT OF CHOROID-SCLERAL INTERFACE VISIBILITY USING THE SEMI-AUTOMATED TECHNIQUE OF ADAPTIVE COMPENSATION

In chapter IV we found that 40% of our EDI-OCT macular images had poorly defined CSI and the variability in the measurement of CT was higher in the images with poorly defined CSI. The results from Chapter IV confirms that clearly visible CSI leads to better delineation of choroidal boundaries in turn leading to accurate measurement of CT. Therefore, in this Chapter we made an attempt to enhance the visibility of macular CSI by employing a novel semi-automated technique of "adaptive compensation".

We observed that compared to macular scans, the visibility of CSI in peripapillary scans were generally very good. In a sample of 100 randomly selected peripapillary scans, nearly all the images had CSI visibility of grade 1 and above. Therefore, we did not proceed further to categorize our peripapillary images into 3 grades of CSI visibility and neither enhanced the visibility of peripapillary CSI.

The manuscript relevant to the contents of this chapter has been published in the journal:

PLoS One

Gupta, P., E. Sidhartha, M. J. Girard, J. M. Mari, T. Y. Wong and C. Y. Cheng. "A Simplified Method to Measure Choroidal Thickness Using Adaptive Compensation in Enhanced Depth Imaging Optical Coherence Tomography." *PLoS One* 2014;9(5):e96661.

5.1 INTRODUCTION

The choroid is important to support retinal and visual function as it supplies nutrients and oxygen to RPE cells and photoreceptors.[1] Therefore, the choroid may play a role in the pathophysiology of many vision threatening retinal diseases such as AMD,[2, 3] PCV,[4, 5] CSCR,[6, 7] Vogt-Koyanagi-Harada[8] disease and myopic macular degeneration.[9-12] To elucidate the mechanisms through which the choroid affects these retinal diseases, quantitative assessment of choroidal characteristics such as CT is required.

However, it was not trivial to image CT because of its posterior location and pigments in the RPE layer,[13] until the advent of SD-OCT with EDI. EDI SD-OCT has provided many new insights into choroidal qualitative morphology. However, to date a notable disparity exists between the CT measurements obtained in different studies. Such variations could be due to unavailability of a standardized and simple to use measurement method and absence of built-in automated software to measure CT in most of the commercially available OCT machines.[14] At present, most of the studies perform the measurements manually by using the in-built caliper system provided by the machine, which is prone to measurement errors. The manual method is also time- and effort-consuming, making it unfeasible especially when dealing with large population data.

As a result, while many studies have published the distribution of CT in patients with retinal diseases and normal controls,[15-19] none of these studies have clearly described the method used in detailed to measure CT. Therefore, the reliability of the CT measurement methods in most of the papers is unknown. In this paper, we describe a simple, semi-automated, time-efficient method to measure CT using images acquired by EDI SD-OCT and available compensation algorithms. We aimed

to assess the reliability of this new CT measurement technique in a sample of healthy eyes.

5.2 MATERIALS AND METHODS

5.2.1 Study Subjects and Design

Data for this analysis were derived from the SiMES, a population-based cross-sectional study of eye diseases in Malay adults, age ranged from 40-80 years living in Singapore. Details of the study design, sampling plan, and methodology have been described in Chapter III and previously elsewhere.[20] In brief, participants recruited in the current study underwent standardized and detailed ophthalmic examination, including Spectralis EDI SD-OCT imaging (see next section). The study was approved by the Institutional Review Board of SERI. It followed the tenants of the Declaration of Helsinki and written informed consent was obtained from the subjects after explanation of the nature and possible consequences of the study.

5.2.2 Inclusion and Exclusion Criteria

Spectralis images of 31 subjects were randomly selected using a random number generated in Stata (College par, Texas, USA). Choroidal images were only selected from right eye of each subject as our measurement technique can be applied uniformly between right and left eyes. Therefore only the right eyes of the subjects were evaluated. In addition, selecting only one eye from individuals would help to avoid inter-eye correlation issue in statistical analysis. “Normal fundus” was defined as free of any macular or vitroretinal diseases on the basis of clinical fundus examination by experienced Ophthalmologist and the results of OCT imaging.

Exclusion criteria for the normal participants included: best corrected LogMAR VA >0.3, evidence of macular or vitroretinal diseases, previous retinal or

refractive surgery, past history of intraocular surgery, or clinical features compatible with a diagnosis of glaucoma suspect or glaucoma.

5.2.3 Intra-grader and Inter-grader Reliability Assessment

To evaluate the intra-grader and inter-grader reliability, 31 Spectralis images were randomly selected for the initial grading phase. Grader A and grader B, masked to subject characteristics and clinical diagnosis, independently graded these images to assess inter-grader reliability of CT measurements. In addition, grader A repeated the measurements after 2 weeks to assess intra-grader reliability. Both graders assessed the same sets of training images before commencing the grading task.

5.2.4 EDI SD-OCT Imaging

CT was obtained using Spectralis SD-OCT (Wavelength: 870 nm; Heidelberg Engineering, Heidelberg, Germany) with EDI modality as specified in details in Chapter III. A single experienced examiner masked to the clinical diagnosis of the subject performed the EDI-OCT examination. Only the horizontal section passing through the center of the fovea was selected for analysis and for each subject their right eye was chosen for subsequent analysis.

5.2.5 Measurement of Choroidal Thickness

The two major steps in our CT semi-automatic measurement protocol are: (A) post processing of images by adaptive compensation technique and (B) quantitative measurement of CT using Photoshop software. On average, measurement of CT at multiple locations (1.5 and 3 mm nasal and temporal to the fovea) requires approximately 1 minute per image.

(A) Adaptive Compensation Technique

An accurate evaluation of the CT with EDI-OCT mainly relies on how well one can delineate the CSI, which anatomically represents the junction between the choroid and the sclera, and is a principal landmark for quantitative measurements of choroid. However, at present identification of CSI is highly variable as there is no algorithm available in Spectralis for its automatic detection. Therefore, in order to accurately determine CT, once the EDI-OCT image was obtained, the CSI was enhanced using a novel post-processing adaptive compensation algorithm[21] which greatly improved the detection of CSI by correcting the deleterious effects of light attenuation.

An adaptive compensation algorithm was developed to over a limitation of standard compensation algorithm that is the overamplification of noise at high depth. Such limitation currently hampers the ability to distinguish the posterior CSI boundary. In adaptive compensation, standard compensation operations are performed until an energy threshold is reached, at which stage the compensation process is stopped to limit noise overamplification in the deeper portion of OCT image.[21] With the above modification adaptive compensation provided significant improvement in visibility of posterior boundary compared to standard compensation. In brief, this novel adaptive compensation algorithm improved the ability to detect and visualize the CSI. First, it removes noise over-amplification at high depth and shadow artifacts casted by blood vessels (thus decreasing the intra-layer contrast of the choroid). Second, it improves the visibility of posterior choroid boundary, by significantly increasing the inter-layer contrast across the CSI (**Figure 5.1**).

(B) Measurement of CT using Photoshop Software

The enhanced images were measured in Photoshop CS6 extended (Adobe Systems Incorporated, San Jose, California). CT at sub-foveal, 1.5 mm and 3 mm

nasal and temporal from the fovea were measured. **Figure 5.2** shows a flow diagram summarizing the CT measurement protocol. The detailed explanation of the steps involved in quantification of CT measurement using Photoshop is as below:

Set the Foveal Reference Line: firstly we opened the image from the file menu, then go the View menu and click on new guides options (**Figure 5.3 A**). In the following window, change the guide orientation to vertical and set the position of the guide and click ok (**Figure 5.3 B**), a reference line is generated (**C**).

Place the Measurement Grid: we used a grid to indicate accurately our measurement points (sub-fovea, 1.5 and 3 mm nasal and temporal to the fovea) and placed it such that the central point on the grid coincides with the reference line (**Figure 5.4**).

Set the Measurement Scale: select Analysis > Set Measurement Scale > Custom to open the Measurement Scale dialog box (**Figure 5.5 A**). Enter the Logical Length and Logical Units that one want to set equal to the Pixel Length. For example, in our case the Pixel Length is 1, and we want to set a scale of 0.0039 mm per pixel, enter 0.0039 for Logical Length, and millimeter for the Logical Units. Click OK in the Measurement Scale dialog box to set the measurement scale on the document (**Figure 5.5 B**). Choose File > Save to save the current measurement scale setting with the document.

Perform Measurement: choose Analysis> Ruler Tool, or Click the Ruler tool in the toolbox (left hand corner), then use the tool to measure the length of the image. Click at the starting location for the measuring line and drag to the end location. Release the mouse button to create the measurement line (**Figure 5.6**).

Display and Export the Measurement Log Data: choose Analysis> Record Measurements, or Click Record Measurements in the Measurement Log panel. Each row in the log represents a measurement set; columns represent the data points in a measurement set (**Figure 5.7A**). One can reorder columns in the log, sort data in the columns, delete rows or columns, or export data from the log to a comma delimited text file. Export data from the Measurement Log into a comma-delimited text file (**Figure 5.7 B**). One can open the text file in a spreadsheet application and perform statistical or analytical calculations from the measurement data.

a. Select one or more rows of data in the log.
b. Choose Export from the Measurement Log options menu or click the Export icon at the top of the panel or right-click in a row, then select Export from the pop-up menu.
c. Enter a filename and location, and click Save.

The measurements are exported to a comma-delimited, UTF‑8 text file.

5.2.6 Statistical Analyses

Statistical analysis was performed using MedCalc Version 12.6 (MedCalc Software, Ostend, Belgium) and SPSS Version 20.0 (SPSS, Inc., Chicago, IL, USA). Shapiro-Wilk tests were used to check the normality of CT data at various locations.

Reliability Assessment of CT: The reliability of the CT measurement was assessed using intra- and inter-grader agreements between two independent graders, measured by the absolute agreement model of the intra-class correlation coefficient (ICC).[22] ICC value of 0.81 – 1.00 indicates almost perfect agreement. Values of less than 0.40 indicate poor to fair agreement. Bland Altman plot analyses[23, 24] were performed to

see if there is any proportional bias between measurements. A two-tailed paired sample *t*-test was used to analyze differences between means in CT by location.

5.3 RESULTS

5.3.1 Baseline Characteristics and CT Measurements

Images from 31 eyes of 31 participants (aged 64.4 ± 7.4 years) were included in the analysis **(Table 5.1)**. The mean (standard deviation) sub-foveal CT in this study was 230.37 (66.66) µm (average of 1st and 2nd measurements of grader A). CT measured by the two graders is summarized in **Table 5.2**. The mean sub-foveal CT measured by grader A for the 1st and 2nd measurements was 229.74 (65.12) µm and 231 (69.14) µm, respectively, and was 232.19 (67.89) µm by grader B.

5.3.2 Intra- and Inter-grader Agreements using Adaptive and Conventional Techniques

Using adaptive compensation both the intra-grader reliability (ICC: 0.95 to 0.97) and inter-grader reliability (ICC: 0.93 to 0.97) were perfect for all five locations of CT (**Table 5.3**). However, with the conventional technique of manual CT measurements using built-in callipers provided with the Heidelberg explorer software, the intra- (ICC: 0.87 to 0.94) and inter-grader reliability (ICC: 0.90 to 0.93) for all the measured locations is lower (**Table 5.4**). Using adaptive compensation, the Bland Altman analysis of intra-grader reliability for sub-foveal CT measurement showed 95% LOA of -33.3 to 30.8 with a mean difference of -1.3 µm (**Figure 5.8**). No significant systemic (except at nasal 3 mm, p = 0.003) and proportional bias was detected in intra-grader CT measurements at all locations. The Bland Altman analysis of inter-grader reliability for sub-foveal CT measurement showed 95% LOA of -36.6

to 34.2 with a mean difference of -1.2 µm (**Figure 5.9**). No significant proportional bias was observed in the inter-grader CT measurements at all locations. Nonetheless, a significant systemic bias at both 1.5 and 3 mm nasal locations was found in the inter-grader CT measurement comparison ($p = 0.001$). However, this could be due to thinnest CT at nasal locations, making it more prone to systemic bias in CT measurements.

5.3.3 Intra- and Inter-layer Contrast Measurement

In addition, the choroid intra-layer contrast (a measure of shadow presence when high) and the CSI inter-layer contrast (a measure of boundary visibility when high) were computed for all images ($n = 31$) before and after applying adaptive compensation (as in [25]). We found that the intra-layer contrast significantly decreased from 0.84 ± 0.07 to 0.60 ± 0.07 ($p < 0.001$; *t*-test), whereas the inter-layer contrast significantly increased from 0.50 ± 0.14 to 0.90 ± 0.10 ($p < 0.001$; paired *t*-test) after applying adaptive compensation (**Table 5**).

5.4 DISCUSSION

Despite significant advances in imaging technology there are considerable variations in CT measurements across clinical studies. In this report, we described a simple, semi-automated method using adaptive compensation to measure CT from images acquired by EDI SD-OCT. The results showed that the method permits a highly reproducible tool for assessing CT from EDI SD-OCT images. Our measurement method is also simple and requires little time to perform (on average ~ 1 minute per image). With these features, our method may have great potential for use in both clinical and population-based studies which involve large number of images.

There are considerable differences in CT measurements across studies. Even though advances in OCT technology have reduced acquisition time, adequate visualization of choroid is still lacking. There are several challenges in imaging the choroid. First, the choroid is located behind the RPE and Bruch's membrane, making it less accessible than the retina and more difficult to be visualized. Second, the pigmentation in the RPE and the choroid itself decreases the signal intensity. Lastly, unlike retinal imaging,[26] wherein the RPE and internal limiting membrane are thin and clearly identifiable, the transition zone between the choroid and sclera (i.e. CSI) has blurred border and is broader, making CSI difficult to identify.

However, it is not always easy to distinguish CSI on acquired images, which may be related to scan quality or anatomic variation. Some choroidal scans have a distinct hypo-reflective line corresponding to the supra-choroidal space, but often this line can be indistinct leading to measurement error.[27] At present, identification of CSI is highly variable. To overcome these challenges, in this study we enhanced choroidal-scleral junction using a post-processing adaptive compensation algorithm.[21] Measurement of CT was performed in the post-processed images using Photoshop (Adobe Systems Incorporated, San Jose, California), a readily available and easy-to-use program.

Adaptive compensation provides two major improvements. First, the intra-layer contrast (of the choroid) significantly decreased after applying adaptive compensation, indicating successful shadow correction within the choroid. Second, the inter-layer contrast (across the CSI) significantly increased after applying adaptive compensation, indicating better visualization of CSI and therefore allowing for precise measurement of CT. These results are consistent with a previous study on standard compensation[25] and indicate significant improvements in image quality.

Also, a study by Lin *et al.* established outer choroidal contrast as a valid quantifiable measure of choroidal image quality and demonstrated that inverted SD-OCT imaging optimizes visualization of CSI and choroidal vessels through improved outer choroid contrast.[28]

With improved intra- and inter-layer contrast, the compensated images are likely more accurate than the non-compensated images as the deleterious effects of OCT light attenuation have been corrected, thus making the CSI more visible. The post-compensation images are more representative of the eye tissue architecture, since better estimates of the ocular tissues optical properties (e.g. reflectivity) are provided. This has been formally demonstrated in the original article by Girard *et al*.,[25] and in the following studies.[21, 29, 30] Lastly, although adaptive compensation is useful in all images, it is likely to be more useful when the CSI is poorly visible, e.g. in images where light attenuation is strong (**Figure 5.1**), emphasizing further the need for compensation for more accurate thickness measurement of the choroid.

Adaptive compensation achieves high intra-grader (ICC: 0.95 to 0.97) and inter-grader (ICC: 0.93 to 0.97) repeatability in CT measurements compared to conventional method (intra-grader ICC: 0.87 to 0.94, inter-grader ICC: 0.90 to 0.93), suggesting the use of adaptive compensation to improve the visualization of CSI and to obtain more reliable CT measurements. However, the high repeatability can be explained by the standardization and strict adherence to a rigorous grading protocol in the present study. In addition, both graders underwent the same training set for standardization purpose before embarking on the actual grading task. The present results are in line in the studies by Ikuno *et al.*[31] and Yamashita *et al.*[32] who reported an inter-grader ICC of 0.97 and 0.94, respectively, for sub-foveal CT measurements. However, in these two previous studies the intra-grader repeatability was not

evaluated, and it is not clear how the choroid images, where CSI could not be clearly visualized, were processed.

But the present study has its own limitations, as the measurement of CT was subjective in nature, and was therefore subject to measurement bias. However, our method may be less prone to observer error because the CSI was enhanced by adaptive compensation to give better visibility. An automated, and thus may be more objective, method of measuring CT would be of potential interest to facilitate, speed-up such analyses.

There are few recent studies on automatic choroidal segmentation in OCT images. Zhang *et al.* proposed an automatic segmentation algorithm for the choroidal vessels using Cirrus OCT in 24 normal subjects. But their aim was to quantify choroidal vasculature thickness and choroicapillaries equivalent thickness rather than the CT [33]. Likewise, Torzicky *et al.*[34] and Duan *et al.*[35] developed the automatic algorithms to detect the boundary between the choroid and sclera based on polarization sensitive OCT which are not commercially available. Although, Tian *et al.*[36] in 2013 proposed an automatic algorithm that could segment choroid in commercially available Spectralis OCT, but their algorithm was tested only on 20 EDI OCT images and need to be validated on more images to prove the robustness of algorithm before its application in clinical studies. While we are preparing the manuscript, a commercially available CT measurement algorithm in swept-source OCT (Topcon Corp., Tokyo, Japan) is being made available. However, in view of lack of supporting agreement studies on the algorithm and manual choroidal segmentation (in both normal and diseased eyes), the accuracy and reliability of automated CT analysis by using swept-source OCT is yet to be established for use in clinical settings.

5.5 CONCLUSIONS

In conclusion, we described a simplified, semi-automated and practical method "adaptive compensation followed by using Photoshop" that gives excellent intra- and inter-grader reliability (ICC>0.93) to quantify CT in the EDI SD-OCT images. This method has great potential usage in both clinical and population based studies, as reliable and accurate measurements of CT from EDI-OCT images are essential in distinguishing clinically significant change of CT and assisting in risk-profiling for various posterior segment diseases.

5.6 REFERENCES

1. Linsenmeier RA, Padnick-Silver L. Metabolic dependence of photoreceptors on the choroid in the normal and detached retina. Invest Ophthalmol Vis Sci 2000;41(10):3117-23.

2. Grossniklaus HE, Green WR. Choroidal neovascularization. Am J Ophthalmol 2004;137(3):496-503.

3. Koizumi H, Yamagishi T, Yamazaki T, et al. Subfoveal choroidal thickness in typical age-related macular degeneration and polypoidal choroidal vasculopathy. Graefes Arch Clin Exp Ophthalmol 2011;249(8):1123-8.

4. Gomi F, Tano Y. Polypoidal choroidal vasculopathy and treatments. Curr Opin Ophthalmol 2008;19(3):208-12.

5. Chung SE, Kang SW, Lee JH, Kim YT. Choroidal thickness in polypoidal choroidal vasculopathy and exudative age-related macular degeneration. Ophthalmology 2011;118(5):840-5.

6. Gupta B, Mohamed MD. Photodynamic therapy for variant central serous chorioretinopathy: efficacy and side effects. Ophthalmologica 2011;225(4):207-10.

7. Imamura Y, Fujiwara T, Margolis R, Spaide RF. Enhanced depth imaging optical coherence tomography of the choroid in central serous chorioretinopathy. Retina 2009;29(10):1469-73.

8. Fong AH, Li KK, Wong D. Choroidal evaluation using enhanced depth imaging spectral-domain optical coherence tomography in Vogt-Koyanagi-Harada disease. Retina 2011;31(3):502-9.

9. Fujiwara T, Imamura Y, Margolis R, et al. Enhanced depth imaging optical coherence tomography of the choroid in highly myopic eyes. Am J Ophthalmol 2009;148(3):445-50.

10. Ikuno Y, Tano Y. Retinal and choroidal biometry in highly myopic eyes with spectral-domain optical coherence tomography. Invest Ophthalmol Vis Sci 2009;50(8):3876-80.

11. Fitzgerald ME, Wildsoet CF, Reiner A. Temporal relationship of choroidal blood flow and thickness changes during recovery from form deprivation myopia in chicks. Exp Eye Res 2002;74(5):561-70.

12. Cheung CM, Loh BK, Li X, et al. Choroidal thickness and risk characteristics of eyes with myopic choroidal neovascularization. Acta Ophthalmol 2013;91(7):e580-1.

13. Povazay B, Hermann B, Unterhuber A, et al. Three-dimensional optical coherence tomography at 1050 nm versus 800 nm in retinal pathologies: enhanced performance and choroidal penetration in cataract patients. J Biomed Opt 2007;12(4):041211.

14. Kahn KN, McKibbin M, Kahn RS. Variability in subfoveal choroidal thickness measurements. Invest Ophthalmol Vis Sci 2011;52(10):7221; author reply

15. Spaide RF, Koizumi H, Pozzoni MC. Enhanced depth imaging spectral-domain optical coherence tomography. Am J Ophthalmol 2008;146(4):496-500.

16. Manjunath V, Fujimoto JG, Duker JS. Cirrus HD-OCT high definition imaging is another tool available for visualization of the choroid and provides agreement with the finding that the choroidal thickness is increased in central serous chorioretinopathy in comparison to normal eyes. Retina 2010;30(8):1320-1; author reply 1-2.

17. Maul EA, Friedman DS, Chang DS, et al. Choroidal thickness measured by spectral domain optical coherence tomography: factors affecting thickness in glaucoma patients. Ophthalmology 2011;118(8):1571-9.

18. Ho J, Branchini L, Regatieri C, et al. Analysis of normal peripapillary choroidal thickness via spectral domain optical coherence tomography. Ophthalmology 2011;118(10):2001-7.

19. Shin JW, Shin YU, Lee BR. Choroidal thickness and volume mapping by a six radial scan protocol on spectral-domain optical coherence tomography. Ophthalmology 2012;119(5):1017-23.

20. Rosman M, Zheng Y, Wong W, et al. Singapore Malay Eye Study: rationale and methodology of 6-year follow-up study (SiMES-2). Clin Experiment Ophthalmol 2012;40(6):557-68.

21. Mari JM, Strouthidis NG, Park SC, Girard MJ. Enhancement of lamina cribrosa visibility in optical coherence tomography images using adaptive compensation. Invest Ophthalmol Vis Sci 2013;54(3):2238-47.

22. Fleiss JL, Cohen J. The Equivalence of Weighted Kappa and the Intraclass Correlation Coefficient as Measures of Reliability. Educational and Psychological Measurement 1973;33(3):613-9.

23. Bland JM, Altman DG. Statistical methods for assessing agreement between two methods of clinical measurement. Lancet 1986;1(8476):307-10.

24. Bland JM, Altman DG. Agreed statistics: measurement method comparison. Anesthesiology 2012;116(1):182-5.

25. Girard MJ, Strouthidis NG, Ethier CR, Mari JM. Shadow removal and contrast enhancement in optical coherence tomography images of the human optic nerve head. Invest Ophthalmol Vis Sci 2011;52(10):7738-48.

26. Hee MR, Puliafito CA, Duker JS, et al. Topography of diabetic macular edema with optical coherence tomography. Ophthalmology 1998;105(2):360-70.

27. Yiu G, Pecen P, Sarin N, et al. Characterization of the choroid-scleral junction and suprachoroidal layer in healthy individuals on enhanced-depth imaging optical coherence tomography. JAMA Ophthalmol 2014;132(2):174-81.

28. Lin P, Mettu PS, Pomerleau DL, et al. Image inversion spectral-domain optical coherence tomography optimizes choroidal thickness and detail through improved contrast. Invest Ophthalmol Vis Sci 2012;53(4):1874-82.

29. Foin N, Mari JM, Davies JE, et al. Imaging of coronary artery plaques using contrast-enhanced optical coherence tomography. Eur Heart J Cardiovasc Imaging 2013;14(1):85.

30. Foin N, Mari JM, Nijjer S, et al. Intracoronary imaging using attenuation-compensated optical coherence tomography allows better visualisation of coronary artery diseases. Cardiovasc Revasc Med 2013;14(3):139-43.

31. Ikuno Y, Maruko I, Yasuno Y, et al. Reproducibility of retinal and choroidal thickness measurements in enhanced depth imaging and high-penetration optical coherence tomography. Invest Ophthalmol Vis Sci 2011;52(8):5536-40.

32. Yamashita T, Yamashita T, Shirasawa M, et al. Repeatability and reproducibility of subfoveal choroidal thickness in normal eyes of Japanese using different SD-OCT devices. Invest Ophthalmol Vis Sci 2012;53(3):1102-7.

33. Zhang L, Lee K, Niemeijer M, et al. Automated segmentation of the choroid from clinical SD-OCT. Invest Ophthalmol Vis Sci 2012;53(12):7510-9.

34. Torzicky T, Pircher M, Zotter S, et al. Automated measurement of choroidal thickness in the human eye by polarization sensitive optical coherence tomography. Opt Express 2012;20(7):7564-74.

35. Duan L, Yamanari M, Yasuno Y. Automated phase retardation oriented segmentation of chorio-scleral interface by polarization sensitive optical coherence tomography. Opt Express 2012;20(3):3353-66.

36. Tian J, Marziliano P, Baskaran M, et al. Automatic segmentation of the choroid in enhanced depth imaging optical coherence tomography images. Biomed Opt Express 2013;4(3):397-411.

CHAPTER V TABLES

Table 5.1 Baseline characteristics of study subjects

Characteristics	**Mean (SD)**
Age, years	64.35 (7.42)
Gender, male	11 (35.48)
Axial length, mm	23.33 (0.88)
Average choroidal thickness,* µm	
Sub-foveal	230.37 (66.66)
Nasal, 1.5 mm	214.33 (74.34)
Nasal, 3 mm	185.77 (69.96)
Temporal, 1.5 mm	224.53 (57.27)
Temporal, 3 mm	229.74 (52.03)

Data are expressed as mean (SD) except for gender, which is expressed as number (%).
*The average of 1st and 2nd measurement of Grader A.

Table 5.2 Summary of choroidal thickness measurements at various locations

Location	Grader A, 1st Measurement	Grader A, 2nd Measurement	Grader B Measurement
Sub-foveal	229.74 (65.12)	231.00(69.14)	232.19 (67.89)
Nasal, 1.5 mm	213.84 (75.12)	214.84(75.49)	221.52(76.08)
Nasal, 3 mm	191.13 (72.79)	180.42(68.25)	187.55(71.06)
Temporal, 1.5 mm	223.94 (56.33)	225.13(59.24)	231.65 (60.82)
Temporal, 3 mm	228.68 (50.64)	230.81(54.57)	230.71 (53.80)

Data are mean (SD).

Table 5.3 Intra- and inter-grader agreements for the choroidal thickness measurement at 5 horizontal locations using adaptive compensation

	Locations, CT measurement	ICC (95% CI)	Mean difference (95% LOA)	P Value[c]	Assessment of proportional bias[d]	
					Pearson's correlation coefficient, r	P Value
Intra-grader Reliability[a]	Sub-foveal	0.97 (0.94 to 0.98)	-1.3 (-33.3 to 30.8)	0.672	0.248	0.179
	Nasal, 1.5 mm	0.95 (0.90 to 0.97)	-1.0 (-48.0 to 46.0)	0.818	-0.160	0.933
	Nasal, 3 mm	0.95 (0.87 to 0.98)	10.7 (-25.3 to 46.7)	0.003	0.249	0.176
	Temporal, 1.5 mm	0.96 (0.92 to 0.98)	-1.2 (-31.9 to 29.5)	0.674	-0.187	0.313
	Temporal, 3 mm	0.95 (0.90 to 0.97)	-2.1 (-33.5 to 29.2)	0.464	-0.248	0.178
Inter-grader Reliability[b]	Sub-foveal	0.96 (0.93 to 0.98)	-1.2 (-36.6 to 34.2)	0.715	0.070	0.708
	Nasal, 1.5 mm	0.97 (0.92 to 0.99)	-9.0 (-34.4 to 16.4)	0.001	-0.127	0.495
	Nasal, 3 mm	0.97 (0.89 to 0.98)	-9.8 (-37.4 to 17.8)	0.001	-0.230	0.212
	Temporal, 1.5 mm	0.93 (0.86 to 0.96)	-6.5 (-48.3 to 35.3)	0.099	-0.075	0.687
	Temporal, 3 mm	0.94 (0.88 to 0.97)	0.1 (-35.5 to 35.7)	0.977	0.043	0.818

LOA, Limits of Agreement; ICC, Intraclass Correlation Coefficient; CI, Confidence Interval.
[a]Mean difference was determined from the1sttime measurement minus the 2ndtime measurement.
[b]Mean difference was determined from Grader A measurement minus Grader B measurement.
[c]P value of one sample t-tests (comparing between mean difference and zero value) to indicate presence of systemic bias
[d]Using Pearson's correlation coefficients of regression line

Table 5.4 Intra- and inter-grader agreements for the choroidal thickness measurement at 5 horizontal locations using Spectralis SD-OCT with conventional manual technique

	Locations, CT measurement	**ICC (95% CI)**	**Mean difference (95% LOA)**
Intra-grader Reliability[a]	Sub-foveal	0.94 (0.87 to 0.97)	9.7 (-30.3 to 49.7)
	Nasal, 1.5 mm	0.92 (0.85 to 0.96)	2.9 (-41.1 to 54.9)
	Nasal, 3 mm	0.92 (0.85 to 0.96)	4.1 (-36.1 to 44.3)
	Temporal, 1.5 mm	0.87 (0.75 to 0.93)	-7.0 (-52.1 to 38.1)
	Temporal, 3 mm	0.88 (0.77 to 0.94)	-1.9 (-44.9 to 48.6)
Inter-grader Reliability[b]	Sub-foveal	0.90 (0.60 to 0.96)	-19.1 (-63.7 to 25.6)
	Nasal, 1.5 mm	0.93 (0.68 to 0.97)	18.3 (-59.7 to 23.2)
	Nasal, 3 mm	0.91 (0.67 to 0.96)	-15 (-54.3 to 24.3)
	Temporal, 1.5 mm	0.91 (0.72 to 0.96)	-12.7 (-49.8 to 24.4)
	Temporal, 3 mm	0.90 (0.58 to 0.96)	-15.7 (-51.3 to 19.9)

CT, Choroidal Thickness; LOA, Limits of Agreement; ICC, Intraclass Correlation Coefficient; CI, Confidence Interval.

[a]Mean difference was determined from the1st time measurement minus the 2nd time measurement.

[b]Mean difference was determined from Grader A measurement minus Grader B measurement.

Table 5.5 Intra- and inter-layer contrast (n = 31 subjects)

		Mean (SD)	P-Value
Intra-layer Contrast	Standard (without compensation)	0.84 (0.07)	<0.001
	Adaptive Compensation	0.60 (0.07)	
Inter-layer Contrast	Standard (without compensation)	0.50 (0.14)	<0.001
	Adaptive Compensation	0.90 (0.10)	

CHAPTER V FIGURES

Figure 5.1 Illustration of the raw versus the compensated image. **(A)** Raw OCT image of a healthy subject. The choroid-scleral interface is only partially visible. Note the presence of blood vessels shadows as indicated by red asterisks. **(B)** Adaptive compensation was applied to the raw image in order to remove blood vessels shadows, enhance contrast and improve visibility of the choroid-scleral interface (more uniform).

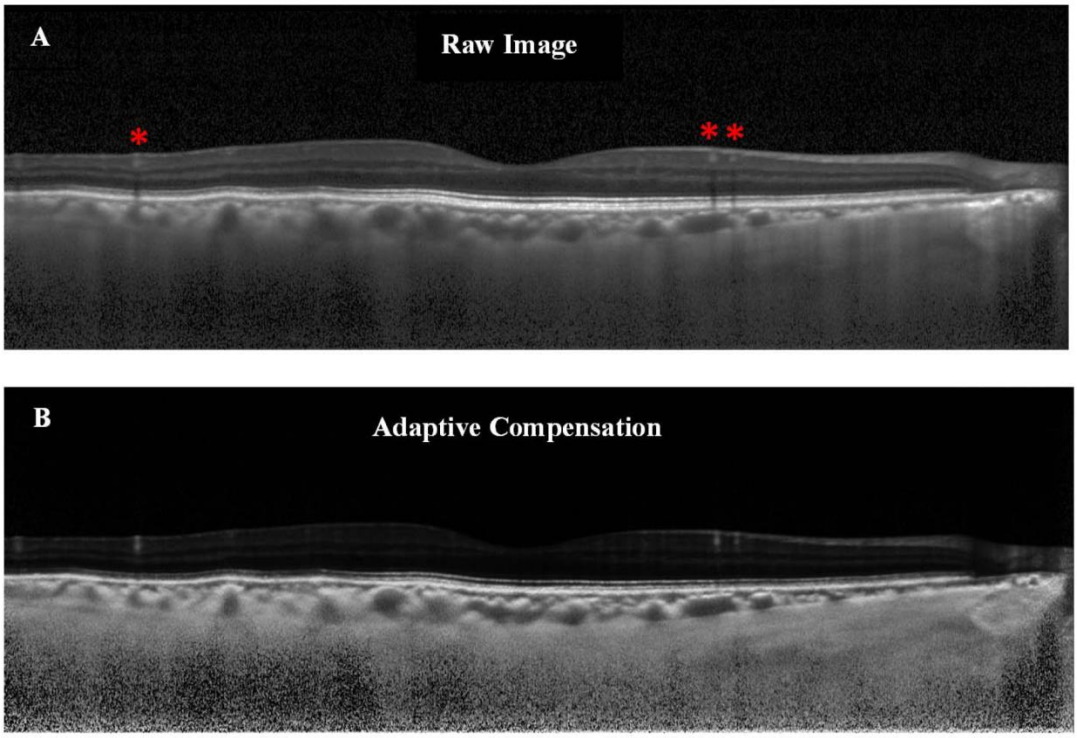

Figure 5.2 Flow diagram of the measurement protocol.

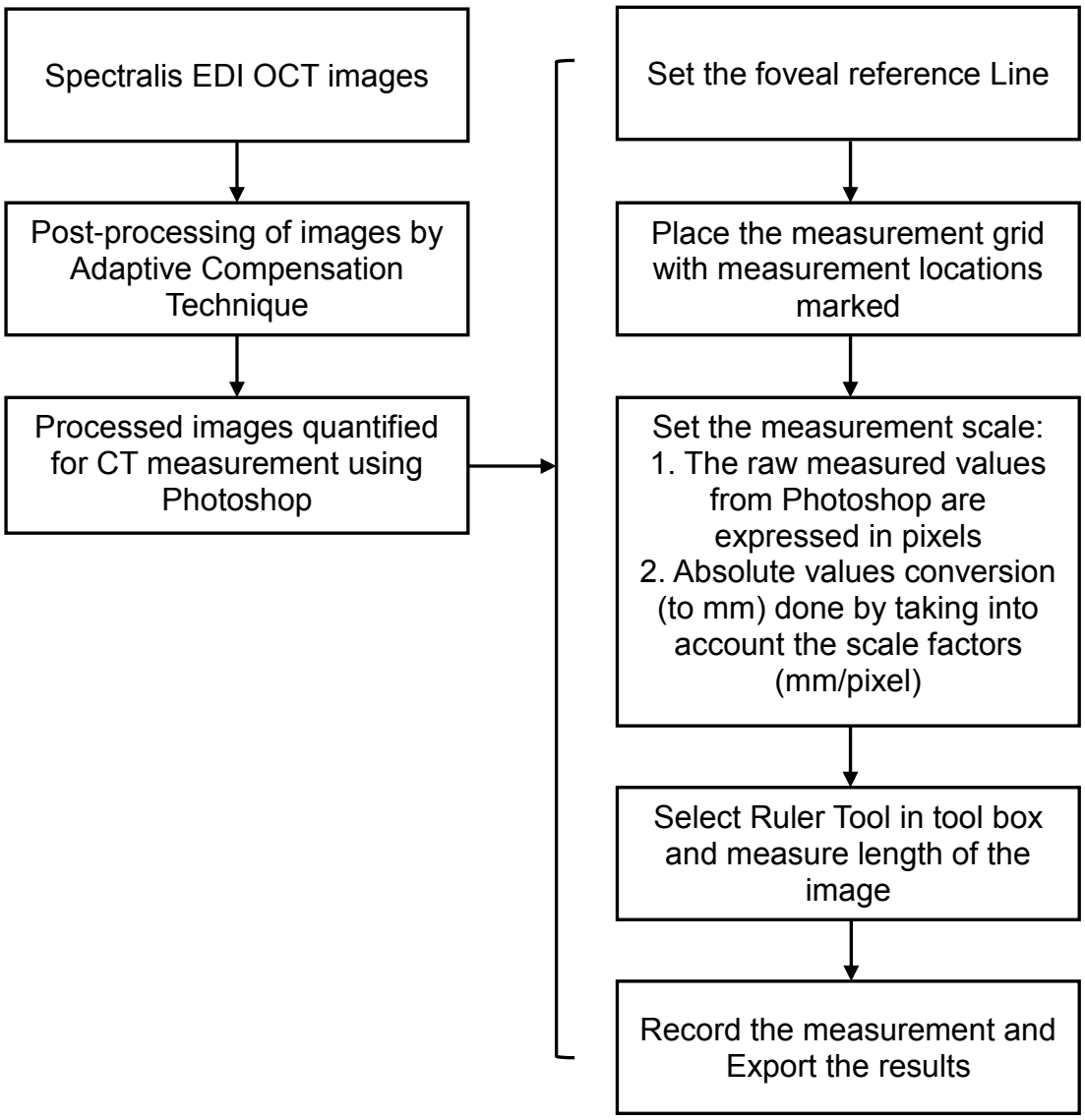

Detailed steps to quantify choroidal thickness using Photoshop

Figure 5.3 Setting of the foveal reference line. Open the image from the file menu, go the view menu and click on new guides options (**A**). Change the guide orientation to vertical (**B**). A foveal reference line is generated (**C**).

A

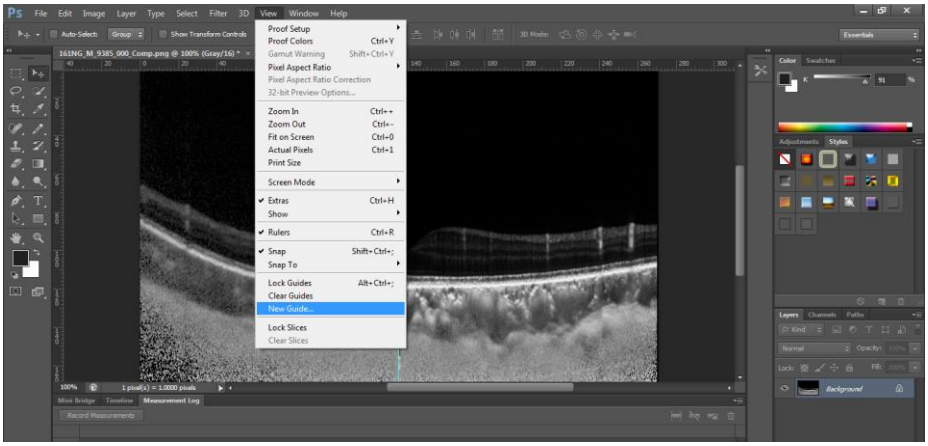

B

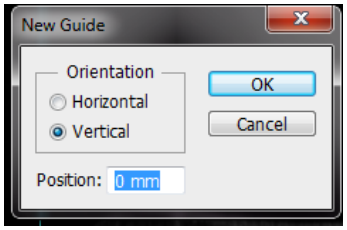

C

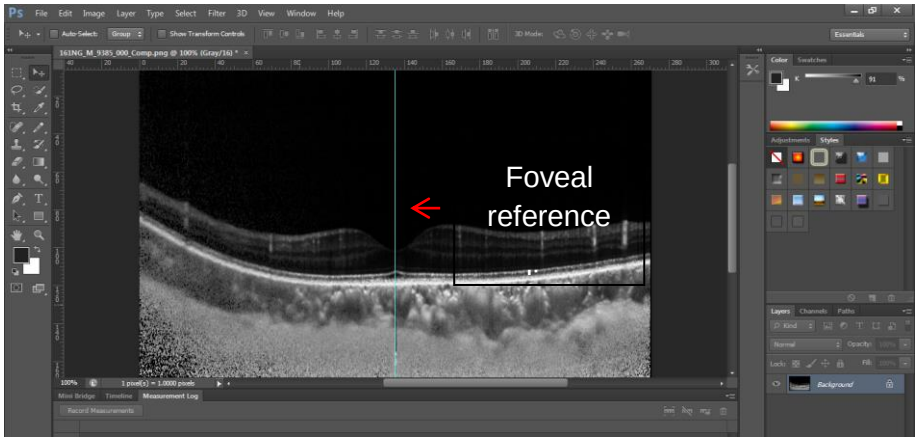

Figure 5.4 Placement of measurement such that the central point on the grid coincides with the foveal reference line.

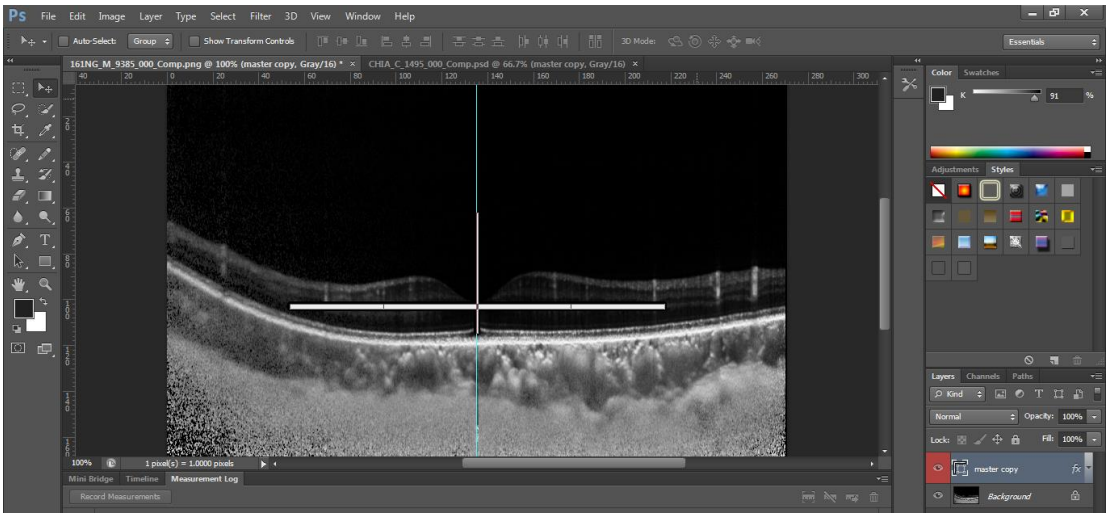

Figure 5.5 Setting of the measurement scale. select *Analysis* > *Set Measurement Scale* > *Custom* to open the measurement scale dialog box (A). Convert the values to desired units (B).

A

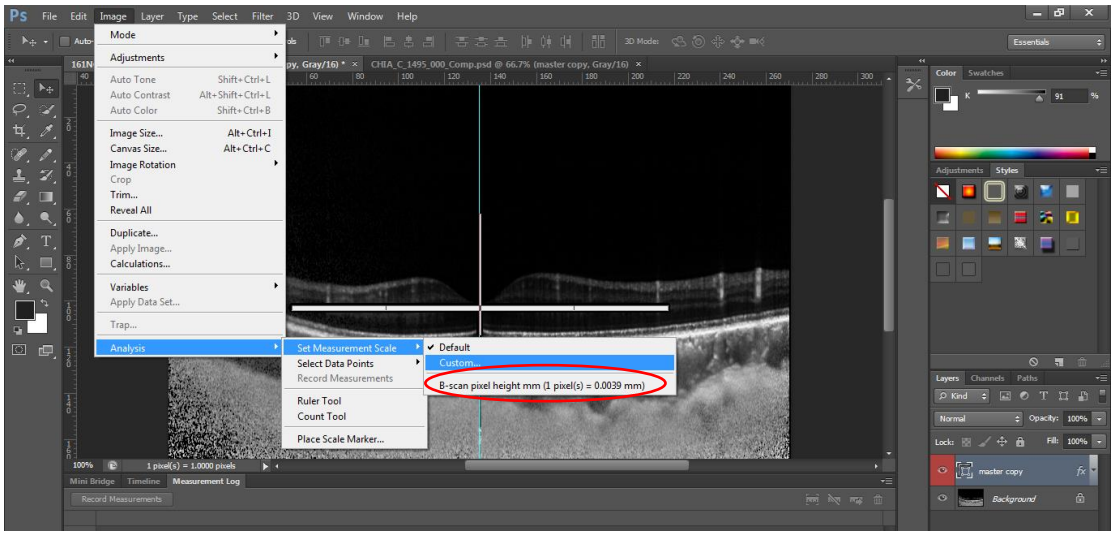

B

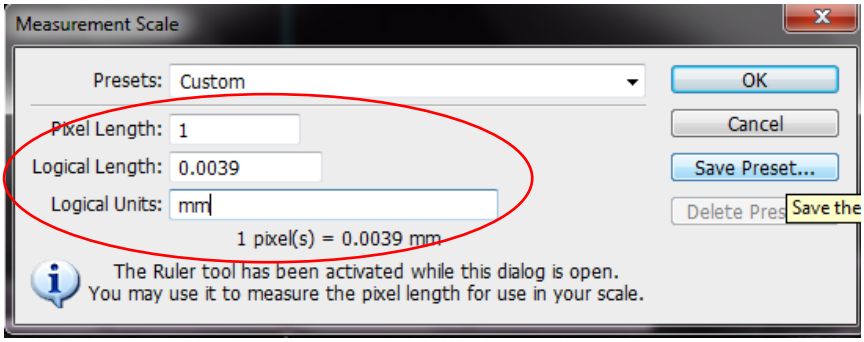

Figure 5.6 Performing measurements using the ruler tool from the analysis tab.

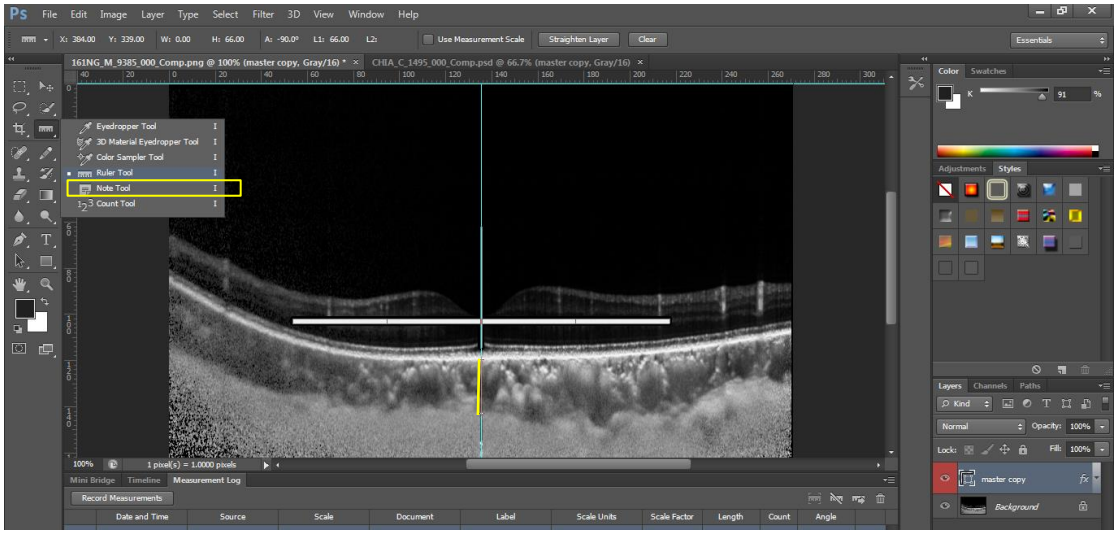

Figure 5.7 Displays recording of the measurements (A) and exporting of the measurement log data (B).

A

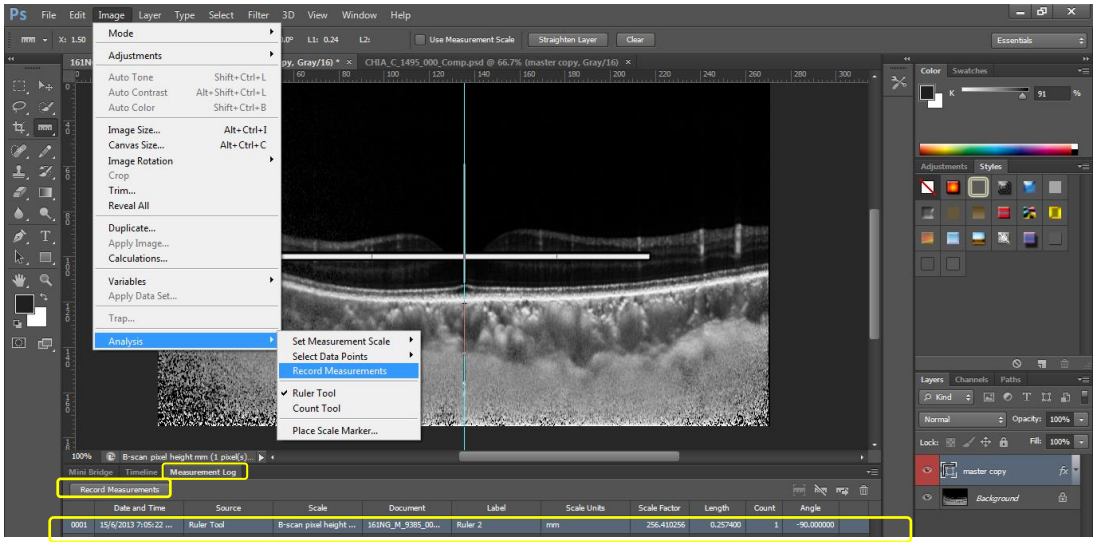

B

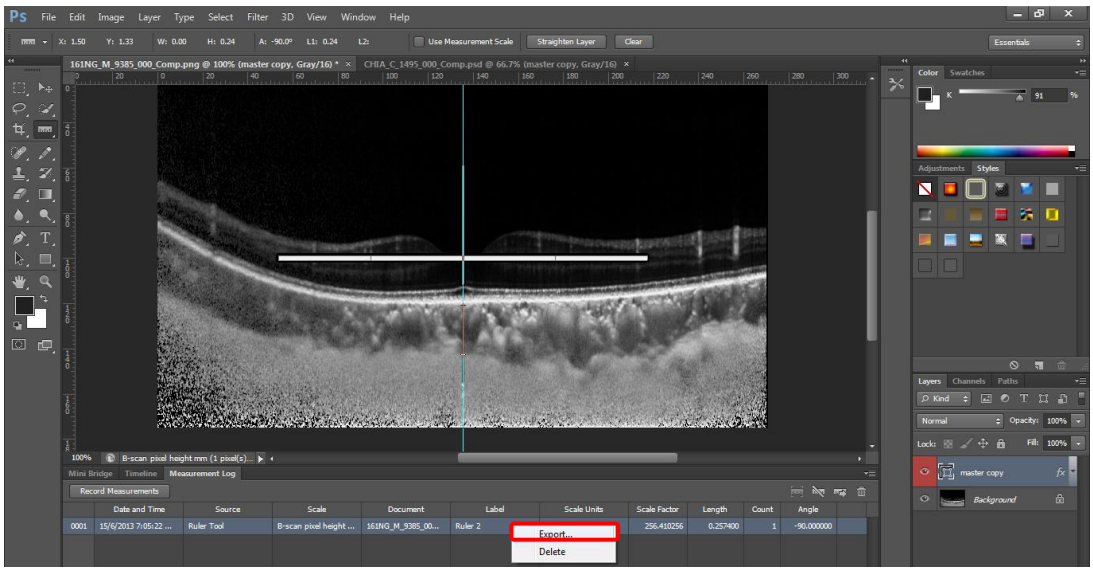

Figure 5.8 Bland Altman plot of intra-grader reliability of sub-foveal choroidal thickness (CT) measurement. The difference was calculated by the 1st measurement minus the 2nd measurement. Pink dashed line represents regression line of difference between 1st and 2nd measurements.

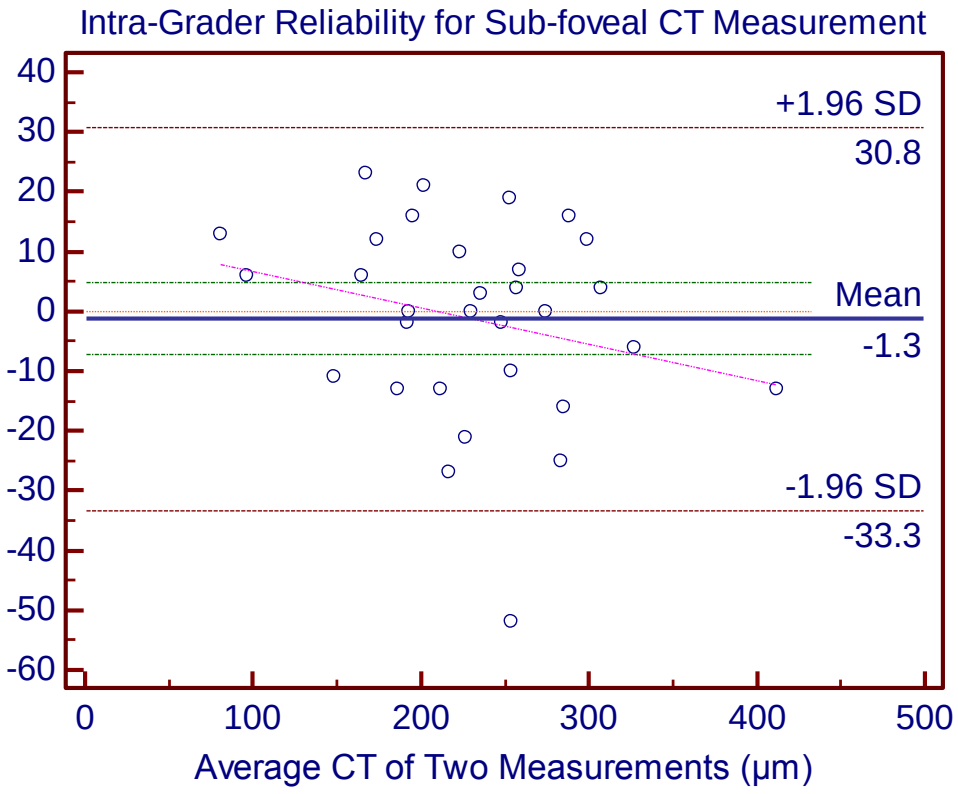

Figure 5.9 Bland Altman plots of inter-grader reliability of sub-foveal choroidal thickness (CT) measurement. The difference was calculated by the grader A measurement minus the grader B measurement. Pink dashed line represents regression line of difference between the two graders measurements.

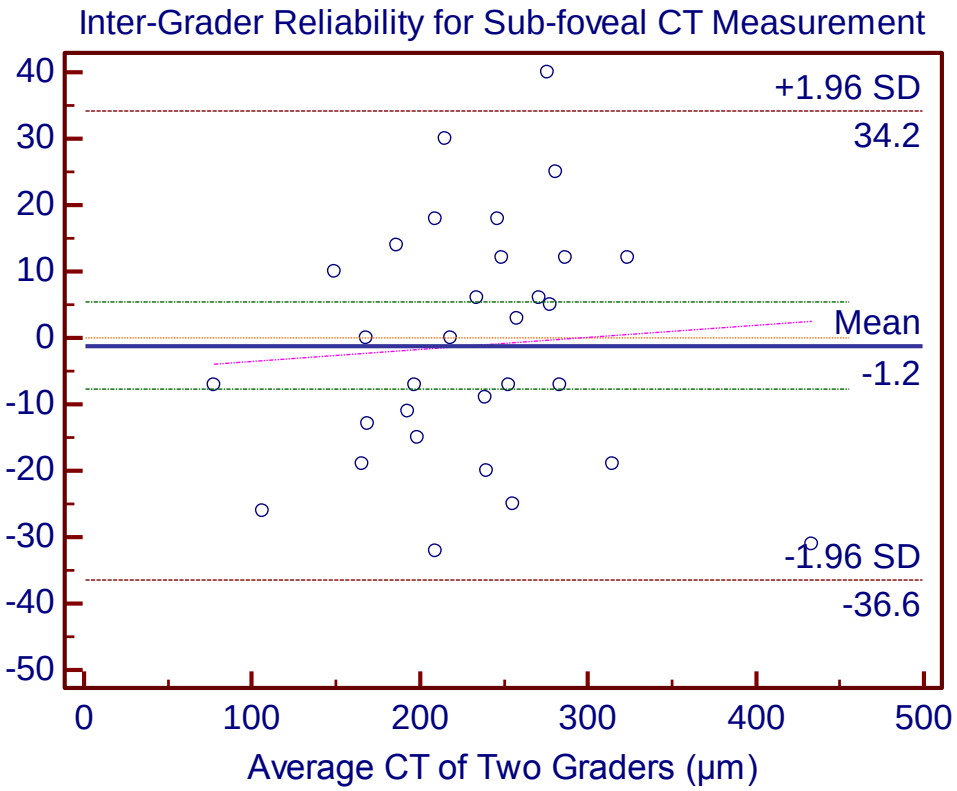

CHAPTER VI

FULLY AUTOMATED CHOROIDAL IMAGE PROCESSING TECHNIQUE TO OVERCOME THE LIMITATIONS OF SEMI-AUTOMATED TECHNIQUE

In chapter V, although we have successfully enhanced the visibility of macular CSI by using novel semi-automated technique of adaptive compensation and our technique was less prone to observer error because the CSI was augmented to give better visibility. But the marking of CSI and measurements of CT were performed manually and thus our semi-automated technique is still subject to measurement errors, limiting its clinical utility. In addition, manual method is also time- and effort-consuming, making it unfeasible especially when dealing with large population data.

Therefore, in order to overcome the limitations of semi-automated technique, in this Chapter, we developed and evaluated novel fully automated choroidal image processing technique which can objectively and accurately define the CSI and objectively measure CT as well as choroidal volume at both macular and peripapillary regions. The measurements obtained by our fully automated choroidal image processing technique are compared with the measurements from reference standard manual method.

6.1 INTRODUCTION

Although the use of EDI in SD-OCT has now allowed better visualization of the choroidal structures,[1] the quantification of CT for evaluating chorioretinal diseases is mostly performed manually and often restricted to one or few points around the foveal center.[2-9] This is due to unavailability of automated choroidal segmentation software, because of which previous investigators have used manual (mostly single point) measurement technique using in-built calipers to evaluate CT.[7, 10-12] However, measurements of a few sampling points are influenced by focal thickening or thinning of the choroid,[13, 14] or by irregularity of the inner chorio-scleral border,[2, 5] and thus highly dependent on location of measurements. In addition, manual methods are further subject to intra- and inter-observer variation. Given the high anatomic variability of choroid, these are impractical for clinical use and epidemiological research involving large samples, which makes the measurements tedious and time-consuming. Thus, an objective and comprehensive assessment of the choroid, such as CT maps and volumetric analysis, is required but is still unavailable.

A few studies have calculated choroidal volume using the built-in software. However, the segmentation of the CSI is still done manually. For EDI SD-OCT to become a clinically practical tool to determine CT, an automatic and accurate measurement algorithm must be developed.

In this study we developed and evaluated novel fully automated choroidal image processing technique which can objectively and accurately define the CSI and objectively measure CT as well as choroidal volume at both macular and peripapillary regions. The measurements obtained by our fully automated choroidal image processing technique are compared with the measurements from reference standard manual method.

6.2 METHODS

6.2.1 Study Subjects

For this analysis we randomly selected (using Strata random number generator) 45 subjects from SiMES-2 (2011 – 2013), a comprehensive detailed population-based cohort study of the Singaporean Malay adults aged 45-85 years.[15] Each subject underwent standardized and detailed ophthalmic examination, including choroidal imaging at macular and optic nerve head region.

6.2.2 Choroidal Image Acquisition Protocol at Macular and Peripapillary Regions

Choroid was imaged using SD-OCT (Spectralis, Heidelberg Engineering, Heidelberg, Germany) with EDI modality after pupil dilation. The detailed choroidal image acquisition protocol for both macular and peripapillary regions have been described in Chapter III of the thesis and elsewhere.[16, 17]

All OCT scans were acquired by a single examiner (PG), who is experienced at performing scans using EDI-Spectralis. After each capture, each of the B-scans was scrutinized manually in each eye by the same examiner, and images of insufficient quality (quality index of < 18 decibels for Spectralis OCT as suggested by the manufacturer for the image quality assurance) were excluded.

6.2.3 Automated Detection of CSI

The changes between choroidal tissue structures create distinct valleys in the OCT A-scans and hence we can delineate CSI as the smooth curve formed by **"valley pixels"**. In our method, valley pixels are defined as the local minima of A-scans and are used as the feature to detect the CSI. However, the valley pixels are also caused by

the speckle noise and the blood vessels in the choroid as shown in **Figure 6.1**. So in order to distinguish the valley pixels caused by CSI from the ones caused by speckle noise and blood vessels, we assume that the CSI is a continuous and smooth curve, the valley pixels caused by it are close to one another and can be connected to form a smooth path between valley pixels on both ends of the image. On the other hand, the valley pixels caused by the speckle noise appears randomly located and the ones caused by blood vessels in the choroid region form short layer segments, which means that the smooth path cannot be formed by these valley pixels as illustrated in **Figure 6.1**.

6.2.4 Automated Measurements of Choroidal Thickness and Volume

The CT at each location was defined as the distance between the Bruch's membrane (lower boundary of RPE) and the CSI. In this study, Bruch's membrane and CSI were delineated with our newly developed automated choroidal image processing technique.

For macular CT, from the 7 serial horizontal B-scans, the scan passing through the fovea was selected by an experienced examiner (PG) and the center of fovea was detected as the lowest points of internal limiting membrane automatically. The CT profile at the fovea and at 500-μm intervals up to 3 mm temporal and nasal to the fovea in horizontal section (**Figure 6.2**), was then automatically measured and created. **Figure 6.3** shows an example of EDI SD-OCT scan of the macula with the automated segmentation lines. Furthermore, the choroidal volume of 7 horizontal B-scans (covering a rectangular region of 8.9 mm x 1.5 mm centered on the fovea) of the region $\{(x,y)| -3mm < x < 3mm, 720\mu m < y < 720\mu m\}$ was calculated with the automatically detected fovea as the center of origin, (0,0) and the measurement points between lines were measured with linear interpolation as illustrated in **Figure 6.4**. In

addition, choroidal volume of 1mm diameter circle at fovea and thickness maps were obtained for each subject.

Likewise, CT (as defined above) in the optic disk region was objectively measured by the automated segmentation software at 12 discrete locations (30^o apart) and at 4 quadrants: superior, nasal, inferior and temporal (**Figure 6.5)**. **Figure 6.6** demonstrates automated peripapillary CT profile measured in the optic disc region.

6.2.5 Agreement and Repeatability of Automated Choroidal Measurements

We evaluated the agreement of automated CT measurements against the manual measurements of CT (ground truth) obtained using in-built calipers of Spectralis OCT in 45 randomly selected subjects at both macular and peripapillary regions.

In addition, we also assessed the intra-session repeatability using EDI SD-OCT and automated choroidal image processing technique. For this images from the same eye of 20 subjects were obtained twice at an interval of 10 minutes. Two images from the same eyes were each measured by automated image processing technique to assess the repeatability of CT and choroidal volume measurements.

6.2.6 Statistical Analyses

Statistical analysis was performed using MedCalc version 12.3 (Medcalc Software, Ostend, Belgium) and SPSS version 20.0 (SPSS, Inc., Chicago, IL, USA). Eyes with other ocular diseases, such as refractive errors, cataract, glaucoma, and retinopathy were not excluded if the quality of OCT image was sufficient to be evaluated.

The agreement and intra-session repeatability of the CT and macular choroidal volume were measured by the absolute agreement model of the intra-class correlation

coefficient (ICC). ICC value of 0.81 – 1.00 indicates good agreement. Values of less than 0.40 indicate poor to fair agreement. We also performed Bland Altman plot analyses to see the mean difference between the repeated measurements. All p values were 2-sided and considered statistically significant when the values were less than 0.05; 95% confidence intervals (CIs) were presented.

6.3 RESULTS

A total of 45 eyes from 45 subjects were included in the study. In none of the images did the automated software fail to detect the RPE and choroidal borders and therefore no eyes were excluded from the analysis.

Table 6.1 shows the agreement between automated and manual CT measurements at 5 horizontal locations. Agreement of CT at 5 measured horizontal locations was excellent (ICC ranging from 0.90 to 0.96). The mean difference (95% limits of agreement) for sub-foveal CT was 2.2 (-61 to 65.5) μm.

Table 6.2 shows the intra-session repeatability of CT and choroidal volume using automated choroidal segmentation software. Repeatability of CT at 5 measured horizontal locations and macular choroidal volume was excellent (ICC ranging from 0.97 to 0.99).

Table 6.3 shows the agreement between automated CT and manual CT at various locations in the optic disc region. The agreement of peripapillary CT was excellent (ICC ranging from 0.95 to 0.99).

Table 6.4 shows the intra-session repeatability of peripapillary CT using automated choroidal segmentation software. Repeatability of peripapillary CT at 4 quadrants was excellent (ICC ranging from 0.9998 to 0.9999). The mean difference (95% limits of agreement) for average peripapillary CT was -0.16 (-1.53 to 1.20) μm.

6.4 DISCUSSION

In this study, we have successfully designed fully automated choroidal image processing technique that can enhance the visualization of CSI, objectively and accurately define the CSI and consistently measure CT (at macular and peripapillary regions) as well as choroidal volume (at macula). Our automated choroidal image processing technique is valid and comparable to existing manual method as our objectively measured macular and peripapillary CT showed good agreement with reference standard manually assessed CT. In addition, the intra-session repeatability of macular and peripapillary CT and macular choroidal volume using automated choroidal image processing technique was excellent.

Although Spectralis OCT with EDI allows visualization of the choroidal structure in detail, the measurement of CT is still performed manually. To date, none of the previous clinical studies used automated measurements of thickness or volume of the choroid because in each of these studies demarcation of CSI, a principal landmark for accurate measurement of the choroid was performed manually.[18-21] This makes the existing measurements not only time and effort consuming but also prone to measurement errors, thereby compromising their validity.

To our best knowledge, this is the first time to use Spectralis OCT with EDI with a fully automated choroidal image processing technique to measure thickness and volume of the choroid. Our fast (processing time ~1.25 seconds per image which comprised of 7 radial scans vs. ~ 2.8 minutes per image comprised of 7 radial scans measured manually), objective and accurate technique has great potential usage in both clinical and population based studies and may improve the diagnosis and management of patients with eye diseases in which the choroid is affected. However,

our study also had limitations. Although the location of the CSI on Spectralis images was determined qualitatively as the junction between posterior choroid and sclera, there was no reference standard to confirm where this structure is actually located in the eye.

6.5 CONCLUSION

In summary, our fully automated choroidal image processing technique allowed fast, reliable and accurate measurements of CT and choroidal volume which are essential in distinguishing clinically significant change in choroid and assisting in risk-profiling for various chorioretinal diseases.

6.6 REFERENCES

1. Spaide RF, Koizumi H, Pozzoni MC. Enhanced depth imaging spectral-domain optical coherence tomography. Am J Ophthalmol 2008;146(4):496-500.

2. Chung SE, Kang SW, Lee JH, Kim YT. Choroidal thickness in polypoidal choroidal vasculopathy and exudative age-related macular degeneration. Ophthalmology 2011;118(5):840-5.

3. Fujiwara T, Imamura Y, Margolis R, et al. Enhanced depth imaging optical coherence tomography of the choroid in highly myopic eyes. Am J Ophthalmol 2009;148(3):445-50.

4. Imamura Y, Fujiwara T, Margolis R, Spaide RF. Enhanced depth imaging optical coherence tomography of the choroid in central serous chorioretinopathy. Retina 2009;29(10):1469-73.

5. Koizumi H, Yamagishi T, Yamazaki T, et al. Subfoveal choroidal thickness in typical age-related macular degeneration and polypoidal choroidal vasculopathy. Graefes Arch Clin Exp Ophthalmol 2011;249(8):1123-8.

6. Fong AH, Li KK, Wong D. Choroidal evaluation using enhanced depth imaging spectral-domain optical coherence tomography in Vogt-Koyanagi-Harada disease. Retina 2011;31(3):502-9.

7. Imamura Y, Iida T, Maruko I, et al. Enhanced depth imaging optical coherence tomography of the sclera in dome-shaped macula. Am J Ophthalmol 2011;151(2):297-302.

8. Mwanza JC, Hochberg JT, Banitt MR, et al. Lack of association between glaucoma and macular choroidal thickness measured with enhanced depth-imaging optical coherence tomography. Invest Ophthalmol Vis Sci 2011;52(6):3430-5.

9. Spaide RF. Enhanced depth imaging optical coherence tomography of retinal pigment epithelial detachment in age-related macular degeneration. Am J Ophthalmol 2009;147(4):644-52.

10. Margolis R, Spaide RF. A pilot study of enhanced depth imaging optical coherence tomography of the choroid in normal eyes. Am J Ophthalmol 2009;147(5):811-5.

11. McCourt EA, Cadena BC, Barnett CJ, et al. Measurement of subfoveal choroidal thickness using spectral domain optical coherence tomography. Ophthalmic Surg Lasers Imaging 2010;41 Suppl:S28-33.

12. Rahman W, Chen FK, Yeoh J, et al. Repeatability of manual subfoveal choroidal thickness measurements in healthy subjects using the technique of enhanced depth imaging optical coherence tomography. Invest Ophthalmol Vis Sci 2011;52(5):2267-71.

13. Yasuno Y, Okamoto F, Kawana K, et al. Investigation of multifocal choroiditis with panuveitis by three-dimensional high-penetration optical coherence tomography. J Biophotonics 2009;2(6-7):435-41.

14. Yeoh J, Rahman W, Chen F, et al. Choroidal imaging in inherited retinal disease using the technique of enhanced depth imaging optical coherence tomography. Graefes Arch Clin Exp Ophthalmol 2010;248(12):1719-28.

15. Rosman M, Zheng Y, Wong W, et al. Singapore Malay Eye Study: rationale and methodology of 6-year follow-up study (SiMES-2). Clin Experiment Ophthalmol 2012;40(6):557-68.

16. Gupta P, Jing T, Marziliano P, et al. Peripapillary choroidal thickness assessed using automated choroidal segmentation software in an Asian population. Br J Ophthalmol 2015.

17. Gupta P, Jing T, Marziliano P, et al. Distribution and determinants of choroidal thickness and volume using automated segmentation software in a population-based study. Am J Ophthalmol 2015;159(2):293-301 e3.

18. Barteselli G, Chhablani J, El-Emam S, et al. Choroidal volume variations with age, axial length, and sex in healthy subjects: a three-dimensional analysis. Ophthalmology 2012;119(12):2572-8.

19. Chhablani J, Barteselli G, Wang H, et al. Repeatability and reproducibility of manual choroidal volume measurements using enhanced depth imaging optical coherence tomography. Invest Ophthalmol Vis Sci 2012;53(4):2274-80.

20. Noori J, Riazi Esfahani M, Hajizadeh F, Zaferani MM. Choroidal mapping; a novel approach for evaluating choroidal thickness and volume. J Ophthalmic Vis Res 2012;7(2):180-5.

21. Shin JW, Shin YU, Lee BR. Choroidal thickness and volume mapping by a six radial scan protocol on spectral-domain optical coherence tomography. Ophthalmology 2012;119(5):1017-23.

CHAPTER VI TABLES

Table 6.1 Agreement between automated versus manual macular choroidal thickness measurement at 5 horizontal locations (n = 45 eyes)

Locations of measurement	Intraclass correlation (95% CI**)**	Mean difference* (95% LOA**)**
Choroidal thickness		
Sub-foveal	0.96 (0.94 to 0.98)	2.2 (-61 to 65.5)
Nasal, 1.5 mm	0.95 (0.92 to 0.97)	-4.3 (-74 to 65.4)
Nasal, 3 mm	0.90 (0.82 to 0.94)	3.9 (-83.6 to 91.4)
Temporal, 1.5 mm	0.94 (0.89 to 0.96)	9 (-59.4 to 77.4)
Temporal, 3 mm	0.93 (0.87 to 0.96)	3 (-62.3 to 68.4)

*Mean difference was determined from the automated measurement minus manual measurement.

Table 6.2 Assessment of intra-session repeatability of macular choroidal thickness (at various horizontal locations) and macular choroidal volume using automated segmentation software (n = 20)

Locations of measurement	Intraclass correlation (95% CI)	Mean difference[a] (95% LOA)
Choroidal thickness		
Sub-foveal	0.996 (0.992 to 0.998)	-0.4 (-21.5 to 20.7)
Nasal, 1.5 mm	0.992 (0.981 to 0.997)	-2.1 (-29.1 to 24.9)
Nasal, 3 mm	0.996 (0.991 to 0.998)	1.6 (-15.6 to 18.8)
Temporal, 1.5 mm	0.995 (0.989 to 0.998)	0.1 (-26.2 to 26.4)
Temporal, 3 mm	0.979 (0.949 to 0.992)	0.5 (-38.2 to 39.2)
Choroidal volume of 7 line scan (8.9 mm x 1.5 mm)	0.999 (0.997 to 0.999)	0.0 (-0.08 to 0.09)

[a]Mean difference was determined from the 1st measurement minus 2nd measurement.

Table 6.3 Agreement between automated versus manual peripapillary choroidal thickness at four optic disc quadrants (n = 45 eyes)

Locations of measurement	Intraclass correlation (95% CI)	Mean difference[a] (95% LOA)
Peripapillary CT		
Inferior Quadrant	0.96 (0.92 to 0.98)	-3.68 (-33.45 to 26.08)
Superior Quadrant	0.99 (0.98 to 0.99)	2.04 (-12.60 to 16.70)
Nasal Quadrant	0.95 (0.91 to 0.97)	-1.94 (-35.62 to 31.72)
Temporal Quadrant	0.97 (0.94 to 0.98)	-3.97 (-37.35 to 29.40)
Average	0.98 (0.96 to 0.99)	-4.05 (-24.36 to 16.25)

[a]Mean difference was determined from the automated measurement minus manual measurement.

Table 6.4 Intra-session repeatability of peripapillary choroidal thickness measurement at four quadrants obtained using automated choroidal segmentation software (n = 30)

Locations of measurement	Intraclass correlation (95% CI)	Mean difference (μm)* (95% LOA)
Peripapillary CT		
Inferior Quadrant	0.99 (0.99 to 0.99)	0.2 (-2.7 to 2.2)
Superior Quadrant	0.99 (0.99 to 1.00)	-0.2 (-2.9 to 2.6)
Nasal Quadrant	0.99 (0.99 to 0.99)	0.3 (-2.9 to 3.4)
Temporal Quadrant	0.99 (0.99 to 0.99)	-0.5 (-3.8 to 2.7)
Average	1.00 (0.99 to 1.00)	-0.1 (-1.5 to 1.2)

*Mean difference was determined from the 1st measurement minus 2nd measurement.

CHAPTER VI FIGURES

Figure 6.1 illustrating automated detection of the choroid-scleral interface (CSI). The valleys (local minimums) of the OCT A-scans are used as the feature to detect the CSI. However, there are also valleys caused by the speckle noise and the blood vessels in the choroid region.

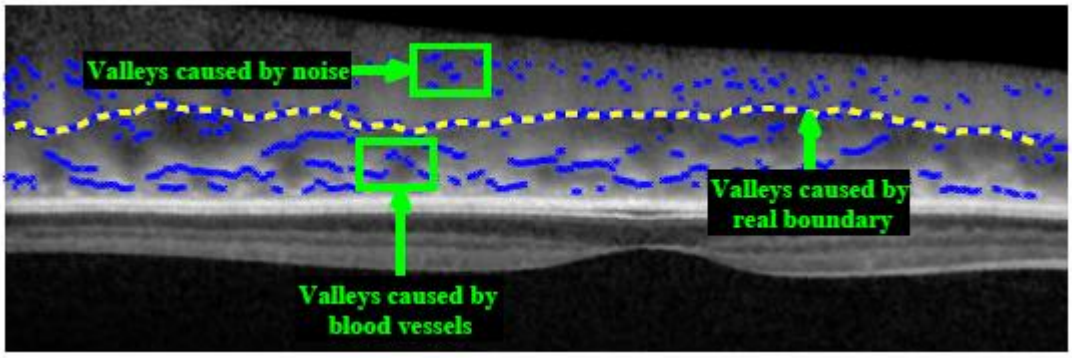

Figure 6.2 EDI-OCT image of the macular region demonstrating automated segmentation of the Bruch's membrane and the choroidal-scleral interface. Choroidal thickness at each measurement points (shown by the numbered grid) was defined as CT (x,y), where x and y are the transversal (from nasal to temporal) and inter-frame (from superior to inferior) direction respectively. The separation between frames is 246 µm.

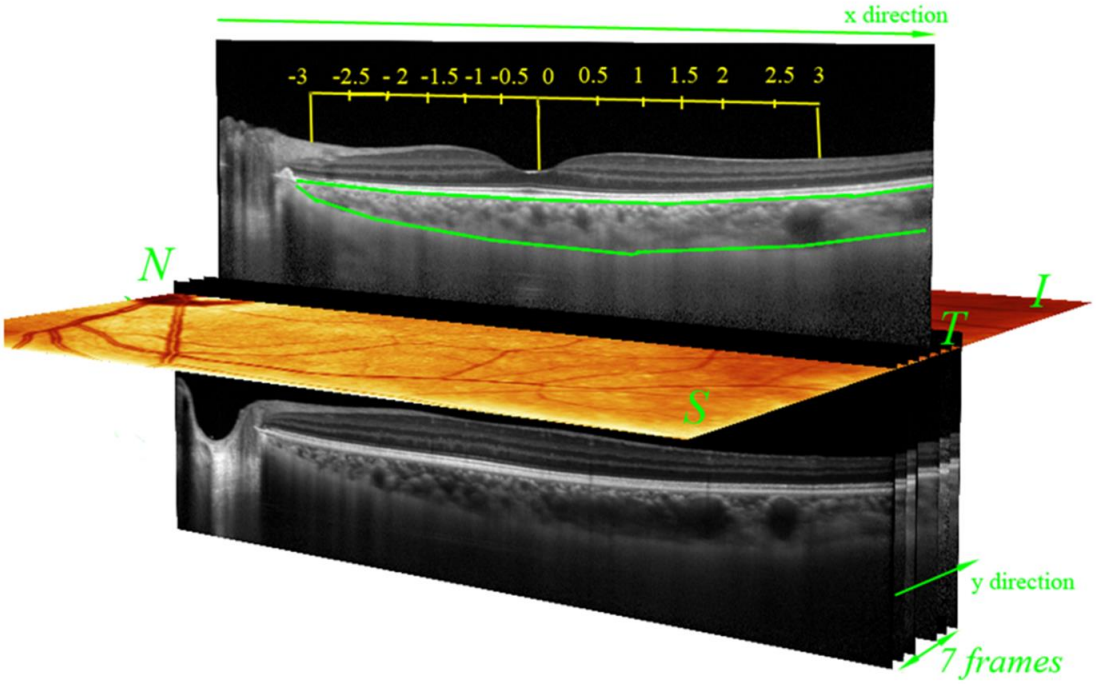

Figure 6.3 EDI-OCT image of the macular region demonstrating automated segmentation of the Bruch's membrane and the choroidal-scleral interface. The horizontal choroidal thickness profile was generated at the fovea (detected as the lowest points of internal limiting membrane automatically) and at 500-µm intervals up to 3 mm temporal and nasal to the fovea.

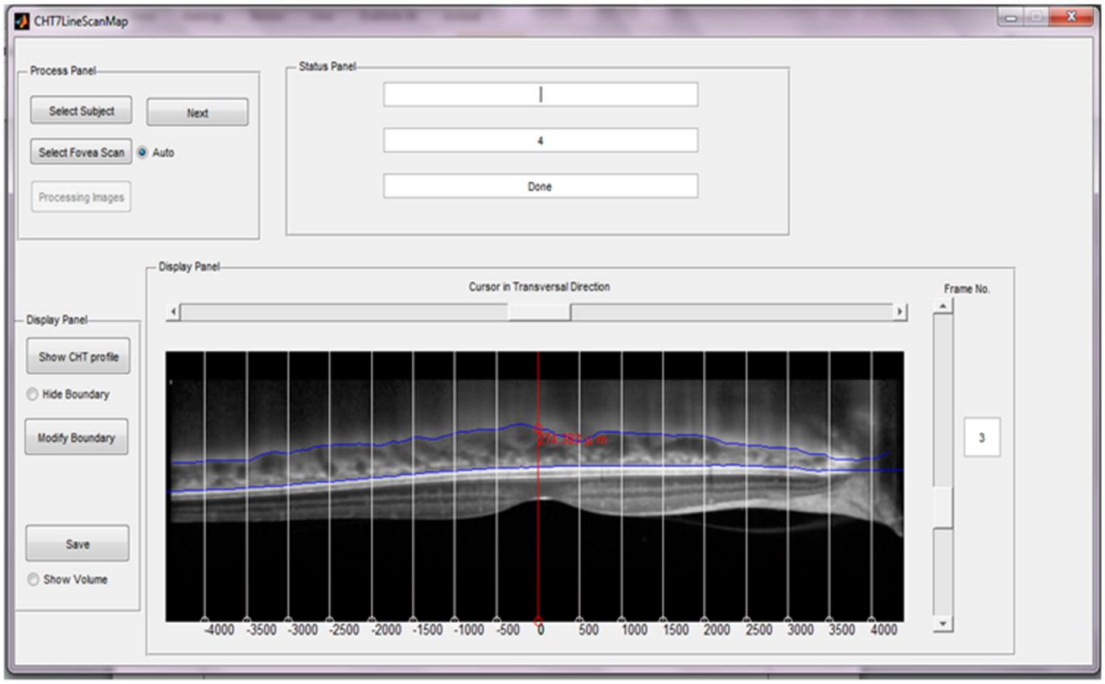

Figure 6.4 An illustration of the color-coded choroidal volume map obtained from the 7 serial horizontal B-scans covering an area of 8.9 x 1.5 mm centered on the fovea. The choroidal volume is expressed in millimeter cube (mm^3) with the warm and the cool colors representing thicker and thinner choroidal volume respectively. X and Y presents the transverse (from nasal to temporal) and inter frame (from superior to inferior) directions respectively.

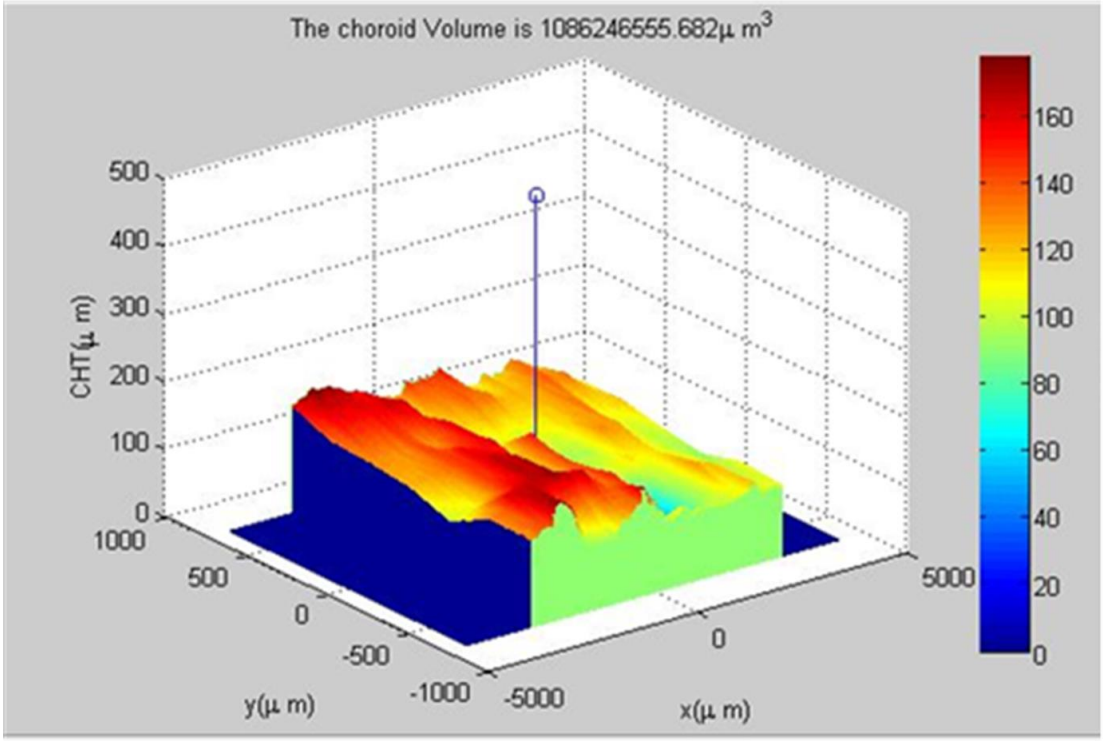

Figure 6.5 EDI-OCT image in the peripapillary region demonstrating automated segmentation of the Bruch's membrane (BM) and the choroidal–scleral interface (CSI).

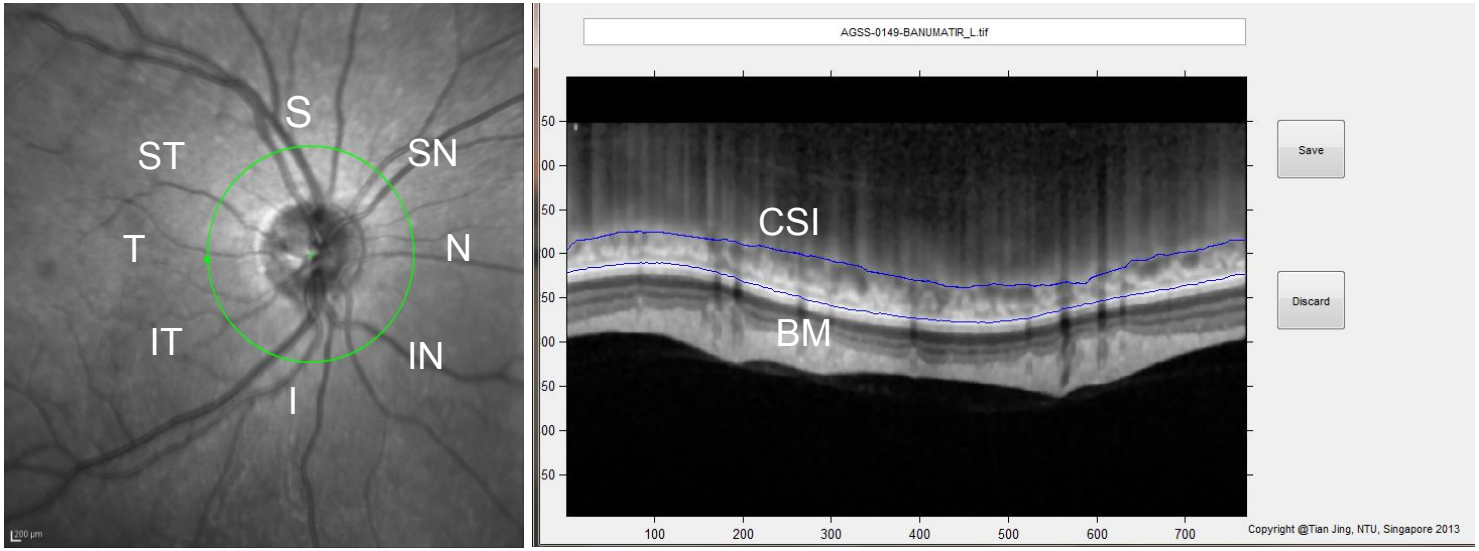

Figure 6.6 Illustration of automated peripapillary choroidal thickness (CHT) measured in the optic disc region. The numbers on the x-axis are locations in clock hour sectors (30° apart). The location of the zero degree is always on the left- most point of the disc circle and the value of degree increases in the clockwise direction. T, temporal; S, superior; N, nasal; I, inferior quadrants.

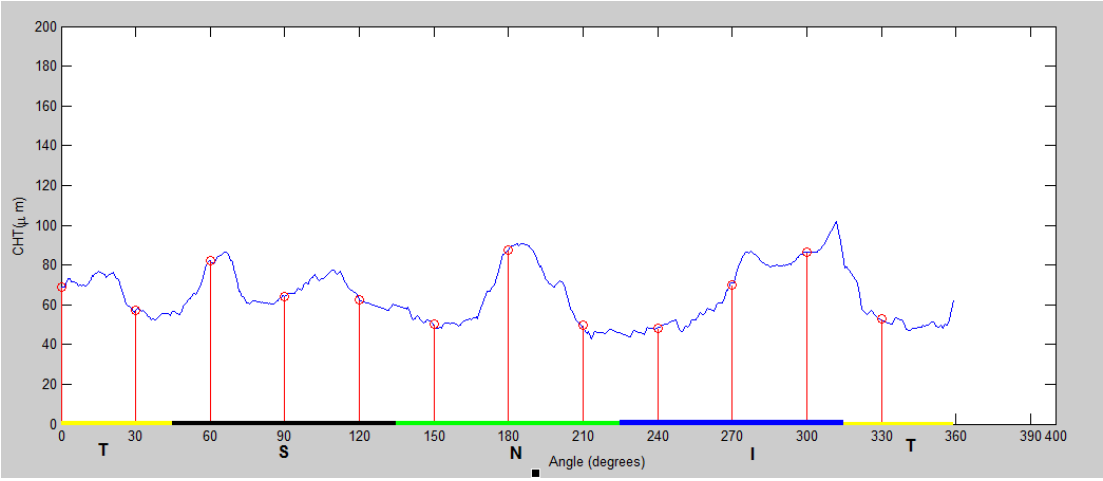

CHAPTER VII

DISTRIBUTION AND DETERMINANTS OF CHOROIDAL THICKNESS AND VOLUME USING AUTOMATED CHOROIDAL IMAGE PROCESSING TECHNIQUE IN A MULTI-ETHNIC POPULATION IN SINGAPORE

In chapter VI, we established that our novel automated choroidal image processing technique which can objectively and accurately define CSI and assess CT is valid and comparable to existing manual CT measurements in both macular and peripapillary regions. In this Chapter, we adapted our validated technique to obtain choroidal measures such as thickness and volume in macular and peripapillary regions in our large population sample in Singapore.

The manuscripts relevant to the contents of previous (Chapter 6) and this chapter have been published in the following journals:

Gupta, P., T. Jing, P. Marziliano, C. Y. Cheung, M. Baskaran, E. L. Lamoureux, T. Y. Wong, C. M. Cheung and C. Y. Cheng. "Distribution and Determinants of Choroidal Thickness and Volume Using Automated Segmentation Software in a Population-Based Study." *American Journal of Ophthalmol*ogy 2015;159(2):293-301.

Gupta, P., T. Jing, P. Marziliano, M. Baskaran, G. C. Cheung, E. L. Lamoureux, C. Y. Cheung, T. Y. Wong, T. Aung and C. Y. Cheng. "Peripapillary Choroidal Thickness Assessed Using Automated Choroidal Segmentation Software in an Asian Population." *British Journal of Ophthalmol*ogy 2015;99(7):920-926.

7.1 INTRODUCTION

Currently there is limited population-based data on CT and volume in Asians. To the best of our knowledge, Beijing eye study is the only population-based study but their measurement of CT was performed manually and was restricted to sub-foveal location only. There is lack of population-based data reporting a series of comprehensive ocular and systemic factors that may influence CT and volume measurements using SD-OCT. To date, it is unknown whether there exists any ethnic variation in CT and volume among Asians. Neither is it known if there are differences in systemic and ocular risk factors of CT and volume in different ethnic groups in Asians. Knowledge of such factors is crucial before drawing inferences on CT and volume by SD-OCT.

Singapore has major racial/ethnic groups, Malay, Indian and Chinese, which provides a unique opportunity to study the effect of ethnic differences on CT and volume in a relatively common geographic and socio-economic environment. The aim was to evaluate the distribution and determinants of macular and peripapillary CT and macular choroidal volume in a multi-ethnic population in Singapore using our novel fully automated choroidal segmentation technique.

7.2 METHODS

7.2.1 Study Subjects

A total of 980 participants were consecutively recruited from the SEED Study, a population-based cohort study, comprising of major ethnic groups in Singapore: Malays (n= 540, from the SiMES, year 2011-2013) and Indians (n= 440 from the SINDI, year 2012-2015). Details of the study design and 3 methodology of the SEED study have been described in Chapter III and elsewhere.[1, 2]

Subjects were excluded if their choroidal images could not be successfully attained due to unstable fixation, opacities of the optic media, such as significant cataract or the available images were not of sufficient quality (quality index below 18 dB), and subjects whose peripapillary atrophy involved the OCT scanning ring. As our aim was to determine the distribution of CT in a general population sample, therefore, any ocular diseases, such as presence of refractive errors, cataract, glaucoma, retinopathy and disorders of the optic nerve or macula, were no reason to exclude a subject if the quality of OCT image was sufficient to be evaluated.

7.2.2 Choroidal Imaging and Measurements

The choroidal image acquisition protocol for both macular and peripapillary regions as well as automated measurements of CT (macular and peripapillary) and macular choroidal volume have been described in detail in Chapter III and VI of the thesis and elsewhere.[3, 4]

7.2.3 Assessment of Ocular and Systemic Factors

Each subject underwent an interview and a detailed systemic and ocular examination including, choroidal imaging at macular and optic nerve head regions using Spectralis SD-OCT.

Detailed descriptions of comprehensive systemic and ocular examinations are described in Chapter III of the thesis.

7.2.4 Statistical Analyses

Statistical analysis was performed using SPSS version 20.0 (SPSS, Inc., Chicago, IL, USA). Demographic, ocular and systemic characteristics of the study participants are presented as means (SD) or number (%) as appropriate. CT at various

locations is expressed as means (SD). Univariate and multiple linear regression analyses were performed to determine the associations of sub-foveal CT, peripapillary CT and macular choroidal volume (dependent variables) with ocular and systemic factors (independent variables). For multiple linear regression, age, gender and factors showing suggestively significant association in univariate analysis ($p<0.10$) were included. In the assessment of associations with ocular and systemic factors, we included glaucoma status, diabetic retinopathy and age related macular degeneration in the regression models to adjust for potential confounding. Generalized estimating equation, exchangeable correlation matrix, was used to account for inter-eye correlations when both eyes of the study subjects were used for analysis.

7.3 RESULTS

We first describe the results of the distribution and determinants of macular CT and volume in ethnic Malays. This was followed by the evaluation of the distribution and determinants of peripapillary CT in ethnic Malays. Next, we performed the above analyses (evaluation of the distribution and determinants of macular and peripapillary CT) in subjects of Indian ethnicity. Furthermore, to elucidate whether the observed differences in CT and volume across ethnic groups are attributable to ethnicity, we compared these choroidal parameters across ethnic groups after adjusting for the population-specific factors.

7.3.1 Distribution and Determinants of Macular CT and Volume in Ethnic Malays

Study Subjects' Characteristics: A total of 540 eyes from 540 consecutive subjects of Malay ethnicity (251 men and 289 women) with a mean (SD) age of 62.70 (8.91)

years were included in the analysis. In none of the images did the automated software fail to detect the RPE and choroidal borders and therefore no eyes were excluded from the analysis. The demographics, ocular and systemic characteristics of the study population are shown in **Table 7.1**.

Distribution of Macular CT and Volume: **Table 7.2** shows the mean CT and choroidal volume. CT was measured at 13 different locations on the horizontal axis. Choroid was thickest at the sub-fovea (242.28±97.58 μm), followed by temporal and thinnest at 3 mm nasal (142.44±79.19 μm) location (which is the last point measured using the software). The mean macular (1 mm diameter) and 7 line scan choroidal volume were 0.185±0.071 mm^3 and 1.889±0.69 mm^3 respectively.

Determinants of Macular CT and Volume: In the univariate analysis (**Table 7.3**), among the ocular factors only SE and AL showed significant association with sub-foveal CT (both $p<0.001$). For each mm increase in AL, sub-foveal CT on average decreased by 19.63 μm ($p<0.001$). A decrease in mean CT by 10.77 μm was observed for each myopic dioptre increase ($p<0.001$). Among the systemic factors, younger age, male gender, higher serum cholesterol or triglycerides levels, current smoking and free of arterial hypertension were found to be significantly associated with thicker sub-foveal CT (all $p<0.05$).

Because of collinearity between AL and SE (correlation coefficient = -0.584), only AL was selected and retained in the multivariate analysis as it had a greater explanatory power on sub-foveal CT change than did SE (standardized β, -0.197 vs. 0.192). In the multiple linear regression model (**Table 7.3**) including all significant factors, only shorter AL ($p<0.001$), younger age ($p<0.001$) and male gender ($p=0.001$) remained significantly associated with thicker sub-foveal CT.

Similarly, in the analysis of the association of choroidal volume at central macular (1 mm diameter) with ocular and systemic factors (**Table 7.4**), only shorter AL, younger age and male gender showed significant association with larger central choroidal volume (all $p<0.001$). Similar factors were associated with greater choroidal volume of 7 line scan (data not shown).

7.3.2 Distribution and Determinants of Peripapillary CT in Ethnic Malays

Of the 540 consecutive subjects (1080 eyes) whose optic disc scans were available, we further excluded 88 subjects because either their choroidal images were not successfully attained (n=47) or the available images were of insufficient quality (n=28) for a reliable determination of the peripapillary choroidal thickness (PPCT) or subjects whose peripapillary atrophy involved the OCT scanning ring (n=13), leaving 452 subjects (904 eyes) with complete data on PPCT for analysis. In none of the images did the automated software fail to detect the Bruch's membrane and choroidal borders and therefore no eyes were excluded from the analysis because of software demarcation error.

Distribution of Peripapillary CT: **Table 7.5** shows the mean PPCT measured at 12 clock hours and four quadrants (superior, nasal, inferior and temporal). The overall mean PPCT in our study subjects was 136.2 ± 56.8 μm. There are regional differences in PPCT among clock hours and different quadrants. Peripapillary choroid was thickest (150.5 ± 59.6 μm) at the superior and thinnest (102.6 ± 51.1 μm) at the inferior quadrant.

Determinants of Peripapillary CT: In the univariate linear regression analysis (**Table 7.6**), AL, IOP, triglycerides levels and diabetes showed significant association with average PPCT (all $p<0.10$). In the multiple linear regression model (**Table 7.6**)

including age, gender and all suggestively significant factors ($p<0.10$) from the univariate analysis, shorter AL ($p=0.002$), younger age ($p<0.018$), lower triglycerides levels ($p=0.015$) and presence of diabetes ($p=0.036$) remained significantly associated with thicker PPCT. The association with IOP was no longer significant ($p=0.407$). For each mm increase in AL and per year increase in age, PPCT on average decreased by 6.59 µm ($p=0.002$) and 0.56 µm ($p=0.018$) respectively. A decrease in mean PPCT by 4.88 µm was observed for each mmol/L increase in triglycerides level ($p=0.015$). Presence of diabetes increased the mean PPCT by 13.73 µm ($p=0.036$). However, if gender and IOP were removed from our multivariate model, presence of diabetes still remained significantly associated with PPCT (regression coefficient = 13.22; 95% CI = 0.42 to 26.02; $p=0.043$).

Table 7.7 presents the multivariate analysis results of the associations of PPCT with ocular and systemic factors by quadrant. In the multivariate models, only younger age and shorter AL was associated with thicker inferior peripapillary choroid; and shorter AL, lower triglycerides level and presence of diabetes were associated with thicker superior peripapillary choroid. IOP was the only significant factor associated with thicker nasal peripapillary choroid. For temporal PPCT, associated factors were similar to those identified from overall PPCT.

7.3.3 Distribution and Determinants of Macular CT and Volume in Ethnic Indians

Study Subjects' Characteristics: A total of 440 eyes from 440 consecutive subjects of Indian ethnicity (231 men and 209 women) with a mean (SD) age of 58.56 (8.18) years were included in the analysis. The demographics, ocular and systemic characteristics of the study population are shown in **Table 7.8**.

Distribution of Macular CT and Volume: **Table 7.9** shows the mean CT and choroidal volume. CT was measured at 13 different locations on the horizontal axis. Choroid was thickest at the sub-fovea 267.23 ±100.99 µm, followed by temporal and thinnest at 3 mm nasal (170.09±88.79 µm) location (which is the last point measured using the software). The mean macular (1 mm diameter) and 7 line scan choroidal volume were 0.209±0.071 mm^3 and 2.167±0.689 mm^3 respectively.

Determinants of Macular CT and Volume: In the univariate analysis (**Table 7.10**), among the ocular factors only AL showed significant association with sub-foveal CT (p=0.001). For each mm increase in AL, sub-foveal CT on average decreased by 15.77 µm (p=0.001). Among the systemic factors, younger age, male gender, higher triglycerides levels, current smoking and free of diabetes mellitus were found to be significantly associated with thicker sub-foveal CT (all p<0.10). In the multiple linear regression model (**Table 7.10**) including all significant factors, only shorter AL (p<0.001), more curved cornea (p<0.001), younger age (p=0.010), male gender (p<0.001) and absence of diabetes (p=0.015) remained significantly associated with thicker sub-foveal CT.

Similarly, in the analysis of the association of choroidal volume at central macular (1 mm diameter) with ocular and systemic factors (**Table 7.11**), only shorter AL, younger age, male gender and higher levels of triglycerides showed significant association with larger central choroidal volume (all p<0.05). Similar factors were associated with greater choroidal volume of 7 line scan (data not shown).

7.3.4 Distribution and Determinants of Peripapillary CT in Ethnic Indians

To assess the distribution and determinants of PPCT in ethnic Indians we analysed 650 Indian eyes.

Distribution of Peripapillary CT: **Table 7.12** shows the mean PPCT measured at 12 clock hours and four quadrants (superior, nasal, inferior and temporal). The overall mean PPCT in our study subjects was 181.74±67.51 μm. There are regional differences in PPCT among clock hours and different quadrants. Peripapillary choroid was thickest (197.50±73.13 μm) at the superior and thinnest (151.09±61.07 μm) at the inferior quadrant.

Determinants of Peripapillary CT: In the univariate linear regression analysis (**Table 7.13**), AL, corneal curvature, age, gender, diastolic BP, HbA1c, triglycerides levels and smokers showed significant association with average PPCT (all $p<0.10$). In the multiple linear regression model (**Table 7.13**) including age, gender and all suggestively significant factors ($p<0.10$) from the univariate analysis, shorter AL ($p<0.001$), younger age ($p<0.001$), male gender ($p<0.001$) and higher HbA1c levels ($p=0.021$) remained significantly associated with thicker PPCT. For each mm increase in AL and per year increase in age, PPCT on average decreased by 18.46 μm ($p<0.001$) and 2.23 μm ($p<0.001$) respectively. Males have 40.08 μm thicker peripapillary choroid than females ($p<0.001$). A decrease in mean PPCT by 5.19 μm was observed for each unit increase in HbA1c level ($p=0.021$).

Table 7.14 presents the multivariate analysis results of the associations of PPCT with ocular and systemic factors by quadrant. In the multivariate models, shorter AL, younger age, male gender and lower HbA1c levels were associated with thicker superior, nasal and temporal peripapillary choroid. For inferior PPCT, except HbA1c, all other factors remained the same.

7.3.5 Comparison of Macular CT and Volume among Ethnic Malays and Indians

To elucidate whether the observed differences in CT and volume across ethnic Malays and Indians are attributable to ethnicity, we compared the above choroidal parameters (CT and volume) between ethnic groups after adjusting for the differences in population-specific factors and other relevant confounders.

Table 7.15 shows the comparison of the baseline characteristics of ethnic Malays and Indians. Indians are significantly younger with more number of male participants of shorter AL, more hyperopic refractive error, lower OPP, SBP, cholesterol and creatinine levels. Compared to Malays, less number of Indians had hypertension.

Table 7.16 shows the unadjusted distribution of macular choroidal volume and CT at various locations in the posterior pole among ethnic Malays and Indians. In general, Indians had significantly thicker choroid at all the measured locations (all $p<0.001$). Likewise they had greater choroidal volume at both 7 line scan region (8.9 x 1.5 mm) and central macular (1mm) region (both $p<0.001$). However after adjusting for population-specific factors which were significantly different between the ethnic groups such as age, gender, AL, corneal curvature, OPP, current smoking, creatinine and cholesterol as well as other potential confounders like presence of AMD, DR and glaucoma, we found that although Indians demonstrated a trend towards thicker choroid at all the locations but it was not statistically significant at most of the locations including sub-foveal. On average, the choroid in Indians is thicker by 12 μm which is statistically significant but this difference is unlikely to be clinically meaningful (**Table 7.17**).

7.3.6 Comparison of Peripapillary CT among Ethnic Malays and Indians

Table 7.18 shows the unadjusted distribution of peripapillary CT at four quadrants among ethnic Malays and Indians. In general, Indians had significantly

thicker peripapillary choroid at all 4 quadrants (all p<0.001). However after adjusting for population-specific factors which were significantly different between the ethnic groups such as age, gender, AL, corneal curvature, OPP, current smoking, alcohol consumption, creatinine, cholesterol and triglycerides as well as other potential confounders like presence of AMD, DR and glaucoma, we found that Indians showed thicker peripapillary choroid at all 4 quadrants. On average, the peripapillary choroid in Indians is thicker by 32 µm which is both statistically and clinically significant (**Table 7.19**).

7.4 DISCUSSION

7.4.1 Macular CT and Volume in Ethnic Malays and Indians

Using the fully automated choroidal image processing technique and after adjusting for the differences in population-specific factors and all other relevant confounders, our results demonstrate the mean macular CT to be 223.44±3.86 µm and 236.13±4.43 µm in ethnic Malays and Indians respectively. Indians had a trend towards thicker choroid at all measured locations but it was not statistically significant at most of the locations including sub-foveal. Although, the difference in mean macular CT of 12 µm between the ethnic groups is statistically significant, it seems to be driven by nasal location. Likewise Indians had greater choroidal volume than ethnic Malays with a mean difference of 0.01 mm^3 (at central 1 mm macular region).

In terms of topographical distribution of macular CT, our results indicate its asymmetric distribution in ethnic Malays and Indians. In both the ethnic groups, the mean CT measurements showed regional differences, being thickest subfoveally, followed by temporal and thinnest at the nasal location.

In both the ethnic groups, male gender, younger age, and shorter axial length are the factors independently associated with thicker choroid and larger choroidal volume. Additionally, higher triglycerides levels and absence of diabetes are associated with thicker choroid in Indians. These factors should be taken into consideration when interpreting EDI SD-OCT based CT and volume measurements in clinics.

7.4.2 Peripapillary CT in Ethnic Malays and Indians

Using our fully automated choroidal image processing technique and after adjusting for the differences in population-specific factors and other likely confounders, our study showed the mean peripapillary CT of 142.56±3.01 μm and 174.49±3.30 μm in ethnic Malays and Indians respectively. The mean difference of 32 μm between the two ethnic groups is both statistically and clinically meaningful.

In relation to the topographical profile of peripapillary choroid, our results exhibit asymmetric distribution of peripapillary CT in ethnic Malays and Indians. In both the ethnic groups, the mean peripapillary CT measurements showed regional differences, being thickest in the superior region and thinnest in the inferior region. However, in ethnic Malays nasal quadrant was thicker than temporal but in Indians temporal region was thicker than nasal.

In both the ethnic groups, younger age and shorter axial length are the factors independently associated with thicker peripapillary choroid. Additionally, male gender and lower HbA1c levels in Malays and lower triglycerides and absence of diabetes in Indians are associated with thicker peripapillary choroid. These factors should be taken into account when interpreting EDI OCT based peripapillary CT measurements in clinics.

7.5 CONCLUSIONS

Our results demonstrate that there exist slight difference in macular CT (mean difference 12 μm), macular choroidal volume (mean difference 0.02 mm^3) and peripapillary CT (mean difference ~32 μm) among ethnic Malays and Indians. Indians tend to have slightly thicker choroid than Malays. With regards to topographical distribution, both macular and peripapillary choroid is asymmetrically distributed (macular: thickest subfoveally and thinnest nasally; peripapillary: thickest superiorly and thinnest inferiorly). However, there is no difference in topographical profile of macular and peripapillary choroid among ethnic Malays and Indians. Factors such as age, gender and axial length are the major determinants of CT and volume among both ethnic groups and should be taken into account when interpreting EDI OCT based CT measurements in clinical settings.

7.6 REFERENCES

1. Lavanya R, Jeganathan VS, Zheng Y, et al. Methodology of the Singapore Indian Chinese Cohort (SICC) eye study: quantifying ethnic variations in the epidemiology of eye diseases in Asians. Ophthalmic Epidemiol 2009;16(6):325-36.

2. Rosman M, Zheng Y, Wong W, et al. Singapore Malay Eye Study: rationale and methodology of 6-year follow-up study (SiMES-2). Clin Experiment Ophthalmol 2012;40(6):557-68.

3. Gupta P, Jing T, Marziliano P, et al. Peripapillary choroidal thickness assessed using automated choroidal segmentation software in an Asian population. Br J Ophthalmol 2015;99(7):920-6.

4. Gupta P, Jing T, Marziliano P, et al. Distribution and determinants of choroidal thickness and volume using automated segmentation software in a population-based study. Am J Ophthalmol 2015;159(2):293-301.

CHAPTER VII TABLES

Table 7.1 Demographic, ocular and systemic characteristics of ethnic Malays (n = 540) for evaluation of choroidal thickness and volume using fully automated choroidal segmentation technique

Characteristics	Included (n = 540)
Age, years	62.70 (8.91)
Gender, % male	251 (46.5)
Axial length, mm	23.59 (0.96)
Anterior chamber depth, mm	3.17 (0.34)
Corneal curvature, mm	7.66 (0.24)
Spherical equivalent, D	0.11 (1.74)
Best corrected visual acuity, Log MAR	0.16 (0.20)
Central corneal thickness, μm	541.76 (35.15)
Intraocular pressure, mmHg	14.49 (3.10)
Ocular perfusion pressure, mmHg	55.55 (8.19)
Systolic blood pressure, mmHg	139.56 (19.68)
Diastolic blood pressure mmHg	76.90 (10.66)
Mean arterial pressure, mmHg	97.78 (12.37)
Body mass index, kg/m^2	26.87 (5.07)
Serum glucose, mmol/L	7.22 (3.52)
HbA1c, %	6.35 (1.43)
Total cholesterol, mmol/L	5.36 (1.29)
Triglycerides, mmol/L	1.92 (1.30)
Blood creatinine, mmol/L	83.23 (41.23)
Current smoking, %	98 (18.1)
Diabetes mellitus, %	143 (26.5)
Arterial hypertension, %	323 (59.8)
Alcohol consumption, %	7 (1.3)

Data are means (standard deviations), except for gender, HbA1c, current smoking, diabetes, arterial hypertension and alcohol consumption which are expressed as number (%).

Table 7.2 Distribution of mean macular choroidal thickness (at various points on the horizontal axis) and volume measurements in ethnic Malays (n = 540) using fully automated choroidal segmentation technique

Location of measurements	Mean (SD)
CHOROIDAL THICKNESS (um)	
Sub-foveal	242.28 (97.58)
Nasal, 0.5 mm	237.11 (97.72)
Nasal, 1 mm	226.68 (98.10)
Nasal, 1.5 mm	208.35 (98.20)
Nasal, 2 mm	187.29 (94.21)
Nasal, 2.5 mm	166.02 (89.72)
Nasal, 3 mm	142.44 (79.19)
Temporal, 0.5 mm	241.93 (96.58)
Temporal, 1 mm	239.39 (92.83)
Temporal, 1.5 mm	232.17 (89.42)
Temporal, 2 mm	221.31 (84.12)
Temporal, 2.5 mm	216.19 (81.93)
Temporal, 3 mm	207.65 (80.98)
CHOROIDAL VOLUME (mm^3)	
Choroidal volume of 7 line scan (8.9 x 1.5 mm)	1.889 (0.693)
Choroidal volume at central macula (1mm diameter circle)	0.185 (0.071)

Data presented are means (standard deviations).

Table 7.3 Univariate and multivariate analysis of the association of ocular and systemic factors with sub-foveal choroidal thickness in ethnic Malays (n = 540) measured using fully automated choroidal segmentation technique

	Univariate analysis			Multivariate analysis[a]		
	Unstandardized β	**Standardized β**	**P-value**	**Unstandardized β**	**Standardized β**	**P-value**
Ocular factors						
Spherical equivalent, D	10.773	0.192	<0.001	-	-	-
Axial length, mm	-19.638	-0.197	<0.001	-32.111	-0.317	**<0.001**
Corneal curvature, mm	-33.037	-0.084	0.063	20.160	0.051	0.303
Anterior chamber depth, mm	0.870	0.003	0.944	-	-	-
Central corneal thickness, μm	0.164	0.059	0.170	-	-	-
Intraocular pressure, mmHg	0.473	0.015	0.727	-	-	-
Ocular perfusion pressure, mmHg	0.269	0.023	0.600	-	-	-
Systemic factors						
Age, years	-3.104	-0.284	<0.001	-4.139	-0.366	**<0.001**
Gender, (female)	-19.432	-0.099	0.021	-30.869	-0.158	**0.001**
Mean arterial pressure, mmHg	0.172	0.022	0.612	-	-	-
Body mass index, kg/m^2	-1.233	-0.064	0.137	-	-	-
Serum glucose, mmol/L	0.556	0.020	0.651	-	-	-
HbA1c, %	3.230	0.047	0.279	-	-	-
Total cholesterol, mmol/L	9.110	0.121	0.005	4.495	0.060	0.163
Triglycerides, mmol/L	7.209	0.096	0.027	4.180	0.057	0.185
Blood creatinine, mmol/L	-0.035	-0.015	0.734	-	-	-
Current smoking, Yes	36.601	0.145	0.001	-1.028	-0.004	0.930
Diabetes mellitus, Yes	1.472	0.007	0.878	-	-	-
Arterial hypertension, Yes	-21.077	-0.106	0.014	-3.723	-0.019	0.678
Alcohol consumption, Yes	34.549	0.040	0.353	-	-	-

[a]Adjusted for glaucoma status, diabetic retinopathy and age-related macular degeneration.

Table 7.4 Univariate and multivariate analysis of the association of ocular and systemic factors with choroidal volume at central macula in ethnic Malays (n = 540) measured using fully automated choroidal segmentation technique

	Univariate analysis			Multivariate analysis[a]		
	Unstandardized β	**Standardized β**	**P-value**	**Unstandardized β**	**Standardized β**	**P-value**
Ocular factors						
Spherical equivalent, D	0.009	0.207	<0.001	-	-	-
Axial length, mm	-0.014	-0.189	<0.001	-0.021	-0.280	**<0.001**
Corneal curvature, mm	-0.014	-0.049	0.274	-	-	-
Anterior chamber depth, mm	0.003	0.013	0.777	-	-	-
Central corneal thickness, per 10 μm	0.000	0.065	0.135	-	-	-
Intraocular pressure, per 10 mmHg	-0.0007	0.003	0.942	-	-	-
Ocular perfusion pressure, per 10 mmHg	0.001	0.011	0.795	-	-	-
Systemic factors						
Age, years	-0.003	-0.320	<0.001	-0.003	-0.396	**<0.001**
Gender, (female vs male)	-0.016	-0.109	0.011	-0.023	-0.159	**<0.001**
Mean arterial pressure, per 10 mmHg	0.0004	0.006	0.886	-	-	-
Body mass index, kg/m^2	-0.001	-0.058	0.177	-	-	-
Serum glucose, mmol/L	0.000	0.007	0.880	-	-	-
HbA1c, %	0.003	0.053	0.227	-	-	-
Total cholesterol, mmol/L	0.007	0.131	0.002	0.003	0.057	0.175
Triglycerides, mmol/L	0.006	0.115	0.008	0.003	0.065	0.122
Blood creatinine, mmol/L	-0.000	0.035	0.420	-	-	-
Current smoking, Yes	0.033	0.175	<0.001	0.006	0.032	0.475
Diabetes mellitus, Yes	-0.000	0.000	0.996	-	-	-
Arterial hypertension, Yes	-0.017	-0.116	0.007	-0.001	-0.007	0.874
Alcohol consumption, Yes	0.018	0.029	0.508	-	-	-

[a]Adjusted for glaucoma status, diabetic retinopathy and age-related macular degeneration.

Table 7.5 Distribution of peripapillary choroidal thickness at clock-hour sectors (30° apart) and four quadrants in ethnic Malays (n = 904 eyes)

Measurement Location	Peripapillary Choroidal Thickness, µm
Clock hour	
1	139.5 (77.0)
2	147.8 (71.0)
3	148.9 (64.9)
4	150.8 (61.9)
5	151.4 (59.3)
6	152.1 (60.8)
7	145.4 (61.7)
8	134.0 (58.6)
9	115.8 (53.5)
10	102.6 (51.1)
11	113.9 (57.3)
12	130.3 (68.6)
Quadrants	
Inferior	111.3 (51.7)
Superior	150.5 (59.6)
Nasal	143.5 (58.4)
Temporal	139.4 (68.9)
Average quadrant thickness	136.2 (56.8)

Data presented are means (standard deviations).
1 o'clock corresponded to the temporal region, 4 o'clock to the superior, 7 o'clock to the nasal, and 10 o'clock to the inferior.

Table 7.6 Associations of average peripapillary choroidal thickness with ocular and systemic factors using generalized estimating equation in Malays (n = 904 eyes)

	Univariate analysis		Multivariate analysis*	
	Beta (95% CI)	**P-value**	**Beta (95% CI)**	**P-value**
Ocular factors				
Spherical equivalent, D	-0.22 (-0.23, 1.88)	0.833	-	-
Axial length, mm	-4.23 (-8.88, 0.40)	0.074	-6.59 (-10.86, -2.33)	**0.002**
Corneal curvature, mm	-13.14 (-30.39, 4.10)	0.135	-	-
Central corneal thickness, μm	-0.01 (-0.14, 0.12)	0.841	-	-
Intraocular pressure, mmHg	1.30 (0.20, 2.40)	0.020	0.60 (-0.82, 2.02)	0.407
Ocular perfusion pressure, mmHg	-0.18 (-0.64, 0.27)	0.436	-	-
Systemic factors				
Age, years	-0.20 (-0.61, 0.19)	0.319	-0.56 (-1.03, -0.09)	**0.018**
Gender, male	-5.63 (-14.53, 3.27)	0.215	5.60 (-5.08, 16.29)	0.304
Systolic blood pressure, mmHg	-0.06 (-0.25, 0.13)	0.538	-	-
Diastolic blood pressure, mmHg	-0.00 (-0.36, 0.34)	0.959	-	-
Mean arterial pressure, mmHg	-0.05 (-0.36, 0.25)	0.718	-	-
Body mass index, kg/m^2	0.18 (-0.55, 0.91)	0.631	-	-
Serum glucose, mmol/L	0.53 (-0.69, 1.76)	0.392	-	-
HbA1c, %	1.13 (-1.83, 4.09)	0.455	-	-
Total cholesterol, mmol/L	0.25 (-3.10, 3.60)	0.883	-	-
Triglycerides, mmol/L	-2.42 (-5.13, 0.29)	0.080	-4.88 (-8.80, -0.95)	**0.015**
Blood creatinine, mmol/L	0.00 (-0.07, 0.08)	0.818	-	-
Current smoking	-2.79 (-13.74, 8.14)	0.616	-	-
Diabetes mellitus	9.39 (-0.73, 19.52)	0.069	13.73 (0.90, 26.34)	**0.036**
Arterial hypertension	3.16 (-5.88, 12.20)	0.493	-	-
Alcohol consumption	-7.99 (-38.18, 22.19)	0.604	-	-

*Adjusted for glaucoma status, diabetic retinopathy and age related macular degeneration; CI = confidence interval.
Beta represents the change in peripapillary choroidal thickness for per unit change in continuous variables and the difference in peripapillary choroidal thickness between groups for categorical variables.

Table 7.7 Multivariate analysis of the associations of regional (inferior, superior, nasal and temporal) peripapillary choroidal thickness (PPCT) with ocular and systemic factors using generalized estimating equation in Malays (n = 904 eyes)

	Inferior PPCT		**Superior PPCT**		**Nasal PPCT**		**Temporal PPCT**	
	Beta (95% CI)	**P-value**	**Beta (95% CI)**	**P-value**	**Beta (95% CI)**	**P-value**	**Beta (95% CI)**	**P-value**
AL, mm	-5.59 (-9.53, -1.65)	**0.005**	-6.03 (-10.56, -1.49)	**0.009**	-	-	-7.96 (-13.34, -2.58)	**0.004**
CC, mm	-	-	-	-	-	-	-3.01 (-28.32, 22.29)	0.815
IOP, mmHg	0.64 (-0.53, 1.83)	0.284	0.51 (-1.04, 2.07)	0.518	1.37 (0.04, 2.70)	**0.044**	0.56 (-1.24, 2.36)	0.543
Age, years	-0.54 (-0.96, -0.11)	**0.012**	-0.44 (-0.94, 0.04)	0.074	-0.28 (-0.71, 0.13)	0.184	-0.68 (-1.27, -0.09)	**0.023**
TG, mmol/L	-	-	-5.15 (-9.26, -1.05)	**0.014**	-	-	-5.96 (-10.51, 1.41)	**0.010**
DM	9.36 (-2.26, 20.99)	0.115	15.15 (2.26, 28.04)	**0.021**	-	-	17.07 (1.82, 32.32)	**0.028**

For inferior, superior, nasal and temporal PPCT age, gender, glaucoma status, diabetic retinopathy, age related macular degeneration and variables with $p<0.10$ in univariate models were included in multivariate models.

CI=confidence interval; PPCT=peripapillary choroidal thickness; AL=axial length; CC=corneal curvature; IOP=intra ocular pressure; TG=triglycerides; DM=diabetes mellitus.

Table 7.8 Baseline characteristics of study subjects of Indian ethnicity

Characteristics	**Included (n = 439)**
Age, years	58.56 (8.18)
Gender, % male	231 (52.6)
Axial length, mm	23.42 (1.00)
Anterior chamber depth, mm	3.23 (0.39)
Corneal curvature, mm	7.61 (0.26)
Spherical equivalent, D	0.33 (1.57)
Best corrected visual acuity Log MAR	0.10 (0.11)
Central corneal thickness, μm	541.99 (33.82)
Intraocular pressure, mmHg	15.12 (2.85)
Ocular perfusion pressure, mmHg	53.87 (7.69)
Systolic blood pressure, mmHg	132.50 (18.43)
Diastolic blood pressure mmHg	77.54 (10.44)
Mean arterial pressure, mmHg	95.86 (11.87)
Body mass index, kg/m^2	26.41 (4.42)
Serum glucose, mmol/L	7.24 (3.76)
HbA1c, %	6.31 (1.37)
Total cholesterol, mmol/L	5.07 (1.25)
Triglycerides, mmol/L	1.99 (1.10)
Blood creatinine, mmol/L	76.13 (43.75)
Current smoking, %	58 (13.2)
Diabetes mellitus, %	158 (36)
Arterial hypertension, %	255 (58.1)
Alcohol consumption, %	55 (12.5)

Data are mean (standard deviations), except for gender, HbA1c, current smoking, diabetes, arterial hypertension and alcohol consumption which are expressed as number (%).

Table 7.9 Mean macular choroidal thickness (at various points on the horizontal axis) and volume measurements in subjects of Indian origin (n = 439) measured using fully automated choroidal segmentation technique

Location of measurements	Mean (SD)
CHOROIDAL THICKNESS (um)	
Sub-foveal	**267.23 (100.99)**
Nasal, 0.5 mm	270.00 (104.54)
Nasal, 1 mm	269.85 (106.46)
Nasal, 1.5 mm	254.59 (107.70)
Nasal, 2 mm	237.70 (107.49)
Nasal, 2.5 mm	209.92 (101.59)
Nasal, 3 mm	**170.09 (88.79)**
Temporal, 0.5 mm	264.16 (96.28)
Temporal, 1 mm	257.76 (91.19)
Temporal, 1.5 mm	249.23 (91.06)
Temporal, 2 mm	241.05 (86.47)
Temporal, 2.5 mm	234.65 (84.30)
Temporal, 3 mm	**230.59 (84.13)**
CHOROIDAL VOLUME (mm^3)	
Choroidal volume of 7 line scan (8.9 x 1.5 mm)	2.167 (0.689)
Choroidal volume at central macula (1mm diameter circle)	0.209 (0.071)

Table 7.10 Univariate and multivariate analysis of the association of ocular and systemic factors with sub-foveal choroidal thickness in Singapore Indians (n = 439)

	Univariate		**Multivariate***	
	Unstandardized β	**P-value**	**Unstandardized β**	**P-value**
Ocular factors				
Spherical equivalent, D	-2.957	0.335	-	-
Axial length, mm	-15.772	0.001	-31.154	**<0.001**
Corneal curvature, mm	-32.039	0.075	53.150	**0.010**
Anterior chamber depth, mm	8.480	0.486	-	-
Central corneal thickness, μm	0.017	0.908	-	-
Intraocular pressure, mmHg	0.974	0.566	-	-
Ocular perfusion pressure, mmHg	0.591	0.347	-	-
Systemic factors				
Age, years	-2.479	<0.001	-2.457	**<0.001**
Gender, (female vs male)	-36.205	<0.001	-41.717	**<0.001**
Mean arterial pressure, mmHg	0.446	0.273	-	-
Body mass index, kg/m^2	-1.515	0.167	-	-
Serum glucose, mmol/L	-1.209	0.357	-	-
HbA1c, %	-5.243	0.138	-	-
Total cholesterol, mmol/L	2.632	0.498	-	-
Triglycerides, mmol/L	12.406	0.005	7.617	0.074
Blood creatinine, mmol/L	0.182	0.102	-	-
Current smoking, Yes	27.665	0.052	10.345	0.481
Diabetes mellitus, Yes	-26.430	0.008	-25.033	**0.015**
Arterial hypertension, Yes	-1.745	0.858	-	-
Alcohol consumption, Yes	1.613	0.912	-	-

*Adjusted for glaucoma status, diabetic retinopathy and age-related macular degeneration.

Table 7.11 Univariate and multivariate analysis of the association of ocular and systemic factors with choroidal volume at central macula in Singapore Indians (n = 437)

	Univariate		**Multivariate***	
	Unstandardized β	**P-value**	**Unstandardized β**	**P-value**
Ocular factors				
Spherical equivalent, D	-0.002	0.362	-	-
Axial length, mm	-0.013	<0.001	-0.019	**<0.001**
Corneal curvature, mm	-0.019	0.147	-	-
Anterior chamber depth, mm	0.003	0.757	-	-
Central corneal thickness, per 10 μm	9.113E-5	0.371	-	-
Intraocular pressure, per 10 mmHg	0.001	0.526	-	-
Ocular perfusion pressure, per 10 mmHg	0.000	0.355	-	-
Systemic factors				
Age, years	-0.002	<0.001	-0.002	**<0.001**
Gender, (female vs male)	-0.028	<0.001	-0.035	**<0.001**
Mean arterial pressure, per 10 mmHg	0.000	0.300	-	-
Body mass index, kg/m^2	-0.001	0.092	0.000	0.550
Serum glucose, mmol/L	-0.001	0.266	-	-
HbA1c, %	-0.005	0.066	-0.004	0.287
Total cholesterol, mmol/L	0.002	0.532	-	-
Triglycerides, mmol/L	0.008	0.007	0.006	**0.038**
Blood creatinine, mmol/L	0.000	0.124	-	-
Current smoking, Yes	0.020	0.051	0.004	0.705
Diabetes mellitus, Yes	-0.021	0.004	-0.011	0.239
Arterial hypertension, Yes	-0.001	0.888	-	-
Alcohol consumption, Yes	0.003	0.764	-	-

*Adjusted for glaucoma status, diabetic retinopathy and age-related macular degeneration.

Table 7.12 Distribution of peripapillary choroidal thickness at clock-hour sectors (30° apart) and four quadrants in Singapore Indians (n = 650 eyes) measured using fully automated choroidal segmentation technique

Measurement Location	Peripapillary Choroidal Thickness, μm
Clock hour	
1	193.80 (89.72)
2	204.32 (82.64)
3	199.64 (78.15)
4	197.29 (75.12)
5	195.44 (74.47)
6	193.54 (76.70)
7	186.20 (76.54)
8	172.47 (71.87)
9	152.14 (63.11)
10	141.23 (60.26)
11	157.36 (67.32)
12	182.64 (80.48)
Quadrants	
Inferior	151.09 (61.07)
Superior	197.50 (73.13)
Nasal	184.03 (72.69)
Temporal	194.33 (78.78)
Average quadrant thickness	181.74 (67.51)

Data presented are means (standard deviations).
1 o'clock corresponded to the temporal region, 4 o'clock to the superior, 7 o'clock to the nasal, and 10 o'clock to the inferior.

Table 7.13 Associations of average peripapillary choroidal thickness with ocular and systemic factors using generalized estimating equation in Singaporean Indians (n = 650 eyes)

	Univariate analysis		Multivariate analysis*	
	Beta (95% CI)	**P-value**	**Beta (95% CI)**	**P-value**
Ocular factors				
Axial length, mm	-15.56 (-23.17, -7.96)	<0.001	-18.46 (-26.47, -10.46)	**<0.001**
Corneal curvature, mm	-26.90 (-51.90, -1.90)	0.035	-13 (-41.03, 15.02)	0.363-
Central corneal thickness, μm	-0.05 (-0.24, 0.13)	0.574	-	-
Intraocular pressure, mmHg	0.93 (-0.88, 2.75)	0.314	-	-
Ocular perfusion pressure, mmHg	-0.07 (-0.85, 0.70)	0.851	-	-
Systemic factors				
Age, years	-1.94 (-2.97, -0.90)	<0.001	-2.23 (-3.37, -1.09)	**<0.001**
Gender, male	29.25 (15.70, 42.81)	<0.001	40.08 (25.60, 54.55)	**<0.001**
Systolic blood pressure, mmHg	-0.30 (-0.67, 0.07)	0.117	-	-
Diastolic blood pressure, mmHg	0.61 (-0.11, 1.34)	0.099	-0.11 (-0.76, 0.53)	0.721
Mean arterial pressure, mmHg	0.05 (-0.45, 0.56)	0.831	-	-
Body mass index, kg/m^2	-0.87 (-2.35, 0.60)	0.246	-	-
Serum glucose, mmol/L	-0.99 (-3.02, 1.03)	0.335	-	-
HbA1c, %	-4.53 (-9.38, 0.31)	0.067	-5.19 (-9.59, -0.78)	**0.021**
Total cholesterol, mmol/L	0.27 (-5.79, 6.35)	0.929	-	-
Triglycerides, mmol/L	4.86 (-0.57, 10.30)	0.080	3.04 (-2.47, 8.55)	0.280
Blood creatinine, mmol/L	0.03 (-0.05, 0.13)	0.445	-	-
Current smoking	25.49 (4.59, 46.39)	0.017	3.37 (-17.67, 24.41)	0.754
Diabetes mellitus	-11.55 (-26.06, 2.95)	0.119	-	-
Arterial hypertension	2.63 (-11.26, 16.54)	0.710	-	-
Alcohol consumption	11.73 (-12.81, 36.27)	0.349	-	-

*Adjusted for glaucoma status, diabetic retinopathy and age related macular degeneration; CI = confidence interval.
Beta represents the change in peripapillary choroidal thickness for per unit change in continuous variables and the difference in peripapillary choroidal thickness between groups for categorical variables.

Table 7.14 Multivariate analysis of the associations of regional (inferior, superior, nasal and temporal) peripapillary choroidal thickness with ocular and systemic factors using generalized estimating equation in Indians (n = 650 eyes)

	Inferior PPCT		**Superior PPCT**		**Nasal PPCT**		**Temporal PPCT**	
	Beta (95% CI)	**P-value**	**Beta (95% CI)**	**P-value**	**Beta (95% CI)**	**P-value**	**Beta (95% CI)**	**P-value**
AL, mm	-14.08 (-20.61, -7.55)	**<0.001**	-19.111 (-27.36, -10.86)	**<0.001**	-16.26 (-23.27, -9.25)	**<0.001**	-21.83 (-30.19, -13.47)	**<0.001**
CC, mm	-10.08 (-35.97, 15.81)	0.445	-12.92 (-44.20, 18.35)	0.481	-	-	-9.28 (-42.87, 24.30)	0.588
Age, years	-1.83 (-2.85, -0.81)	**<0.001**	-2.43 (-3.57, -1.29)	**<0.001**	-2.19 (-3.25, -1.13)	**<0.001**	-2.31 (-3.55, -1.06)	**<0.001**
Gender (male)	28.18 (16.44, 39.92)	**<0.001**	39.97 (25.39, 54.54)	**<0.001**	42.54 (28.57, 56.13)	**<0.001**	49.89 (34.95, 64.82)	**<0.001**
SBP, mmHg	-	-	-	-	-	-	-2.72 (-0.68, 0.13)	0.193
DBP, mmHg	-	-	0.02 (-0.67, 0.71)	0.954	-	-		
HbA1c, %	-3.72 (-7.72, 0.27)	0.068	-5.22 (-10.06, -0.37)	**0.035**	-5.29 (-10.24, -0.35)	**0.036**	-5.44 (-10.35, -0.52)	**0.030**
TG, mmol/L	-	-	-	-	2.27 (-3.35, 8.79)	0.380	2.79 (-3.28, 8.88)	0.367

For inferior, superior, nasal and temporal PPCT age, gender, glaucoma status, diabetic retinopathy, age related macular degeneration and variables with p<0.10 in univariate models were included in multivariate models.

CI=confidence interval; PPCT=peripapillary choroidal thickness, AL=axial length; CC=corneal curvature; SBP=systolic blood pressure; DBP=diastolic blood pressure; HbA1c= hemoglobin A1c; TG=triglycerides.

Table 7.15 Comparison of the baseline characteristics of ethnic Malays (n = 540) and Indians (n = 439)

Characteristics	Malays (n = 540)	Indians (n = 439)	P-value*
Age, years	62.70 (8.91)	58.56 (8.18)	**<0.001**
Gender, % male	251 (46.5)	231 (52.6)	**0.046**
Axial length, mm	23.59 (0.96)	23.42 (1.00)	**0.012**
Corneal curvature, mm	7.66 (0.24)	7.61 (0.26)	**0.003**
Spherical equivalent, D	0.11 (1.74)	0.33 (1.57)	**0.039**
OPP, mmHg	55.55 (8.19)	53.29 (7.12)	**0.001**
SBP, mmHg	139.56 (19.68)	132.80 (17.32)	**<0.001**
DBP, mmHg	76.90 (10.66)	77.72 (9.77)	0.209
BMI, kg/m^2	26.87 (5.07)	26.41 (4.42)	0.133
HbA1c, %	6.35 (1.43)	6.31 (1.37)	0.678
Total cholesterol, mmol/L	5.36 (1.29)	5.07 (1.25)	**0.001**
Triglycerides, mmol/L	1.92 (1.30)	1.99 (1.10)	0.410
Blood creatinine, mmol/L	83.23 (41.23)	76.13 (43.75)	**0.010**
Diabetes mellitus, %	220 (42.1)	199 (45.3)	0.328
Hypertension, %	385 (71.3)	255 (58.2)	**<0.001**
Diabetic retinopathy, %	30 (5.6)	26 (5.9)	0.890
AMD, %	1 (0.2)	1 (0.2)	0.887
Glaucoma, %	5 (5.3)	6 (9.2)	0.359
Current smoking, %	98 (18.1)	59 (13.4)	0.054

Data presented are means (standard deviations) or number (%).
*Based on independent sample t-test for continuous variables or Chi-square/Fisher's exact test for categorical variables.
OPP=ocular perfusion pressure; SBP=systolic blood pressure; DBP=diastolic blood pressure; BMI=body mass index; HbA1c=haemoglobin A1c; AMD=age related macular degeneration.

Table 7.16 Comparison of the distribution of mean unadjusted macular choroidal thickness and volume in ethnic Malays and Indians using fully automated choroidal segmentation technique.

Macular Choroidal Thickness (μm)	**Malays (n = 540)**	**Indians (n = 439)**	**P-value***
Average	212.99 (79.72)	242.83 (81.73)	**<0.001**
Sub-foveal	242.28 (97.58)	267.23 (100.99)	**<0.001**
Nasal, 1.5 mm	142.44 (79.19)	170.09 (88.79)	**<0.001**
Nasal, 3 mm	208.35 (98.20)	254.59 (107.70)	**<0.001**
Temporal, 1.5 mm	232.17 (89.42)	249.23 (91.06)	**<0.001**
Temporal, 3 mm	207.65 (80.98)	230.59 (84.13)	**<0.001**
Choroidal Volume (mm^3)			
Choroidal volume of 7 line scan (8.9 x 1.5 mm)	1.88 (0.69)	2.16 (0.68)	**<0.001**
Choroidal volume at central macula (1mm)	0.185 (0.072)	0.209 (0.071)	**<0.001**

Data are means (standard devaitions).
*Based on independent sample t-test

Table 7.17 Comparison of the distribution of mean adjusted macular choroidal thickness and volume in ethnic Malays and Indians using fully automated choroidal segmentation technique.

Macular Choroidal Thickness (μm)	**Malays (n = 540)**	**Indians (n = 439)**	**P-value***
Average	223.44 (3.86)	236.13 (4.43)	**0.011**
Sub-foveal	253.40 (4.95)	261.72 (5.69)	0.195
Nasal, 1.5 mm	224.44 (4.92)	250.19 (5.56)	**<0.001**
Nasal, 3 mm	151.75 (4.11)	163.16 (4.72)	**0.032**
Temporal, 1.5 mm	240.21 (4.54)	241.80 (5.21)	0.787
Temporal, 3 mm	212.18 (4.21)	222.12 (4.84)	0.069
Choroidal Volume (mm^3)			
Choroidal volume of 7 line scan (8.9 x 1.5 mm)	1.99 (0.032)	2.12 (0.037)	**0.002**
Choroidal volume at central macula (1mm)	0.195 (0.003)	0.205 (0.004)	**0.023**

Data are mean (standard error).
*Adjusted for age, gender, AL, corneal curvature, OPP, current smoking, creatinine, cholesterol, AMD, DR and glaucoma status.

Table 7.18 Comparison of the distribution of mean unadjusted peripapillary choroidal thickness in ethnic Malays and Indians using fully automated choroidal segmentation technique.

Peripapillary CT (µm)	Malays (n = 904 eyes)	Indians (n = 650 eyes)	P-value*
Superior	150.53 (2.31)	196.87 (3.80)	**<0.001**
Nasal	143.53 (2.26)	183.63 (3.79)	**<0.001**
Inferior	111.34 (2.01)	150.63 (3.15)	**<0.001**
Temporal	139.47 (2.71)	193.86 (4.07)	**<0.001**
Average	136.22 (2.23)	181.09 (3.55)	**<0.001**

Data are mean (standard error).
*Based on generalized estimating equations

Table 7.19 Comparison of the distribution of mean adjusted peripapillary choroidal thickness in ethnic Malays and Indians using fully automated choroidal segmentation technique.

Peripapillary CT (µm)	Malays* (n = 904 eyes)	Indians* (n = 650 eyes)	P-value*
Superior	156.51 (3.19)	190.93 (3.50)	**<0.001**
Nasal	150.06 (3.17)	175.79 (3.48)	**<0.001**
Inferior	116.71 (2.71)	144.94 (2.98)	**<0.001**
Temporal	146.75 (3.51)	186.67 (3.85)	**<0.001**
Average	142.56 (3.01)	174.49 (3.30)	**<0.001**

Data are mean (standard error).
* Adjusted for age, gender, AL, corneal curvature, OPP, creatinine, cholesterol, triglycerides, current smoking, alcohol consumption, glaucoma status, AMD and DR.

CHAPTER VIII

DISTRIBUTION AND DETERMINATS OF CHOROIDAL VASCULATURE IN POPULATION-BASED STUDY

In Chapter VII, we have evaluated choroidal parameters such as CT and volume in our multi-ethnic population. However, given that the choroid is predominantly composed of blood vessels (~85%) surrounded by stromal tissues, a detailed analysis of the choroid in terms of its vasculature may be a more suitable way to assess choroidal health and to better understand its role in diseases where choroid is implicated in the pathophysiology.

Therefore, in this Chapter, we assessed vascular status of the choroid through image binarization of EDI SD-OCT images in healthy eyes from a population-based study. To represent vascular status of the choroid we computed OCT derived quantitative parameter called "choroidal vascularity index (CVI)". We also evaluated the ocular and systemic determinants of CVI in our population-based sample.

The manuscript relevant to the contents of this chapter has been published in the journal:

Scientific Reports

Agrawal, R.,[#] **P. Gupta**,[#] K. A. Tan, C. M. Cheung, T. Y. Wong and C. Y. Cheng. "Choroidal Vascularity Index as a Measure of Vascular Status of the Choroid: Measurements in Healthy Eyes from a Population-Based Study." *Scientific Reports* Feb 2016 [Epub ahead of print].

#: Joint first authors.

8.1 INTRODUCTION

The choroid is the vascular layer of eye, with one of the highest blood flow of any tissue in the body.[1] The choroid is predominantly composed of blood vessels surrounded by stromal tissue comprising of connective tissue, melanocytes, nerves and extracellular fluid.[2] The vascular layer of the choroid may be differentiated into 3 layers from internal to external, with increasing luminal diameter. The innermost layer is the choriocapillaris, the middle is Sattler's layer with medium vessels, and the outer is Haller's layer, with large vessels.[1]

Being a major vascular layer of the eye the choroid plays an important role in ocular health, and is involved in the pathogenesis of many intraocular diseases such as AMD, PCV, CSCR and myopic macular degeneration.[3-9] There is evidence from histological studies that the disease processes affect the stroma and vasculature of the choroid.[10-12] However, shrinkage occurs during the fixation of the tissues during the histological process, making it difficult to study the changes in vascular tone of the choroid.[13]

CT has been reported as an indicator of ocular[14-17] and systemic health.[18-22] Although, many studies have now reported changes in the thickness of the choroid in various ocular and systemic diseases[8-12] and proposed CT as a marker to assess these disease conditions, there exists a notable disparity in CT in various clinical studies. One such example is diabetes mellitus,[23-27] where there has been no consensus as to whether it causes an increase or decrease in CT. This raises the question of what structures in the choroid changes with increasing or decreasing CT and if there is a more robust marker to assess choroid health.

To answer this question, morphological and vascular analyses of the choroid may provide some clues and lead to the development of a more stable marker. The

advent of EDI OCT has allowed more precise non-invasive quantitative assessment of the choroid.[28] Using EDI OCT, there have been attempts to assess the choroidal stromal and vascular structures.[13,29-32] Recently Sonoda et al. described a method for computing luminal and interstitial areas in the choroid as a means to quantify vascular status of the choroid.[30,31]

Adapting the image segmentation technique proposed by Sonoda et al.,[30,31] we further propose a new quantitative parameter called choroidal vascularity index (CVI) to assess vascular status of the choroid through image binarization of EDI SD-OCT images in healthy eyes. Furthermore, we aimed to determine the ocular and systemic factors affecting the CVI as well as CT in subjects enrolled from a population-based study in Singapore. This index may provide additional information on the morphology and physiology of the choroid and may be a more robust marker compared to CT.

8.2 METHODS

8.2.1 Study Population

The data for this study was derived from SiMES-2, a population based cohort study of 45 – 85 years old Malay adults living in Singapore**.** This study was conducted as per the tenets set forth in the Declaration of Helsinki, and ethics committee approval was obtained from the Institutional Review Board of SERI. Written informed consent was obtained from the subjects after explanation about the details of the study and any potential risks involved with the study and consequences of the study.

8.2.2 Study Subjects

Details of the study design, and methodology have been reported in detail in Chapter III and elsewhere.[33] In this study, we enrolled 400 consecutive participants

from February 2012 to April 2013. Exclusion criteria included: logMAR visual acuity >0.30, SE <-6 D, evidence of vitreo-retinal diseases such as AMD and DR, previous ocular surgery or clinical features compatible with a diagnosis of glaucoma and Spectralis OCT imaging with a quality index <18 decibels. Glaucoma was defined as described in Chapter III and elsewhere.[34]

8.2.3 Choroidal Thickness Assessment

The choroid was imaged using the EDI mode of SD-OCT (Spectralis, Heidelberg Engineering, Heidelberg, Germany) explained in detail in Chapter III. In our study, Bruch's membrane and the CSI were delineated with our automatic segmentation algorithm[35] which demonstrated excellent repeatability in our previously reported population-based study.[36] Although measurements of both eyes of each study participant were obtained, due to inter eye correlation only the right eye was used for further analysis.

8.2.4 Image Binarization Details

The same raster scan passing through the fovea was selected for binarization. It was segmented using the protocol described by Sonoda et al.[30-31] with minor modifications. The image binarization was done using public domain software, Image J (version 1.47; http://imagej.nih.gov/ij/). The subfoveal choroidal area with a width of 1.5 mm, centred at the fovea, was selected (**Figure 8.1A**) and this constituted the region of interest. Only 1.5 mm of the macular area on the single line scan was selected as a representative segment of the macular region due to segmental nature of the choroidal blood supply as described by Hayreh.[37] The posterior ciliary arteries and their branches along with terminal choroidal arterioles, the choriocapillaris, and the vortex veins have a segmental or lobular distribution in the choroid.

Image binarization techniques can be used to convert grey scale images into binarized images. This facilitates tasks such as image layout analysis and image skew estimation. An appropriate image binarization technique, taking into account the uneven illumination, image contrast variation and poor image resolution, is essential to accurately apply a threshold to an image. Different image binarization or thresholding techniques like Otsu's, Bernsen's and Niblack's autolocal thresholding techniques were hence attempted.[38,39] Otsu's is a global thresholding technique while Bernsen's is local thresholding technique. After comparing the different image segmentation techniques, we adopted Niblack's autolocal threshold technique in our current study. This is because it takes into consideration the mean and standard deviation of all the pixels in the region of interest. In addition, given that binarization could be influenced by the variation in the amount of melanin in RPE in different eyes, and also affected by the direction of light and focusing issues, these were taken into account by using a distinct binarization threshold for individual subject.

Using Niblack's autolocal threshold tool, the image was first binarized to get a clear view of the choroid-scleral interface (**Figure 8.1B**). This was to allow more precise selection of the subfoveal choroid area. This is in contrast to Sonoda's et al[30,31] protocol in which the polygonal area was selected prior to image binarization. In addition, we did not preselect vessels of size more than 100 um.

With the upper border marked at the RPE and the lower border the line of light pixels at the choroid scleral junction, the choroidal area was selected using polygon tool and added to the region of interest manager (**Figure 8.1B**). The image was then converted to RGB (red, green, blue) colour to allow the colour threshold tool to select the dark pixels (**Figure 8.1C**). The total subfoveal circumscribed choroidal area (TCA) and the area of dark pixels were calculated. The luminal area (LA) was defined

as the area of dark pixels. Stromal area (SA) was further calculated by subtracting LA from TCA. To determine the vascularity status of the choroid, CVI was computed by dividing LA by TCA. In addition, the proportion of dark (LA) to light areas (SA) was also computed. **Figure 8.1D** represents the overlay image of the region on interest on the original EDI OCT scan.

The detailed step by step process of image binarization technique using Image J is as explained below:

Firstly, the 1x1 pixel image of the OCT was opened in Image J, and the scale was set. The line tool was used to measure the pixel length of 200 um as given in the scale at the bottom of the OCT scan image (**Figure 8.2**). To set the scale, the option Analyse > Set Scale was selected, and the known distance was set to 2 mm. For future images, the "Disable Global Calibration" was unchecked when the images were opened.

Secondly, a 1.5mm line was drawn above the fovea, with the center of the fovea. The lines were drawn by first using the Colour Picker tool to select white, then, using the line tool, 1.5mm was measured parallel to the retinal pigment epithelium and drawn with the centre of the line just above the of the fovea, above the retina. "Command-D" was keyed in to leave a mark where the line was initially drawn. Thirdly, auto local threshold was applied. Image > Type > 8 bit was first applied (**Figure 8.3A**), followed by Image > Adjust > Auto Local Threshold (**Figure 8.3B**). Niblack was selected as the method (**Figure 8.3C**).

Next, the polygon tool was used to draw a polygon under the lines drawn, to select the subfoveal choroid (**Figure 8.4A**). The area of the choroid under the retinal pigment epithlium was selected. The upper border was marked at the retinal pigment epithelium and the lower border area was below the line of light pixels at the choroid

scleral junction. The area was saved in the ROI manager by selecting the option Analyse > Tools > ROI manager, and Add [t] (**Figure 8.4B**). Fifthly, the area of vascularity was highlighted by selecting Image > Type > RGB colour, and Image > Adjust > Colour Threshold. The first bar under Brightness was adjusted to 0, and the second bar was adjusted to 254 (**Figure 8.5A**). After clicking Select (**Figure 8.5B**), the area was added to the ROI manager.

After clicking Select in the above figure, the area was added to the ROI manager by selecting Add [t] to determine the area of vascularity within the initially selected polygon, both areas in the ROI manager were selected (**Figure 8.6A**) and merged by selecting More > AND (**Figure 8.6B**). The composite third area was added to the ROI manager by selecting Add [t] (**Figure 8.6C**). Lastly, the first and third areas were selected and measured using the ROI manager. The first area represents the total area of choroid selected, and the third composite area is the vascular area.

8.2.5 Inter-rater and Intra-rater Agreement

10% of the total images (35 images), were initially segmented by two graders (KAT and RA) to determine inter-rater agreement. The same set of images was segmented by one grader (KAT) after an interval of one week to compute intra-rater reliability. The intra- and inter-rater reliability for the image binarization was measured by the absolute agreement model of the intra-class correlation coefficient (ICC).[40] ICC value of 0.81 – 1.00 indicates good agreement. Values of less than 0.40 indicate poor to fair agreement. We also performed Bland-Altman plot analyses[41,42] to determine the mean difference between the measurements. The Bland-Altman plots were constructed using MedCalc version 12.3 (Medcalc Software, Ostend, Belgium) software. Moreover, random scans, including those with thick and thin choroid, were further reviewed by both graders to ensure good inter-rater agreement. After obtaining

good inter-rater and intra-rater agreement, all the scans were binarized by single author (KAT).

8.2.6 Measurement of Ocular and Systemic Factors

Each participant underwent a detailed interview and a standardized examination for comprehensive assessment of various ocular and systemic factors. Measurement of ocular and systemic factors has been explained in detail in Chapter III of this thesis.

8.2.7 Statistical Methods

Statistical analysis was performed using SPSS version 20.0 (SPSS, Inc., Chicago, IL, USA). Since CVI and subfoveal choroidal thickness (SFCT) have different measurement units, we used the coefficient of variation (COV) to compare the variability between CVI and SFCT. Univariate and multiple linear regression analyses were performed to determine the associations of SFCT and CVI (dependent variables) with ocular and systemic factors (independent variables). For multiple linear regression, factors showing significant association in univariate analysis ($p<0.10$) were included. All p values were 2-sided and considered statistically significant when the values were less than 0.05.

8.3 RESULTS

A total of 400 subjects were recruited for this study. We excluded 55 subjects for the following reasons: visual acuity worse than 0.30 (n=9), SE < -6 D (n=7), glaucoma (n=6), presence of macular or vitreo-retinal diseases (n=18) and poor OCT image quality (n=15). A total of 345 eyes from 345 subjects were included in the final analysis; 190 (55%) subjects were female. The demographics, ocular, systemic and

choroidal characteristics of the study subjects are shown in **Table 8.1**. In terms of choroidal characteristics, mean TCA was 0.74±0.21mm^2 and mean LA was 0.49±0.15mm^2. Mean SFCT was 241.34±97.11μm (range, 40.24 - 519.48μm) and mean CVI was 65.61±2.33% (range, 60.07 - 71.27%).

CVI was found to have lower COV (3.55) than SFCT (COV = 40.30), indicating CVI to be less variable than SFCT. The histogram plots (**Figure 8.7A and Figure 8.7B**) represent the distribution of SFCT and CVI in relation to normal density plot.

Using image binarization, the intra- (ICC: 0.97 to 0.99 for TCA and ICC: 0.91 to 0.98 for LA) and inter-grader reliability (ICC: 0.90 to 0.97 for TCA and ICC: 0.89 to 0.97 for LA) were excellent for both TCA and LA (**Table 8.2**). Bland Altman plot analysis of intra- and inter-rater reliability for TCA (**Figures 8.8A and 8.8B**) and LA (**Figures 8.8C and 8.8D)** at sub-foveal location was excellent.

In **Table 8.3**, the multiple regression model shows younger age, shorter AL, higher IOP, higher LA and lower systolic blood pressure to be significantly ($p<0.05$) associated with thicker sub-foveal choroid. However, among factors associated with CVI (**Table 8.4**), in the multiple regression model, SFCT was the only factor associated with CVI. A thicker sub-foveal choroid was significantly ($p<0.001$) associated with higher CVI. There were no other statistically significant association between CVI and any other factors (**Table 8.4**).

8.4 DISCUSSION

In this population-based study, using the modified Sonoda's image binarization technique for EDI SD-OCT scans, we propose an OCT based metric termed "CVI" to assess vascularity of the choroid. Our results validated the findings

obtained by Sonoda et al. and found that on a single cross sectional scan, nearly two third (~66%) of the subfoveal choroid is vascular in healthy eyes. Importantly, CVI showed lesser variability and was influenced by fewer physiologic factors as opposed to CT, indicating CVI to be a relatively stable index for studying the changes in the choroid. As the choroid is primarily a vascular structure, understanding of this new vascular index may help to further elucidate the role of vascular processes within the choroid in disease development and progression. We hence propose CVI as an independent surrogate marker to assess choroidal health in future studies.

Several studies have assessed the vascular structures of the choroid by OCT,[13,29] but they required customized software that limited their widespread use. There are reports[30,31]on the differentiation and quantification of the structural components of the choroid (luminal and interstitial areas), using freely and easily accessible software, *Image J,* these studies were performed in clinic-based settings with a potential selection and sampling biases. We have highlighted the significant differences in our protocol with that proposed by Sonoda et al.[30,31] in **Table 8.5**. Our modification of applying auto local threshold prior to image binarization enabled us to accurately localise choroid scleral interface giving more precise selection of the choroid. In addition, the simple binarization technique without pre-selection of larger choroidal vessels allowed nearly accurate estimation of vascularity of the choroid even with a very simple algorithm, which can be reproduced by the wider research community.

Although there is no concrete evidence that the dark areas represented the vascular areas and the light areas the stromal areas, the findings of earlier studies and that of numerous empirical observations suggest that the dark areas were the vascular components in the binarized images.[13,29] In addition, a comparison of the original

EDI-OCT images to the binary images (**Figure 8.1**) revealed that the dark areas corresponded with vascular components of the choroid, including both the larger and smaller choroidal vessels. Therefore, the binarization technique developed by Sonoda et al.,[30,31] which was further simplified by us, is valid and offers precise segmentation of choroidal vasculature from stroma.

Interestingly, when comparing the factors affecting SFCT to those that affect CVI, we found SFCT to be associated with many physiological factors such as age, AL, IOP and, most significantly, the vascular area in the choroid (LA), whereas stromal area did not have a significant association with SFCT. On the other hand, CVI was only affected by SFCT, but was not affected by most of the physiological variables. Moreover, SFCT demonstrated relatively greater variability (mean SFCT was 241.34±97.11µm, COV=40.30) compared to CVI (mean CVI was 65.61±2.33%, COV=3.55). Thus our results suggest CVI to be a better and relatively more stable marker to monitor choroid compared to CT, which is affected by more variables and demonstrated greater variability. Clinically, measuring the proportion of vascularity of the eye would provide us with a deeper understanding of how disease processes affect different structures in the eye, and therefore may be more informative compared to CT measurements alone.

We have demonstrated a significant association of SFCT with vascular area of the choroid. This signifies the fact that the vascular area is the predominant segment influencing the CT in normal population. An increase in CVI reflects either an increase in the number of blood vessels or in the diameter of the choroidal blood vessels within a designated area. Hayreh [37] demonstrated the vulnerability of submacular choroidal supply to generalised chronic ischaemic disorders (age related macular degeneration), due to numerous watershed zones of the short posterior ciliary

arteries in the choroid. There can be potential clinical implications of the CVI, which can be explored in further studies. A decrease in CVI on EDI OCT scans at baseline may be an indicator of choroidal ischemia in patients with macular disorders like age related macular degeneration or diabetes. On the other hand, we may use CVI to determine increase in vascularity of the choroid in posterior uveitis or central serous chorioretinopathy. CVI can also be used as a follow up tool for treatment response and resolution of diseases.

The strengths of our study include a large sample size with a single common ethnicity. Hence, our findings were unlikely to be confounded by ethnic heterogeneity. Standardized clinical examination protocols, as well as reliable differentiation and quantifications of choroidal morphometric parameters and OCT parameters were used in our study. Nevertheless, this study has few limitations. First, binarization of choroidal images was performed only in the right eye of each study subject. There may exist inter-eye differences, yet such differences should be small. Second, the CT measurements in our study were not performed at the same time of the day; each participant underwent the OCT examination in a randomized manner with respect to when the readings were obtained. It seems unlikely that circadian changes may have influenced the results of our investigation. Third, although our images were binarized at standard threshold, there is a possibility of over or underestimation of both SA and LA.

8.5 CONCLUSIONS

In conclusion, in this population-based study, we introduced a novel OCT based marker termed “CVI” to assess vascularity of the subfoveal choroid. Our result

showed that on a single cross sectional EDI-OCT image, two-third (~66%) of the subfoveal choroid is vascular in healthy eyes. This index should provide a new means of studying the pathophysiology of human choroid in greater detail. However, larger studies for different disease models are warranted to further validate the application of this index in clinical practice. Whether CVI is a complimentary or substitute tool to CT can only be answered based on the proposed studies in choroidal diseases.

8.6 REFERENCES

1. Alm A, Bill A. Ocular and optic nerve blood flow at normal and increased intraocular pressures in monkeys (Macaca irus): a study with radioactively labelled microspheres including flow determinations in brain and some other tissues. Exp Eye Res 1973;15(1):15-29.

2. Nickla DL, Wallman J. The multifunctional choroid. Prog Retin Eye Res 2010;29(2):144-68.

3. Chung SE, Kang SW, Lee JH, Kim YT. Choroidal thickness in polypoidal choroidal vasculopathy and exudative age-related macular degeneration. Ophthalmology 2011;118(5):840-5.

4. Fujiwara T, Imamura Y, Margolis R, et al. Enhanced depth imaging optical coherence tomography of the choroid in highly myopic eyes. Am J Ophthalmol 2009;148(3):445-50.

5. Gomi F, Tano Y. Polypoidal choroidal vasculopathy and treatments. Curr Opin Ophthalmol 2008;19(3):208-12.

6. Grossniklaus HE, Green WR. Choroidal neovascularization. Am J Ophthalmol 2004;137(3):496-503.

7. Gupta B, Mohamed MD. Photodynamic therapy for variant central serous chorioretinopathy: efficacy and side effects. Ophthalmologica 2011;225(4):207-10.

8. Ikuno Y, Tano Y. Retinal and choroidal biometry in highly myopic eyes with spectral-domain optical coherence tomography. Invest Ophthalmol Vis Sci 2009;50(8):3876-80.

9. Koizumi H, Yamagishi T, Yamazaki T, et al. Subfoveal choroidal thickness in typical age-related macular degeneration and polypoidal choroidal vasculopathy. Graefes Arch Clin Exp Ophthalmol 2011;249(8):1123-8.

10. Lutty GA, Cao J, McLeod DS. Relationship of polymorphonuclear leukocytes to capillary dropout in the human diabetic choroid. Am J Pathol 1997;151(3):707-14.

11. Fryczkowski AW, Sato SE, Hodes BL. Changes in the diabetic choroidal vasculature: scanning electron microscopy findings. Ann Ophthalmol 1988;20(8):299-305.

12. Sakamoto T, Murata T, Inomata H. Class II major histocompatibility complex on melanocytes of Vogt-Koyanagi-Harada disease. Arch Ophthalmol 1991;109(9):1270-4.

13. Branchini LA, Adhi M, Regatieri CV, et al. Analysis of choroidal morphologic features and vasculature in healthy eyes using spectral-domain optical coherence tomography. Ophthalmology 2013;120(9):1901-8.

14. Lindner M, Bezatis A, Czauderna J, et al. Choroidal thickness in geographic atrophy secondary to age-related macular degeneration. Invest Ophthalmol Vis Sci 2015;56(2):875-82.

15. Young M, Fallah N, Forooghian F. Choroidal degeneration in birdshot chorioretinopathy. Retina 2015;35(4):798-802.

16. Tseng CC, Chen SN. Long-term efficacy of half-dose photodynamic therapy on chronic central serous chorioretinopathy. Br J Ophthalmol 2015.

17. Gupta P, Saw S, Cheung CY, et al. Choroidal thickness and high myopia: a case-control study of young Chinese men in Singapore. Acta Ophthalmol 2015;93(7):585-92.

18. Kim JT, Lee DH, Joe SG, et al. Changes in choroidal thickness in relation to the severity of retinopathy and macular edema in type 2 diabetic patients. Invest Ophthalmol Vis Sci 2013;54(5):3378-84.

19. Wong IY, Wong RL, Zhao P, Lai WW. Choroidal thickness in relation to hypercholesterolemia on enhanced depth imaging optical coherence tomography. Retina 2013;33(2):423-8.

20. Ahn SJ, Woo SJ, Park KH. Retinal and choroidal changes with severe hypertension and their association with visual outcome. Invest Ophthalmol Vis Sci 2014;55(12):7775-85.

21. Sizmaz S, Kucukerdonmez C, Pinarci EY, et al. The effect of smoking on choroidal thickness measured by optical coherence tomography. Br J Ophthalmol 2013;97(5):601-4.

22. Takahashi H, Takase H, Ishizuka A, et al. Choroidal thickness in convalescent vogt-koyanagi-harada disease. Retina 2014;34(4):775-80.

23. Lee HK, Lim JW, Shin MC. Comparison of choroidal thickness in patients with diabetes by spectral-domain optical coherence tomography. Korean J Ophthalmol 2013;27(6):433-9.

24. Unsal E, Eltutar K, Zirtiloglu S, et al. Choroidal thickness in patients with diabetic retinopathy. Clin Ophthalmol 2014;8:637-42.

25. Gerendas BS, Waldstein SM, Simader C, et al. Three-dimensional automated choroidal volume assessment on standard spectral-domain optical coherence tomography and correlation with the level of diabetic macular edema. Am J Ophthalmol 2014;158(5):1039-48.

26. Adhi M, Brewer E, Waheed NK, Duker JS. Analysis of morphological features and vascular layers of choroid in diabetic retinopathy using spectral-domain optical coherence tomography. JAMA Ophthalmol 2013;131(10):1267-74.

27. Farias LB, Lavinsky D, Schneider WM, et al. Choroidal thickness in patients with diabetes and microalbuminuria. Ophthalmology 2014;121(10):2071-3.

28. Spaide RF, Koizumi H, Pozzoni MC. Enhanced depth imaging spectral-domain optical coherence tomography. Am J Ophthalmol 2008;146(4):496-500.

29. Sohrab M, Wu K, Fawzi AA. A pilot study of morphometric analysis of choroidal vasculature in vivo, using en face optical coherence tomography. PLoS One 2012;7(11):e48631.

30. Sonoda S, Sakamoto T, Yamashita T, et al. Choroidal structure in normal eyes and after photodynamic therapy determined by binarization of optical coherence tomographic images. Invest Ophthalmol Vis Sci 2014;55(6):3893-9.

31. Sonoda S, Sakamoto T, Yamashita T, et al. Luminal and stromal areas of choroid determined by binarization method of optical coherence tomographic images. Am J Ophthalmol 2015;159(6):1123-31 e1.

32. Iwata A, Mitamura Y, Niki M, et al. Binarization of enhanced depth imaging optical coherence tomographic images of an eye with Wyburn-Mason syndrome: a case report. BMC Ophthalmol 2015;15(1):19.

33. Foong AW, Saw SM, Loo JL, et al. Rationale and methodology for a population-based study of eye diseases in Malay people: The Singapore Malay eye study (SiMES). Ophthalmic Epidemiol 2007;14(1):25-35.

34. Foster PJ, Buhrmann R, Quigley HA, Johnson GJ. The definition and classification of glaucoma in prevalence surveys. Br J Ophthalmol 2002;86(2):238-42.

35. Tian J, Marziliano P, Baskaran M, et al. Automatic segmentation of the choroid in enhanced depth imaging optical coherence tomography images. Biomed Opt Express 2013;4(3):397-411.

36. Gupta P, Jing T, Marziliano P, et al. Distribution and determinants of choroidal thickness and volume using automated segmentation software in a population-based study. Am J Ophthalmol 2015;159(2):293-301 e3.

37. Hayreh SS. Segmental nature of the choroidal vasculature. Br J Ophthalmol 1975;59(11):631-48.

38. Bernsen J. Dynamic thresholding of grey-level images. Eighth Internation Conference of Pattern Recognition, France, Paris:Conference Proceedings 1986.

39. Niblack W. An Introduction to Digital Image Processing. Englewood Cliffs, New Jersey: Prentice Hall International Inc., 1986.

40. Fleiss JL, Cohen J. The Equivalence of Weighted Kappa and the Intraclass Correlation Coefficient as Measures of Reliability. Educational and Psychological Measurement 1973;33(3):613-9.

41. Bland JM, Altman DG. Statistical methods for assessing agreement between two methods of clinical measurement. Lancet 1986;1(8476):307-10.

42. Bland JM, Altman DG. Agreed statistics: measurement method comparison. Anesthesiology 2012;116(1):182-5.

CHAPTER VIII TABLES

Table 8.1 Demographics, clinical and choroidal characteristics of study subjects (n = 345)

Characteristics	**Mean ± SD**	**Range**
Age, yrs	61.53 ± 8.77	47.19 to 86.72
Gender, male (%)	155 (44.9%)	
Axial length, mm	23.58 ± 0.96	21.60 to 27.89
IOP, mm Hg	14.41 ± 2.84	6 to 20
Ocular perfusion pressure, mmHg	55.68 ± 8.39	37.44 to 96.11
Systolic blood pressure, mmHg	139.21 ±20.63	95 to 226.50
Diastolic blood pressure mmHg	77.27±10.85	54.50 to 133
Body mass index, kg/m^2	26.75 ±5.13	12.15 to 52.95
Serum glucose, mmol/L	6.98 ± 3.35	2.8 to 22.9
HbA1c, %	6.26 ± 1.27	4.3 to 11.7
Total cholesterol, mmol/L	5.43 ± 1.26	2.49 to 10.40
Triglycerides, mmol/L	1.95 ± 1.38	0.42 to 14.95
Blood creatinine, mmol/L	78.92 ± 33.11	30 to 412
Current smoking, %	68 (19.8%)	
Alcohol consumption, %	5 (1.5%)	
Choroidal Parameters		
TCA, mm^2	0.74±0.21	0.198 to 1.237
LA, mm^2	0.49± 0.15	0.122 to 0.817
SA, mm^2	0.25±0.06	0.076 to 0.441
CVI (LA/TCA)	65.61±2.33	60.07 to 71.27
LA/SA	1.92±0.20	1.50, 2.48
SFCT, μm	241.34±97.11	40.24, 519.48

Data presented are means ± standard deviations (SD), except for gender, HbA1c, current smoking and alcohol consumption which are number (%).
TCA, total sub-foveal choroidal area; LA, luminal area; SA, stromal area; CVI, choroidal vascularity index; LA/SA, luminal area/ stromal area; SFCT, sub-foveal choroidal thickness.

Table 8.2 Intra- and inter-grader reliability assessment of choroidal parameters in 35 subjects

	Intra Rater		Inter Rater	
	ICC (95% CI)	**Mean difference (95% LOA)**	**ICC (95% CI)**	**Mean difference (95% LOA)**
TCA	0.99 (0.97 to 0.99)	-0.01 (-0.16 to 0.13)	0.94 (0.90 to 0.97)	0 (-0.06 to 0.07)
LA	0.96 (0.91 to 0.98)	-0.01 (-0.11 to 0.09)	0.94 (0.89 to 0.97)	0.01 (-0.07 to 0.10)

TCA, total sub-foveal choroidal area; LA, luminal area; ICC, intraclass correlation coefficient; CI, confidence interval; LOA, limits of agreement.

Table 8.3 Linear regression analyses of ocular and systemic factors associated with sub-foveal choroidal thickness

	Univariate			Multivariate*		
	Unstandardized β	**Standardized β**	**P-value**	**Unstandardized β**	**Standardized β**	**P-value**
Ocular factors						
Axial length, mm	-15.348	-0.155	**0.005**	-10.508	-0.105	**0.002**
IOP, mmHg	3.160	0.092	**0.087**	3.619	0.105	**0.002**
OPP, mm Hg	-0.354	-0.031	0.572	-	-	-
LA, mm^2	523.214	0.814	**<0.001**	459.729	0.714	**<0.001**
SA, mm^2	1132.841	0.787	**<0.001**	68.271	0.047	0.669
Systemic factors						
Age, yrs	-3.986	-0.360	**<0.001**	-0.856	-0.077	**0.041**
Gender, female	-22.274	-0.114	**0.034**	-13.171	-0.068	0.068
Body mass index, kg/m^2	-1.173	-0.062	0.252	-	-	-
Systolic blood pressure, mmHg	-0.499	-0106	**0.050**	-0.328	-0.071	**0.043**
Diastolic blood pressure mmHg	0.749	0.084	0.122	-	-	-
Serum glucose, mmol/L	0.102	0.004	0.949	-	-	-
HbA1c, %	5.913	0.077	0.157	-	-	-
Total cholesterol, mmol/L	8.092	0.106	**0.052**	-0.525	-0.007	0.836
Triglycerides, mmol/L	3.456	0.049	0.366	-	-	-
Blood creatinine, mmol/L	-0.050	-0.017	0.754	-	-	-
Current smoking, Yes	28.392	0.116	**0.031**	-11.737	-0.049	0.187
Alcohol consumption, Yes	-19.833	0.024	0.651	-	-	-

*Adjusted for variables with a p-value<0.10 in the univariate analysis.
β, regression coefficient.

Table 8.4 Linear regression analyses of ocular and systemic factors associated with choroidal vascularity index

	Univariate			Multivariate*		
	Unstandardized β	**Standardized β**	**P-value**	**Unstandardized β**	**Standardized β**	**P-value**
Ocular factors						
Axial length, mm	-0.274	-0.113	**0.039**	-0.106	-0.004	0.375
IOP, mmHg	-0.014	-0.018	0.745	-	-	-
OPP, mmHg	0.022	0.080	0.136	-	-	-
SFCT, µm	0.012	0.519	**<0.001**	0.012	0.484	**<0.001**
Systemic factors						
Age, yrs	-0.057	-0.215	**<0.001**	-0.001	-0.003	0.950
Gender, female	-0.706	-0.151	**0.005**	-0.183	-0.039	0.482
Body mass index, kg/m^2	-0.026	-0.058	0.283	-	-	-
Systolic blood pressure, mmHg	-0.001	-0.012	0.818	-	-	-
Diastolic blood pressure mmHg	0.031	0.145	**0.007**	0.019	0.089	0.072
Serum glucose, mmol/L	0.025	0.036	0.511	-	-	-
HbA1c, %	0.034	0.018	0.736	-	-	-
Total cholesterol, mmol/L	0.115	0.062	0.256	-	-	-
Triglycerides, mmol/L	0.130	0.077	0.158	-	-	-
Blood creatinine, mmol/L	0.003	0.035	0.516	-	-	-
Current smoking, Yes	1.098	0.187	**<0.001**	0.535	0.092	0.088
Alcohol consumption, Yes	1.004	0.051	0.341	-	-	-

*Adjusted for variables with a p-value<0.10 in the univariate analysis.
β, regression coefficient.

Table 8.5 Image binarization protocol in Sonoda et al. vs. current study

	Sonoda et al (2014)[30]	**Sonoda et al (2015)[31]**	**Current study**
Study sample size	15 eyes of 15 subjects	180 eyes of 180 subjects	345 eyes of 345 subjects
Choroidal area measured	1.5 mm	7.5 mm	1.5 mm
Location of measurement	Centered on fovea , 1500 um	Entire raster scan, 7500 um	Centered on fovea (1500 um) due to the segmental nature of choroidal blood supply as described by Hayreh et al.[37]
Pre-selection of vessels	3 choroidal vessels with lumens > 100 mm were randomly selected and the average reflectivity of these areas was determined by the software		Used autolocal threshold techniques to allow binarization of smaller choroidal vessels or choriocapillaris.
Brightness adjustment	Average brightness was set as the minimum value		Brightness was not adjusted as it would reduce the contrast between luminal and stromal areas and possibly affect the autolocal threshold.
Order of binarization	Region of interest selected prior to image binarization		To get a clear view of the choroid-scleral interface, image binarization was performed prior to area selection.
Image segmentation time	~ 5 minutes per image		~1 minute per image

CHAPTER VIII FIGURES

Figure 8.1 Image binarization for choroid with normal choroidal thickness. (A) Original SD OCT image. (B) 1.5 mm segmentation block of the subfoveal choroidal area. (C) Segmented OCT image using modified image binarization approach. (D) Overlay of region of interest created after image binarization was performed on the SD OCT image.

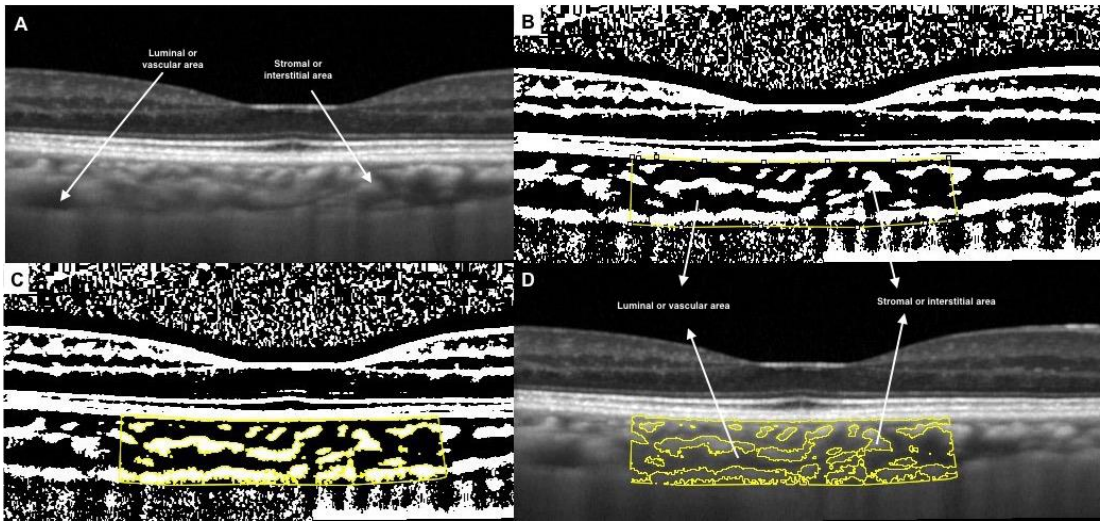

Step by step process for binarizing the image using image J software

Figure 8.2 To set the scale, the option Analyse > Set Scale was selected, and the known distance was set to 2 mm.

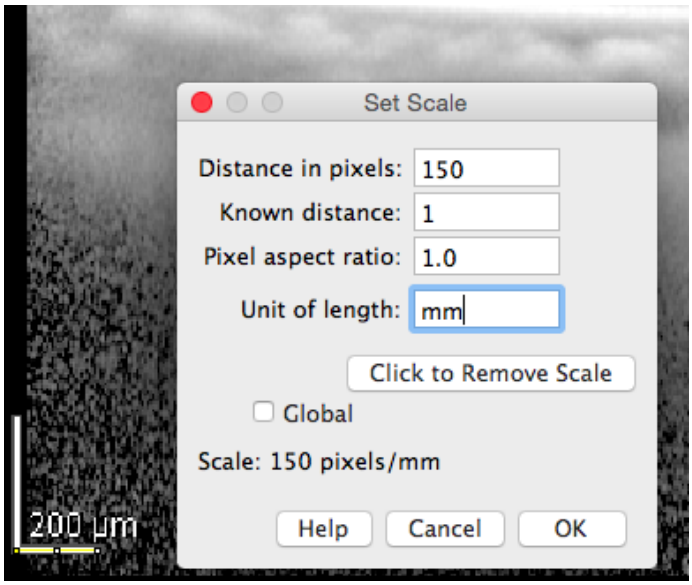

Figure 8.3 Auto local threshold was applied. Image > Type > 8 bit was first applied (**A**), followed by Image > Adjust > Auto Local Threshold (**B**). Niblack was selected as the method (**C**).

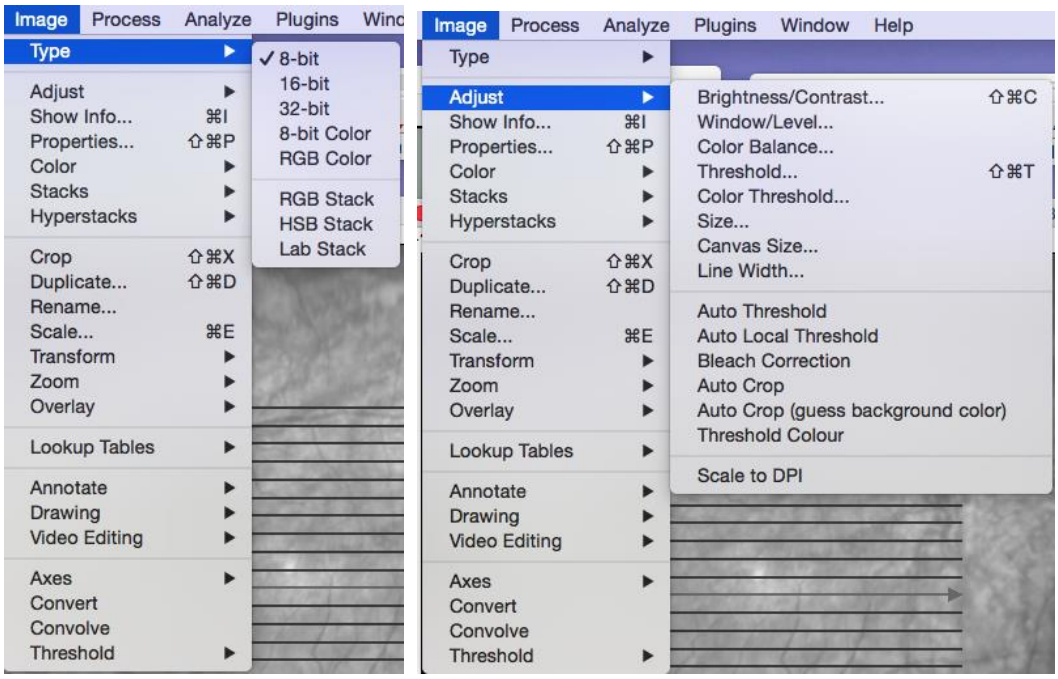

(A) **(B)**

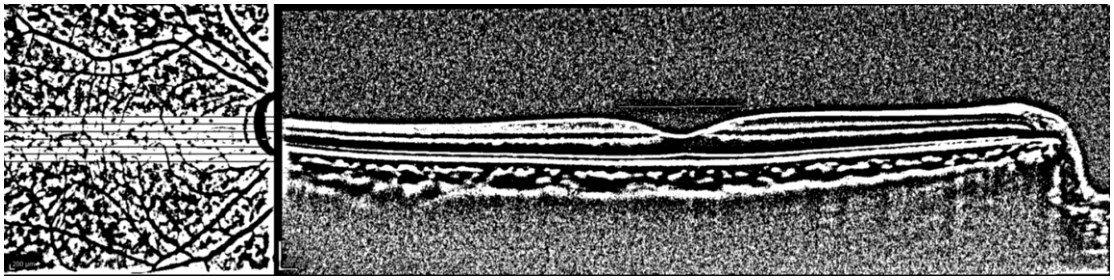

(C)

Figure 8.4 The polygon tool was used to draw a polygon under the lines drawn, to select the subfoveal choroid (**A**). The area of the choroid under the retinal pigment epithlium was selected. The upper border was marked at the retinal pigment epithelium and the lower border area was below the line of light pixels at the choroid scleral junction. The area was saved in the ROI manager by selecting the option Analyse > Tools > ROI manager, and Add [t] (**B**).

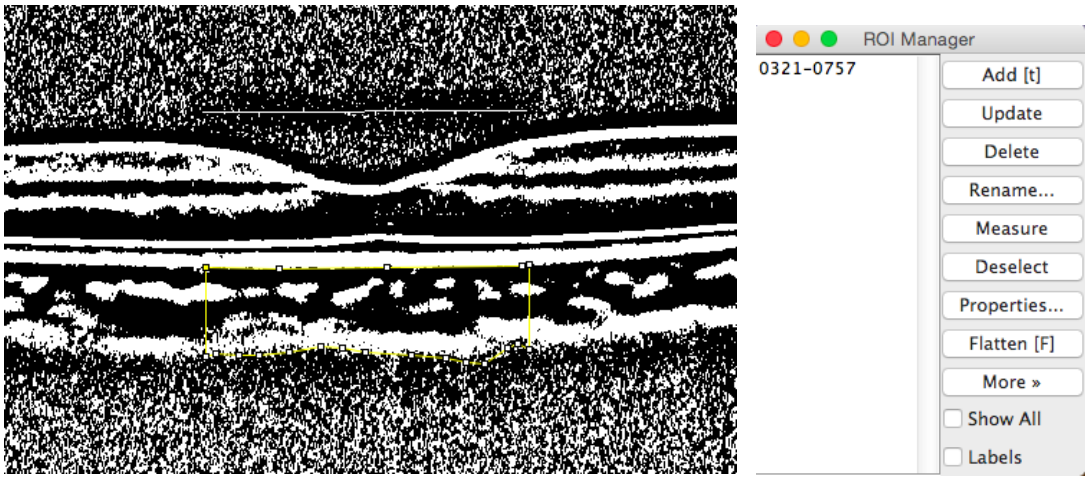

(A) **(B)**

Figure 8.5 Fifthly, the area of vascularity was highlighted by selecting Image > Type > RGB colour, and Image > Adjust > Colour Threshold. The first bar under Brightness was adjusted to 0, and the second bar was adjusted to 254 (**A**). After clicking Select (**B**), the area was added to the ROI manager.

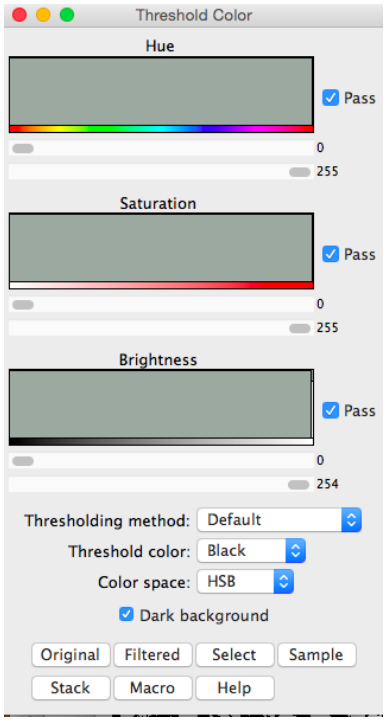

(A)

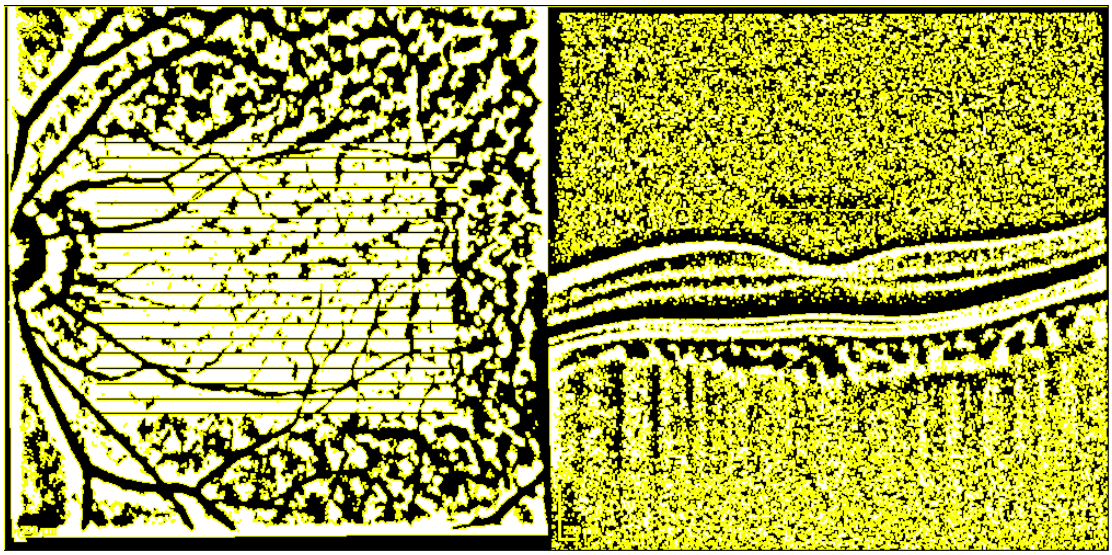

(B)

Figure 8.6 After clicking Select in the above figure, the area was added to the ROI manager by selecting Add [t]. to determine the area of vascularity within the initially selected polygon, both areas in the ROI manager were selected (**A**) and merged by selecting More > AND (**B**). The composite third area was added to the ROI manager by selecting Add [t] (**C**). Lastly, the first and third areas were selected and measured using the ROI manager. The first area represents the total area of choroid selected, and the third composite area is the vascular area.

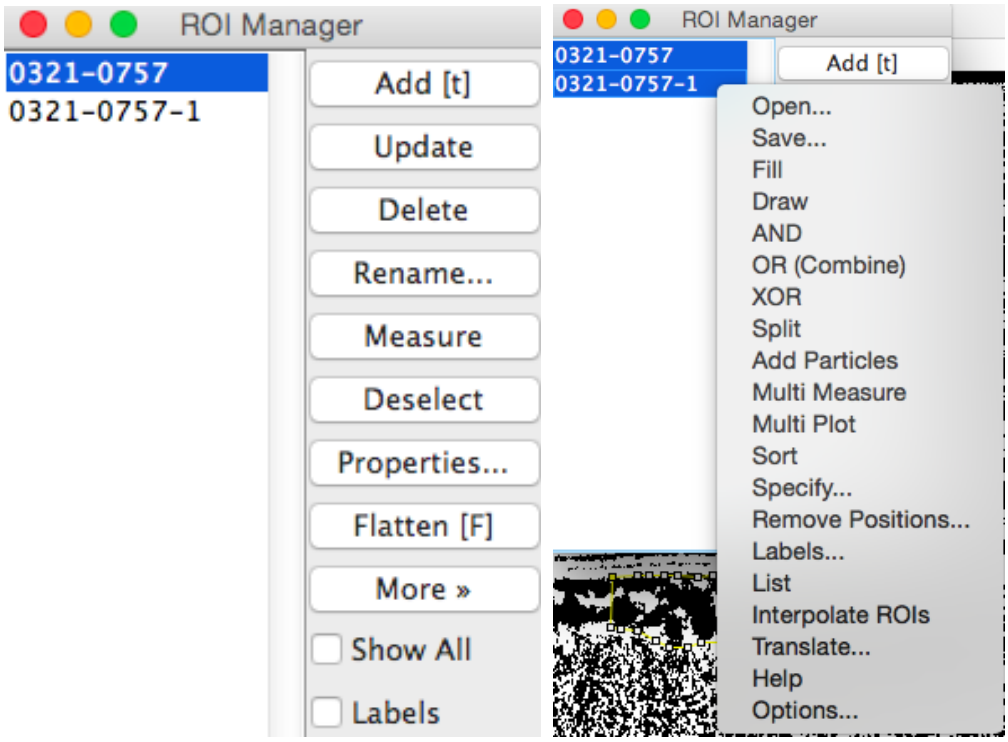

(A) **(B)**

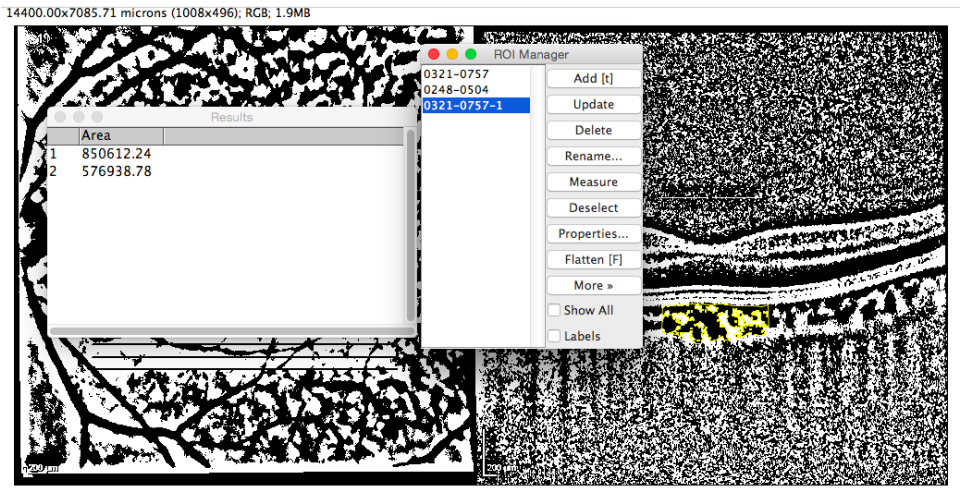

(C)

Figure 8.7 Distribution of subfoveal choroidal thickness **(A)** and choroidal vascularity index **(B)** across the population.

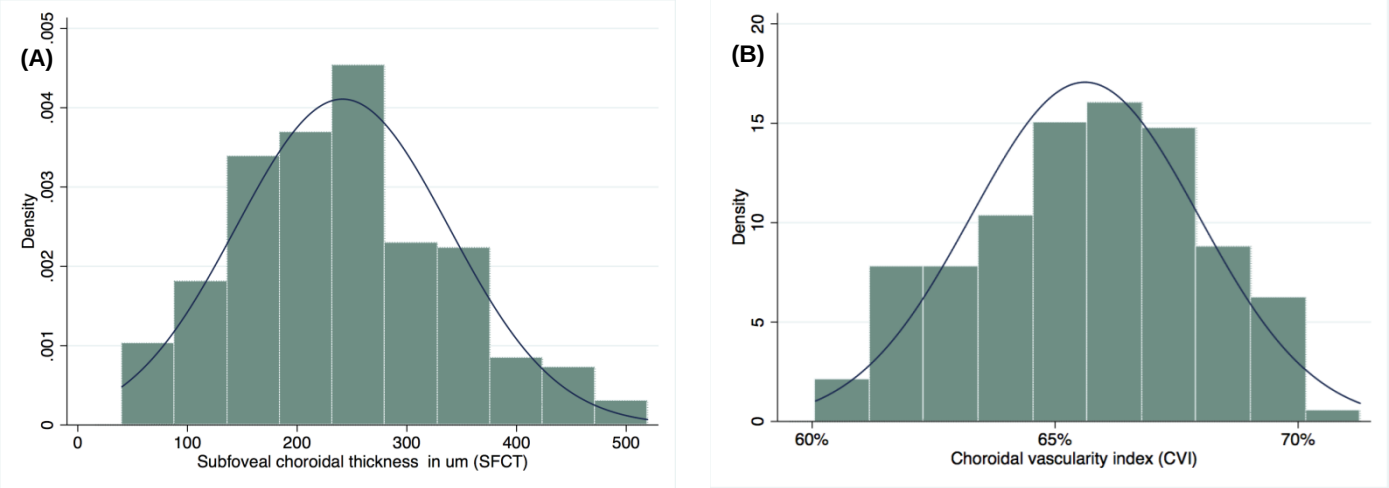

Figure 8.8 Bland Altman plots of total choroidal area and luminal area. **(A)** and **(B)** shows intra- and inter- rater reliability for total choroidal area respectively. **(C)** and **(D)** shows intra- and inter- rater reliability for luminal area respectively.
For intra-rater reliability, the difference was calculated by the 1st measurement minus the 2nd measurement. Pink dashed line represents regression line of difference between 1st and 2nd measurements. For inter-rater reliability, the difference was calculated by the grader 1 measurement minus the grader 2 measurement. Pink dashed line represents regression line of difference between the two graders measurements.

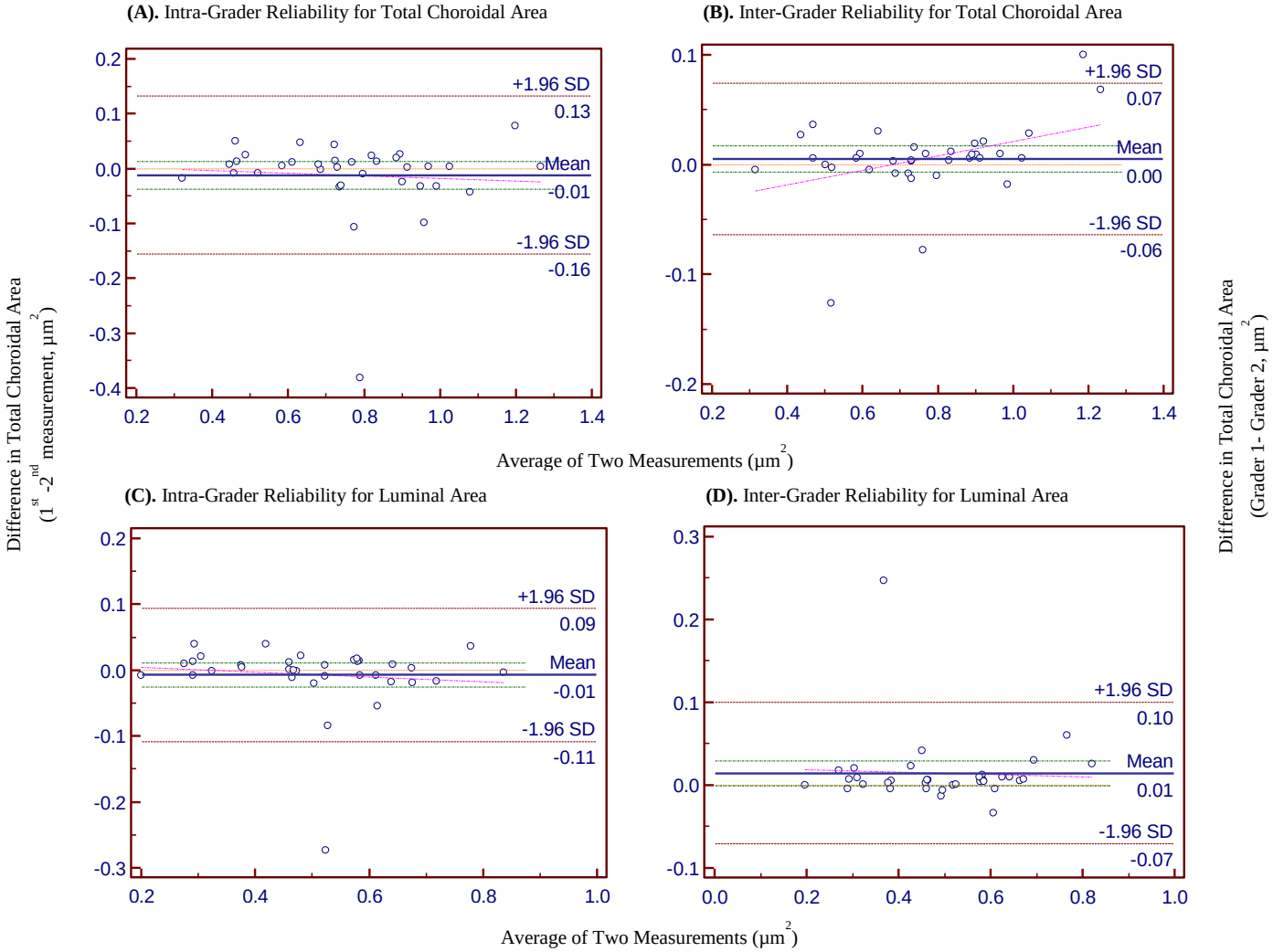

CHAPTER IX

CHARACTERIZATION OF CHOROID IN HIGH MYOPES

Until now we have addressed the technological challenges in the field of choroidal imaging by our novel semi- and fully-automated choroidal image processing techniques as well as objectively and reliably quantified choroidal parameters such as thickness, volume and vasculature in our multi-ethnic populations in Singapore.

However, we postulate that due to axial elongation of the globe in eyes with high myopia, the above choroidal traits and in particular other morphological and vascular attributes of the choroid such as CSI curvature, inflection point, and vascular area might be altered in eyes with high myopia. Therefore, in this Chapter we characterized the choroid including its detailed morphological and vascular analysis in young high myopes.

The manuscripts relevant to the contents of this chapter have been published in the following journals:

Gupta, P., S. Saw, C. Y. Cheung, M. J. Girard, J. M. Mari, M. Bhargava, C. Tan, M. Tan, A. Yang, F. Tey, G. Nah, P. Zhao, T. Y. Wong and C. Y. Cheng. "Choroidal Thickness and High Myopia: A Case-Control Study of Young Chinese Men in Singapore." *Acta Ophthalmologica* 2015;93(7):585-592.

Gupta, P., C. Y. Cheung, S. M. Saw, M. Bhargava, C. S. Tan, M. Tan, A. Yang, F. Tey, G. Nah, P. Zhao, T. Y. Wong and C. Y. Cheng. "Peripapillary Choroidal Thickness in Young Asians with High Myopia." *Investigative Ophthalmology and Vision Sci*ence 2015;56(3):1475-1481.

Gupta, P., S. Saw, C. Y. Cheung, M. J. Girard, J. M. Mari, M. Bhargava, C. Tan, M. Tan, A. Yang, F. Tey, G. Nah, P. Zhao, T. Y. Wong and C. Y. Cheng. "Choroidal Thickness is not a Predictor of Visual Acuity in Young High Myopes." *Acta Ophthalmol*ogica May 2016; 94(8) [Epub ahead of print].

Gupta, P., S. G. Thakku, S. Saw, M. Tan, E. Lim, M. Tan, C. M. G. Cheung, T. Y. Wong and C. Y. Cheng. "Detailed Phenotyping and Characterization of Choroidal Morphological and Vascular Features in Young Men with High Myopia using Spectral Domain Optical Coherence Tomography." *American Journal of Ophthalmology* 2016 (under review).

9.1 INTRODUCTION

High myopia (defined as -6 D or more) is a major cause of visual impairment in the world[1-3] and the prevalence is especially high in East Asia.[4-7] In particular, in Singapore, the prevalence of pathological myopia or high myopia in young adults is high ~14.7%.[8] In high myopia, excessive axial elongation of globe can cause biomechanical stretching and thinning of not only the RPE layers[9, 10] but also the choroid,[11-13] leading to increased risk of various chorioretinal complications[14-17] which may lead to vision loss. Thus, the changes in the choroid are significant but they are not well studied.

Because, the choroid contributes blood supply not only to the outer retina[18] but also to the prelaminar portion of the optic nerve,[19] a variety of ocular pathologies including glaucoma[20, 21] and high myopia[11] occur in the peripapillary choroidal region. Given that high myopia is associated with a high prevalence of retinal complications such as posterior staphyloma,[22, 23] lacquer cracks,[16] chorio-retinal atrophy as well as optic disc changes, such as oval configuration, larger area of peripapillary atrophy, disc tilt and rotation,[24] these may potentially affect the characteristics of both macular and peripapillary choroid such as its thickness and distribution profile. As some of the earliest changes in high myopia begin in the choroid, characterization of the choroid may help elucidate the mechanisms through which the choroid affects these diseases.

Since choroid supports the metabolic demands of the RPE and photoreceptors,[25] disturbances in choroidal morphology and circulation may account, in part, for outer retinal dysfunction and vision loss in high myopia. Thus, we hypothesize a relationship between CT and VA in high myopes.

With the advancement in imaging technology, OCT based EDI [26] provides an easy and non-invasive way to quantify CT. Although, using EDI, SD-OCT various investigators have measured CT in the macular area in high myopes but these studies were either conducted on small sample populations[11, 12] or were mainly limited in their assessment of CT to horizontal locations only.[27, 28] To the best of our knowledge, there are no studies which investigated CT by severity of myopia, the distribution of CT, and assessed ocular factors associated with CT in Asian eyes. Knowledge of such factors is crucial before drawing inferences on how CT influences the development of pathological myopia. In addition, none of the studies have explored the distribution of CT around the optic disc in high myopes.

There is now evidence from recent studies that suggest CT to be a predictor of VA and thinner choroid to be associated with poorer VA.[27, 29-31] However, these studies included only older participants mostly above 40 years, and their results may be confounded by other ocular comorbidities due to aging. In addition, in some studies[27, 30] the association was tested using univariate analysis only, thus it remained unclear whether the observed association between VA and CT was a primary relationship or was due to confounding effects from other myopia-related changes, such as elongated AL. Finally, these studies were performed in myopic eyes free of myopic macular degeneration. It is unclear whether CT influences VA in the presence of myopic macular degeneration.

Therefore, in this Chapter we evaluated various choroidal characteristics including, thickness (at both macular and peripapillary regions), morphology and vasculature in young, high myopes and compared them with emmetropes. We first quantified and compared the distribution of macular CT in myopes with varying degree of myopic refractive error and emmetropes. This was followed by the

evaluation of ocular determinants of sub-foveal CT in high myopes. We then performed the distribution and determinants of peripapillary CT in this cohort. This was followed by the detailed morphological and vascular analyses of the choroid in the sub-foveal (1.5 mm) and macular (6 mm) regions. And finally, we examined the potential influence of sub-foveal CT on VA in young, extremely high myopic persons (more than -10 D) with and without myopic macular degeneration changes. We used a case-control study approach of young, highly myopic and emmetropic healthy male adults in Singapore.

9.2 MATERIALS AND METHODS

9.2.1 Study Population

A total of 28,908 male adults were screened for myopia (mean age ± SD: 19.8 ± 1.2 years; range: 17-29 years) from 2009 to 2010 as part of a mandatory medical eye review for employment purposes. Measured using non-cycloplegic autorefraction (Huvitz MRK-3100P), 2,584 persons were identified to have myopia with SE of -6.0 D or worse. Of these 2,584 persons, 719 were selected on the basis of a refractive error-stratified random sampling strategy and underwent a further comprehensive ophthalmologic examination at SERI from December 2011 to June 2012. Their SE was further confirmed by subjective refraction, and those with SE >-6.0 D (n =96) were excluded, leaving 623 subjects with high myopia (251 with SE between -6.0 D and -8.0 D; 207 with SE between -8.0 D and -10.0 D; 165 with SE -10.0 D or worse). In addition, 151 emmetropes who had SE less than 0.5 D in both eyes measured using autorefraction were recruited as controls and went through a similar ophthalmologic examination. Subjects were also excluded if they did not give consent to take part in

this medical review, had any previous ocular trauma or surgery, and those with other clinically significant ocular co-morbidity.

Written informed consent was obtained from the subjects and their parents/guardians (if they were 21 years old and below). Ethics approval was obtained from the Institutional Review Board of DSO National Laboratories, Singapore. The study was conducted in accordance with the tenets of the World Medical Association's Declaration of Helsinki.

9.2.2 Clinical Examination

The detailed ophthalmic examination and the methods involved are explained in Chapter III of the thesis. In brief, before dilation following ocular examinations were performed: objective and subjective refraction, ocular biometry, IOP and contrast sensitivity (CS) evaluation.

CS was measured using the Rabin super vision test (Rabin et al. 2004), with and without a night vision goggle filter (SVT-NVG) and low and high luminance log CS were taken for this test. The NVG filter used was a dark green, low-luminance filter which slides in place in front of the illuminated chart, reducing chart luminance (from 100 to 4 cd/m^2) to simulate the low-luminance (i.e., wearing NVG). In order to minimize memorization of optotypes, two different sequences were displayed for right and left eyes and measurement of CS were recorded by counting the number of letters correctly read by the subjects using the Conversion Table.

Subjects underwent slit lamp examination. Binocular indirect ophthalmoscopy was performed approximately 30 minutes after topical instillation of 3 drops of tropicamide and 2.5% phenylephrine, given 5 minutes apart. Dilated fundus examination was carried out by ophthalmologists. The presence and type of peripheral

retinal degenerations and vitreous degenerations were systematically documented. Fundus photography was performed using non-mydriatic retinal camera (Canon CR-DGi with a 10-DSLR back, Japan).

9.2.3 OCT Imaging

The retinal and choroidal (macular and peripapillary) architectural parameters were determined using SD-OCT (Spectralis, Wavelength: 870 nm; Heidelberg Engineering, Heidelberg, Germany) after pupil dilation. Choroid was imaged with EDI modality whereas retina was imaged without EDI. Please see Chapter III for imaging details. Since Spectralis OCT does not allow AL to be input, our methods may still have residual errors (2% to 7%)[32] due to ocular magnification from methods that additionally uses AL. Although, imaging of both eyes of each subject was performed, only right eye was chosen for subsequent analysis.

Macular Choroidal Scan: Radial scan consisting of six sections, each comprising 100 averaged scans (using the automatic averaging and eye tracking features of the proprietary device), were obtained in an angle of 30° centered onto the fovea (30° angles between the lines). Only the horizontal and vertical section passing through the center of the fovea was selected for analysis.

Peripapillary Choroidal Scan: The peripapillary region was scanned using a 360°, 3.5 mm diameter circle centered on the optic disc (**Figure 9.1**), each comprising 100 averaged scans (using the proprietary automatic averaging and eye tracking features of the SD-OCT device).

9.2.4 Measurement of Choroidal Thickness

Both macular and peripapillary CT was measured manually using the Heidelberg Eye Explorer software (version 1.5.12.0; Heidelberg Engineering) as the perpendicular distance between the outer portion of the hyperreflective line corresponding to the RPE (automatically detected by the instrument) to the hyporeflective line or margin corresponding to the sclerochoroidal interface (manually drawn by an experienced grader, who was masked to subject characteristics and clinical diagnosis).

Macular Choroidal Thickness: An accurate evaluation of the CT with EDI-OCT relies mainly on the visibility of CSI, which anatomically represents the junction between the choroid and the sclera and is a principal landmark for quantitative measurements of choroid. Therefore, in our study, in order to accurately determine CT, CSI was enhanced using our novel technique of adaptive compensation described in detail in Chapter V and elsewhere.[33-35] Our method has shown higher intra- and inter-grader reliability of CT measurements compared to conventional method.[33]

The CT in the enhanced images was measured at the following locations: sub-fovea and 1.5 and 3 mm nasal, temporal, superior and inferior to fovea. As there was no significant difference between the horizontal and vertical sub-foveal CT (mean horizontal SFCT=225.87 µm, mean vertical SFCT=232.09 µm, p=0.399), only horizontal SFCT was used for analysis. **Figure 9.2** shows an EDI-OCT scan comparing CT between a young emmetrope and a young myope. In addition, we evaluated the intra-observer reliability of CT measurements in both the myopic and emmetropic group. 40 randomly selected Spectralis images (20 from each group) were assessed again by the same grader (grader 1 vs. grader 1) after an interval of one week.

Peripapillary Choroidal Thickness: The PPCT was measured at the following locations around the optic disc: temporal, superotemporal, superior, superonasal, nasal, inferonasal, inferior and inferotemporal. Furthermore, the intra-observer reliability of PPCT measurements was assessed in 40 randomly selected Spectralis images (20 from each myopic and emmetropic group) after an interval of one week.

9.2.5 Assessment of Myopic Macular Degeneration

The colour fundus photos were graded similar to previously established grading techniques by a single trained grader masked to the participant characteristics.[36] Adjudication was performed by an experienced medical retina specialist from an accredited fundus photo grading centre. The main findings which were graded included myopia-related macular pathology, including staphyloma, lacquer crack and peripapillary atrophy (PPA). Presence of lacquer crack, its location, and number were evaluated. Curtin and Karlin classification was used to determine the subtype and position of PPA.[37] Staphyloma was determined by visualizing the border of the ectasia, then its location and type were documented based on the Curtin classification.[38]

Inter-grader reliability in grading for the aforementioned features was assessed with additional grading of 100 randomly selected eyes by trained graders, and reliability was found to be good (all intra-class correlation coefficient above 0.75). To confirm the presence of posterior staphyloma, the cross-sectional images from SD-OCT was graded by a medical retinal specialist. **Figure 9.3** shows the presence of posterior staphyloma on horizontal scan of the macular central on the fovea (20°) obtained using SD-OCT. The presence of posterior staphyloma was defined as curvature of the RPE layer, with a foveal depth of $\geq$ 500 μm relative to the 3 mm

periphery of the OCT B-scan. This allows posterior staphyloma with more gentle and subtle sloping edges to be detected.

9.2.6 Measurement of Choroidal Morphological and Vascular Parameters

For each eye, the horizontal cross-sectional scan passing through the fovea was identified. Based on this cross-sectional scan, we defined and calculated (in MATLAB) the following choroidal morphological and vascular parameters (**Figure 9.4**).

CSI Curvature: When compared to a healthy choroid, myopic eyes may have irregularities in the choroidal boundary, including thinning underneath the macula. In order to quantify these irregularities, we used parameters such as curvature and number of inflection points at the CSI. Curvature of the CSI gives an overall measure of the CSI shape (flat, 'U' shaped, inverted 'U' shape). In order to measure overall curvature, the best-fitting circular arc to the marked CSI points was identified. The reciprocal of the radius of this best-fitting circular arc was reported as CSI curvature. The sign of the curvature indicated the direction of the arc (positive denotes an anteriorly curved, and negative a posteriorly curved arc).

Number of Inflection Points: The number of inflection point measures the extent of local irregularities. A more irregular CSI would have greater local variations and hence more inflection points. Mathematically an inflection point is a point on a curve at which the curve changes from being concave to convex, or vice versa. An inflection point represents the contour of the CSI, with >1 point signaling irregular shape.

Thickest Point Distance from the Fovea: CT varies within the macular region. In order to quantify the position of the region with the thickest choroid, the distance of this point from the foveal center was measured.

Choroidal Thickness and Volume: CT was defined as the distance between the RPE layer and the CSI. The average thickness within the macular (6mm centered on fovea) and foveal (1.5mm centered on fovea) regions were reported as mean CT. Choroidal volume was measured by the summation the area enclosed between the RPE layer and the CSI for each of the radial scans multiplied by the distance between consecutive scans.

Choroidal Vascular Area within Foveal and Macular Regions: Based on the marking of the choroidal region in the horizontal scan passing through the fovea, image binarization was used to distinguish between the vascular and stromal areas of the choroid. The Niblack local thresholding technique was used, similar to that described in previous papers.[39] Black spaces within the choroid after binarization were assumed to represent vascular regions. The area of this region was measured within the sub-fovea as well as the macula, and defined as vascular area.

Validation of Image Binarization: The Niblack local thresholding technique[39] used to identify stromal and luminal areas within the choroid was validated against manual delineations. On a set of 8 randomly chosen cross-sectional scans of the choroid, the 3 or 4 best visible blood vessels were delineated. 4 similarly sized regions corresponding to the stroma were also marked. The automatically binarized images were compared to these manual markings. In the binarized image, black regions correspond to the lumen and white regions to the stroma. Overlaying the manually marked luminal and stromal regions, we compared the extent to which the two methods agreed (**Figure 9.5**). We found that 2.5% of the luminal area and 4.1% of the stromal area were incorrectly identified.

9.2.7 Statistical Analyses

Subjects were excluded from analysis if they had any history of anterior ocular diseases, previous ocular trauma, evidence of macular or vitreoretinal diseases or any form of refractive surgery done in their eyes. However, conditions such as, peripapillary atrophy, lacquer crack, posterior staphyloma or chorio-retinal atrophy were not excluded, as they are commonly seen in high myopic eyes. Statistical analysis was performed using SPSS version 17.0 (SPSS, Inc., Chicago, IL, USA) and MedCalc version 12.3 (Medcalc Software, Ostend, Belgium). A p-value of <0.05 was considered statistically significant. For the purpose of analyses, myopic eyes were divided into three groups based on SE: <-6 to -8D, <-8 to -10D, and <-10D.

I. The demographics and ocular parameters between myopic and control eyes were compared using independent samples Student t-tests.

II. The intra-session repeatability of the CT was measured by the absolute agreement model of the intra-class correlation coefficient (ICC).[40]

III. Generalized linear model was used to assess the mean CT across different locations in eyes with varying degree of myopia and conditions such as posterior staphyloma and chorio-retinal atrophy were included to adjust for potential residual confounding.

IV. Repeated measures analysis of variance (ANOVA) with Bonferroni post-test was used to compare mean thickness at various locations within each group.

V. Univariate and multiple linear regression analyses were performed to determine the association of ocular factors (independent variables) with CT measurements (dependent variables). For multiple linear regression, age and factors which showed significant association in univariate analysis ($p<0.05$) were included.

9.3 RESULTS

We first describe the results of the distribution and determinants of macular CT in a larger sample of highly myopic Asian eyes and its comparison with control eyes. This is followed by the topographical distribution and predictors of peripapillary CT in high myopic eyes. We then we performed the morphological and vascular analysis of the choroid. Lastly we describe the impact of subfoveal CT on BCVA in a group of extremely high (SE<-10D) myopic eyes.

9.3.1 Macular Choroidal Thickness in High Myopes

Of the 623 eligible high myopes (SE ≤-6.0 D), we further excluded 103 subjects because either their choroidal images were not successfully attained (n=69) or the available images were not of optimal quality to perform accurate measurements (n=31) or they did not meet the inclusion criteria (n=3), leaving 648 subjects (520 high myopes and 128 emmetropes) with complete data on CT for analysis.

Subject Demographics: The mean age of included myopic and emmetropic subjects was 21.59 ± 1.15 years and 22.06 ±0.97 years respectively. The mean SE was -8.68±2.05 diopters (range, -6 to -23 D) for myopic group, and 0.12±0.24 diopters for emmetropic group. Among the myopic group, all our subjects had peri-papillary atrophy, 35.6% had posterior staphyloma, 6.5% had chorio-retinal atrophy and 2% had lacquer cracks. The demographics and ocular characteristics of the study population are shown in **Table 9.1**.

Reliability Assessment of Macular Choroidal Thickness: In terms of reliability of CT measurements, the intra-observer reliability for myopic (ICC: 0.95 to 0.98) and

emmetropic group (ICC: 0.95 to 0.97) was excellent for all locations of CT (**Table 9.2**).

Distribution Profile of Macular Choroidal Thickness: CT varied significantly across the myopic sub-groups and the emmetropic control group at all the locations (p for trend <0.001 for all locations, **Table 9.3**). It was significantly thinner in the more myopic eyes over a range of eccentricities and the pattern of distribution was different from emmetropes **(Figure 9.6A and 9.6B)**. Across the three myopic sub-groups, CT was found to be thickest at the superior location, followed by the temporal, sub-foveal, inferior and the nasal locations (p<0.001 by repeated measures ANOVA). In comparison, the choroid in emmetropic eyes was thickest at the fovea, followed by the superior, inferior, temporal and the nasal locations (p<0.001 by repeated measures ANOVA). However in both the myopia and emmetropic groups, choroid was thinnest at the nasal location being 108.85 µm and 238.25 µm in myopic and emmetropic group respectively **(Figure 9.6A and 9.6B)**.

Determinants of Macular Choroidal Thickness: In the univariate analysis, SE, AL, corneal curvature, presence of posterior staphyloma and chorio-retinal atrophy were significantly associated with SFCT (all p<0.05, **Table 9.4** and **Figure 9.7**). For each mm increase in AL and corneal curvature, SFCT on average decreased by 32.31 µm (p<0.001) and 84.31 µm (p<0.001) respectively. A decrease in mean SFCT by 13.10 µm was observed for each myopic diopter increase (p<0.001). Presence of posterior staphyloma and chorio-retinal atrophy decreased the mean SFCT by 22.69 µm and 26.91 µm respectively. Both AL and SE influenced CT but a larger extent from AL. The results remained similar after adjusting for age (data not shown).

Because of collinearity between AL and SE (correlation coefficient = -0.65), only AL was selected and retained in the multivariate analysis as it had a greater

explanatory power on CT change than did SE (standardized β, -0.489 vs.0.348). In the multiple linear regression analysis, AL, presence of posterior staphyloma and chorio-retinal atrophy remained significantly associated with CT (all $p<0.05$), whereas the association with corneal curvature was abolished ($p=0.975$). However, there was no change in results after adjusting for age.

In addition, SFCT correlated negatively with the logMAR visual acuity ($r=-0.085$, $p=0.054$) and log low luminance contrast sensitivity ($r=-0.115$, $p=0.009$) although the association was not statistically significant in multivariate analysis (**Figure 9.8**).

9.3.2 Peripapillary Choroidal Thickness in High Myopes

Of the 623 eligible high myopes (SE ≤-6.0 D), we further excluded 175 subjects because their choroidal images were not successfully attained due to unstable fixation (n = 62), the available images were not of optimal quality (a quality index of < 25 decibels as suggested by the manufacturer for the image quality assurance, n = 39), those where the choroid-scleral interface was not clearly delineated (n = 21) to perform accurate measurements, subjects whose peripapillary atrophy involved the OCT scanning ring (n=30) or they did not meet the inclusion criteria (n = 23), leaving 448 high myopes with complete data on PPCT for analysis. Of the 151 emmetropes recruited, 35 were found to have SE greater than ±0.5 D on subjective refraction and were excluded, leaving 116 emmetropes for analysis.

Subject Demographics: The mean age of included myopic and emmetropic subjects was 21.63 ± 1.15 years and 22.03 ± 0.96 years ($p<0.001$), respectively. The mean SE was -8.52 ± 1.80 D (range, -6 to -18.25 D) for myopic group, and 0.11 ± 0.24 D for emmetropic group. Among the myopic group, nearly all our subjects (97.3%) had

peri-papillary atrophy, 41.3% had posterior staphyloma, 6.3% had chorio-retinal atrophy, 0.4% had lacquer cracks and 22.5% had tilted disc. The demographics and ocular characteristics of the study population are shown in **Table 9.5**.

Reliability Assessment of Peripapillary Choroidal Thickness: In terms of reliability of PPCT measurements, the intra-observer reliability for myopic (ICC: 0.96 to 0.98) and emmetropic (ICC: 0.95 to 0.98) group was excellent for all locations of PPCT (**Table 9.6**).

Topographical Distribution of Peripapillary Choroidal Thickness: PPCT varied significantly across the myopic sub-groups and the emmetropic group at all the locations (p for trend <0.001 for all locations, **Table 9.7**). PPCT was significantly thinner in the more myopic eyes over a range of eccentricities and their pattern of distribution was different from emmetropes (**Figure 9.9**). Across the three myopic sub-groups, peripapillary choroid was thickest (163.41 ± 50.43 µm) at the superior location whereas in emmetropes it was thickest (207 ± 58.01 µm) at the temporal location. Peripapillary choroid was thinnest in both myopes (109.98 ± 37.30 µm) and control eyes (137.90 ± 44.53 µm) at the inferior location.

Predictors of Peripapillary Choroidal Thickness: In the univariate analysis, SE, AL, corneal curvature, IOP, average RNFL thickness and presence of posterior staphyloma and chorio-retinal atrophy were significantly associated with PPCT (all p<0.05, **Table 9.8**). For each mm increase in AL and corneal curvature, PPCT on average decreased by 13.02 µm (p<0.001) and 36.72 µm (p<0.001) respectively. A decrease in mean PPCT by 5.39 µm was observed for each myopic dioptre increase (p<0.001). Each mm Hg increase in IOP increased the PPCT by 1.40 µm whereas for each µm increase in average RNFL thickness, PPCT increased by 0.74 µm. Presence

of posterior staphyloma and chorio-retinal atrophy decreased the PPCT by 15.29 μm and 14.76 μm respectively (both p<0.001). The results remained similar after adjusting for age (data not shown).

Because of collinearity between AL and SE (correlation coefficient = -0.574), only AL was selected and retained in the multivariate analysis as it had a greater explanatory power on PPCT change than did SE (standardized β, -0.319 vs. 0.222). There was no collinearity between posterior staphyloma and chorio-retinal atrophy as variance inflation factor (VIF) was close to 1. In the multiple linear regression analysis, AL (p=0.001), IOP (p=0.006), presence of posterior staphyloma (p=<0.001) and chorio-retinal atrophy (p=0.032), remained significantly associated with PPCT, whereas the association with corneal curvature (p=0.062) and RNFL thickness was abolished (p=0.156). The results remained similar after adjusting for age. However, on performing a linear regression analysis between IOP and average PPCT in the emmetropic group we found no significant association (p = 0.964; regression coefficient = -0.075; 95% CI, -3.334 to 3.183).

9.3.3 Morphological and Vascular Analyses of Choroid in High Myopes

Table 9.9 shows the comparison of clinical characteristics in myopes vs. emmetropes. The mean age of included myopic and emmetropic subjects was 21.61±1.14 years and 21.59±1.15 years respectively. The mean SE was -8.66±2.00 D (range, -6 to -23 D) for the high myopic group, and 0.13±0.24 D for the emmetropic control group. Among the high myopic group, nearly all the subjects (99%) had PPA, 55.2% had posterior staphyloma, 9.2% had chorio-retinal atrophy and 1.2% had lacquer cracks.

Table 9.10 shows choroidal morphological and vascular characteristics of eyes with high myopia and control eyes with emmetropia. The choroid was

significantly thinner in high myopic eyes compared to control eyes (mean CT: 257.19±68.23 μm vs. 371.33±63.35 μm, p<0.001). In myopes, choroid was thickest temporally compared to sub-foveal location in emmetropes (thickest point distance from fovea -1.51±1.42 mm vs. -0.53±1.06 mm, p<0.001).

There was significant reduction in total choroidal, vascular and stromal areas respectively in high myopic eyes compared to control eyes (Table 2; all p<0.001). Choroidal vascularity was greater in the high myopic eyes, compared to the control eyes (55.4±0.40 vs. 52.2±3.30, p<0.001).

In the multiple regression analysis after adjusting for age, both vascular and stromal areas were significantly lower (vascular area: β=-0.306, stromal area: β=-0.377, both p<0.001; Model 1, Table 3) at macular region in high myopic eyes, compared to control eyes. Further adjusting vascular and stromal areas for choroidal thickness, the vascular area increased (β=0.027, p<0.001) and the stromal area showed a decrease (β=-0.027, p<0.001) in myopic eyes (Model 2); suggesting that thinning in myopes was actually due to reduction in stromal component. Compared to control eyes, choroidal vascularity was greater in myopic eyes (β=0.032, p<0.001). Similar findings were observed for sub-foveal region (**Table 9.11**).

9.3.4 Impact of Choroidal Thickness on Visual Acuity

The purpose of this study was to examine the potential influence of CT on VA in young, extremely high myopic persons (SE ≤ -10 D) with and without myopic macular degeneration changes. Extremely high myopic subjects were chosen as we conceived that if there exists an association between CT and VA, it would be more apparent in this group of subjects.

Of the 520 myopic (SE ≤ -6 D) subjects, we therefore selected 118 subjects with SE -10.0 D or worse in both eyes (mean SE in the right and left eyes was -11.56 ± 2.04 D and -11.26 ±2.30 D respectively) as cases for the current analysis. We also selected 55 emmetropic male subjects with SE less than ± 0.5 D in both eyes (mean SE in the right and left eyes was 0.14 ± 0.25 D and 0.16 ± 0.26 D respectively) as controls. Of the 118 subjects who had SE -10.0 D or worse, 13 subjects were excluded as their choroidal images were not successfully attained (n= 8) due to unstable fixation, those where the CSI was not clearly delineated (n= 4) to perform accurate measurements or they did not meet the study inclusion criteria (n=1), leaving 105 highly myopic subjects with complete data on CT for analysis.

Subject Demographics: The mean age of included myopic and emmetropic subjects was 21.51 ± 1.22 years and 21.96 ± 0.89 years respectively. The mean SE was -11.56 ± 2.04 D (range, -10 to -23 D) for myopic group, and 0.14 ± 0.25 D for emmetropic group (**Table 9.13**). Among the high myopic group, nearly all the subjects (99%) had PPA, 66.7% had posterior staphyloma, 22.9% had chorio-retinal atrophy and 4.8% had lacquer cracks.

Distribution Profile of Choroidal and Retinal Thicknesses: **Table 9.14** shows the distribution profile of choroidal and retinal thicknesses at different locations in both high myopic and emmetropic groups. In the highly myopic group, the mean CT was 194.81 ± 57.78 µm and the mean retinal thickness was 287.39 ± 31.75 µm. Choroid was significantly thinner in the highly myopic eyes over a range of eccentricities and the pattern of distribution was different from emmetropes (**Figure 9.10A**). Among the high myopes, choroid was found to be thickest at the superior location, followed by the temporal, sub-foveal, inferior and the nasal locations ($p<0.001$ by repeated

measures ANOVA). In comparison, the choroid in emmetropic eyes was thickest at the fovea, followed by the superior, inferior, temporal and the nasal locations ($p<0.001$ by repeated measures ANOVA). However in both the highly myopic and emmetropic groups, choroid was thinnest at the 3 mm nasal location being 87.34 µm and 237.10 µm respectively (**Figure 9.10A**). Retinal thickness in both myopes and emmetropes showed similar distribution pattern, being thickest in the nasal location and thinnest subfoveally (**Figure 9.10B**).

Both AL and SE influenced BCVA but a larger extent from SE (standardized β, -0.505 vs. 0.214), thus only SE was selected and retained in the multivariate analysis due to collinearity between AL and SE (correlation coefficient = -0.638).

Association of Sub-foveal Choroidal Thickness with BCVA: **Table 9.15** shows the linear regression analyses of the associations of sub-foveal CT (exposure variable of interest) evaluated against BCVA (dependent variable) to calculate regression coefficients (β). In model 1, (univariate analysis) sub-foveal CT was significantly associated with BCVA ($\beta = -0.039$, $p = 0.015$). However, after adjusting for SE (model 2), sub-foveal CT was no more significantly associated with BCVA ($p = 0.761$). In model 3, including both SE and presence of any pathological myopia lesions such as posterior staphyloma, lacquer cracks or chorio-retinal atrophy, we found that sub-foveal CT was not independently associated with BCVA ($p = 0.937$). There was no significant interactions between sub-foveal CT and SE or sub-foveal CT and pathological myopia lesions on BCVA (*both p interaction >0.05*). Furthermore, the association between BCVA and sub-foveal CT in a group of 33 highly myopic subjects without any pathological myopic lesions (except PPA) was found to be insignificant ($\beta = 0.012$, $p = 0.776$).

It is speculated that if there exist any association between CT and VA, it would most likely concern the subfoveal CT due to maximum number of photoreceptors at sub-fovea. To confirm whether the distribution pattern of CT has influence on BCVA, we analyzed the association of CT at different locations (nasal, temporal, superior and inferior) with BCVA. However, we found no significant associations (all $p>0.05$) between CT at different locations and BCVA (data not shown).

9.4 DISCUSSION

Although the understanding of the characteristics of the in-vivo choroid has increased substantially in recent years, to date, only a few studies have examined macular CT in high myopia. None of previous studies so far have explored the profile of peripapillary choroid in high myopia and only a limited number of studies have reported the distribution of peripapillary choroid in emmetropic eyes. To our best knowledge, this study measured CT directly with EDI SD-OCT in the largest group of young, high myopic Asian subjects at both macular and peripapillary regions. Our study provided new data on CT and severity of myopia. In addition we performed a detailed morphological and vascular analysis of the choroid. Lastly, we examined the impact of CT on BCVA in a group of extremely high myopes (SE<-10D).

9.4.1 Macular Choroidal Thickness in Myopes vs. Emmetropes

Macular CT in the myopic group was significantly lower than that of the emmetropic control group at all eccentricities and there was a further decrease in CT with increase in degree of myopic refractive error. The mean sub-foveal CT in myopic group was 225.87±5.51 μm, which is much thicker than those reported in previous

studies that showed a mean CT of 93.2[11] to 115.5[28] µm (**Table 9.5**). The mean SFCT in emmetropes was 375.15 µm which is also thicker than previous studies that reported a mean thickness of 272 to 354 µm.[26, 41-43]

The differences in CT in our study compared to other studies could be because of differences in participants' characteristics, such as age, refractive error, and ethnicity. Our study participants are twice as young, mean age 21.63 years compared to other studies.[11, 12, 28, 41-43] In addition, there were variations in OCT device characteristics such as wavelength, eye tracking method, and averaging software among studies. In our results, CT decreased with increase in severity of myopic refractive error. The findings suggest that thinning or abnormalities of choroid plays a role in the pathogenesis of myopic degeneration and thus visual impairment.

Distribution Profile of Macular Choroidal Thickness: We found that CT in highly myopic eyes was thickest superiorly and thinnest nasally. In comparison, the choroid in normal eyes was thickest at the fovea and thinnest nasally. The observed pattern of CT distribution in our study is similar to the previous studies, in both myopes[12, 44] and emmetropes.[41] Two possible reasons for the relative choroidal thinning nasally and inferiorly in normal eyes are the choroidal watershed and the fetal choroidal fissure, which closes inferiorly at 7 weeks.[45]

Determinants of Macular Choroidal Thickness: Among the range of ocular factors studied, AL, presence of posterior staphyloma and chorio-retinal atrophy were the significant predictors of CT. In **Table 9.16**, on performing a meta-regression on various studies to quantify the change in mean CT with SE adjusting for age we found no significant association between SE and mean CT (β=0.429, p=0.952) indicating AL to be a more important predictor of CT than SE.

Longer Axial Length is associated with Choroidal Thinning: We found a significant negative association of SFCT with AL. In high myopia because of axial elongation, both the retina and choroid are stretched [9, 10, 46] leading to thinning.[11, 12, 41] However, thinner choroid is still adequate to nourish proportionally thin retina which is consistent with fairly normal visual functions in adolescents and young adults with high myopia than their aged counterparts which undergoes further age-related reduction in choroid.[11] In contrast, in non-myopic elderly eyes thinner choroid may not be adequate to supply the relatively thick retina which might in turn influence visual function. We therefore speculate that the relatively thin choroid in young myopes may be physiologically sufficient, although the same CT may be considered pathologic in older eyes without myopia.

Presence of Posterior Staphyloma is associated with Choroidal Thinning: Presence of posterior staphyloma, a hallmark of high myopia was significantly associated with choroidal thinning. Similar results were reported in the previous studies which demonstrated posterior staphyloma formation as a key factor in choroidal thinning in highly myopic eyes.[11, 12] This association is probably because in myopic eyes with posterior staphyloma, choroidal circulation is altered with marked attenuation and reduction in number of large choroidal vessels.[47] In addition, there is a shift in the entry site of the posterior ciliary arteries towards the staphyloma's border leading to scarce choroidal arterial network in the area occupied by staphyloma.[48] Thus, all these changes lead to choroidal thinning in eyes with staphyloma.

9.4.2 Peripapillary Choroidal Thickness in Myopes vs. Emmetropes

Peripapillary choroid in myopic group was significantly thinner than emmetropic control group at any locations. The mean PPCT in myopes and emmetropes was 142.62 ± 43.84 µm and 181.90 ± 46.43 µm respectively. We

demonstrated further decrease in PPCT with increase in degree of myopic refractive error. The mean PPCT in emmetropes of 181.90 ± 46.43 μm is in concurrence with former studies showing a mean thickness of 165.03[49] to 191.62[50] μm (**Table 9.17**).

Distribution Profile of Peripapillary Choroidal Thickness: In terms of distribution of PPCT, in both myopic and emmetropic eyes, peripapillary choroid was thinnest inferiorly. Studies done so far have consistently shown inferior region to be the thinnest among other regions of the posterior pole.[49-52] As optic fissure is located in the inferior aspect of the optic cup and is the last part of the globe to close,[53] this regional difference in ocular development may contribute to the thinner choroid found in inferior region. Thinner choroid would lead to decreased blood flow in choriocapillaris which nourishes the prelaminar portion of the optic disk, making it more susceptible to hypoxia or to elevated IOP. This is supported by a very common observation that glaucoma typically affects the inferior optic disc region first.[51, 54] The possible role of thinner choroid in glaucoma development is further supported by the findings of Usui et al.[55] and Hirooka et al.[54] who reported significant choroidal thinning in myopic normal tension glaucoma damage eyes as compared to myopic controls. Likewise, a substantial reduction in PPCT in patients with glaucoma who have sclerotic optic disc was demonstrated by Robert et al.[21]

We found peripapillary choroid in highly myopic eyes was thickest superiorly whereas in emmetropic eyes was thickest temporally. This variation in the refractive error differences in CT profile could be attributed to the presence of posterior staphyloma in highly myopic eyes. Although staphylomas may have various morphologic features, the most common types involve the macular and optic nerve regions.[56] Similar to our observation in emmetropes, Oh et al.[50] also reported peripapillary choroid to be thickest temporally. However, the observed pattern of

PPCT distribution in emmetropes in our study differs from most of the previous studies in healthy eyes which reported choroid to be thickest superiorly.[21, 49, 51, 52, 54, 57] Although, the magnitude of the difference in thickness of the thickest point is not clinically significant (ranges between 15 to 20 µm). The differences in PPCT profile in our study compared to other studies could be because of the differences in age of our study participants. Our study participants are twice as young, mean age 22 years compared to other studies.[21, 49, 51, 52, 54, 57] Thus, the exact reason for the variations in topographic profile of PPCT is not clear and further studies on a wide range of age group are needed.

Determinants of Peripapillary Choroidal Thickness: Among the range of ocular factors studied, AL, IOP and presence of posterior staphyloma and chorio-retinal atrophy were the significant factors associated with PPCT

Longer Axial Length is associated with Thinner Peripapillary Choroid: PPCT was significantly thinner in eyes with longer AL. The possible reason might be the anatomic differences in eyes of different refractive status with more stretched and therefore thinner peripapillary choroid in longer eyes. Therefore, AL deserves consideration in a normative database of PPCT measurement and should be taken into account while interpreting the results.

Greater IOP is associated with Thicker Peripapillary Choroid: Interestingly, we found a positive association between PPCT and IOP in high myopes. Our results are in concordance with previous studies,[58] which using the pressure-volume relationship of the eye,[59] estimated that to produce an IOP increase of 5 mm Hg from the average IOP of 15 mm Hg, the choroid would need to expand uniformly by approximately 10 µm. Our subjects had a mean choroidal thickness increase of 2.38 µm for every mm

Hg increase in IOP supporting the conclusion that the IOP increase resulted from choroidal thickness increase.

Posterior Staphyloma is associated with Thinner Peripapillary Choroid: Similar to macular CT, we found presence of posterior staphyloma was significantly associated with choroidal thinning in high myopes in the peripapillary region as well.

9.4.3 Morphological and Vascular Analyses of the Choroid in High Myopes

Our study provides detailed phenotyping and characterization of the morphology and vasculature of the choroid in eyes with high myopia measured using image binarization from choroidal scans obtained using EDI-OCT. Our results indicate that while the choroidal thinning in high myopic eyes was associated with a reduction in both choroidal vascular and stromal areas, the primary component that was reduced was its stromal component. This was further supported by higher choroidal vascularity in myopic eyes compared to control eyes.

9.4.4 Visual Acuity is Independent of Choroidal Thickness

Our results suggest that CT alone is not an independent indicator of VA in these young, highly myopic eyes, and factors such as SE still remains to be more important predictors of BCVA.

Our finding of no independent association between sub-foveal CT and VA is in contrast to most of the previous hospital-based investigations.[27, 29, 30] Nishida and colleagues in 145 myopic eyes (≥ -6 D) with no other retinal or optic nerve pathology demonstrated CT to be an important predictor of VA. The discrepancy may be due to differences in age groups between our study and Nishida's study. Our study participants are much younger with mean age of 22 years compared to Nishida's study (mean age 57 years). With the advancing age, the choroid may undergo further age-related attenuation.[11, 13] Therefore in Nishida's study choroidal thinning is

attributed to dual factors: myopic refractive error and older age. In addition, with advancing age other myopic maculopathy and severity develop progressively,[60] which may lead to reduced VA. In contrast, our young subjects with relatively thicker choroid retained their visual function and therefore enjoyed better vision.

In the Beijing Eye Study,[31] better BCVA was found to be associated with thicker sub-foveal CT after adjusting for age, AL and other parameters. However, Beijing Eye Study is a population-based study with a mean age of participant's being 64.3 years and a mean refractive error (SE) of -0.18 D. The observed association between sub-foveal CT and VA could be due to residual confounding effects of AL which was taken as a binary variable (> 26 mm vs. <=26 mm).

Flores-Moreno and colleagues examined 60 eyes of 46 highly myopic subjects (SE ≥ -6 D; mean age 45.9 years) without macular diseases and found that in univariate analysis, BCVA (logMAR) was significantly correlated with thinner sub-foveal CT (correlation coefficient r = -0.36; p = 0.004). Similarly, Ho and coworkers evaluated 56 myopic subjects (SE ≥ -6 D; mean age 50.4 years) and found that in univariate analysis sub-foveal CT was correlated with logMAR VA (r^2 = 0.295, p = 0.008). In both studies the association between BCVA and sub-foveal CT was tested in univariate analysis only, without taking into account other potential confounders, such as SE, AL and other ocular comorbidities due to ageing. By contrast, our study involved younger subjects with little ocular comorbidity, and thus, the results are less complicated by confounding factors.

The results of our study are in concordance with the results of a recent study by Pang et al.[61] who reported no significant reduction in VA (mean VA = 20/30) in highly myopic eyes (mean AL = 30.7 mm) with extreme choroidal thinning (mean sub-foveal CT = 14 ±6 μm), suggesting CT alone is not a reliable indicator of visual

function. However, their study involved relatively small sample size (36 eyes of 20 myopic subjects) and older subjects (mean age of 71 years) with ocular comorbidities, and thus, their results may be complicated by confounding factors. In addition, use of manual calipers to measure very small CT might have introduced some measurement errors.

It is interesting that although previous studies[27, 29-31] have concluded sub-foveal CT to be inversely correlated to VA, this study has shown that there are clear exceptions to these observations. We did not find any significant association between decreased VA and thinner choroid in our young, extremely high myopic subjects with or without myopic maculopathy. Although retinal thickness was reduced in myopic eyes (average thickness 287 μm) than in a comparable group of control eyes (average thickness 307 μm), thinning of 20 μm may not be clinically meaningful and photoreceptor layer might not have been disrupted maintaining a fairly normal visual functions in adolescents and young adults with high myopia than their aged counterparts in which both severity of myopia and other myopic maculopathy increases with advancing age leading to reduced VA.

In myopic eyes with choroidal thinning, the good VA in face of thinner choroid may be explained by intact choroidal perfusion from larger patent choroidal vessels, which are typically in Haller's layer and located eccentric to the subfoveal area.[25] However, this study lacks choroidal blood flow measurements, and future studies of choroidal circulation will be useful to correlate CT with perfusion in normal eyes and in high myopes with choroidal thinning.

9.5 SUMMARY AND CONCLUSIONS

In summary, we found that macular and peripapillary CT is significantly lower in high myopic eyes over a range of eccentricities. Mean sub-foveal CT in myopes was 225.87 ± 5.51 μm as compared to 375.15 ± 6.58 μm in emmetropes. Mean PPCT in myopes was 142.62 ± 43.84 μm vs. 181.90 ± 46.43 μm in emmetropes. We demonstrated further decrease in macular and peripapillary CT with increase in severity of myopia.

Macular and peripapillary CT distribution follows a different profile in high myopia compared to emmetropes. Macular CT in myopic eyes was thickest superiorly whereas in emmetropes it was thickest at the fovea. However, in both the groups macular choroid was thinnest nasally. Peripapillary choroid was thickest at the superior location in myopic eyes, whereas in emmetropes it was thickest at the temporal location. However, in both the groups peripapillary choroid was thinnest inferiorly.

AL, presence of posterior staphyloma and chorio-retinal atrophy are the significant predictors of macular CT in high myopia. For PPCT; AL, IOP and presence of posterior staphyloma are independent determinants. These factors must be taken into account when interpreting the data on CT. Given the large number of people with myopia in the world, these findings seem to have widespread implications.

Our result demonstrates significant alterations in choroidal morphological and vascular features in high myopes. Choroidal thinning in high myopic eyes was associated with a reduction in both choroidal vascular and stromal areas, the primary component that was reduced was its stromal component. This was further supported by higher choroidal vascularity in myopic eyes compared to control eyes.

We further report that high myopic eyes had thinner choroid but CT is not an independent predictor of VA. Other factors related to myopia are likely responsible for the diminished VA in young highly myopic eyes.

9.6 STRENGTHS

The study has several strengths. Our EDI SD-OCT images were enhanced using adaptive compensation[33] to improve CSI visibility. Therefore, the CT measurements obtained in our study are likely more reliable and accurate. Our study is one of the most large-scale, prospective studies conducted to investigate the topography and predictors of macular and peripapillary CT in myopic subjects. Unlike other studies, our study included an emmetropic group and therefore we could examine the differences between highly myopic eyes and non-myopic eyes in our case-control study. Furthermore, we involved a group of young, healthy, male, Asian subjects of uniform age and were thus free of confounding factors.

9.7 LIMITATIONS

The study also has some limitations. Inclusion of only male Asian subjects may limit the application of our data to females and subjects of other groups or ethnicities. Further studies in other ethnic populations are warranted to confirm the results. Choroidal characteristics were assessed only in the right eye of each study subject. There may exist inter-eye differences, yet such differences should be small. Although our images were binarized at standard threshold, there is a possibility of over or under estimation of both vascular and avascular areas. Recently, diurnal fluctuation of choroidal thickness was reported[62] and this could have impacted our results, though any impact of diurnal variation should be randomly distributed among

myopic and emmetropic eyes. Another limitation is that the cause-effect relationship cannot be ascertained due to the cross-sectional nature of our study.

9.8 REFERENCES

1. Iwano M, Nomura H, Ando F, et al. Visual acuity in a community-dwelling Japanese population and factors associated with visual impairment. Jpn J Ophthalmol 2004;48(1):37-43.

2. Klaver CC, Wolfs RC, Vingerling JR, et al. Age-specific prevalence and causes of blindness and visual impairment in an older population: the Rotterdam Study. Arch Ophthalmol 1998;116(5):653-8.

3. Liu JH, Cheng CY, Chen SJ, Lee FL. Visual impairment in a Taiwanese population: prevalence, causes, and socioeconomic factors. Ophthalmic Epidemiol 2001;8(5):339-50.

4. Wu HM, Seet B, Yap EP, et al. Does education explain ethnic differences in myopia prevalence? A population-based study of young adult males in Singapore. Optom Vis Sci 2001;78(4):234-9.

5. Wong TY, Foster PJ, Hee J, et al. Prevalence and risk factors for refractive errors in adult Chinese in Singapore. Invest Ophthalmol Vis Sci 2000;41(9):2486-94.

6. Wong TY, Ferreira A, Hughes R, et al. Epidemiology and disease burden of pathologic myopia and myopic choroidal neovascularization: an evidence-based systematic review. Am J Ophthalmol 2014;157(1):9-25 e12.

7. Morgan IG, Ohno-Matsui K, Saw SM. Myopia. Lancet 2012;379(9827):1739-48.

8. Koh V, Yang A, Saw SM, et al. Differences in prevalence of refractive errors in young Asian males in Singapore between 1996-1997 and 2009-2010. Ophthalmic Epidemiol 2014;21(4):247-55.

9. Lim MC, Hoh ST, Foster PJ, et al. Use of optical coherence tomography to assess variations in macular retinal thickness in myopia. Invest Ophthalmol Vis Sci 2005;46(3):974-8.

10. Lam DS, Leung KS, Mohamed S, et al. Regional variations in the relationship between macular thickness measurements and myopia. Invest Ophthalmol Vis Sci 2007;48(1):376-82.

11. Fujiwara T, Imamura Y, Margolis R, et al. Enhanced depth imaging optical coherence tomography of the choroid in highly myopic eyes. Am J Ophthalmol 2009;148(3):445-50.

12. Ikuno Y, Tano Y. Retinal and choroidal biometry in highly myopic eyes with spectral-domain optical coherence tomography. Invest Ophthalmol Vis Sci 2009;50(8):3876-80.

13. Spaide RF. Enhanced depth imaging optical coherence tomography of retinal pigment epithelial detachment in age-related macular degeneration. Am J Ophthalmol 2009;147(4):644-52.

14. Neelam K, Cheung CM, Ohno-Matsui K, et al. Choroidal neovascularization in pathological myopia. Prog Retin Eye Res 2012;31(5):495-525.

15. Ohno-Matsui K, Kawasaki R, Jonas JB, et al. International photographic classification and grading system for myopic maculopathy. Am J Ophthalmol 2015;159(5):877-83 e7.

16. Jonas JB, Holbach L, Panda-Jonas S. Bruch's membrane thickness in high myopia. Acta Ophthalmol 2014.

17. Cheung CM, Loh BK, Li X, et al. Choroidal thickness and risk characteristics of eyes with myopic choroidal neovascularization. Acta Ophthalmol 2013;91(7):e580-1.

18. Linsenmeier RA, Padnick-Silver L. Metabolic dependence of photoreceptors on the choroid in the normal and detached retina. Invest Ophthalmol Vis Sci 2000;41(10):3117-23.

19. Hayreh SS. Blood supply of the optic nerve head and its role in optic atrophy, glaucoma, and oedema of the optic disc. Br J Ophthalmol 1969;53(11):721-48.

20. Yin ZQ, Vaegan, Millar TJ, et al. Widespread choroidal insufficiency in primary open-angle glaucoma. J Glaucoma 1997;6(1):23-32.

21. Roberts KF, Artes PH, O'Leary N, et al. Peripapillary choroidal thickness in healthy controls and patients with focal, diffuse, and sclerotic glaucomatous optic disc damage. Arch Ophthalmol 2012;130(8):980-6.

22. Curtin BJ. Posterior staphyloma development in pathologic myopia. Ann Ophthalmol 1982;14(7):655-8.

23. Curtin BJ, Karlin DB. Axial length measurements and fundus changes of the myopic eye. Am J Ophthalmol 1971;71(1 Pt 1):42-53.

24. Jonas JB, Gusek GC, Naumann GO. Optic disk morphometry in high myopia. Graefes Arch Clin Exp Ophthalmol 1988;226(6):587-90.

25. Nickla DL, Wallman J. The multifunctional choroid. Prog Retin Eye Res 2010;29(2):144-68.

26. Spaide RF, Koizumi H, Pozzoni MC. Enhanced depth imaging spectral-domain optical coherence tomography. Am J Ophthalmol 2008;146(4):496-500.

27. Ho M, Liu DT, Chan VC, Lam DS. Choroidal thickness measurement in myopic eyes by enhanced depth optical coherence tomography. Ophthalmology 2013;120(9):1909-14.

28. Flores-Moreno I, Lugo F, Duker JS, Ruiz-Moreno JM. The relationship between axial length and choroidal thickness in eyes with high myopia. Am J Ophthalmol 2013;155(2):314-9 e1.

29. Nishida Y, Fujiwara T, Imamura Y, et al. Choroidal thickness and visual acuity in highly myopic eyes. Retina 2012;32(7):1229-36.

30. Flores-Moreno I, Ruiz-Medrano J, Duker JS, Ruiz-Moreno JM. The relationship between retinal and choroidal thickness and visual acuity in highly myopic eyes. Br J Ophthalmol 2013;97(8):1010-3.

31. Shao L, Xu L, Wei WB, et al. Visual acuity and subfoveal choroidal thickness: the Beijing Eye Study. Am J Ophthalmol 2014;158(4):702-9 e1.

32. Garway-Heath DF, Rudnicka AR, Lowe T, et al. Measurement of optic disc size: equivalence of methods to correct for ocular magnification. Br J Ophthalmol 1998;82(6):643-9.

33. Gupta P, Sidhartha E, Girard MJ, et al. A simplified method to measure choroidal thickness using adaptive compensation in enhanced depth imaging optical coherence tomography. PLoS One 2014;9(5):e96661.

34. Girard MJ, Strouthidis NG, Ethier CR, Mari JM. Shadow removal and contrast enhancement in optical coherence tomography images of the human optic nerve head. Invest Ophthalmol Vis Sci 2011;52(10):7738-48.

35. Mari JM, Strouthidis NG, Park SC, Girard MJ. Enhancement of lamina cribrosa visibility in optical coherence tomography images using adaptive compensation. Invest Ophthalmol Vis Sci 2013;54(3):2238-47.

36. Vongphanit J, Mitchell P, Wang JJ. Prevalence and progression of myopic retinopathy in an older population. Ophthalmology 2002;109(4):704-11.

37. Curtin BJ, Karlin DB. Axial length measurements and fundus changes of the myopic eye. I. The posterior fundus. Trans Am Ophthalmol Soc 1970;68:312-34.

38. Curtin BJ. The posterior staphyloma of pathologic myopia. Trans Am Ophthalmol Soc 1977;75:67-86.

39. Niblack W. An Introduction to Digital Image Processing. Englewood Cliffs, New Jersey: Prentice Hall International Inc., 1986.

40. Fleiss JL, Cohen J. The Equivalence of Weighted Kappa and the Intraclass Correlation Coefficient as Measures of Reliability. Educational and Psychological Measurement 1973;33(3):613-9.

41. Margolis R, Spaide RF. A pilot study of enhanced depth imaging optical coherence tomography of the choroid in normal eyes. Am J Ophthalmol 2009;147(5):811-5.

42. Manjunath V, Taha M, Fujimoto JG, Duker JS. Choroidal thickness in normal eyes measured using Cirrus HD optical coherence tomography. Am J Ophthalmol 2010;150(3):325-9 e1.

43. Esmaeelpour M, Povazay B, Hermann B, et al. Three-dimensional 1060-nm OCT: choroidal thickness maps in normal subjects and improved posterior segment visualization in cataract patients. Invest Ophthalmol Vis Sci 2010;51(10):5260-6.

44. Goldenberg D, Moisseiev E, Goldstein M, et al. Enhanced depth imaging optical coherence tomography: choroidal thickness and correlations with age, refractive error, and axial length. Ophthalmic Surg Lasers Imaging 2012;43(4):296-301.

45. Sadler TW. Langman's Medical Embryology. 10th ed. ed. Baltimore: Lippincott Williams and Wilkins, 2006.

46. Yanoff M, Fine BS. Ocular Pathology: A Text and Atlas. 3rd ed. ed: JB Lippincott, 1989.

47. Quaranta M, Arnold J, Coscas G, et al. Indocyanine green angiographic features of pathologic myopia. Am J Ophthalmol 1996;122(5):663-71.

48. Moriyama M, Ohno-Matsui K, Futagami S, et al. Morphology and long-term changes of choroidal vascular structure in highly myopic eyes with and without posterior staphyloma. Ophthalmology 2007;114(9):1755-62.

49. Huang W, Wang W, Zhou M, et al. Peripapillary choroidal thickness in healthy Chinese subjects. BMC Ophthalmol 2013;13:23.

50. Oh J, Yoo C, Yun CM, et al. Simplified method to measure the peripapillary choroidal thickness using three-dimensional optical coherence tomography. Korean J Ophthalmol 2013;27(3):172-7.

51. Tanabe H, Ito Y, Terasaki H. Choroid is thinner in inferior region of optic disks of normal eyes. Retina 2012;32(1):134-9.

52. Ho J, Branchini L, Regatieri C, et al. Analysis of normal peripapillary choroidal thickness via spectral domain optical coherence tomography. Ophthalmology 2011;118(10):2001-7.

53. Schoenwolf G, Bleyl S, Brauer P, P F-W. Larsen's human Embrology. Philadelphia: Elsevier, 2009.

54. Hirooka K, Tenkumo K, Fujiwara A, et al. Evaluation of peripapillary choroidal thickness in patients with normal-tension glaucoma. BMC Ophthalmol 2012;12:29.

55. Usui S, Ikuno Y, Miki A, et al. Evaluation of the choroidal thickness using high-penetration optical coherence tomography with long wavelength in highly myopic normal-tension glaucoma. Am J Ophthalmol 2012;153(1):10-6 e1.

56. Hsiang HW, Ohno-Matsui K, Shimada N, et al. Clinical characteristics of posterior staphyloma in eyes with pathologic myopia. Am J Ophthalmol 2008;146(1):102-10.

57. Li L, Bian A, Zhou Q, Mao J. Peripapillary choroidal thickness in both eyes of glaucoma patients with unilateral visual field loss. Am J Ophthalmol 2013;156(6):1277-84 e1.

58. Arora KS, Jefferys JL, Maul EA, Quigley HA. Choroidal thickness change after water drinking is greater in angle closure than in open angle eyes. Invest Ophthalmol Vis Sci 2012;53(10):6393-402.

59. Silver DM, Geyer O. Pressure-volume relation for the living human eye. Curr Eye Res 2000;20(2):115-20.

60. Chang L, Pan CW, Ohno-Matsui K, et al. Myopia-related fundus changes in Singapore adults with high myopia. Am J Ophthalmol 2013;155(6):991-9 e1.

61. Pang CE, Sarraf D, Freund kb. Extreme choroidal thinning in high myopia. Retina 2014.

62. Tan CS, Ouyang Y, Ruiz H, Sadda SR. Diurnal variation of choroidal thickness in normal, healthy subjects measured by spectral domain optical coherence tomography. Invest Ophthalmol Vis Sci 2012;53(1):261-6.

63. Takahashi A, Ito Y, Iguchi Y, et al. Axial length increases and related changes in highly myopic normal eyes with myopic complications in fellow eyes. Retina 2012;32(1):127-33.

64. Chen W, Wang Z, Zhou X, et al. Choroidal and photoreceptor layer thickness in myopic population. Eur J Ophthalmol 2012;22(4):590-7.

CHAPTER IX TABLES

Table 9.1 Baseline characteristics of study subjects for macular choroidal thickness

	Myopes (n=520)	Emmetropes (n=128)	P value
Age, years	21.59 (1.15)	22.06 (0.97)	<0.001
Axial length, mm	27.32 (1.16)	23.69 (0.62)	<0.001
Anterior chamber depth, mm	3.74 (0.25)	3.46 (0.27)	<0.001
Corneal curvature, mm	7.76 (0.25)	7.85 (0.41)	0.137
Spherical equivalent, D	-8.68 (2.05)	0.12 (0.24)	<0.001
Best corrected visual acuity Log MAR	0.01 (0.08)	-0.09 (0.06)	<0.001
Log low luminance contrast sensitivity	0.36 (0.28)	0.50 (0.20)	<0.001
Log high luminance contrast sensitivity	0.66 (0.33)	0.88 (0.21)	<0.001
Intraocular pressure, mmHg	16.12 (2.94)	15.26 (2.74)	0.002

Data are means (standard deviations).

Table 9.2 Intra-grader reliability of macular choroidal thickness measurements at different locations in myopic and emmetropic group

	Myopes		Emmetropes	
Locations of measurement	ICC (95% CI)	Mean difference (μm)* (SD)	ICC (95% CI)	Mean difference (μm)* (SD)
Choroidal thickness				
Sub-foveal	0.98 (0.96 to 0.99)	9.9 (11.3)	0.97 (0.95 to 0.99)	11.5 (17.7)
Nasal, 1.5 mm	0.96 (0.93 to 0.98)	9.6 (14.8)	0.96 (0.93 to 0.98)	10.1 (20.6)
Nasal, 3 mm	0.94 (0.87 to 0.97)	8.0 (14.4)	0.96 (0.93 to 0.98)	-15.0 (20.8)
Temporal, 1.5 mm	0.97 (0.93 to 0.98)	9.1 (14.8)	0.97 (0.94 to 0.98)	14.3 (19.4)
Temporal, 3 mm	0.97 (0.94 to 0.98)	10.8 (13.0)	0.96 (0.91 to 0.98)	11.1 (18.5)
Superior, 1.5 mm	0.96 (0.93 to 0.98)	-7.5 (16.2)	0.95 (0.90 to 0.98)	13.2 (20.4)
Superior, 3 mm	0.95 (0.90 to 0.98)	9.2 (17.8)	0.97 (0.94 to 0.99)	-14.9 (17.2)
Inferior, 1.5 mm	0.97 (0.95 to 0.99)	11.0 (13.5)	0.96 (0.92 to 0.98)	14.7 (18.0)
Inferior, 3 mm	0.96 (0.93 to 0.98)	-8.6 (17.0)	0.97 (0.94 to 0.99)	13.1 (18.5)

ICC= intra-class correlation coefficient; CI= confidence interval; SD = standard deviation.
*Mean difference was determined from the 1st measurement minus 2nd measurement.

Table 9.3 Distribution of mean adjusted macular choroidal thickness (CT) at different locations across the myopic and control groups using generalized linear model

Location	Emmetropes (n=128)	Myopia, -6 to -8(D) (n=233)	Myopia, <-8 to -10(D) (n=169)	Myopia, <-10(D) (n=118)	All Myopes (n=520)	Changes in CT across 3 myopic groups	
						† Beta	† P trend
Subfoveal	375.15 (6.58)	241.54 (6.63)	223.90 (7.14)	210.60 (7.13)	225.87 (5.51)	-15.74	<0.001
Nasal, 1.5 mm	324.01 (6.59)	187.01 (6.17)	165.27 (6.66)	150.70 (6.64)	168.35 (5.18)	-18.60	<0.001
Nasal, 3 mm	238.25 (6.72)	121.19 (4.76)	106.90 (5.13)	97.13 (5.12)	108.85 (3.97)	-12.30	<0.001
Temporal, 1.5 mm	359.27 (6.51)	249.52 (6.38)	235.82 (6.87)	223.47 (6.85)	236.64 (5.27)	-13.10	<0.001
Temporal, 3 mm	328.41 (6.04)	251.51 (6.02)	243.83 (6.49)	235.77 (6.47)	243.88 (4.94)	-07.84	<0.001
Superior, 1.5 mm	365.01 (5.66)	263.84 (7.05)	250.70 (7.59)	238.81 (7.57)	251.47 (5.81)	-12.59	<0.001
Superior, 3 mm	358.03 (5.74)	278.23 (7.25)	263.61 (7.81)	254.64 (7.79)	265.97 (5.97)	-12.14	<0.001
Inferior, 1.5 mm	358.93 (6.14)	243.27 (6.32)	219.94 (6.81)	202.87 (6.79)	222.74 (5.32)	-20.59	<0.001
Inferior, 3 mm	339.41 (6.30)	232.76 (6.25)	214.86 (6.74)	199.84 (6.72)	216.32 (5.21)	-16.63	<0.001
	P<0.001*	P<0.001*	P<0.001*	P<0.001*	P<0.001*		

Data are mean (standard error) in µm, adjusted for presence of posterior staphyloma and chorio-retinal atrophy.

† Adjusted for presence of posterior staphyloma and chorio-retinal atrophy.

*Repeated measures ANOVA, comparing the distribution of choroidal thickness across fovea, nasal (3 mm), temporal (3 mm), superior (3 mm), and inferior (3 mm) locations.

CT=choroidal thickness.

Table 9.4 Association of ocular factors with sub-foveal choroidal thickness in all myopes (n =520)

	Univariate analysis			Multivariate analysis		
	Unstandardized β Coefficient	**Standardized β Coefficient**	**P-value**	**Unstandardized β Coefficient**	**Standardized β Coefficient**	**P-value**
Ocular factors						
Spherical equivalent, D	13.109	0.348	<0.001	-	-	-
Axial length, mm	-32.319	-0.489	<0.001	-24.232	-0.370	**<0.001**
Corneal curvature, mm	-84.318	-0.279	<0.001	0.397	0.001	0.975
Anterior chamber depth, mm	-8.200	-0.027	0.541	-	-	-
Intraocular pressure, mmHg	0.714	0.027	0.535	-	-	-
Posterior Staphyloma	-22.698	-0.443	<0.001	-15.642	-0.306	**<0.001**
Chorio-retinal atrophy	-26.910	-0.289	<0.001	-10.585	-0.114	**0.003**

Table 9.5 Clinical characteristics of the study subjects for peripapillary choroidal thickness

	Myopes (n=448)	Emmetropes (n=116)	P value*
Age, years	21.63 (1.15)	22.03 (0.96)	<0.001
Axial length, mm	27.23 (1.07)	23.70 (0.61)	<0.001
Anterior chamber depth, mm	3.74 (0.25)	3.46 (0.27)	<0.001
Corneal curvature, mm	7.76 (0.25)	7.81 (0.41)	0.123
Spherical equivalent, D	-8.52 (1.80)	0.11 (0.24)	<0.001
Best corrected visual acuity, logMAR	0.01 (0.07)	-0.09 (0.06)	<0.001
Intraocular pressure, mmHg	16.11 (2.95)	15.22 (2.64)	0.003
RNFL thickness, µm	87.21 (8.94)	103.76 (9.99)	<0.001

Data presented are means (standard deviations).
D = dioptre; logMAR = logarithm of the minimum angle of resolution; RNFL = retinal nerve fiber layer thickness.
*Based on independent sample t-test.

Table 9.6 Intra-grader reliability of peripapillary choroidal thickness measurements at different locations in myopic and emmetropic group

Locations of measurement	Myopes ICC (95% CI)	Emmetropes ICC (95% CI)
Peripapillary choroidal thickness		
Temporal, 360°	0.97 (0.92 to 0.98)	0.96 (0.90 to 0.98)
Superotemporal, 45°	0.97 (0.94 to 0.99)	0.98 (0.95 to 0.99)
Superior, 90°	0.98 (0.96 to 0.99)	0.96 (0.90 to 0.98)
Superionasal, 135°	0.98 (0.96 to 0.99)	0.97 (0.92 to 0.98)
Nasal, 180°	0.97 (0.93 to 0.99)	0.96 (0.90 to 0.98)
Inferonasal, 225°	0.96 (0.92 to 0.98)	0.96 (0.91 to 0.98)
Inferior, 270°	0.96 (0.91 to 0.98)	0.95 (0.88 to 0.98)
Inferotemporal, 315°	0.96 (0.90 to 0.98)	0.96 (0.90 to 0.98)

ICC = Intraclass correlation coefficient; CI = confidence interval.

Table 9.7 Distribution of mean peripapillary choroidal thickness at different locations across the three myopic and control groups

Locations	Emmetropes (n = 116)	High Myopia				
		All (n = 448)	SE <-6 to -8 D (n = 211)	SE <-8 to -10 D (n = 143)	SE <-10 D (n = 94)	P for trend†
Temporal, 360°	207.00 (58.01)	138.47 (58.57)	151.30 (62.21)	132.45 (51.00)	118.85 (54.41)	<0.001
Superotemporal, 45°	201.89 (53.13)	150.32 (54.10)	160.10 (57.14)	144.51 (49.02)	137.23 (50.82)	<0.001
Superior, 90°	188.18 (50.17)	163.41 (50.43)	170.60 (52.08)	160.88 (47.30)	151.14 (49.03)	<0.001
Superionasal, 135°	189.15 (52.85)	162.21 (50.50)	169.58 (52.26)	159.19 (47.63)	150.24 (48.45)	<0.001
Nasal, 180°	189.24 (53.17)	161.97 (51.82)	170.66 (55.30)	157.36 (47.22)	149.51 (47.30)	<0.001
Inferonasal, 225°	168.68 (50.38)	137.82 (46.16)	146.83 (50.15)	132.62 (41.11)	125.53 (40.04)	<0.001
Inferior, 270°	137.90 (44.53)	109.98 (37.30)	117.01 (39.41)	106.91 (33.54)	98.88 (34.80)	<0.001
Inferotemporal, 315°	173.17 (52.10)	116.81 (49.12)	128.19 (54.12)	110.73 (41.25)	100.52 (42.05)	<0.001
Average	181.90 (46.43)	142.62 (43.84)	151.78 (46.79)	138.08 (38.53)	128.99 (40.20)	<0.001
	P<0.001*	P<0.001*	P<0.001*	P<0.001*	P<0.001*	

Data presented are mean (standard deviations) in μm.

* Repeated Measures ANOVA, comparing the distribution of peripapillary choroidal thickness at various locations within each group.

† Peripapillary choroidal thickness varied significantly across the myopic sub-groups and the emmetropic group at all the locations (p for trend <0.001 for all locations).

Table 9.8 Association of ocular factors with average peripapillary choroidal thickness in all myopes (n = 448)

	Univariate analysis			Multivariate analysis		
	Unstandardized β Coefficient	**Standardized β Coefficient**	**P-value**	**Unstandardized β Coefficient**	**Standardized β Coefficient**	**P-value**
Ocular factors						
Age, years	-0.412	-0.011	0.818	-	-	-
Spherical equivalent, D	5.396	0.222	<0.001	-	-	-
Axial length, mm	-13.029	-0.319	<0.001	-7.090	-0.175	**0.001**
Corneal curvature, mm	-36.720	-0.216	<0.001	-4.456	-0.026	0.602
Anterior chamber depth, mm	-3.989	-0.023	0.631	-	-	-
Intraocular pressure, mmHg	1.407	0.095	0.045	1.628	0.111	**0.006**
Average RNFL thickness, µm	0.745	0.152	0.001	0.287	0.059	0.156
Posterior staphyloma	-15.296	-0.519	<0.001	-12.160	-0.433	**<0.001**
Chorio-retinal atrophy	-14.768	-0.247	<0.001	-0.533	-0.089	**0.032**
Tilted disc	-2.814	-0.081	0.088	-	-	-

D = dioptre; RNFL = retinal nerve fiber layer thickness.
For multivariate analysis after adjusting for age there was no change in the result.

Table 9.9 Clinical characteristic of study subjects with high myopia (n=515 eyes) and controls with emmetropia (n=88 eyes).

	Subjects with High Myopia (n=515 eyes)	**Controls with Emmetropia (n=88 eyes)**	**P-value[a]**
Age, years	21.59 (1.15)	22.02 (1.05)	**0.001**
Axial length, mm	27.31 (1.14)	23.70 (0.63)	**<0.001**
Corneal curvature, mm	7.76 (0.25)	7.85 (0.41)	**<0.001**
Spherical equivalent, Diopter	-8.66 (2.00)	0.13 (0.24)	**<0.001**
BCVA, LogMAR	0.01 (0.08)	-0.10 (0.06)	**<0.001**
Intraocular pressure, mmHg	16.12 (2.90)	15.19 (2.74)	**0.005**

Data presented are means (standard deviations).
BCVA=best corrected visual acuity; LogMAR = logarithm of the minimum angle of resolution.
[a]Based on independent sample t-test.

Table 9.10 Choroidal morphologic and vascular characteristics in high myopic and control eyes.

Choroidal Characteristics	Subjects with High Myopia (n=515 eyes)	Control with Emmetropia (n=88 eyes)	P-value[a]
MORPHOLOGICAL			
Mean choroidal thickness, µm	257.19 (68.23)	371.33 (63.35)	<**0.001**
Choroidal volume, mm^3	7.27 (1.92)	10.49 (1.79)	<**0.001**
Thickest point distance from fovea, mm	-1.51 (1.42)	-0.53 (1.06)	<**0.001**
VASCULAR			
Sub Foveal (1.5 mm region)			
Total choroidal area, mm^2	0.416 (0.114)	0.608 (0.102)	<**0.001**
Vascular area, mm^2	0.236 (0.059)	0.314 (0.044)	<**0.001**
Stromal area, mm^2	0.179 (0.062)	0.293 (0.066)	<**0.001**
Choroidal vascularity	0.575 (0.057)	0.520 (0.040)	<**0.001**
Macular (6 mm region)			
Total choroidal area, mm^2	1.543 (0.409)	2.228 (0.380)	<**0.001**
Vascular area, mm^2	0.851 (0.211)	1.156 (0.167)	<**0.001**
Stromal area, mm^2	0.692 (0.212)	1.071 (0.233)	<**0.001**
Choroidal vascularity	0.554 (0.040)	0.522 (0.033)	<**0.001**

Data presented are means (standard deviations) or number (%).
[a]Based on independent sample t-test.

Table 9.11 Multiple regression analysis of choroidal attributes such as vascular area, stromal area and vascularity (dependent variables) in high myopic eyes (n=515) with reference to control eyes (n=88).

	Vascular Area, mm^2		**Stromal Area, mm^2**		**Choroidal Vascularity**	
Sub Foveal (1.5 mm region)	**Beta (95% CI)**	**P-value**	**Beta (95% CI)**	**P-value**	**Beta (95% CI)**	**P-value**
Model 1	-0.078 (-0.091, -0.065)	<0.001	-0.114 (-0.129, -0.100)	<0.001	0.054 (0.042, 0.067)	<0.001
Model 2	0.013 (0.007, 0.018)	<0.001	-0.013 (-0.018, -0.007)	<0.001	--	--
Macular (6 mm region)						
Model 1	-0.306 (-0.353, -0.259)	<0.001	-0.377 (-0.426, -0.328)	<0.001	0.032 (0.023, 0.041)	<0.001
Model 2	0.027 (0.012, 0.042)	0.001	-0.027 (-0.042, -0.012)	0.001	--	--

Beta represents differences in choroidal vascular area, stromal area and vascularity in high myopic eyes with reference to control eyes.
Model 1: adjusted for age.
Model 2: adjusted for age and choroidal thickness. However, choroidal vascularity was only adjusted for age.
CI: confidence interval.

Table 9.12 Association of axial length with choroidal traits such as vascular area, stromal area and vascularity (dependent variables) in high myopic eyes (n=515).

	Vascular Area, mm^2			Stromal Area, mm^2			Choroidal vascularity		
	Beta (95% CI)	**Standardized Beta**	**P-value**	**Beta (95% CI)**	**Standardized Beta**	**P-value**	**Beta (95% CI)**	**Standardized Beta**	**P-value**
Sub Foveal (1.5 mm)	-0.020 (-0.025, -0.016)	-0.396	**<0.001**	-0.023 (-0.027, -0.019)	-0.421	**<0.001**	0.011 (0.007, 0.016)	0.229	**<0.001**
Macular (6 mm)	-0.077 (-0.092, -0.063)	-0.418	**<0.001**	-0.081 (-0.095, -0.066)	-0.433	**<0.001**	0.007 (0.004, 0.010)	0.210	**<0.001**

Beta represents change in choroidal traits (vascular area, stromal area and vascularity) per mm change in axial length in high myopic eyes.
CI: confidence interval.

Table 9.13 Baseline characteristics of extremely high (<-10 D) myopic subjects

	Myopes (n=105)	**Emmetropes (n=55)**	**P-value***
Age, years	21.51 (1.22)	21.96 (0.89)	0.033
Axial length, mm	28.46 (1.23)	23.65 (0.58)	<0.001
Anterior chamber depth, mm	3.74 (0.22)	3.47 (0.29)	<0.001
Corneal curvature, mm	7.76 (0.24)	7.79 (0.44)	0.686
Spherical equivalent, Diopter	-11.56 (2.04)	0.14 (0.25)	<0.001
BCVA, LogMAR	0.07 (0.09)	-0.10 (0.05)	<0.001
Intraocular pressure, mmHg	16.42 (3.04)	15.28 (2.78)	0.035

Data presented are means (standard deviations).
BCVA=best corrected visual acuity; LogMAR = logarithm of the minimum angle of resolution.
*P value was obtained with independent sample t-test.

Table 9.14 Distribution of choroidal and retinal thicknesses at different locations across the extremely high myopic (<-10D) and control groups

	Choroidal Thickness			Retinal Thickness		
Locations	High Myopes (n=105)	Emmetropes (n=55)	P-Value*	Myopes (n=105)	Emmetropes (n=55)	P-Value*
Subfoveal	194.81 (57.78)	377.98 (77.61)	<0.001	237.19 (22.24)	224.36 (19.31)	<0.001
Nasal, 1.5 mm	136.69 (54.650	325.67 (71.93)	<0.001	338.51 (24.22)	361.70 (21.19)	<0.001
Nasal, 3 mm	87.34 (39.39)	237.10 (69.49)	<0.001	291.00 (31.56)	312.90 (22.05)	<0.001
Temporal, 1.5 mm	210.48 (60.17)	358.60 (73.62)	<0.001	315.84 (19.11)	337.94 (13.72)	<0.001
Temporal, 3 mm	225.30 (62.57)	316.69 (68.28)	<0.001	250.47 (27.89)	273.67 (14.73)	<0.001
Superior, 1.5 mm	225.67 (76.06)	370.58 (67.58)	<0.001	327.36 (19.89)	349.70 (23.92)	<0.001
Superior, 3 mm	242.82 (84.77)	355.63 (72.81)	<0.001	273.15 (20.14)	288.10 (13.14)	<0.001
Inferior, 1.5 mm	188.21 (60.68)	362.23 (67.49)	<0.001	316.29 (19.13)	344.52 (16.90)	<0.001
Inferior, 3 mm	188.50 (69.05)	338.50 (81.60)	<0.001	259.16 (18.46)	274.43 (13.99)	<0.001
Average	188.85 (55.78)	338.11 (59.69)	<0.001	287.39 (31.75)	307.48 (18.87)	<0.001

Data presented are means (standard deviations) in µm.

*P-value was obtained from independent sample T-test.

†For both choroidal and retinal thicknesses repeated measures ANOVA showed significant difference between the mean location measures within myopes and emmetropes.

Table 9.15 Association of subfoveal choroidal thickness with best corrected visual acuity in young, extremely high myopic eyes (SE<-10D, n = 105)

	Best corrected visual acuity (LogMAR)		
	B	**95% CI**	**P-value**
Model 1			
SFCT	-0.039	-0.070 to -0.008	0.015
Model 2			
SFCT + SE	0.005	-0.027 to 0.037	0.761
Model 3			
SFCT + SE + presence of any pathological myopia lesions*	-0.001	-0.036 to 0.033	0.937

Model 1: univariate
Model 2: adjusted for SE
Model 3: adjusted for SE and presence of any pathological myopia lesions* (posterior staphyloma, lacquer cracks or chorio-retinal atrophy).
SFCT was analysed per 100 μm.
SFCT = subfoveal choroidal thickness (μm); SE = spherical equivalent (diopter); LogMAR = logarithm of minimal angle of resolution.

Table 9.16 Summary of macular choroidal thickness and other variables in various studies in high myopia

Study	No of eyes	Mean age, years	AL, mm	SE, diopters	OCT Machine	EDI (Yes/No)	Mean CT,* µm
Current study	520	21.59	27.32	-8.68	Spectralis SD-OCT	Yes	225.87 (5.51)
Flores-Moreno et al. 2013[28]	120	54.4	29.17	-14.34	Topcon 3D-2000 OCT	No	115.5 (85.3)
Fujiwara et al. 2009[11]	55	59.7	-	-11.9	Spectralis SD-OCT	Yes	93.2 (62.5)
Ikuno et al. 2009[12]	31	51.7	29.6	-15.5	Cirrus SD-OCT	No	99.3 (58.8)
Takahashi et al. 2012[63]	20	63.4	28.37	-10.8	Cirrus SD-OCT	No	68.1 (10.5)
Chen et al. 2012[64]	20	28.8	-	-9.29	Spectralis SD-OCT	Yes	156.07 (86.3)

EDI = enhanced depth imaging; SD-OCT = spectral domain optical coherence tomography; AL = axial length; CT = choroidal thickness; SE = spherical equivalent; "-"not available.

* Data are mean (SD) except current study which is mean (standard error).

Table 9.17 Summary of peripapillary choroidal thickness and other variables in various studies in normal eyes

Study	No of eyes	Mean age, years	AL, mm	SE, diopters	OCT Machine	EDI (Yes/No)	Mean PPCT,* µm
Current study (Myopes)	448	21.63 (1.15)	27.23 (1.07)	-8.52 (1.80)	Spectralis SD-OCT	Yes	142.62 (43.84)
Current study (Emmetropes)	116	22.03 (0.96)	23.70 (0.61)	0.11 (0.24)	Spectralis SD-OCT	Yes	181.90 (46.43)
Huang et al. 2013[13]	76	56.95 (12.99)	23.20	0.31 (1.12)	Spectralis SD-OCT	Yes	165.03 (40.37)
Oh et al. 2013[14]	40	41.2 (20.6)	-	-0.4 (1.1)	Topcon 3D- OCT	No	191.2 (62)
Tanabe et al. 2012[11]	28	54.1 (20.0)	-	-3.6 (4.1)	Spectralis SD-OCT	Yes	-
Ho et al. 2011[12]	36	48 (16)	-	-	Cirrus SD-OCT	No	-

AL = axial length; SE = spherical equivalent; EDI = enhanced depth imaging; PPCT = peripapillary choroidal thickness; "-" not available.
* Data presented are means (standard deviations).

CHAPTER IX FIGURES

Figure 9.1 Enhanced depth imaging optical coherence tomography image demonstrating peripapillary region scanned using a 360°, 3.5 mm diameter circle centered on the optic disc. The peripapillary choroidal thickness was measured as the perpendicular distance between Bruch's membrane and the choroid-scleral interface at the following locations: T = temporal; ST = superotemporal; S = superior; SN = superonasal; N = nasal; IN = inferonasal; I = inferior; IT = inferotemporal.

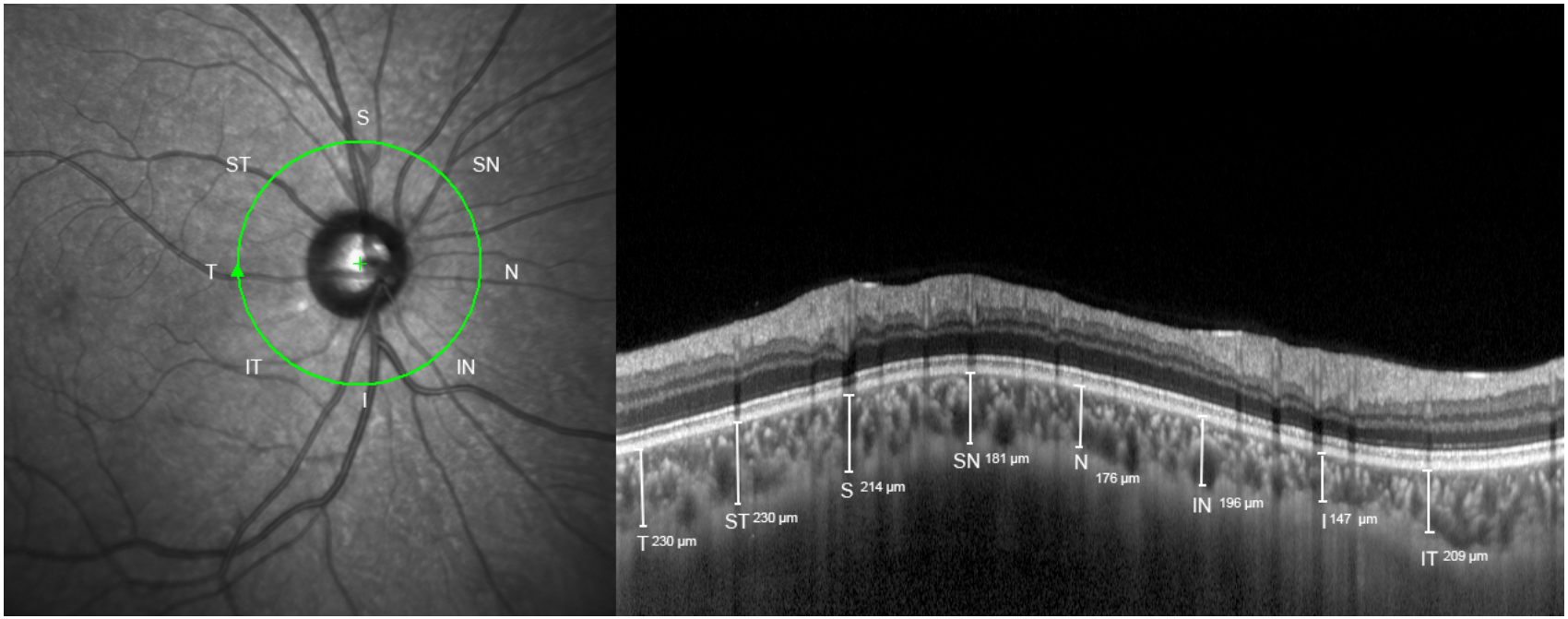

Figure 9.2 Comparison of EDI-OCT scans of choroidal thickness between emmetrope and myope. **(A)** A 22-year-old male with no refractive error (AL = 23.61 mm) and an average choroidal thickness of 325 µm. **(B)** A 23-year-old male with SE of -12.25D (AL = 29.35 mm) and an average choroidal thickness of 117 µm.

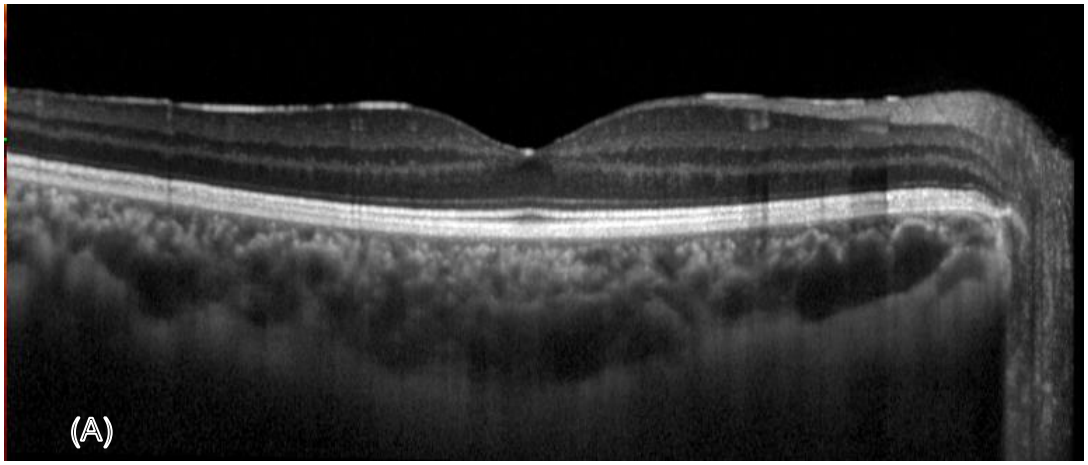

(A) A 22-year-old male with no refractive error (AL = 23.61 mm) and an average choroidal thickness of 325 µm.

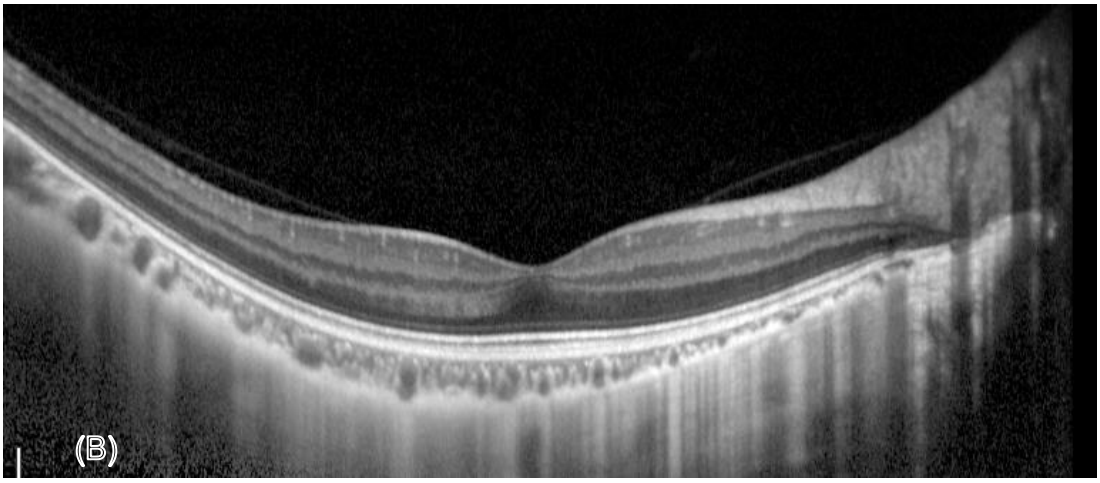

(B) A 23-year-old male with SE of -12.25D (AL = 29.35 mm) and an average choroidal thickness of 117 µm.

Figure 9.3 shows the presence of posterior staphyloma on horizontal scan of the macular central on the fovea (20°) obtained using SD-OCT.

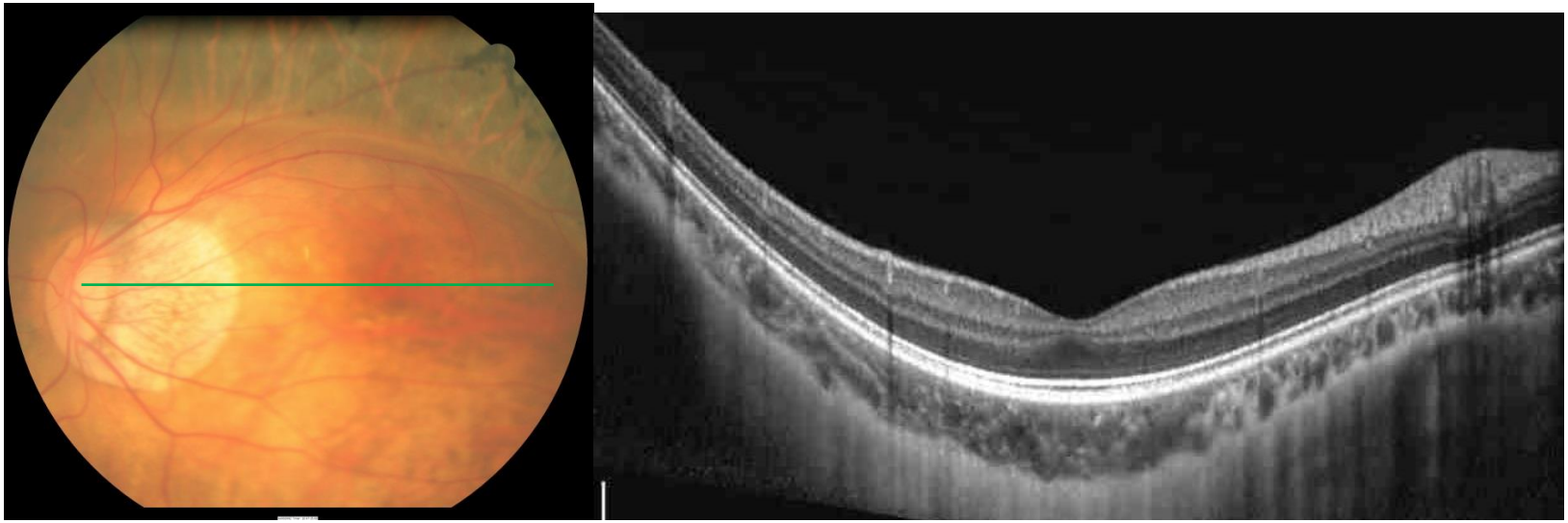

Figure 9.4 Visualization of choroid morphological and vascular parameters obtained by our custom-written application on MATLAB on choroidal images acquired by EDI, SD-OCT.

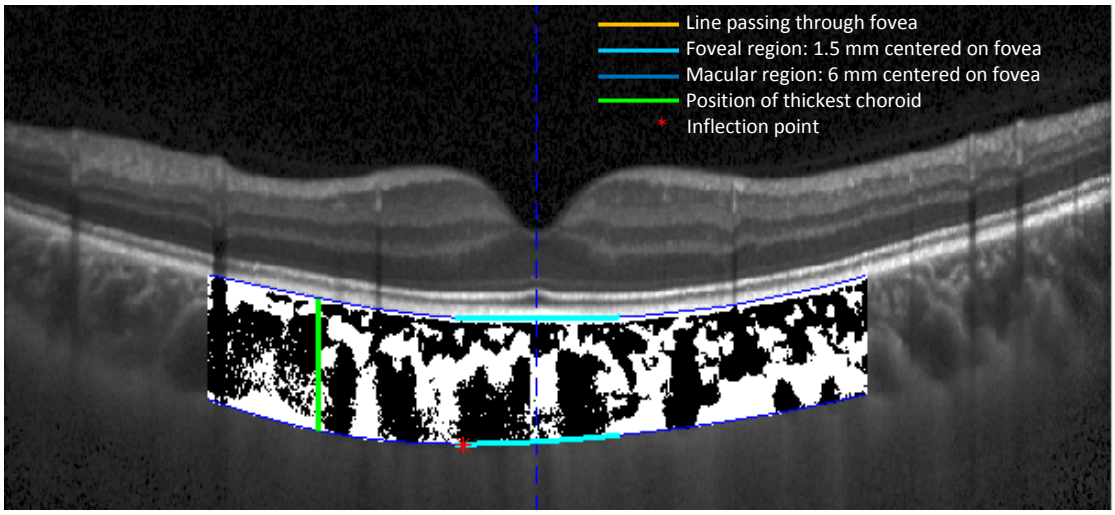

Figure 9.5 Validation of Niblack binarization against manual delineation of stromal areas; (A) Original choroid cross-sectional scans with RPE choroid-scleral boundaries; (B) Identification of choroid vasculature by automated binarization with overlayed manual delineation of four blood vessels.

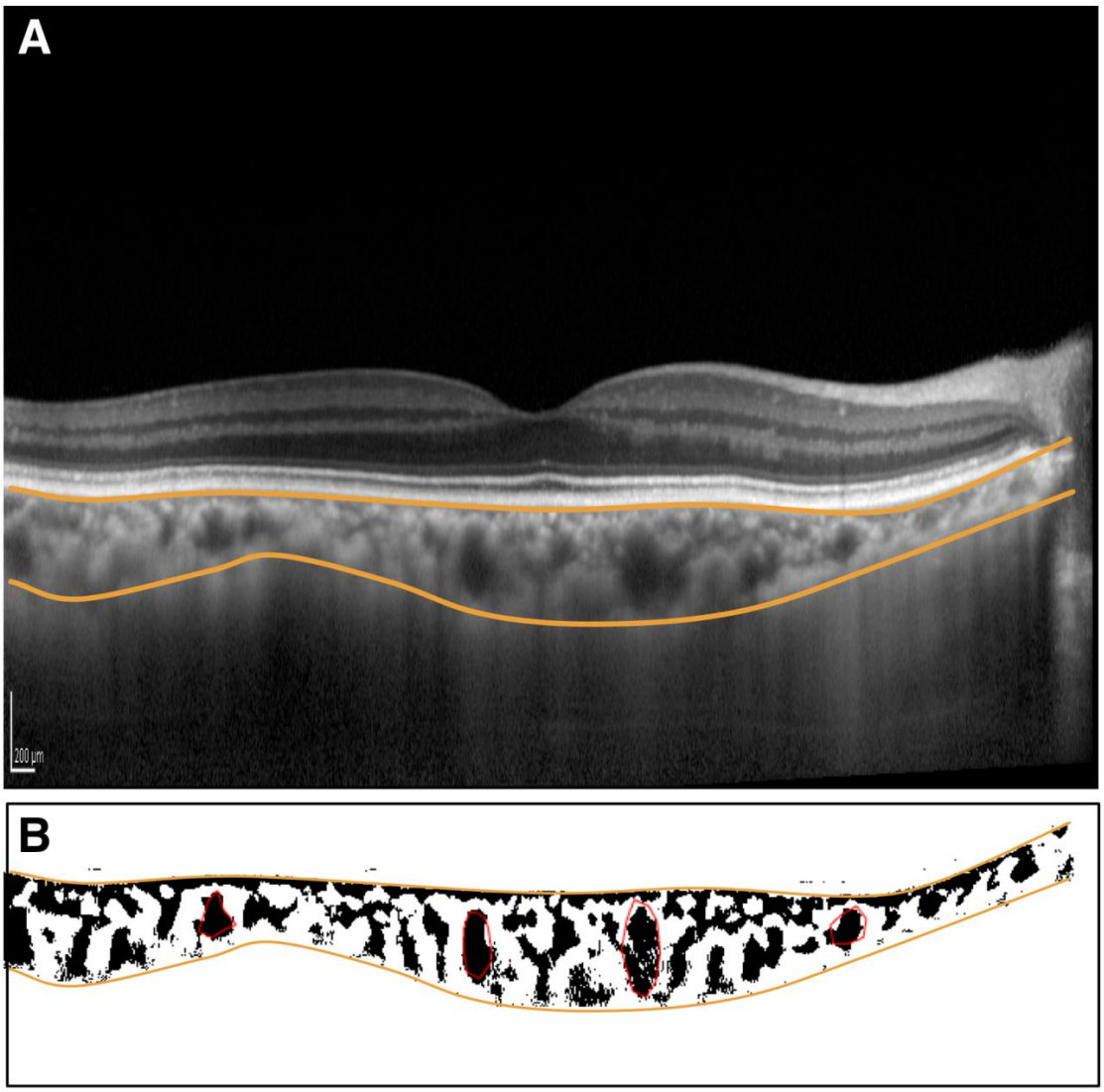

Figure 9.6 Graph showing the differences in macular choroidal thickness in the high myopic groups and emmetropic group along the horizontal axis (**A**) and vertical axis (**B**). Mean thickness at each of the nasal, temporal, superior, and inferior locations measured at 1.5 mm and 3 mm intervals eccentric to the sub-foveal area. Error bars indicate standard error. SFCT is sub-foveal choroidal thickness.

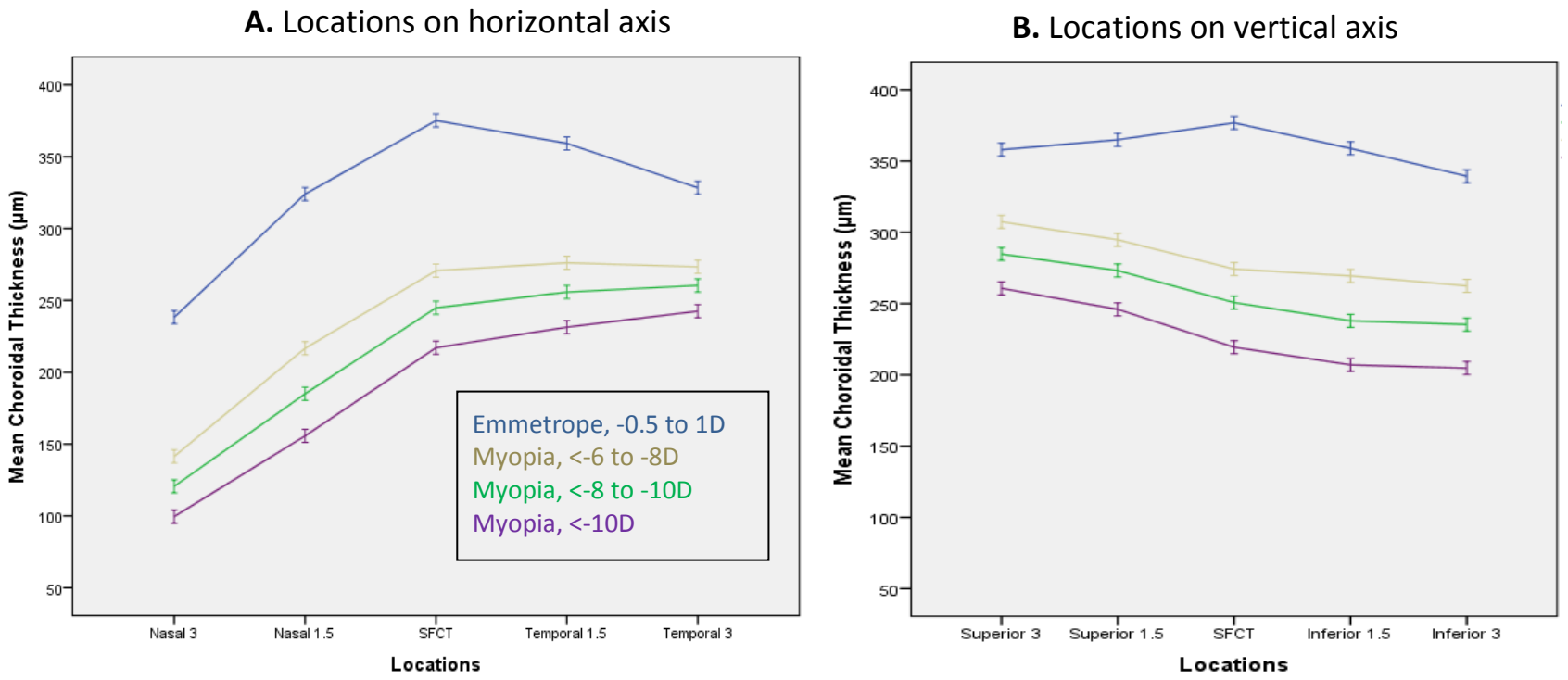

Figure 9.7 (**A**) Scatterplot showing negative correlation between subfoveal choroidal thickness and axial length in all myopes. (**B**). Scatterplot showing positive correlation between subfoveal choroidal thickness and spherical equivalent in all myopes. (**C**). Scatterplot showing negative correlation between subfoveal choroidal thickness and corneal curvature in all myopes.

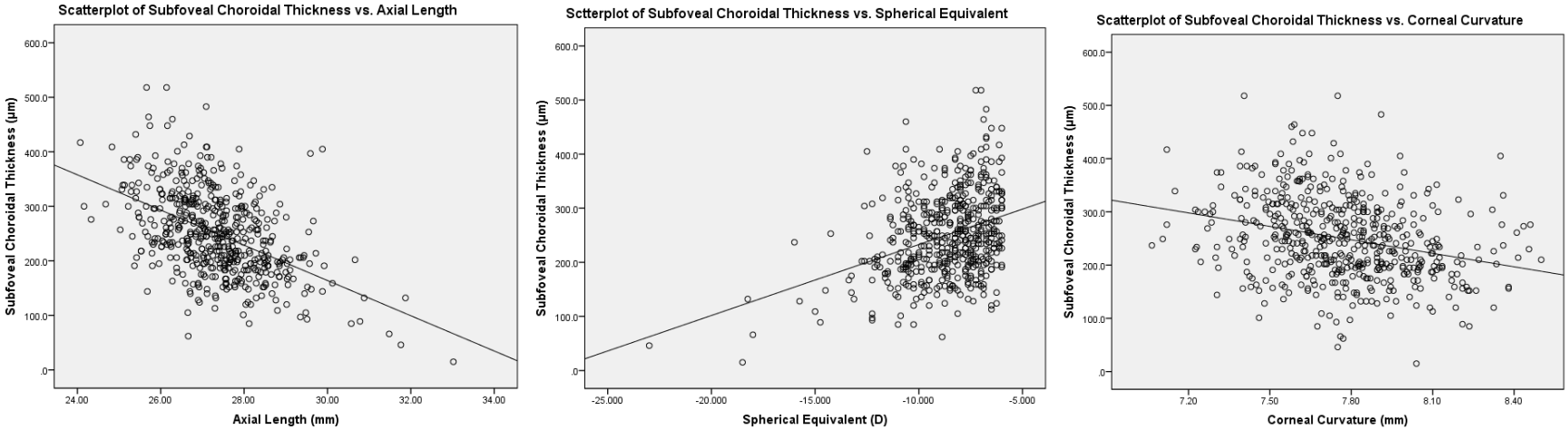

Figure 9.8 (**A**) Scatterplot showing negative correlation between LogMAR visual acuity and subfoveal choroidal thickness in all myopes. (**B**). Scatterplot showing negative correlation between Log contrast sensitivity and subfoveal choroidal thickness in all myopes.

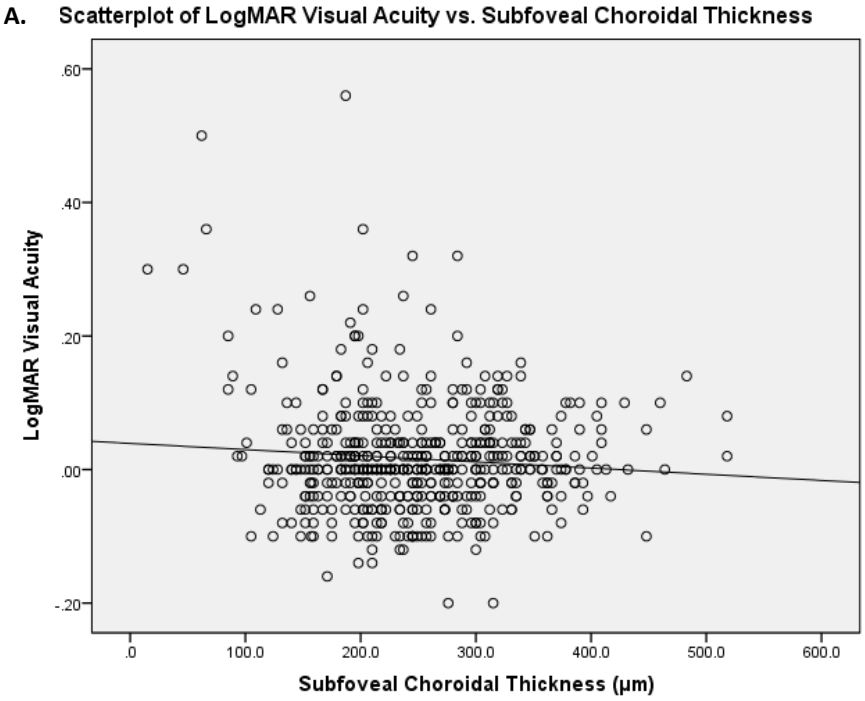

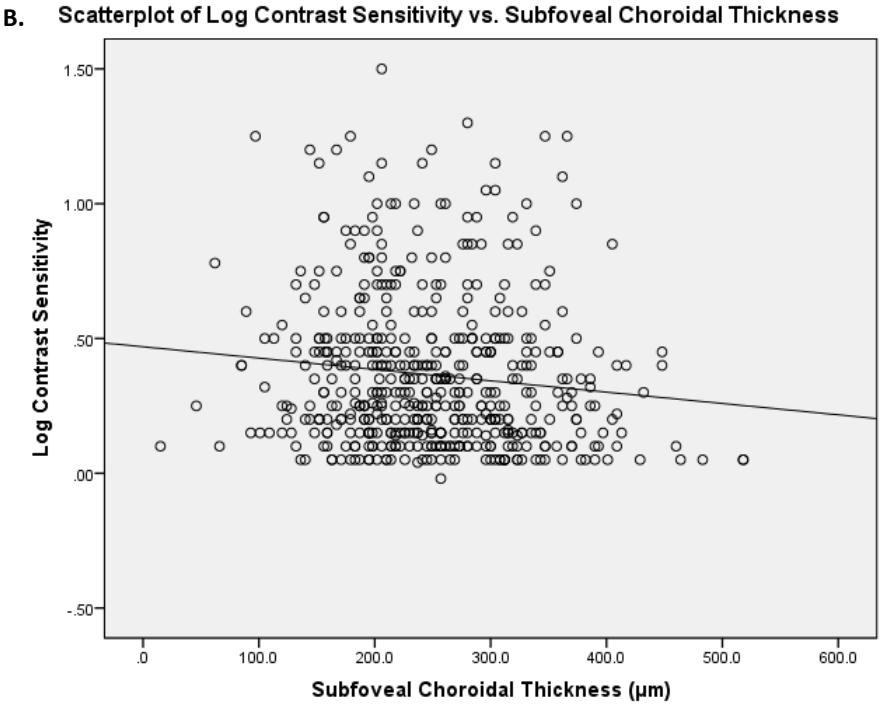

Figure 9.9 Graph showing the distribution of mean peripapillary choroidal thickness (micrometer, μm) in high myopic and emmetropic groups at different locations around the optic disc. The x-axis represents the locations of the measurements of peripapillary choroidal thickness around the optic disc. T = temporal, ST = superiotemporal, S = superior, SN = superionasal, N = nasal, IN = inferonasal, I = inferior, IT = inferotemporal. Error bars indicate standard error.

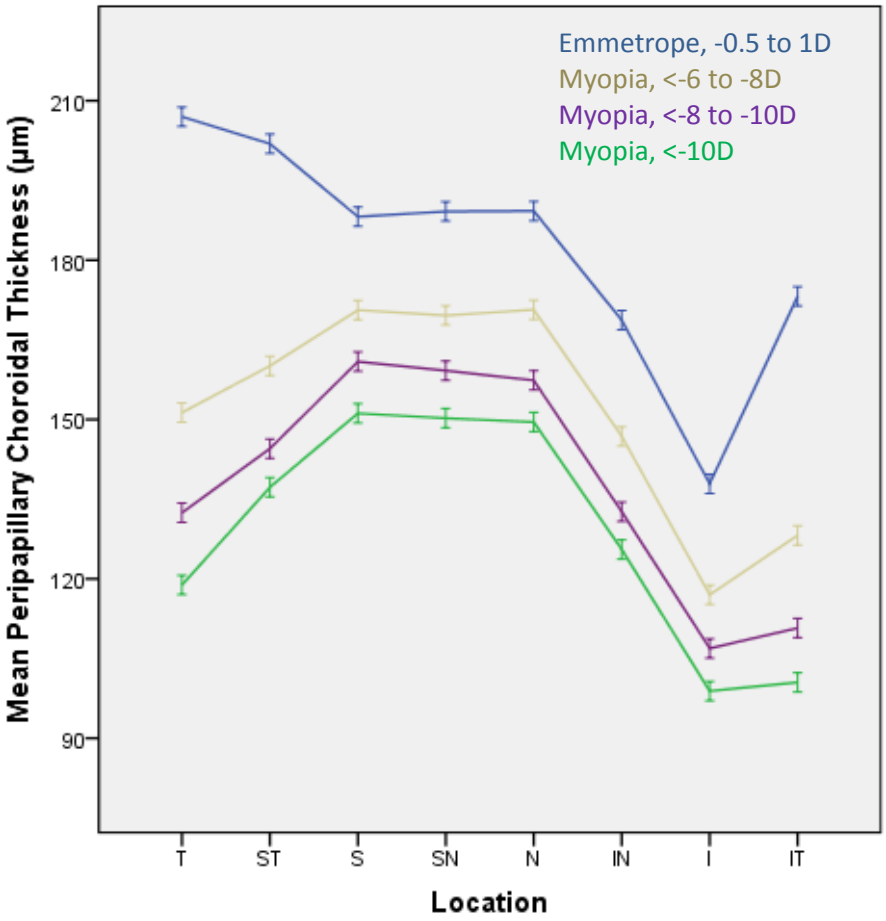

Figure 9.10 Distribution profiles of choroidal and retinal thicknesses at different locations in high myopic and emmetropic groups. Mean thickness at each of the nasal, temporal, superior, and inferior locations was measured at 1.5 mm and 3 mm intervals eccentric to the sub-foveal area. Error bars indicate standard error. SFCT=sub-foveal choroidal thickness; SFRT=sub-foveal retinal thickness; N=nasal; T=temporal; S=superior; I=inferior.

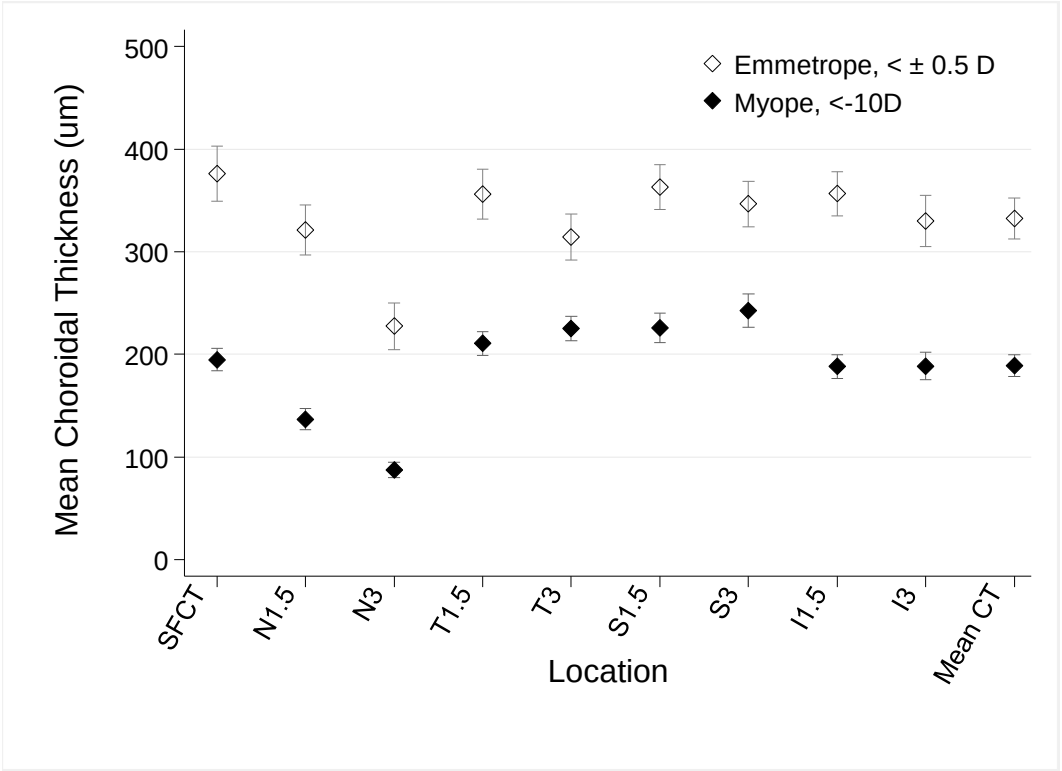

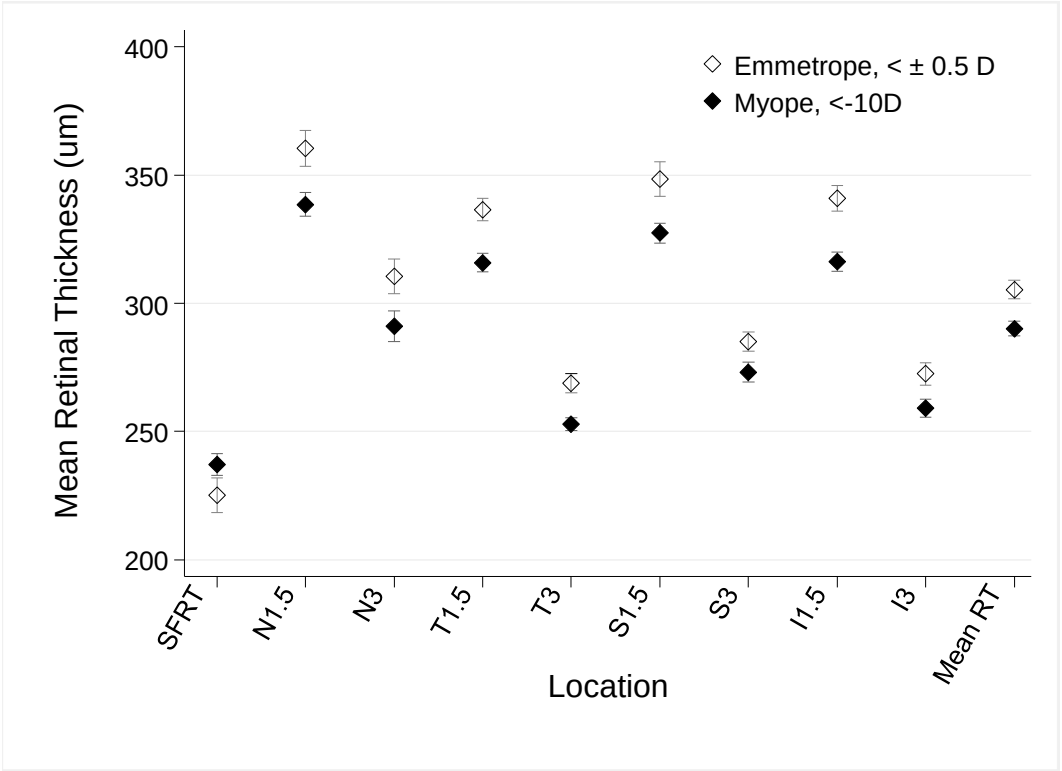

CHAPTER X

CHARACTERIZATION OF CHOROID IN DIABETES AND DIABETIC RETINOPATHY

In Chapter IX, we demonstrated that choroidal attributes, in particular, curvature of the CSI, inflection points and vascular area are significantly altered in high myopes. Given that choroid is implicated in the pathogenesis of diabetes and DR, in this Chapter, we performed characterization of morphological and vascular traits of the choroid in subjects with diabetes and DR. Since both diabetes and DR are accompanied by focal changes in the choroid, we hypothesize that the above choroidal features might be altered in these diseases.

The manuscript relevant to the contents of this chapter has been published in:

British Journal of Ophthalmology

Gupta, P., S. G. Thakku, C. Sabanayagam, G. Tan, G. M. Cheung, E. L. Lamoureux, T. Y. Wong and C. Y. Cheng. "Characterization of Choroidal Morphology and Vasculature in Diabetes and Diabetic Retinopathy." *British Journal of Ophthalmology 2016*

10.1 INTRODUCTION

Diabetes mellitus is a metabolic disease characterized by both macrovascular and microvascular complications.[1] Diabetic retinopathy (DR) is the most common microvascular complication, primarily caused by chronic hyperglycemia leading to loss of pericytes of retinal capillaries and subsequent ischemia.[2] The pathogenesis and clinical features of DR are primarily attributed to retinal vascular damage;[3] however, there is increasing evidence of choroidal involvement as persons with diabetes have been found to have various choroidal abnormalities including choroidal vascular degeneration, choroidal aneurysms, choroidal neovascularization, obstruction of the choriocapillaris, and increased tortuosity and narrowing of the choroidal vessels.[4-6]

The choroid is an integral part of metabolic exchange in the outer retina, in particular, foveal avascular zone, due to lack of retinal vasculature and a high metabolic demand from an increased photoreceptor density.[7, 8] Therefore, the choroid plays an important physiological role in ocular health, and is involved in the pathogenesis of many ocular diseases including DR.[9-13]

The recent availability of enhanced depth imaging (EDI) optical coherence tomography (OCT) has allowed the non-invasive quantitative assessment of the choroid.[14] Since then various studies have proposed choroidal thickness (CT) as a marker to assess different disease conditions[15-19] including diabetes. However, reports on CT in diabetes have been contradictory with studies reporting increase,[13] decrease[9, 11] or even no change.[20] This could possibly be due to confounding effects from factors such as age, gender, refractive error, axial length, diurnal variation etc. which have been shown to influence CT.[21-24] Thus measurements of CT alone may not be sufficient to reflect the structural changes within the choroid, which is a complex, 3-

dimentional structure predominantly composed of interconnected network of blood vessels surrounded by stromal tissue.[7] Thus, a more detailed investigation of choroidal structure and vasculature may provide better understanding of the choroid in diseases such as diabetes and DR where to date there has been no consensus as to whether there is increase or decrease in CT.

Nevertheless, there are limited in-vivo reports on a few choroidal morphological features and vessel layer measurements in DR.[25, 26] There has been no attempt to define and quantify morphological traits such as curvature of the choroid-scleral interface (CSI) and vascularity of the choroid in persons with diabetes and DR. In view of paucity of data on these features and given the rising trend in the prevalence of both diabetes and DR among Asian,[27, 28] it is imperative to have in-vivo baseline measurements of the choroidal morphometric and vascular features in persons with diabetes and DR.

The aim of this study was to characterize the morphological and vascular features of the choroid in a sample of Indian adults with diabetes and DR using novel segmentation methods on choroidal images obtained by EDI SD-OCT.

10.2 MATERIALS AND METHODS

10.2.1 Study Subjects

In this cross-sectional study, 500 consecutive subjects were recruited during their 6-year follow-up examination from a total of 2200 subjects who participated in Singapore Indian Eye Study-2 (SINDI-2, 2013-2015), a population-based cohort study conducted at the Singapore Eye Research Institute. Details of the baseline study

design, sampling plan, and methodology (SINDI-1, 2007-2009) have been reported elsewhere.[29]

Each subject underwent an interview and detailed ocular examination according to a standardized study protocol,[29] including imaging of the choroid using Spectralis SD-OCT with EDI (Spectralis SD-OCT; Heidelberg Engineering GmbH, Heidelberg, Germany). The study protocol was approved by the SingHealth Centralized Institutional Review Board and adhered to the ethical principles outlined in the Declaration of Helsinki, 2008. Written voluntary informed consent was obtained from each subject.

10.2.2 Exclusion Criteria

Among non-diabetic and diabetic group (including those with and without DR), subjects with refractive error <-6.00 diopters, age related macular degeneration (AMD), glaucoma and those whose choroidal images were of insufficient quality (quality index of < 18 decibels for Spectralis OCT as suggested by the manufacturer for the image quality assurance) were excluded. However, subjects with DR that had received treatments such as intravitreal injections or laser photocoagulation (more than 6 months of their participation into the study) were not excluded.

10.2.3 Ocular and Systemic Examination

Each subject underwent an interview and detailed systemic and ocular examination according to a standardized study protocol, as described in Chapter III of the thesis.

10.2.4 OCT Image Acquisition and Delineation

The choroid was imaged using EDI mode of Spectralis SD-OCT. The details on choroidal image acquisition protocol have been described in Chapter III of the thesis. Although choroidal images of both eyes of each study subject were obtained, due to strong inter-eye correlation only the right eye of each subject was delineated for detailed morphological and vascular analyses. Raw OCT images were loaded on a custom-written application on MATLAB that enabled delineation of RPE and CSI (described in detail in Chapter IX).

10.2.5 Measurement of Choroidal Morphological and Vascular Parameters

For each eye, the horizontal cross-sectional scan passing through the fovea was identified. Based on this cross-sectional scan, we defined and calculated (in MATLAB) the following choroidal morphological and vascular parameters: CSI curvature, inflection points, thickest point distance from the fovea, CT, choroidal volume and choroidal vascular area within foveal and macular regions. Our technique of image binarization to identify stromal and luminal areas within the choroid was validated against manual delineations. The above choroidal morphological and vascular features and validation of image binarization technique are both described in detail in Chapter IX of this thesis and in Figures 9.4 and 9.5.

10.2.6 Statistical Analyses

To compare the characteristics of participants among groups, independent *t*-test was performed for continuous variables and chi-square tests or Fisher's exact test for categorical variables. Data was expressed as mean ± standard deviation (SD). Multiple linear regression analysis was used to assess differences in choroidal characteristics by diabetes (in reference to no diabetes) and DR (in reference to no DR) after adjusting for factors with $p < 0.1$ in the univariate analysis and biologically

plausible factors such as age, sex and AL. Statistical significance was set at $p < 0.05$ unless otherwise indicated. All statistical analyses were carried out using SPSS (v 20.0; Chicago, IL, USA).

10.3 RESULTS

Of the 500 subjects initially enrolled, 37 were excluded based on our clinical exclusion criteria; myopia <-6.00 D (n=6), age related macular degeneration (n=4), glaucoma or glaucoma suspect (n=13) and poor OCT image quality (n=14), leaving 463 subjects for analysis. Of the 463 subjects included, 273 had no diabetes, 100 had diabetes but no DR, and 89 had DR.

The demographic, clinical and choroidal characteristics of the subjects with and without diabetes are depicted in **Table 10.1**. There were significant differences in characteristics (clinical and choroidal) between the two groups. Total choroidal area, vascular area and choroidal vascularity was lower in subjects with diabetes compared to non-diabetics (all $p<0.001$). There was no significant difference in choroidal stromal area between the two groups. Of the subjects, 86.4% without diabetes had one inflection point vs. 24% of those with diabetes.

In the multiple regression analysis after accounting for relevant confounders such as age, gender, SBP, DBP, ocular perfusion pressure (OPP), HbA1c and presence of hypertension (Model 2), subjects with diabetes had significantly thinner CT at all the studied locations (all $p<0.001$), including thinner mean CT (mean difference [MD]=-25.19µm, $p=0.001$), lesser choroidal volume (MD=-0.23mm^3, $p=0.003$) and more inflection points (MD=1.78, $p<0.001$) compared to those without

diabetes (**Table 10.2**). They also had lesser total choroidal area, choroidal vascular area and choroidal vascularity within the foveal and macular regions.

Of the diabetics, subjects with DR had significantly thicker choroid, greater choroidal volume, more posteriorly curved CSI and lesser inflection points (all $p<0.05$). Total choroidal, vascular and stromal areas within foveal and macular regions were significantly greater in those with the DR compared with those without (**Table 10.3**).

In the multiple regression analysis after adjusting for potential confounders such as age, gender, axial length, SBP, HbA1c, duration of diabetes and insulin use (Model 2), compared to diabetic subjects with no DR, those with DR exhibited significantly thicker CT at all the studied locations (all $p<0.001$) including, thicker mean CT (MD=25.91µm, $p=0.001$), greater choroidal volume (MD=0.24mm^3, $p=0.009$) and lesser inflection points (MD=-0.478, $p=0.045$). In addition, they demonstrated greater total choroidal, vascular and stromal areas at foveal and macular regions (all $p<0.05$). However, at the macular region, choroid was less vascular in subjects with DR (**Table 10.4**).

DR subjects were classified according to their stage of DR. Of the 89 subjects with DR, 58 (65.1%) had minimal to mild DR, 24 (26.9%) had moderate non proliferative DR, while none of our subjects had severe non proliferative DR and 7 (7.8%) subjects had proliferative DR. Comparison of choroidal traits across different DR severity groups showed no significant trend in any of the choroidal attributes (p for trend >0.05 for all traits, **Table 10.5**).

Given laser treatments in particular PRP have been shown to result in choroidal thinning,[25] we examined the effect of any previous laser treatments in

diabetic subjects with DR. However, since two third of our subjects had only minimal to mild DR, number of subjects with laser treatment is also limited. Of the 89 subjects with DR, 74 (83.14%) had no previous laser treatment while 13 (14.6%) subjects had undergone focal laser and only 2 (2.24%) had PRP done. Comparison of choroidal features between subjects who had previous laser treatments (focal or PRP) vs. those with no laser treatment showed no significant difference in any of their choroidal traits (all $p>0.05$, **Table 10.6**). Similar results were observed when further adjusted for DR stages.

10.4 DISCUSSION

To the best of our knowledge, this is the first study to characterize morphology and vasculature of the choroid in persons with diabetes and DR using the technique of image binarization in choroidal images obtained using EDI, SD-OCT. Our results demonstrated significant alterations in choroidal structural and vascular characteristics in both diabetes and DR. As speculated, subjects with diabetes showed significantly thinner choroid and lower vascular area, which is consistent with capillary drop-out wherein decreased choroidal blood flow plays a key role in the pathogenesis. Conversely, among the diabetic group, subjects with DR displayed thicker choroid and significantly higher vascular area compared to no DR. These findings indicate that the choroidal morphology and function are distinctly different in two conditions.

Knowledge about choroidal structural and vascular traits in-vivo remains limited. There are only couple of reports on some of the choroidal morphological features and vessel layer thickness measurements in healthy and DR eyes using Cirrus OCT.[25, 30] However, Cirrus OCT is not adequate to visualize the entire choroidal

structures, as the line of peak sensitivity is placed at posterior vitreous, allowing better visualization of retinal structures.[31] This gives a poor quality of choroidal image, compromising the validity of existing studies, in particular their vascular analysis. In addition, there is no report on choroidal features in diabetic persons, except for CT. Given the increasing trend in the prevalence and severity of diabetes and DR among Asians, it is important to have in-vivo baseline measurements of choroidal traits to provide better insight into the choroidal angiopathy associated with the disease.

We demonstrated that in persons with diabetes there is significant increase in inflection points indicating irregular contour of the CSI. This finding is supported by the clinical observation of focal changes (either thickening or thinning) in the choroid of diabetic persons.[32] In terms of CT our finding are consistent with the existing studies which reported choroidal thinning in diabetes.[9, 11] Distribution profiles of CT in persons with diabetes are similar to that in non-diabetic eyes; the choroid was thickest subfoveally and thins out much more nasally than temporally. Our results are congruent to what was observed in few other studies of horizontal variation in CT among subjects with diabetes.[10, 12] Since the blood supply for the choroid originates from the posterior ciliary arteries in the macula and then travels to the so-called "watershed zones" of the choroid periphery, this may be the reason for the reduction in CT towards the nasal regions.[33]

Interestingly, in comparison to non-diabetic eyes, choroidal vascular area was markedly reduced in persons with diabetes. In view of contradictory results of current studies on CT in diabetes[9, 11, 13, 20] it is still uncertain how diabetes affects the choroid. Because diabetes is primarily a vascular disease affecting both retinal and choroidal vasculature, knowledge of individual components of the choroid in particular vascular area may provide a better measure of the influence of diabetes on choroid. We

speculated reduction in luminal area in diabetes as there is narrowing of choroidal arterioles, choriocapillaris atrophy, and capillary dropout (shown by histologic studies),[5, 34] which in turn leads to a decreased choroidal blood flow in diabetic eyes (shown by circulatory studies using Laser Doppler Flowmetry).[35] The results of this study support our hypothesis of reduced choroidal vascularity in diabetic subjects.

On the other hand, compared to subjects without DR, persons with DR showed decrease in inflection points. Although, there was a displacement of the thickest point of choroid from under the foveal centre towards temporal location, the displacement was lesser compared to that seen in subjects with diabetes and was not significant. Contrary to diabetes (without DR), there was a significant increase in CT (at all the locations), choroidal volume and vascular area within foveal and macular regions in DR. We hypothesize that the increase production of VEGF or other cytokines in DR might result in choroidal vasodilation and elevation in choroidal blood flow, which subsequently increase the thickness and vascular area of the choroid.

There was no significant difference in any of the choroidal traits in DR subjects with or without laser treatment. We speculate the reason for no difference in choroidal features across the two groups to be the lesser number of subjects in treatment group compared to no treatment. It is more likely a power issue and we recommend future studies with more number of subjects in treatment group to study the likely effect of lasers on choroidal attributes.

The strengths of our study included a relatively large sample size with a single common ethnicity, standardized clinical examination protocols, reliable differentiation and quantifications of choroidal parameters. Furthermore, our analysis included a comprehensive list of potential confounding factors; choroidal characteristics in different groups were confirmed after adjusting for effect of these

factors. However, this study also has limitations. Our OCT images were binarized at standard threshold, yet there was a possibility of over or under estimation of both vascular and avascular areas. Choroidal attributes were assessed from a horizontal cross-sectional scan passing through the fovea. Future studies using more dense volume scan protocols are warranted. Also future improved software will be able to perform binarization of volume scans and will provide data not limited to single scan. We did not have information on prior intravitreal anti-VEGF injection for our diabetic subjects with DR. However, given that two third of our subjects had only minimum to mild DR, it is unlikely to influence our findings. DR subjects were classified according to their stage of DR. However, the statistical power to perform subgroup analysis by stage may be limited. Future studies with large sample in different DR severity groups are warranted. Choroidal scans were only performed for one time point in the day. The effect of diurnal variation on choroidal features[22, 36] could not be assessed due to the inherent limitation of our study design.

10.5 CONCLUSION

In conclusion, we report significant alterations in choroidal morphometric and vascular attributes in persons with diabetes and DR. These findings will be useful in further understanding the role and contribution of choroidal measures in the pathogenesis of diabetes and DR.

10.6 REFERENCES

1. Zoungas S, Woodward M, Li Q, et al. Impact of age, age at diagnosis and duration of diabetes on the risk of macrovascular and microvascular complications and death in type 2 diabetes. Diabetologia 2014;57(12):2465-74.

2. Cheung N, Mitchell P, Wong TY. Diabetic retinopathy. The Lancet;376(9735):124-36.

3. Antonetti DA, Klein R, Gardner TW. Diabetic retinopathy. N Engl J Med 2012;366(13):1227-39.

4. Cao J, McLeod S, Merges CA, Lutty GA. Choriocapillaris degeneration and related pathologic changes in human diabetic eyes. Arch Ophthalmol 1998;116(5):589-97.

5. Hidayat AA, Fine BS. Diabetic choroidopathy. Light and electron microscopic observations of seven cases. Ophthalmology 1985;92(4):512-22.

6. McLeod DS, Lutty GA. High-resolution histologic analysis of the human choroidal vasculature. Invest Ophthalmol Vis Sci 1994;35(11):3799-811.

7. Nickla DL, Wallman J. The multifunctional choroid. Prog Retin Eye Res 2010;29(2):144-68.

8. Linsenmeier RA, Padnick-Silver L. Metabolic dependence of photoreceptors on the choroid in the normal and detached retina. Invest Ophthalmol Vis Sci 2000;41(10):3117-23.

9. Esmaeelpour M, Povazay B, Hermann B, et al. Three-dimensional 1060-nm OCT: choroidal thickness maps in normal subjects and improved posterior segment visualization in cataract patients. Invest Ophthalmol Vis Sci 2010;51(10):5260-6.

10. Kim JT, Lee DH, Joe SG, et al. Changes in choroidal thickness in relation to the severity of retinopathy and macular edema in type 2 diabetic patients. Invest Ophthalmol Vis Sci 2013;54(5):3378-84.

11. Querques G, Lattanzio R, Querques L, et al. Enhanced depth imaging optical coherence tomography in type 2 diabetes. Invest Ophthalmol Vis Sci 2012;53(10):6017-24.

12. Regatieri CV, Branchini L, Carmody J, et al. Choroidal thickness in patients with diabetic retinopathy analyzed by spectral-domain optical coherence tomography. Retina 2012;32(3):563-8.

13. Xu J, Xu L, Du KF, et al. Subfoveal choroidal thickness in diabetes and diabetic retinopathy. Ophthalmology 2013;120(10):2023-8.

14. Spaide RF, Koizumi H, Pozzoni MC. Enhanced depth imaging spectral-domain optical coherence tomography. Am J Ophthalmol 2008;146(4):496-500.

15. Fujiwara T, Imamura Y, Margolis R, et al. Enhanced depth imaging optical coherence tomography of the choroid in highly myopic eyes. Am J Ophthalmol 2009;148(3):445-50.

16. Gupta P, Saw S, Cheung CY, et al. Choroidal thickness and high myopia: a case-control study of young Chinese men in Singapore. Acta Ophthalmol 2014.

17. Chung SE, Kang SW, Lee JH, Kim YT. Choroidal thickness in polypoidal choroidal vasculopathy and exudative age-related macular degeneration. Ophthalmology 2011;118(5):840-5.

18. Imamura Y, Fujiwara T, Margolis R, Spaide RF. Enhanced depth imaging optical coherence tomography of the choroid in central serous chorioretinopathy. Retina 2009;29(10):1469-73.

19. Koizumi H, Yamagishi T, Yamazaki T, et al. Subfoveal choroidal thickness in typical age-related macular degeneration and polypoidal choroidal vasculopathy. Graefes Arch Clin Exp Ophthalmol 2011;249(8):1123-8.

20. Vujosevic S, Martini F, Cavarzeran F, et al. Macular and peripapillary choroidal thickness in diabetic patients. Retina 2012;32(9):1781-90.

21. Gupta P, Jing T, Marziliano P, et al. Distribution and determinants of choroidal thickness and volume using automated segmentation software in a population-based study. Am J Ophthalmol 2015;159(2):293-301 e3.

22. Tan CS, Ouyang Y, Ruiz H, Sadda SR. Diurnal variation of choroidal thickness in normal, healthy subjects measured by spectral domain optical coherence tomography. Invest Ophthalmol Vis Sci 2012;53(1):261-6.

23. Tan CS, Cheong KX. Macular choroidal thicknesses in healthy adults--relationship with ocular and demographic factors. Invest Ophthalmol Vis Sci 2014;55(10):6452-8.

24. Barteselli G, Chhablani J, El-Emam S, et al. Choroidal volume variations with age, axial length, and sex in healthy subjects: a three-dimensional analysis. Ophthalmology 2012;119(12):2572-8.

25. Adhi M, Brewer E, Waheed NK, Duker JS. Analysis of Morphological Features and Vascular Layers of Choroid in Diabetic Retinopathy Using Spectral-Domain Optical Coherence Tomography. JAMA Ophthalmol 2013.

26. Sim DA, Keane PA, Mehta H, et al. Repeatability and reproducibility of choroidal vessel layer measurements in diabetic retinopathy using enhanced depth optical coherence tomography. Invest Ophthalmol Vis Sci 2013;54(4):2893-901.

27. Huang OS, Tay WT, Ong PG, et al. Prevalence and determinants of undiagnosed diabetic retinopathy and vision-threatening retinopathy in a multiethnic Asian cohort: the Singapore Epidemiology of Eye Diseases (SEED) study. Br J Ophthalmol 2015;99(12):1614-21.

28. Sivaprasad S, Gupta B, Crosby-Nwaobi R, Evans J. Prevalence of diabetic retinopathy in various ethnic groups: a worldwide perspective. Surv Ophthalmol 2012;57(4):347-70.

29. Lavanya R, Jeganathan VS, Zheng Y, et al. Methodology of the Singapore Indian Chinese Cohort (SICC) eye study: quantifying ethnic variations in the epidemiology of eye diseases in Asians. Ophthalmic Epidemiol 2009;16(6):325-36.

30. Branchini LA, Adhi M, Regatieri CV, et al. Analysis of choroidal morphologic features and vasculature in healthy eyes using spectral-domain optical coherence tomography. Ophthalmology 2013;120(9):1901-8.

31. Mrejen S, Spaide RF. Optical coherence tomography: imaging of the choroid and beyond. Surv Ophthalmol 2013;58(5):387-429.

32. Manjunath V, Taha M, Fujimoto JG, Duker JS. Choroidal thickness in normal eyes measured using Cirrus HD optical coherence tomography. Am J Ophthalmol 2010;150(3):325-9 e1.

33. Hayreh SS. In vivo choroidal circulation and its watershed zones. Eye (Lond) 1990;4 (Pt 2):273-89.

34. Lutty GA, Cao J, McLeod DS. Relationship of polymorphonuclear leukocytes to capillary dropout in the human diabetic choroid. Am J Pathol 1997;151(3):707-14.

35. Nagaoka T, Kitaya N, Sugawara R, et al. Alteration of choroidal circulation in the foveal region in patients with type 2 diabetes. Br J Ophthalmol 2004;88(8):1060-3.

36. Chakraborty R, Read SA, Collins MJ. Diurnal variations in axial length, choroidal thickness, intraocular pressure, and ocular biometrics. Invest Ophthalmol Vis Sci 2011;52(8):5121-9.

CHAPTER X TABLES

Table 10.1 Clinical and choroidal characteristics of study subjects in the non-diabetic and diabetic groups

	Without Diabetes (n = 273)	**With Diabetes (n = 189)**	**P-value[a]**
Age, years	60.10 (6.82)	62.14 (6.81)	<**0.001**
Gender, male (%)	138 (50.9)	103 (54.5)	0.507
Axial length, mm	23.38 (1.11)	23.22 (0.95)	**0.019**
BMI, kg/m^2	26.16 (4.63)	27.05 (3.90)	**0.031**
SBP, mmHg	132.32 (17.66)	135.66 (17)	**0.043**
DBP, mmHg	78.80 (9.87)	73.99 (7.47)	<**0.001**
MOPP, mmHg	54.48 (7.35)	52.20 (6.28)	<**0.001**
HbA1c, %	5.60 (0.43)	7.74 (1.53)	<**0.001**
Duration of diabetes, years	-	15.23 (8.52)	-
Insulin use (Y)	-	43 (22.75)	-
Hypertension (Y)	141 (51.6)	142 (75.1)	<**0.001**
Choroidal Characteristics			
Mean CT, µm	276.11 (56.02)	249 (54.30)	<**0.001**
Sub-foveal CT, µm	301.92 (63.10)	269.46 (61.02)	<**0.001**
Nasal 3 mm CT, µm	269.04 (67.09)	241.41 (64.64)	<**0.001**
Temporal 3 mm CT, µm	283.23 (53.20)	256.63 (51.86)	<**0.001**
Choroidal volume, mm^3	2.42 (0.48)	2.195 (0.605)	<**0.001**
CSI curvature, mm^{-1}	-0.093 (0.044)	-0.087 (0.040)	0.097
No of inflection points	1.16 (0.45)	2.70 (1.47)	<**0.001**
Thickest point distance from fovea, mm	0.026 (1.038)	-0.436 (1.46)	<**0.001**
Sub Foveal (1.5 mm region)			
Total choroidal area, mm^2	0.452 (0.094)	0.404 (0.091)	<**0.001**
Vascular area, mm^2	0.241 (0.052)	0.196 (0.047)	<**0.001**
Stromal area, mm^2	0.211 (0.087)	0.207 (0.051)	0.617
Choroidal vascularity	0.555 (0.214)	0.485 (0.052)	<**0.001**
Macular (6 mm region)			
Total choroidal area, mm^2	1.670 (0.327)	1.494 (0.325)	<**0.001**
Vascular area, mm^2	0.884 (0.185)	0.719 (0.167)	<**0.001**
Stromal area, mm^2	0.786 (0.302)	0.774 (0.174)	0.608
Choroidal vascularity	0.548 (0.199)	0.480 (0.039)	<**0.001**

Data presented are means (standard deviations) or number (%).

[a] Based on independent sample t-test for continuous variables or Chi-square/Fisher's exact test for categorical variables.

BMI=body mass index; SBP=systolic blood pressure; DBP=diastolic blood pressure; MOPP=mean ocular perfusion pressure; HbA1c=haemoglobin A1c; CT=choroidal thickness; CSI=choroid scleral interface.

Table 10.2 Differences in choroidal characteristics (dependent variables) in subjects with diabetes (n = 189), compared to those without diabetes (n = 273)

	Model 1		Model 2	
Choroidal Characteristics	**Beta coefficient[a] (95% CI)**	**P-value**	**Beta coefficient[a] (95% CI)**	**P-value**
Mean CT, µm	-17.82 (-28.05, -7.60)	**<0.001**	-25.19 (-40.37, -10.02)	**0.001**
Sub-foveal CT, µm	-23.44 (-35.07, -11.82)	**<0.001**	-29.13 (-46.45, -11.81)	**0.001**
Nasal 3 mm CT, µm	-17.69 (-29.79, -5.58)	**0.004**	-27.73 (-45.40, -10.06)	**0.002**
Temporal 3 mm CT, µm	-17.97 (-27.89, -8.06)	**<0.001**	-22.67 (-37.71, -7.63)	**0.003**
Choroidal volume, mm^3	-0.142 (-0.243, -0.041)	**0.006**	-0.230 (-0.384, -0.077)	**0.003**
CSI curvature, mm^{-1}	0.007 (-0.001, 0.016)	0.092	0.009 (-0.004, 0.022)	0.173
No of inflection points	1.487 (1.292, 1.682)	**<0.001**	1.780 (1.48, 2.07)	**<0.001**
Thickest point distance from fovea, mm	-0.426 (-0.660, -0.192)	**<0.001**	-0.233 (-0.584, 0.119)	0.194
Sub Foveal (1.5 mm region)				
Total choroidal area, mm^2	-0.035 (-0.053, -0.018)	**<0.001**	-0.044 (-0.070, -0.018)	**0.001**
Vascular area, mm^2	-0.042 (-0.052, -0.032)	**<0.001**	-0.043 (-0.058, -0.028)	**<0.001**
Stromal area, mm^2	0.007 (-0.007, 0.021)	0.344	-0.001 (-0.022, 0.020)	0.935
Choroidal vascularity	-0.090 (-0.123. -0.058)	**<0.001**	-0.077 (-0.124, -0.031)	**0.001**
Macular (6 mm region)				
Total choroidal area, mm^2	-0.120 (-0.181, -0.060)	**<0.001**	-0.159 (-0.250, -0.069)	**0.001**
Vascular area, mm^2	-0.151 (-0.185, -0.117)	**<0.001**	-0.160 (-0.212, -0.107)	**<0.001**
Stromal area, mm^2	0.031 (-0.017, 0.079)	0.210	0.000 (-0.071, 0.072)	0.991
Choroidal vascularity	-0.088 (-0.117, -0.058)	**<0.001**	-0.077 (-0.121, -0.033)	**0.001**

Model 1: adjusted for age and sex.
Model 2: adjusted for age, sex, axial length, BMI, MOPP, HbA1c, and hypertension.
[a] Beta coefficient represents difference in choroidal characteristics in subjects with diabetes with reference to non-diabetes.
CI=confidence interval; CT=choroidal thickness; CSI=choroid scleral interface.

Table 10.3 Clinical and choroidal characteristics of study diabetic subjects without and with diabetic retinopathy

	Without DR (n = 100)	**With DR (n = 89)**	**P-value[a]**
Age, years	61.85 (7.47)	62.48 (6.01)	0.525
Gender, male (%)	49 (49)	54 960.7)	0.108
Axial length, mm	23.38 (1.11)	23.04 (0.70)	**0.015**
BMI, kg/m^2	26.89 (3.43)	27.23 (4.39)	0.555
SBP, mmHg	132.19 (15.75)	139.56 (17.58)	**0.003**
DBP, mmHg	73.81 (7.28)	74.19 (7.71)	0.727
MOPP, mmHg	51.67 (5.91)	52.81 (6.66)	0.213
HbA1c, %	7.49 (1.33)	8.02 (1.69)	**0.019**
Duration of diabetes, years	14.71 (8.63)	15.83 (8.40)	0.366
Insulin use (Y)	14 (14)	29 (33)	**0.002**
Hypertension (Y)	73 (73)	69 (77.5)	0.472
Choroidal Characteristics			
Mean CT, µm	233.50 (47.09)	266.41 (56.78)	**<0.001**
Sub-foveal CT, µm	251.79 (52.72)	289.31 (63.83)	**<0.001**
Nasal 3 mm CT, µm	224.38 (57)	260.54 (67.60)	**<0.001**
Temporal 3 mm CT, µm	242.66 (46.71)	272.33 (53.11)	**<0.001**
Choroidal volume, mm^3	2.05 (0.43)	2.35 (0.72)	**<0.001**
CSI curvature, mm^{-1}	-0.081 (0.042)	-0.093 (0.037)	**0.033**
No of inflection points	2.96 (1.44)	2.41 (1.46)	**0.001**
Thickest point distance from fovea, mm	-0.56 (1.51)	-0.29 (1.39)	0.200
Sub Foveal (1.5 mm region)			
Total choroidal area, mm^2	0.377 (0.079)	0.433 (0.095)	**<0.001**
Vascular area, mm^2	0.186 (0.045)	0.207 (0.048)	**0.002**
Stromal area, mm^2	0.191 (0.042)	0.226 (0.054)	**<0.001**
Choroidal vascularity	0.491 (0.055)	0.478 (0.049)	0.102
Macular (6 mm region)			
Total choroidal area, mm^2	1.401 (0.282)	1.598 (0.340)	**<0.001**
Vascular area, mm^2	0.682 (0.150)	0.760 (0.176)	**0.001**
Stromal area, mm^2	0.718 (0.148)	0.837 (0.180)	**<0.001**
Choroidal vascularity	0.485 (0.040)	0.473 (0.037)	**0.049**

Data presented are means (standard deviations) or number (%).

[a] Based on independent sample t-test for continuous variables or Chi-square/Fisher's exact test for categorical variables.

DR=diabetic retinopathy; BMI=body mass index; SBP=systolic blood pressure; DBP=diastolic blood pressure; MOPP=mean ocular perfusion pressure; HbA1c=haemoglobin A1c; CT=choroidal thickness; CSI=choroid scleral interface.

Table 10.4 Difference in choroidal characteristics (dependent variables) in diabetic subjects with diabetic retinopathy (n = 89), compared to those without diabetic retinopathy (n = 100)

	Model 1		Model 2	
Choroidal Characteristics	**Beta coefficient[a] (95% CI)**	**P-value**	**Beta coefficient[a] (95% CI)**	**P-value**
Mean CT, µm	32.75 (19.11, 46.40)	**<0.001**	25.91 (11.12, 40.69)	**0.001**
Sub-foveal CT, µm	36.71 (21.07, 52.35)	**<0.001**	30.50 (13.61, 47.39)	**<0.001**
Nasal 3 mm CT, µm	34.92 (18.61, 51.22)	**<0.001**	23.93 (6.44, 41.43)	**0.008**
Temporal 3 mm CT, µm	30.60 (17.10, 44.10)	**<0.001**	27.89 (13.06, 43.73)	**<0.001**
Choroidal volume, mm^3	0.310 (-0.148, 0.472)	**<0.001**	0.240 (0.06, 0.41)	**0.009**
CSI curvature, mm^{-1}	-0.013 (-0.014, 0.009)	**0.030**	-0.008 (-0.021, 0.004)	0.201
No of inflection points	-0.586 (-1.00, -1.67)	**0.006**	-0.478 (-0.944, -0.011)	**0.045**
Thickest point distance from fovea, mm	0.209 (-0.206, 0.624)	0.322	0.021 (-0.426, 0.469)	0.926
Sub Foveal (1.5 mm region)				
Total choroidal area, mm^2	0.055 (0.032, 0.079)	**<0.001**	0.046 (0.020, 0.071)	**<0.001**
Vascular area, mm^2	0.021 (0.009, 0.033)	**0.001**	0.016 (0.003, 0.030)	**0.019**
Stromal area, mm^2	0.034 (0.021, 0.048)	**<0.001**	0.030 (0.015, 0.044)	**<0.001**
Choroidal vascularity	-0.013 (-0.028, 0.002)	0.081	-0.014 (-0.029, 0.002)	0.087
Macular (6 mm region)				
Total choroidal area, mm^2	0.197 (0.115, 0.278)	**<0.001**	0.155 (0.067, 0.244)	**0.001**
Vascular area, mm^2	0.078 (0.036, 0.120)	**<0.001**	0.057 (0.011, 0.102)	**0.016**
Stromal area, mm^2	0.119 (0.074, 0.164)	**<0.001**	0.099 (0.051, 0.147)	**<0.001**
Choroidal vascularity	-0.012 (-0.023, -0.001)	**0.038**	-0.012 (-0.024, -0.001)	**0.036**

Model 1: adjusted for age and sex.
Model 2: adjusted for age, sex, axial length, SBP, HbA1c, duration of diabetes and insulin use.
[a] Beta coefficient represents difference in choroidal characteristics in diabetic subjects with DR in reference to those without DR.
CI=confidence interval; CT=choroidal thickness; CSI=choroid scleral interface.

Table 10.5. Choroidal characteristics of study subjects in the diabetic group with stages of diabetic retinopathy (minimal-mild DR, moderate NPDR and PDR).

				Changes in choroidal traits across DR stages	
Choroidal Characteristics	**Minimal-Mild DR (n = 58)**	**Moderate NPDR (n = 24)**	**PDR (n = 7)**	**Beta**	**P for trend**
Mean CT, µm	268.10 (56.70)	267.97 (60.57)	262.11 (65.84)	-1.915	0.847
Sub-foveal CT, µm	290.57 (63.23)	289.17 (68.66)	294.22 (75.84)	0.605	0.957
Nasal 3 mm CT, µm	261.82 (63.90)	264.78 (78.48)	255.32 (78.74)	-0.910	0.938
Temporal 3 mm CT, µm	274.43 (55.03)	271.21 (53.38)	268.96 (59.71)	-2.916	0.753
Choroidal volume, mm^3	2.38 (0.84)	2.33 (0.54)	2.27 (0.59)	-0.054	0.672
CSI curvature, mm^{-1}	-0.08 (0.03)	-0.09 (0.03)	-0.11 (0.03)	-0.009	0.166
No of inflection points	2.53 (1.62)	2.42 (1.24)	2.00 (1.00)	-0.207	0.412
Thickest point distance from fovea, mm	-0.26 (1.40)	-0.26 (1.52)	-0.42 (1.34)	-0.024	0.831
Sub Foveal (1.5 mm region)					
Total choroidal area, mm^2	0.435 (0.094)	0.433 (0.102)	0.441 (0.113)	0.001	0.957
Vascular area, mm^2	0.208 (0.047)	0.204 (0.050)	0.210 (0.058)	-0.001	0.921
Stromal area, mm^2	0.227 (0.053)	0.229 (0.062)	0.230 (0.059)	0.002	0.855
Choroidal vascularity	0.478 (0.043)	0.471 (0.053)	0.475 (0.355)	-0.003	0.690
Macular (6 mm region)					
Total choroidal area, mm^2	1.608 (0.340)	1.607 (0.363)	1.572 (0.395)	-0.011	0.847
Vascular area, mm^2	0.761 (0.172)	0.766 (0.188)	0.723 (0.227)	-0.010	0.736
Stromal area, mm^2	0.846 (0.184)	0.841 (0.186)	0.849 (0.172)	-0.001	0.971
Choroidal vascularity	0.472 (0.037)	0.474 (0.031)	0.452 (0.041)	-0.006	0.361

Data presented are means (standard deviations).
DR= diabetic retinopathy; NPDR= non proliferative diabetic retinopathy; PDR= proliferative diabetic retinopathy.

Table 10.6. Choroidal characteristics of subjects with DR who had laser treatment (focal or grid) vs. those with no laser treatment.

Choroidal Characteristics	**No laser treatment (n = 74)**	**Lasers (focal or PRP) (n = 15)**	**P-value[a]**	**P-value[b]**
Mean CT, µm	270.13 (59.08)	248.59 (45.83)	0.272	0.222
Sub-foveal CT, µm	292.95 (66.55)	272.16 (51.44)	0.346	0.225
Nasal 3 mm CT, µm	265.57 (68.83)	236.60 (65.36)	0.213	0.136
Temporal 3 mm CT, µm	274.73 (56.39)	260.62 (34.65)	0.444	0.474
Choroidal volume, mm^3	2.39 (0.77)	2.16 (0.44)	0.361	0.413
CSI curvature, mm^{-1}	-0.90 (0.03)	-0.106 (0.03)	0.227	0.633
No of inflection points	2.51 (1.53)	2.00 (0.81)	0.305	0.506
Thickest point distance from fovea, mm	-0.21 (1.41)	-0.70 (1.46)	0.312	0.273
Sub Foveal (1.5 mm region)				
Total choroidal area, mm^2	0.439 (0.099)	0.408 (0.077)	0.346	0.225
Vascular area, mm^2	0.208 (0.049)	0.201(0.048)	0.675	0.656
Stromal area, mm^2	0.231 (0.057)	0.206 (0.031)	0.198	0.082
Choroidal vascularity	0.474 (0.049)	0.488 (0.036)	0.379	0.164
Macular (6 mm region)				
Total choroidal area, mm^2	1.620 (0.354)	1.491 (0.275)	0.272	0.222
Vascular area, mm^2	0.766 (0.180)	0.709 (0.175)	0.348	0.361
Stromal area, mm^2	0.854 (0.188)	0.782 (0.111)	0.242	0.154
Choroidal vascularity	0.471 (0.035)	0.470 (0.044)	0.908	0.592

Data presented are means (standard deviations).

[a] Based on independent sample t test.

[b] Adjusted for DR stages.

CHAPTER XI

CHARACTERIZATION OF CHOROID IN AGE-RELATED MACULAR DEGENERATION AND POLYPOIDAL CHOROIDAL VASCULOPATHY

In Chapter X, we demonstrated significant alterations in choroidal morphological and vascular characteristics in persons with diabetes and DR. Given the involvement of choroid in the pathogenesis of AMD and PCV, in this Chapter, we extended the characterization of morphological and vascular traits of the choroid in subjects with AMD and PCV with a hypothesis that the above choroidal features will be altered in these diseases.

The manuscript relevant to the contents of this chapter has been published in journal:

Retina

Gupta, P., D.W. Ting, S. G. Thakku, T. Y. Wong, C. Y. Cheng, E. Wong, R. Mathur, D. Wong, G. M. Cheung. "Detailed Characterization of Choroidal Morphological and Vascular Features in Age-Related Macular Degeneration and Polypoidal Choroidal Vasculopathy." *Retina 2016*

11.1 INTRODUCTION

Age related macular degeneration (AMD), a leading cause of blindness in the elderly population globally,[1-3] is traditionally characterized by changes seen in the retinal pigment epithelium (RPE) and Bruch's membrane.[4] With the advent of spectral-domain optical coherence tomography (SD-OCT), coupled with the enhanced depth imaging (EDI) mode, changes in the choroid such as choroidal thickness (CT), have been increasingly recognized as another key feature in the evolution and possibly pathogenesis of AMD.[5-8] Polypoidal choroidal vasculopathy (PCV) is a subtype of AMD, more commonly seen in Asians than white Caucasian populations, which is often associated with thickened choroid and choroidal hyperpermeability compared to typical AMD.[5, 8-11] In this regard, histological studies of eyes with PCV reported abnormal dilatation of choroidal vessels with hyalinization, arteriosclerosis, exudation and loss of smooth muscles.[12-14] Furthermore, several groups have reported that anti-vascular endothelial growth factor (VEGF) therapy is less effective in eyes with PCV with thickened choroid.[15]

Although the choroid is predominantly composed of blood vessels surrounded by stromal tissues, and CT and choroidal hyperpermeability have been shown to be closely related,[9, 15, 16] measurement of CT alone may not capture the specific changes within the choroid, .[17] A wide variation in CT exists even within the subgroup of eyes classified to have PCV. Therefore a method to analyze details of the choroid in terms of its morphometric and vascular features is essential to better understand the role of choroid in typical AMD and PCV. The pachychoroid phenotype has recently been characterized to include not only increased CT, but also the presence of pathologically dilated outer choroidal vessel (pachyvessels), attenuation and thinning of choriocapillaris and Sattler vessels, regional choroidal hyperpermeability.[18] Based on

these features, a subtype of PCV, called "polypoidal choroidal neovascularization (CNV)" may be classified based on presence of polypoidal lesions in the absence of pachychoroidal features. It has been proposed that polypoidal lesions in polypoidal CNV may represent a structural variant of neovascular tissue.[19]

The detailed analysis of choroidal morphometric features such as presence of pachyvessels can be subjective and lack quantitative endpoints. Recently Sonodo et al. described a method to separately quantify choroidal luminal and interstitial areas in eyes with AMD.[20] In this study, we aim to apply the binarization of OCT images technology to characterize detailed morphological and vascular features of the choroid in eyes with typical exudative AMD and PCV, and to investigate whether PCV can be sub-classified into typical PCV and polypoidal CNV based on these choroidal vascular features. Our hypothesis is that eyes with PCV may be sub-classified into 2 subgroups, with different functional and anatomical characteristics in choroidal vasculature.

11.2 METHODS

11.2.1 Study Subjects

The data for this study was taken from a prospective, observational cohort study involving patients with exudative AMD in the Asian AMD Phenotyping Study.[21] Detailed methodology has been published elsewhere.[21-23] The study was approved by the Centralized Institutional Review Board (CIRB) of SingHealth, Singapore (protocol number R697/47/2009) and conducted in accordance with the Declaration of Helsinki. Written informed consent was obtained from each participant.

11.2.2 Clinical Examination and Diagnosis

At baseline, all patients underwent an interview and comprehensive ocular examination including best corrected visual acuity testing using logarithm of the minimal angle of resolution (logMAR), refraction, slit-lamp biomicroscopy examination, and imaging according to standardized protocol, which included color fundus photography and angiography with fluorescein and indocyanine green (TRC-50X/ IMAGEnet 2000; Topcon, Tokyo, Japan or Spectralis; Heidelberg Engineering, Heidelberg, Germany). Information including medical history and smoking was obtained using standardized questionnaire.

Patients were classified as typical AMD and PCV based on fundus fluorescein angiogram and indocyanine green (ICG) angiogram as described in detail previously.[24-27] Briefly, typical AMD is graded based on presence or absence of CNV according to the Macular Photocoagulation Study.[24] PCV is diagnosed based on presence of characteristic polypoidal lesions seen in ICG.[25-27]

To study the differences in choroidal traits between AMD and PCV subtypes, patients with PCV were further categorized on the basis of CT into typical PCV (with CT≥250um) and PCV without thick choroid.

11.2.3 Ocular and Systemic Examination

Each subject underwent an interview and detailed systemic and ocular examination according to a standardized study protocol, as described in Chapter III of the thesis.

11.2.4 OCT Image Acquisition and Delineation

The choroid was imaged using EDI mode of Spectralis SD-OCT. OCT raster scans with EDI were acquired at the macular region of both eyes of each subject. Each set of images comprised 25 serial horizontal B-scans (each composed of 1536 A-scans) covering a rectangular region of 20º X 20º centered on the fovea. Distance between consecutive scans was on average about 240 μm and each scan was 8.9 mm in length. To reduce speckle noise, each B-scan was averaged 9 times during acquisition. OCT images were loaded on a custom-written application on MATLAB that enabled delineation for detailed morphological and vascular analyses (described in detail in Chapter IX).

11.2.5 Measurement of Choroidal Morphological and Vascular Parameters

For each eye, the horizontal cross-sectional scan passing through the fovea was identified. Based on this cross-sectional scan, we defined and calculated (in MATLAB) choroidal morphological and vascular parameters such as CSI curvature, number of inflection points, thickest point distance from the fovea, CT and choroidal vascular area within foveal and macular regions. Our technique of image binarization to identify stromal and luminal areas within the choroid was validated against manual delineations. The above choroidal morphological and vascular features and validation of image binarization technique are both described in detail in Chapter IX of this thesis and in Figures 9.4 and 9.5.

11.2.6 Statistical Analyses

To compare the clinical and choroidal characteristics of AMD and PCV eyes, independent *t*-test was performed for continuous variables and chi-square tests or Fisher's exact test for categorical variables. All data were expressed as mean ± standard deviation (SD) or number (%). In order to study the choroidal characteristics

of subtypes of PCV, we divided them into two groups based on their mean CT: typical PCV (with mean CT ≥ 250 μm) and PCV without thick choroid (CT < 250 μm). Multiple linear regression analysis was performed to assess differences in choroidal characteristics between patients with typical AMD and different PCV subtypes after adjusting for the effect of confounding factors which were significantly different (p ≤0.05) between the groups. All statistical analyses were carried out using SPSS (v 20.0; Chicago, IL, USA) and a p value <0 .05 was considered to be statistically significant.

11.3 RESULTS

A total of 156 eyes of 156 patients (78 affected eyes of 78 patients with typical AMD and 78 affected eyes of 78 patients with PCV) were analyzed. Baseline demographics are summarized in **Table 11.1**. Patients with PCV were significantly younger than patients with typical AMD (66.3 vs. 71.8 years, P < 0.001). There was no significant difference in gender, refractive error and other clinical characteristics between the two study groups. After adjusting for age and gender, patients with PCV were more likely to have hypertension (47.2 vs. 74.6%, P=0.001) and had lower total cholesterol (5.31 vs 5.67 mmol/L, p=0.011) compared to patients with typical AMD. Best corrected visual acuity was similar between the two groups.

In terms of baseline choroidal characteristics, eyes with PCV generally had thicker baseline CT at all the measured locations across the macula than eyes with typical AMD. Likewise, choroidal vascular area within the macular (6 mm centered on fovea) and foveal (1.5 mm centered on fovea) regions was significantly greater (both p<0.05) in eyes with PCV compared to typical AMD. However, after adjusting

for differences in age and hypertension, only CT in nasal location remained significantly thicker in the PCV group (**Table 11.2**). There were no significant variations in other morphological traits such as curvature of the CSI and inflection points between the groups.

We further divided PCV group into typical PCV (with CT≥250um) and PCV without thick choroid. Eyes with typical PCV (n=40) had significantly greater choroidal vascular area within the macular and foveal regions in addition to having thicker choroid at all the measured locations (all P<0.001) compared to eyes with AMD (**Table 11.3**). In contrast, eyes with PCV without thick choroid (n=38) had low choroidal vascular area which were similar to those in eyes with AMD (**Table 11.4**).

11.4 DISCUSSION

Our understanding of the pathogenesis and characteristics of AMD continues to evolve, with observations that some of the changes seen occur in the choroid. To the best of our knowledge, our study is the first to provide characterization of detailed morphology and vasculature of the choroid in Asian patients with typical AMD and PCV subtypes using the technique of image binarization in choroidal images obtained using EDI, SD-OCT. Our results demonstrate that although eyes with PCV had thicker choroid than typical AMD, the difference in choroidal morphologic and vascular attributes were not significantly different after adjustment for major confounding parameters such as age and hypertension. Therefore CT measurement may not entirely reflect the detailed structural and functional alterations within the choroid in different exudative maculopathy. Compared to eyes with PCV, eyes with AMD had more inflection points indicating more variation in CSI and the CSI was less posteriorly curved, these differences were not significant. In addition, we

observed that there is significant heterogeneity within the PCV group, suggesting two subtypes with different choroidal features. As we hypothesized, patients with typical PCV with thick choroid had significantly higher vascular area, which is consistent with the pachychoroid spectrum in which choroidal vessel dilatation plays a key role in the pathogenesis. Both CT and vascular area were significantly higher in eyes with typical PCV compared to eyes with AMD, indicating that the choroidal morphology and function are distinctly different from that in eyes with typical AMD. The pathogenic mechanisms that account for dilated choroidal vessels and pachychoroid remain unclear. Among the various plausible hypotheses for the pathogenesis of PCV; engorgement of the vortex vein,[28] choroidal vascular hyperpermeability[15] and choroidal venous hypertension[29] have been proposed but remain to be validated further.

In contrast to typical PCV, choroidal features in eyes with PCV without thick choroid are less well understood. It has been suggested that the pachychoroid phenotype may have normal or low CT when luminal volume increases secondary to choroidal vessel dilation occur concurrently with reduction in tissue volume from atrophy of the choriocapillaris.[19] We were interested to investigate whether this subgroup of PCV eyes had features suggestive of choroidal vessel dilatation despite thin choroid. Studying vascular area offered a novel, objective, semi-automated technique for this purpose. Our results indicate that eyes with PCV and thin choroid had significantly lower vascular area than typical PCV group, and vascular area measurements were similar to that in eyes with typical AMD. These findings suggest this subtype of PCV does not fall within the pachychoroid spectrum and may be more appropriately considered polypoidal CNV. The pathogenesis of this subtype is expected to be similar to neovascular AMD, in which choroidal vessel dilatation plays

less important role than in typical PCV. Accordingly, treatment response in polypoidal CNV can be expected to be similar to that in neovascular AMD, but different to eyes with typical PCV. Similarly, the benefit of photodynamic therapy polypoidal CNV is less clear compared to typical PCV.[30, 31]

Our findings in the present study are important for clinicians as our results further confirm that differences in choroidal vascular attributes have important implications in the pathogenesis and possibly treatment response in AMD and PCV subtypes. The OCT binarization technique provides an objective measure of choroidal vascularity which can help to determine whether an eye belongs to the pachychoroid spectrum. There are currently no clear definition of what constitutes a 'pachyvessel' and grading may lack objectivity and repeatability. Similarly grading of choroidal hyperpermeability based on indocyanine green angiography is subjective and also dependent on the phase of angiography and instrument used for image acquisition (camera-based versus scanning laser ophthalmoscopy based).

The strengths of our study include the prospective nature of recruitment and relatively large sample size. Hence, our findings were unlikely to be confounded by selection bias. Standardized clinical examination protocols, reliable differentiation and quantifications of choroidal parameters were used in our study. Unlike other studies where the choroidal characteristics in particular CT, were evaluated post treatment and were thus biased, our study assessed choroidal attributes in treatment naïve eyes. Furthermore, our analysis included a comprehensive list of potential confounding factors; choroidal characteristics in different groups were confirmed after adjusting for effect of these factors. However, this study also has limitations. Although our images were binarized at standard threshold, there is a possibility of over or under estimation of both vascular and avascular areas. Choroidal scans were

only performed for one time point in the day. The effect of diurnal variation on choroidal features[32, 33] could not be assessed due to the inherent limitation of our study design. We acknowledge the choice of choroidal thickness of 250um as cut-off between two subtypes of PCV was an arbitrary definition. Lastly, the cross-sectional design of our study prevented inferring causality.

11.5 CONCLUSIONS

In conclusion, our findings indicate significant alterations in specific choroidal characteristics in addition to CT, in typical PCV compared to typical AMD. Choroidal vascular characteristics can be used to sub-classify PCV into two subtypes. The subtype of PCV without thick choroid (polypoidal CNV) has similar choroidal vascular characteristics to eyes with AMD. This subtype, unlike typical PCV, does not fall within the pachychoroid spectrum. Our results highlight the relevance of further understanding phenotypic manifestations of choroidal vasculature in the diagnostic criteria for PCV subtypes and AMD. Thus, the diagnostic criteria for PCV should incorporate the phenotypic manifestations of the choroidal vasculature that are unique to this disease, as it likely will affect optimal management.

11.6 REFERENCES

1. Kawasaki R, Yasuda M, Song SJ, et al. The prevalence of age-related macular degeneration in Asians: a systematic review and meta-analysis. Ophthalmology 2010;117(5):921-7.

2. Wong TY, Loon SC, Saw SM. The epidemiology of age related eye diseases in Asia. Br J Ophthalmol 2006;90(4):506-11.

3. Wong WL, Su X, Li X, et al. Global prevalence of age-related macular degeneration and disease burden projection for 2020 and 2040: a systematic review and meta-analysis. Lancet Glob Health 2014;2(2):e106-16.

4. Bird AC, Bressler NM, Bressler SB, et al. An international classification and grading system for age-related maculopathy and age-related macular degeneration. The International ARM Epidemiological Study Group. Surv Ophthalmol 1995;39(5):367-74.

5. Koizumi H, Yamagishi T, Yamazaki T, et al. Subfoveal choroidal thickness in typical age-related macular degeneration and polypoidal choroidal vasculopathy. Graefes Arch Clin Exp Ophthalmol 2011;249(8):1123-8.

6. Manjunath V, Goren J, Fujimoto JG, Duker JS. Analysis of choroidal thickness in age-related macular degeneration using spectral-domain optical coherence tomography. Am J Ophthalmol 2011;152(4):663-8.

7. Chung SE, Kang SW, Lee JH, Kim YT. Choroidal thickness in polypoidal choroidal vasculopathy and exudative age-related macular degeneration. Ophthalmology 2011;118(5):840-5.

8. Kim SW, Oh J, Kwon SS, et al. Comparison of choroidal thickness among patients with healthy eyes, early age-related maculopathy, neovascular age-related

macular degeneration, central serous chorioretinopathy, and polypoidal choroidal vasculopathy. Retina 2011;31(9):1904-11.

9. Jirarattanasopa P, Ooto S, Nakata I, et al. Choroidal thickness, vascular hyperpermeability, and complement factor H in age-related macular degeneration and polypoidal choroidal vasculopathy. Invest Ophthalmol Vis Sci 2012;53(7):3663-72.

10. Li Y, You QS, Wei WB, et al. Polypoidal choroidal vasculopathy in adult chinese: the Beijing Eye Study. Ophthalmology 2014;121(11):2290-1.

11. Rishi P, Rishi E, Mathur G, Raval V. Ocular perfusion pressure and choroidal thickness in eyes with polypoidal choroidal vasculopathy, wet-age-related macular degeneration, and normals. Eye (Lond) 2013;27(9):1038-43.

12. Okubo A, Sameshima M, Uemura A, et al. Clinicopathological correlation of polypoidal choroidal vasculopathy revealed by ultrastructural study. Br J Ophthalmol 2002;86(10):1093-8.

13. Terasaki H, Miyake Y, Suzuki T, et al. Polypoidal choroidal vasculopathy treated with macular translocation: clinical pathological correlation. Br J Ophthalmol 2002;86(3):321-7.

14. Nakashizuka H, Mitsumata M, Okisaka S, et al. Clinicopathologic findings in polypoidal choroidal vasculopathy. Invest Ophthalmol Vis Sci 2008;49(11):4729-37.

15. Koizumi H, Yamagishi T, Yamazaki T, Kinoshita S. Relationship between clinical characteristics of polypoidal choroidal vasculopathy and choroidal vascular hyperpermeability. Am J Ophthalmol 2013;155(2):305-13 e1.

16. Maruko I, Iida T, Sugano Y, et al. Subfoveal retinal and choroidal thickness after verteporfin photodynamic therapy for polypoidal choroidal vasculopathy. Am J Ophthalmol 2011;151(4):594-603 e1.

17. Nickla DL, Wallman J. The multifunctional choroid. Prog Retin Eye Res 2010;29(2):144-68.

18. Dansingani KK, Balaratnasingam C, Naysan J, Freund kb. En face imaging of pachychoroid spectrum disorders with swept-source optical coherence tomography. Retina 2016;36(3):499-516.

19. Balaratnasingam C, Lee WK, Koizumi H, et al. Polypoidal Choroidal Vasculopathy: A Distinct Disease or Manifestation of Many? Retina 2016;36(1):1-8.

20. Sonoda S, Sakamoto T, Yamashita T, et al. Choroidal structure in normal eyes and after photodynamic therapy determined by binarization of optical coherence tomographic images. Invest Ophthalmol Vis Sci 2014;55(6):3893-9.

21. Cheung CM, Bhargava M, Laude A, et al. Asian age-related macular degeneration phenotyping study: rationale, design and protocol of a prospective cohort study. Clin Experiment Ophthalmol 2012;40(7):727-35.

22. Cheung CM, Li X, Mathur R, et al. A prospective study of treatment patterns and 1-year outcome of Asian age-related macular degeneration and polypoidal choroidal vasculopathy. PLoS One 2014;9(6):e101057.

23. Cheung CM, Bhargava M, Xiang L, et al. Six-month visual prognosis in eyes with submacular hemorrhage secondary to age-related macular degeneration or polypoidal choroidal vasculopathy. Graefes Arch Clin Exp Ophthalmol 2013;251(1):19-25.

24. Laser photocoagulation of subfoveal neovascular lesions in age-related macular degeneration. Results of a randomized clinical trial. Macular Photocoagulation Study Group. Arch Ophthalmol 1991;109(9):1220-31.

25. [Criteria for diagnosis of polypoidal choroidal vasculopathy]. Nippon Ganka Gakkai Zasshi 2005;109(7):417-27.

26. Cheung CM, Lai TY, Chen SJ, et al. Understanding indocyanine green angiography in polypoidal choroidal vasculopathy: the group experience with digital fundus photography and confocal scanning laser ophthalmoscopy. Retina 2014;34(12):2397-406.

27. Cheung CM, Laude A, Wong W, et al. Improved specificity of polypoidal choroidal vasculopathy diagnosis using a modified everest criteria. Retina 2015;35(7):1375-80.

28. Chung SE, Kang SW, Kim JH, et al. Engorgement of vortex vein and polypoidal choroidal vasculopathy. Retina 2013;33(4):834-40.

29. Yu PK, Tan PE, Cringle SJ, et al. Phenotypic heterogeneity in the endothelium of the human vortex vein system. Exp Eye Res 2013;115:144-52.

30. Wong CW, Cheung CM, Mathur R, et al. Three-year results of polypoidal choroidal vasculopathy treated with photodynamic therapy: Retrospective Study and Systematic Review. Retina 2015;35(8):1577-93.

31. Spaide RF, Donsoff I, Lam DL, et al. Treatment of polypoidal choroidal vasculopathy with photodynamic therapy. Retina 2002;22(5):529-35.

32. Tan CS, Ouyang Y, Ruiz H, Sadda SR. Diurnal variation of choroidal thickness in normal, healthy subjects measured by spectral domain optical coherence tomography. Invest Ophthalmol Vis Sci 2012;53(1):261-6.

33. Chakraborty R, Read SA, Collins MJ. Diurnal variations in axial length, choroidal thickness, intraocular pressure, and ocular biometrics. Invest Ophthalmol Vis Sci 2011;52(8):5121-9.

CHAPTER X1 TABLES

Table 11.1 Clinical characteristics of study subjects between AMD and PCV

Clinical Characteristics	AMD (N=78)	PCV (N=78)	P value*	P value**
Age, yrs	71.80 (9.19)	66.30 (9.69)	**<0.001**	-
Gender, male (%)	45 (57.7)	42 (53.8)	0.747	-
Hypertension, yes	53 (74.6)	34 (47.2)	**0.001**	**0.015**
Diabetes, yes	24 (33.8)	25 (34.2)	1.000	0.594
Current smoker, yes	12 (15.4)	12 (16.4)	1.000	0.963
Hba1c, %	6.16 (1.14)	5.98 (0.88)	0.337	0.579
Total cholesterol, mmol/l	5.67 (1.32)	5.31 (1.09)	0.095	**0.011**
Spherical equivalent, diopter	-0.18 (1.40)	-0.06 (2.19)	0.684	0.764
Best-corrected visual acuity, logMAR	0.85 (0.54)	0.86 (0.55)	0.884	0.868

Data presented are means (SD) or number (%)

* Based on independent sample t-test for continuous variables or Chi-square/Fisher's exact test for categorical variables

** Age and gender adjusted

Table 11.2 Choroidal characteristics of study subjects between AMD and PCV

	Unadjusted			Adjusted	
Choroidal Characteristics	**All AMD (N=78)**	**All PCV (N=78)**	**P value***	**Difference† (95% CI)**	**P value****
Mean CT, um	224.33 (72.67)	263.62 (93.79)	**0.004**	23.17 (-4.65, 51.00)	0.102
Sub-foveal CT, um	243.47 (80.79)	288.54 (99.04)	**0.002**	29.61 (-0.511, 59.73)	0.054
Mean nasal CT, um	205.66 (75.49)	257.52 (107.95)	**0.001**	34.21 (3.48, 64.94)	**0.029**
Mean temporal CT, um	243.10 (77.66)	269.82 (86.22)	**0.044**	12.16 (-15.58, 39.91)	0.388
CSI curvature, mm^-1	0.578 (0.264)	0.532 (0.280)	0.300	-0.034 (-0.132, 0.065)	0.477
No of inflection point	1.92 (1.33)	1.88 (1.33)	0.858	0.043 (-0.426, 0.513)	0.855
Thickest point distance from fovea	-0.003 (1.63)	0.350 (1.27)	0.134	0.192 (-0.315, 0.699)	0.455
Vascular area (sub-fovea), mm^2	0.148 (0.053)	0.177 (0.064)	**0.003**	0.020 (0.000, 0.040)	0.053
Vascular area (6 mm region), mm^2	0.554 (0.195)	0.639 (0.227)	**0.013**	0.051 (-0.020, 0.122)	0.158

Data presented are means (SD)

*P value calculated are based on independent t-test

** P value are based on linear regression after adjusting for age and hypertension

† Difference in choroidal characteristics of PCV with reference to AMD

Table 11.3 Choroidal characteristics of study subjects between AMD and typical PCV (choroidal thickness ≥250μm)

	Unadjusted			Adjusted	
Choroidal Characteristics	**AMD (N=78)**	**Typical PCV (N=40)**	**P value***	**Difference† (95% CI)**	**P value****
Mean CT, um	224.33 (72.67)	334.45 (72.26)	**<0.001**	89.89 (59.43, 120.35)	**<0.001**
Sub-foveal CT, um	243.47 (80.79)	361.16 (75.53)	**<0.001**	98.04 (64.91, 131.16)	**<0.001**
Mean nasal CT, um	205.66 (75.49)	334.50 (92.60)	**<0.001**	107.23 (73.21, 141.26)	**<0.001**
Mean temporal CT, um	243.10 (77.66)	334.52 (62.98)	**<0.001**	72.58 (41.13, 104.03)	**<0.001**
CSI curvature, mm^-1	0.578 (0.264)	0.522 (0.280)	0.289	-0.039 (-0.161, 0.083)	0.530
No of inflection point	1.92 (1.33)	1.75 (1.31)	0.505	0.123 (-0.711, 0.464)	0.678
Thickest point distance from fovea	-0.003 (1.63)	0.377 (1.186)	0.151	0.136 (-0.516, 0.787)	0.680
Vascular area (sub-fovea), mm^2					
Mean (SD)	0.148 (0.053)	0.215 (0.061)	**<0.001**	0.053 (0.029, 0.077)	**<0.001**
Lowest quartile	0.085 (0.019)	0.150 (0.018)	**<0.001**	0.072 (0.056, 0.087)	**<0.001**
Highest quartile	0.217 (0.033)	0.291 (0.061)	**<0.001**	0.076 (0.035, 0.116)	**0.001**
Vascular area (6 mm region), mm^2					
Mean (SD)	0.554 (0.195)	0.797 (0.191)	**<0.001**	0.195 (0.113, 0.278)	**<0.001**
Lowest quartile	0.329 (0.061)	0.594 (0.057)	**<0.001**	0.276 (0.223, 0.328)	**<0.001**
Highest quartile	0.810 (0.138)	1.040 (0.160)	**<0.001**	0.211 (0.093, 0.329)	**0.001**

Data presented are means (SD)

*P value calculated are based on independent t-test

** P value are based on linear regression after adjusting for age and hypertension

† Difference in choroidal characteristics of typical PCV (CT≥250 μm) with reference to AMD

Table 11.4 Choroidal characteristics of study subjects between AMD and PCV without thick choroid (choroidal thickness<250µm)

	Unadjusted			Adjusted	
Choroidal Characteristics	**AMD (N=78)**	**PCV without thick choroid (N=38)**	**P value***	**Difference† (95% CI)**	**P value****
Mean CT, um	224.33 (72.67)	189.05 (40.84)	**0.002**	-33.86 (-61.15, -6.56)	**0.016**
Sub-foveal CT, um	243.47 (80.79)	212.09 (51.95)	**0.042**	-27.78 (-58.65, 3.07)	0.077
Mean nasal CT, um	205.66 (75.49)	176.49 (45.44)	**0.016**	-29.53 (-58.71, -0.350)	**0.047**
Mean temporal CT, um	243.10 (77.66)	201.72 (44.76)	**0.001**	-38.16 (-66.87, -9.45)	**0.010**
CSI curvature, mm^-1	0.578 (0.264)	0.543 (0.283)	0.481	-0.031 (-0.149, 0.087)	0.604
No of inflection point	1.92 (1.33)	2.03 (1.36)	0.662	-0.103 (-0.467, 0.673)	0.721
Thickest point distance from fovea	-0.003 (1.63)	0.320 (1.375)	0.307	-0.206 (-0.443, 0.854)	0.531
Vascular area (sub-fovea), mm^2					
Mean (SD)	0.148 (0.053)	0.136 (0.037)	0.282	-0.008 (-0.029, 0.013)	0.451
Lowest quartile	0.085 (0.019)	0.091 (0.013)	0.292	0.003 (-0.004, 0.010)	0.447
Highest quartile	0.217 (0.033)	0.185 (0.013)	**0.001**	-0.019 (-0.031, -0.007)	**0.004**
Vascular area (6 mm region), mm^2					
Mean (SD)	0.554 (0.195)	0.473 (0.116)	**0.011**	-0.07 (-0.143, 0.003)	0.060
Lowest quartile	0.329 (0.061)	0.315 (0.035)	0.448	-0.007 (-0.729, 0.473)	**0.009**
Highest quartile	0.810 (0.138)	0.606 (0.047)	**<0.001**	-0.123 (-0.172, -0.073)	**<0.001**

Data presented are means (SD)

*P value calculated are based on independent t-test

** P value are based on linear regression after adjusting for age and hypertension

† Difference in choroidal characteristics of PCV without thick choroid (<250µm) with reference to AMD

CHAPTER XI FIGURES

Figure 11.1 Comparison of FFA, ICG, choroidal thickness and vascular area across AMD and PCV subtypes.

11.1A Typical AMD with thin choroid and low vascular area. Choroidal thickness: 136um; vascular area 0.37mm^2

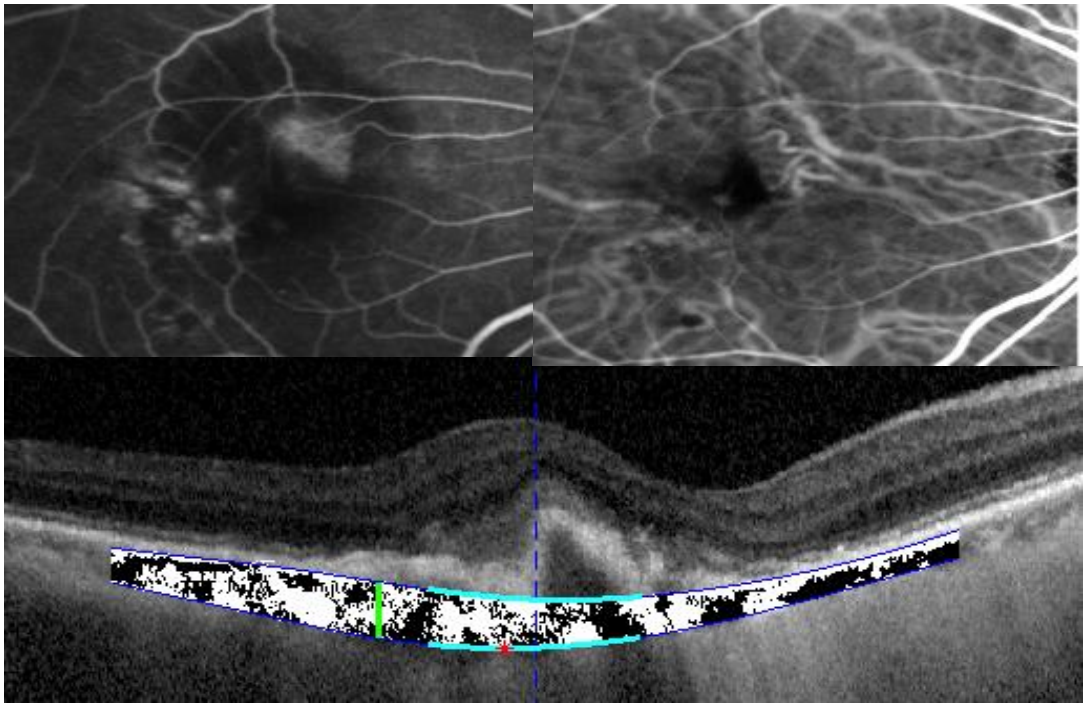

11.1B Typical PCV with thick choroid and high vascular area. Choroidal thickness: 486um; vascular area: 0.96mm^2

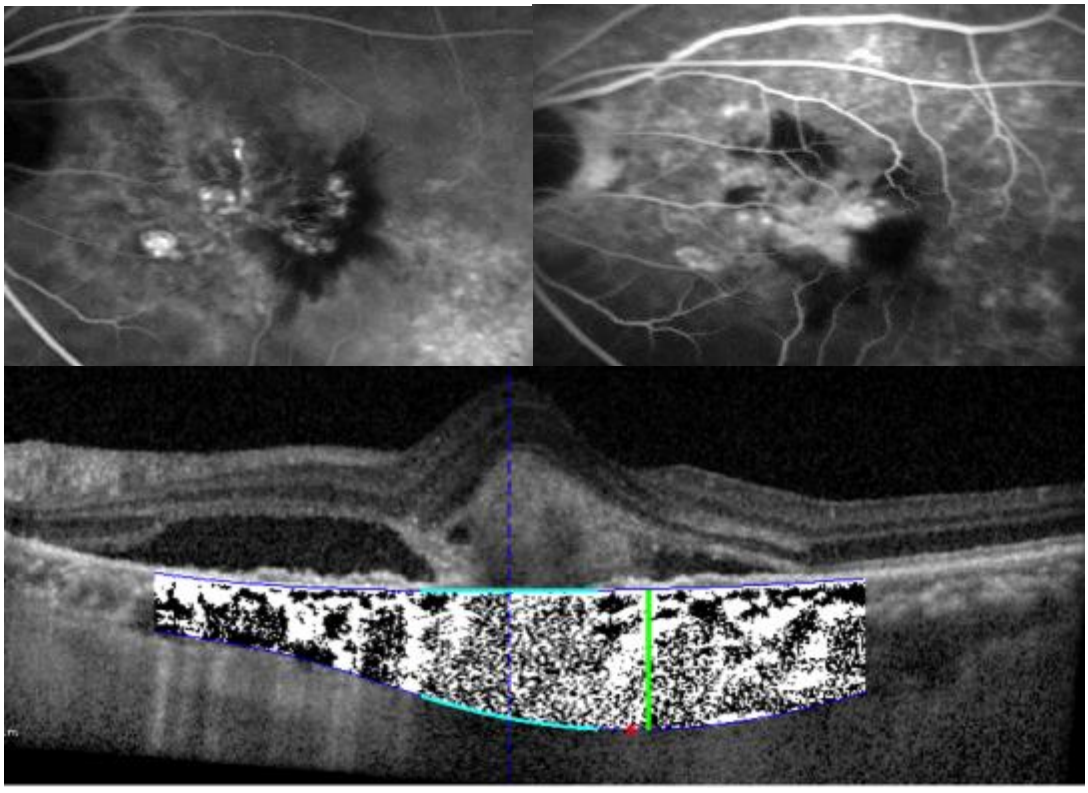

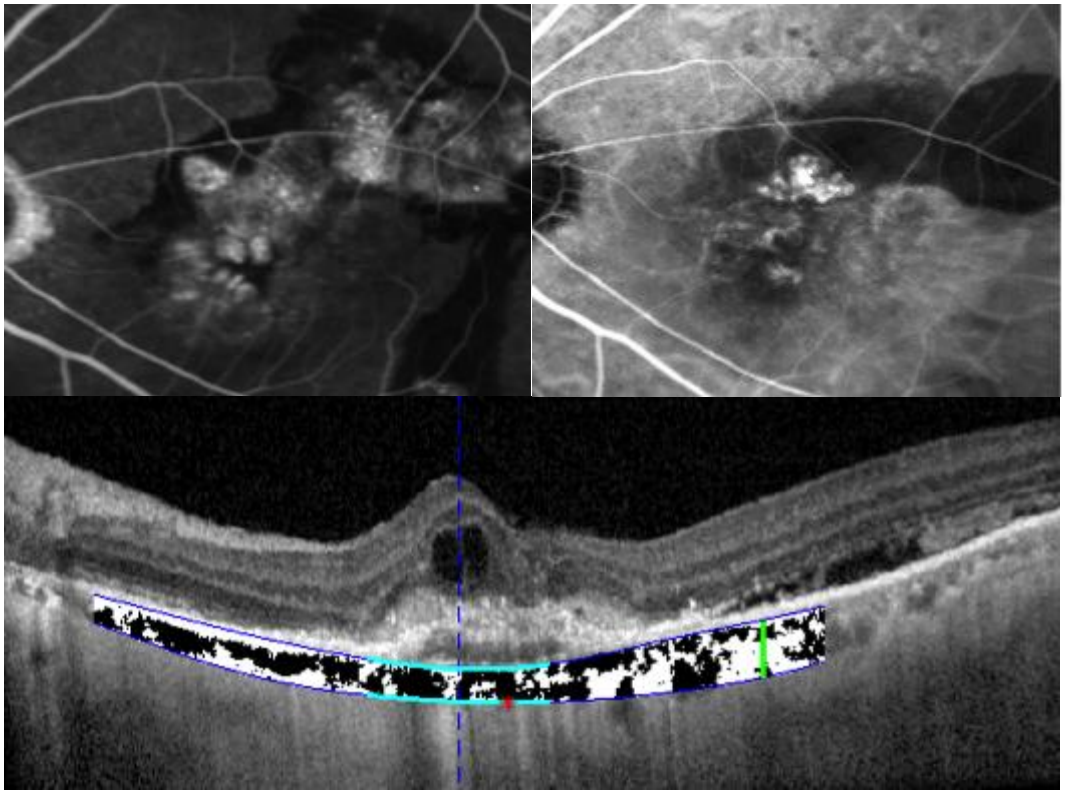

11.3 C PCV with thin choroid and low vascular area. Choroidal thickness: 110 um; vascular area: 0.33mm^2

CHAPTER 12

DISCUSSION AND FUTURE DIRECTIONS

12.1 SUMMARY OF THE FINDINGS

In this doctoral work, we have successfully developed novel (semi- and fully-automated) image processing techniques to provide fast, reliable and comprehensive assessment of the choroid in-vivo. Using our fully automated choroidal segmentation technique we performed a population-based evaluation of the distribution and determinants of most commonly used macular and peripapillary choroidal traits: thickness and volume. Distribution and determinants of these traits were then established in most common chorio-retinal diseases such as myopia, AMD and DR. Lastly, in addition to CT and volume (which may not capture the specific changes within the choroid), we performed detailed characterization of choroidal morphometric and vascular attributes in the above eye diseases and their comparison with healthy eyes.

The salient findings from our various studies are summarized below:

We found that only 60% of EDI images had well-defined CSI and the variability in CT measurement was higher in the images with poorly defined CSI (ICC: 0.97 for images with well-defined CSI vs. ICC: 0.51 for images with poorly defined CSI), highlighting that visibility of CSI was critical for accurate determination of CT (Chapter 4).

We overcame the primary challenge of poor CSI visibility by enhancing the visualization of CSI by our novel technique of “adaptive compensation” (Chapter 5).

After applying adaptive compensation to enhance our images, the contrast between choroid and sclera was significantly increased (from 0.50 ± 0.14 to 0.90 ± 0.10, $p < 0.001$; paired *t*-test) and CT measurements were more reliable (ICC: 0.93 to 0.97) than the non-enhanced images (ICC: 0.90 to 0.93). Nevertheless, such technique still required manual input to mark the CSI and measure CT, thus subject to measurement errors, limiting its clinical utility.

To overcame the above limitations of the semi-automated technique, we further developed and evaluated novel fully automated choroidal image processing technique which defined the CSI and measured CT as well as choroidal volume at both macular and peripapillary regions objectively (Chapter 6). Comparing our automated technique with the reference standard (manual measurement by trained readers), we found excellent agreement (ICC: 0.90 to 0.96) between the 2 assessments, demonstrating that our automated choroidal image processing technique was valid and comparable to existing manual CT measurement.

We adapted our validated fully automated choroidal image processing technique to obtain distribution and determinants of choroidal measures such as thickness and volume (in macular and peripapillary regions) in a multi-ethnic population in Singapore (Chapter 7). After adjusting for the differences in population specific characteristics, we observed slight ethnic difference in macular CT (mean difference 12 µm, p=0.011), macular choroidal volume (mean difference 0.02 $mm^{3,}$ p=0.002) and peripapillary CT (mean difference ~32 µm, p<0.001) among ethnic Malays and Indians. Indians tend to have slightly thicker choroid than Malays.

With regards to topographical distribution, both macular and peripapillary choroid was asymmetrically distributed (macular: thickest subfoveally and thinnest nasally; peripapillary: thickest superiorly and thinnest inferiorly). However, there was

no difference in topographical profile of macular and peripapillary choroid among ethnic Malays and Indians.

Factors such as age, gender and AL were the major determinants of CT and volume among both ethnic groups and should be taken into account when interpreting EDI OCT based CT measurements in clinical settings.

We assessed vascular status of the choroid through image binarization of EDI SD-OCT images in healthy eyes from a population-based study (Chapter 8). To represent vascular status of the choroid we computed OCT derived quantitative parameter called "choroidal vascularity index (CVI)". Two-third (~66%) of the subfoveal choroid was found to be vascular in healthy eyes.

On performing detailed characterization of choroidal morphological and vascular traits in young, high myopes (Chapter 9) we found that macular and peripapillary CT was significantly lower in high myopic eyes over a range of eccentricities. Mean sub-foveal CT in myopes was 225.87 ± 5.51 µm as compared to 375.15 ± 6.58 µm in emmetropes. Mean PPCT in myopes was 142.62 ± 43.84 µm vs. 181.90 ± 46.43 µm in emmetropes. There was further decrease in macular and peripapillary CT with increase in severity of myopia.

Macular and peripapillary CT distribution followed a different profile in high myopes compared to emmetropes. Macular CT in myopic eyes was thickest superiorly whereas in emmetropes it was thickest at the fovea. However, in both the groups macular choroid was thinnest nasally. Peripapillary choroid was thickest at the superior location in myopic eyes, whereas in emmetropes it was thickest at the temporal location. However, in both the groups peripapillary choroid was thinnest inferiorly.

AL, presence of posterior staphyloma and chorio-retinal atrophy were the significant predictors of macular CT in high myopia. For PPCT: AL, IOP and presence of posterior staphyloma were independent determinants. These factors must be taken into account when interpreting the data on CT. Given the large number of people with myopia in the world, these findings seem to have widespread implications.

Our result demonstrates significant alterations in choroidal morphological and vascular features in high myopes. CSI was less curved posteriorly and had more inflection points in high myopes with myopic macular degeneration. Choroidal vasculature was significantly reduced in high myopic eyes; however, this was more prevalent in eyes with myopic macular degeneration.

We further report that high myopic eyes had thinner choroid but CT was not an independent predictor of visual acuity. Other factors related to myopia were likely responsible for the diminished visual acuity in young highly myopic eyes.

There were significant alterations in choroidal structural and vascular characteristics in both diabetes and DR (Chapter 10). As speculated, subjects with diabetes showed significantly thinner choroid and lower vascular area, which is consistent with capillary drop-out wherein decreased choroidal blood flow plays a key role in the pathogenesis. Conversely, among the diabetic group, subjects with DR displayed thicker choroid and significantly higher vascular area compared to no DR.

Although eyes with PCV had thicker choroid than typical AMD, the difference in choroidal morphologic and vascular attributes were not significantly different after adjustment for major confounding parameters such as age and hypertension (Chapter 11).

We observed significant heterogeneity within the PCV group, suggesting two subtypes with different choroidal features: typical PCV with thick choroid and PCV without thick choroid (polypoidal CNV). Both CT and vascular area were significantly higher in eyes with typical PCV compared to eyes with AMD, indicating that the choroidal morphology and function are distinctly different from that in eyes with typical AMD. PCV and thin choroid had significantly lower vascular area than typical PCV group, and vascular area measurements were similar to that in eyes with typical AMD.

12.2 CLINICAL SIGNIFICANCE

1. Good visibility of CSI is critical for accurate measurement of CT. But despite the technique of EDI in SD-OCT, CSI is not clearly visible. We used adaptive compensation technique to enhance the contrast at the CSI which significantly reduced the variability in manual measurements of CT, making CT an important diagnostic parameter for evaluating diseases where choroid is implicated in pathophysiology.
2. We developed automated choroidal segmentation software which provided fast (~1 second vs. ~3-4 minute per image manually) and accurate measurements of CT at both macular and peripapillary locations. This will help in distinguishing clinically significant change of CT as well as in risk-profiling of various diseases. Furthermore, our automated software provided comprehensive assessment of the choroid in terms of choroidal volume which can better reflect the profile of the entire choroid. Therefore, our fast, reliable and comprehensive assessment of the choroid is useful in both clinical and population studies.

3. We provide race-specific clinical information to better understand the chorio-retinal pathologies in different ethnic groups.
4. Information on distribution and determinants of CT and CV is useful for clinicians to better diagnose the disease.
5. Given choroidal vascular dysfunction are thought to be associated with many pathologic conditions our detailed characterization of the choroidal vascular area, stromal area and vascularity is useful to study specific changes in the choroid. Particularly choroidal vascularity index is used to gain insight into the vascular status of the choroid.
6. Detailed characterization of various morphological and vascular traits of the choroid has important implication in the pathogenesis and possibly the treatment response.
7. We found significant alteration in choroidal structural and vascular characteristics in diseases such as high myopia, diabetic retinopathy, AMD and PCV. These specific changes in choroidal traits highlight the relevance of further understanding phenotypic manifestations of choroidal vasculature in the diagnostic criteria for these diseases.

12.3 STUDY LIMITATIONS

1. Although the location of the CSI on Spectralis images was determined qualitatively as the junction between posterior choroid and sclera, there was no reference standard to confirm where this structure is actually located in the eye.
2. Single line scan protocol was used to determine the CT profile. Future studies using denser scanning protocols to determine the topographical

thickness profile of the choroid, will likely provide additional insights into the changes in the choroid associated with diseases.

3. The study population only consisted of subjects of Malay and Indian ethnicities, and the findings may vary in other racial groups. Further studies in other ethnic populations, in particular Chinese are thus warranted.
4. As in any population based study, our investigation included all eligible and participating subjects from the study. Some of them have eye diseases that may have changed choroidal traits. Therefore, the distribution of choroidal traits determined in this study may represent the choroidal attributes not in healthy eyes but in eyes of the general adult and elderly populations. However, this would not affect the observed associations because, in our multiple regression analysis model, we have adjusted for the potential ocular diseases in elderly people that might influence choroidal features.
5. For detailed characterization of the choroid, although our images were binarized at standard threshold, there is a possibility of over or underestimation of both luminal and stromal areas.
6. Our subjects were examined only at a single time point, and thus we are not able to take the diurnal variation of choroidal thickness into account. However, the CT measurements in our study were not performed at the same time of the day; each participant underwent the OCT examination in a randomized manner with respect to when the readings were obtained. It seems unlikely that circadian changes may have influenced the results of our investigation.

7. Due to our cross-sectional study design, we were unable to determine the causal relationships between the various risk factors and choroidal traits. Longitudinal studies to determine the sequence of changes as they relate to disease progression would prove beneficial.

12.4 FUTURE DIRECTIONS

Outcomes from this dissertation provide some interesting opportunities to explore important future directions in the field of choroidal imaging. Some of these studies have commenced while other ideas can be explored in future.

We have characterized various choroidal morphological and vascular traits using our novel image processing techniques. We established the topographical distribution as well as ocular and systemic risk factors for the most commonly used choroidal attributes such as thickness and volume in a multi-ethnic population in Singapore. Singapore has 3 major racial/ethnic groups: Malays, Indians and Chinese. This gives us a unique opportunity to study the effect of ethnic variation in CT among Asians in a relatively common geographic and socio-economic environment. However, this doctoral work was confined to only two ethnic groups: Malays and Indians. Due to time constraints we could not evaluate the distribution and determinants of choroid in ethnic Chinese. Since Chinese ethnic group accounts for ~80% of the population of Singapore, we therefore, are expanding our work to evaluate choroidal characteristics in Chinese.

In order to better understand the chorio-retinal pathologies in Asians and Caucasians (such as PCV), next step could be to compare choroidal attributes between races. Knowledge of such features would help to effectively identify optimal race-specific treatment.

In our algorithm for detailed analyses of the choroid, delineation of CSI was based on markings of few most prominent points at the junction of the choroid and the sclera. These were further extrapolated to mark the entire CSI. Future algorithm marking the CSI without extrapolating the points would result in a more precise assessment of the choroid.

For the myopic group, all our study subjects were males, and thus, some of our findings may not be generalized to females. Future studies involving females in different degree of myopic refractive error would give better understanding of the choroid in myopia.

In diabetes, to date, there is no consensus as to whether there is thinning or thickening of the choroid. However, it has been postulated that blood flow may play a crucial role in the variation of CT. Therefore, newer imaging techniques such as choroidal angiography may be explored to explain this further. Although, we did study the effect of severity of DR on choroidal features but our analysis was limited by sample size. Further studies to correlate the severity of DR with choroidal traits in larger sample may provide a better insight into the choroidal angiopathy associated with DR and its effect on the progression of the disease.

Likewise, the effect of different treatment modalities such as intravitreal injections, lasers such as focal or PRP on choroidal parameters was investigated but again we did not find significant difference in any of the choroidal traits in DR subjects with or without laser treatment. We speculate the reason for no difference in choroidal features across the two groups to be the lesser number of subjects in treatment group compared to no treatment. It is more likely a power issue and we

recommend future studies with more number of subjects in treatment group to study the likely effect of lasers on choroidal attributes.

Lastly, recent innovations in technology such as longer wavelength OCT including swept source (SS) technology along with OCT angiograpgy (OCT-A) and en-face imaging may provide an even better understanding of choroidal involvement in retinal diseases due to following features:

Longer Wavelength and Swept Source Technology: OCT systems using longer wavelength (1050 nm) and SS-OCT technology have demonstrated an enhanced visualization of the choroid, even through opaque media.[1] Swept laser light sources can rapidly sweep the required frequencies, the acquisition of scans is much faster with axial scan rates of up to 100 000–236 000 A-scans per second (5 to 10 times that of the SD-OCT), and can achieve axial resolutions of 11 μm in tissue.[2] Because data can be acquired much faster, volumetric assessment of the choroid is also feasible.[3]

Significant improvement in the visualization of CSI using these techniques is important in diseases such as CSCR, where the choroid is thicker than normal, and thus difficult to evaluate across its entire width. In addition, volumetric analysis of the choroid, as well as that of the various pathological features such as CNV and subretinal/intraretinal fluid, may be possible. Such a volumetric analysis is expected to help with monitoring the progression of diseases such as wet AMD, CSCR and DR, as well as assessment of the response to treatments such as anti-VEGF agents, laser photocoagulation and PDT.

OCT Angiography (OCT-A): In contrast to ICG and FFA, which are two-dimensional investigations for blood flow analysis, OCT-A emerges as a novel, high-resolution, non-invasive imaging modality which can ‘visualize’ ocular blood flow in

retinal and choroidal vessels and potentially identify angiographic abnormalities in the retinal and choroidal microvasculature. The novel OCT-A adopts the split-spectrum amplitude-decorrelation angiography (SSADA) technology and detects blood flow through motion contrast generated by moving red blood cells at various retinal and choroidal layers.[4, 5] This new technology allows OCT-A to characterize vascular information in various segmented retinal and choroidal layers and provide unprecedented quantitative measurements of retinal and choroidal microcirculation by generating retinal/choroidal vascular perfusion density parameters which are proxy measures of retinal/choroidal blood flow. Thus OCT-A's retinal vascular perfusion parameter can be potentially used as an imaging diagnostic tool.

En-face Imaging: This allows the clinician to visualize three-dimensional data in a fundus projection. Although cross-sectional images (B-scans) have helped delineate pathological features in retinal diseases, microstructural changes and morphology of the retinal and choroidal vasculature are difficult to evaluate using B-scans. This is expected to improve as en-face imaging provides further detail about the subtle pathological features in the retina and choroid in diseased states.[6] In addition, the involvement of the specific vascular layers of the choroid in different diseases is expected to delineate in further detail using this technique. We hypothesize that such an attempt can be useful not only as an adjunctive diagnostic tool, but it can also lead to more targeted approaches to treating various chorio-retinal pathologies.

12.5 REFERENCES

1. Povazay B, Hermann B, Unterhuber A, et al. Three-dimensional optical coherence tomography at 1050 nm versus 800 nm in retinal pathologies: enhanced performance and choroidal penetration in cataract patients. J Biomed Opt 2007;12(4):041211.

2. Srinivasan VJ, Huber R, Gorczynska I, et al. High-speed, high-resolution optical coherence tomography retinal imaging with a frequency-swept laser at 850 nm. Opt Lett 2007;32(4):361-3.

3. Drexler W, Fujimoto JG. State-of-the-art retinal optical coherence tomography. Prog Retin Eye Res 2008;27(1):45-88.

4. Jia Y, Tan O, Tokayer J, et al. Split-spectrum amplitude-decorrelation angiography with optical coherence tomography. Opt Express 2012;20(4):4710-25.

5. Jia Y, Bailey ST, Wilson DJ, et al. Quantitative optical coherence tomography angiography of choroidal neovascularization in age-related macular degeneration. Ophthalmology 2014;121(7):1435-44.

6. Srinivasan VJ, Adler DC, Chen Y, et al. Ultrahigh-speed optical coherence tomography for three-dimensional and en face imaging of the retina and optic nerve head. Invest Ophthalmol Vis Sci 2008;49(11):5103-10.

Available online at www.sciencedirect.com
ScienceDirect
journal homepage: www.elsevier.com/locate/survophthal

Major review

State of science: Choroidal thickness and systemic health

Kara-Anne Tan, MBBS[a], *Preeti Gupta, MOpt*[a,b], *Aniruddha Agarwal, MD*[c], *Jay Chhablani, MS*[d], *Ching-Yu Cheng, PhD*[b,e,f], *Pearse A. Keane, FRCOphth*[g], *Rupesh Agrawal, FRCS*[b,e,f,*]

[a] *Yong Loo Lin School of Medicine, National University of Singapore, Singapore, Singapore*
[b] *Singapore Eye Research Institute and Singapore National Eye Centre, Singapore, Singapore*
[c] *Stanley M. Truhlsen Eye Institute, University of Nebraska Medical Center, Omaha, Nebraska, USA*
[d] *Department of Vitreoretina Services, L.V. Prasad Eye Institute, Hyderabad, Telangana, India*
[e] *Department of Ophthalmology, Yong Loo Lin School of Medicine, National University of Singapore and National University Health System, Singapore, Singapore*
[f] *Duke-NUS Graduate Medical School, Singapore, Singapore*
[g] *Department of Medical Retina, Moorfields Eye Hospital, NHS Foundation Trust, London, United Kingdom*

ARTICLE INFO

Article history:
Received 27 June 2015
Received in revised form 28 February 2016
Accepted 29 February 2016
Available online xxx

Keywords:
choroidal thickness
systemic disease
vascular layer
EDI-OCT
age
diurnal variation
physiological
metabolic
inflammatory

ABSTRACT

The choroid is a highly vascular structure; therefore, a wide range of systemic conditions can affect it. Conversely, choroid health may also give us insight into systemic health. With the emergence of optical coherence tomography, there has been a surge in the research on choroidal thickness and factors affecting it. Studies regarding the effect of systemic health on the choroid have largely been in the form of cross-sectional, prospective, and case studies. We offer a summary of recent findings on the topic.

Kara-Anne Tan and Preeti Gupta are joint first authors.

* Corresponding author: Rupesh Agrawal, FRCS, Consultant, National Healthcare Group Eye Institute, Tan Tock Seng Hospital, Singapore 308433.
E-mail address: Rupesh_agrawal@ttsh.com.sg (R. Agrawal).

0039-6257/$ – see front matter
http://dx.doi.org/10.1016/j.survophthal.2016.02.007

1. Introduction

The choroid is the most vascular layer of the eye and plays an instrumental role in the physiology of the eye and in the pathogenesis of various ocular diseases. Per unit weight, the choroid has the highest blood flow of any tissue in the body[7] and is the vascular supply to the outer retina, retinal pigment epithelium, possibly a portion of the optic nerve,[44] and is the only source of metabolic exchange for the avascular fovea.[80]

A structurally and functionally normal choroidal vasculature is essential for retinal function. Abnormal choroidal blood volume and/or compromised flow may result in photoreceptors dysfunction and death with resultant vision loss.[16] Consequently, the choroid plays a vital role in the pathophysiology of many conditions, such as central serous chorioretinopathy,[27] choroidal neovascularization related to age-related macular degeneration,[68,74] polypoidal choroidal vasculopathy,[68,74] multifocal choroiditis,[55] angioid streaks,[6] and high myopia-related chorioretinal atrophy.[20] In addition, the high flow of blood in the choroid predisposes it as a site for metastatic and embolic spread of tumors and infections.[80] Basically, as a result of the vascular nature of the choroid, potentially any disease affecting vasculature could also affect choroid health.

Quantitative assessment of the choroid has always been a challenging task with conventional imaging modalities such as indocyanine green angiography and ultrasonography because of limited image resolution and repeatability.[22,43] Histological evaluation is difficult because of the lack of samples and may not be accurate owing to changes in the choroid after fixation; however, our understanding of the choroid has been vastly augmented in recent times since the introduction of imaging the choroid *in vivo* using enhanced depth imaging technique of optical coherence tomography (EDI-OCT).[104]

This innovation in technology has sparked a rise in the amount of research done with regard to choroidal thickness,[71,86,104] which is measured on the EDI-OCT from the outer border of the retinal pigment epithelium, represented by a hyperreflective line, to the inner border of the suprachoroidal space, represented by a hyporeflective line. There is, however, only limited literature published on systemic diseases affecting choroidal health.[10] We consolidate the current knowledge on the effects of systemic health on choroidal thickness and attempt to provide insights on how choroid thickness may be an indicator of systemic health (Table 1). Infections and diseases limited to the eye without any systemic involvement have been excluded.

2. Physiological changes in choroidal thickness

2.1. Diurnal variation

There have been few studies determining the diurnal variation of choroidal thickness in healthy patients.[17,106,109,113] A prospective study conducted by Tan et al of 12 healthy volunteers studied the choroidal thickness over 2 separate days in 5 fixed, 2-hour intervals.[106] This study revealed that there is a significant variation in choroidal thickness, with mean amplitude of 33.7 ± 21.5 μm. A progressive decrease in choroidal thickness occurred from 9 AM till 5 PM, with good reproducibility of the diurnal pattern between 2 visits. A study conducted in Japanese patients by Usui et al[113] performed over a 24-hour period showed a similar decreasing trend in choroidal thickness from 9 AM to 6 PM The amplitude reported, 33.0 ± 14.3 μm, was also similar to the reported values in Tan et al. In contrast, a study by Toyokawa et al[109] on Japanese subjects showed a smaller mean amplitude of 20.3 μm and an apparent increase in choroidal thickness from morning to evening. Current literature suggests that there is pattern of change of choroidal thickness; however, the exact pattern remains uncertain. Findings suggest that the time of measurements is important to consider when assessing choroidal thickness in clinical practice and in trials. A possible hypothesis is that diurnal variation occurs because of the circadian rhythm of hormonal changes affecting the blood supply of the body,[67] reflected in the vascular supply of the choroid, influencing its thickness. Increased vascular supply from sympathetic over activity in the morning[67] may be reflected in the vascularity of the choroid and hence results in a thicker choroid in the morning.

2.2. Age-related changes

Age is one of the biggest contributing factors to choroidal thickness (Fig. 1).[37,102] Previous histologic studies have shown a decrease in vascular density, overall luminal area, and diameter of the choriocapillaris with age.[34,87,97] This leads to a decrease in physiological functions of the choroid, that is, the ability of the choroid to provide sufficient levels of oxygen and other metabolites to the retinal pigment epithelium and outer retina may decrease,[104] contributing to the onset of many diseases in the elderly. Similar to histologic studies, age-related choroidal thinning in healthy eyes is confirmed by numerous clinical studies.[11,37,49,70,71,91,96] In healthy eyes, Margolis et al and Ikuno et al reported a decrease in choroidal thickness by 15.6 μm and 14 μm, respectively, for each decade of life.[49,71] Ding et al reported that age-related thinning occurs only after age 60.[31] Barteselli et al reported decrease in choroidal volume by 7.32% for every decade.[11] There are increasing data from recent population-based studies that indicate that both choroidal thickness and choroidal volume decrease with advancing age.[42,115]

A study[84] involving 96 eyes from 48 healthy children (mean age of 6.7 years) and 54 eyes from 27 healthy adults (mean age of 30.7 years) analyzed the choroidal thickness of the 2 populations and found that choroidal thickness was significantly greater in adults than in children. Thus, it is essential that age be taken into consideration when choroidal thickness is evaluated; however, no nomogram with age existents, and it may be time to develop one.

2.3. Gender differences

There are gender differences in the epidemiology of certain macular diseases. For example, a large number of studies have shown that central serous chorioretinopathy is more common in men, with a male-to-female ratio of up to 8:1.[66] Several

Table 1 – Summary and possible mechanisms of choroidal changes in health and disease

Physiological changes	Increase in choroidal thickness	Decrease in choroidal thickness	Proposed mechanism(s)
Diurnal variation		Decrease in thickness may be observed until evening, although there may be fluctuations	Circadian rhythm and hormonal influences; increased vascular supply due to sympathetic over activity during daytime[17,67,106,109,113]
Age		Choroidal thinning is associated with increasing age	Decrease in vascular density, luminal area, and diameter of the choriocapillaris with advancing age[11,37,49,70,71,84,91,96,115]
Gender	Choroid is thicker in men than in women		Lower basal sympathetic tone in men[23,65,83,110,121]
Female and hormonal changes			
Menstrual cycle		Decrease in thickness during the midluteal phase	Hormonal changes affecting choroidal vasculature[78,112]
Pregnancy	Increase in thickness during the second trimester		Pregnancy-related fluid retention during the second trimester; hormonal changes[8,40,98]
Preeclampsia	Increase in thickness may be less than normal pregnant women	In a few patients, thinning of the choroid may occur	Changes may depend on severity of preeclampsia; decreased thickness may be linked with generalized systemic vasospasm[8,38,98]
Metabolic diseases			
Diabetes mellitus		Decrease in thickness compared to nondiabetic healthy controls	Possible relationship with diabetic microangiopathy[33,60,85,90,114,120]
Hypercholesterolemia	Increased thickness compared to healthy controls		Further studies needed to confirm association and possible mechanisms[118]
Cardiovascular diseases			
Hypertension	Increased thickness compared to healthy controls		Interstitial fluid accumulation; further studies needed to confirm possible mechanisms[3]
Respiratory diseases			
Smoking		Significant decrease in thickness compared to nonsmokers	Vascular dysfunction caused by decrease in nitric oxide bioavailability; increased systemic vascular resistance[100,101,111]
Systemic inflammatory conditions			
Ankylosing spondylitis	Increased thickness		Inflammation of the uveal tract[63]
Raynaud's phenomenon		Decrease in thickness	Gender association; higher basal sympathetic tone; systemic vasospasm or sclerosis associated[23,50]
Vogt-Koyanagi-Harada syndrome	Increased thickness during active disease	Decreased thickness during chronic, resolution phase	Inflammation of the uveal tract[25,72,105]
Behçet's disease	Variable; but reports suggest increased thickness during active disease		Inflammation of the uveal tract[24,48,52,61]
Sarcoidosis	Increased thickness is usually associated with presence of lesions such as granulomas		Presence of lesions in the choroid resulting in increased volume[79,92]
Tumors			
Metastatic cancer	Localized increased thickness with dome or plateau-shaped elevation; skin melanomas and breast metastasis are flattest, whereas lung, gastrointestinal, kidney and prostate metastasis are thicker		Presence of lesions in the choroid resulting in increased volume[5,90]

(*continued on next page*)

Table 1 (continued)

Physiological changes	Increase in choroidal thickness	Decrease in choroidal thickness	Proposed mechanism(s)
Sturge-Weber syndrome	Increased thickness associated with diffuse choroidal hemangiomas that reduces after photodynamic therapy		Presence of vascular lesions in the choroid resulting in increased volume[15]
Hematological diseases			
Sickle cell disease		Decrease in thickness may occur in some patients	Microvascular occlusions; vasospasm related[73]
Leukemia	Possible increase		Mechanisms not clear; changes may be highly variable[9]
Neurological diseases			
Alzheimer's disease		Decrease in thickness	Mechanisms not clear[39]
Migraine		Possible decrease during an attack	Mechanisms not clear; possible vasospasm related[29,30,32,122]

studies have reported gender differences in choroidal thickness or volume, for instance, Barteselli et al[11] reported men have a 7.4% greater choroidal volume than women. Two of the population-based studies, the Beijing Eye Study involving 3,233 subjects and the Singapore Malay Eye Study involving 540 subjects, showed male gender to be significantly associated with thicker choroid after adjusting for relevant confounders such as age and axial length.[115] Similarly, Li et al reported that choroidal thickness was 18% higher in men than in women after accounting for age and axial length.[65] Similarly, many other studies in healthy subjects determined subfoveal choroidal thickness to be higher in men than in women.[83,110,121] In contrast, there are 2 studies that showed no statistically significant difference in choroidal thickness measurements between men and women[94,96]; however, as most existing studies reporting thicker choroid in men than in women, gender differences should be considered when interpreting an EDI SD-OCT scan of the choroid. This difference in the thickness of the choroid between men and women might also explain the gender differences in the epidemiology of macular diseases. The difference in choroidal thickness in men and women may be explained by the higher basal sympathetic tone in women.[23]

2.4. *Activity of the sympathetic system*

The tone of the sympathetic system may have an important bearing on the thickness of the choroid. As described in the preceding sections, the basal tone of the sympathetic system may be responsible, at least in part, for physiological variations such as diurnal changes and gender-based differences. Studies have shown that sympathetic innervation of the choroid may be a protective mechanism against overperfusion in conditions with acute rise in systemic blood pressure.[14] Experimental models have shown that stimulation of the cervical sympathetic chain results in frequency-dependent vasoconstriction and reduction in choroidal blood flow.[14] Adrenergic innervation of the choroid that originates from superior cervical ganglion has been also demonstrated in a chicken model.[41] Similarly, in a pigeon model, stimulation of the parasympathetic Edinger-Westphal nucleus dramatically increased choroidal blood flow. Such findings were also confirmed using histology.[35] As the basal tone of the sympathetic system may have a significant role in maintaining the choroidal blood flow and thickness, various conditions that affect the ocular sympathetic innervation may have a direct bearing on choroidal thickness.

3. Choroidal thickness in women

3.1. *Menstrual cycle*

Complex hormonal changes occur during the menstrual cycle, and these fluctuations can affect vascular physiology and cause hemodynamic changes during different phases of the cycle.[76,77] To assess the systemic hemodynamic changes via choroidal vascular changes, a single prospective study[112] looked at 23 eyes of 23 women with regular menstrual cycles. This study showed that, compared to the early follicular

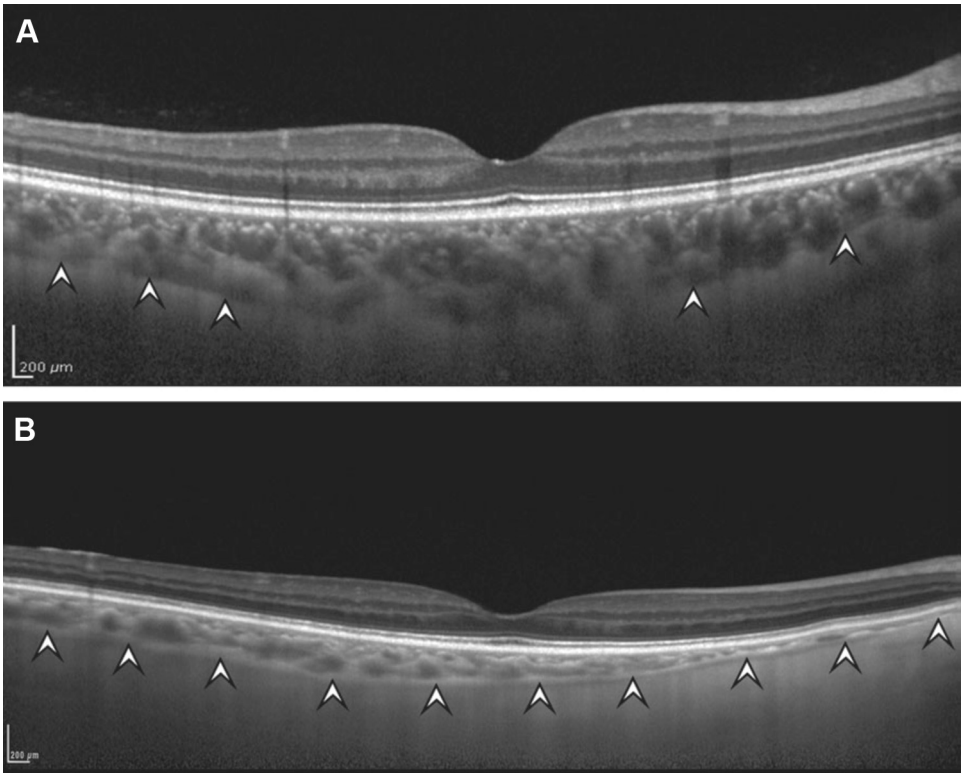

Fig. 1 – Comparison of choroidal thickness obtained using EDI-OCT scans in 2 subjects of different ages. *A*: A 46-year-old man with subfoveal choroidal thickness of 326 μm. *B*: An 83-year-old man with subfoveal choroidal thickness of 163 μm. EDI-OCT, enhanced depth imaging technique of optical coherence tomography.

and ovulatory phases, choroidal thickness decreased significantly during the midluteal phase. Choroidal thickness reduced by 6.47% between the early follicular and midluteal phase. The difference in choroidal thickness between the early follicular phase and ovulatory phase was, however, not statistically significant but suggests that the blood supply during these phases may result in fluctuation of choroidal vascularity and hence affecting the choroidal thickness. Hormonal changes in menstruation have been associated with altered sympathetic outflow.[78] The altered sympathetic outflow may affect choroidal flow, which is possibly reflected in choroidal thickness. These findings show that it may be important to consider menstrual phase of the woman when interpreting choroidal thickness measurements.

3.2. *Pregnancy*

Many ocular changes may occur in pregnancy, including changes in vision, ocular blood flow,[21] decrease in intraocular pressure,[4,46,57] and an increase in central cornea thickness[116] and curvature.[46] Two studies from Atas et al[8] and Sayin et al[98] with 76 and 119 participants, respectively, similarly showed that the choroidal thickness was greater in normal pregnant women than in normal, nonpregnant women. A prospective study[40] involving 90 healthy pregnant women in their first, second, or third trimester and 30 nonpregnant healthy women compared the choroidal thickness in these 4 groups. There was increased choroidal thickness in women in the second trimester as compared to nonpregnant women. There was no significant difference of choroidal thickness among the other groups. This suggests that choroidal thickening can occur in the second trimester. A likely mechanism for this finding is the increase of pregnancy-related fluid retention in the choroid.[8]

3.3. *Pre-eclampsia*

Pre-eclampsia is an obstetrical complication characterized by placental ischemia and systemic inflammation and vascular changes that lead to widespread vasoconstriction and systemic hypertension and proteinuria.[47] Patients with severe preeclampsia may have cerebral or visual disturbances, pulmonary edema, impaired liver function, and thrombocytopenia. Approximately 40% of women with preeclampsia report subjective visual disturbances.[93]

Atas et al[8] and Sayin et al[98] studied the effect of pre-eclampsia on choroidal thickness and found that the increase of choroidal thickness in pre-eclamptic patients was significantly less than in normal pregnant patients and was similar to the choroidal thickness in normal, nonpregnant women. A study[38] was conducted based on 15 severe preeclampsia cases and 15 healthy subjects of matched ethnicity and parity. A reference group of 19 age-matched, nongravid normotensive women was also studied. Severe pre-eclampsia cases demonstrated greater mean choroidal thickness than controls.

The difference in findings may be the result of the difference in severity of the preeclampsia. On one hand, increased vascular permeability may increase the choroidal volume and thickness

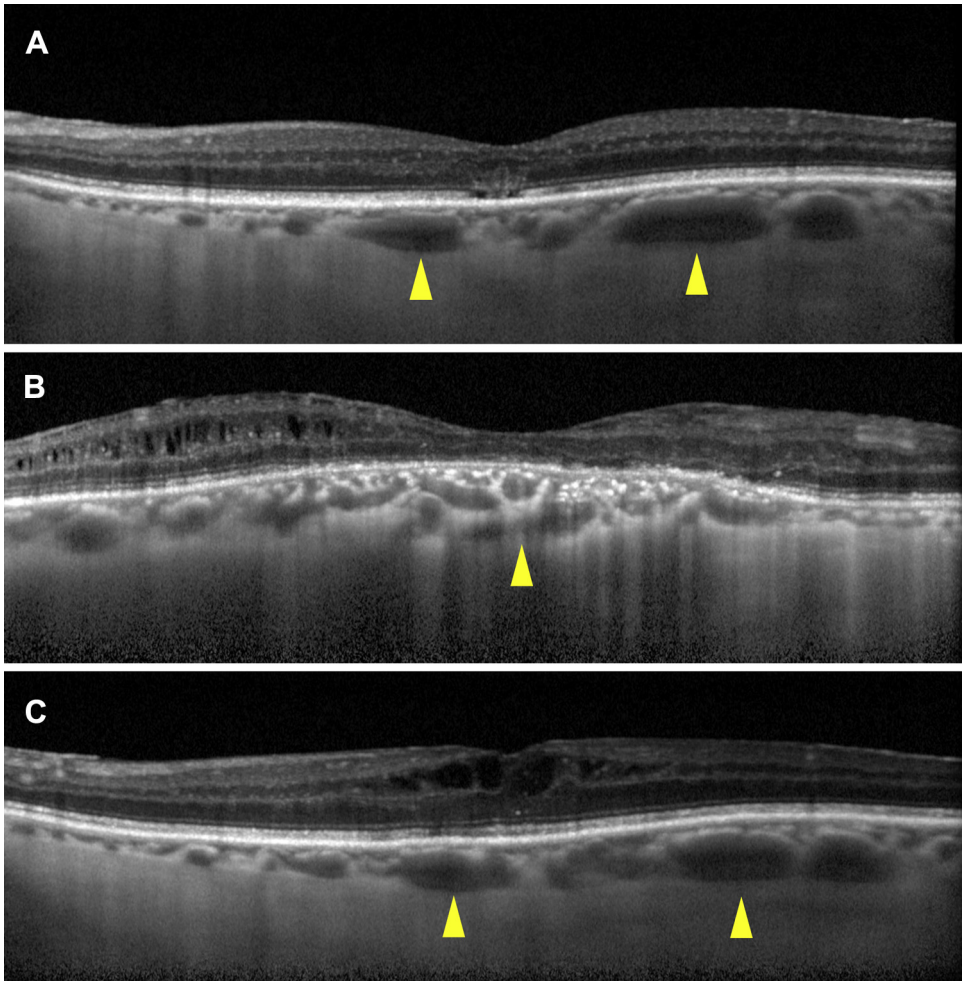

Fig. 2 – A–C: Enhanced depth imaging optical coherence tomography scans of 3 patients with idiopathic panuveitis. The figure demonstrates increased choroidal thickness that correlates with disease activity and presence of macular edema and/or disruption of the outer retinal layers. The yellow arrowheads indicate dilated choroidal vasculature.

because of vascular leakage, whereas decrease in choroidal thickness among patients with pre-eclampsia may be the result of the increased systemic vascular vasospasm.[8] The exact mechanism resulting in decreased choroidal thickness from vasospasm in pre-eclampsia is not understood. Increased systemic vasospasm may decrease choroidal blood flow, resulting in decreased choroidal thickness. Thus, choroidal thickness may be a useful tool to screen for pre-eclampsia.

4. Choroidal thickness in metabolic diseases

4.1. *Diabetes mellitus*

Diabetes mellitus is a vascular disease characterized by macrovascular and microvascular abnormalities. In diabetic eyes, in addition to changes in retinal circulation, alterations to the underlying choroidal vasculature also seem to play a vital role as studies on diabetic eyes have reported various abnormalities, including choroidal vascular degeneration, choroidal aneurysms, choroidal neovascularization, obstruction of the choriocapillaris, and increased tortuosity and narrowing of the choroidal vessels.[16,45,75] Given that choroid is an integral part of the nutrient and oxygen exchange with the outer third of the retina[82] and choroidal thickness is considered proxy measure of choroidal blood flow, compromised choroidal circulation might lead to structural changes in the choroid including choroidal thickness.

Although various studies have reported choroidal thickness in patients with diabetes mellitus, the results have been somewhat contradictory. Vujosevic et al did not find any significant difference in the mean choroidal thickness between their controls and diabetic patients.[114] Regatieri et al reported similar choroidal thickness between their controls and nonproliferative diabetic retinopathy.[90] Meanwhile, Esmaeelpour et al and Querques et al both showed that patients with diabetes mellitus had significantly thinner choroids than nondiabetics regardless of their diabetic retinopathy status.[33,85] In contrast, Kim et al showed that early diabetic retinopathy patients had thinner choroids compared to nondiabetics, but there was progressively thickening with increasing severity of diabetic retinopathy.[60] Xu et al in the Beijing Eye Study measured choroidal thickness in 246 subjects with diabetes mellitus and concluded subfoveal choroid to be thicker in

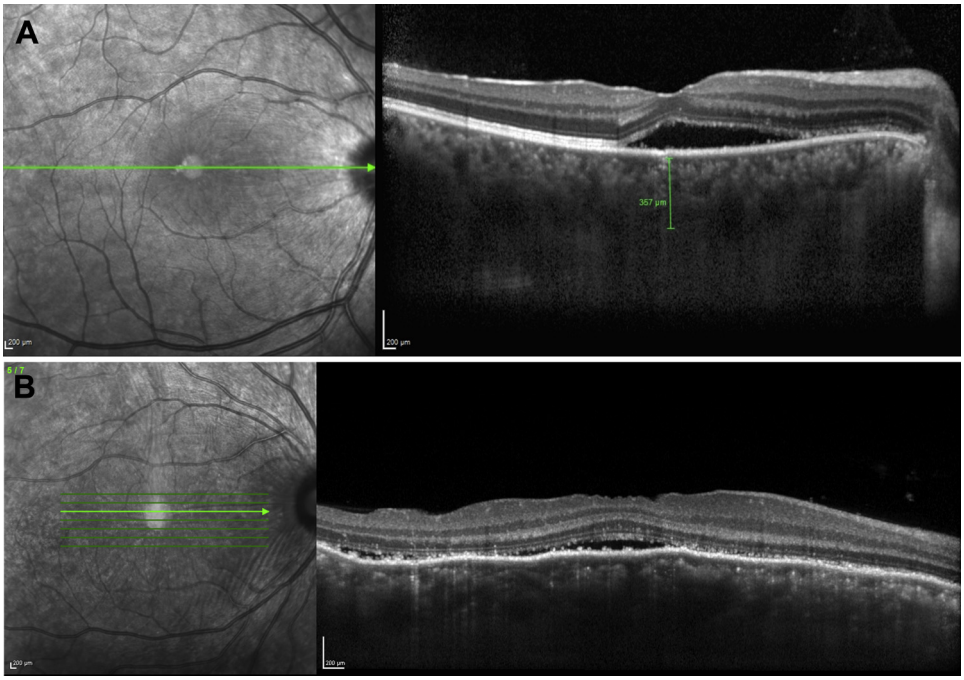

Fig. 3 – *A and B:* Enhanced depth imaging OCT scan of 2 patients with Vogt-Koyanagi-Harada syndrome demonstrates an increased choroidal thickness during the active stage of the disease along with presence of subretinal fluid.

those with diabetes, whereas the presence and stage of diabetic retinopathy were not associated with change in subfoveal choroidal thickness after accounting for relevant confounders.[120] Thus, the effect of diabetes on the choroid is still not clear. The general consensus is that diabetes causes a decrease in choroidal thickness; however, different ocular parameters need to be explored to understand the pathophysiology of diabetes mellitus in the choroid.

4.2. *Hypercholesterolemia*

Because of its high blood flow, the choroid has been considered as a potential site for the atherosclerotic changes[95] that occur in presence of hypercholesterolemia; however, to date, there is only one study[118] on the effect of hypercholesterolemia on choroidal thickness. Wong et al did a cross-sectional observational study on 322 healthy eyes of 161 subjects (mean age 60 years) found subfoveal choroidal thickness to be significantly higher in subjects with hypercholesterolemia (306 ± 111 µm) than controls (258 ± 97 µm). Thus, hypercholesterolemia might be an important factor to be taken into consideration when analyzing choroidal thickness; however, further studies are needed to confirm this association.

5. Choroidal thickness in cardiovascular diseases

5.1. *Hypertension*

Hypertension is a known cause of pathology in vascular systems in the heart, brain, kidneys, and eyes. Ocular changes in hypertension include retinal hemorrhages, cotton wool spots, intraretinal lipid accumulation, and vessel closure in the retinal capillaries and the choriocapillaris. Although both retinal and choroidal changes are observed in hypertension, the mechanism of choroidal damage remains unknown. Ahn et al[3] in 42 eyes with hypertensive retinopathy demonstrated significant increase in subfoveal choroidal thickness, possibly due to interstitial fluid accumulation in the choroid caused by choroidal permeability changes. Thus, hypertension may be considered as a potential determinant of the thickness of the choroid; however, further prospective studies with a larger sample size and longer follow-up periods are needed to confirm this finding.

6. Choroidal thickness in respiratory diseases

6.1. *Smoking*

Smoking, an important modifiable risk factor for many cardiovascular, respiratory, and other systemic diseases,[119] is also a risk factor for ocular vascular diseases such as hypertensive retinopathy, age-related macular degeneration, and anterior ischemic optic neuropathy.[18,19,59] Smoking cause vascular alterations, including decrease in retinal and choroidal blood flow.[58,64,117] Because smoking influences choroidal vasculature, this in turn might lead to structural changes in the choroid. Several studies have now shown significant decrease in choroidal thickness in smokers.[100,101,111] These studies proposed reduction in choroidal thickness caused by smoking to be related to vascular dysfunction caused by decrease in

nitric oxide bioavailability. This leads to peripheral vasoconstriction, causing an increase in the peripheral resistance to flow and thereby a decrease in choroidal thickness.

7. Choroidal thickness in systemic inflammatory conditions

Systemic inflammatory conditions may affect the ocular tissues and result in choroidal changes that often relate to the disease activity. Choroidal changes in such inflammatory conditions are demonstrated in Figure 2.

7.1. *Ankylosing spondylitis*

Ankylosing spondylitis is a chronic inflammatory disease that may also involve the eye, causing anterior uveitis. Uveitis is one of the classification criteria for seronegative spondyloarthritis and is its most common extra-articular manifestation. To date, only 1 study[63] was done to determine the effect of ankylosing spondylitis on the choroid. They studied 168 eyes of 84 ankylosing spondylitis patients and 126 eyes of 63 healthy subjects and found that choroidal thickness was increased. There was, however, no correlation between choroidal thicknesses and the severity or duration of ankylosing spondylitis. The inflammation of the uveal tract may explain the increase in choroidal thickness. Choroidal thickness may, therefore, be a good indicator of ankylosing spondylitis disease activity and could help in identifying cases in which uveitis may develop.

7.2. *Raynaud phenomenon*

Raynaud phenomenon is a reversible vasospastic response of the extremities to cold or emotion and is a recognized early manifestation of systemic sclerosis. The effect on vasodilation and vasoconstriction is not limited to skin in the peripheries but also is known to affect other organs, such as the choroidal plexus of the eye. A study[50] was done, involving 30 patients without visual symptoms, classified as primary Raynaud phenomenon, Raynaud phenomenon secondary to suspected systemic sclerosis, and overt systemic sclerosis, and 27 normal subjects. In patients with primary Raynaud phenomenon, a thinning of choroidal thickness was observed. The thinning is more severe in Raynaud phenomenon secondary to suspected systemic sclerosis and in overt systemic sclerosis. Perhaps, the thinning of choroid in Raynaud phenomenon is reflection of the systemic hemodynamic changes. The effect of blood circulation in Raynaud phenomenon has also been investigated, and it has an association with basal sympathetic tone, also it has a higher incidence in women.[23] Altered choroidal thickness once again may be an index of systemic blood circulation.

7.3. *Vogt-Koyanagi-Harada syndrome*

Vogt-Koyanagi-Harada (VKH) syndrome is a multisystemic, autoimmune, granulomatous inflammatory disease affecting the melanocyte-containing tissues such as the uvea, ear, skin, and meninges. In the eye, VKH causes bilateral granulomatous panuveitis initially presenting as diffuse choroiditis with multifocal serous detachments that may result in serous retinal detachment. In the later stages of the disease, there is chorioretinal depigmentation, sunset glow fundus, or perilimbal vitiligo.[88] There are 4 phases of the disease: prodromal, acute uveitis, convalescent, and chronic-recurrent phases.

In 8 patients with active VKH syndrome, EDI-OCT measurements found that their mean choroidal thickness was 805 $\pm$ 173 μm, which is much thicker than in normal eyes.[72] The choroidal thickness decreased in response to corticosteroid treatment to 341 $\pm$ 70 μm by the 14th day.

Takashi et al[105] studied 1 randomly selected eye from 19 patients with VKH syndrome of duration more than 3 years, of which 12 eyes had severe sunset glow fundus and 7 with little or no depigmentation. The mean choroidal thickness of the 12 eyes with severe sunset glow fundus was 144 $\pm$ 72 μm, which

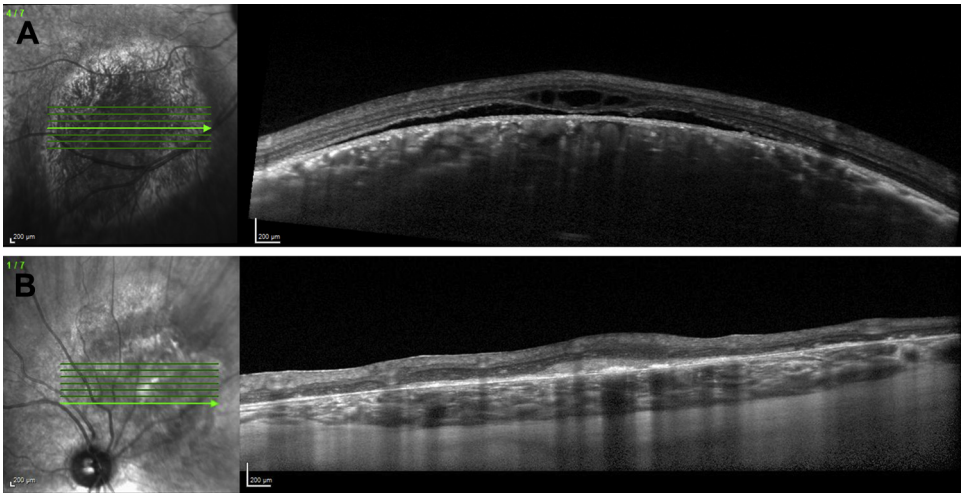

Fig. 4 – *A and B*: Enhanced depth imaging OCT scans of 2 patients with choroidal hemangioma demonstrates retinochoroidal changes such as increased choroidal thickness, altered pattern of choroidal vasculature, and elevation of the choroid due to the tumor mass.

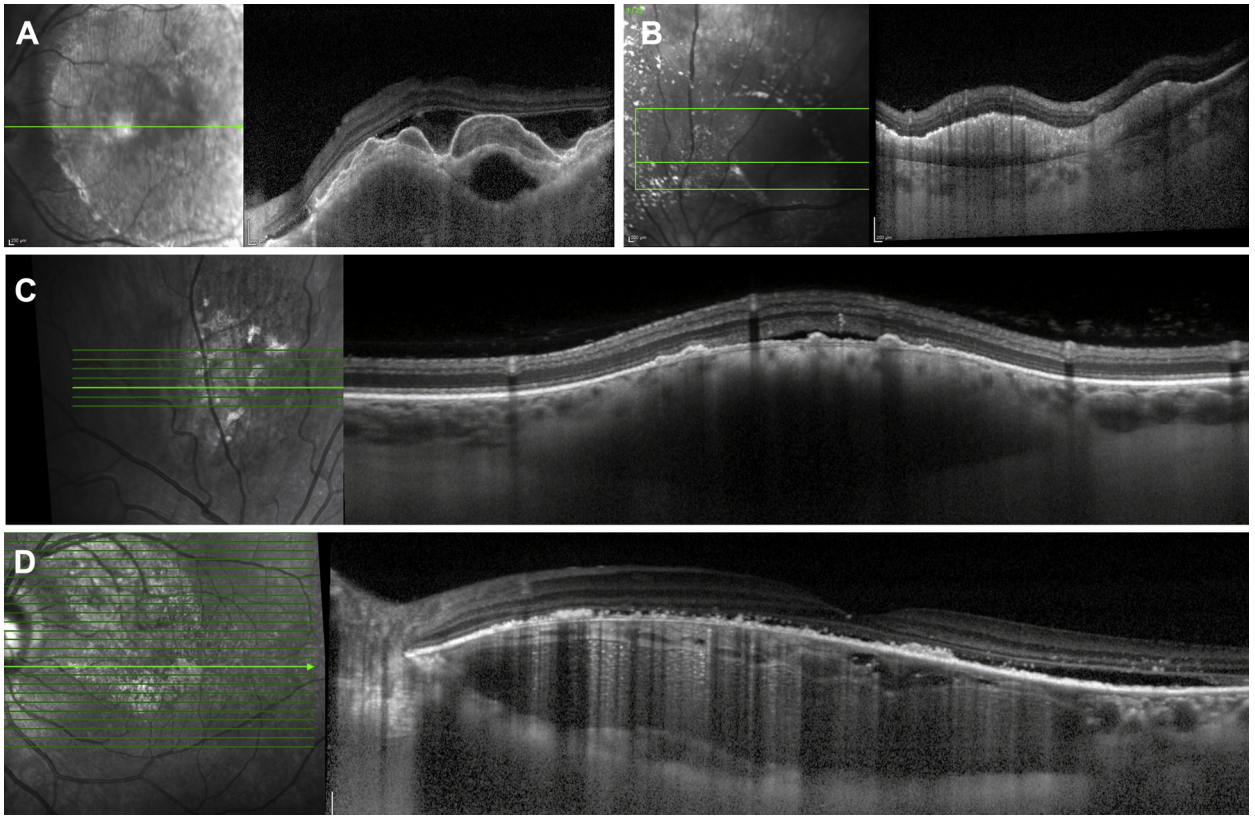

Fig. 5 – *A:* Optical coherence tomography (OCT) of a patient with choroidal metastasis secondary to breast carcinoma shows presence of choroidal infiltration with undulating and seasick appearance of the choroid. *B:* OCT scan of a patient with metastatic lymphoma showing presence of lymphoid infiltration and collection of metastatic material at the level of the retinal pigment epithelium. *C:* Appearance of a choroidal nevus on OCT. *D:* OCT appearance of a choroidal osteoma in the posterior pole.

was significantly thinner than that of the 7 eyes with little or no depigmentation. It was found that choroidal thickness was inversely correlated with disease duration and the degree of depigmentation.

Similarly, a prospective case-control study[25] was conducted on 16 patients (30 eyes) with VKH syndrome for more than 6 months and 17 normal individuals (32 eyes). Their eyes were examined by the EDI-OCT, and choroidal thickness was correlated to disease duration, clinical disease activity, and severity. The mean subfoveal choroidal thickness in the control group was 333 μm (±85.8), compared to 250.7 μm (±93.3) in VKH patients. Choroidal thickness was significantly decreased in patients with VKH, with a negative correlation between choroidal thickness and disease duration.

These studies demonstrate an increase in choroidal thickness during periods of active inflammation and a reduction during the chronic phase (Fig. 3). Choroidal thickness measurement may be a noninvasive tool to monitor disease activity and guide treatment decisions.

7.4. *Behçet disease*

Behçet disease is an idiopathic, multisystem disease characterized by recurrent orogenital ulceration and vasculitis involving small, medium, and large veins and arteries. Ocular complications occur in 95% of men and 70% of women. It usually presents bilaterally and can cause acute panuveitis, retinitis, retinal vasculitis, and vitritis. End-stage disease is marked by vascular occlusion, optic atrophy, and gliotic sheathing.[81]

In 30 patients with Behçet disease, the mean subfoveal choroidal thickness in affected eyes was significantly greater in the acute phase of disease than the quiescent phase (398.77 ± 155.59 μm vs 356.72 ± 141.09 μm).[61] Even during the quiescent phase, the choroidal thickness in affected eyes was thicker in patients with Behçet disease than the general population (259.96 ± 65.16 μm). Interestingly, the uninvolved eye in patients with Behçet disease also had a greater choroidal thickness as compared to the general population, suggesting that there may be choroidal infiltration even in the clinically uninvolved eye. A second study[52] conducted on 23 eyes of 13 patients similarly observed a dilation of choroidal vessels during the active phase of uveitis, with the choroidal thickness being significantly greater than when the disease was in remission. In addition, the choroidal thickness was significantly reduced after treatment with infliximab. Iccarino et al[48] confirmed these results, with 23.3% of the 30 eyes from 15 patients having no increase in choroidal thickness and 76% with an increase in choroidal thickness.

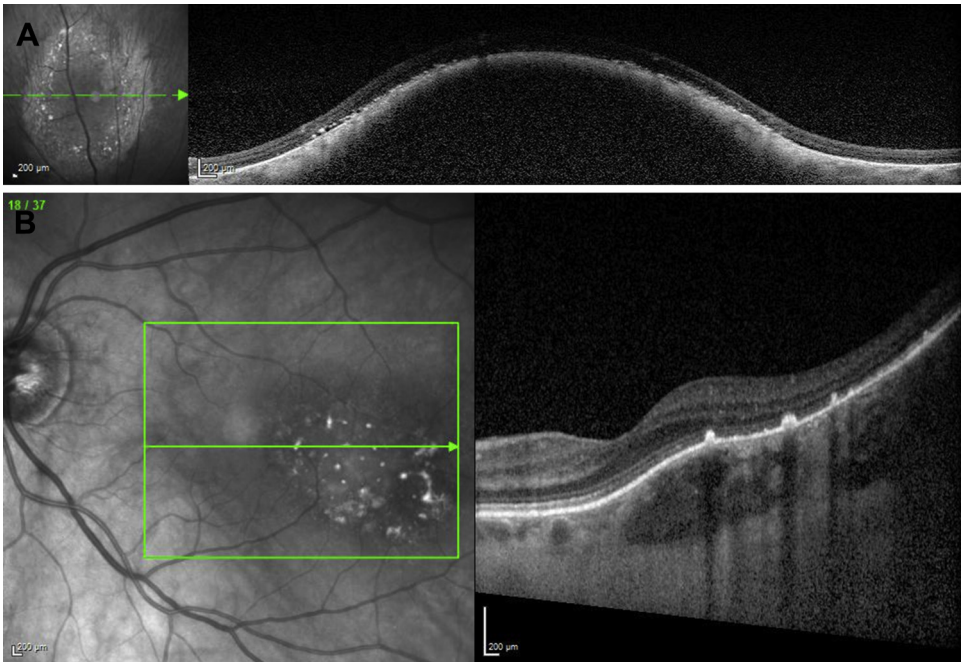

Fig. 6 – Imaging of metastatic melanoma in 2 patients using enhanced depth imaging OCT. *A:* Large metastatic choroidal melanoma in a patient superior to the optic nerve head and *B:* appearance of a metastatic choroidal melanoma after treatment with radiotherapy and systemic chemotherapy.

In contrast, another study[24] on 35 patients with Behçet disease found that choroidal thickness was significantly reduced as compared to normal controls. This difference may be explained by the disease duration. In the first 2–3 years of Behçet disease, there is progressive fibrosis and thinning of choroid due to ischemic changes in the choroid from the recurrent inflammation.

7.5. *Sarcoidosis*

Sarcoidosis is a multisystemic T-cell mediated granulomatous inflammatory disorder of unknown cause. There is a wide spectrum of disease, potentially affecting the mediastinal and superficial lymph nodes, lungs, liver, spleen, skin, parotid glands, pharyngeal bones, and the eye. In the eye, it has variable manifestations as anterior, intermediate, or panuveitis. Choroidal and optic disc granulomas, multifocal choroiditis, and segmental and rarely occlusive phlebitis may also be seen.

Only isolated case reports have described the imaging of choroid and assessment of choroid involvement in sarcoidosis. In the first study,[79] the eye of a 63-year-old woman with biopsy-proven sarcoidosis was examined with EDI-OCT. She presented with unilateral multifocal choroidal granuloma, which was seen as a homogenous hyporeflective lesion with choriocapillaris thinning. The surrounding choroid was spared. The choroidal granuloma decreased in size after treatment with immunosuppressive agents.

In a second case study,[92] a 49-year-old woman with a choroidal granuloma secondary to sarcoidosis, the choroidal granuloma appeared as a localized hyporeflective choroidal thickening. The choroidal thickness decreased after 2 weeks of systemic corticosteroid treatment from 568 µm to 356 µm; after 5 months, it decreased to 274 µm, and after 11 months, it reached 150 µm.

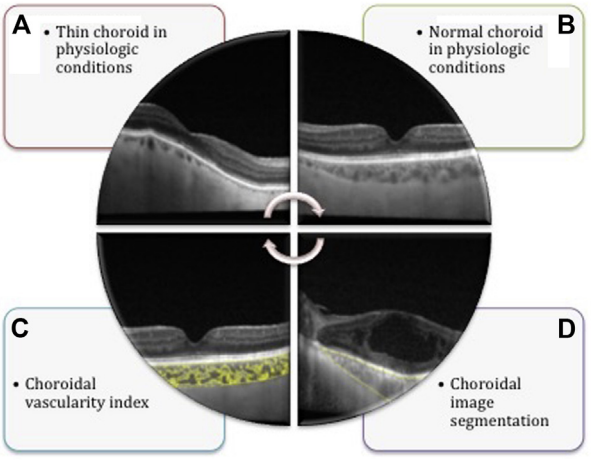

Fig. 7 – *A and B:* Composite image matrix representing variations in choroidal thickness in physiologic conditions on EDI-OCT scans. Image segmentation tools are used to demarcate the *C:* choroid and further segment the choroid into vascular and stromal segments using image binarization techniques facilitating calculation of proportion of vascular channels in the choroid, which can be further termed as Choroidal Vascularity Index. *D:* Segmenting the choroid on EDI OCT scans. EDI-OCT, enhanced depth imaging technique of optical coherence tomography.

8. Choroidal thickness in tumors

8.1. Metastasis

The choroid is the most common site for uveal metastases, accounting for approximately 90%, followed by the iris and ciliary body. The most common primary site is breast, followed by lung. Other possible primary sites are the gastrointestinal tract, kidney, skin melanoma, and, rarely, the prostate. Metastasis to the choroid may occur unilaterally or bilaterally and may be multifocal or unifocal. As such, unlike other systemic diseases, choroid metastases do not cause generalized increase or decrease in choroidal thickness. Shields et al[99] examined 520 eyes and found that most metastatic choroid tumors are dome or plateau shaped and measured 3-mm thick. The tumors were differentiated according to their primary sites, and it was found that the choroidal metastatic tumors from breast cancer are usually bilateral and multifocal, with a flatter tumor of 2 mm at the thickest tumor focus. Thicker tumors were more often found in lung, gastrointestinal, kidney, and prostate cancers, with the mean thickness in gastrointestinal and kidney cancers being 4 mm. Metastatic tumors from skin melanomas were the flattest, with a mean thickness of 1 mm. A study[5] that aimed to describe imaging features of choroidal metastasis using EDI-OCT examined 31 eyes with choroidal metastasis and found that the tumor has a characteristic "lumpy bumpy" anterior surface, with outer retina layer disruption, but preservation of inner layers of the retina. It also found that the choroidal metastases had an average thickness of 987 μm. The conclusion was that SD EDI-OCT allows visualization and imaging of choroid metastases.

The appearance of choroid in hemangioma and metastasis is demonstrated in Figures 4–6.

8.2. Sturge-Weber syndrome

Sturge-Weber syndrome involves congenital hamartomatous malformations that affect the eye, central nervous system, and eye. The most prevalent ocular malformation is the choroidal hemangioma, which usually enlarges slowly and affects over half of the choroid. Diffuse choroidal hemangiomas occur almost exclusively in patients with Sturge-Weber syndrome and associated with serous retinal detachment. This disease is known to cause an increase in choroidal thickness due to the vascular malformations.

An 18-year-old white boy with a known diagnosis of Sturge-Weber syndrome had diffused choroidal hemangiomas and serous retinal detachment treated with photodynamic therapy.[15] Optical coherence tomography examinations were done at baseline and 3 and 12 months after photodynamic therapy. The subfoveal choroidal thickness showed a reduction in thickness from 251 to 83 μm after photodynamic therapy. Thus, choroidal thickness measurement might be a beneficial parameter to follow the response to treatment for patients with diffuse choroidal hemangiomas.

9. Choroidal thickness in hematological diseases

9.1. Sickle cell disease

Sickle cell disease is caused by abnormal hemoglobins, which cause the red blood cells to assume an abnormal shape. This is characterized by the presence of mutant hemoglobin S. Because of their abnormal shape, the red blood cells may cause vaso-occlusion, producing tissue hypoxia and ischemia.[89] Sickle cell disease can cause either proliferative or nonproliferative sickle cell retinopathy.

A study conducted on 208 eyes of 107 patients referred for screening of sickle cell disease[3] found that choroidal thickness was significantly decreased in patients with sickle cell disease as compared to age, gender, and ethnicity matched controls. This may be the result of the slower blood flow in the choriocapillaris because of the sickling of the red blood cells. Interestingly, there was no difference in choroidal thickness between eyes in patients with sickle cell disease eyes with and without macular thinning. This indicates that microarteriolar occlusions in the macula are independent of changes in the choroidal circulation.

9.2. Leukemia

Leukemia is a disease of the hematopoietic stem cells, causing abnormal proliferation of white blood cells. Ocular involvement may occur in virtually any part of the eye and is more common in acute than in chronic leukemias. Primary leukemic infiltration is rare and must be differentiated from the chronic sequelae of the disease in the form of anemia, thrombocytopenia, hyperviscosity, and opportunistic infections. Choroidal deposits may occur, and present with a "leopard skin" appearance.

The effect of leukemia on choroidal thickness has not been extensively studied, possibly because of the many other secondary complications that would affect results. One 52-year-old man newly diagnosed with acute lymphocytic leukemia had EDI-OCT imaging that showed diffuse choroidal thickening in both eyes, with subfoveal choroidal thickness being 500 and 503 μm for the right and left eye, respectively.[9] After 4 weeks of systemic chemotherapy, there was a marked decrease in choroidal thickness bilaterally (315 and 325 μm). This suggests that choroidal thickness measurements could be a noninvasive tool to monitor disease activity and treatment outcomes in patients with leukemia; however, since this is only one case report.

10. Choroidal thickness in neurological diseases

10.1. Alzheimer disease

Cerebral vascular impairment is one of the earliest pathological features in Alzheimer disease,[12,28] and recent studies have speculated that retinal vasculature changes show similar pathogenetic alterations as cerebral vasculature.[13,36] One

prospective study[39] involving 42 eyes of 21 patients with a diagnosis of mild-to-moderate Alzheimer disease, and 42 eyes of 21 age-matched normal subjects showed that choroidal thickness was significantly decreased in Alzheimer disease ($P < 0.05$). This suggests that choroidal thickness may be a noninvasive parameter to diagnose and monitor treatment progression in Alzheimer disease.

10.2. *Migraine*

Migraine, an episodic chronic neovascular disorder with recurrent throbbing, often severe, headaches, is divided into 2 main clinical subtypes based on the presence or absence of an aura.[51] Patients with migraine commonly have visual symptoms and have an increased prevalence of visual field defects and glaucoma.[62] The visual aura and headaches experienced by patients with migraine are explained by vasospasm, and this in turn may affect choroid vasculature.

Four studies by Ekinci et al, Dervisogullari et al, Dermircan et al, and Zengin et al determined that patients with migraine had a significantly thinner choroid as compared either to controls or to themselves when they were not having an attack.[29,30,32,122] Zengin et al and Dervisogullari et al found that patients with migraine had choroidal thinning during their attacks as compared to controls.[30,122] Interestingly, Zengin also studied 5 patients both while they were having an attack and when they were not and determined that there was a sharp decrease in choroidal thickness during the attack.[122] This suggests that there may be decreased ocular blood flow from vasospasm during a migraine attack. Demircan and Ekinci conducted their study on patients with a history of migraine and similarly determined that there was choroid thinning in patients with migraine.[29,32] This suggests that the effects of the migraine on the choroid is not limited to the time of the attack, but causes long-term effects.

In contrast, 2 studies by Karalezli et al and Dadaci et al determined that there was choroid thickening in patients with migraine[26,56]; however, because there is much more evidence for choroid thinning in patients with migraine, it is more likely that conclusion is accurate. The knowledge of the effect of migraine on choroidal thickness allows us to better understand the pathophysiology behind the disease. Clinically, it is important to take into account a history of migraine when using choroidal thickness measurements.

11. Future scope

A recent further development is image segmentation of EDI-OCT scans, which allows for analysis of structures within the choroid (Fig. 7). This analysis may determine which structures, vascular or interstitial, in the choroid change in these diseases, giving us a better understanding of the pathophysiology of the change in choroid thickness. Moreover, assessing the proportion of vasculature in the choroid, which can be termed as "Choroidal Vascularity Index" may provide a noninvasive tool to screen for and monitor diseases not just restricted to the eye but for systemic microcirculatory disorders (Fig. 7). Choroidal Vascularity Index is a method to quantify choroidal blood flow by calculating the proportion of luminal area to the total subfoveal choroidal area using semi-automated image analysis of EDI-OCT scans. The methodology and applications of Choroidal Vascularity Index in panuveitis have been recently described.[1,2] This technique involves binarization of the EDI-OCT scan using a detailed image analysis algorithm.[107]

Recently, there has been interest in the field of noninvasive retinochoroidal imaging using OCT angiography and swept-source optical coherence tomography. OCT angiography is based on split-spectrum amplitude-decorrelation angiography that allows detection of endoluminal flow without a need to inject fluorescein dye.[53,103] The technique of OCT angiography has been shown to be useful in detection of various abnormalities such as irregular flow patterns that correspond well with invasive imaging techniques like indocyanine green angiography in conditions such as central serous chorioretinopathy and choroidal neovascularization.[54,108] Swept-source OCT provides a deeper range of imaging in the eye with a fast scanning speed. This technology has been used to obtain valuable information in various choroidal pathologies such as choroidal tumors.[69]

12. Conclusions

The study of choroidal thickness is a relatively new and exciting one, owing to the recent development of OCT. There has been a recent surge in research on the effects of systemic health on choroidal thickness. It is clear that many systemic and physiological conditions impacting hemodynamics have consequential effect on choroidal thickness (Table 1), although the pattern of these effects may not yet be certain. We consolidate current knowledge to give a clearer picture of the future of choroidal research, in particular, in the understanding of the effects of systemic health on choroidal thickness. We feel that choroidal has promise as a disease-monitoring tool and that systemic conditions must be considered when conducting future studies on choroidal thickness.

13. Method of literature search

A systematic literature search of the Medline/PubMed database (www.ncbi.nlm.nih.gov/pubmed) was performed in May 2015, using the following search parameters: Choroid thickness in combination with diurnal variation, age, gender, menstrual cycle, pregnancy, preeclampsia, diabetes mellitus, hypercholesterolemia, hypertension, smoking, ankylosing spondylitis, Raynaud's phenomenon, Vogt-Koyanagi-Harada syndrome, Behçet's disease, sarcoidosis, metastatic cancer, tumors, Sturge-Weber syndrome, sickle cell disease, leukemia, Alzheimer's disease, and migraine. The reference lists of

the identified publications provided additional information and related sources.

14. Disclosures

Dr. Keane has received a proportion of his funding from the Department of Health's NIHR Biomedical Research Centre for Ophthalmology at Moorfields Eye Hospital and UCL Institute of Ophthalmology. The views expressed in the publication are those of the author and not necessarily those of the Department of Health. The authors report no conflicts of interest. The authors alone are responsible for the content and preparation of this article. The authors have no financial disclosure/proprietary interest.

REFERENCES

1. Agrawal R, Salman M, Tan KA, et al. Choroidal Vascularity Index (CVI)—a novel optical coherence tomography parameter for monitoring patients with panuveitis? PLoS One. 2016;11:e0146344
2. Agrawal R, Gupta P, Tan KA, Cheung CM, Wong TY, Cheng CY. Choroidal vascularity index as a measure of vascular status of the choroid: measurements in healthy eyes from a population-based study. Sci Rep. 2016;6:21090
3. Ahn SJ, Woo SJ, Park KH. Retinal and choroidal changes with severe hypertension and their association with visual outcome. Invest Ophthalmol Vis Sci. 2014;55:7775–85
4. Akar Y, Yucel I, Akar ME, et al. Effect of pregnancy on intraobserver and intertechnique agreement in intraocular pressure measurements. Ophthalmologica. 2005;219:36–42
5. Al-Dahmash SA, Shields CL, Kaliki S, et al. Enhanced depth imaging optical coherence tomography of choroidal metastasis in 14 eyes. Retina. 2014;34:1588–93
6. Al-Rashaed S, Arevalo JF. Long-term follow-up of choroidal neovascularization secondary to angioid streaks: case series and literature review. Clin Ophthalmol. 2012;6:1029–34
7. Alm A, Bill A. Ocular and optic nerve blood flow at normal and increased intraocular pressures in monkeys (Macaca irus): a study with radioactively labelled microspheres including flow determinations in brain and some other tissues. Exp Eye Res. 1973;15:15–29
8. Atas M, Acmaz G, Aksoy H, et al. Evaluation of the macula, retinal nerve fiber layer and choroid in preeclampsia, healthy pregnant and healthy non-pregnant women using spectral-domain optical coherence tomography. Hypertens Pregnancy. 2014;33:299–310
9. Bajenova NV, Vanderbeek BL, Johnson MW. Change in choroidal thickness after chemotherapy in leukemic choroidopathy. Retina. 2012;32:203–5
10. Baltmr A, Lightman S, Tomkins-Netzer O. Examining the choroid in ocular inflammation: a focus on enhanced depth imaging. J Ophthalmol. 2014;2014:459136
11. Barteselli G, Chhablani J, El-Emam S, et al. Choroidal volume variations with age, axial length, and sex in healthy subjects: a three-dimensional analysis. Ophthalmology. 2012;119:2572–8
12. Bell RD, Zlokovic BV. Neurovascular mechanisms and blood-brain barrier disorder in Alzheimer's disease. Acta Neuropathol. 2009;118:103–13
13. Berisha F, Feke GT, Trempe CL, et al. Retinal abnormalities in early Alzheimer's disease. Invest Ophthalmol Vis Sci. 2007;48:2285–9
14. Bill A, Sperber GO. Control of retinal and choroidal blood flow. Eye. 1990;4:319–25
15. Cacciamani A, Scarinci F, Parravano M, et al. Choroidal thickness changes with photodynamic therapy for a diffuse choroidal hemangioma in Sturge-Weber syndrome. Int Ophthalmol. 2014;34:1131–5
16. Cao J, McLeod S, Merges CA, Lutty GA. Choriocapillaris degeneration and related pathologic changes in human diabetic eyes. Arch Ophthalmol. 1998;116:589–97
17. Chakraborty R, Read SA, Collins MJ. Diurnal variations in axial length, choroidal thickness, intraocular pressure, and ocular biometrics. Invest Ophthalmol Vis Sci. 2011;52:5121–9
18. Chakravarthy U, Augood C, Bentham GC, et al. Cigarette smoking and age-related macular degeneration in the EUREYE Study. Ophthalmology. 2007;114:1157–63
19. Chakravarthy U, Wong TY, Fletcher A, et al. Clinical risk factors for age-related macular degeneration: a systematic review and meta-analysis. BMC Ophthalmol. 2010;10:31
20. Chang L, Pan CW, Ohno-Matsui K, et al. Myopia-related fundus changes in Singapore adults with high myopia. Am J Ophthalmol. 2013;155:991–9.e991
21. Chen HC, Newsom RS, Patel V, et al. Retinal blood flow changes during pregnancy in women with diabetes. Invest Ophthalmol Vis Sci. 1994;35:3199–208
22. Coleman DJ, Lizzi FL. In vivo choroidal thickness measurement. Am J Ophthalmol. 1979;88:369–75
23. Cooke JP, Creager MA, Osmundson PJ, Shepherd JT. Sex differences in control of cutaneous blood flow. Circulation. 1990;82:1607–15
24. Coskun E, Gurler B, Pehlivan Y, et al. Enhanced depth imaging optical coherence tomography findings in Behcet disease. Ocul Immunol Inflamm. 2013;21:440–5
25. da Silva FT, Sakata VM, Nakashima A, et al. Enhanced depth imaging optical coherence tomography in long-standing Vogt-Koyanagi-Harada disease. Br J Ophthalmol. 2013;97:70–4
26. Dadaci Z, Doganay F, Oncel Acir N, et al. Enhanced depth imaging optical coherence tomography of the choroid in migraine patients: implications for the association of migraine and glaucoma. Br J Ophthalmol. 2014;98:972–5
27. Daruich A, Matet A, Dirani A, et al. Central serous chorioretinopathy: recent findings and new physiopathology hypothesis. Prog Retin Eye Res. 2015;48:82–112
28. de la Torre JC. Alzheimer disease as a vascular disorder: nosological evidence. Stroke. 2002;33:1152–62
29. Demircan S, Atas M, Arik Yuksel S, et al. The impact of migraine on posterior ocular structures. J Ophthalmol. 2015;2015:868967
30. Dervisogullari MS, Totan Y, Gencler OS. Choroid thickness and ocular pulse amplitude in migraine during attack. Eye (Lond). 2015;29:371–5
31. Ding X, Li J, Zeng J, et al. Choroidal thickness in healthy Chinese subjects. Invest Ophthalmol Vis Sci. 2011;52:9555–60
32. Ekinci M, Ceylan E, Cagatay HH, et al. Retinal nerve fibre layer, ganglion cell layer and choroid thinning in migraine with aura. BMC Ophthalmol. 2014;14:75
33. Esmaeelpour M, Povazay B, Hermann B, et al. Three-dimensional 1060-nm OCT: choroidal thickness maps in normal subjects and improved posterior segment visualization in cataract patients. Invest Ophthalmol Vis Sci. 2010;51:5260–6
34. Feeney-Burns L, Burns RP, Gao CL. Age-related macular changes in humans over 90 years old. Am J Ophthalmol. 1990;109:265–78

35. Fitzgerald ME, Vana BA, Reiner A. Control of choroidal blood flow by the nucleus of Edinger-Westphal in pigeons: a laser Doppler study. Invest Ophthalmol Vis Sci. 1990;31:2483–92
36. Frost S, Kanagasingam Y, Sohrabi H, et al. Retinal vascular biomarkers for early detection and monitoring of Alzheimer's disease. Transl Psychiatry. 2013;3:e233
37. Fujiwara T, Imamura Y, Margolis R, et al. Enhanced depth imaging optical coherence tomography of the choroid in highly myopic eyes. Am J Ophthalmol. 2009;148:445–50
38. Garg A, Wapner RJ, Ananth CV, et al. Choroidal and retinal thickening in severe preeclampsia. Invest Ophthalmol Vis Sci. 2014;55:5723–9
39. Gharbiya M, Trebbastoni A, Parisi F, et al. Choroidal thinning as a new finding in Alzheimer's disease: evidence from enhanced depth imaging spectral domain optical coherence tomography. J Alzheimers Dis. 2014;40:907–17
40. Goktas S, Basaran A, Sakarya Y, et al. Measurement of choroid thickness in pregnant women using enhanced depth imaging optical coherence tomography. Arq Bras Oftalmol. 2014;77:148–51
41. Guglielmone R, Cantino D. Autonomic innervation of the ocular choroid membrane in the chicken: a fluorescence-histochemical and electron-microscopic study. Cell Tissue Res. 1982;222:417–31
42. Gupta P, Jing T, Marziliano P, et al. Distribution and determinants of choroidal thickness and volume using automated segmentation software in a population-based study. Am J Ophthalmol. 2015;159:293–301.e293
43. Guyer DR, Puliafito CA, Mones JM, et al. Digital indocyanine-green angiography in chorioretinal disorders. Ophthalmology. 1992;99:287–91
44. Hayreh SS. The blood supply of the optic nerve head and the evaluation of it - myth and reality. Prog Retin Eye Res. 2001;20:563–93
45. Hidayat AA, Fine BS. Diabetic choroidopathy. Light and electron microscopic observations of seven cases. Ophthalmology. 1985;92:512–22
46. Horven I, Gjonnaess H. Corneal indentation pulse and intraocular pressure in pregnancy. Arch Ophthalmol. 1974;91:92–8
47. American College of Obstetricians and Gynecologists; Task Force on Hypertension in Pregnancy. Hypertension in pregnancy. Report of the American College of Obstetricians and Gynecologists' Task Force on Hypertension in Pregnancy. Obstet Gynecol. 2013;122:1122–31
48. Iaccarino G, Cennamo G, Forte R, Cennamo G. Evaluation of posterior pole with echography and optical coherence tomography in patients with Behcet's disease. Ophthalmologica. 2009;223:250–5
49. Ikuno Y, Kawaguchi K, Nouchi T, Yasuno Y. Choroidal thickness in healthy Japanese subjects. Invest Ophthalmol Vis Sci. 2010;51:2173–6
50. Ingegnoli F, Gualtierotti R, Pierro L, et al. Choroidal impairment and macular thinning in patients with systemic sclerosis: the acute study. Microvasc Res. 2015;97:31–6
51. Headache Classification Committee of the International Headache Society (IHS). The International Classification of Headache Disorders, 3rd edition (beta version). Cephalalgia. 2013;33:629–808
52. Ishikawa S, Taguchi M, Muraoka T, et al. Changes in subfoveal choroidal thickness associated with uveitis activity in patients with Behcet's disease. Br J Ophthalmol. 2014;98:1508–13
53. Jia Y, Tan O, Tokayer J, et al. Split-spectrum amplitude-decorrelation angiography with optical coherence tomography. Opt Express. 2012;20:4710–25
54. Jia Y, Bailey ST, Wilson DJ, et al. Quantitative optical coherence tomography angiography of choroidal neovascularization in age-related macular degeneration. Ophthalmology. 2014;121:1435–44
55. Joondeph BC, Tessler HH. Multifocal choroiditis. Int Ophthalmol Clin. 1990;30:286–90
56. Karalezli A, Simsek C, Celik G, Eroglu FC. Evaluation of choroidal thickness using spectral-domain optical coherence tomography in migraine patients during acute migraine attacks: a comparative study. Eye (Lond). 2014;28:1477–81
57. Kass MA, Sears ML. Hormonal regulation of intraocular pressure. Surv Ophthalmol. 1977;22:153–76
58. Kergoat H, Faucher C. Effects of oxygen and carbogen breathing on choroidal hemodynamics in humans. Invest Ophthalmol Vis Sci. 1999;40:2906–11
59. Khan JC, Thurlby DA, Shahid H, et al. Smoking and age related macular degeneration: the number of pack years of cigarette smoking is a major determinant of risk for both geographic atrophy and choroidal neovascularisation. Br J Ophthalmol. 2006;90:75–80
60. Kim JT, Lee DH, Joe SG, et al. Changes in choroidal thickness in relation to the severity of retinopathy and macular edema in type 2 diabetic patients. Invest Ophthalmol Vis Sci. 2013;54:3378–84
61. Kim M, Kim H, Kwon HJ, et al. Choroidal thickness in Behcet's uveitis: an enhanced depth imaging-optical coherence tomography and its association with angiographic changes. Invest Ophthalmol Vis Sci. 2013;54:6033–9
62. Klein BE, Klein R, Meuer SM, Goetz LA. Migraine headache and its association with open-angle glaucoma: the Beaver Dam Eye Study. Invest Ophthalmol Vis Sci. 1993;34:3024–7
63. Kola M, Kalkisim A, Karkucak M, et al. Evaluation of choroidal thickness in ankylosing spondylitis using optical coherence tomography. Ocul Immunol Inflamm. 2014;22:434–8
64. Langhans M, Michelson G, Groh MJ. Effect of breathing 100% oxygen on retinal and optic nerve head capillary blood flow in smokers and non-smokers. Br J Ophthalmol. 1997;81:365–9
65. Li XQ, Larsen M, Munch IC. Subfoveal choroidal thickness in relation to sex and axial length in 93 Danish university students. Invest Ophthalmol Vis Sci. 2011;52:8438–41
66. Liegl R, Ulbig MW. Central serous chorioretinopathy. Ophthalmologica. 2014;232:65–76
67. Linsell CR, Lightman SL, Mullen PE, et al. Circadian rhythms of epinephrine and norepinephrine in man. J Clin Endocrinol Metab. 1985;60:1210–5
68. Ma L, Tang SM, Rong SS, et al. Association of PEDF polymorphisms with age-related macular degeneration and polypoidal choroidal vasculopathy: a systematic review and meta-analysis. Sci Rep. 2015;5:9497
69. Maloca P, Gyger C, Hasler PW. A pilot study to image the vascular network of small melanocytic choroidal tumors with speckle noise-free 1050-nm swept source optical coherence tomography (OCT choroidal angiography). Graefes Arch Clin Exp Ophthalmol 2016 Feb 4;. [Epub ahead of print].
70. Manjunath V, Taha M, Fujimoto JG, Duker JS. Choroidal thickness in normal eyes measured using Cirrus HD optical coherence tomography. Am J Ophthalmol. 2010;150:325–9.e321
71. Margolis R, Spaide RF. A pilot study of enhanced depth imaging optical coherence tomography of the choroid in normal eyes. Am J Ophthalmol. 2009;147:811–5
72. Maruko I, Iida T, Sugano Y, et al. Subfoveal choroidal thickness after treatment of Vogt-Koyanagi-Harada disease. Retina. 2011;31:510–7
73. Mathew R, Bafiq R, Ramu J, et al. Spectral domain optical coherence tomography in patients with sickle cell disease. Br J Ophthalmol. 2015;99:967–72

74. Matsuoka M, Ogata N, Otsuji T, et al. Expression of pigment epithelium derived factor and vascular endothelial growth factor in choroidal neovascular membranes and polypoidal choroidal vasculopathy. Br J Ophthalmol. 2004;88:809–15
75. McLeod DS, Lutty GA. High-resolution histologic analysis of the human choroidal vasculature. Invest Ophthalmol Vis Sci. 1994;35:3799–811
76. Mills PJ, Nelesen RA, Ziegler MG, et al. Menstrual cycle effects on catecholamine and cardiovascular responses to acute stress in black but not white normotensive women. Hypertension. 1996;27:962–7
77. Mills PJ, Ziegler MG, Nelesen RA, Kennedy BP. The effects of the menstrual cycle, race, and gender on adrenergic receptors and agonists. Clin Pharmacol Ther. 1996;60:99–104
78. Minson CT, Halliwill JR, Young TM, Joyner MJ. Influence of the menstrual cycle on sympathetic activity, baroreflex sensitivity, and vascular transduction in young women. Circulation. 2000;101:862–8
79. Modi YS, Epstein A, Bhaleeya S, et al. Multimodal imaging of sarcoid choroidal granulomas. J Ophthalmic Inflamm Infect. 2013;3:58
80. Mrejen S, Spaide RF. Optical coherence tomography: imaging of the choroid and beyond. Surv Ophthalmol. 2013;58:387–429
81. Muhaya M, Lightman S, Ikeda E, et al. Behcet's disease in Japan and in Great Britain: a comparative study. Ocul Immunol Inflamm. 2000;8:141–8
82. Nickla DL, Wallman J. The multifunctional choroid. Prog Retin Eye Res. 2010;29:144–68
83. Ooto S, Hangai M, Yoshimura N. Effects of sex and age on the normal retinal and choroidal structures on optical coherence tomography. Curr Eye Res. 2015;40:213–25
84. Park KA, Oh SY. An optical coherence tomography-based analysis of choroidal morphologic features and choroidal vascular diameter in children and adults. Am J Ophthalmol. 2014;158:716–23.e712
85. Querques G, Lattanzio R, Querques L, et al. Enhanced depth imaging optical coherence tomography in type 2 diabetes. Invest Ophthalmol Vis Sci. 2012;53:6017–24
86. Rahman W, Chen FK, Yeoh J, et al. Repeatability of manual subfoveal choroidal thickness measurements in healthy subjects using the technique of enhanced depth imaging optical coherence tomography. Invest Ophthalmol Vis Sci. 2011;52:2267–71
87. Ramrattan RS, van der Schaft TL, Mooy CM, et al. Morphometric analysis of Bruch's membrane, the choriocapillaris, and the choroid in aging. Invest Ophthalmol Vis Sci. 1994;35:2857–64
88. Read RW, Holland GN, Rao NA, et al. Revised diagnostic criteria for Vogt-Koyanagi-Harada disease: report of an international committee on nomenclature. Am J Ophthalmol. 2001;131:647–52
89. Rees DC, Williams TN, Gladwin MT. Sickle-cell disease. Lancet. 2010;376:2018–31
90. Regatieri CV, Branchini L, Carmody J, et al. Choroidal thickness in patients with diabetic retinopathy analyzed by spectral-domain optical coherence tomography. Retina. 2012;32:563–8
91. Rhodes LA, Huisingh C, Johnstone J, et al. Peripapillary choroidal thickness variation with age and race in normal eyes. Invest Ophthalmol Vis Sci. 2014;56:1872–9
92. Rostaqui O, Querques G, Haymann P, et al. Visualization of sarcoid choroidal granuloma by enhanced depth imaging optical coherence tomography. Ocul Immunol Inflamm. 2014;22:239–41
93. Royburt M, Seidman DS, Serr DM, Mashiach S. Neurologic involvement in hypertensive disease of pregnancy. Obstet Gynecol Surv. 1991;46:656–64
94. Ruiz-Medrano J, Flores-Moreno I, Pena-Garcia P, et al. Macular choroidal thickness profile in a healthy population measured by swept-source optical coherence tomography. Invest Ophthalmol Vis Sci. 2014;55:3532–42
95. Salazar JJ, Ramirez AI, de Hoz R, et al. Alterations in the choroid in hypercholesterolemic rabbits: reversibility after normalization of cholesterol levels. Exp Eye Res. 2007;84:412–22
96. Sanchez-Cano A, Orduna E, Segura F, et al. Choroidal thickness and volume in healthy young white adults and the relationships between them and axial length, ammetropy and sex. Am J Ophthalmol. 2014;158:574–83.e571
97. Sarks SH. Ageing and degeneration in the macular region: a clinico-pathological study. Br J Ophthalmol. 1976;60:324–41
98. Sayin N, Kara N, Pirhan D, et al. Subfoveal choroidal thickness in preeclampsia: comparison with normal pregnant and nonpregnant women. Semin Ophthalmol. 2014;29:11–7
99. Shields CL, Shields JA, Gross NE, et al. Survey of 520 eyes with uveal metastases. Ophthalmology. 1997;104:1265–76
100. Sigler EJ, Randolph JC, Calzada JI, Charles S. Smoking and choroidal thickness in patients over 65 with early-atrophic age-related macular degeneration and normals. Eye (Lond). 2014;28:838–46
101. Sizmaz S, Kucukerdonmez C, Pinarci EY, et al. The effect of smoking on choroidal thickness measured by optical coherence tomography. Br J Ophthalmol. 2013;97:601–4
102. Spaide RF. Age-related choroidal atrophy. Am J Ophthalmol. 2009;147:801–10
103. Spaide RF, Klancnik JM Jr, Cooney MJ. Retinal vascular layers imaged by fluorescein angiography and optical coherence tomography angiography. JAMA Ophthalmol. 2015;133:45–50
104. Spaide RF, Koizumi H, Pozzoni MC. Enhanced depth imaging spectral-domain optical coherence tomography. Am J Ophthalmol. 2008;146:496–500
105. Takahashi H, Takase H, Ishizuka A, et al. Choroidal thickness in convalescent vogt-koyanagi-harada disease. Retina. 2014;34:775–80
106. Tan CS, Ouyang Y, Ruiz H, Sadda SR. Diurnal variation of choroidal thickness in normal, healthy subjects measured by spectral domain optical coherence tomography. Invest Ophthalmol Vis Sci. 2012;53:261–6
107. Tan KA, Agrawal R. Luminal and stromal areas of choroid determined by binarization method of optical coherence tomographic images. Am J Ophthalmol. 2015;160:394
108. Teussink MM, Breukink MB, van Grinsven MJ, et al. OCT angiography compared to fluorescein and indocyanine green angiography in chronic central serous chorioretinopathy. Invest Ophthalmol Vis Sci. 2015;56:5229–37
109. Toyokawa N, Kimura H, Fukomoto A, Kuroda S. Difference in morning and evening choroidal thickness in Japanese subjects with no chorioretinal disease. Ophthalmic Surg Lasers Imaging. 2012;43:109–14
110. Tuncer I, Karahan E, Zengin MO, et al. Choroidal thickness in relation to sex, age, refractive error, and axial length in healthy Turkish subjects. Int Ophthalmol. 2015;35:403–10
111. Ulas F, Celik F, Dogan U, Celebi S. Effect of smoking on choroidal thickness in healthy smokers. Curr Eye Res. 2014;39:504–11
112. Ulas F, Dogan U, Duran B, et al. Choroidal thickness changes during the menstrual cycle. Curr Eye Res. 2013;38:1172–81

113. Usui S, Ikuno Y, Akiba M, et al. Circadian changes in subfoveal choroidal thickness and the relationship with circulatory factors in healthy subjects. Invest Ophthalmol Vis Sci. 2012;53:2300–7
114. Vujosevic S, Martini F, Cavarzeran F, et al. Macular and peripapillary choroidal thickness in diabetic patients. Retina. 2012;32:1781–90
115. Wei WB, Xu L, Jonas JB, et al. Subfoveal choroidal thickness: the Beijing Eye Study. Ophthalmology. 2013;120:175–80
116. Weinreb RN, Lu A, Beeson C. Maternal corneal thickness during pregnancy. Am J Ophthalmol. 1988;105:258–60
117. Wimpissinger B, Resch H, Berisha F, et al. Response of choroidal blood flow to carbogen breathing in smokers and non-smokers. Br J Ophthalmol. 2004;88:776–81
118. Wong IY, Wong RL, Zhao P, Lai WW. Choroidal thickness in relation to hypercholesterolemia on enhanced depth imaging optical coherence tomography. Retina. 2013;33:423–8
119. World Health Organisation. WHO global report: mortality attributable to tobacco. WHO Press, Geneva, Switzerland; 2012, p 362
120. Xu J, Xu L, Du KF, et al. Subfoveal choroidal thickness in diabetes and diabetic retinopathy. Ophthalmology. 2013;120:2023–8
121. Zeng J, Liu R, Zhang XY, et al. [Relationship between gender and posterior pole choroidal thickness in normal eyes]. Zhonghua Yan Ke Za Zhi. 2012;48:1093–6
122. Zengin MO, Elmas Z, Cinar E, Kucukerdonmez C. Choroidal thickness changes in patients with migraine. Acta Neurol Belg. 2015;115:33–7

OPEN ACCESS Freely available online

PLOS ONE

A Simplified Method to Measure Choroidal Thickness Using Adaptive Compensation in Enhanced Depth Imaging Optical Coherence Tomography

Preeti Gupta[1,2], Elizabeth Sidhartha[1,2], Michael J. A. Girard[1,3], Jean Martial Mari[4], Tien-Yin Wong[1,2,5,6], Ching-Yu Cheng[1,2,5,6]*

1 Singapore Eye Research Institute and Singapore National Eye Centre, Singapore, Singapore, **2** Department of Ophthalmology, Yong Loo Lin School of Medicine, National University of Singapore and National University Health System, Singapore, Singapore, **3** Department of Biomedical Engineering, Faculty of Engineering, National University of Singapore, Singapore, **4** Department of Bioengineering, Faculty of Engineering Science, University College London, London, United Kingdom, **5** Saw Swee Hock School of Public Health, National University of Singapore and National University Health System, Singapore, Singapore, **6** Centre for Quantitative Medicine, Office of Clinical Sciences, Duke-NUS Graduate Medical School, Singapore, Singapore

Abstract

Purpose: To evaluate a simplified method to measure choroidal thickness (CT) using commercially available enhanced depth imaging (EDI) spectral domain optical coherence tomography (SD-OCT).

Methods: We measured CT in 31 subjects without ocular diseases using Spectralis EDI SD-OCT. The choroid-scleral interface of the acquired images was first enhanced using a post-processing compensation algorithm. The enhanced images were then analysed using Photoshop. Two graders independently graded the images to assess inter-grader reliability. One grader re-graded the images after 2 weeks to determine intra-grader reliability. Statistical analysis was performed using intra-class correlation coefficient (ICC) and Bland-Altman plot analyses.

Results: Using adaptive compensation both the intra-grader reliability (ICC: 0.95 to 0.97) and inter-grader reliability (ICC: 0.93 to 0.97) were perfect for all five locations of CT. However, with the conventional technique of manual CT measurements using built-in callipers provided with the Heidelberg explorer software, the intra- (ICC: 0.87 to 0.94) and inter-grader reliability (ICC: 0.90 to 0.93) for all the measured locations is lower. Using adaptive compensation, the mean differences (95% limits of agreement) for intra- and inter-grader sub-foveal CT measurements were −1.3 (−3.33 to 30.8) μm and −1.2 (−36.6 to 34.2) μm, respectively.

Conclusions: The measurement of CT obtained from EDI SD-OCT using our simplified method was highly reliable and efficient. Our method is an easy and practical approach to improve the quality of choroidal images and the precision of CT measurement.

Citation: Gupta P, Sidhartha E, Girard MJA, Mari JM, Wong T-Y, et al. (2014) A Simplified Method to Measure Choroidal Thickness Using Adaptive Compensation in Enhanced Depth Imaging Optical Coherence Tomography. PLoS ONE 9(5): e96661. doi:10.1371/journal.pone.0096661

Editor: Yingfeng Zheng, Zhongshan Ophthalmic Center, China

Received September 30, 2013; **Accepted** April 10, 2014; **Published** May 5, 2014

Funding: This study was supported by a grant (R760/44/2010) from National Medical Research Council, Singapore. Image post-processing techniques were supported by the Ministry of Education, Academic Research Funds, Tier 1, Singapore (MJAG). The funders had no role in study design, data collection and analysis, decision to publish, or preparation of the manuscript.

Competing Interests: The authors have declared that no competing interests exist.

* E-mail: ching-yu_cheng@nuhs.edu.sg

Introduction

The choroid is important to support retinal and visual function as it supplies nutrients and oxygen to retinal pigment epithelial (RPE) cells and photoreceptors [1]. Therefore, the choroid may play a role in the pathophysiology of many vision threatening retinal diseases such as age-related macular degeneration [2,3], polypoidal choroidal vasculopathy [4,5], central serous chorioretinopathy [6,7], Vogt-Koyanagi-Harada [8] disease and myopic macular degeneration [9–12]. To elucidate the mechanisms through which the choroid affects these retinal diseases, quantitative assessment of choroidal characteristics such as choroidal thickness (CT) is required.

However, it was not trivial to image CT because of its posterior location and pigments in the RPE layer [13], until the advent of spectral domain optical coherence tomography (SD-OCT) with enhanced depth imaging (EDI). EDI SD-OCT has provided many new insights into choroidal qualitative morphology. However, to date a notable disparity exists between the CT measurements obtained in different studies. Such variations could be due to unavailability of a standardized and simple to use measurement method and absence of built-in automated software to measure CT in most of the commercially available OCT machines [14]. At present, most of the studies perform the measurements manually by using the in-built caliper system provided by the machine, which is prone to measurement errors. The manual method is also

time- and effort-consuming, making it unfeasible especially when dealing with large population data.

As a result, while many studies have published the distribution of CT in patients with retinal diseases and normal controls [15–19], none of these studies have clearly described the method used in detailed to measure CT. Therefore, the reliability of the CT measurement methods in most of the papers is unknown. In this paper, we describe a simple, semi-automated, time-efficient method to measure CT using images acquired by EDI SD-OCT and available compensation algorithms. We aimed to assess the reliability of this new CT measurement technique in a sample of healthy eyes.

Materials and Methods

Study Subjects and Design

Data for this analysis were derived from the Singapore Malay Eye Study (SiMES), a population-based cross-sectional study of eye diseases in Malay adults, age ranged from 40–80 years living in Singapore. Details of the study design, sampling plan, and methodology have been reported elsewhere [20]. In brief, participants recruited in the current study underwent standardized and detailed ophthalmic examination, including Spectralis EDI SD-OCT imaging (see next section). The study was approved by the Institutional Review Board of Singapore Eye Research Institute. It followed the tenants of the Declaration of Helsinki and written informed consent was obtained from the subjects after explanation of the nature and possible consequences of the study.

Spectralis images of 31 subjects were randomly selected using a random number generated in Stata (College par, Texas, USA). Choroidal images were only selected from right eye of each subject as our measurement technique can be applied uniformly between right and left eyes. Therefore only the right eyes of the subjects were evaluated. In addition, selecting only one eye from individuals would help to avoid inter-eye correlation issue in statistical analysis. "Normal fundus" was defined as free of any macular or vitroretinal diseases on the basis of clinical fundus examination by experienced Ophthalmologist and the results of OCT imaging. Exclusion criteria for the normal participants included: best corrected LogMAR VA >0.3, evidence of macular or vitroretinal diseases, previous retinal or refractive surgery, past history of intraocular surgery, or clinical features compatible with a diagnosis of glaucoma suspect or glaucoma.

To evaluate the intra-grader and inter-grader reliability, 31 Spectralis images were randomly selected for the initial grading

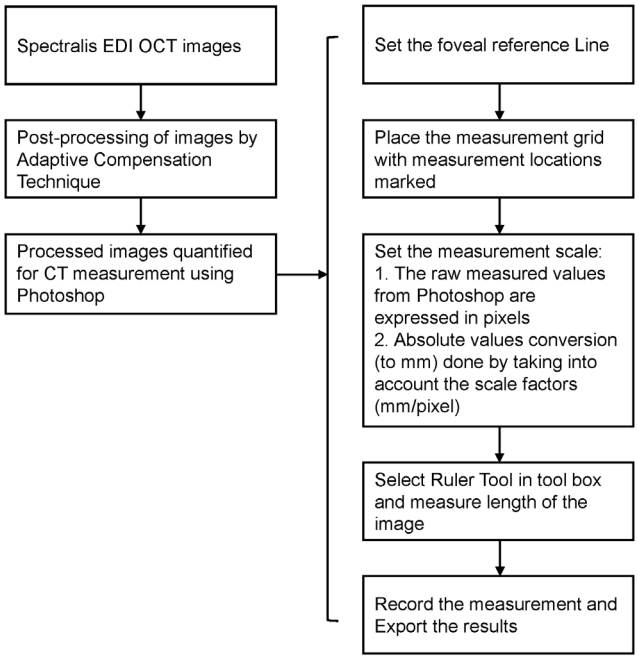

Figure 2. Flow diagram of the measurement protocol.
doi:10.1371/journal.pone.0096661.g002

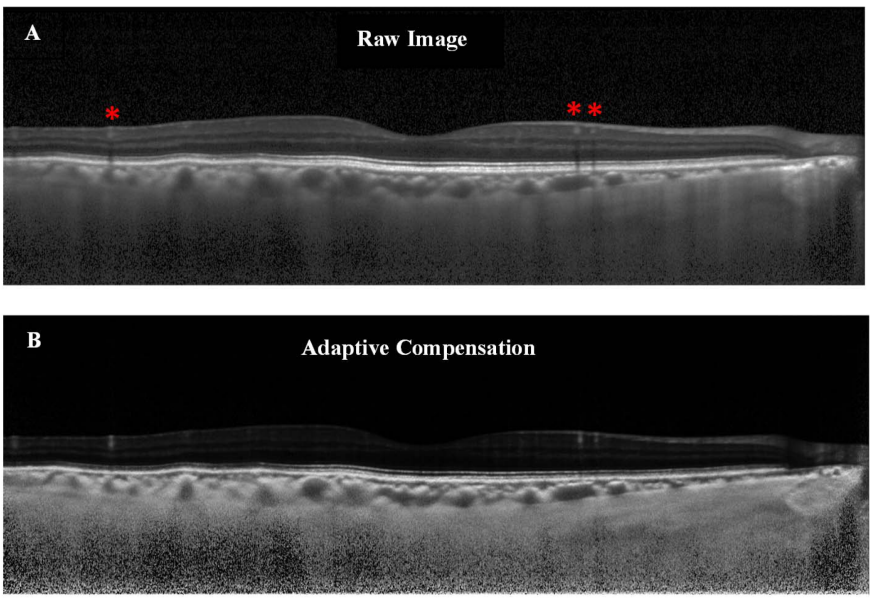

Figure 1. Illustration of the raw versus the compensated image. (A) Raw OCT image of a healthy subject. The choroid-scleral interface is only partially visible. Note the presence of blood vessels shadows as indicated by red asterisks. (B) Adaptive compensation was applied to the raw image in order to remove blood vessels shadows, enhance contrast and improve visibility of the choroid-scleral interface (more uniform).
doi:10.1371/journal.pone.0096661.g001

phase. Grader A and grader B, masked to subject characteristics and clinical diagnosis, independently graded these images to assess inter-grader reliability. In addition, grader A repeated the measurements after 2 weeks to assess intra-grader reliability. Both graders assessed the same sets of training images before commencing the grading task.

EDI SD-OCT Imaging

CT was obtained using Spectralis SD-OCT with EDI modality (Wavelength: 870 nm; Heidelberg Engineering, Heidelberg, Germany) after pupil dilation using tropicamide 1% and phenylephrine hydrochloride 2.5%. Subjects' keratometry readings and the refraction data were entered into the software program to estimate optical magnification and, therefore, to allow for more accurate comparisons across individuals. A single experienced examiner masked to the clinical diagnosis of the subject performed the EDI-OCT examination. Seven sections, each comprising 100 averaged scans (using the automatic averaging and eye tracking features of the proprietary device), were obtained in an angle of 5°–30° rectangle centered at the fovea. The horizontal section passing through the center of the fovea was selected for analysis. For each subject only the right eye was chosen for subsequent analysis.

Measurement of Choroidal Thickness

The two major steps in our CT semi-automatic measurement protocol are: (A) post processing of images by adaptive compensation technique and (B) quantitative measurement of CT using Photoshop software. On average, measurement of CT at multiple locations (1.5 and 3 mm nasal and temporal to the fovea) requires approximately 1 minute per image.

(A) Adaptive compensation technique. An accurate evaluation of the CT with EDI-OCT mainly relies on how well one can delineate the choroid-scleral interface (CSI), which anatomically represents the junction between the choroid and the sclera, and is a principal landmark for quantitative measurements of choroid. However, at present identification of CSI is highly variable as there is no algorithm available in Spectralis for its automatic detection. Therefore, in order to accurately determine CT, once the EDI-OCT image was obtained, the CSI was enhanced using a novel post-processing compensation algorithm [21] which greatly improved the detection of CSI by correcting the deleterious effects of light attenuation. In brief, this novel adaptive compensation algorithm improved the ability to detect and visualize the CSI. First, it removes noise over-amplification at high depth and shadow artifacts casted by blood vessels (thus decreasing the intra-layer contrast of the choroid). Second, it improves the visibility of posterior choroid boundary, by significantly increasing the inter-layer contrast across the CSI (**Figure 1**).

(B) Measurement of CT using photoshop software. The enhanced images were measured in Photoshop CS6 extended (Adobe Systems Incorporated, San Jose, California). CT at subfoveal, 1.5 mm and 3 mm nasal and temporal from the fovea were measured. **Figure 2** shows a flow diagram summarizing the CT measurement protocol. The detailed explanation of the steps involved in quantification of CT measurement using Photoshop is provided in Appendix S1.

Statistical Analysis

Statistical analysis was performed using MedCalc Version 12.6 (MedCalc Software, Ostend, Belgium) and SPSS Version 20.0 (SPSS, Inc., Chicago, IL, USA). Shapiro-Wilk tests were used to check the normality of CT data at various locations. The reliability of the CT measurement was assessed using intra- and inter-grader agreements between two independent graders, measured by the absolute agreement model of the intra-class correlation coefficient (ICC) [22]. ICC value of 0.81–1.00 indicates almost perfect agreement. Values of less than 0.40 indicate poor to fair agreement. Bland Altman plot analyses [23,24] were performed to see if there is any proportional bias between measurements. A two-tailed paired sample *t*-test was used to analyze differences between means in CT by location.

Results

Images from 31 eyes of 31 participants (aged 64.4±7.4 years) were included in the analysis (**Table 1**). The mean (standard deviation) sub-foveal CT in this study was 230.37 (66.66) μm (average of 1st and 2nd measurements of grader A). CT measured by the two graders is summarized in **Table 2**. The mean subfoveal CT measured by grader A for the 1st and 2nd measurements was 229.74 (65.12) μm and 231 (69.14) μm, respectively, and was 232.19 (67.89) μm by grader B.

Using adaptive compensation both the intra-grader reliability (ICC: 0.95 to 0.97) and inter-grader reliability (ICC: 0.93 to 0.97) were perfect for all five locations of CT (**Table 3**). However, with the conventional technique of manual CT measurements using

Table 1. Baseline characteristics of study subjects.

Characteristics	Mean (SD)
Age, years	64.35 (7.42)
Gender, male	11 (35.48)
Axial length, mm	23.33 (0.88)
Average choroidal thickness,* μm	
Sub-foveal	230.37 (66.66)
Nasal, 1.5 mm	214.33 (74.34)
Nasal, 3 mm	185.77 (69.96)
Temporal, 1.5 mm	224.53 (57.27)
Temporal, 3 mm	229.74 (52.03)

Data are expressed as mean (SD) except for gender, which is expressed as number (%).
*The average of 1st and 2nd measurement of Grader A.
doi:10.1371/journal.pone.0096661.t001

Table 2. Summary of choroidal thickness measurements at various locations.

Location	Grader A, 1st Measurement	Grader A, 2nd Measurement	Grader B Measurement
Sub-foveal	229.74 (65.12)	231.00(69.14)	232.19 (67.89)
Nasal, 1.5 mm	213.84 (75.12)	214.84(75.49)	221.52(76.08)
Nasal, 3 mm	191.13 (72.79)	180.42(68.25)	187.55(71.06)
Temporal, 1.5 mm	223.94 (56.33)	225.13(59.24)	231.65 (60.82)
Temporal, 3 mm	228.68 (50.64)	230.81(54.57)	230.71 (53.80)

Data are mean (SD).
doi:10.1371/journal.pone.0096661.t002

built-in callipers provided with the Heidelberg explorer software, the intra- (ICC: 0.87 to 0.94) and inter-grader reliability (ICC: 0.90 to 0.93) for all the measured locations is lower (**Table 4**). Using adaptive compensation, the Bland Altman analysis of intra-grader reliability for sub-foveal CT measurement showed 95% LOA of −33.3 to 30.8 with a mean difference of −1.3 μm (**Figure 3**). No significant systemic (except at nasal 3 mm, $p = 0.003$) and proportional bias was detected in intra-grader CT measurements at all locations. The Bland Altman analysis of inter-grader reliability for sub-foveal CT measurement showed 95% LOA of −36.6 to 34.2 with a mean difference of −1.2 μm (**Figure 4**). No significant proportional bias was observed in the inter-grader CT measurements at all locations. Nonetheless, a significant systemic bias at both 1.5 and 3 mm nasal locations was found in the inter-grader CT measurement comparison ($p = 0.001$). However, this could be due to thinnest CT at nasal locations, making it more prone to systemic bias in CT measurements.

In addition, the choroid intra-layer contrast (a measure of shadow presence when high) and the CSI inter-layer contrast (a measure of boundary visibility when high) were computed for all images ($n = 31$) before and after applying adaptive compensation (as in [25]). We found that the intra-layer contrast significantly decreased from 0.84±0.07 to 0.60±0.07 ($p<0.001$; *t*-test), whereas the inter-layer contrast significantly increased from 0.50±0.14 to 0.90±0.10 ($p<0.001$; paired *t*-test) after applying adaptive compensation (**Table 5**).

Discussion

Despite significant advances in imaging technology there are considerable variations in CT measurements across clinical studies. In this report, we described a simple, semi-automated method using adaptive compensation to measure CT from images acquired by EDI SD-OCT. The results showed that the method permits a highly reproducible tool for assessing CT from EDI SD-OCT images. Our measurement method is also simple and requires little time to perform (on average ~1 minute per image). With these features, our method may have great potential for use in both clinical and population-based studies which involve large number of images.

Table 3. Intra- and inter-grader agreements for the choroidal thickness measurement at 5 horizontal locations using adaptive compensation.

					Assessment of proportional bias[d]	
	Locations, CT measurement	ICC (95% CI)	Mean difference (95% LOA)	P Value[c]	Pearson's correlation coefficient, r	P Value
Intra-grader Reliability[a]	Sub-foveal	0.97 (0.94 to 0.98)	−1.3 (−33.3 to 30.8)	0.672	0.248	0.179
	Nasal, 1.5 mm	0.95 (0.90 to 0.97)	−1.0 (−48.0 to 46.0)	0.818	−0.160	0.933
	Nasal, 3 mm	0.95 (0.87 to 0.98)	10.7 (−25.3 to 46.7)	0.003	0.249	0.176
	Temporal, 1.5 mm	0.96 (0.92 to 0.98)	−1.2 (−31.9 to 29.5)	0.674	−0.187	0.313
	Temporal, 3 mm	0.95 (0.90 to 0.97)	−2.1 (−33.5 to 29.2)	0.464	−0.248	0.178
Inter-grader Reliability[b]	Sub-foveal	0.96 (0.93 to 0.98)	−1.2 (−36.6 to 34.2)	0.715	0.070	0.708
	Nasal, 1.5 mm	0.97 (0.92 to 0.99)	−9.0 (−34.4 to 16.4)	0.001	−0.127	0.495
	Nasal, 3 mm	0.97 (0.89 to 0.98)	−9.8 (−37.4 to 17.8)	0.001	−0.230	0.212
	Temporal, 1.5 mm	0.93 (0.86 to 0.96)	−6.5 (−48.3 to 35.3)	0.099	−0.075	0.687
	Temporal, 3 mm	0.94 (0.88 to 0.97)	0.1 (−35.5 to 35.7)	0.977	0.043	0.818

LOA, Limits of Agreement; ICC, Intraclass Correlation Coefficient; CI, Confidence Interval.
[a]Mean difference was determined from the1st time measurement minus the 2nd time measurement.
[b]Mean difference was determined from Grader A measurement minus Grader B measurement.
[c]P value of one sample t-tests (comparing between mean difference and zero value) to indicate presence of systemic bias.
[d]Using Pearson's correlation coefficients of regression line.
doi:10.1371/journal.pone.0096661.t003

Table 4. Intra- and inter-grader agreements for the choroidal thickness measurement at 5 horizontal locations using Spectralis SD-OCT with conventional manual technique.

	Locations, CT measurement	ICC (95% CI)	Mean difference (95% LOA)
Intra-grader Reliability[a]	Sub-foveal	0.94 (0.87to 0.97)	9.7 (−30.3 to 49.7)
	Nasal, 1.5 mm	0.92 (0.85 to 0.96)	2.9 (−41.1 to 54.9)
	Nasal, 3 mm	0.92 (0.85 to 0.96)	4.1 (−36.1 to 44.3)
	Temporal, 1.5 mm	0.87 (0.75 to 0.93)	−7.0 (−52.1 to 38.1)
	Temporal, 3 mm	0.88 (0.77 to 0.94)	−1.9 (−44.9 to 48.6)
Inter-grader Reliability[b]	Sub-foveal	0.90 (0.60 to 0.96)	−19.1 (−63.7 to 25.6)
	Nasal, 1.5 mm	0.93 (0.68 to 0.97)	18.3 (−59.7 to 23.2)
	Nasal, 3 mm	0.91 (0.67 to 0.96)	−15 (−54.3 to 24.3)
	Temporal, 1.5 mm	0.91 (0.72 to 0.96)	−12.7 (−49.8 to 24.4)
	Temporal, 3 mm	0.90 (0.58 to 0.96)	−15.7 (−51.3 to 19.9)

LOA, Limits of Agreement; ICC, Intraclass Correlation Coefficient; CI, Confidence Interval.
[a]Mean difference was determined from the1st time measurement minus the 2nd time measurement.
[b]Mean difference was determined from Grader A measurement minus Grader B measurement.
doi:10.1371/journal.pone.0096661.t004

There are considerable differences in CT measurements across studies. Even though advances in OCT technology have reduced acquisition time, adequate visualization of choroid is still lacking. There are several challenges in imaging the choroid. First, the choroid is located behind the RPE and Bruch's membrane, making it less accessible than the retina and more difficult to be visualized. Second, the pigmentation in the RPE and the choroid itself decreases the signal intensity. Lastly, unlike retinal imaging [26], wherein the RPE and internal limiting membrane are thin and clearly identifiable, the transition zone between the choroid and sclera (i.e. CSI) has blurred border and is broader, making CSI difficult to identify.

However, it is not always easy to distinguish CSI on acquired images, which may be related to scan quality or anatomic variation. Some choroidal scans have a distinct hypo-reflective line corresponding to the supra-choroidal space, but often this line can be indistinct leading to measurement error [27]. At present, identification of CSI is highly variable. To overcome these challenges, in this study we enhanced choroidal-scleral junction using a post-processing adaptive compensation algorithm [21]. Measurement of CT was performed in the post-processed images using Photoshop (Adobe Systems Incorporated, San Jose, California), a readily available and easy-to-use program.

Adaptive compensation provides two major improvements. First, the intra-layer contrast (of the choroid) significantly decreased after applying adaptive compensation, indicating successful shadow correction within the choroid. Second, the inter-layer contrast (across the CSI) significantly increased after applying adaptive compensation, indicating better visualization of CSI and therefore allowing for precise measurement of CT. These results are consistent with a previous study on standard compensation [25] and indicate significant improvements in image quality. Also, a study by Lin *et al.* established outer choroidal contrast as a valid quantifiable measure of choroidal

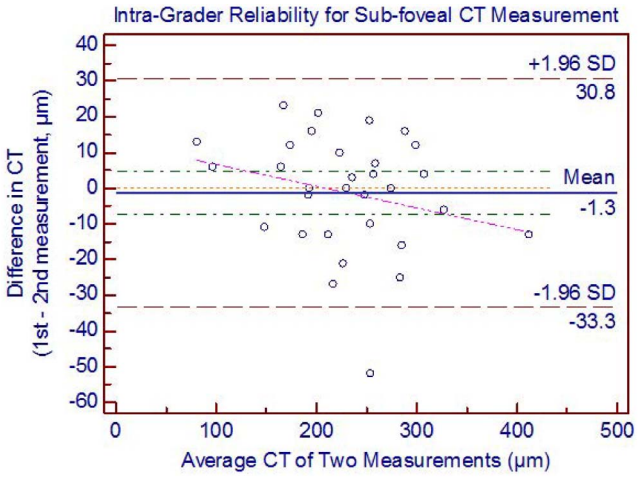

Figure 3. Bland Altman plot of intra-grader reliability of sub-foveal choroidal thickness (CT) measurement. The difference was calculated by the 1st measurement minus the 2nd measurement. Pink dashed line represents regression line of difference between 1st and 2nd measurements.
doi:10.1371/journal.pone.0096661.g003

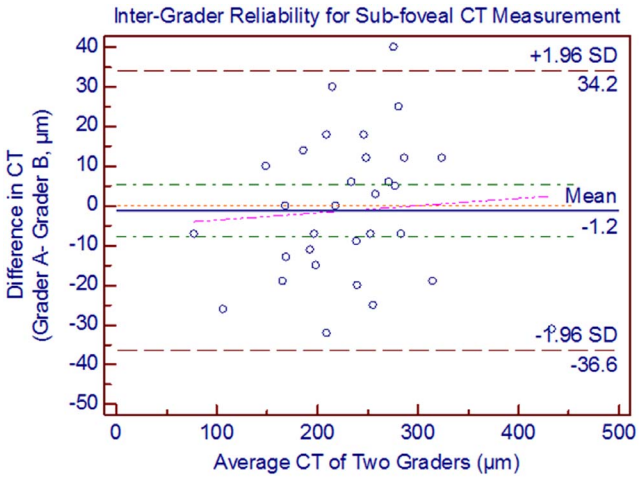

Figure 4. Bland Altman plots of inter-grader reliability of sub-foveal choroidal thickness (CT) measurement. The difference was calculated by the grader A measurement minus the grader B measurement. Pink dashed line represents regression line of difference between the two graders measurements.
doi:10.1371/journal.pone.0096661.g004

Table 5. Intra- and inter-layer contrast (n = 31 subjects).

		Mean (SD)	P-Value
Intra-layer Contrast	Standard (without compensation)	0.84 (0.07)	<0.001
	Adaptive Compensation	0.60 (0.07)	
Inter-layer Contrast	Standard (without compensation)	0.50 (0.14)	<0.001
	Adaptive Compensation	0.90 (0.10)	

doi:10.1371/journal.pone.0096661.t005

image quality and demonstrated that inverted SD-OCT imaging optimizes visualization of CSI and choroidal vessels through improved outer choroid contrast [28].

With improved intra- and inter-layer contrast, the compensated images are likely more accurate than the non-compensated images as the deleterious effects of OCT light attenuation have been corrected, thus making the CSI more visible. The post-compensation images are more representative of the eye tissue architecture, since better estimates of the ocular tissues optical properties (e.g. reflectivity) are provided. This has been formally demonstrated in the original article by Girard *et al.* [25], and in the following studies [21,29,30]. Lastly, although adaptive compensation is useful in all images, it is likely to be more useful when the CSI is poorly visible, e.g. in images where light attenuation is strong (**Figure 1**), emphasizing further the need for compensation for more accurate thickness measurement of the choroid.

Adaptive compensation achieves high intra-grader (ICC: 0.95 to 0.97) and inter-grader (ICC: 0.93 to 0.97) repeatability in CT measurements compared to conventional method (intra-grader ICC: 0.87 to 0.94, inter-grader ICC: 0.90 to 0.93), suggesting the use of adaptive compensation to improve the visualization of CSI and to obtain more reliable CT measurements. However, the high repeatability can be explained by the standardization and strict adherence to a rigorous grading protocol in the present study. In addition, both graders underwent the same training set for standardization purpose before embarking on the actual grading task. The present results are in line in the studies by Ikuno *et al.* [31] and Yamashita *et al.* [32] who reported an inter-grader ICC of 0.97 and 0.94, respectively, for sub-foveal CT measurements. However, in these two previous studies the intra-grader repeatability was not evaluated, and it is not clear how the choroid images, where CSI could not be clearly visualized, were processed.

But the present study has its own limitations, as the measurement of CT was subjective in nature, and was therefore subject to measurement bias. However, our method may be less prone to observer error because the CSI was enhanced by adaptive compensation to give better visibility. An automated, and thus may be more objective, method of measuring CT would be of potential interest to facilitate, speed-up and render operator-independent such analyses.

There are few recent studies on automatic choroidal segmentation in OCT images. Zhang *et al.* proposed an automatic segmentation algorithm for the choroidal vessels using Cirrus OCT in 24 normal subjects. But their aim was to quantify choroidal vasculature thickness and choroicapillaries equivalent thickness rather than the CT [33]. Likewise, Torzicky *et al.* [34] and Duan *et al.* [35] developed the automatic algorithms to detect the boundary between the choroid and sclera based on polarization sensitive OCT which are not commercially available. Although, Tian *et al.* [36] in 2013 proposed an automatic algorithm that could segment choroid in commercially available Spectralis OCT, but their algorithm was tested only on 20 EDI OCT images and need to be validated on more images to prove the robustness of algorithm before its application in clinical studies. While we are preparing the manuscript, a commercially available CT measurement algorithm in swept-source OCT (Topcon Corp., Tokyo, Japan) is being made available. However, in view of lack of supporting agreement studies on the algorithm and manual choroidal segmentation (in both normal and diseased eyes), the accuracy and reliability of automated CT analysis by using swept-source OCT is yet to be established for use in clinical settings.

In conclusion, we described a simplified, semi-automated and practical method "adaptive compensation followed by using Photoshop" that gives excellent intra- and inter-grader reliability (ICC>0.93) to quantify CT in the EDI SD-OCT images. This method has great potential usage in both clinical and population based studies, as reliable and accurate measurements of CT from EDI-OCT images are essential in distinguishing clinically significant change of CT and assisting in risk-profiling for various posterior segment diseases.

Supporting Information

Appendix S1 Detailed steps to quantify choroidal thickness using Photoshop.
(DOCX)

Author Contributions

Conceived and designed the experiments: PG ES MJG JMM TYW CYC. Performed the experiments: PG ES CYC. Analyzed the data: PG CYC. Contributed reagents/materials/analysis tools: JMM MJG. Wrote the paper: PG CYC. Designed the software used in analysis: MJG JMM.

References

1. Linsenmeier RA, Padnick-Silver L (2000) Metabolic dependence of photoreceptors on the choroid in the normal and detached retina. Invest Ophthalmol Vis Sci 41: 3117–3123.
2. Grossniklaus HE, Green WR (2004) Choroidal neovascularization. Am J Ophthalmol 137: 496–503.
3. Koizumi H, Yamagishi T, Yamazaki T, Kawasaki R, Kinoshita S (2011) Subfoveal choroidal thickness in typical age-related macular degeneration and polypoidal choroidal vasculopathy. Graefes Arch Clin Exp Ophthalmol 249: 1123–1128.
4. Gomi F, Tano Y (2008) Polypoidal choroidal vasculopathy and treatments. Curr Opin Ophthalmol 19: 208–212.
5. Chung SE, Kang SW, Lee JH, Kim YT (2011) Choroidal thickness in polypoidal choroidal vasculopathy and exudative age-related macular degeneration. Ophthalmology 118: 840–845.
6. Gupta B, Mohamed MD (2011) Photodynamic therapy for variant central serous chorioretinopathy: efficacy and side effects. Ophthalmologica 225: 207–210.
7. Imamura Y, Fujiwara T, Margolis R, Spaide RF (2009) Enhanced depth imaging optical coherence tomography of the choroid in central serous chorioretinopathy. Retina 29: 1469–1473.

8. Fong AH, Li KK, Wong D (2011) Choroidal evaluation using enhanced depth imaging spectral-domain optical coherence tomography in Vogt-Koyanagi-Harada disease. Retina 31: 502–509.
9. Fujiwara T, Imamura Y, Margolis R, Slakter JS, Spaide RF (2009) Enhanced depth imaging optical coherence tomography of the choroid in highly myopic eyes. Am J Ophthalmol 148: 445–450.
10. Ikuno Y, Tano Y (2009) Retinal and choroidal biometry in highly myopic eyes with spectral-domain optical coherence tomography. Invest Ophthalmol Vis Sci 50: 3876–3880.
11. Fitzgerald ME, Wildsoet CF, Reiner A (2002) Temporal relationship of choroidal blood flow and thickness changes during recovery from form deprivation myopia in chicks. Exp Eye Res 74: 561–570.
12. Cheung CM, Loh BK, Li X, Mathur R, Wong E, et al. (2013) Choroidal thickness and risk characteristics of eyes with myopic choroidal neovascularization. Acta Ophthalmol.
13. Povazay B, Hermann B, Unterhuber A, Hofer B, Sattmann H, et al. (2007) Three-dimensional optical coherence tomography at 1050 nm versus 800 nm in retinal pathologies: enhanced performance and choroidal penetration in cataract patients. J Biomed Opt 12: 041211.
14. Kahn KN, McKibbin M, Kahn RS (2011) Variability in subfoveal choroidal thickness measurements. Invest Ophthalmol Vis Sci 52: 7221; author reply 7221.
15. Spaide RF, Koizumi H, Pozzoni MC (2008) Enhanced depth imaging spectral-domain optical coherence tomography. Am J Ophthalmol 146: 496–500.
16. Manjunath V, Taha M, Fujimoto JG, Duker JS (2010) Choroidal thickness in normal eyes measured using Cirrus HD optical coherence tomography. Am J Ophthalmol 150: 325–329 e321.
17. Maul EA, Friedman DS, Chang DS, Boland MV, Ramulu PY, et al. (2011) Choroidal thickness measured by spectral domain optical coherence tomography: factors affecting thickness in glaucoma patients. Ophthalmology 118: 1571–1579.
18. Ho J, Branchini L, Regatieri C, Krishnan C, Fujimoto JG, et al. (2011) Analysis of normal peripapillary choroidal thickness via spectral domain optical coherence tomography. Ophthalmology 118: 2001–2007.
19. Shin JW, Shin YU, Lee BR (2012) Choroidal thickness and volume mapping by a six radial scan protocol on spectral-domain optical coherence tomography. Ophthalmology 119: 1017–1023.
20. Rosman M, Zheng Y, Wong W, Lamoureux E, Saw SM, et al. (2012) Singapore Malay Eye Study: rationale and methodology of 6-year follow-up study (SiMES-2). Clin Experiment Ophthalmol 40: 557–568.
21. Mari JM, Strouthidis NG, Park SC, Girard MJ (2013) Enhancement of lamina cribrosa visibility in optical coherence tomography images using adaptive compensation. Invest Ophthalmol Vis Sci 54: 2238–2247.
22. Fleiss JL, Cohen J (1973) The Equivalence of Weighted Kappa and the Intraclass Correlation Coefficient as Measures of Reliability. Educational and Psychological Measurement 33: 613–619.
23. Bland JM, Altman DG (1986) Statistical methods for assessing agreement between two methods of clinical measurement. Lancet 1: 307–310.
24. Bland JM, Altman DG (2012) Agreed statistics: measurement method comparison. Anesthesiology 116: 182–185.
25. Girard MJ, Strouthidis NG, Ethier CR, Mari JM (2011) Shadow removal and contrast enhancement in optical coherence tomography images of the human optic nerve head. Invest Ophthalmol Vis Sci 52: 7738–7748.
26. Hee MR, Puliafito CA, Duker JS, Reichel E, Coker JG, et al. (1998) Topography of diabetic macular edema with optical coherence tomography. Ophthalmology 105: 360–370.
27. Yiu G, Pecen P, Sarin N, Chiu SJ, Farsiu S, et al. (2014) Characterization of the choroid-scleral junction and suprachoroidal layer in healthy individuals on enhanced-depth imaging optical coherence tomography. JAMA Ophthalmol 132: 174–181.
28. Lin P, Mettu PS, Pomerleau DL, Chiu SJ, Maldonado R, et al. (2012) Image inversion spectral-domain optical coherence tomography optimizes choroidal thickness and detail through improved contrast. Invest Ophthalmol Vis Sci 53: 1874–1882.
29. Foin N, Mari JM, Davies JE, Di Mario C, Girard MJ (2013) Imaging of coronary artery plaques using contrast-enhanced optical coherence tomography. Eur Heart J Cardiovasc Imaging 14: 85.
30. Foin N, Mari JM, Nijjer S, Sen S, Petraco R, et al. (2013) Intracoronary imaging using attenuation-compensated optical coherence tomography allows better visualisation of coronary artery diseases. Cardiovasc Revasc Med 14: 139–143.
31. Ikuno Y, Maruko I, Yasuno Y, Miura M, Sekiryu T, et al. (2011) Reproducibility of retinal and choroidal thickness measurements in enhanced depth imaging and high-penetration optical coherence tomography. Invest Ophthalmol Vis Sci 52: 5536–5540.
32. Yamashita T, Yamashita T, Shirasawa M, Arimura N, Terasaki H, et al. (2012) Repeatability and reproducibility of subfoveal choroidal thickness in normal eyes of Japanese using different SD-OCT devices. Invest Ophthalmol Vis Sci 53: 1102–1107.
33. Zhang L, Lee K, Niemeijer M, Mullins RF, Sonka M, et al. (2012) Automated segmentation of the choroid from clinical SD-OCT. Invest Ophthalmol Vis Sci 53: 7510–7519.
34. Torzicky T, Pircher M, Zotter S, Bonesi M, Gotzinger E, et al. (2012) Automated measurement of choroidal thickness in the human eye by polarization sensitive optical coherence tomography. Opt Express 20: 7564–7574.
35. Duan L, Yamanari M, Yasuno Y (2012) Automated phase retardation oriented segmentation of chorio-scleral interface by polarization sensitive optical coherence tomography. Opt Express 20: 3353–3366.
36. Tian J, Marziliano P, Baskaran M, Tun TA, Aung T (2012) Automatic measurements of choroidal thickness in EDI-OCT images. Conf Proc IEEE Eng Med Biol Soc 2012: 5360–5363.

Acta Ophthalmologica

Relationship of ocular and systemic factors to the visibility of choroidal–scleral interface using spectral domain optical coherence tomography

Preeti Gupta,[1,2] Ching-Yu Cheng,[1,2,3,4] Chui Ming Gemmy Cheung,[1,2,4] Hla Myint Htoon,[1,4] Yingfeng Zheng,[1] Ecosse L. Lamoureux,[1,2,4] Tin Aung,[1,2,4] Tien-Yin Wong[1,2,4] and Carol Y. Cheung[1,2,4]

[1]Singapore Eye Research Institute and Singapore National Eye Centre, Singapore, Singapore
[2]Department of Ophthalmology, Yong Loo Lin School of Medicine, National University of Singapore and National University Health System, Singapore, Singapore
[3]Saw Swee Hock School of Public Health, National University of Singapore and National University Health System, Singapore, Singapore
[4]Office of Clinical Sciences, Duke-NUS Graduate Medical School, Singapore, Singapore

ABSTRACT.

Purpose: **To assess the visibility of the choroidal–scleral interface (CSI) from spectral domain optical coherence tomography (SD-OCT) and evaluate the ocular and systemic factors influencing the visibility of CSI in healthy eyes from population-based Malay sample.**

Methods: **Participants were consecutively recruited from the population-based Singapore Malay Eye Study-2 (SiMES-2). SD-OCT images were obtained by Spectralis OCT with enhanced depth imaging (EDI) mode. Visibility of CSI was assessed by a grading system ranging from 0 to 2 scores. The reliability of choroidal thickness measurement in different grades of CSI visibility was assessed using intraclass correlation coefficient. Ordinal regression analyses were performed to evaluate a range of ocular and systemic factors influencing the visibility of CSI.**

Results: **A total of 176 healthy eyes were analysed, and 59.1% of our subjects had well-defined CSI (score 2), 8.5% had poorly defined CSI (score 0), and 32.4% had CSI between well and poorly defined (score 1). The reliability of subfoveal choroidal thickness measurement decreased with each grade of CSI visibility score. Decreased axial length (AL) (estimate of ordinal regression [OR] = 0.465, p = 0.003), thicker retinal thickness (estimate of OR = −0.030, p = 0.004), younger age (estimate of OR = 0.045, p = 0.030) and diabetes (estimate of OR = −0.746, p = 0.004) were associated with lower CSI visibility score.**

Conclusions: **Only 60% of normal healthy eyes had well-defined CSI from SD-OCT images. Our data suggest that choroidal thickness measurements can be substantially affected by the visibility of CSI. The visibility of CSI varies with AL, retinal thickness, age and diabetes.**

Key words: choroidal thickness – choroid–scleral interface – EDI SD-OCT – visibility of choroid-scleral interface

Acta Ophthalmol.

doi: 10.1111/aos.12777

Introduction

The choroid is a major vascular layer of the eye which provides oxygen and nourishment to the outer layers of the retina including the photoreceptors (Linsenmeier & Padnick-Silver 2000). Abnormalities in choroidal vasculature (e.g. vascular hyperpermeability, vascular changes and loss, and thinning) are of importance in the pathophysiology of a number of retinal diseases such as age-related macular degeneration (Grossniklaus & Green 2004; Koizumi et al. 2011), polypoidal choroidal vasculopathy (Gomi & Tano 2008; Chung et al. 2011), central serous chorioretinopathy (Gupta & Mohamed 2011; Imamura et al. 2009) and high myopia-related chorioretinal atrophies (Fitzgerald et al. 2002; Fujiwara et al. 2009; Ikuno & Tano 2009). To elucidate the mechanisms how the choroid may affect chorioretinal diseases, an easy, objective and quantitative analysis of the choroid is required. Indocyanine green angiography and, to a lesser extent, fluorescein angiography are the current standards to evaluate the choroidal circulation in clinic; however, they are invasive and can only provide qualitative assessment of choroid.

Since the introduction of optical coherence tomography-based enhanced

depth imaging (EDI-OCT) by Spaide and colleagues (Spaide et al. 2008), this technique has been used to study the changes in choroidal thickness in many conditions (Chung et al. 2011; Fujiwara et al. 2009; Gomi & Tano 2008; Grossniklaus & Green 2004; Ikuno & Tano 2009; Imamura et al. 2009) as well as other ocular abnormalities (Beck et al. 2015). Nonetheless, an accurate estimation of choroidal thickness with EDI-OCT relies mainly on the visibility of choroid–scleral interface (CSI), which anatomically represents the junction between the choroid and the sclera and is a principal landmark for quantitative measurements of choroid. However, unlike retinal layers, the contrast between the choroid and scleral border is weak (Chiu et al. 2010; Ghorbel et al. 2011; Duan et al. 2012; Kajic et al. 2012), giving CSI a variable visibility leading to variations and inaccuracy in choroidal thickness measurements across the clinical studies. There have been no studies which investigate factors which may determine the visibility of the CSI.

The aim of this study was to assess the visibility of CSI in EDI-OCT images in healthy eyes and to determine the effects of a range of ocular and systemic factors on CSI visibility in the population-based sample.

Methods

Study population

Data for this analysis were derived from the Singapore Malay Eye Study-2 (SiMES-2), a population-based cohort study of eye diseases in Malay adults aged 46–86 years living in Singapore. Details of the baseline study design, sampling plan and methodology (SiMES-1), conducted in 2004–6, have been reported elsewhere (Foong et al. 2007). The follow-up examination, SiMES-2, is ongoing (Rosman et al. 2012). For this analysis, we enrolled 176 consecutive participants of the SiMES-2 from June 2012 to January 2013. Participants recruited in this phase underwent standardized and detailed ophthalmic examination, including Spectralis EDI SD-OCT.

Normal participants had no history of ocular disease except cataract. Participants were excluded based on the following characteristics: best-corrected LogMAR VA >0.3, evidence of macular or vitreoretinal diseases, diabetic retinopathy, previous retinal or refractive surgery, past history of intraocular surgery, or clinical features compatible with a diagnosis of glaucoma suspect or glaucoma. A glaucoma suspect was defined as having any of the following criteria in the presence of normal visual field: (1) abnormal anterior segment signs consistent with pseudoexfoliation or pigment dispersion syndrome, (2) narrow angles (posterior trabecular meshwork visible for <180 degrees during static gonioscopy), (3) vertical cup-to-disc ratio (VCDR) > 0.6 or VCDR asymmetry >0.2 and (4) peripheral anterior synechiae or other findings consistent with secondary glaucoma (Shen et al. 2008). Glaucoma was diagnosed and classified using the International Society of Geographic and Epidemiological Ophthalmology (ISGEO) scheme (Foster et al. 2002), based on the findings from gonioscopy, optic disc characteristics and visual fields results. The study was approved by the Institutional Review Board of Singapore Eye Research Institute. It followed the tenants of the Declaration of Helsinki, and written informed consent was obtained from the subjects.

EDI-OCT imaging

Choroidal thickness was obtained using a SD-OCT (Spectralis, Heidelberg Engineering, Heidelberg, Germany) with EDI modality after pupil dilation using tropicamide 1% and phenylephrine hydrochloride 2.5%. The EDI mode places the retinal pigmented epithelium near the zero-delay line while producing an upright enhanced choroidal images. Seven sections, each comprising 100 averaged scans (using the automatic averaging and eye tracking features of the proprietary device), were obtained in an angle of 5–30° rectangle centred onto the fovea. According to Spectralis user manual guidelines, subjects' keratometry readings and the most recent refraction were entered into the software program to estimate optical magnification and, therefore, to allow for more accurate comparisons across individuals. All the scans included in the study had signal strength of at least 18, which is considered as acceptable quality. One of the authors (PG) who was masked to subject characteristics and clinical diagnosis performed the EDI-OCT examination. Only the horizontal section passing through the centre of the fovea was selected for analysis.

Image analysis

Choroidal thickness measurement

Using the Spectralis linear measurement tool, a single observer (PG) measured choroidal thickness perpendicularly from the outer portions of the hyper-reflective line, corresponding to the retinal pigment epithelium (automatically detected by the instrument), to the hyporeflective line or margin corresponding to the sclerochoroidal interface (drawn manually) at subfoveal location.

CSI visibility grading system

We developed a new grading system to assess the visibility of CSI for EDI-OCT images. Two blinded observers evaluated all the OCT scans to locate the CSI on each EDI-OCT image. The CSI was defined as a hyporeflective line between the large vessel layer of the choroid and the sclera (Fig. 1). For the grading of CSI visibility, the EDI-OCT images were given a score between 0 and 2. A score of '2' was assigned if the image contained a well-defined CSI. A score of '1' was assigned if the visibility of CSI was between well-defined and poorly defined CSI, and a score of '0' was given if the image had poorly defined CSI visibility, that is no clearly identifiable border between the choroid and sclera was seen. Figure 1 demonstrates examples of well-defined, moderately defined and poorly defined CSI in EDI-OCT images in the SiMES-2 cohort.

Reliability assessment

We evaluated both the intra- and interobserver reliability in assessing CSI visibility. For intra-observer reliability, 176 Spectralis images were assessed again by the same grader (grader 1 versus grader 1) after an interval of 1 week. Two independent graders (grader 1 versus grader 2) assessed the interobserver reliability of CSI visibility in 176 Spectralis images.

In addition, subfoveal choroidal thickness at the foveal centre was measured twice by the same grader to assess the reliability of choroidal thickness measurement in each score of CSI visibility (15 images for each score).

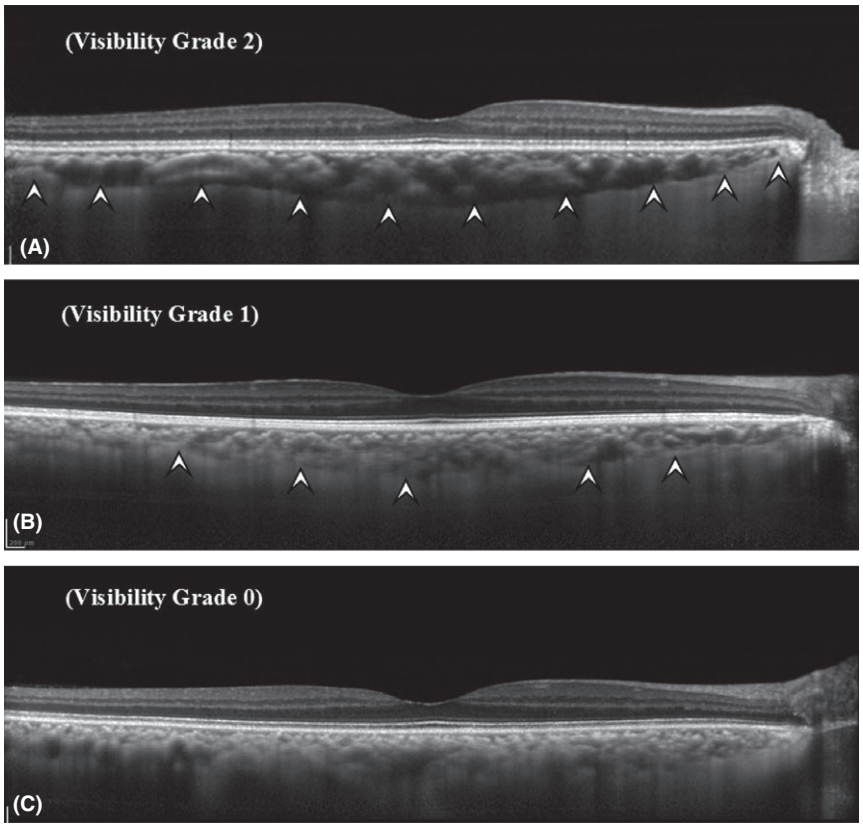

Fig. 1. The choroidal–scleral interface (CSI) is indicated by hyper-reflective line shown by arrowheads. (A) demonstrates an example of a well-defined CSI, (B) shows a moderately defined CSI, and (C) a poorly defined CSI in EDI-OCT image in the SiMES-2 cohort.

Measurement of ocular factors

All participants underwent an extensive and standardized examination procedure, which included measurement of visual acuity monocularly using LogMAR number chart (Lighthouse International, New York, NY, USA) at a distance of 4 m. Intraocular pressure was measured with a Goldmann applanation tonometer (Haag-Streit, Bern, Switzerland) before pupil dilation. The static refraction of each eye was measured using an autorefractor (Canon RK 5 Auto Ref-Keratometer, Canon Inc. Ltd., Tochigiken, Japan). Spherical equivalent refraction was calculated as the sum of the value of the spherical value and half of the cylindrical value. Central corneal thickness was measured with an ultrasound pachymeter (Advent, Mentor O & O, Norwell, MA, USA), and the mean of five measurements was used in the analysis. Axial length (AL), corneal curvature and anterior chamber depth were measured with a non-contact partial coherence laser interferometry (IOLMaster V3.01, Carl Zeiss Meditec AG, Jena, Germany), and the mean of five measurements was used in the analysis. Lens opacity was assessed by trained ophthalmologists using Lens Opacities Classification System (LOCS) III (Chylack et al. 1993) with a Haag-Streit slit-lamp microscope (model BQ-900) in comparison with standard photographic slides for nuclear opalescence, nuclear colour, cortical and posterior subcapsular (PSC) cataract. Retinal thickness of central 1-mm region was obtained from Spectralis OCT after pupil dilation.

Assessment of demographic, lifestyle and systemic factors

All participants underwent a detailed interview using standardized questionnaires. Information on socio-demographic status, lifestyle risk factors (e.g. smoking, alcohol consumption), medication use and self-reported history of systemic disease was collected. Systolic and diastolic blood pressures were measured using a digital automatic blood pressure monitor (Dinamap model Pro Series DP110X-RW, 100V2; GE Medical Systems Information Technologies, Inc., Milwaukee, WI, USA), after subjects were seated for at least 5 min. Body mass index (BMI) was calculated as body weight (in kilograms) divided by body height (in metres) squared. Smoking status was defined as those currently smoking, ex-smokers and non-smokers. The number of packs smoked per week was recorded. Non-fasting venous blood samples were analysed at the National University Hospital Reference Laboratory for biochemical testing of serum total cholesterol, high-density lipoprotein (HDL) cholesterol, low-density lipoprotein (LDL) cholesterol, triglycerides, glycosylated haemoglobin (HbA1c), glucose and creatinine.

Statistical analysis

Statistical analysis was performed using MEDCALC version 12.3 (Medcalc Software, Ostend, Belgium) and SPSS version 20.0 (SPSS, Inc., Chicago, IL, USA). The intra–inter grader reliability in assessing CSI visibility was measured by weighted kappa statistics (K_w) (Fleiss & Cohen 1973). K_w values of 0.81–1.00 indicate almost perfect agreement, values of 0.61–0.80 indicate good agreement, and values of 0.41–0.60 indicate moderate agreement. Values of less than 0.40 indicate poor to fair agreement. The reliability of choroidal thickness measurement in each score of CSI visibility was measured by the absolute agreement model of the intra-class correlation coefficient (ICC). ICC value of 0.81–1.00 indicates almost perfect agreement. Values of less than 0.40 indicate poor-to-fair agreement.

As the dependent variable (CSI visibility scores 0, 1 & 2) is ordinal in nature, we used ordinal regression for our analysis. Univariate and multiple ordinal regression analyses were performed to assess the ocular and systemic factors (independent variables) related to the CSI visibility (dependent variable). For multiple regression analysis, gender and factors which showed significant association in univariate analysis were included. The three groups (CSI visibility score 0, 1 & 2) were not evenly distributed. Thus, the Logit link function could not be used, and instead, complementary log–log (higher scores more probable) was used. However, this function could only determine the direction of the relationship between each predictor and the ordinal nature of categorical

outcome. A p-value of < 0.05 was considered statistically significant. Right eye ($n = 161$) of each subject was selected for the analysis. However, when images of right eye were not available, then the images of left eye ($n = 15$) were used.

Results

Table 1 shows the baseline characteristics and the distribution of CSI visibility grade of the study subjects. A total of 176 eyes from 176 subjects (85 men and 91 women) with a mean ± SD (standard deviation) age of 60.44 ± 8.19 years (range, 48–86 years) were included in the study. The CSI was clearly identifiable (score 2) in 59.1% (104/176 eyes), poorly defined (score 0) in 8.5% (15/176 eyes) and was between clearly and poorly defined (score 1) in 32.4% (57/176 eyes) of our subjects.

Table 1. A summary of subjects' demographics, ocular parameters and systemic factors.

	Included ($n = 176$)
Age, years	60.44 (8.19)
Gender, % male	48.3
Spherical equivalent, D	0.03 (2.03)
Best-corrected visual acuity, logMAR	0.13 (0.10)
Axial length, mm	23.62 (1.07)
Anterior chamber depth, mm	3.22 (.35)
Corneal curvature, mm	7.45 (1.19)
Intraocular pressure, mmHg	14.90 (2.94)
Central corneal thickness, μm	541.15 (35.68)
LOCS III nuclear cataract, %	35 (19.9)
LOCS III cortical, %	56 (38.8)
LOCS III PSC, %	8 (4.5)
Retinal thickness, μm	261.25 (21.17)
Subfoveal choroidal thickness, μm	244.36 (95.31)
OCT signal strength	30.56 (5.08)
Systolic blood pressure, mmHg	137.23 (19.50)
Body mass index, kg/m^2	77.52 (9.84)
Current smoking, %	36 (20.05)
Diabetes mellitus, %	51 (29.0)
Hypertension, %	74 (42.0)
Visibility grade	
Grade 0	15 (8.5)
Grade 1	57 (32.4)
Grade 2	104 (59.1)

Data are mean (SD), except for gender, cataracts, HbA1c, current smoking, diabetes hypertension and visibility grades which are expressed as number (%).

Table 2 shows the intra- and intergrader reliability assessment of CSI visibility. Both the intra- and interobserver reliability was moderate to good (Kw = 0.78, 95% CI: 0.70–0.85 and Kw = 0.74, 95% CI: 0.64-0.83 for intra- and interobserver reliability, respectively).

The reliability of subfoveal choroidal thickness measurement was highest for CSI visibility score 2 (ICC = 0.977, 95% CI, 0.935–0.992) followed by score 1 (ICC = 0.734, 95% CI, 0.585–0.940) and score 0 (ICC = 0.514, 95% CI, 0.058–0.853), respectively. In addition, in our previously published paper (Gupta et al. 2014), we have reported that both the intragrader reliability (ICC: 0.87–0.94) and intergrader reliability (ICC: 0.90–0.93) for the choroidal thickness measurement using Spectralis SD-OCT were excellent.

Among the ocular factors, decreased AL ($p = 0.006$), thicker retinal ($p < 0.001$) and choroidal ($p = 0.012$) thicknesses were more likely to have lower CSI visibility score. Among other factors, young individuals ($p = 0.003$) and those with diabetes ($p = 0.033$) were associated with lower CSI visibility score. We did not observe any associations between CSI visibility with other factors, for example gender, BMI, systolic and diastolic blood pressure, HDL and LDL cholesterol, blood creatinine, triglycerides, serum blood glucose level, HbA1c, smoking status and hypertension (all $p > 0.10$) (Table 3). Factors with $p < 0.10$ in the univariate analysis were further included into the multivariate analysis. However, because of the collinearity between AL and spherical equivalent, only AL was selected and retained in the multivariate analysis.

In the multivariate-adjusted model, decreased AL (estimate of ordinal regression = 0.465, p = 0.003), thicker retinal thickness (estimate of ordinal regression = −0.030, p = 0.004), younger age (estimate of ordinal regression = 0.045, p = 0.030) and diabetes (estimate of ordinal regression = −0.746, p = 0.004) were significantly and independently associated with lower CSI visibility score (Table 4).

In this sample, we found that 10.9% of younger people (age less than 60 years), 12.5% of those with thicker retinal thickness (≥280 μm), 11.8% of those with shorter AL (≤23 mm) and 11.76% of those with diabetes had poor CSI visibility (grade 0).

Discussion

In this study, we found that only 60% of subjects had well-delineated CSI that allowed good visualization of the choroid, and the choroidal thickness measurements had higher variability in the images with poor visualization of CSI. Moreover, we demonstrated that the visualization of CSI was poorer in eyes with shorter eye ball, thicker retinal thickness, and in younger persons and persons with diabetes.

Correct identification and knowledge of factors determining CSI visibility is essential for the accuracy and performance of imaging programs that aim to automatically detect this anatomical structure. We found that younger age was associated with poorer identification of choroid scleral junction (Fig. 2). Previous histologic studies have shown a decrease in vascular density, overall luminal area and diameter of chorio-capillary vessels with increase in age (Sarks 1976; Feeney-Burns et al. 1990; Ramrattan et al. 1994). This leads to a decrease in physiological functions of the choroid, that is the ability of the choroid to provide sufficient levels of oxygen and other metabolites to the RPE, and outer retina may decrease (Spaide et al. 2008) contributing to the onset of many diseases in elderly people. There

Table 2. Intra- and interobserver reliability assessment of CSI visibility.

Inter- and intragrader reliability	Intergrader				Intragrader			
	Score 0	Score 1	Score 2	Total	Score 0	Score 1	Score 2	Total
Score 0	12	4	1	17	8	10	0	18
Score 1	5	35	12	52	3	39	13	55
Score 2	1	10	96	107	0	10	93	103
Total	18	49	109	176	11	59	106	176

Gray shades indicate agreement of CSI visibility scores between the graders (intra and inter).

Table 3. Univariate analysis between ocular and systemic factors with visibility of choroidal–scleral interface (CSI).

Choroid–scleral interface visibility				
			95% Confidence interval	
	Estimate	p-value	Lower bound	Upper bound
Ocular factors				
Axial length (mm)	0.375	**0.006**	0.106	0.645
Spherical equivalent (D)	−0.143	0.054	−2.88	0.003
Anterior chamber depth (mm)	−0.290	0.383	−0.942	0.362
Central corneal thickness (μm)	0.004	0.229	−0.003	0.011
Corneal curvature (mm)	0.104	0.197	−0.054	0.262
Intraocular pressure (mmHg)	0.021	0.605	−0.059	0.101
LOCS III nuclear cataract (no versus yes)	−0.683	0.056	−1.382	0.017
LOCS III cortical (no versus yes)	0.011	0.966	−0.487	0.509
LOCS III PSC (no versus yes)	0.546	0.261	−0.406	1.498
Retinal thickness (μm)	−0.034	**< 0.001**	−0.052	−0.016
Subfoveal choroidal thickness (μm)	−0.003	**0.012**	−0.006	−0.001
OCT signal strength	0.022	0.352	−0.024	0.068
Systemic factors				
Age (years)	0.048	**0.003**	0.016	0.080
Diabetes mellitus (yes versus no)	−0.524	**0.033**	−1.006	−0.042

Bolded font indicates statistical significance.

Table 4. Multivariate analysis of ocular and systemic factors with visibility of choroidal–scleral interface (CSI).

Choroid–scleral interface visibility				
			95% Confidence interval	
	Estimate	p-value	Lower bound	Upper bound
Axial length (mm)	0.465	**0.003**	0.160	0.771
LOCS III nuclear cataract (no versus yes)	−0.104	0.795	−0.891	0.683
Age (years)	0.045	**0.030**	0.004	0.086
Retinal thickness (μm)	−0.030	**0.004**	−0.050	−0.009
Subfoveal choroidal thickness (μm)	−0.002	0.278	−0.005	0.001
Gender (male versus female)	0.218	0.413	−0.304	0.740
Diabetes mellitus (yes versus no)	−0.746	**0.004**	−1.256	−0.236

Bolded font indicates statistical significance.

is an increasing trend of data from other older adult studies which states that choroidal thickness decreases with age (Fujiwara et al. 2012; Margolis & Spaide 2009). Thicker choroid in younger age would undergo more attenuation of incident light resulting in poor visualization of the CSI. Nevertheless, we did not find any significant association between CSI visibility score and choroidal thickness in the multiple regression model (Table 4). Another possible explanation of poorer CSI visibility at younger age is higher concentration of choroidal melanin pigments in young individuals, which tend to progressively decrease with advancing age (Weiter et al. 1986).

In addition to age, persons with diabetes had poorer visibility of choroid–scleral junction. There is inconsistency in literature in terms of choroidal blood flow, which is reported to decrease, increase and remain unchanged in patients with diabetes (Langham et al. 1991; MacKinnon et al. 1997; Schmidt et al. 2000). However, many studies have demonstrated significant decrease in choroidal blood flow in diabetic patients, especially those with macular oedema (Langham et al. 1991; Geyer et al. 1999). However, in our cohort, none of the diabetic subjects had diabetic macular oedema or intraretinal cystic changes. While comparing the retinal thickness in diabetics (259.15 μm) and non-diabetics (262.12 μm), we found no significant difference ($p = 0.402$) in thickness. Thus, the reasons for diabetic people having poor CSI visibility are still unclear. We can only speculate that poor CSI visibility in diabetics might be associated with blood flow changes in choroid, but unfortunately, in our study, we did not obtain any information pertaining to blood flow. An alternative explanation could be the hyper-reflectivity of incident light from the intraretinal fluid which can lead to a shadowing effect of the deeper layers resulting in poorer CSI visibility (Adhi et al. 2013).

Another reason for diabetic subjects having poor CSI visibility could be the fact that diabetes leads to a faster development of cataract which in turn might be associated with poorer visibility of CSI. However, in a subgroup analysis in diabetic subjects with cataracts, we found no significant association between the presence of cataract and CSI visibility score ($p = 0.074$, chi-square test), indicating that the presence of cataract in diabetic subjects does not affect the visibility of CSI. In our study, we also found that thicker retinal thickness was associated with poorer CSI visibility. It is noted that there were no relationships between CSI visibility with most systemic factors such as BMI, blood pressure, cholesterol, glucose and smoking.

Among the ocular factors, the visibility of CSI was influenced by AL. CSI was poorly distinct in eyes with shorter AL (Fig. 3). Our results are compatible with histologic findings that in eyes with greater AL, the elongation of the eyeball leads to mechanical stretching and thinning of retina (Lim et al. 2005; Lam et al. 2007). The excessive

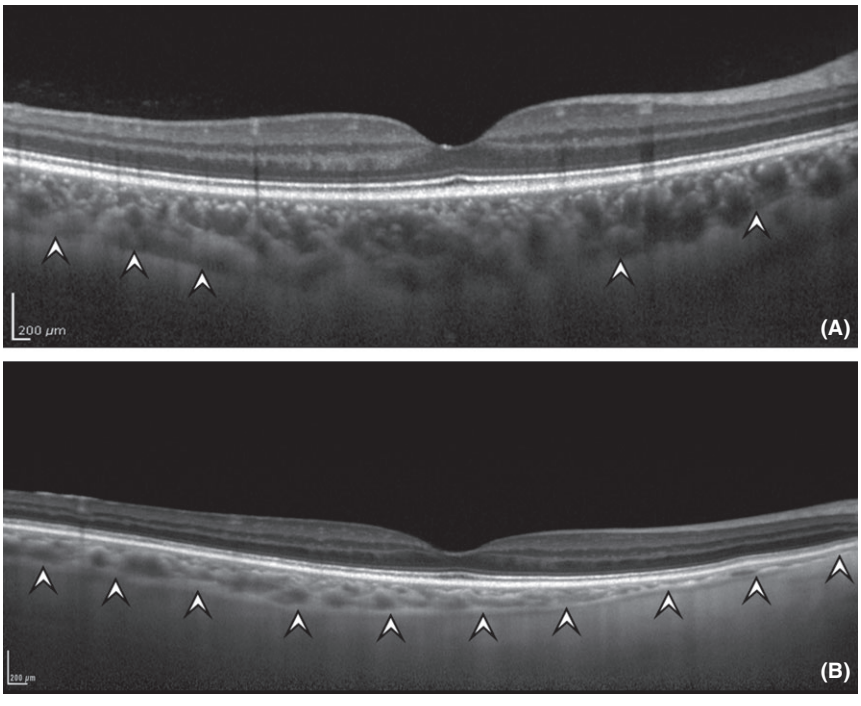

Fig. 2. Comparison of CSI visibility between EDI-OCT scans in two subjects of different ages. (A) A 46-year-old male with poorly demarcated CSI (subfoveal choroidal thickness of 326 μm). (B) A 83-year-old man with CSI distinctly visible (subfoveal choroidal thickness of 163 μm).

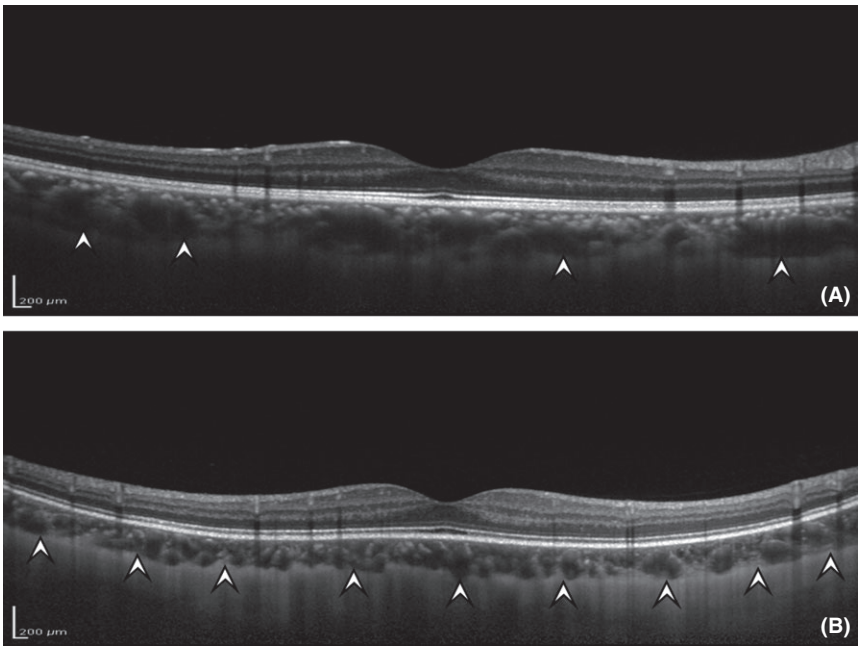

Fig. 3. Comparison of CSI visibility between EDI-OCT scans in two subjects according to refractive status. (A) A 46-year-old male with no refractive error (AL = 23.41) and a poorly demarcated CSI (subfoveal choroidal thickness of 275 μm). (B) A 46-year-old male with myopia (AL = 29.57) with a well-defined CSI (subfoveal choroidal thickness of 165 μm).

elongation affects not only the retina but also the choroid and Bruch membrane. There is found to be choroidal thinning in eyes with high myopia (T. Fujiwara et al. 2009; Ikuno et al. 2010; Ikuno & Tano 2009; Margolis & Spaide 2009) due to significant thinning of the choriocapillaris and focal lack of vessels (Okabe et al. 1982; Grossniklaus & Green 1992; Hirata & Negi 1998). The sclera is also weaker in myopes with a correlation between high myopes and scleral thinning found in human eyes (Avetisov et al. 1983). The choroid adheres to the sclera because of the fixed position of the blood vessels passing through the sclera, and it is likely that the choroid is stretched in myopic eyes (Wildsoet 1998). This allows more penetration of light into the deep choroid giving greater resolution and potentially better specification of the posterior choroidal border. In addition, myopic subjects usually have less pigmented RPE which facilitates detection of the scleral interface.

An important factor in standardizing choroidal thickness measurements is the definition of the choroid–scleral junction. While most EDI-OCT studies, including the landmark Spaide et al. study, define the choroidal–scleral junction as the inner border of the sclera, a recent study by Yiu et al. (2014) reported the presence of a hyporeflective band likely corresponding to the suprachoroidal layer (SCL). However, it is often difficult to visualize SCL, and in Yiu et al. study, SCL was visible in only 45% of their healthy Caucasian subjects. In contrast, in our cohort of healthy Asian subjects, we could not appreciate the presence of SCL, and therefore, like majority of other EDI-OCT studies on choroidal thickness assessment, we considered inner border of the sclera as posterior boundary of the choroid. A probable reason for invisible SCL in our subjects of Asian descent is the presence of greater pigmentation in Asian eyes compared to Caucasians, thereby affecting the visibility of SCL.

The strengths of this study include its unselected population-based sample, standardized assessment of systemic and ocular factors, and laboratory investigations. Our study had some limitations. Although the location of the CSI on Spectralis images was determined qualitatively as the junction between posterior choroid and sclera, there was no reference standard to confirm where this structure is actually located in the eye. The study population only consisted of subjects of Malay ethnicity, and the findings may vary in other racial groups. Further studies in other ethnic populations are thus warranted. Although we performed a 7-line scan, only the horizontal section passing

through the centre of the fovea was used to evaluate the CSI. It is ideal to assess intrasession repeatability. However, in this study, we did not assess intrasession repeatability, the CSI visibility. Knowing that subject pigmentation might influence signal penetration thus affecting the visibility of CSI, it was not considered in our study. However, all our subjects were of Malay ethnicity having more or less similar pigmentation; therefore, there should be no impact of pigmentation on our results. Visualization of the choroidal scleral boundary may vary across different OCT modalities. However, this study only described the visibility of CSI using the Spectralis OCT. Lastly, even though we have explored series of ocular and systemic factors affecting CSI, reflectivity of the choroid might have influenced the visibility of CSI.

Conclusions

In summary, we found that only 60% of our images had well-delineated CSI and the variability in the measurement of choroidal thickness was higher in the images with poorly defined CSI. The factors associated with poorer CSI visibility are younger age, shorter AL, thicker retinal thickness and diabetes. The CSI visibility is critical for accurate determination of choroidal thickness which can help clinicians evaluate chorioretinal disorders such as age-related macular degeneration, central serous chorioretinopathy as well as monitoring the effect of therapeutic interventions.

References

Adhi M, Brewer E, Waheed NK & Duker JS (2013): Analysis of morphological features and vascular layers of choroid in diabetic retinopathy using spectral-domain optical coherence tomography. JAMA Ophthalmol **131**: 1267–1274.

Avetisov ES, Savitskaya NF, Vinetskaya MI & Iomdina EN (1983): A study of biochemical and biomechanical qualities of normal and myopic eye sclera in humans of different age groups. Metab Pediatr Syst Ophthalmol **7**: 183–188.

Beck M, Schlatter B, Wolf S & Zinkernagel MS (2015): Senile scleral plaques imaged with enhanced depth optical coherence tomography. Acta Ophthalmol **93**: 188–192.

Chiu SJ, Li XT, Nicholas P, Toth CA, Izatt JA & Farsiu S (2010): Automatic segmentation of seven retinal layers in SDOCT images congruent with expert manual segmentation. Opt Express **18**: 19413–19428.

Chung SE, Kang SW, Lee JH & Kim YT (2011): Choroidal thickness in polypoidal choroidal vasculopathy and exudative age-related macular degeneration. Ophthalmology **118**: 840–845.

Chylack LT Jr, Wolfe JK, Singer DM et al. (1993): The lens opacities classification system III. The longitudinal study of cataract study group. Arch Ophthalmol **111**: 831–836.

Duan L, Yamanari M & Yasuno Y (2012): Automated phase retardation oriented segmentation of chorio-scleral interface by polarization sensitive optical coherence tomography. Opt Express **20**: 3353–3366.

Feeney-Burns L, Burns RP & Gao CL (1990): Age-related macular changes in humans over 90 years old. Am J Ophthalmol **109**: 265–278.

Fitzgerald ME, Wildsoet CF & Reiner A (2002): Temporal relationship of choroidal blood flow and thickness changes during recovery from form deprivation myopia in chicks. Exp Eye Res **74**: 561–570.

Fleiss JL & Cohen J (1973): The equivalence of weighted kappa and the intraclass correlation coefficient as measures of reliability. Educ Psychol Measur **33**: 613–619.

Foong AW, Saw SM, Loo JL et al. (2007): Rationale and methodology for a population-based study of eye diseases in Malay people: the Singapore Malay eye study (SiMES). Ophthalmic Epidemiol **14**: 25–35.

Foster PJ, Buhrmann R, Quigley HA & Johnson GJ (2002): The definition and classification of glaucoma in prevalence surveys. Br J Ophthalmol **86**: 238–242.

Fujiwara T, Imamura Y, Margolis R, Slakter JS & Spaide RF (2009): Enhanced depth imaging optical coherence tomography of the choroid in highly myopic eyes. Am J Ophthalmol **148**: 445–450.

Fujiwara A, Shiragami C, Shirakata Y, Manabe S, Izumibata S & Shiraga F (2012): Enhanced depth imaging spectral-domain optical coherence tomography of subfoveal choroidal thickness in normal Japanese eyes. Jpn J Ophthalmol **56**: 230–235.

Geyer O, Neudorfer M, Snir T, Goldstein M, Rock T, Silver DM & Bartov E (1999): Pulsatile ocular blood flow in diabetic retinopathy. Acta Ophthalmol Scand **77**: 522–525.

Ghorbel I, Rossant F, Bloch I, Tick S & Paques M (2011): Automated segmentation of macular layers in OCT images and quantitative evaluation of performances. Pattern Recogn **44**: 1590–1603.

Gomi F & Tano Y (2008): Polypoidal choroidal vasculopathy and treatments. Curr Opin Ophthalmol **19**: 208–212.

Grossniklaus HE & Green WR (1992): Pathologic findings in pathologic myopia. Retina **12**: 127–133.

Grossniklaus HE & Green WR (2004): Choroidal neovascularization. Am J Ophthalmol **137**: 496–503.

Gupta B & Mohamed MD (2011): Photodynamic therapy for variant central serous chorioretinopathy: efficacy and side effects. Ophthalmologica **225**: 207–210.

Gupta P, Sidhartha E, Girard MJ, Mari JM, Wong TY & Cheng CY (2014): A simplified method to measure choroidal thickness using adaptive compensation in enhanced depth imaging optical coherence tomography. PLoS ONE **9**: e96661.

Hirata A & Negi A (1998): Morphological changes of choriocapillaris in experimentally induced chick myopia. Graefes Arch Clin Exp Ophthalmol **236**: 132–137.

Ikuno Y & Tano Y (2009): Retinal and choroidal biometry in highly myopic eyes with spectral-domain optical coherence tomography. Invest Ophthalmol Vis Sci **50**: 3876–3880.

Ikuno Y, Kawaguchi K, Nouchi T & Yasuno Y (2010): Choroidal thickness in healthy Japanese subjects. Invest Ophthalmol Vis Sci **51**: 2173–2176.

Imamura Y, Fujiwara T, Margolis R & Spaide RF (2009): Enhanced depth imaging optical coherence tomography of the choroid in central serous chorioretinopathy. Retina **29**: 1469–1473.

Kajic V, Esmaeelpour M, Povazay B, Marshall D, Rosin PL & Drexler W (2012): Automated choroidal segmentation of 1060 nm OCT in healthy and pathologic eyes using a statistical model. Biomed Opt Express **3**: 86–103.

Koizumi H, Yamagishi T, Yamazaki T, Kawasaki R & Kinoshita S (2011): Subfoveal choroidal thickness in typical age-related macular degeneration and polypoidal choroidal vasculopathy. Graefes Arch Clin Exp Ophthalmol **249**: 1123–1128.

Lam DS, Leung KS, Mohamed S et al. (2007): Regional variations in the relationship between macular thickness measurements and myopia. Invest Ophthalmol Vis Sci **48**: 376–382.

Langham ME, Grebe R, Hopkins S, Marcus S & Sebag M (1991): Choroidal blood flow in diabetic retinopathy. Exp Eye Res **52**: 167–173.

Lim MC, Hoh ST, Foster PJ, Lim TH, Chew SJ, Seah SK & Aung T (2005): Use of optical coherence tomography to assess variations in macular retinal thickness in myopia. Invest Ophthalmol Vis Sci **46**: 974–978.

Linsenmeier RA & Padnick-Silver L (2000): Metabolic dependence of photoreceptors on the choroid in the normal and detached retina. Invest Ophthalmol Vis Sci **41**: 3117–3123.

MacKinnon JR, O'Brien C, Swa K, Aspinall P, Butt Z & Cameron D (1997): Pulsatile ocular blood flow in untreated diabetic retinopathy. Acta Ophthalmol Scand **75**: 661–664.

Margolis R & Spaide RF (2009): A pilot study of enhanced depth imaging optical coher-

ence tomography of the choroid in normal eyes. Am J Ophthalmol **147**: 811–815.

Okabe S, Matsuo N, Okamoto S & Kataoka H (1982): Electron microscopic studies on retinochoroidal atrophy in the human eye. Acta Med Okayama **36**: 11–21.

Ramrattan RS, van DST, Mooy CM, de BW, Mulder PG & de JP (1994): Morphometric analysis of Bruch's membrane, the choriocapillaris, and the choroid in aging. Invest Ophthalmol Vis Sci **35**: 2857–2864.

Rosman M, Zheng Y, Wong W et al. (2012): Singapore Malay Eye Study: rationale and methodology of 6-year follow-up study (SiMES-2). Clin Experiment Ophthalmol **40**: 557–568.

Sarks SH (1976): Ageing and degeneration in the macular region: a clinico-pathological study. Br J Ophthalmol **60**: 324–341.

Schmidt KG, von Ruckmann A, Kemkes-Matthes B & Hammes HP (2000): Ocular pulse amplitude in diabetes mellitus. Br J Ophthalmol **84**: 1282–1284.

Shen SY, Wong TY, Foster PJ et al. (2008): The prevalence and types of glaucoma in malay people: the Singapore Malay eye study. Invest Ophthalmol Vis Sci **49**: 3846–3851.

Spaide RF, Koizumi H & Pozzoni MC (2008): Enhanced depth imaging spectral-domain optical coherence tomography. Am J Ophthalmol **146**: 496–500.

Weiter JJ, Delori FC, Wing GL & Fitch KA (1986): Retinal pigment epithelial lipofuscin and melanin and choroidal melanin in human eyes. Invest Ophthalmol Vis Sci **27**: 145–152.

Wildsoet CF (1998): Myopia and nearwork. Oxford: Butterworth-Heinemann.

Yiu G, Pecen P, Sarin N, Chiu SJ, Farsiu S, Mruthyunjaya P & Toth CA (2014): Characterization of the choroid-scleral junction and suprachoroidal layer in healthy individuals on enhanced-depth imaging optical coherence tomography. JAMA Ophthalmol **132**: 174–181.

Received on August 18th, 2014.
Accepted on May 11th, 2015.

Correspondence:
Carol Y. Cheung, PhD
Academic Medicine Research Institute
Duke-NUS Graduate Medical School
Head, Ocular Imaging Group
Singapore Eye Research Institute
20 College Road, The Academia
Level 6 Discovery Tower
Singapore 169856
Singapore
Tel: +65 6576 7233
Fax: +65 6225 2568
Email: carol.cheung.y.l@seri.com.sg

This study was supported by a grant from National Medical Research Council, Singapore [Grant No. NMRC R760/44/2010]. The funding organization had no role in the design or conduct of this research.

Distribution and Determinants of Choroidal Thickness and Volume Using Automated Segmentation Software in a Population-Based Study

PREETI GUPTA, TIAN JING, PINA MARZILIANO, CAROL Y. CHEUNG, MANI BASKARAN, ECOSSE L. LAMOUREUX, TIEN YIN WONG, CHUI MING GEMMY CHEUNG, AND CHING-YU CHENG

• PURPOSE: To objectively quantify choroidal thickness and choroidal volume using fully automated choroidal segmentation software applied to images obtained from enhanced depth imaging spectral-domain optical coherence tomography (EDI SD OCT) in a population-based study; and evaluate the ocular and systemic determinants of choroidal thickness and choroidal volume.

• DESIGN: Prospective cross-sectional study.

• METHODS: Participants ranging in age from 45 to 85 years were recruited from the Singapore Malay Eye Study-2 (SiMES-2), a follow-up population-based study. All participants (n = 540) underwent a detailed ophthalmic examination, including EDI SD OCT for measurements of thickness and volume of the choroid.

• RESULTS: The intrasession repeatability of choroidal thickness at 5 measured horizontal locations and macular choroidal volume using automated choroidal segmentation software was excellent (intraclass correlation coefficient, 0.97-0.99). Choroid was significantly thicker under the fovea (242.28 ± 97.58 μm), followed by 3 mm temporal (207.65 ± 80.98 μm), and was thinnest at 3 mm nasal (142.44 ± 79.19 μm) location. The mean choroidal volume at central macular region (within a circle of 1 mm diameter) was 0.185 ± 0.69 mm^3. Among the range of ocular and systemic factors studied, age, sex, and axial length were the only significant predictors of choroidal thickness and choroidal volume (all $P < .05$).

• CONCLUSIONS: Using a new automated choroidal segmentation software, we provide fast, reliable, and objective measurements of choroidal thickness and volume in a population-based sample. Male sex, younger age, and shorter axial length are the factors independently associated with thicker choroid and larger choroidal volume. These factors should be taken into consideration when interpreting EDI SD OCT–based choroidal thickness measurements in clinics. (Am J Ophthalmol 2015;159:293–301. © 2015 by Elsevier Inc. All rights reserved.)

THE CHOROID CONTRIBUTES BLOOD SUPPLY TO THE outer retina[1] and is therefore associated with the pathogenesis of major diseases of the posterior segment of the eye.[2–10] Until recently, the choroid was imaged by invasive techniques with limited image resolution.[11,12] Although the use of enhanced depth imaging (EDI) in spectral-domain optical coherence tomography (SD OCT) is noninvasive and has now allowed visualization of the choroidal structure in detail,[13] the quantification of choroidal thickness for evaluating chorioretinal diseases is mostly performed manually and often at 1 or few points around the foveal center.[2,4,9,10,14–16]

Owing to unavailability of automated choroidal segmentation software, previous investigators have used a manual (mostly single-point) measurement technique using built-in calipers to evaluate choroidal thickness.[17–20] However, measurements of a few sampling points are influenced by focal thickening or thinning of the choroid,[21,22] or by irregularity of the inner chorioscleral border,[2,10] and thus are highly dependent on location of measurements. In addition, manual methods are further subject to intra- and interobserver variation. Given the high anatomic variability of choroid, these are impractical for clinical use and epidemiologic research involving large samples, which makes the measurements tedious and time consuming. Thus, an objective and comprehensive assessment of the choroid, such as choroidal thickness maps and volumetric analysis, is required but is still unavailable.

A few studies[23–26] have calculated choroidal volume using the built-in software. However, the segmentation of the choroid-scleral interface (CSI) is still done manually. For EDI SD OCT to become a clinically practical tool to determine choroidal thickness, an automatic and accurate measurement algorithm must be developed.

AJO.com Supplemental Material available at AJO.com.

Accepted for publication Oct 29, 2014.

From Singapore Eye Research Institute and Singapore National Eye Centre (P.G., C.Y.Cheung, M.B., E.L.L., T.Y.W., C.M.G.C., C.-Y.Cheng); Department of Ophthalmology, Yong Loo Lin School of Medicine, National University of Singapore and National University Health System (P.G., C.Y.Cheung, M.B., E.L.L., T.Y.W., C.M.G.C., C.-Y.Cheng); Saw Swee Hock School of Public Health, National University of Singapore (T.Y.W., C.-Y.Cheng); Office of Clinical Sciences, Duke-NUS Graduate Medical School (C.Y.Cheung, M.B., E.L.L., T.Y.W., C.M.G.C., C.-Y.Cheng); and School of Electrical and Electronic Engineering, Nanyang Technological University (T.J., P.M.), Singapore.

Inquiries to Dr Ching-Yu Cheng, Singapore Eye Research Institute, The Academia, 20 College Road, Discovery Tower, Level 6, Singapore 169856; e-mail: ching-yu_cheng@nuhs.edu.sg

0002-9394/$36.00
http://dx.doi.org/10.1016/j.ajo.2014.10.034

This study used new, fully automated choroidal segmentation software to objectively quantify choroidal thickness and choroidal volume in the macular area, acquired using EDI SD OCT in a population-based setting. We aimed to obtain accurate distribution of choroidal thickness and choroidal volume and to determine their associations with ocular and systemic determinants at the macula. In addition, we also assessed the intrasession repeatability of both choroidal thickness and choroidal volume measures.

SUBJECTS AND METHODS

• **STUDY POPULATION:** Data for this analysis were derived from the Singapore Malay Eye Study-2 (SiMES-2), a comprehensive, detailed population-based cohort study of 3280 Singaporean Malay adults aged 45-85 years. Details of the baseline study design, sampling plan, and methodology (SiMES-1 2004-2006) have been reported elsewhere.[27] The follow-up examination, SiMES-2, started from 2011 and is ongoing.[28] For this analysis, we enrolled consecutive participants of the SiMES-2 from February 2012 to April 2013. Participants recruited in SiMES-2 underwent standardized and detailed ophthalmic examination, including Spectralis EDI SD OCT. Ethics approval was obtained from the institutional review board (IRB) of the Singapore Eye Research Institute, and the IRB approved a protocol for the prospective study. The study was conducted in accordance with the World Medical Association's Declaration of Helsinki. Written informed consent was obtained from all subjects.

• **ENHANCED DEPTH IMAGING OPTICAL COHERENCE TOMOGRAPHY IMAGE ACQUISITION PROTOCOL:** Choroidal thickness was obtained using SD OCT (Spectralis; Heidelberg Engineering, Heidelberg, Germany) with EDI modality after pupil dilation using tropicamide 1% and phenylephrine hydrochloride 2.5%. A 7-horizontal-line scan (30 × 5 degrees) centered on the fovea was performed, with 100 frames averaged in each B-scan. Each scan was 8.9 mm in length and spaced 240 μm apart from each other.

All OCT scans were acquired by a single examiner (P.G.), who is experienced at performing scans using EDI-Spectralis. After each capture, each of 7 B-scans was scrutinized manually in each eye by the same examiner (P.G.), and images that had motion artifacts (n = 14) or were poorly focused (n = 26) were excluded from the analysis. Measurements of both eyes of each study participant were obtained. However, because of intereye correlation issues, only the right eye was used for this analysis.

• **MEASUREMENTS OF CHOROIDAL THICKNESS AND VOLUME:** Following Spectralis user manual guidelines, subjects' keratometry readings and the most recent refraction were entered into the software program to estimate optical magnification and, therefore, to allow for more accurate comparisons across individuals. The choroidal thickness at each location was defined as the distance between the Bruch membrane (lower boundary of retinal pigment epithelium [RPE]) and the CSI. In our study, Bruch membrane and CSI were delineated with the automatic segmentation algorithm developed by Tian and associates.[29] The authors evaluated the accuracy of their algorithm with the ground truth (manual measurement of choroidal thickness) and demonstrated good consistency between the manual labelings and their algorithm (the average of the Dice coefficients over 45 tested images was 90.5% with standard deviation of 3%).[29]

In our study, from the 7-horizontal-line scan, the line passing through the fovea was selected by an experienced examiner and the center of the fovea was detected as the lowest point of internal limiting membrane automatically. The choroidal thickness profile at the fovea and at 500-μm intervals up to 3 mm temporal and nasal to the fovea in horizontal section (Supplemental Figure; available at AJO.com) was then automatically measured and created. Figure 1 shows an example of an EDI SD OCT scan of the macula with the automated segmentation lines. Furthermore, the choroidal volume of the 7-line scan (8.9 mm × 1.5 mm) of the region $\{(x,y)|\ -3\ \text{mm} < x < 3\ \text{mm}, 720\ \mu\text{m} < y < 720\ \mu\text{m}\}$ was calculated with the automatically detected fovea as the center of origin, (0,0), and the measurement points between lines were measured with linear interpolation as illustrated in Figure 2. In addition, choroidal volume in a 1-mm-diameter circle at the fovea and thickness maps were obtained for all subjects.

• **ASSESSMENT OF REPEATABILITY OF AUTOMATED MEASUREMENTS:** To access the intrasession repeatability using EDI SD OCT and automated choroidal segmentation software, images from the same eye of 20 subjects were obtained twice at an interval of 10 minutes. Two images from the same eyes were each measured by segmentation software to assess the repeatability of choroidal thickness and choroidal volume measurements.

• **MEASUREMENT OF OCULAR FACTORS:** All participants underwent a standardized examination procedure. The refraction of each eye was measured using an autorefractor (Canon RK 5 Auto Ref-Keratometer; Canon Inc Ltd, Tochigiken, Japan). Spherical equivalent (SE) was calculated as the sum of the spherical power and half of the cylinder power. Best-corrected visual acuity (BCVA) was measured monocularly using a logarithm of the minimal angle of resolution (logMAR) chart (Lighthouse International, New York, New York, USA) at a distance of 4 m. Biometry measurements (ie, axial length [AL], corneal curvature, and anterior chamber depth [ACD]) were measured with noncontact partial coherence laser interferometry (IOL Master V3.01; Carl Zeiss Meditec AG, Jena, Germany) and the mean of 5 measurements was used in the

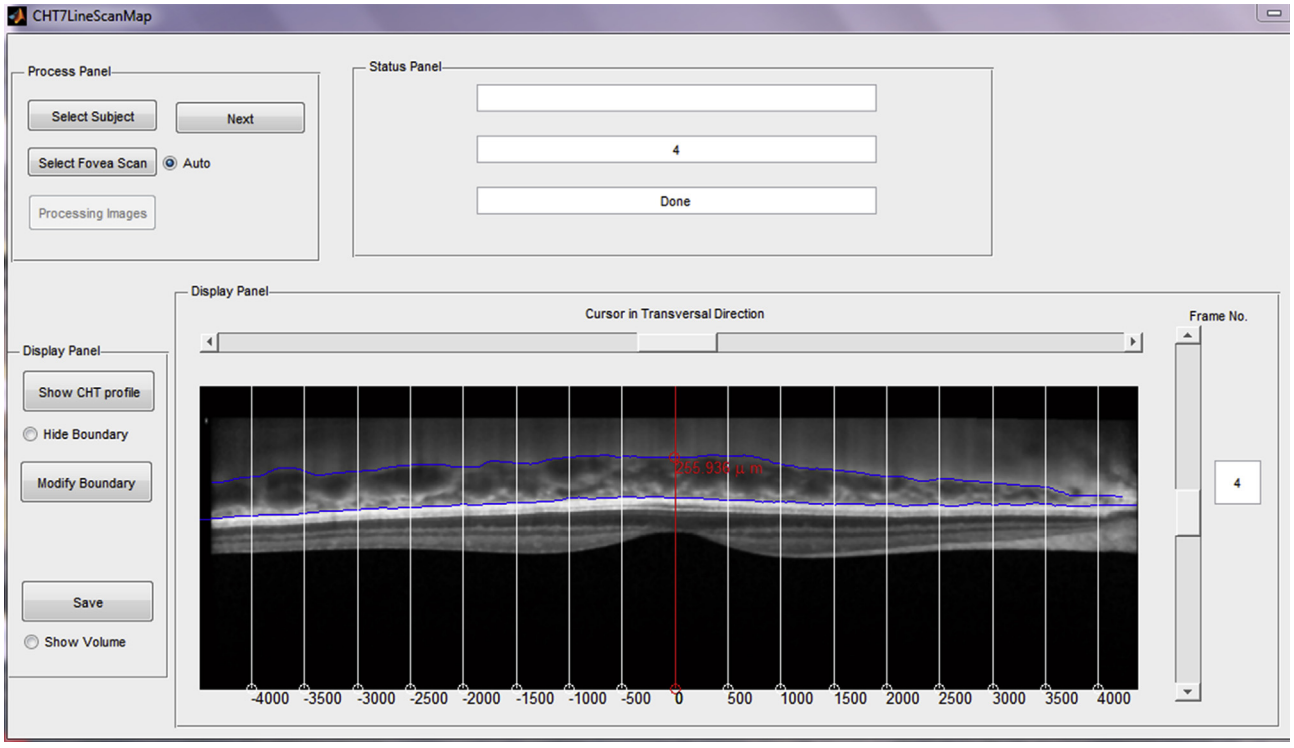

FIGURE 1. Enhanced depth imaging optical coherence tomography image in the macular region demonstrating automated segmentation of the Bruch membrane and the choroidal-scleral interface. The choroidal thickness was measured in the fovea (detected as the lowest points of internal limiting membrane automatically) and at 500-μm intervals up to 3 mm temporal and nasal to the fovea in horizontal section.

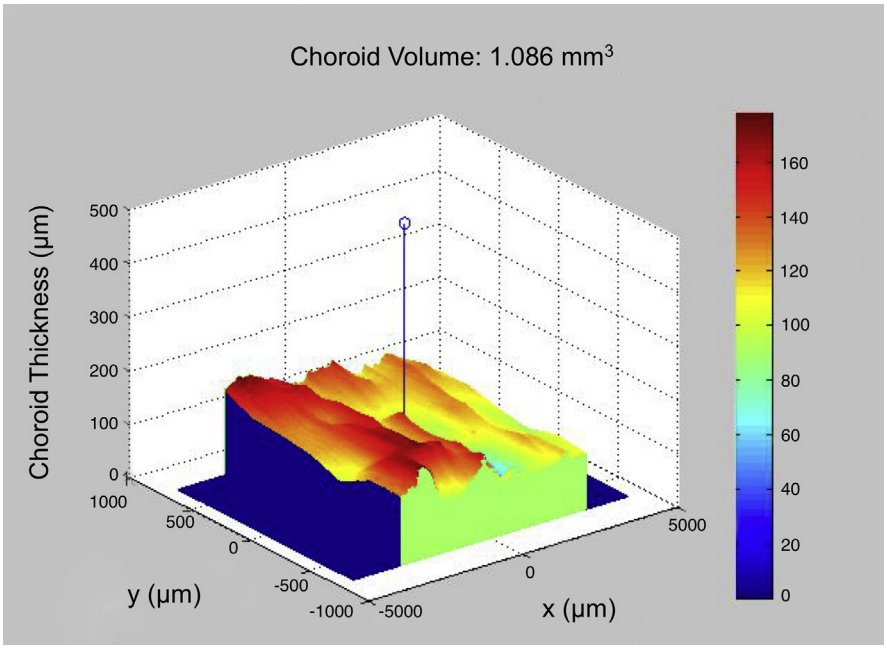

FIGURE 2. An illustration of the color-coded choroidal volume map obtained from the 7-line scans covering an area of 8.9 × 1.5 mm. The choroidal volume is expressed in millimeters cubed (mm^3), with the warm and the cool colors representing thicker and thinner choroidal volume, respectively. X and Y presents the transverse (from nasal to temporal) and interframe (from superior to inferior) directions, respectively.

TABLE 1. Demographic, Ocular, and Systemic Characteristics of the 540 Study Participants in the Singapore Malay Eye Study for Evaluation of Choroidal Thickness and Volume Using Automated Segmentation Software

Characteristic	Value (N = 540 Subjects)
Age (y)	62.70 (8.91)
Sex, male	251 (46.5)
Axial length, mm	23.59 (0.96)
Anterior chamber depth, mm	3.17 (0.34)
Corneal curvature, mm	7.66 (0.24)
Spherical equivalent, D	0.11 (1.74)
Best-corrected visual acuity, logMAR	0.16 (0.20)
Central corneal thickness, μm	541.76 (35.15)
Intraocular pressure, mm Hg	14.49 (3.10)
Ocular perfusion pressure, mm Hg	55.55 (8.19)
Systolic blood pressure, mm Hg	139.56 (19.68)
Diastolic blood pressure mm Hg	76.90 (10.66)
Mean arterial pressure, mm Hg	97.78 (12.37)
Body mass index, kg/m^2	26.87 (5.07)
Serum glucose, mmol/L	7.22 (3.52)
HbA1c, %	6.35 (1.43)
Total cholesterol, mmol/L	5.36 (1.29)
Triglycerides, mmol/L	1.92 (1.30)
Blood creatinine, mmol/L	83.23 (41.23)
Current smoking, %	98 (18.1)
Diabetes mellitus, %	143 (26.5)
Arterial hypertension, %	323 (59.8)
Alcohol consumption, %	7 (1.3)

D = diopter.

Data are mean (SD), except for sex, HbA1c, current smoking, diabetes, arterial hypertension, and alcohol consumption which are expressed as number (%).

TABLE 2. Assessment of Intrasession Repeatability of Choroidal Thickness (at Various Horizontal Locations) and Choroidal Volume Using Automated Segmentation Software (n = 20)

Locations of Measurement	Intraclass Correlation (95% Confidence Interval)	Mean Difference[a] (95% Limits of Agreement)
Choroidal thickness		
Subfoveal	0.996 (0.992-0.998)	−0.4 (−21.5 to 20.7)
Nasal, 1.5 mm	0.992 (0.981-0.997)	−2.1 (−29.1 to 24.9)
Nasal, 3 mm	0.996 (0.991-0.998)	1.6 (−15.6 to 18.8)
Temporal, 1.5 mm	0.995 (0.989-0.998)	0.1 (−26.2 to 26.4)
Temporal, 3 mm	0.979 (0.949-0.992)	0.5 (−38.2 to 39.2)
Choroidal volume of 7-line scan (8.9 mm × 1.5 mm)	0.999 (0.997-0.999)	0.0 (−0.08 to 0.09)

[a]Mean difference was determined from the first measurement minus second measurement.

TABLE 3. Distribution of Mean Choroidal Thickness (at Various Locations on the Horizontal Axis) and Volume Measurements Using Automated Segmentation Software (N = 540 Subjects)

Location of Measurements	Mean (SD)
Choroidal thickness in μm	
Subfoveal	242.28 (97.58)
Nasal, 0.5 mm	237.11 (97.72)
Nasal, 1 mm	226.68 (98.10)
Nasal, 1.5 mm	208.35 (98.20)
Nasal, 2 mm	187.29 (94.21)
Nasal, 2.5 mm	166.02 (89.72)
Nasal, 3 mm	142.44 (79.19)
Temporal, 0.5 mm	241.93 (96.58)
Temporal, 1 mm	239.39 (92.83)
Temporal, 1.5 mm	232.17 (89.42)
Temporal, 2 mm	221.31 (84.12)
Temporal, 2.5 mm	216.19 (81.93)
Temporal, 3 mm	207.65 (80.98)
Choroidal volume in mm^3	
Choroidal volume of 7-line scan (8.9 × 1.5 mm)	1.889 (0.693)
Choroidal volume at central macula (within 1-mm-diameter circle)	0.185 (0.071)

analysis. Intraocular pressure (IOP) was measured using Goldmann applanation tonometry (Haag-Streit, Bern, Switzerland) before pupil dilation. Central corneal thickness (CCT) was measured with an ultrasound pachymeter (Advent; Mentor O & O, Norwell, Massachusetts, USA) and the mean of 5 measurements was used in the analysis.

• **ASSESSMENT OF DEMOGRAPHIC, LIFESTYLE, AND SYSTEMIC FACTORS:** All study participants underwent a detailed interview using standardized questionnaires. Information on demographic status, lifestyle risk factors (eg, smoking, alcohol consumption), medication use, and self-reported history of systemic diseases such as arterial hypertension and diabetes mellitus were collected. Systolic and diastolic blood pressures (BP) were measured using a digital automatic blood pressure monitor (Dinamap model Pro Series DP110X-RW, 100V2; GE Medical Systems Information Technologies, Inc, Milwaukee, Wisconsin, USA), after subjects were seated for at least 5 minutes with legs uncrossed. A total of 3 measurements were taken, and the average of the 2 closest BP readings was taken as each participant's BP. Mean ocular perfusion pressure (OPP) was calculated using the following equation: mean OPP = (2/3 × MAP – IOP), where MAP (mean arterial pressure) = diastolic BP + (1/3 × [systolic BP – diastolic BP]). Systolic and diastolic OPP were calculated using the following equations: systolic OPP = systolic BP – IOP and diastolic OPP = diastolic BP –IOP, respectively. Body mass index (BMI) was calculated as body weight (in kilograms) divided by body height (in meters) squared. Smoking status was defined as those currently smoking,

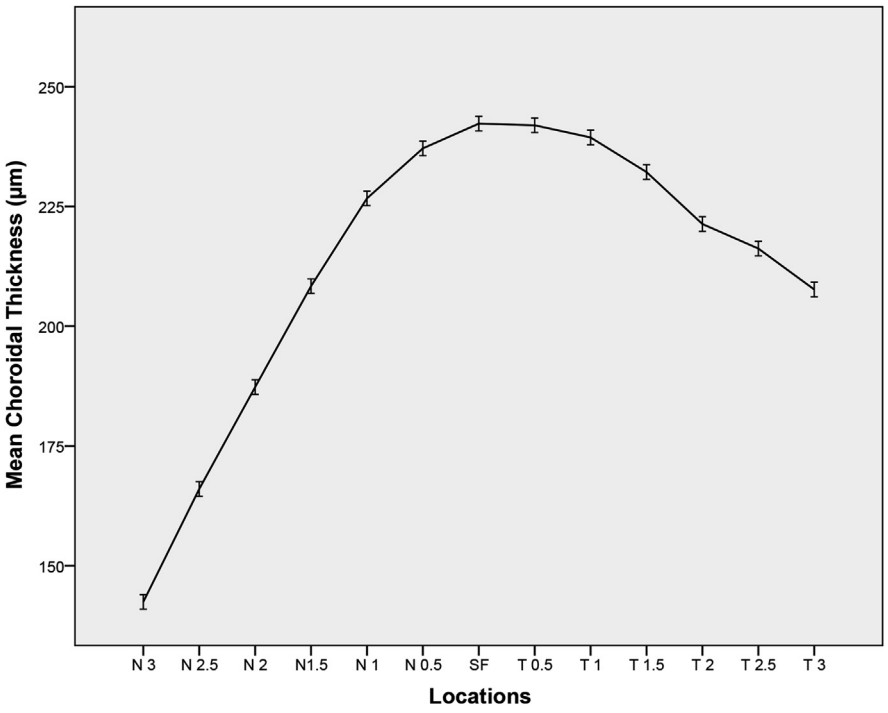

FIGURE 3. Graph showing the distribution of mean choroidal thickness in micrometers (µm) at each of the studied locations in 500-µm (0.5 mm) intervals, up to 3 mm nasal and temporal to the fovea. The numbers on the x-axis are locations in mm from the fovea. SF = subfoveal; N = nasal; T = temporal. The choroid was thickest at the subfoveal region, followed by temporal, and was thinnest at the nasal location.

ex-smokers, and nonsmokers. Nonfasting venous blood samples were analyzed at the National University Hospital Reference Laboratory for biochemical testing of serum total cholesterol, high-density lipoprotein (HDL) cholesterol, low-density lipoprotein (LDL) cholesterol, triglycerides, glycosylated hemoglobin (HbA1c), glucose, and creatinine.

• **STATISTICAL ANALYSIS:** Statistical analysis was performed using MedCalc version 12.3 (Medcalc Software, Ostend, Belgium) and SPSS version 20.0 (SPSS, Inc, Chicago, Illinois, USA). Univariate and multiple linear regression analyses were performed to determine the associations of subfoveal choroidal thickness and choroidal volume (dependent variables) with ocular and systemic factors (independent variables). For multiple linear regression, factors showing suggestively significant association in univariate analysis ($P < .10$) were included. Eyes with other ocular diseases, such as refractive errors, cataract, glaucoma, and retinopathy, were not excluded if the quality of OCT image was sufficient to be evaluated, as we aimed to determine the choroidal thickness distribution in a general population sample. In the assessment of associations with ocular and systemic factors, we included glaucoma status, diabetic retinopathy, and age-related macular degeneration in the regression models to adjust for potential confounding.

The intrasession repeatability of the choroidal thickness and choroidal volume were measured by the absolute agreement model of the intraclass correlation coefficient (ICC).[30] An ICC value of 0.81-1.00 indicates good agreement. Values of less than 0.40 indicate poor to fair agreement. We also performed Bland-Altman plot analyses[31,32] to see the mean difference between the repeated measurements. All *P* values were 2-sided and considered statistically significant when the values were less than .05; 95% confidence intervals (CIs) were presented.

RESULTS

A TOTAL OF 540 EYES FROM 540 CONSECUTIVE SUBJECTS (251 men and 289 women) with a mean (SD) age of 62.70 (8.91) years were included in the study. In none of the images did the automated software fail to detect the RPE and choroidal borders; therefore, no eyes were excluded from the analysis. The demographics and ocular and systemic characteristics of the study population are shown in Table 1.

Table 2 shows the intrasession repeatability of measurements of choroidal thickness and choroidal volume using automated choroidal segmentation software. Repeatability of choroidal thickness at 5 measured horizontal locations and macular choroidal volume was excellent (ICC ranging from 0.97 to 0.99).

TABLE 4. Univariate and Multivariate Analysis of the Association of Ocular and Systemic Factors With Subfoveal Choroidal Thickness Measured Using Automated Segmentation Software (N = 540 Subjects)

	Univariate Analysis			Multivariate Analysis[a]		
	Unstandardized Beta Coefficient	Standardized Beta Coefficient	*P* Value	Unstandardized Beta Coefficient	Standardized Beta Coefficient	*P* Value[b]
Ocular factors						
Spherical equivalent, D	10.773	0.192	<.001	-	-	-
Axial length, mm	−19.638	−0.197	<.001	−32.111	−0.317	<.001[b]
Corneal curvature, mm	−33.037	−0.084	.063	20.160	0.051	.303
Anterior chamber depth, mm	0.870	0.003	.944	-	-	-
Central corneal thickness, μm	0.164	0.059	.170	-	-	-
Intraocular pressure, mm Hg	0.473	0.015	.727	-	-	-
Ocular perfusion pressure, mm Hg	0.269	0.023	.600	-	-	-
Systemic factors						
Age, y	−3.104	−0.284	<.001	−4.139	−0.366	<.001[b]
Sex (female vs male)	−19.432	−0.099	.021	−30.869	−0.158	.001[b]
Mean arterial pressure, mmHg	0.172	0.022	.612	-	-	-
Body mass index, kg/m^2	−1.233	−0.064	.137	-	-	-
Serum glucose, mmol/L	0.556	0.020	.651	-	-	-
HbA1c, %	3.230	0.047	.279	-	-	-
Total cholesterol, mmol/L	9.110	0.121	.005	4.495	0.060	.163
Triglycerides, mmol/L	7.209	0.096	.027	4.180	0.057	.185
Blood creatinine, mmol/L	−0.035	−0.015	.734	-	-	-
Current smoking, (yes vs no)	36.601	0.145	.001	−1.028	−0.004	.930
Diabetes mellitus, (yes vs no)	1.472	0.007	.878	-	-	-
Arterial hypertension, (yes vs no)	−21.077	−0.106	.014	−3.723	−0.019	.678
Alcohol consumption, (yes vs no)	34.549	0.040	.353	-	-	-

D = diopter.
[a]Adjusted for glaucoma status, diabetic retinopathy, and age-related macular degeneration.
[b]The values indicate statistically significant results.

Table 3 shows the mean choroidal thickness and choroidal volume. Choroidal thickness was measured at 13 different locations on the horizontal axis (Figure 3). Choroid was thickest at the subfovea (242.28 ± 97.58 μm), followed by temporal, and thinnest at the 3 mm nasal (142.44 ± 79.19 μm) location (which is the last point measured using the software). The mean macular (1 mm diameter) and 7-line-scan choroidal volume were 0.185 ± 0.071 mm^3 and 1.889 ± 0.69 mm^3, respectively.

In the univariate analysis (Table 4), among the ocular factors only SE and AL showed significant association with subfoveal choroidal thickness (both $P < .001$). For each 1-mm increase in AL, subfoveal choroidal thickness on average decreased by 19.63 μm ($P < .001$). A decrease in mean choroidal thickness by 10.77 μm was observed for each myopic diopter increase ($P < .001$). Among the systemic factors, younger age, male sex, higher serum cholesterol or triglyceride levels, current smoking, and lack of arterial hypertension were found to be significantly associated with thicker subfoveal choroidal thickness (all $P < .05$).

Because of collinearity between AL and SE (correlation coefficient = −0.584), only AL was selected and retained in the multivariate analysis, as it had a greater explanatory power on subfoveal choroidal thickness change than did SE (standardized β, −0.197 vs 0.192). In the multiple linear regression model (Table 4) including all significant factors, only shorter AL ($P < .001$), younger age ($P < .001$), and male sex ($P = .001$) remained significantly associated with thicker subfoveal choroidal thickness.

Similarly, in the analysis of the association of choroidal volume at central macula (1 mm diameter) with ocular and systemic factors (Table 5), only shorter AL, younger age, and male sex showed significant association with larger central choroidal volume (all $P < .001$). Similar factors were associated with greater choroidal volume of 7-line scan (data not shown).

DISCUSSION

ALTHOUGH SPECTRALIS OCT WITH EDI ALLOWS VISUALIZATION of the choroidal structure in detail, the measurement of choroidal thickness is still performed manually. To date, none of the previous clinical studies used automated measurements of thickness and volume of choroid, as in

TABLE 5. Univariate and Multivariate Analysis of the Association of Ocular and Systemic Factors With Choroidal Volume at Central Macula Measured Using Automated Segmentation Software (N = 540 Subjects)

	Univariate Analysis			Multivariate Analysis[a]		
	Unstandardized Beta Coefficient	Standardized Beta Coefficient	*P* Value	Unstandardized Beta Coefficient	Standardized Beta Coefficient	*P* Value[b]
Ocular factors						
Spherical equivalent, D	0.009	0.207	<.001	-	-	-
Axial length, mm	−0.014	−0.189	<.001	−0.021	−0.280	<.001[b]
Corneal curvature, mm	−0.014	−0.049	.274	-	-	-
Anterior chamber depth, mm	0.003	0.013	.777	-	-	-
Central corneal thickness, per 10 μm	0.000	0.065	.135	-	-	-
Intraocular pressure, per 10 mm Hg	−0.0007	0.003	.942	-	-	-
Ocular perfusion pressure, per 10 mm Hg	0.001	0.011	.795	-	-	-
Systemic factors						
Age, y	−0.003	−0.320	<.001	−0.003	−0.396	<.001[b]
Sex, (female vs male)	−0.016	−0.109	.011	−0.023	−0.159	<.001[b]
Mean arterial pressure, per 10 mm Hg	0.0004	0.006	.886	-	-	-
Body mass index, kg/m^2	−0.001	−0.058	.177	-	-	-
Serum glucose, mmol/L	0.000	0.007	.880	-	-	-
HbA1c, %	0.003	0.053	.227	-	-	-
Total cholesterol, mmol/L	0.007	0.131	.002	0.003	0.057	.175
Triglycerides, mmol/L	0.006	0.115	.008	0.003	0.065	.122
Blood creatinine, mmol/L	−0.000	0.035	.420	-	-	-
Current smoking, (yes vs no)	0.033	0.175	<.001	0.006	0.032	.475
Diabetes mellitus, (yes vs no)	−0.000	0.000	.996	-	-	-
Arterial hypertension, (yes vs no)	−0.017	−0.116	.007	−0.001	−0.007	.874
Alcohol consumption, (yes vs no)	0.018	0.029	.508	-	-	-

D = diopter.
[a]Adjusted for glaucoma status, diabetic retinopathy, and age-related macular degeneration.
[b]The values indicate statistically significant results.

all of these studies demarcation of CSI, a principal landmark for accurate measurement of the choroid, was performed manually. To our best knowledge, this is the first study to use Spectralis OCT with EDI with a fully automated choroidal segmentation software to measure choroidal thickness and choroidal volume in subjects from a population-based study. Our fast (processing time ~1 second) and accurate algorithm has great potential usage in both clinical and population-based studies and may improve the diagnosis and management of patients with eye diseases in which the choroid is affected. We found the choroid to be significantly thicker under the fovea, followed by the temporal location, and thinnest at the nasal location. Among the range of ocular and systemic factors studied, age, sex, and AL were the only significant predictors of choroidal thickness and choroidal volume measurements.

Although previous studies have reported thickness and volume of the choroid using SD OCT[23,24,26,33] and Swept Source OCT,[25] their measurements were performed manually by displacing the built-in reference line of the retinal boundary to the CSI, making it not only time consuming but also prone to measurement errors. For example, in a study by Shin and associates,[26] choroidal volume measurements took ~2.8 minutes per image for 6-radial B-scan[26] vs 1.25 seconds per image for 7-line scan in our study.[29] These limitations compromised the validity of existing studies. On top of this, such time-consuming manual methods make the measurements impractical for both large-scale clinical and epidemiologic studies. We have recently successfully designed an algorithm that can consistently measure choroidal thickness and volume automatically.[29] In this study, we further extend our experience using this automated program in a large population.

We reported automated choroidal volume at the central macula (within 1 mm diameter) of 0.185 ± 0.071 mm^3. Although previous clinic-based, small-scale studies have reported choroidal volume, they used a manual choroidal segmentation approach. For example, Hirata and associates[25] in 31 healthy Japanese (mean age 64.6 years) and Chhablani and associates[24] in 60 eyes of 32 subjects (mean age 44 years) reported choroidal volume of the center 1-mm-diameter ETDRS ring to be 159 ± 0.066 mm^3 and 0.28-0.29 mm^3, respectively. In addition to the central macula, we also reported choroidal volume of 7-line scan (8.9 × 1.5 mm) centered on the fovea of 1.889 ±

0.693 mm^3. Our measurements of choroidal volume were limited to the posterior pole and not over the entire retinal area, but were in the region of clinically significant changes in most of the posterior segment diseases.

Our results have confirmed the asymmetric distribution of macular choroidal thickness. The mean choroidal thickness measurements showed regional differences, being thickest subfoveally, followed by temporally, and thinnest at the nasal location. These observations are similar to the results of previous EDI-OCT studies in normal eyes, which have shown highest choroidal thickness at the fovea, decreasing gradually on both temporal and nasal sides, but more so nasally.[13,18,34] The loss of choroidal tissue in the nasal location could be a contributing cause for the development of peripapillary atrophy and may play a role in glaucoma, as previously speculated by Spaide and associates.[13]

Among the ocular factors, the choroid was thicker and choroidal volume was greater in eyes with shorter AL. Our results are in concordance with histologic findings that in eyes with greater AL, the elongation of the eyeball leads to mechanical stretching and thinning of the retina[35,36] and choroid. Choroidal thinning was observed in eyes with myopic refraction[4,8,18,37] owing to significant thinning of the choriocapillaris and focal lack of vessels.[38–40]

We acknowledge limitations to our study. Although the location of the CSI on Spectralis images was determined qualitatively as the junction between posterior choroid and sclera, there was no reference standard to confirm where this structure is actually located in the eye. Measurement of choroidal thickness and choroidal volume was performed only in the right eye of each study subject. There may exist intereye differences, yet such differences should be small. We have not analyzed the influence of lens opacity, which was shown to affect the delineation of CSI and the thickness measurements,[41] on the measurements in this study. Our subjects were examined only at a single time point, and thus we are not able to take the diurnal variation of choroidal thickness into account. As in any population-based study, our investigation included all eligible and participating subjects from the study. Some of them have eye diseases that may have changed choroidal thickness. Therefore, the distribution of choroidal thickness determined in this study may represent the choroidal thickness not in healthy eyes but in eyes of the general adult and elderly populations.

In conclusion, we objectively demonstrate a mean subfoveal choroidal thickness of 242.28 ± 97.58 μm and a choroidal volume at central macula of 0.185 ± 0.69 mm^3 in ethnic Malay adults. Male sex, younger age and shorter AL are the factors that were independently associated with thicker choroid and greater volume measures. Our fully automated choroidal segmentation software allows highly reliable and accurate measurements of choroidal thickness and choroidal volume, which are essential in distinguishing clinically significant changes in the choroid and assisting in risk profiling for various chorioretinal diseases.

ALL AUTHORS HAVE COMPLETED AND SUBMITTED THE ICMJE FORM FOR DISCLOSURE OF POTENTIAL CONFLICTS OF INTEREST. Financial disclosures: T.Y.W.: received grant support from National Medical Research Council (NMRC) and Biomedical Research Council, Singapore directed to Singapore Eye Research Institute, Advisory Board member for Abbot, Novartis, Pfizer, Allergan, and Bayer, independent consultant for Abbot, Novartis, Pfizer, Allergan, and Bayer; C.M.G. Cheung: independent consultant for Bayer and Novartis; C.-Y. Cheng: received grant support from National Medical Research Council (NMRC) and Biomedical Research Council, Singapore directed to Singapore Eye Research Institute. This study was supported by a grant from National Medical Research Council (Singapore) and National Research Foundation University Fund (Singapore). The sponsor or funding organization had no role in the design or conduct of this research. Contributions of authors: design of the study (P.G., T.Y.W., C.-Y. Cheng); conduct of the study (P.G., T.J., P.M., C.Y. Cheung, T.Y.W., C.-Y. Cheng); collection (P.G.); management (P.G.); analysis (P.G., C.-Y. Cheng); interpretation of the data (P.G., C.-Y. Cheng); preparation of manuscript (P.G., C.-Y. Cheng); review of the manuscript (P.G., T.J., P.M., C.Y. Cheung, M.B., E.L.L., T.Y.W., C.M.G.C., C.-Y. Cheng); approval of the manuscript (P.G., T.J., P.M., C.Y. Cheung, M.B., E.L.L., T.Y.W., C.M.G.C., C.-Y. Cheng).

REFERENCES

1. Linsenmeier RA, Padnick-Silver L. Metabolic dependence of photoreceptors on the choroid in the normal and detached retina. *Invest Ophthalmol Vis Sci* 2000;41(10):3117–3123.
2. Chung SE, Kang SW, Lee JH, Kim YT. Choroidal thickness in polypoidal choroidal vasculopathy and exudative age-related macular degeneration. *Ophthalmology* 2011;118(5):840–845.
3. Fitzgerald ME, Wildsoet CF, Reiner A. Temporal relationship of choroidal blood flow and thickness changes during recovery from form deprivation myopia in chicks. *Exp Eye Res* 2002;74(5):561–570.
4. Fujiwara T, Imamura Y, Margolis R, Slakter JS, Spaide RF. Enhanced depth imaging optical coherence tomography of the choroid in highly myopic eyes. *Am J Ophthalmol* 2009;148(3):445–450.
5. Gomi F, Tano Y. Polypoidal choroidal vasculopathy and treatments. *Curr Opin Ophthalmol* 2008;19(3):208–212.
6. Grossniklaus HE, Green WR. Choroidal neovascularization. *Am J Ophthalmol* 2004;137(3):496–503.
7. Gupta B, Mohamed MD. Photodynamic therapy for variant central serous chorioretinopathy: efficacy and side effects. *Ophthalmologica* 2011;225(4):207–210.
8. Ikuno Y, Tano Y. Retinal and choroidal biometry in highly myopic eyes with spectral-domain optical coherence tomography. *Invest Ophthalmol Vis Sci* 2009;50(8):3876–3880.
9. Imamura Y, Fujiwara T, Margolis R, Spaide RF. Enhanced depth imaging optical coherence tomography of the choroid in central serous chorioretinopathy. *Retina* 2009;29(10):1469–1473.

10. Koizumi H, Yamagishi T, Yamazaki T, Kawasaki R, Kinoshita S. Subfoveal choroidal thickness in typical age-related macular degeneration and polypoidal choroidal vasculopathy. *Graefes Arch Clin Exp Ophthalmol* 2011; 249(8):1123–1128.
11. Coleman DJ, Silverman RH, Chabi A, et al. High-resolution ultrasonic imaging of the posterior segment. *Ophthalmology* 2004;111(7):1344–1351.
12. Guyer DR, Puliafito CA, Mones JM, Friedman E, Chang W, Verdooner SR. Digital indocyanine-green angiography in chorioretinal disorders. *Ophthalmology* 1992;99(2):287–291.
13. Spaide RF, Koizumi H, Pozzoni MC. Enhanced depth imaging spectral-domain optical coherence tomography. *Am J Ophthalmol* 2008;146(4):496–500.
14. Fong AH, Li KK, Wong D. Choroidal evaluation using enhanced depth imaging spectral-domain optical coherence tomography in Vogt-Koyanagi-Harada disease. *Retina* 2011; 31(3):502–509.
15. Mwanza JC, Hochberg JT, Banitt MR, Feuer WJ, Budenz DL. Lack of association between glaucoma and macular choroidal thickness measured with enhanced depth-imaging optical coherence tomography. *Invest Ophthalmol Vis Sci* 2011; 52(6):3430–3435.
16. Spaide RF. Enhanced depth imaging optical coherence tomography of retinal pigment epithelial detachment in age-related macular degeneration. *Am J Ophthalmol* 2009; 147(4):644–652.
17. Imamura Y, Iida T, Maruko I, Zweifel SA, Spaide RF. Enhanced depth imaging optical coherence tomography of the sclera in dome-shaped macula. *Am J Ophthalmol* 2011; 151(2):297–302.
18. Margolis R, Spaide RF. A pilot study of enhanced depth imaging optical coherence tomography of the choroid in normal eyes. *Am J Ophthalmol* 2009;147(5):811–815.
19. McCourt EA, Cadena BC, Barnett CJ, Ciardella AP, Mandava N, Kahook MY. Measurement of subfoveal choroidal thickness using spectral domain optical coherence tomography. *Ophthalmic Surg Lasers Imaging* 2010;41(Suppl): S28–33.
20. Rahman W, Chen FK, Yeoh J, Patel P, Tufail A, Da Cruz L. Repeatability of manual subfoveal choroidal thickness measurements in healthy subjects using the technique of enhanced depth imaging optical coherence tomography. *Invest Ophthalmol Vis Sci* 2011;52(5):2267–2271.
21. Yasuno Y, Okamoto F, Kawana K, Yatagai T, Oshika T. Investigation of multifocal choroiditis with panuveitis by three-dimensional high-penetration optical coherence tomography. *J Biophotonics* 2009;2(6-7):435–441.
22. Yeoh J, Rahman W, Chen F, et al. Choroidal imaging in inherited retinal disease using the technique of enhanced depth imaging optical coherence tomography. *Graefes Arch Clin Exp Ophthalmol* 2010;248(12):1719–1728.
23. Barteselli G, Chhablani J, El-Emam S, et al. Choroidal volume variations with age, axial length, and sex in healthy subjects: a three-dimensional analysis. *Ophthalmology* 2012; 119(12):2572–2578.
24. Chhablani J, Barteselli G, Wang H, et al. Repeatability and reproducibility of manual choroidal volume measurements using enhanced depth imaging optical coherence tomography. *Invest Ophthalmol Vis Sci* 2012;53(4):2274–2280.
25. Hirata M, Tsujikawa A, Matsumoto A, et al. Macular choroidal thickness and volume in normal subjects measured by swept-source optical coherence tomography. *Invest Ophthalmol Vis Sci* 2011;52(8):4971–4978.
26. Shin JW, Shin YU, Lee BR. Choroidal thickness and volume mapping by a six radial scan protocol on spectral-domain optical coherence tomography. *Ophthalmology* 2012;119(5):1017–1023.
27. Foong AW, Saw SM, Loo JL, et al. Rationale and methodology for a population-based study of eye diseases in Malay people: The Singapore Malay eye study (SiMES). *Ophthalmic Epidemiol* 2007;14(1):25–35.
28. Rosman M, Zheng Y, Wong W, et al. Singapore Malay Eye Study: rationale and methodology of 6-year follow-up study (SiMES-2). *Clin Experiment Ophthalmol* 2012;40(6):557–568.
29. Tian J, Marziliano P, Baskaran M, Tun TA, Aung T. Automatic segmentation of the choroid in enhanced depth imaging optical coherence tomography images. *Biomed Opt Express* 2013;4(3):397–411.
30. Fleiss JL, Cohen J. The equivalence of weighted kappa and the intraclass correlation coefficient as measures of reliability. *Educational and Psychological Measurement* 1973;33(3): 613–619.
31. Bland JM, Altman DG. Statistical methods for assessing agreement between two methods of clinical measurement. *Lancet* 1986;1(8476):307–310.
32. Bland JM, Altman DG. Agreed statistics: measurement method comparison. *Anesthesiology* 2012;116(1):182–185.
33. Noori J, Riazi Esfahani M, Hajizadeh F, Zaferani MM. Choroidal mapping; a novel approach for evaluating choroidal thickness and volume. *J Ophthalmic Vis Res* 2012; 7(2):180–185.
34. Manjunath V, Taha M, Fujimoto JG, Duker JS. Choroidal thickness in normal eyes measured using Cirrus HD optical coherence tomography. *Am J Ophthalmol* 2010;150(3): 325–329.e321.
35. Lam DS, Leung KS, Mohamed S, et al. Regional variations in the relationship between macular thickness measurements and myopia. *Invest Ophthalmol Vis Sci* 2007;48(1):376–382.
36. Lim MC, Hoh ST, Foster PJ, et al. Use of optical coherence tomography to assess variations in macular retinal thickness in myopia. *Invest Ophthalmol Vis Sci* 2005;46(3):974–978.
37. Ikuno Y, Kawaguchi K, Nouchi T, Yasuno Y. Choroidal thickness in healthy Japanese subjects. *Invest Ophthalmol Vis Sci* 2010;51(4):2173–2176.
38. Grossniklaus HE, Green WR. Pathologic findings in pathologic myopia. *Retina* 1992;12(2):127–133.
39. Hirata A, Negi A. Morphological changes of choriocapillaris in experimentally induced chick myopia. *Graefes Arch Clin Exp Ophthalmol* 1998;236(2):132–137.
40. Okabe S, Matsuo N, Okamoto S, Kataoka H. Electron microscopic studies on retinochoroidal atrophy in the human eye. *Acta Med Okayama* 1982;36(1):11–21.
41. Maul EA, Friedman DS, Chang DS, et al. Choroidal thickness measured by spectral domain optical coherence tomography: factors affecting thickness in glaucoma patients. *Ophthalmology* 2011;118(8):1571–1579.

Biosketch

Preeti Gupta graduated with masters in Optometry from Queensland University of Technology, Australia in 2008. She then joined the Ocular Epidemiology Research Group at Singapore Eye Research Institute, Singapore, where she conducts and coordinates epidemiological and population-based projects under the Singapore Epidemiology of Eye Disease programme. Her area of interest includes epidemiology of major eye diseases and ocular imaging using novel image processing techniques.

Biosketch

Ching-Yu Cheng leads Ocular Epidemiology Research group at Singapore Eye Research Institute and co-directs the Singapore Epidemiology of Eye Diseases (SEED) program. His primary research interests are related to epidemiology and genetics of major eye diseases. His current work involves a variety of epidemiological, clinical, and image research on glaucoma; and identification of susceptibility genes for complex ocular diseases, such as glaucoma, macular degeneration and cataract, using both genome-wide association approaches and next-generation sequencing technology.

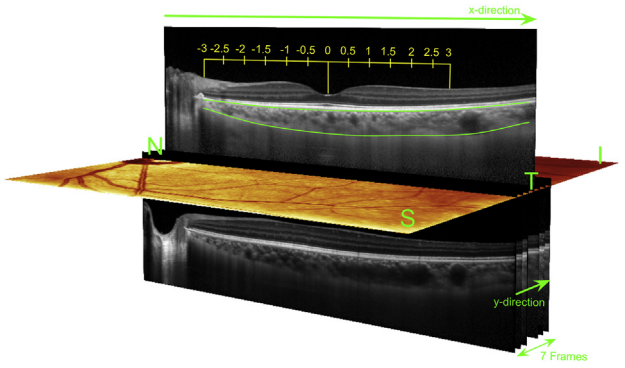

SUPPLEMENTAL FIGURE. Enhanced depth imaging optical coherence tomography image with automatically segmented Bruch membrane and the choroidal-scleral interface. Choroidal thickness at each measurement point (shown by the numbered grid) was defined as CT (x,y), where x and y are the transverse (from nasal to temporal) and interframe (from superior to inferior) directions, respectively. The separation between frames is 246 μm.

Peripapillary choroidal thickness assessed using automated choroidal segmentation software in an Asian population

Preeti Gupta,[1,2] Tian Jing,[3] Pina Marziliano,[3] Mani Baskaran,[1,2,4] Gemmy C M Cheung,[1,4] Ecosse L Lamoureux,[1,4] Carol Y Cheung,[1,3] Tien Yin Wong,[1,2,4] Tin Aung,[1,2,4] Ching-Yu Cheng[1,2,4]

[1]Singapore Eye Research Institute and Singapore National Eye Centre, Singapore, Singapore
[2]Department of Ophthalmology, Yong Loo Lin School of Medicine, National University of Singapore and National University Health System, Singapore, Singapore
[3]School of Electrical and Electronic Engineering, Nanyang Technological University, Singapore, Singapore
[4]Duke-NUS Graduate Medical School, Singapore, Singapore

Correspondence to
Dr Cheng-Yu Cheng, Ocular Epidemiology Research Group & Statistics Unit, Singapore Eye Research Institute, 20 College Road, The Academia, Level 6, Discovery Tower, Singapore 169856, Singapore;
ching-yu_cheng@nuhs.edu.sg

Received 17 September 2014
Revised 11 November 2014
Accepted 12 December 2014
Published Online First 22 January 2015

ABSTRACT

Aims To objectively quantify the thickness of peripapillary choroid using spectral-domain optical coherence tomography (SD-OCT) with enhanced depth imaging (EDI) followed by a novel automated choroidal segmentation software in Asian eyes and to evaluate its systemic and ocular determinants.

Methods We recruited 520 subjects (1040 eyes) from the Singapore Malay Eye Study, a cross-sectional population-based study. Subjects underwent standardised detailed ophthalmic examination including SD-OCT (Spectralis) with EDI for measurement of peripapillary choroidal thickness (PPCT).

Results The mean age of the subjects was 66.7 ±10.4 years (range 47–88 years) and the mean spherical equivalent was −0.01±2.28 D (range −18.50 to +7.00 D). The intra-session repeatability of PPCT measurements at four quadrants using automated choroidal segmentation software was excellent (intraclass correlation coefficient 0.9998–0.9999). The overall mean PPCT was 136.2±56.8 μm. Peripapillary choroid showed geographical differences among the four quadrants, being thickest in the superior quadrant (150.5 ±59.6 μm), followed by the nasal (143.5±58.4 μm) and temporal quadrants (139.4±68.9 μm), and thinnest in the inferior quadrant (111.3±51.7 μm). Among the range of ocular and systemic factors studied, shorter axial length (p=0.002), younger age (p=0.018), lower triglyceride level (p=0.015) and the presence of diabetes (p=0.036) were the only significant predictors of thicker peripapillary choroid.

Conclusions Using novel automated choroidal segmentation software, we provide reliable objective measurements of PPCT in a population-based setting. Shorter axial length, younger age, lower triglyceride levels and the presence of diabetes are the factors independently associated with thicker PPCT. These factors should be taken into consideration when interpreting Spectralis EDI SD-OCT-based PPCT measurements in clinics.

INTRODUCTION

The choroid supplies blood to the outer retina[1] and also to the anterior optic nerve head (ONH).[2 3] Although the circulation of the posterior ciliary artery is the main source of blood supply to the ONH, the prelaminar region of the ONH is mainly nourished by the peripapillary choroid.[3–5] Using spectral domain optical coherence tomography (SD-OCT), studies have shown that the peripapillary choroid is altered in eyes with glaucoma[6–8] and high myopia.[9] Glaucoma eyes were found to have a thinner peripapillary choroid,[6–8] and an abnormal choroidal blood supply has been suggested as one factor responsible for the occurrence of glaucomatous optic neuropathy in patients with glaucoma.[3] Knowledge of the distribution of peripapillary choroidal thickness (PPCT) in the population may therefore be useful in facilitating the detection of abnormal changes in PPCT and thus help in elucidating the pathophysiology of such eye diseases.

However, to date only a few studies[10–12] have measured PPCT in normal healthy subjects using different OCT devices, and these studies measured PPCT manually with a relatively small sample size in a clinic-based setting. With the limitation of manual measurements being tedious, time consuming, lacking objectivity and therefore having potential intra- and inter-operator variability, regular assessment of PPCT using SD-OCT is impractical for both clinical and large-scale quantitative studies.

This study used a novel automated choroidal segmentation software to objectively quantify the PPCT acquired using SD-OCT with enhanced depth imaging (EDI) in a population-based setting. We aimed to obtain an accurate distribution of PPCT and to determine its associated systemic and ocular factors.

MATERIALS AND METHODS

Study population

The subjects in this study were enrolled from the Singapore Malay Eye Study (SiMES), a population-based cohort study of eye diseases in the Malay population aged 40–80 years in Singapore.[13] The baseline examination was conducted between 2004 and 2006 and a follow-up examination of the SiMES participants has been conducted since January 2011, 6 years after the baseline examination. For this study, we consecutively recruited 540 subjects from SiMES participants who attended the follow-up examination from February 2012 to July 2013. Subjects were excluded if their choroidal images could not be successfully attained due to unstable fixation, opacities of the optic media such as significant cataract, or if the available images were not of sufficient quality (quality index <28 dB), and those whose peripapillary atrophy involved the OCT scanning ring. As our aim is to determine the distribution of PPCT in a general

To cite: Gupta P, Jing T, Marziliano P, *et al*. *Br J Ophthalmol* 2015;**99**:920–926.

population sample, any ocular disease including disorders of the optic nerve or macula was not a reason to exclude a subject if the quality of the OCT image was sufficient to be evaluated.

Subjects underwent standardised ophthalmic examination including Spectralis EDI SD-OCT (Heidelberg Engineering, Heidelberg, Germany).

Peripapillary choroidal imaging

Peripapillary choroid was imaged using the EDI modality of SD-OCT (wavelength 870 nm) after pupil dilation using tropicamide 1% and phenylephrine hydrochloride 2.5%. Following the guidelines of the Spectralis user manual, the subjects' keratometry readings and the most recent refraction were entered into the software program to estimate optical magnification and, therefore, to allow for more accurate comparisons across individuals. For measurements of PPCT, the peripapillary region was scanned using a 360° 3.6 mm diameter circle that was centred on the optic disc, each comprising 100 averaged scans (using the automatic averaging and eye tracking features of the proprietary device).

Examinations were performed by a single experienced examiner and measurements of PPCT on both eyes of the study subjects were obtained and used for this analysis.

Automated measurement of PPCT

In our study, Bruch's membrane and the choroidal–scleral interface (CSI) were delineated with the automatic segmentation algorithm recently developed by Tian *et al*[14] (figure 1). This algorithm demonstrated good consistency with the manual measurements of choroidal thickness (mean (SD) Dice coefficient over 45 tested images was 90.5 (3)%).[14]

The PPCT at each location was defined as the distance between the Bruch's membrane and the CSI. Here we define locations in the radial scan in terms of the angle with the fixed diameter of 3.6 mm. The PPCT in the optic disc region was automatically measured at the 12 discrete locations (30° apart) as indicated by 12 vertical lines in figure 2. The mean PPCT values in the temporal (T), superior (S), nasal (N) and inferior (I) quadrants were also calculated (figure 2).

Repeatability of PPCT measurements

To assess the intra-session repeatability using EDI SD-OCT and automated choroidal segmentation software, images from the same eye of 30 subjects were obtained twice at an interval of 10 min. Two images from the same eyes were each measured by segmentation software to assess the repeatability of PPCT measurements.

Assessment of ocular factors

The refraction of each eye was measured using an autorefractor (Canon RK 5 Auto Ref-Keratometer; Canon, Tochigiken, Japan). The spherical equivalent was calculated as the sum of the spherical power and half of the cylinder power. Best-corrected visual acuity was measured monocularly using a logarithm of the minimum angle of resolution (LogMAR) chart (Lighthouse International, New York, USA) at a distance of 4 m. Biometry measurements— that is, axial length (AL), corneal curvature and anterior chamber depth—were measured with a non-contact partial coherence laser interferometry (IOLMaster V.3.01; Carl Zeiss Meditec, Jena, Germany) and the mean of five measurements was used in the analysis. Intraocular pressure (IOP) was measured using Goldmann applanation tonometry (Haag-Streit, Bern, Switzerland) before pupil dilation. Central corneal thickness was measured with an ultrasound pachymeter (Advent; Mentor O & O, Norwell, Massachusetts, USA) and the mean of five measurements was used in the analysis.

Assessment of demographic, lifestyle and systemic factors

All study participants also underwent a detailed interview using standardised questionnaires. Information on demographic status, lifestyle risk factors (eg, smoking, alcohol consumption), medication use and self-reported history of systemic diseases such as arterial hypertension and diabetes mellitus were collected. Systolic and diastolic blood pressures (BPs) were measured using a digital automatic BP monitor (Dinamap model Pro Series DP110X-RW, 100V2; GE Medical Systems Information Technologies, Milwaukee, Wisconsin, USA). A total of three measurements were taken, and the average of the two closest BP readings was taken as each participant's BP. Mean ocular perfusion pressure (OPP) was calculated using the following equation: mean OPP=(2/3×mean arterial pressure − IOP), where MAP=diastolic BP + (1/3 × [systolic BP − diastolic BP]). Body mass index (BMI) was calculated as kg/m^2. Smoking status was defined as currently smokers, ex-smokers and non-smokers. Non-fasting venous blood samples were collected for biochemical testing of serum total cholesterol, high-density lipoprotein cholesterol, low-density lipoprotein cholesterol, triglycerides, glycosylated haemoglobin (HbA1c), glucose and creatinine.

Statistical analysis

Statistical analysis was performed using MedCalc V.12.3 (Medcalc Software, Ostend, Belgium) and SPSS V.20.0 (SPSS, Chicago, Illinois, USA). Both eyes of the study subjects were included in the analysis. Univariate and multiple linear regression analyses were used to assess the association between ocular and systemic factors (independent variables) and average PPCT

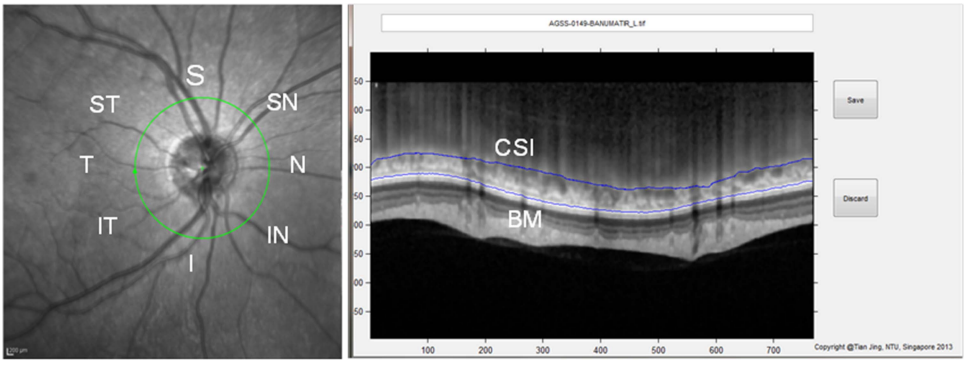

Figure 1 Enhanced depth imaging optical coherence tomography image in the peripapillary region demonstrating automated segmentation of the Bruch's membrane (BM) and the choroidal–scleral interface (CSI). The peripapillary choroidal thickness at each measured location was defined as the distance between BM and the CSI.

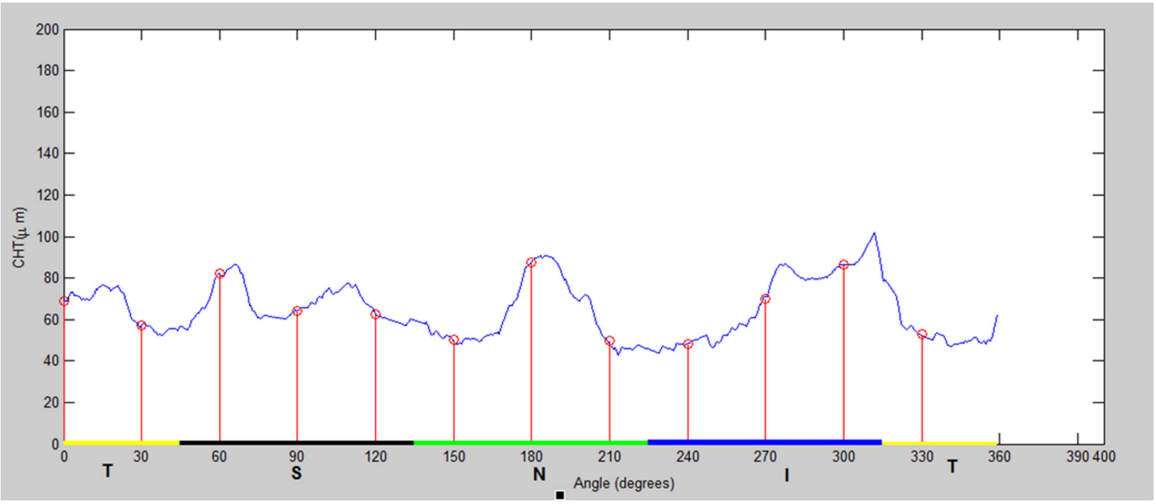

Figure 2 Illustration of automated peripapillary choroidal thickness (CHT) measured in the optic disc region. The numbers on the x-axis are locations in clock hour sectors (30° apart). The location of the zero degree is always on the left-most point of the disc circle and the value of degree increases in the clockwise direction. T, temporal; S, superior; N, nasal; I, inferior quadrants.

(dependent variable), adjusted for potential confounders such as glaucoma status, diabetic retinopathy and age-related macular degeneration. For multiple linear regression, age, gender and factors showing suggestively significant association in univariate analysis ($p<0.10$) were included. Eyes with other ocular diseases such as refractive errors, cataract, glaucoma and retinopathy were not excluded if the quality of the OCT image was sufficient to be evaluated, as we aimed to determine the PPCT distribution in a general population sample. Generalised estimating equation, exchangeable correlation matrix, was used to account for inter-eye correlations.

We assessed the intrasession repeatability of PPCT using the intraclass correlation coefficient (ICC).[15] We also performed Bland–Altman plot analyses[16] to see the mean difference between the repeated measurements. All p values were two-sided and considered statistically significant when the values were <0.05.

RESULTS

Of the 1750 subjects from the SiMES-2 study, approximately a quarter of our subjects had Spectralis OCT imaging performed. Of the 520 subjects (1040 eyes) who had Spectralis OCT images and were therefore recruited to this study, we further excluded

Table 1 Comparison of baseline characteristics of study subjects versus subjects excluded from the Singapore Malay Eye Study (SiMES-2) population

Characteristics	Total (n=1750)	Included (n=452)	Excluded (n=1298)	p Value*
Age, years	63.30 (10.20)	66.76 (10.45)	62.09 (9.83)	<0.001
Gender, % male	801 (45.8)	179 (39.6)	622 (47.9)	0.002
Axial length, mm	23.61 (1.11)	23.61 (1.08)	23.61 (1.12)	0.972
Anterior chamber depth, mm	3.14 (0.37)	3.11 (0.38)	3.15 (0.36)	0.064
Corneal curvature, mm	7.65 (0.25)	7.67 (0.25)	7.64 (0.25)	0.021
Spherical equivalent, D	−0.122 (2.40)	−0.60 (2.34)	−0.143 (2.42)	0.542
Central corneal thickness, μm	540.11 (33.74)	538.37 (32.80)	540.85 (34.12)	0.196
Intraocular pressure, mm Hg	14.49 (3.15)	14.38 (3.23)	14.53 (3.12)	0.400
Ocular perfusion pressure, mm Hg	55.97 (8.14)	55.46 (9.05)	56.15 (7.79)	0.154
Systolic blood pressure, mm Hg	141.05 (20.24)	141.52 (21.52)	140.89 (19.78)	0.583
Diastolic blood pressure mm Hg	77.11 (10.58)	75.55 (11.53)	77.65 (10.17)	0.001
Mean arterial pressure, mm Hg	98.42 (12.29)	97.54 (13.49)	98.73 (11.83)	0.097
Body mass index, kg/m^2	26.85 (5.20)	26.29 (5.68)	27.04 (5.01)	0.015
Serum glucose, mmol/L	7.08 (3.39)	7.19 (3.52)	7.04 (3.35)	0.399
HbA1c, %	6.32 (1.40)	6.28 (1.36)	6.33 (1.41)	0.590
Total cholesterol, mmol/L	5.36 (1.26)	5.35 (1.32)	5.37 (1.23)	0.761
Triglycerides, mmol/L	1.88 (1.22)	1.84 (1.36)	1.89 (1.17)	0.396
Blood creatinine, mmol/L	87.08 (65.98)	90.09 (59.95)	86.03 (67.92)	0.264
Current smoking, %	288 (16.5)	77 (17.0)	211 (16.3)	0.710
Diabetes mellitus, %	506 (28.9)	129 (28.5)	377 (29)	0.422
Arterial hypertension, %	1120 (64.0)	307 (67.9)	813 (62.6)	0.047
Alcohol consumption, %	15 (0.9)	5 (1.1)	10 (0.8)	0.553

Data presented are mean (SD) or n (%), as appropriate.
Ocular characteristics are presented for right eye only.
*p Value was obtained with independent sample t test for continuous variables and with χ^2 tests for categorical variables.

68 subjects because either their choroidal images were not successfully attained (n=37), the available images were of insufficient quality (n=22) for a reliable determination of the PPCT or their peripapillary atrophy involved the OCT scanning ring (n=9), leaving 452 subjects (904 eyes) with complete data on PPCT for analysis. In none of the images did the automated software fail to detect the Bruch's membrane and choroidal borders and therefore no eyes were excluded from the analysis because of software demarcation error.

Table 1 presents the baseline characteristics of the study subjects included versus the subjects excluded from the SiMES-2 population. Compared with those SiMES-2 subjects excluded from the analysis, the 452 study subjects tended to be older, female, with steeper corneal curvature, lower diastolic BP and BMI and tended to have hypertension.

Table 2 shows the profile of major eye diseases among our study cohort. A total of 351 (77.7%) participants did not have any eye diseases; the remaining 101 (22.7%) had eye diseases including diabetic retinopathy (8.4%), glaucoma (4.6%), high myopia (4%) and early (4.9%) and late (0.4%) age-related macular degeneration.

Table 3 shows the intra-session repeatability of PPCT measurement using automated choroidal segmentation software. The repeatability of PPCT at the four quadrants was excellent (ICC 0.9998–0.9999). The mean difference (95% limits of agreement) for mean PPCT was −0.16 (−1.53 to 1.20) μm.

Table 4 shows the mean PPCT measured at 12 clock hours and four quadrants (superior, nasal, inferior and temporal). The overall mean PPCT in our study subjects was 136.2±56.8 μm. There were regional differences in PPCT among clock hours and different quadrants (figure 3A, B). Peripapillary choroid was thickest (150.5±59.6 μm) at the superior quadrant and thinnest (102.6±51.1 μm) at the inferior quadrant.

In the univariate linear regression analysis (table 5), AL, IOP, triglyceride levels and diabetes showed a significant association with mean PPCT (all p<0.10). In the multiple linear regression model (table 5) including age, gender and all suggestively significant factors (p<0.10) from the univariate analysis, shorter AL (p=0.002), younger age (p<0.018), lower triglyceride levels (p=0.015) and the presence of diabetes (p=0.036) remained significantly associated with thicker PPCT. The association with IOP was no longer significant (p=0.407). For each increase in AL of 1 mm and increase in age of 1 year, PPCT on average decreased by 6.59 μm (p=0.002) and 0.56 μm (p=0.018), respectively. A decrease in mean PPCT by 4.88 μm was observed for each mmol/L increase in triglyceride level (p=0.015). The presence of diabetes increased the mean PPCT by 13.73 μm (p=0.036). However, if gender and IOP were removed from our multivariate model, the presence of diabetes still remained significantly associated with PPCT (regression coefficient 13.22, 95% CI 0.42 to 26.02, p=0.043). Table 6 presents the multivariate analysis results of the association of PPCT with ocular and systemic factors by quadrant. In the multivariate models, only younger age and shorter AL were associated with a thicker inferior peripapillary choroid and shorter AL, lower triglyceride level and the presence of diabetes were associated with a thicker superior peripapillary choroid. IOP was the only significant factor associated with a thicker nasal peripapillary choroid. For temporal PPCT, associated factors were similar to those identified from overall PPCT.

Table 2 Major eye diseases in the study population (n=452)

Presence of eye diseases	N (%)
None	351 (77.7)
Diabetic retinopathy	38 (8.4)
Age-related macular degeneration (ARMD)	
Early ARMD	22 (4.9)
Late ARMD	2 (0.4)
Glaucoma	21 (4.6)
High myopia (−6 dioptres or more)	18 (4.0)

Data presented are n (%).

Table 3 Intra-session repeatability of peripapillary choroidal thickness measurement at four quadrants by automated choroidal segmentation software (n=30)

Locations of measurement	Intraclass correlation (95% CI)	Mean (95% CI) difference (μm)*
Peripapillary choroidal thickness		
Inferior quadrant	0.99 (0.99 to 0.99)	0.2 (−2.7 to 2.2)
Superior quadrant	0.99 (0.99 to 1.00)	−0.2 (−2.9 to 2.6)
Nasal quadrant	0.99 (0.99 to 0.99)	0.3 (−2.9 to 3.4)
Temporal quadrant	0.99 (0.99 to 0.99)	−0.5 (−3.8 to 2.7)
Average	1.00 (0.99 to 1.00)	−0.1 (−1.5 to 1.2)

*Mean difference was determined from the first measurement minus the second measurement.

DISCUSSION

To the best of our knowledge, this is the first study to use Spectralis OCT with EDI with an automated choroidal segmentation software to measure PPCT in subjects from a population-based study. We found the peripapillary choroid to be significantly thicker in the superior quadrant and thinnest at

Table 4 Distribution of peripapillary choroidal thickness at clock hour sectors (30° apart) and four quadrants (n=904 eyes)

Measurement location	Peripapillary choroidal thickness, μm
Clock hour	
1	139.5 (77.0)
2	147.8 (71.0)
3	148.9 (64.9)
4	150.8 (61.9)
5	151.4 (59.3)
6	152.1 (60.8)
7	145.4 (61.7)
8	134.0 (58.6)
9	115.8 (53.5)
10	102.6 (51.1)
11	113.9 (57.3)
12	130.3 (68.6)
Quadrants	
Inferior	111.3 (51.7)
Superior	150.5 (59.6)
Nasal	143.5 (58.4)
Temporal	139.4 (68.9)
Average quadrant thickness	136.2 (56.8)

Data presented are mean (SD).
1 o'clock corresponds to the temporal region, 4 o'clock to the superior region, 7 o'clock to the nasal region and 10 o'clock to the inferior region.

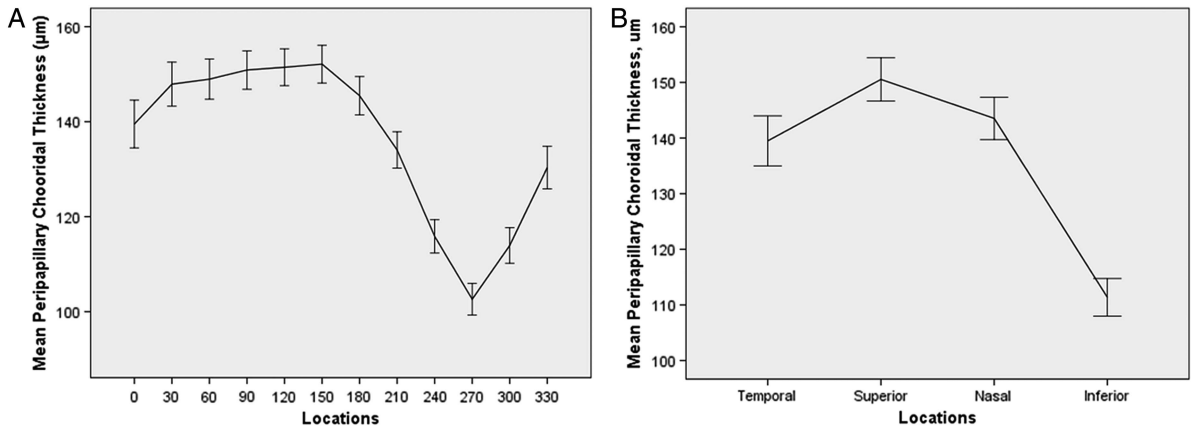

Figure 3 Variation trend of peripapillary choroidal thickness in µm. Distribution of mean peripapillary choroidal thickness at (A) clock hour sectors (30° apart) and (B) four quadrants (inferior, superior, nasal and temporal) in 904 eyes. Error bars represents standard error.

the inferior quadrant. Among the range of ocular and systemic factors studied, AL, age, triglyceride level and diabetes were the only significant determinants of PPCT.

Previous studies have characterised the thickness and profile of peripapillary choroid in normal eyes but with limited validity.[10–12] There are several reasons for compromised validity. First, their measurements were not automated but involved manual adjustment of the choroidal boundaries, making it time-consuming and also prone to measurement errors. Second, these studies were performed in clinic-based settings with a potential selection bias and involved a smaller sample size, affecting their generalisability. To address these issues we therefore developed and used a novel technique of automated choroidal segmentation[14] to objectively and efficiently obtain the PPCT in a population-based sample.

Our study showed a mean PPCT of 136.2±56.8 µm. Previous studies have reported a mean thickness of 165–191.6 µm.[10 11] The disparities in PPCT in our study compared with other studies may be due to differences in the demographic data of enrolled subjects such as ethnicity and age. Different studies may have different age groups of study participants and, with advancing age, the choroid may undergo further age-related attenuation. The mean age of our participants was 67 years, compared with 57 and 48 years in the studies by Huang *et al*[11]

Table 5 Associations of average peripapillary choroidal thickness (PPCT) with ocular and systemic factors using generalised estimating equation (n=904 eyes)

	Univariate analysis		Multivariate analysis*	
	β (95% CI)	p Value	β (95% CI)	p Value
Ocular factors				
Spherical equivalent, D	−0.22 (−0.23 to 1.88)	0.833	–	–
Axial length, mm	−4.23 (−8.88 to 0.40)	0.074	−6.59 (−10.86 to −2.33)	**0.002**
Corneal curvature, mm	−13.14 (−30.39 to 4.10)	0.135	–	–
Central corneal thickness, µm	−0.01 (−0.14 to 0.12)	0.841	–	–
Intraocular pressure, mm Hg	1.30 (0.20 to 2.40)	0.020	0.60 (−0.82 to 2.02)	0.407
Ocular perfusion pressure, mm Hg	−0.18 (−0.64 to 0.27)	0.436	–	–
Systemic factors				
Age, years	−0.20 (−0.61 to 0.19)	0.319	−0.56 (−1.03 to −0.09)	**0.018**
Gender, male	−5.63 (−14.53 to 3.27)	0.215	5.60 (−5.08 to 16.29)	0.304
Systolic blood pressure, mm Hg	−0.06 (−0.25 to 0.13)	0.538	–	–
Diastolic blood pressure, mm Hg	−0.00 (−0.36 to 0.34)	0.959	–	–
Mean arterial pressure, mm Hg	−0.05 (−0.36 to 0.25)	0.718	–	–
Body mass index, kg/m^2	0.18 (−0.55 to 0.91)	0.631	–	–
Serum glucose, mmol/L	0.53 (−0.69 to 1.76)	0.392	–	–
HbA1c, %	1.13 (−1.83 to 4.09)	0.455	–	–
Total cholesterol, mmol/L	0.25 (−3.10 to 3.60)	0.883	–	–
Triglycerides, mmol/L	−2.42 (−5.13 to 0.29)	0.080	−4.88 (−8.80 to −0.95)	**0.015**
Blood creatinine, mmol/L	0.00 (−0.07 to 0.08)	0.818	–	–
Current smoking	−2.79 (−13.74 to 8.14)	0.616	–	–
Diabetes mellitus	9.39 (−0.73 to 19.52)	0.069	13.73 (0.90 to 26.34)	**0.036**
Arterial hypertension	3.16 (−5.88 to 12.20)	0.493	–	–
Alcohol consumption	−7.99 (−38.18 to 22.19)	0.604	–	–

Bold type indicates statistical significance.
β represents the change in PPCT per unit change in continuous variables and the difference in PPCT between groups for categorical variables.
*Adjusted for glaucoma status, diabetic retinopathy and age-related macular degeneration.

Table 6 Multivariate analysis of the associations of regional (inferior, superior, nasal and temporal) peripapillary choroidal thickness (PPCT) with ocular and systemic factors using generalised estimating equation (n=904 eyes)

	Inferior PPCT		Superior PPCT		Nasal PPCT		Temporal PPCT	
	β (95% CI)	p value	β (95% CI)	p Value	β (95% CI)	p Value	β (95% CI)	p Value
Axial length, mm	−5.59 (−9.53 to −1.65)	**0.005**	−6.03 (−10.56 to −1.49)	**0.009**	–	–	−7.96 (−13.34 to −2.58)	**0.004**
Corneal curvature, mm	–	–	–	–	–	–	−3.01 (−28.32 to 22.29)	0.815
Intraocular pressure, mm Hg	0.64 (−0.53 to 1.83)	0.284	0.51 (−1.04 to 2.07)	0.518	1.37 (0.04 to 2.70)	**0.044**	0.56 (−1.24 to 2.36)	0.543
Age, years	−0.54 (−0.96 to −0.11)	**0.012**	−0.44 (−0.94 to 0.04)	0.074	−0.28 (−0.71 to 0.13)	0.184	−0.68 (−1.27 to −0.09)	**0.023**
Triglycerides, mmol/L	–	–	−5.15 (−9.26 to −1.05)	**0.014**	–	–	−5.96 (−10.51 to 1.41)	**0.010**
Diabetes mellitus	9.36 (−2.26 to 20.99)	0.115	15.15 (2.26 to 28.04)	**0.021**	–	–	17.07 (1.82 to 32.32)	**0.028**

Bold type indicates statistical significance.
For inferior, superior, nasal and temporal PPCT, age, gender, glaucoma status, diabetic retinopathy, age-related macular degeneration and variables with p<0.10 in univariate models were included in multivariate models.

and Ho *et al*,[10] respectively. In addition, differences in the choroidal segmentation method, which was fully automated in our study and was manual in previous studies, variations in OCT device characteristics such as wavelength, eye tracking method and averaging software among studies might contribute to the observed variations in thickness across studies.

With regard to the profile of the peripapillary choroid, our results confirmed the asymmetrical distribution of PPCT. The mean PPCT measurements showed regional differences, being thickest in the superior region, followed by the nasal and temporal quadrants and thinnest in the inferior region. These observations are similar to the results of previous EDI-OCT studies in normal eyes which have consistently shown the inferior region to be thinner than other regions.[10 11 17] The thinner choroid in the inferior region makes this area more susceptible to retinal and choroidal diseases. Several studies[10 18] have hypothesised that the thinnest peripapillary choroid in the inferior quadrant may represent an area of lower blood supply which may predispose the inferior region of the optic nerve to glaucomatous ischaemic damage, suggesting a possible explanation for the well-known observation that glaucoma typically affects the inferior optic nerve region first.

Among the other ocular factors, the peripapillary choroid was thinner in eyes with longer AL, which is in agreement with previous studies on macular choroidal thickness that have shown a decrease in choroid in elongated eyes.[9 19] In eyes with greater AL, the elongation of the eyeball leads to mechanical stretching and thinning of the retina[20 21] and choroid due to significant thinning of the choriocapillaris and focal lack of vessels.[22–24]

We found that the peripapillary choroid thinned with age, similar to the findings of previous studies on PPCT.[11 12] Thinning results in a reduced ability of the choroid to provide sufficient levels of oxygen and other metabolites to the ONH. We speculate that such a gradual loss in physiological functions of the peripapillary choroid may contribute to the onset of glaucoma in elderly people.

In addition, we observed thickening of the peripapillary choroid in persons with diabetes. However, the reasons for diabetic people having thicker peripapillary choroid are still unclear as there is inconsistency in the literature in terms of choroidal blood flow, which is reported to decrease, increase and remain unchanged in patients with diabetes.[25–27] This statistically significant finding could therefore be seen as exploratory and confirmatory studies are necessary to evaluate the results.

Tan *et al* reported that arterial BP had an effect on subfoveal choroidal thickness. They found that a change in choroidal thickness was positively correlated with the change in systolic BP.[28] However, in our study we did not find any significant association between BP and PPCT. Lastly, in our study lower levels of triglyceride were associated with thicker PPCT. However, the reasons for such an association are unknown and further studies are needed to confirm this relationship.

We acknowledge limitations to our study. First, recent studies have reported diurnal fluctuations in choroidal thickness in the macular region.[28–30] To the best of our knowledge there are no data on the association between diurnal variation and choroidal thickness in the peripapillary region. Our subjects were examined only at a single time point and thus we are not able to take account of any diurnal variation of PPCT. Second, our investigation included consecutive participating subjects from a population-based study and thus some of them had eye diseases that might have changed choroidal thickness. The distribution of PPCT determined in this study may not therefore represent the PPCT in healthy eyes but in general adult and elderly populations. However, this would not affect the observed associations because, in our multiple regression analysis model, we have adjusted for the potential ocular diseases in elderly people that might influence choroidal thickness.

In conclusion, we objectively demonstrated a mean PPCT of 136.2±56.8 μm in an Asian population. Shorter AL, younger age, lower triglyceride levels and the presence of diabetes were the factors independently associated with thicker peripapillary choroid. Automated choroidal segmentation software allows highly reliable, faster and more objective evaluation of choroid, which may help provide further insight into diseases such as glaucoma and myopia.

Contributors All the authors contributed to the preparation of the manuscript.

Funding This study was supported by a grant from the National Medical Research Council, Singapore (grant No. NMRC R760/44/2010).

Competing interests None.

Patient consent Written informed consent was obtained from all study participants.

Ethics approval The study adhered to the tenets of the Declaration of Helsinki and ethics approval was obtained from the Singapore Eye Research Institute Institutional Review Board.

Provenance and peer review Not commissioned; externally peer reviewed.

REFERENCES

1 Linsenmeier RA, Padnick-Silver L. Metabolic dependence of photoreceptors on the choroid in the normal and detached retina. *Invest Ophthalmol Vis Sci* 2000;41:3117–23.

2 Flammer J, Orgul S, Costa VP, *et al*. The impact of ocular blood flow in glaucoma. *Prog Retin Eye Res* 2002;21:359–93.
3 Hayreh SS. Blood supply of the optic nerve head and its role in optic atrophy, glaucoma, and oedema of the optic disc. *Br J Ophthalmol* 1969;53:721–48.
4 Hayreh SS. The 1994 Von Sallman Lecture. The optic nerve head circulation in health and disease. *Exp Eye Res* 1995;61:259–72.
5 Hayreh SS. The blood supply of the optic nerve head and the evaluation of it—myth and reality. *Prog Retin Eye Res* 2001;20:563–93.
6 Roberts KF, Artes PH, O'Leary N, *et al*. Peripapillary choroidal thickness in healthy controls and patients with focal, diffuse, and sclerotic glaucomatous optic disc damage. *Arch Ophthalmol* 2012;130:980–6.
7 Yin ZQ, Vaegan, Millar TJ, *et al*. Widespread choroidal insufficiency in primary open-angle glaucoma. *J Glaucoma* 1997;6:23–32.
8 Hirooka K, Tenkumo K, Fujiwara A, *et al*. Evaluation of peripapillary choroidal thickness in patients with normal-tension glaucoma. *BMC Ophthalmol* 2012;12:29.
9 Fujiwara T, Imamura Y, Margolis R, *et al*. Enhanced depth imaging optical coherence tomography of the choroid in highly myopic eyes. *Am J Ophthalmol* 2009;148:445–50.
10 Ho J, Branchini L, Regatieri C, *et al*. Analysis of normal peripapillary choroidal thickness via spectral domain optical coherence tomography. *Ophthalmology* 2011;118:2001–7.
11 Huang W, Wang W, Zhou M, *et al*. Peripapillary choroidal thickness in healthy Chinese subjects. *BMC Ophthalmol* 2013;13:23.
12 Oh J, Yoo C, Yun CM, *et al*. Simplified method to measure the peripapillary choroidal thickness using three-dimensional optical coherence tomography. *Korean J Ophthalmol* 2013;27:172–7.
13 Rosman M, Zheng Y, Wong W, *et al*. Singapore Malay Eye Study: rationale and methodology of 6-year follow-up study (SiMES-2). *Clin Experiment Ophthalmol* 2012;40:557–68.
14 Tian J, Marziliano P, Baskaran M, *et al*. Automatic segmentation of the choroid in enhanced depth imaging optical coherence tomography images. *Biomed Opt Express* 2013;4:397–411.
15 Fleiss JL, Cohen J. The equivalence of weighted kappa and the intraclass correlation coefficient as measures of reliability. *Educ Psychol Meas* 1973;33:613–19.
16 Bland JM, Altman DG. Statistical methods for assessing agreement between two methods of clinical measurement. *Lancet* 1986;1:307–10.
17 Tanabe H, Ito Y, Terasaki H. Choroid is thinner in inferior region of optic disks of normal eyes. *Retina* 2012;32:134–9.
18 Schwartz B, Harris A, Takamoto T, *et al*. Regional differences in optic disc and retinal circulation. *Acta Ophthalmol Scand* 2000;78:627–31.
19 Flores-Moreno I, Lugo F, Duker JS, *et al*. The relationship between axial length and choroidal thickness in eyes with high myopia. *Am J Ophthalmol* 2013;155:314–19.
20 Lam DS, Leung KS, Mohamed S, *et al*. Regional variations in the relationship between macular thickness measurements and myopia. *Invest Ophthalmol Vis Sci* 2007;48:376–82.
21 Lim MC, Hoh ST, Foster PJ, *et al*. Use of optical coherence tomography to assess variations in macular retinal thickness in myopia. *Invest Ophthalmol Vis Sci* 2005;46:974–8.
22 Grossniklaus HE, Green WR. Pathologic findings in pathologic myopia. *Retina* 1992;12:127–33.
23 Hirata A, Negi A. Morphological changes of choriocapillaris in experimentally induced chick myopia. *Graefes Arch Clin Exp Ophthalmol* 1998;236:132–7.
24 Okabe S, Matsuo N, Okamoto S, *et al*. Electron microscopic studies on retinochoroidal atrophy in the human eye. *Acta Med Okayama* 1982;36:11–21.
25 Langham ME, Grebe R, Hopkins S, *et al*. Choroidal blood flow in diabetic retinopathy. *Exp Eye Res* 1991;52:167–73.
26 MacKinnon JR, O'Brien C, Swa K, *et al*. Pulsatile ocular blood flow in untreated diabetic retinopathy. *Acta Ophthalmol Scand* 1997;75:661–4.
27 Schmidt KG, von Ruckmann A, Kemkes-Matthes B, *et al*. Ocular pulse amplitude in diabetes mellitus. *Br J Ophthalmol* 2000;84:1282–4.
28 Tan CS, Ouyang Y, Ruiz H, *et al*. Diurnal variation of choroidal thickness in normal, healthy subjects measured by spectral domain optical coherence tomography. *Invest Ophthalmol Vis Sci* 2012;53:261–6.
29 Chakraborty R, Read SA, Collins MJ. Diurnal variations in axial length, choroidal thickness, intraocular pressure, and ocular biometrics. *Invest Ophthalmol Vis Sci* 2011;52:5121–9.
30 Usui S, Ikuno Y, Akiba M, *et al*. Circadian changes in subfoveal choroidal thickness and the relationship with circulatory factors in healthy subjects. *Invest Ophthalmol Vis Sci* 2012;53:2300–7.

Peripapillary choroidal thickness assessed using automated choroidal segmentation software in an Asian population

Preeti Gupta, Tian Jing, Pina Marziliano, Mani Baskaran, Gemmy C M Cheung, Ecosse L Lamoureux, Carol Y Cheung, Tien Yin Wong, Tin Aung and Ching-Yu Cheng

Br J Ophthalmol 2015 99: 920-926 originally published online January 21, 2015
doi: 10.1136/bjophthalmol-2014-306152

SCIENTIFIC REPORTS

OPEN

Choroidal vascularity index as a measure of vascular status of the choroid: Measurements in healthy eyes from a population-based study

Received: 19 August 2015
Accepted: 07 January 2016
Published: 12 February 2016

Rupesh Agrawal[1,2,*], Preeti Gupta[1,3,*], Kara-Anne Tan[3], Chui Ming Gemmy Cheung[1,3,4], Tien-Yin Wong[1,3,4] & Ching-Yu Cheng[1,3,4]

The vascularity of the choroid has been implicated in the pathogenesis of various eye diseases. To date, no established quantifiable parameters to estimate vascular status of the choroid exists. Choroidal vascularity index (CVI) may potentially be used to assess vascular status of the choroid. We aimed to establish normative database for CVI and identify factors associated with CVI in healthy eyes. In this population-based study on 345 healthy eyes, choroidal enhanced depth imaging optical coherence tomography scans were segmented by modified image binarization technique. Total subfoveal choroidal area (TCA) was segmented into luminal (LA) and stromal (SA) area. CVI was calculated as the proportion of LA to TCA. Linear regression was used to identify ocular and systemic factors associated with CVI and subfoveal choroidal thickness (SFCT). Subfoveal CVI ranged from 60.07 to 71.27% with a mean value of 65.61 ± 2.33%. CVI was less variable than SFCT (coefficient of variation for CVI was 3.55 vs 40.30 for SFCT). Higher CVI was associated with thicker SFCT, but not associated with most physiological variables. CVI was elucidated as a significant determinant of SFCT. While SFCT was affected by many factors, CVI remained unaffected suggesting CVI to be a more robust marker of choroidal diseases.

The choroid is the vascular layer of eye, with one of the highest blood flow of any tissue in the body[1]. The choroid is predominantly composed of blood vessels surrounded by stromal tissue comprising of connective tissue, melanocytes, nerves and extracellular fluid[2]. The vascular layer of the choroid may be differentiated into 3 layers from internal to external, with increasing luminal diameter. The innermost layer is the choriocapillaris, the middle is Sattler's layer with medium vessels, and the outer is Haller's layer, with large vessels[1].

Being a major vascular layer of the eye the choroid plays an important role in ocular health, and is involved in the pathogenesis of many intraocular diseases such as age-related macular degeneration, polypoidal choroidal vasculopathy, central serous chorioretinopathy and myopic macular degeneration[3–9]. There is evidence from histological studies that the disease processes affect the stroma and vasculature of the choroid[10–12]. However, shrinkage occurs during the fixation of the tissues during the histological process, making it difficult to study the changes in vascular tone of the choroid[13].

Choroid thickness (CT) has been reported as an indicator of ocular[14–17] and systemic health[18–22]. Although, many studies have now reported changes in the thickness of the choroid in various ocular and systemic diseases[8–12] and proposed CT as a marker to assess these disease conditions, there exists a notable disparity in CT in various clinical studies. One such example is diabetes mellitus[23–27], where there has been no consensus as to whether it causes an increase or decrease in CT. This raises the question of what structures in the choroid changes with increasing or decreasing CT and if there is a more robust marker to assess choroid health.

To answer this question, morphological and vascular analyses of the choroid may provide some clues and lead to the development of a more stable marker. The advent of enhanced depth imaging (EDI) optical coherence

[1]Singapore Eye Research Institute and Singapore National Eye Center, Singapore. [2]National Healthcare Group Eye Institute, Tan Tock Seng Hospital, Singapore. [3]Department of Ophthalmology, Yong Loo Lin School of Medicine, National University of Singapore and National University Health System, Singapore. [4]Duke-NUS Graduate Medical School, Singapore. *These authors contributed equally to this work. Correspondence and requests for materials should be addressed to C-Y.C. (email: ching-yu_cheng@nuhs.edu.sg)

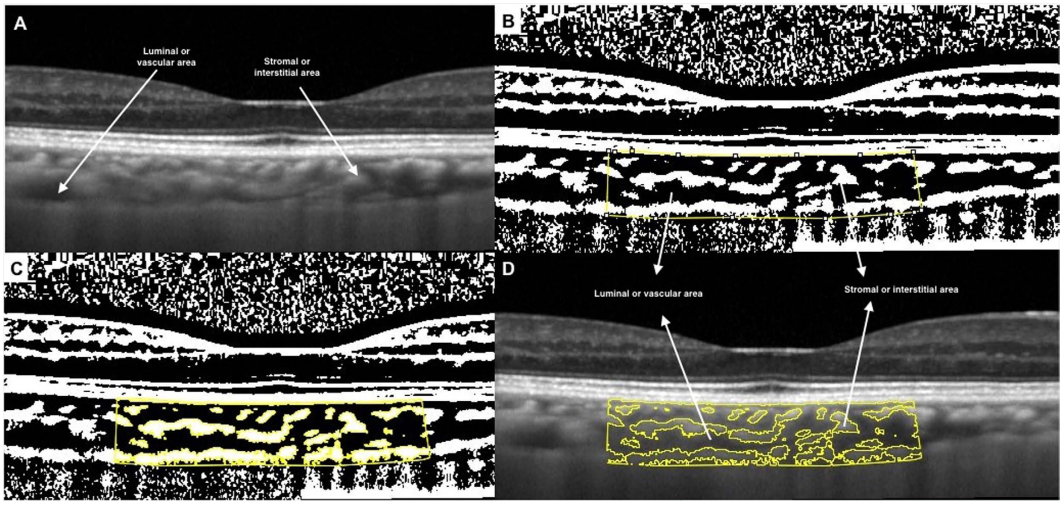

Figure 1. Image binarization for choroid with normal choroidal thickness. (**A**) Original SD OCT image. (**B**) 1.5 mm segmentation block of the subfoveal choroidal area. (**C**) Segmented OCT image using modified image binarization approach. (**D**) Overlay of region of interest created after image binarization was performed on the SD OCT image.

tomography (OCT) has allowed more precise non-invasive quantitative assessment of the choroid[28]. Using EDI OCT, there have been attempts to assess the choroidal stromal and vascular structures[13,29–32]. Recently Sonoda *et al.* described a method for computing luminal and interstitial areas in the choroid as a means to quantify vascular status of the choroid[30,31].

Adapting the image segmentation technique proposed by Sonoda *et al.*[30,31], we further propose a new quantitative parameter called choroidal vascularity index (CVI) to assess vascular status of the choroid through image binarization of EDI SD-OCT images in healthy eyes. Furthermore, we aimed to determine the ocular and systemic factors affecting the CVI as well as CT in subjects enrolled from a population-based study in Singapore. This index may provide additional information on the morphology and physiology of the choroid and may be a more robust marker compared to CT.

Methods

Study population. The data for this study was derived from the Singapore Malay Eye Study-2 (SiMES-2), a population based cohort study of 45–85 years old Malay adults living in Singapore. This study was conducted as per the tenets set forth in the Declaration of Helsinki, and ethics committee approval was obtained from the Institutional Review Board of Singapore Eye Research Institute. Written informed consent was obtained from the subjects after explanation about the details of the study and any potential risks involved with the study and consequences of the study.

Study subjects. Details of the study design, and methodology have been reported elsewhere[33]. In this study, we enrolled 400 consecutive participants from February 2012 to April 2013. Exclusion criteria included: logarithmic minimum angle of resolution (logMAR) visual acuity >0.30, spherical equivalent (SE) <-6 diopter, evidence of vitreo-retinal diseases such as age related macular degeneration and diabetic retinopathy, previous ocular surgery or clinical features compatible with a diagnosis of glaucoma and Spectralis OCT imaging with a quality index <18 decibels. Glaucoma was defined using the International Society of Geographic and Epidemiological Ophthalmology scheme[34], based on findings from gonioscopy, optic disc characteristics, and visual fields results.

Choroidal thickness assessment. The choroid was imaged using the EDI mode of SD-OCT (Spectralis, Heidelberg Engineering, Heidelberg, Germany). The macular region was scanned using a 7 horizontal line scan ($30° \times 5°$) centred on the fovea, with 100 frames averaged in each B-scan. Each scan was 8.9 mm in length and spaced 240 μm apart from each other. In our study, Bruch's membrane and the choroid-scleral interface were delineated with the automatic segmentation algorithm developed by Tian *et al.*[35] which demonstrated excellent repeatability in our previously reported population-based study[36]. The choroidal thickness was automatically measured as the distance between the Bruch's membrane (lower boundary of retinal pigmented epithelium [RPE]) and the choroid-scleral interface. Although measurements of both eyes of each study participant were obtained, due to inter eye correlation only the right eye was used for further analysis.

Image binarization details. The same raster scan passing through the fovea was selected for binarization. It was segmented using the protocol described by Sonoda *et al.*[30–31] with minor modifications. The image binarization was done using public domain software, Image J (version 1.47; http://imagej.nih.gov/ij/). The subfoveal choroidal area with a width of 1.5 mm, centred at the fovea, was selected (Fig. 1A) and this constituted the region of interest. Only 1.5 mm of the macular area on the single line scan was selected as a representative segment of the

macular region due to segmental nature of the choroidal blood supply as described by Hayreh[37]. The posterior ciliary arteries and their branches along with terminal choroidal arterioles, the choriocapillaris, and the vortex veins have a segmental or lobular distribution in the choroid.

Image binarization techniques can be used to convert grey scale images into binarized images. This facilitates tasks such as image layout analysis and image skew estimation. An appropriate image binarization technique, taking into account the uneven illumination, image contrast variation and poor image resolution, is essential to accurately apply a threshold to an image. Different image binarization or thresholding techniques like Otsu's, Bernsen's and Niblack's autolocal thresholding techniques were hence attempted[38,39]. Otsu's is a global thresholding technique while Bernsen's is local thresholding technique. After comparing the different image segmentation techniques, we adopted Niblack's autolocal threshold technique in our current study. This is because it takes into consideration the mean and standard deviation of all the pixels in the region of interest. In addition, given that binarization could be influenced by the variation in the amount of melanin in RPE in different eyes, and also affected by the direction of light and focussing issues, these were taken into account by using a distinct binarization threshold for individual subject.

Using Niblack's autolocal threshold tool, the image was first binarized to get a clear view of the choroid-scleral interface (Fig. 1B). This was to allow more precise selection of the subfoveal choroid area. This is in contrast to Sonoda's *et al.*[30,31] protocol in which the polygonal area was selected prior to image binarization. In addition, we did not preselect vessels of size more than 100 um.

With the upper border marked at the RPE and the lower border the line of light pixels at the choroid scleral junction, the choroidal area was selected using polygon tool and added to the region of interest manager (Fig. 1B). The image was then converted to RGB (red, green, blue) colour to allow the colour threshold tool to select the dark pixels (Fig. 1C). The total subfoveal circumscribed choroidal area (TCA) and the area of dark pixels were calculated. The luminal area (LA) was defined as the area of dark pixels. Stromal area (SA) was further calculated by subtracting LA from TCA. To determine the vascularity status of the choroid, CVI was computed by dividing LA by TCA. In addition, the proportion of dark (LA) to light areas (SA) was also computed. Fig. 1D represents the overlay image of the region on interest on the original EDI OCT scan.

Inter-rater and Intra-rater agreement. 10% of the total images (35 images), were initially segmented by two graders (KAT and RA) to determine inter-rater agreement. The same set of images was segmented by one grader (KAT) after an interval of one week to compute intra-rater reliability. The intra- and inter-rater reliability for the image binarization was measured by the absolute agreement model of the intra-class correlation coefficient (ICC)[40]. ICC value of 0.81–1.00 indicates good agreement. Values of less than 0.40 indicate poor to fair agreement. We also performed Bland-Altman plot analyses[41,42] to determine the mean difference between the measurements. The Bland-Altman plots were constructed using MedCalc version 12.3 (Medcalc Software, Ostend, Belgium) software. Moreover, random scans, including those with thick and thin choroid, were further reviewed by both graders to ensure good inter-rater agreement. After obtaining good inter-rater and intra-rater agreement, all the scans were binarized by single author (KAT).

Measurement of ocular factors. Each participant underwent a standardized examination. Refraction and corneal curvature were measured using an auto-keratorefractor (Canon RK 5 Auto Ref-Keratometer, Canon Inc. Ltd., Tochigiken, Japan). SE was calculated as the sum of the spherical power and half of the cylinder power. Best-corrected visual acuity was measured monocularly using a LogMAR chart (Lighthouse International, New York, USA) at a distance of 4 meters. Ocular biometry, including axial length (AL), was measured using non-contact partial coherence interferometry (IOL Master V3.01, Carl Zeiss Meditec AG, Jena, Germany). Intraocular pressure (IOP) was measured using Goldmann applanation tonometry (Haag-Streit, Bern, Switzerland) before pupil dilation. Standardized visual field testing was performed with static automated white-on-white threshold perimetry (SITA Fast 24-2, Humphrey Field Analyzer II; Carl Zeiss Meditec, Inc., Oberkochen, Germany). Slit-lamp biomicroscopy (Haag-Streit model BQ-900; Haag-Streit, Switzerland) was performed by the study ophthalmologists to examine the anterior chamber and lens after pupil dilation with tropicamide 1% and phenylephrine hydrochloride 2.5%.

Measurement of systemic factors. A detailed interviewer-administered questionnaire was used to collect demographic data, lifestyle risk factors (e.g. smoking, alcohol consumption), medical history (e.g. hypertension, diabetes), ocular history (e.g. glaucoma), and medication use from all participants. Systolic and diastolic blood pressures (BP) were measured using a digital automatic blood pressure monitor (Dinamap model Pro Series DP110X-RW, 100V2; GE Medical Systems Information Technologies, Inc., Milwaukee, WI), after subjects were seated for at least five minutes. BP was measured twice, with measurements 5 minutes apart. A third measurement was taken if the previous 2 systolic BP readings differed by more than 10 mmHg or the diastolic BP differed by more than 5 mmHg. The mean of the two closest BP readings was taken as each participant's BP.

Mean ocular perfusion pressure (OPP) was calculated using the following equation: mean OPP = (2/3 × mean arterial pressure [MAP] – IOP), where MAP = diastolic BP + (1/3 × [systolic BP – diastolic BP]). Body mass index (BMI) was calculated as body weight (in kilograms) divided by body height (in meters) squared. Smoking status was defined as those currently smoking, ex-smokers and non-smokers. Nonfasting venous blood samples were analysed at the National University Hospital Reference Laboratory for biochemical testing of serum total cholesterol, triglycerides, glycosylated haemoglobin (HbA1c), serum glucose level and creatinine.

Statistical methods. Statistical analysis was performed using SPSS version 20.0 (SPSS, Inc., Chicago, IL, USA). Since CVI and subfoveal choroidal thickness (SFCT) have different measurement units, we used the coefficient of variation (COV) to compare the variability between CVI and SFCT. Univariate and multiple linear

Characteristics	Mean ± SD	Range
Age, yrs	61.53 ± 8.77	47.19 to 86.72
Gender, male (%)	155 (44.9%)	
Axial length, mm	23.58 ± 0.96	21.60 to 27.89
IOP, mm Hg	14.41 ± 2.84	6 to 20
Ocular perfusion pressure, mmHg	55.68 ± 8.39	37.44 to 96.11
Systolic blood pressure, mmHg	139.21 ± 20.63	95 to 226.50
Diastolic blood pressure mmHg	77.27 ± 10.85	54.50 to 133
Body mass index, kg/m^2	26.75± 5.13	12.15 to 52.95
Serum glucose, mmol/L	6.98 ± 3.35	2.8 to 22.9
HbA1c, %	6.26 ± 1.27	4.3 to 11.7
Total cholesterol, mmol/L	5.43 ± 1.26	2.49 to 10.40
Triglycerides, mmol/L	1.95 ± 1.38	0.42 to 14.95
Blood creatinine, mmol/L	78.92 ± 33.11	30 to 412
Current smoking, %	68 (19.8%)	
Alcohol consumption, %	5 (1.5%)	
Choroidal Parameters		
TCA, mm^2	0.74 ± 0.21	0.198 to 1.237
LA, mm^2	0.49 ± 0.15	0.122 to 0.817
SA, mm^2	0.25 ± 0.06	0.076 to 0.441
CVI (LA/TCA)	65.61 ± 2.33	60.07 to 71.27
LA/SA	1.92 ± 0.20	1.50, 2.48
SFCT, μm	241.34 ± 97.11	40.24, 519.48

Table 1. Demographics, clinical and choroidal characteristics of study subjects (n = 345). Data presented are means ± standard deviations, except for gender, HbA1c , current smoking and alcohol consumption which are number (%). TCA, total sub-foveal choroidal area; LA, luminal area; SA, stromal area; CVI, choroidal vascularity index; LA/SA, luminal area/ stromal area; SFCT, sub-foveal choroidal thickness.

regression analyses were performed to determine the associations of SFCT and CVI (dependent variables) with ocular and systemic factors (independent variables). For multiple linear regression, factors showing significant association in univariate analysis ($p < 0.10$) were included. All p values were 2-sided and considered statistically significant when the values were less than 0.05.

Results

A total of 400 subjects were recruited for this study. We excluded 55 subjects for the following reasons: visual acuity worse than 0.30 (n = 9), SE < −6 diopter (n = 7), glaucoma (n = 6), presence of macular or vitreo-retinal diseases (n = 18) and poor OCT image quality (n = 15). A total of 345 eyes from 345 subjects were included in the final analysis; 190 (55%) subjects were female. The demographics, ocular, systemic and choroidal characteristics of the study subjects are shown in Table 1. In terms of choroidal characteristics, mean TCA was 0.74 ± 0.21 mm^2 and mean LA was 0.49 ± 0.15 mm^2. Mean SFCT was 241.34 ± 97.11 μm (range, 40.24–519.48 μm) and mean CVI was 65.61 ± 2.33% (range, 60.07–71.27%).

CVI was found to have lower COV (3.55) than SFCT (COV = 40.30), indicating CVI to be less variable than SFCT. The histogram plots (Fig. 2A,B) represent the distribution of SFCT and CVI in relation to normal density plot.

Using image binarization, the intra- (ICC: 0.97 to 0.99 for TCA and ICC: 0.91 to 0.98 for LA) and inter-grader reliability (ICC: 0.90 to 0.97 for TCA and ICC: 0.89 to 0.97 for LA) were excellent for both TCA and LA (Table 2). Bland Altman plot analysis of intra- and inter-rater reliability for TCA (Fig. 3A,B) and LA (Fig. 3C,D) at sub-foveal location was excellent.

In Table 3, the multiple regression model shows younger age, shorter AL, higher IOP, higher LA and lower systolic blood pressure to be significantly ($p < 0.05$) associated with thicker sub-foveal choroid. However, among factors associated with CVI (Table 4), in the multiple regression model, SFCT was the only factor associated with CVI. A thicker sub-foveal choroid was significantly ($p < 0.001$) associated with higher CVI. There were no other statistically significant association between CVI and any other factors (Table 4).

Discussion

In this population-based study, using the modified Sonoda's image binarization technique for EDI SD-OCT scans, we propose an OCT based metric termed "CVI" to assess vascularity of the choroid. Our results validated the findings obtained by Sonoda *et al.* and found that on a single cross sectional scan, nearly two third (~66%) of the subfoveal choroid is vascular in healthy eyes. Importantly, CVI showed lesser variability and was influenced by fewer physiologic factors as opposed to CT, indicating CVI to be a relatively stable index for studying the changes in the choroid. As the choroid is primarily a vascular structure, understanding of this new vascular index may

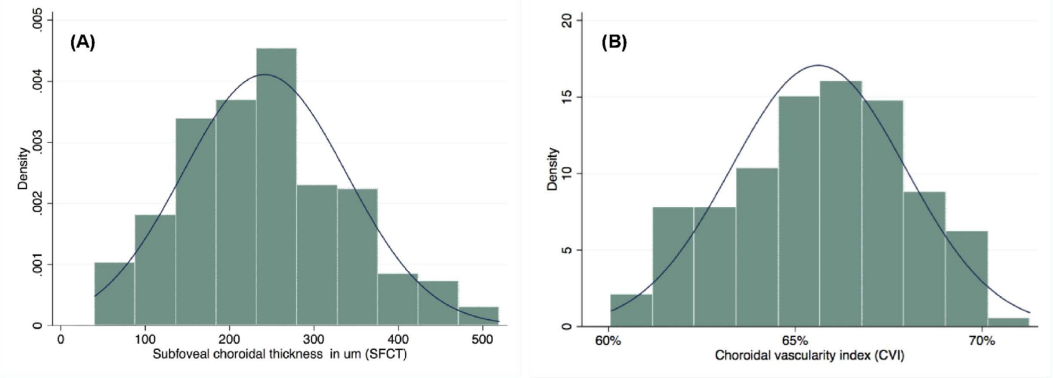

Figure 2. Distribution of subfoveal choroidal thickness (**A**) and choroidal vascularity index (**B**) across the population.

	Intra Rater		Intra Rater	
	ICC (95% CI)	Mean difference (95% LOA)	ICC (95% CI)	Mean difference (95% LOA)
TCA	0.99 (0.97 to 0.99)	−0.01 (−0.16 to 0.13)	0.94 (0.90 to 0.97)	0 (−0.06 to 0.07)
LA	0.96 (0.91 to 0.98)	−0.01 (−0.11 to 0.09)	0.94 (0.89 to 0.97)	0.01 (−0.07 to 0.10)

Table 2. Intra- and inter-grader reliability assessment of choroidal parameters in 35 subjects. TCA, total sub-foveal choroidal area; LA, luminal area; ICC, intraclass correlation coefficient; CI, confidence interval; LOA, limits of agreement.

help to further elucidate the role of vascular processes within the choroid in disease development and progression. We hence propose CVI as an independent surrogate marker to assess choroidal health in future studies.

Several studies have assessed the vascular structures of the choroid by OCT[13,29], but they required customized software that limited their widespread use. There are reports[30,31] on the differentiation and quantification of the structural components of the choroid (luminal and interstitial areas), using freely and easily accessible software, *Image J,* these studies were performed in clinic-based settings with a potential selection and sampling biases. We have highlighted the significant differences in our protocol with that proposed by Sonoda *et al.*[30,31] in Table 5. Our modification of applying auto local threshold prior to image binarization enabled us to accurately localise choroid scleral interface giving more precise selection of the choroid. In addition, the simple binarization technique without pre-selection of larger choroidal vessels allowed nearly accurate estimation of vascularity of the choroid even with a very simple algorithm, which can be reproduced by the large research community.

Although there is no concrete evidence that the dark areas represented the vascular areas and the light areas the stromal areas, the findings of earlier studies and that of numerous empirical observations suggest that the dark areas were the vascular components in the binarized images[13,29]. In addition, a comparison of the original EDI-OCT images to the binary images (Fig. 1) revealed that the dark areas corresponded with vascular components of the choroid, including both the larger and smaller choroidal vessels. Therefore, the binarization technique developed by Sonoda *et al.*[30,31], which was further simplified by us, is valid and offers precise segmentation of choroidal vasculature from stroma.

Interestingly, when comparing the factors affecting SFCT to those that affect CVI, we found SFCT to be associated with many physiological factors such as age, AL, IOP and, most significantly, the vascular area in the choroid (LA), whereas stromal area did not have a significant association with SFCT. On the other hand, CVI was only affected by SFCT, but was not affected by most of the physiological variables. Moreover, SFCT demonstrated relatively greater variability (mean SFCT was $241.34 \pm 97.11\,\mu m$, COV = 40.30) compared to CVI (mean CVI was $65.61 \pm 2.33\%$, COV = 3.55). Thus our results suggest CVI to be a better and relatively more stable marker to monitor choroid compared to CT, which is affected by more variables and demonstrated greater variability. Clinically, measuring the proportion of vascularity of the eye would provide us with a deeper understanding of how disease processes affect different structures in the eye, and therefore may be more informative compared to CT measurements alone.

We have demonstrated a significant association of SFCT with vascular area of the choroid. This signifies the fact that the vascular area is the predominant segment influencing the CT in normal population. An increase in CVI reflects either an increase in the number of blood vessels or in the diameter of the choroidal blood vessels within a designated area. Hayreh[37] demonstrated the vulnerability of submacular choroidal supply to generalised chronic ischaemic disorders (age related macular degeneration), due to numerous watershed zones of the short posterior ciliary arteries in the choroid. There can be potential clinical implications of the CVI, which can be explored in further studies. A decrease in CVI on EDI OCT scans at baseline may be an indicator of choroidal ischemia in patients with macular disorders like age related macular degeneration or diabetes. On the other hand,

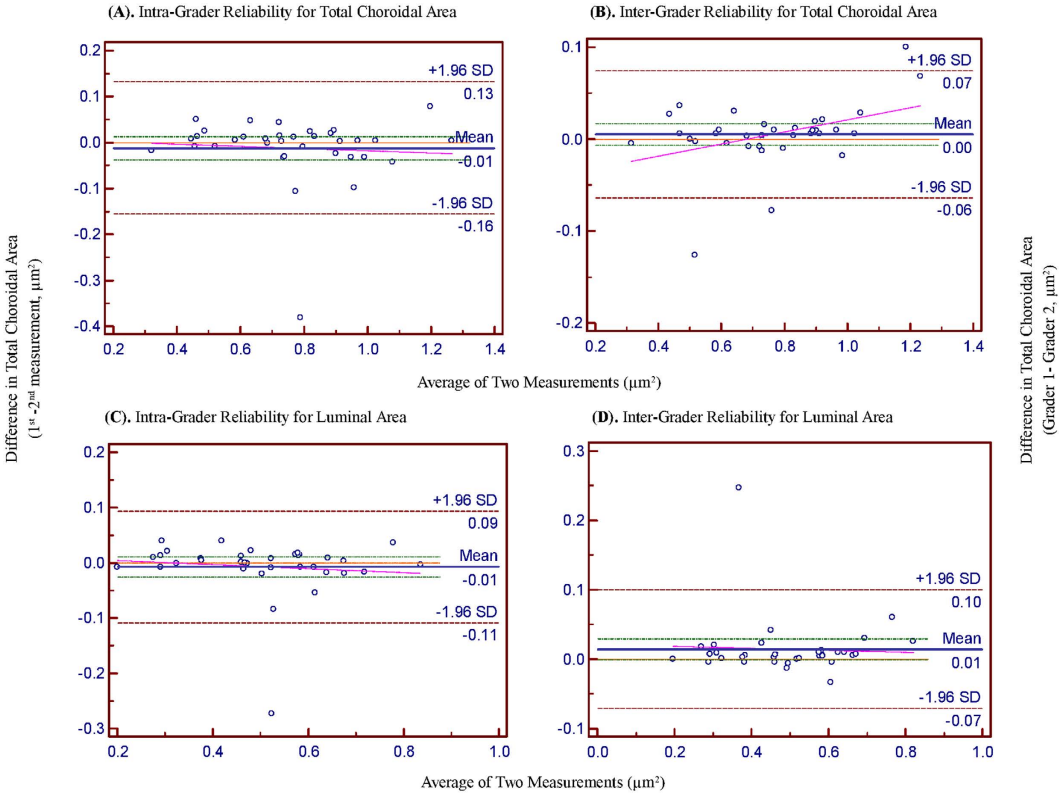

Figure 3. Bland Altman plots of total choroidal area and luminal area. (**A**) and (**B**) shows intra- and inter- rater reliability for total choroidal area respectively. (**C**) and (**D**) shows intra- and inter- rater reliability for luminal area respectively. For intra-rater reliability, the difference was calculated by the 1st measurement minus the 2nd measurement. Pink dashed line represents regression line of difference between 1st and 2nd measurements. For inter-rater reliability, the difference was calculated by the grader 1 measurement minus the grader 2 measurement. Pink dashed line represents regression line of difference between the two graders measurements.

	Univariate			Multivariate*		
	Unstandardized β	Standardized β	P-value	Unstandardized β	Standardized β	P-value
Ocular factors						
Axial length, mm	−15.348	−0.155	0.005	−10.508	−0.105	0.002
IOP, mmHg	3.160	0.092	0.087	3.619	0.105	0.002
OPP, mm Hg	−0.354	-0.031	0.572	–	–	–
LA, mm^2	523.214	0.814	<0.001	459.729	0.714	<0.001
SA, mm^2	1132.841	0.787	<0.001	68.271	0.047	0.669
Systemic factors						
Age, yrs	−3.986	−0.360	<0.001	−0.856	−0.077	0.041
Gender, female	−22.274	−0.114	0.034	−13.171	−0.068	0.068
Body mass index, kg/m^2	−1.173	−0.062	0.252	–	–	–
Systolic blood pressure, mmHg	−0.499	−0106	0.050	−0.328	−0.071	0.043
Diastolic blood pressure mmHg	0.749	0.084	0.122	–	–	–
Serum glucose, mmol/L	0.102	0.004	0.949	–	–	–
HbA1c, %	5.913	0.077	0.157	–	–	–
Total cholesterol, mmol/L	8.092	0.106	0.052	−0.525	−0.007	0.836
Triglycerides, mmol/L	3.456	0.049	0.366	–	–	–
Blood creatinine, mmol/L	-0.050	-0.017	0.754	–	–	–
Current smoking, (yes vs no)	28.392	0.116	0.031	−11.737	−0.049	0.187
Alcohol consumption, (yes vs no)	−19.833	0.024	0.651	–	–	–

Table 3. Linear regression analyses of ocular and systemic factors associated with sub-foveal choroidal thickness. *Adjusted for variables with a p-value < 0.10 in the univariate analysis. β, regression coefficient.

	Univariate			Multivariate*		
	Unstandardized β	Standardized β	P-value	Unstandardized β	Standardized β	P-value
Ocular factors						
Axial length, mm	−0.274	−0.113	0.039	−0.106	−0.004	0.375
IOP, mmHg	−0.014	−0.018	0.745	–	–	–
OPP, mmHg	0.022	0.080	0.136	–	–	–
SFCT, μm	0.012	0.519	<0.001	0.012	0.484	<0.001
Systemic factors						
Age, yrs	−0.057	−0.215	<0.001	−0.001	−0.003	0.950
Gender, female	−0.706	−0.151	0.005	−0.183	−0.039	0.482
Body mass index, kg/m^2	−0.026	−0.058	0.283	–	–	–
Systolic blood pressure, mmHg	−0.001	−0.012	0.818	–	–	–
Diastolic blood pressure mmHg	0.031	0.145	0.007	0.019	0.089	0.072
Serum glucose, mmol/L	0.025	0.036	0.511	–	–	–
HbA1c, %	0.034	0.018	0.736	–	–	–
Total cholesterol, mmol/L	0.115	0.062	0.256	–	–	–
Triglycerides, mmol/L	0.130	0.077	0.158	–	–	–
Blood creatinine, mmol/L	0.003	0.035	0.516	–	–	–
Current smoking, (yes vs no)	1.098	0.187	<0.001	0.535	0.092	0.088
Alcohol consumption, (yes vs no)	1.004	0.051	0.341	–	–	–

Table 4. Linear regression analyses of ocular and systemic factors associated with choroidal vascularity index. *Adjusted for variables with a p-value < 0.10 in the univariate analysis. β, regression coefficient.

	Sonoda *et al.* (2014)[30]	Sonoda *et al.* (2015)[31]	Current study
Study sample size	15 eyes of 15 subjects	180 eyes of 180 subjects	345 eyes of 345 subjects
Choroidal area measured	1.5 mm	7.5 mm	1.5 mm
Location of measurement	Centered on fovea , 1500 um	Entire raster scan, 7500 um	Centered on fovea (1500 um) due to the segmental nature of choroidal blood supply as described by Hayreh *et al.*[37]
Pre-selection of vessels	3 choroidal vessels with lumens >100 mm were randomly selected and the average reflectivity of these areas was determined by the software		Used autolocal threshold techniques to allow binarization of smaller choroidal vessels or choriocapillaris.
Brightness adjustment	Average brightness was set as the minimum value		Brightness was not adjusted as it would reduce the contrast between luminal and stromal areas and possibly affect the autolocal threshold.
Order of binarization	Region of interest selected prior to image binarization		To get a clear view of the choroid-scleral interface, image binarization was performed prior to area selection.
Image segmentation time	~5 minutes per image		~1 minute per image

Table 5. Image binarization protocol in Sonoda *et al.* vs current study.

we may use CVI to determine increase in vascularity of the choroid in posterior uveitis or central serous chorioretinopathy. CVI can also be used as a follow up tool for treatment response and resolution of diseases.

The strengths of our study include a large sample size with a single common ethnicity. Hence, our findings were unlikely to be confounded by ethnic heterogeneity. Standardized clinical examination protocols, as well as reliable differentiation and quantifications of choroidal morphometric parameters and OCT parameters were used in our study. Nevertheless, this study has few limitations. First, binarization of choroidal images was performed only in the right eye of each study subject. There may exist inter-eye differences, yet such differences should be small. Second, the CT measurements in our study were not performed at the same time of the day; each participant underwent the OCT examination in a randomized manner with respect to when the readings were obtained. It seems unlikely that circadian changes may have influenced the results of our investigation. Third, although our images were binarized at standard threshold, there is a possibility of over or underestimation of both SA and LA.

In conclusion, in this population-based study, we introduced a novel OCT based marker termed "CVI" to assess vascularity of the subfoveal choroid. Our result showed that on a single cross sectional EDI-OCT image, two-third (~66%) of the subfoveal choroid is vascular in healthy eyes. This index should provide a new means of studying the pathophysiology of human choroid in greater detail. However, larger studies for different disease models are warranted to further validate the application of this index in clinical practice. Whether CVI is a complimentary or substitute tool to CT can only be answered based on the proposed studies in choroidal diseases.

References

1. Alm, A. & Bill, A. Ocular and optic nerve blood flow at normal and increased intraocular pressures in monkeys (Macaca irus): a study with radioactively labelled microspheres including flow determinations in brain and some other tissues. *Exp Eye Res* **15,** 15–29 (1973).
2. Nickla, D. L. & Wallman, J. The multifunctional choroid. *Prog Retin Eye Res* **29,** 144–168 (2010).
3. Chung, S. E., Kang, S. W., Lee, J. H. & Kim, Y. T. Choroidal thickness in polypoidal choroidal vasculopathy and exudative age-related macular degeneration. *Ophthalmology* **118,** 840–845 (2011).
4. Fujiwara, T., Imamura, Y., Margolis, R., Slakter, J. S. & Spaide, R. F. Enhanced depth imaging optical coherence tomography of the choroid in highly myopic eyes. *Am J Ophthalmol* **148,** 445–450 (2009).
5. Gomi, F. & Tano, Y. Polypoidal choroidal vasculopathy and treatments. *Curr Opin Ophthalmol* **19,** 208–212 (2008).
6. Grossniklaus, H. E. & Green, W. R. Choroidal neovascularization. *Am J Ophthalmol* **137,** 496–503 (2004).
7. Gupta, B. & Mohamed, M. D. Photodynamic therapy for variant central serous chorioretinopathy: efficacy and side effects. *Ophthalmologica* **225,** 207–210 (2011).
8. Ikuno, Y. & Tano, Y. Retinal and choroidal biometry in highly myopic eyes with spectral-domain optical coherence tomography. *Invest Ophthalmol Vis Sci* **50,** 3876–3880 (2009).
9. Koizumi, H., Yamagishi, T., Yamazaki, T., Kawasaki, R. & Kinoshita, S. Subfoveal choroidal thickness in typical age-related macular degeneration and polypoidal choroidal vasculopathy. *Graefes Arch Clin Exp Ophthalmol* **249,** 1123–1128 (2011).
10. Lutty, G. A., Cao, J. & McLeod, D. S. Relationship of polymorphonuclear leukocytes to capillary dropout in the human diabetic choroid. *Am J Pathol* **151,** 707–714 (1997).
11. Fryczkowski, A. W., Sato, S. E. & Hodes, B. L. Changes in the diabetic choroidal vasculature: scanning electron microscopy findings. *Ann Ophthalmol* **20,** 299–305 (1988).
12. Sakamoto, T., Murata, T. & Inomata, H. Class II major histocompatibility complex on melanocytes of Vogt-Koyanagi-Harada disease. *Arch Ophthalmol* **109,** 1270–1274 (1991).
13. Branchini, L. A. *et al.* Analysis of choroidal morphologic features and vasculature in healthy eyes using spectral-domain optical coherence tomography. *Ophthalmology* **120,** 1901–1908 (2013).
14. Lindner, M. *et al.* Choroidal thickness in geographic atrophy secondary to age-related macular degeneration. *Invest Ophthalmol Vis Sci* **56,** 875–882 (2015).
15. Young, M., Fallah, N. & Forooghian, F. Choroidal degeneration in birdshot chorioretinopathy. *Retina* **35,** 798–802 (2015).
16. Tseng, C. C. & Chen, S. N. Long-term efficacy of half-dose photodynamic therapy on chronic central serous chorioretinopathy. *Br J Ophthalmol* **99,** 1070–1077(2015).
17. Gupta, P. *et al.* Choroidal thickness and high myopia: a case-control study of young Chinese men in Singapore. *Acta ophthalmol*, doi: 10.1111/aos12631 (2014).
18. Kim, J. T., Lee, D. H., Joe, S. G., Kim, J. G. & Yoon, Y. H. Changes in choroidal thickness in relation to the severity of retinopathy and macular edema in type 2 diabetic patients. *Invest Ophthalmol Vis Sci* **54,** 3378–3384 (2013).
19. Wong, I. Y., Wong, R. L., Zhao, P. & Lai, W. W. Choroidal thickness in relation to hypercholesterolemia on enhanced depth imaging optical coherence tomography. *Retina* **33,** 423–428 (2013).
20. Ahn, S. J., Woo, S. J. & Park, K. H. Retinal and choroidal changes with severe hypertension and their association with visual outcome. *Invest Ophthalmol Vis Sci* **55,** 7775–7785 (2014).
21. Sizmaz, S. *et al.* The effect of smoking on choroidal thickness measured by optical coherence tomography. *Br J Ophthalmol* **97,** 601–604 (2013).
22. Takahashi, H. *et al.* Choroidal thickness in convalescent vogt-koyanagi-harada disease. *Retina* **34,** 775–780 (2014).
23. Lee, H. K., Lim, J. W. & Shin, M. C. Comparison of choroidal thickness in patients with diabetes by spectral-domain optical coherence tomography. *Korean J Ophthalmol* **27,** 433–439 (2013).
24. Unsal, E. *et al.* Choroidal thickness in patients with diabetic retinopathy. *Clin Ophthalmol* **8,** 637–642, (2014).
25. Gerendas, B. S. *et al.* Three-dimensional automated choroidal volume assessment on standard spectral-domain optical coherence tomography and correlation with the level of diabetic macular edema. *Am J Ophthalmol* **158,** 1039–1048 (2014).
26. Adhi, M., Brewer, E., Waheed, N. K. & Duker, J. S. Analysis of morphological features and vascular layers of choroid in diabetic retinopathy using spectral-domain optical coherence tomography. *JAMA Ophthalmol* **131,** 1267–1274 (2013).
27. Farias, L. B. *et al.* Choroidal thickness in patients with diabetes and microalbuminuria. *Ophthalmology* **121,** 2071–2073 (2014).
28. Spaide, R. F., Koizumi, H. & Pozzoni, M. C. Enhanced depth imaging spectral-domain optical coherence tomography. *Am J Ophthalmol* **146,** 496–500 (2008).
29. Sohrab, M., Wu, K. & Fawzi, A. A. A pilot study of morphometric analysis of choroidal vasculature *in vivo*, using en face optical coherence tomography. *PLoS One* **7,** doi: 10.1371/journal.pone.0048631 (2012).
30. Sonoda, S. *et al.* Choroidal structure in normal eyes and after photodynamic therapy determined by binarization of optical coherence tomographic images. *Invest Ophthalmol Vis Sci* **55,** 3893–3899 (2014).
31. Sonoda, S. *et al.* Luminal and stromal areas of choroid determined by binarization method of optical coherence tomographic images. *Am J Ophthalmol* **159,** 1123–1131 (2015).
32. Iwata, A. *et al.* Binarization of enhanced depth imaging optical coherence tomographic images of an eye with Wyburn-Mason syndrome: a case report. *BMC Ophthalmol* **15,** (2015).
33. Foong, A. W. *et al.* Rationale and methodology for a population-based study of eye diseases in Malay people: The Singapore Malay eye study (SiMES). *Ophthalmic Epidemiol* **14,** 25–35 (2007).
34. Foster, P. J., Buhrmann, R., Quigley, H. A. & Johnson, G. J. The definition and classification of glaucoma in prevalence surveys. *Br J Ophthalmol* **86,** 238–242 (2002).
35. Tian, J., Marziliano, P., Baskaran, M., Tun, T. A. & Aung, T. Automatic segmentation of the choroid in enhanced depth imaging optical coherence tomography images. *Biomed Opt Express* **4,** 397–411 (2013).
36. Gupta, P. *et al.* Distribution and determinants of choroidal thickness and volume using automated segmentation software in a population-based study. *Am J Ophthalmol* **159,** 293–301 (2015).
37. Hayreh, S. S. Segmental nature of the choroidal vasculature. *Br J Ophthalmol* **59,** 631–648 (1975).
38. Bernsen, J. Dynamic thresholding of grey-level images. Eighth International Conference of Pattern Recognition, France. Paris: Conference proceedings. doi: 10.5120/18107-9291 (1986 Oct).
39. Niblack, W. In *An Introduction to Digital Image Processing*. (Prentice Hall International Inc., 1986).
40. Fleiss, J. L. & Cohen, J. The Equivalence of Weighted Kappa and the Intraclass Correlation Coefficient as Measures of Reliability. *Educational and Psychological Measurement* **33,** 613–619 (1973).
41. Bland, J. M. & Altman, D. G. Statistical methods for assessing agreement between two methods of clinical measurement. *Lancet* **1,** 307–310 (1986).
42. Bland, J. M. & Altman, D. G. Agreed statistics: measurement method comparison. *Anesthesiology* **116,** 182–185 (2012).

Acknowledgements

This study was supported by a grant from National Medical Research Council, Singapore [Grant No. NMRC R760/44/2010]. The funding organization had no role in the design or conduct of this research.

Author Contributions

R.A.: conceived and designed the study, collected the data, analysed and interpreted the data, wrote the main manuscript text as well as reviewed the manuscript. P.G.: conceived and designed the study, collected the data, analysed and interpreted the data, wrote the main manuscript text as well as reviewed the manuscript. K-A.T.: collected the data and wrote the main manuscript text. C.M.G.C.: Reviewed the manuscript T.Y.W.: Reviewed the manuscript C-Y.C.: conceived and designed the study, analysed and interpreted the data, wrote the main manuscript text and reviewed the manuscript.

Additional Information

Competing financial interests: The authors declare no competing financial interests.

How to cite this article: Agrawal, R. *et al.* Choroidal vascularity index as a measure of vascular status of the choroid: Measurements in healthy eyes from a population-based study. *Sci. Rep.* **6**, 21090; doi: 10.1038/srep21090 (2016).

Relationship Between Peripapillary Choroid and Retinal Nerve Fiber Layer Thickness in a Population-Based Sample of Nonglaucomatous Eyes

PREETI GUPTA, CAROL Y. CHEUNG, MANI BASKARAN, JING TIAN, PINA MARZILIANO, ECOSSE L. LAMOUREUX, CHUI MING GEMMY CHEUNG, TIN AUNG, TIEN YIN WONG, AND CHING-YU CHENG

• PURPOSE: To describe the relationship between peripapillary choroidal thickness and retinal nerve fiber layer (RNFL) thickness in a population-based sample of nonglaucomatous eyes.

• DESIGN: Population-based, cross-sectional study.

• METHODS: A total of 478 nonglaucomatous subjects aged over 40 years were recruited from the Singapore Malay Eye Study (SiMES-2). All participants underwent a detailed ophthalmic examination, including Cirrus and Spectralis optical coherence tomography (OCT) for the measurements of RNFL thickness and peripapillary choroidal thickness, respectively. Associations between peripapillary choroidal thickness and RNFL thickness were assessed using linear regression models with generalized estimating equations.

• RESULTS: Of the 424 included subjects (843 nonglaucomatous eyes), 60.9% were women, and the mean (SD) age was 66.74 (10.44) years. The mean peripapillary choroidal thickness was 135.59 ± 56.74 μm and the mean RNFL thickness was 92.92 ± 11.41 μm. In terms of distribution profile, peripapillary choroid was thickest (150.04 ± 59.72 μm) at the superior and thinnest (110.71 ± 51.61 μm) at the inferior quadrant, whereas RNFL was thickest (118.60 ± 19.83 μm) at the inferior and thinnest (67.36 ± 11.36 μm) at the temporal quadrant. We found that thinner peripapillary choroidal thickness (PPCT) was independently associated with thinner RNFL thickness globally (regression coefficient [β] = −1.334 μm for per-SD decrease in PPCT, $P = .003$), and in the inferior (β = −2.565, $P = .001$) and superior (β = −2.340, $P = .001$) quadrants even after adjusting for potential confounders.

• CONCLUSIONS: Thinner peripapillary choroid was independently associated with thinner RNFL globally and in the inferior and superior regions. This structure-structure relationship may need further exploration in glaucomatous eyes prior to its application in clinical settings. (Am J Ophthalmol 2015;■:■–■. © 2015 by Elsevier Inc. All rights reserved.)

RETINAL NERVE FIBER LAYER (RNFL) THICKNESS changes are the earliest signs of glaucoma. These precede even optic nerve head (ONH) and visual field changes,[1,2] making the evaluation of RNFL thickness a crucial assessment in the early diagnosis of glaucoma.[3–5] Among the various factors associated with the development and progression of glaucoma, vascular and hemodynamic factors have been suggested to play an important role.[6,7] Studies[8,9] have now demonstrated vascular insufficiency of the ONH to be an important parameter in the pathogenesis of glaucomatous optic neuropathy. Since RNFL is formed by the expansion of the fibers of the optic nerve, any insufficient blood supply to the ONH could lead to thinner RNFL causing glaucomatous optic neuropathy.

Because of the common source of blood supply to the ONH and peripapillary choroid via the short posterior ciliary arteries,[10–13] it is likely that a relationship exists between peripapillary choroid and RNFL thickness. However, to date, no studies have explored the quantitative relationship between these parameters in normal subjects, particularly in the general population. Evaluation of the association between peripapillary choroidal thickness and RNFL thickness may help better elucidate the relationship between the structural parameters that may be useful clinically for assessment of ONH damage in glaucoma.

With the recent advancement in imaging technology using spectral-domain optical coherence tomography (SD OCT), in particular the enhanced depth imaging (EDI)

Accepted for publication Sep 11, 2015.

From the Singapore Eye Research Institute, Singapore National Eye Centre (P.G., C.Y.C., M.B., E.L.L., C.M.G.C., T.A., T.Y.W., C.-Y.C.); Department of Ophthalmology, Yong Loo Lin School of Medicine, National University of Singapore and National University Health System (P.G., C.Y.C., M.B., E.L.L., C.M.G.C., T.A., T.Y.W., C.-Y.C.); Duke-NUS Graduate Medical School (C.Y.C., M.B., E.L.L., C.M.G.C., T.A., T.Y.W., C.-Y.C.); and School of Electrical and Electronic Engineering, Nanyang Technological University (J.T., P.M.), Singapore.

Inquiries to Ching-Yu Cheng, Associate Professor, Academic Medicine Research Institute, Duke-NUS Graduate Medical School, Head, Ocular Epidemiology Research Group & Statistics Unit, Singapore Eye Research Institute, 20 College Road, The Academia, Level 6, Discovery Tower, Singapore 169856; e-mail: chingyu.cheng@duke-nus.edu.sg

0002-9394/$36.00
http://dx.doi.org/10.1016/j.ajo.2015.09.018

technique of SD OCT, objective and quantitative assessment of the peripapillary choroidal thickness is now possible. The purpose of this population-based, cross-sectional study was to evaluate the relationship between peripapillary choroidal thickness and RNFL thickness as measured by SD OCT in a large population sample of nonglaucomatous subjects. We further report the distribution profile of peripapillary choroidal thickness obtained using our automated choroidal segmentation software[14] and RNFL thickness in our population.

METHODS

• **STUDY POPULATION AND DESIGN:** Subjects of this study were enrolled from the Singapore Malay Eye Study (SiMES), a population-based cohort study of eye diseases in a Malay population aged 40–80 years in Singapore. The baseline examination was conducted between 2004 and 2006 and a follow-up examination of the SiMES participants was conducted between January 2011 and December 2013.[15] For this study, we consecutively recruited 478 subjects from SiMES participants who attended the follow-up examination from February 2012 to July 2013. Written informed consent was obtained from all participants after explanation of the nature and possible consequences of the study. The study adhered to the tenets of the Declaration of Helsinki, and ethics approval was obtained from the Singapore Eye Research Institute Institutional Review Board.

• **OCULAR EXAMINATIONS:** Each study participant underwent a standard ophthalmic examination including measurement of refraction and visual acuity, slit-lamp biomicroscopy, tonometry, pachymetry, perimetry, ocular biometry, fundus examination, and SD OCT imaging. Refraction and corneal curvature were measured using an autokeratorefractometer (Canon RK 5 Auto Ref-Keratometer; Canon Inc Ltd, Tochigiken, Japan). Spherical equivalent (SE) was calculated as the sum of the spherical power and half of the cylinder power. Best-corrected visual acuity (BCVA) was measured monocularly using a logarithm of the minimal angle of resolution (logMAR) chart (Lighthouse International, New York, New York, USA) at a distance of 4 m. Central corneal thickness was measured using an ultrasound pachymeter (Advent; Mentor O & O Inc, Norwell, Massachusetts, USA). Ocular biometry, including axial length (AL), was measured using noncontact partial coherence interferometry (IOL Master V3.01; Carl Zeiss Meditec AG, Jena, Germany). Intraocular pressure (IOP) was measured using Goldmann applanation tonometry (Haag-Streit, Bern, Switzerland) before pupil dilation. Standardized visual field testing was performed with static automated white-on-white threshold perimetry (SITA Fast 24-2, Humphrey Field Analyzer II; Carl Zeiss Meditec, Inc, Oberkochen, Germany). Slit-lamp biomicroscopy (Haag-Streit model BQ-900; Haag-Streit) was performed by the study ophthalmologists to examine the anterior chamber and lens after pupil dilation with tropicamide 1% and phenylephrine hydrochloride 2.5%.

Glaucoma was defined using the International Society of Geographic and Epidemiological Ophthalmology scheme,[16] based on findings from gonioscopy, optic disc characteristics, and visual fields results (as described below).

• **VISUAL FIELD EXAMINATION:** Standardized visual field testing was performed with static automated perimetry (Swedish Interactive Threshold Algorithm standard 24-2, Humphery Field Analyzer II; Carl Zeiss Meditec, Dublin, California, USA). A visual field was defined as reliable when fixation losses were less than 20%, and false-positive and false-negative rates were less than 33%. A glaucomatous visual field defect was defined as the presence of 3 or more significant ($P < .05$) nonedge continuous points with at least 1 at the $P < .01$ level on the same side of the horizontal meridian in the pattern deviation plot, and classified as "outside normal limits" on the Glaucoma Hemifield Test, confirmed on 2 consecutive visual field examinations.

SiMES is part of the Singapore Epidemiology Eye Diseases (SEED) study.[17] For the purpose of conformity between other studies in SEED, we have used Cirrus HD-OCT for RNFL thickness measurements and Spectralis SD OCT with EDI for choroidal measurements. In addition, we believe that the use of 2 SD OCT machines has its own advantages, as systematic measurement error in 1 machine, if existing, could lead to a biased association between peripapillary choroidal thickness and RNFL thickness, whereas this could be taken care of by the use of 2 machines.

• **RETINAL NERVE FIBER LAYER IMAGING AND MEASUREMENT:** Cirrus HD-OCT (software version 6.0; Carl Zeiss Meditec, Inc, Dublin, California, USA) was used to measure peripapillary RNFL. After pupil dilation, RNFL scan acquisitions were performed for each participant using an optic disc cube 200 × 200 scan protocol, which generates a cube of data in a 6 mm × 6 mm grid with 200 × 200 axial measurements. In brief, the subject's pupil was first centered and focused in an iris viewing camera on the acquire screen, and the line scanning ophthalmoscope (LSO) with "auto focus" mode was then used to optimize the view of the retina. The "center" and "enhance" modes were used to optimize the Z-offset and scan polarization, respectively, for the OCT scan to maximize the OCT signal. Rescanning was performed if a motion artifact or saccades through the calculation circle (3.46 mm diameter around the ONH) were detected. The OCT scans were excluded if there was the presence of RNFL or ONH

algorithm segmentation failure. All the OCT scans included in the study had signal strength of at least 6, which is considered as acceptable quality. RNFL thicknesses (average, clock hours, and quadrants) were derived automatically from a single scan using the in-built automated software for segmentation and parameter measurements without manual operator adjustment.

• **PERIPAPILLARY CHOROIDAL THICKNESS IMAGING AND MEASUREMENT:** Peripapillary choroid was imaged using the EDI mode of the Spectralis SD OCT. EDI is a method that improves resolution of choroidal details as the zero-delay line with the highest sensitivity is closer to the choroid, and more accurate image acquisition is possible in comparison with those of standard retinal SD OCT methods.[18] Following the Spectralis user manual guidelines, subjects' keratometry readings and the refraction data were entered into the machine to estimate optical magnification and, therefore, to allow for more accurate comparisons across individuals. The peripapillary region was scanned using a 360 degree, 3.4-mm-diameter circle that was centered on the optic disc, each comprising 100 averaged scans (using the proprietary automatic averaging and eye tracking features of the device). Scans were centered using an internal fixation and centering was confirmed by a scanning laser ophthalmoscope integrated into the instrument.

In our study, the Bruch membrane and choroidal-scleral interface were delineated with the automatic segmentation algorithm developed by Tian and associates.[14] This algorithm demonstrated good consistency with the manual measurements of choroidal thickness (the average of the Dice coefficients over 45 tested images was 90.5% with standard deviation of 3%).[14] The peripapillary choroidal thickness in the optic disc region was automatically measured as the perpendicular distance between the outer portion of the hyperreflective line corresponding to the RPE and the hyporeflective line or margin corresponding to the choroidal-scleral interface at the 12 discrete locations (30 degrees apart) and the 4 quadrants. In our recently published paper[19] using automated choroidal segmentation software we have demonstrated excellent intra-session repeatability (intraclass correlation coefficient ranging from 0.9998 to 0.999) of peripapillary choroidal thickness measurement at all 4 quadrants.

• **EXCLUSION CRITERIA:** For our analyses, we excluded subjects based on the following criteria: best-corrected logMAR visual acuity >0.30, SE greater than 6 diopter, and clinical features compatible with a diagnosis of glaucoma. The quality of the SD OCT image was assessed prior to the analysis, and images that had motion artifacts or were of insufficient quality (signal strength of <6 for Cirrus OCT and a quality index of <25 decibels for Spectralis OCT, as suggested by the manufacturer, for the image quality assurance) for a reliable determination of RNFL thickness and peripapillary choroidal thickness were excluded. Of the 478 total subjects (947 eyes) examined, 104 eyes were excluded (5 eyes with best-corrected logMAR visual acuity >0.30, 14 eyes with SE greater than -6 diopter, 42 eyes with a diagnosis of glaucoma, and 43 eyes with poor OCT image quality), leaving 843 nonglaucomatous eyes for final analysis.

• **STATISTICAL ANALYSIS:** Mean and standard deviation (SD) of both peripapillary choroidal thickness and RNFL thickness was calculated in all subjects for clock hours and 4 quadrants. Associations of peripapillary choroidal thickness (independent variable of interest) with RNFL thicknesses (dependent variable) were assessed using linear regression. Generalized estimating equations (exchangeable correlation matrix) were used to account for the correlation between pairs of eyes for each individual. Factors such as age, sex, AL, IOP, diabetic retinopathy, and age-related macular degeneration were included in the multivariate model to adjust for potential confounding. Statistical significance was set at $P < .05$ unless otherwise indicated. The data were analyzed with MedCalc version 12.3 (Medcalc Software, Ostend, Belgium) and SPSS version 20.0 (SPSS, Inc, Chicago, Illinois, USA).

RESULTS

A TOTAL OF 843 EYES FROM 424 SUBJECTS WERE INCLUDED IN the study. Of the 424 subjects, 363 (85.6%) did not have any eye diseases; the remaining 61 (14.4%) had eye diseases including diabetic retinopathy (8.5%) and early (5.2%) and late (0.6%) age-related macular degeneration. The included participants' mean age was 66.74 ± 10.44 years and 258 (60.9%) participants were female. The clinical characteristics of the included and excluded eyes are shown in Table 1. Compared to the eyes included in the analysis, excluded eyes were more myopic and had poor BCVA.

Table 2 presents the distribution of mean peripapillary choroidal thickness and RNFL thickness measured at 12 clock hours and 4 quadrants (superior, nasal, inferior, and temporal). The average peripapillary choroidal thickness was 135.59 ± 56.74 μm and the average RFNL thickness was 92.92 ±11.41 μm. There are variations in the topographic profile of peripapillary choroidal thickness and RNFL thickness among clock hours and different quadrants. Peripapillary choroid was thickest (150.04 ± 59.72 μm) at the superior quadrant and thinnest (110.71 ± 51.61) at the inferior quadrant, whereas RNFL was thickest (118.60 ± 19.83 μm) at the inferior and thinnest (67.36 ± 11.36) at the temporal quadrant.

Table 3 shows the linear regression analyses of the associations of peripapillary choroidal thickness (exposure variable of interest) by locations evaluated against RNFL thicknesses (dependent variable) from the same location

TABLE 1. Comparison of Ocular Characteristics of Included and Excluded Eyes in Evaluating the Relationship Between Peripapillary Choroid and Retinal Nerve Fiber Layer Thickness

Characteristics	Included (n = 843 Eyes)	Excluded (n = 61 Eyes)	*P* Value[a]
Axial length, mm	23.56 (0.98)	24.27 (1.92)	.198
Anterior chamber depth, mm	3.14 (0.38)	3.00 (0.42)	.185
Corneal curvature, mm	7.67 (0.25)	7.64 (0.24)	.876
Spherical equivalent, D	0.23 (1.57)	−3.19 (5.54)	.002
BCVA, logMAR	0.28 (0.45)	0.55 (0.78)	.028
Central corneal thickness, μm	539.72 (32.64)	536.10 (32.16)	.063
Intraocular pressure, mm Hg	14.30 (3.17)	15.48 (4.92)	.150
Average RNFL thickness, μm	92.92 (11.41)	93.11 (11.09)	.923

BCVA = best-corrected visual acuity; D = diopter; logMAR = logarithm of the minimal angle of resolution; RNFL = retinal nerve fiber layer.

Data presented are means (standard deviations).

[a]*P* value was obtained with generalized estimating equation.

TABLE 2. Distribution of Peripapillary Choroid and Retinal Nerve Fiber Layer Thickness in Nonglaucomatous Eyes at Clock-Hour Sectors (30 Degrees Apart) and 4 Quadrants, With 360-Degree, 3.4-mm-Diameter Peripapillary Circle Scans (N = 843 Eyes)

Measurement Location	Peripapillary Choroidal Thickness (μm) Mean (SD)	Retinal Nerve Fiber Layer Thickness (μm) Mean (SD)
Clock hours		
1	138.61 (77.01)	56.95 (11.08)
2	147.09 (70.88)	81.10 (16.00)
3	148.38 (65.03)	115.72 (23.97)
4	150.46 (62.21)	116.95 (26.79)
5	151.06 (59.39)	115.26 (24.91)
6	151.68 (61.06)	81.07 (16.87)
7	145.17 (61.97)	57.38 (11.06)
8	133.58 (58.49)	67.01 (14.72)
9	115.32 (53.67)	113.61 (30.65)
10	102.01 (51.07)	127.30 (28.03)
11	113.25 (57.11)	115.00 (30.08)
12	129.24 (68.31)	67.53 (14.04)
Quadrants		
Superior	150.04 (59.72)	116.05 (18.42)
Nasal	143.12 (58.46)	69.69 (11.28)
Inferior	110.71 (51.61)	118.60 (19.83)
Temporal	138.47 (68.65)	67.36 (11.36)
Average thickness	135.59 (56.74)	92.92 (11.41)

SD = standard deviation.

One o'clock corresponded to the temporal region, 4 o'clock to the superior, 7 o'clock to the nasal, and 10 o'clock to the inferior.

(Figure) to calculate regression coefficients (β). In Model 1, including age, sex, and AL, we found that thinner peripapillary choroidal thickness was independently associated with thinner RNFL thickness globally (β = −1.364 μm for per-SD decrease in peripapillary choroidal thickness, $P = .002$) and in the inferior (β = −2.539, $P = .001$) and superior (β = −2.492, $P = .001$) quadrants. In Model 2, including age, sex, AL, IOP, diabetic retinopathy, and age-related macular degeneration, thinner peripapillary choroidal thickness was independently associated with thinner RNFL thickness globally (β = −1.329 μm for per-SD decrease in peripapillary choroidal thickness, $P = .003$) and in the inferior (β = −2.566, $P < .001$) and superior (β = −2.348, $P = .001$) quadrants. In order to control for potential confounding effect from OCT signal strengths, we further included signal strength from both Cirrus and Spectralis OCT in our regression analyses. The results remained similar after further adjustment for signal strength (Model 3 in Table 3). However, in all models, the association was not present in the temporal quadrant.

DISCUSSION

OUR STUDY PROVIDES THE POPULATION-BASED DATA ON the quantitative relationship between peripapillary choroidal thickness and RNFL thickness measured by SD OCT in nonglaucomatous subjects. We found that thinner peripapillary choroidal thickness was independently associated with thinner RNFL thickness globally, in the inferior and superior quadrants, even after adjusting for relevant confounders. The results of this study provide evidence that thinning of the peripapillary choroid is associated with corresponding RNFL thinning. In terms of topographic profile, the peripapillary choroid was thickest at the superior and thinnest at the inferior quadrants, whereas RNFL was thickest at the inferior and thinnest at the temporal quadrants. Thinnest peripapillary choroid in the inferior quadrant may explain the susceptibility of the inferior optic nerve region to glaucoma.

To date, none of the studies has thoroughly investigated the quantitative relationship between peripapillary choroidal thickness and RNFL thickness in normal subjects, particularly in the general population. Only a few studies,[20,21] when analyzing RNFL as one of the covariates associated with peripapillary choroidal thickness, reported no significant correlation, a finding contrary to our results. Similarly, Maul and associates in a cross-sectional study of 74 suspects and glaucoma patients reported no significant association of peripapillary choroidal thickness with either degree of glaucoma damage

TABLE 3. The Associations of Peripapillary Choroidal Thickness With Retinal Nerve Fiber Layer Thickness in a Population-Based Sample of Nonglaucomatous Eyes (N = 843) Using Generalized Estimating Equation

	Model 1[a]		Model 2[b]		Model 3[c]	
	Retinal Nerve Fiber Layer Thickness		Retinal Nerve Fiber Layer Thickness		Retinal Nerve Fiber Layer Thickness	
	Beta (95% CI)	*P* Value	Beta (95% CI)	*P* Value	Beta (95% CI)	*P* Value
Average peripapillary choroidal thickness	−1.364 (0.497, 2.232)	.002	−1.329 (0.463, 2.196)	.003	−1.334 (0.464, 2.205)	.003
Inferior peripapillary choroidal thickness	−2.539 (1.099, 3.979)	.001	−2.566 (1.124, 4.009)	<.001	−2.565 (1.119, 4.010)	.001
Superior peripapillary choroidal thickness	−2.492 (1.086, 3.898)	.001	−2.348 (0.937, 3.760)	.001	−2.340 (0.923, 3.757)	.001

CI = confidence interval.

Average, inferior, and superior peripapillary choroidal thickness was regressed with average, inferior, and superior retinal nerve fiber layer thickness, respectively.

Average, inferior, and superior peripapillary choroidal thicknesses were analyzed per standard deviation decrease.

[a]Adjusted for age, sex, and axial length.

[b]Adjusted for age, sex, axial length, intraocular pressure, diabetic retinopathy, and age-related macular degeneration.

[c]Adjusted for age, sex, axial length, intraocular pressure, diabetic retinopathy, age-related macular degeneration, and signal strength from Cirrus and Spectralis optical coherence tomography.

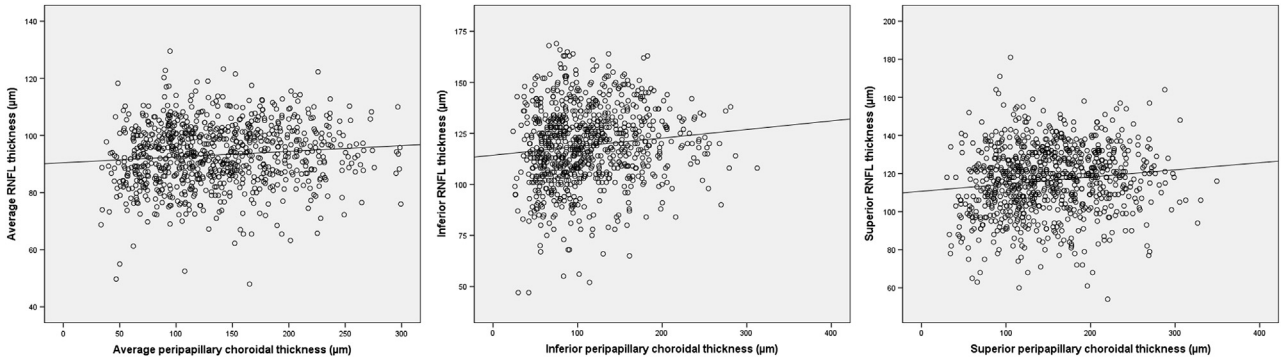

FIGURE. Scatterplot showing positive correlation of (Left) average retinal nerve fiber layer (RNFL) thickness with average peripapillary choroidal thickness, (Middle) inferior RNFL thickness with inferior peripapillary choroidal thickness, and (Right) superior RNFL thickness with superior peripapillary choroidal thickness.

or RNFL thickness.[22] There are several reasons for this. First, their peripapillary choroidal thickness measurements were not automated but involved manual delineation of the choroidal boundaries, making it not only time consuming, but also prone to measurement errors. Second, these studies were performed in clinic-based settings with a potential selection bias and involved smaller sample sizes (36 and 76 normal subjects in studies by Ho and associates and Huang and associates, respectively).[20,21] To address these issues, we therefore developed and used a novel technique of automated choroidal segmentation[14,19] to objectively and efficiently obtain the thickness of the peripapillary choroid and investigate its association with RNFL thickness in a population-based sample.

Interestingly, our results demonstrate significant positive association between inferior, superior, and average peripapillary choroidal thickness and RNFL thickness (ie, thinner peripapillary choroid in these quadrants was associated with thinner RNFL). A possible reason for the positive association between these structural features could be because both ONH and peripapillary choroid shares the common source of blood supply via the short posterior ciliary arteries.[10–13] Our study supports the hypothesis that since glaucomatous neurodegeneration occurs at the ONH,[23] it is likely that concurrent choroidal changes would also occur in the peripapillary region underlying areas of RNFL thinning. It is also interesting to note that although the association between peripapillary choroidal thickness and RNFL in the temporal region was significant in the univariate analysis, it was abolished after incorporating age, sex, and AL. We believe that the association in the temporal region is primarily driven by AL, given that the temporal region is most influenced by AL measurements compared to the other regions.

In terms of topographic profile of peripapillary choroid and RNFL thicknesses, our results confirmed the asymmetric distribution of both the peripapillary choroid and RNFL thicknesses.[19,24–26] The mean peripapillary choroidal thickness and RNFL thickness measurements showed regional differences, peripapillary choroid being thickest superiorly and thinnest inferiorly, whereas RNFL was thickest inferiorly and thinnest temporally. Our observations of the distribution of peripapillary choroidal thickness are similar to the results of previous EDI-OCT studies in normal eyes, which have consistently shown the inferior region to be the thinnest, compared to other regions.[19–21,27,28] Although it remains unclear why the inferior choroid demonstrates such prominent thinning, we favor the theory that both the vascular watershed zone and the embryonic location of the optic fissure closure may be responsible.[29] As the optic fissure is located in the inferior aspect of the optic cup and is the last part of the globe to close,[30] this regional difference in ocular development may contribute to the thinner choroid found in the inferior region. Therefore, development of the ONH and peripapillary choroid needs to be considered to explain the spatial distribution of peripapillary choroidal thickness at different sectors.

Despite RNFL being thickest in the inferior quadrant, this region is most vulnerable to glaucomatous damage. Selective and predominant inferior RNFL loss in early glaucoma is multifactorial. One of the known reasons for the vulnerability of the inferior region is that the lamina cribrosa of the inferior pole has larger pores and thinner connective tissue and glial support for passing retinal ganglion cell axons.[31–33] Based on our findings, this could also possibly be because of the thinnest peripapillary choroid in the inferior region. We speculate that thinnest peripapillary choroid in the inferior quadrant, which represents an area of lower blood supply, may predispose the inferior region of the optic nerve to glaucomatous ischemic damage, suggesting a possible explanation for the observation that glaucoma typically affects the inferior optic nerve region first. Peripapillary choroidal thickness as a surrogate to vascular supply[12,13] found a mild to moderate association, more so with inferior RNFL thickness, in our study of nonglaucomatous eyes. The magnitude of association is weak, thus again suggesting involvement of multiple factors related to inferior RNFL susceptibility in glaucoma pathogenesis. Further examination in glaucoma patients would be needed to confirm this association and to see whether such association is stronger in glaucomatous eyes.

The strengths of this study include its population-based design and a relatively large sample size with a single common ethnicity. Hence, our findings were unlikely to be confounded by ethnic heterogeneity. Unlike other studies, which involved manual delineation of choroidal boundaries, we used an automated choroidal segmentation technique to objectively obtain the thickness of the peripapillary choroid. Therefore, our measurements of peripapillary choroidal thickness are less prone to measurement errors. The relationship between peripapillary choroidal thickness and RNFL was confirmed after adjusting for potential clinical factors. Nevertheless, this study has a few limitations. First, recent studies have reported diurnal fluctuations in choroidal thickness in the macular region.[34–36] To the best of our knowledge, there are no data on the association between diurnal variation and choroidal thickness in the peripapillary region. Our subjects were examined only at a single time point, and thus we are not able to take account of any diurnal variation of peripapillary choroidal thickness. However, the peripapillary choroidal thickness measurements in our study were not performed at the same time of the day; each participant underwent the OCT examination in a randomized manner with respect to when the readings were obtained. It seems unlikely that circadian changes may have influenced the results of our investigation. Second, owing to the cross-sectional nature of our study we could identify a structural relationship between peripapillary choroidal thickness and RNFL thickness, but cannot address the temporal relationship between these structures. More longitudinal data are needed to clarify this relationship. Last, our investigation included consecutive participating subjects from a population-based study and thus some of them had eye diseases. Therefore, the distribution of peripapillary choroidal thickness and RNFL thickness determined in this study may represent the thickness not in healthy eyes but in the general adult and elderly populations. However, this would not affect the observed associations, because in the multiple regression analysis models we have adjusted for the potential ocular diseases in elderly people that might influence peripapillary choroidal thickness.

In conclusion, the current study demonstrates significant positive associations between peripapillary choroid and RNFL thicknesses and examines this structure-structure relationship. Understanding of the relationship between these structural parameters may be useful clinically for assessment of ONH damage in glaucoma. However, this relationship needs to be explored further in glaucomatous eyes of varying severity before it is applied in clinical settings.

FUNDING/SUPPORT: THIS STUDY WAS SUPPORTED BY A GRANT FROM NATIONAL MEDICAL RESEARCH COUNCIL (SINGAPORE) and National Research Foundation University Fund (Singapore). The sponsor or funding organization had no role in the design or conduct of this research. Financial Disclosures: C.Y. Cheung: received grant support from National Medical Research Council (NMRC) and Biomedical Research Council, Singapore directed to Singapore Eye Research Institute; T.A.: received grant support from National Medical Research Council (NMRC) and Biomedical Research Council, Singapore directed to Singapore Eye Research Institute; T.Y.W.: received grant support from National Medical Research Council

(NMRC) and Biomedical Research Council, Singapore directed to Singapore Eye Research Institute; Advisory Board member for Abbot, Novartis, Pfizer, Allergan, and Bayer; independent consultant for Abbot, Novartis, Pfizer, Allergan, and Bayer; C.Y. Cheng: received grant support from National Medical Research Council (NMRC) and Biomedical Research Council, Singapore directed to Singapore Eye Research Institute. All authors attest that they meet the current ICMJE requirements to qualify as authors.

REFERENCES

1. Sommer A, Katz J, Quigley HA, et al. Clinically detectable nerve fiber atrophy precedes the onset of glaucomatous field loss. *Arch Ophthalmol* 1991;109(1):77–83.
2. Tuulonen A, Lehtola J, Airaksinen PJ. Nerve fiber layer defects with normal visual fields. Do normal optic disc and normal visual field indicate absence of glaucomatous abnormality? *Ophthalmology* 1993;100(5):587–597.
3. Bowd C, Weinreb RN, Williams JM, Zangwill LM. The retinal nerve fiber layer thickness in ocular hypertensive, normal, and glaucomatous eyes with optical coherence tomography. *Arch Ophthalmol* 2000;118(1):22–26.
4. Schuman JS, Hee MR, Puliafito CA, et al. Quantification of nerve fiber layer thickness in normal and glaucomatous eyes using optical coherence tomography. *Arch Ophthalmol* 1995; 113(5):586–596.
5. Zangwill LM, Williams J, Berry CC, Knauer S, Weinreb RN. A comparison of optical coherence tomography and retinal nerve fiber layer photography for detection of nerve fiber layer damage in glaucoma. *Ophthalmology* 2000;107(7): 1309–1315.
6. Chen FK, Yeoh J, Rahman W, Patel PJ, Tufail A, Da Cruz L. Topographic variation and interocular symmetry of macular choroidal thickness using enhanced depth imaging optical coherence tomography. *Invest Ophthalmol Vis Sci* 2012; 53(2):975–985.
7. Horecky J, Baciak L, Kasparova S, Pacheco G, Aliev G, Vancova O. Minimally invasive surgical approach for three-vessel occlusion as a model of vascular dementia in the rat-brain bioenergetics assay. *J Neurol Sci* 2009;283(1-2): 178–181.
8. Hayreh SS. Blood supply of the optic nerve head and its role in optic atrophy, glaucoma, and oedema of the optic disc. *Br J Ophthalmol* 1969;53(11):721–748.
9. Nicolela MT, Hnik P, Drance SM. Scanning laser Doppler flowmeter study of retinal and optic disk blood flow in glaucomatous patients. *Am J Ophthalmol* 1996;122(6): 775–783.
10. Duijm HF, van den Berg TJ, Greve EL. Choroidal haemodynamics in glaucoma. *Br J Ophthalmol* 1997;81(9):735–742.
11. Flammer J, Orgul S, Costa VP, et al. The impact of ocular blood flow in glaucoma. *Prog Retin Eye Res* 2002;21(4): 359–393.
12. Hayreh SS. The blood supply of the optic nerve head and the evaluation of it - myth and reality. *Prog Retin Eye Res* 2001; 20(5):563–593.
13. Hayreh SS. The 1994 Von Sallman Lecture. The optic nerve head circulation in health and disease. *Exp Eye Res* 1995; 61(3):259–272.
14. Tian J, Marziliano P, Baskaran M, et al. Automatic segmentation of the choroid in enhanced depth imaging optical coherence tomography images. *Biomed Opt Express* 2013; 4(3):397–411.
15. Rosman M, Zheng Y, Wong W, et al. Singapore Malay Eye Study: rationale and methodology of 6-year follow-up study (SiMES-2). *Clin Experiment Ophthalmol* 2012;40(6): 557–568.
16. Foster PJ, Buhrmann R, Quigley HA, Johnson GJ. The definition and classification of glaucoma in prevalence surveys. *Br J Ophthalmol* 2002;86(2):238–242.
17. Chua J, Tham YC, Liao J, et al. Ethnic differences of intraocular pressure and central corneal thickness: the Singapore Epidemiology of Eye Diseases study. *Ophthalmology* 2014; 121(10):2013–2022.
18. Spaide RF, Koizumi H, Pozzoni MC. Enhanced depth imaging spectral-domain optical coherence tomography. *Am J Ophthalmol* 2008;146(4):496–500.
19. Gupta P, Jing T, Marziliano P, et al. Peripapillary choroidal thickness assessed using automated choroidal segmentation software in an Asian population. *Br J Ophthalmol* 2015;99(7):920–926.
20. Ho J, Branchini L, Regatieri C, Krishnan C, Fujimoto JG, Duker JS. Analysis of normal peripapillary choroidal thickness via spectral domain optical coherence tomography. *Ophthalmology* 2011;118(10):2001–2007.
21. Huang W, Wang W, Zhou M, et al. Peripapillary choroidal thickness in healthy Chinese subjects. *BMC Ophthalmol* 2013;13:23.
22. Maul EA, Friedman DS, Chang DS, et al. Choroidal thickness measured by spectral domain optical coherence tomography: factors affecting thickness in glaucoma patients. *Ophthalmology* 2011;118(8):1571–1579.
23. Jonas JB, Budde WM, Panda-Jonas S. Ophthalmoscopic evaluation of the optic nerve head. *Surv Ophthalmol* 1999;43(4): 293–320.
24. Wang YX, Pan Z, Zhao L, You QS, Xu L, Jonas JB. Retinal nerve fiber layer thickness. The Beijing Eye Study 2011. *PLoS One* 2013;8(6):e66763.
25. Zhao L, Wang Y, Chen CX, Xu L, Jonas JB. Retinal nerve fibre layer thickness measured by Spectralis spectral-domain optical coherence tomography: The Beijing Eye Study. *Acta Ophthalmol* 2014;92(1):e35–e41.
26. Cheung CY, Chen D, Wong TY, et al. Determinants of quantitative optic nerve measurements using spectral domain optical coherence tomography in a population-based sample of non-glaucomatous subjects. *Invest Ophthalmol Vis Sci* 2011; 52(13):9629–9635.
27. Tanabe H, Ito Y, Terasaki H. Choroid is thinner in inferior region of optic disks of normal eyes. *Retina* 2012;32(1): 134–139.
28. Ouyang Y, Heussen FM, Mokwa N, et al. Spatial distribution of posterior pole choroidal thickness by spectral domain optical coherence tomography. *Invest Ophthalmol Vis Sci* 2011; 52(9):7019–7026.
29. Ikuno Y, Kawaguchi K, Nouchi T, Yasuno Y. Choroidal thickness in healthy Japanese subjects. *Invest Ophthalmol Vis Sci* 2010;51(4):2173–2176.

30. Schoenwolf G, Bleyl S, Brauer P, Francis-West P. Larsen's Human Embrology. Philadelphia: Elsevier; 2009:602–616.
31. Jonas JB, Mardin CY, Schlotzer-Schrehardt U, Naumann GO. Morphometry of the human lamina cribrosa surface. *Invest Ophthalmol Vis Sci* 1991;32(2):401–405.
32. Quigley HA, Addicks EM. Regional differences in the structure of the lamina cribrosa and their relation to glaucomatous optic nerve damage. *Arch Ophthalmol* 1981;99(1):137–143.
33. Radius RL, Gonzales M. Anatomy of the lamina cribrosa in human eyes. *Arch Ophthalmol* 1981;99(12):2159–2162.
34. Chakraborty R, Read SA, Collins MJ. Diurnal variations in axial length, choroidal thickness, intraocular pressure, and ocular biometrics. *Invest Ophthalmol Vis Sci* 2011;52(8):5121–5129.
35. Tan CS, Ouyang Y, Ruiz H, Sadda SR. Diurnal variation of choroidal thickness in normal, healthy subjects measured by spectral domain optical coherence tomography. *Invest Ophthalmol Vis Sci* 2012;53(1):261–266.
36. Usui S, Ikuno Y, Akiba M, et al. Circadian changes in subfoveal choroidal thickness and the relationship with circulatory factors in healthy subjects. *Invest Ophthalmol Vis Sci* 2012;53(4):2300–2307.

Biosketch

Preeti Gupta graduated with masters in Optometry from Queensland University of Technology, Australia in 2008. She then joined the Ocular Epidemiology Research Group at Singapore Eye Research Institute, Singapore, where she conducts and coordinates epidemiological and population-based projects under the Singapore Epidemiology of Eye Disease programme. Her area of interest includes epidemiology of major eye diseases and ocular imaging using novel image processing techniques.

Biosketch

Ching-Yu Cheng leads Ocular Epidemiology Research group at Singapore Eye Research Institute and co-directs the Singapore Epidemiology of Eye Diseases (SEED) program. His primary research interests are related to epidemiology and genetics of major eye diseases. His current work involves a variety of epidemiological, clinical, and image research on glaucoma; and identification of susceptibility genes for complex ocular diseases, such as glaucoma, macular degeneration and cataract, using both genome-wide association approaches and next-generation sequencing technology.

Acta Ophthalmologica

Choroidal thickness and high myopia: a case–control study of young Chinese men in Singapore

Preeti Gupta,[1,2] Seang-Mei Saw,[1,2,3] Carol Y. Cheung,[1,2,4] Michael J. A. Girard,[1,5] Jean Martial Mari,[6] Mayuri Bhargava,[1,2] Colin Tan,[7] Mellisa Tan,[8] Adeline Yang,[8] Frederick Tey,[8] Gerard Nah,[9] Paul Zhao,[9] Tien Yin Wong[1,2,3,4] and Ching-Yu Cheng[1,2,3,4]

[1]Singapore Eye Research Institute and Singapore National Eye Centre, Singapore
[2]Department of Ophthalmology, Yong Loo Lin School of Medicine, National University of Singapore and National University Health System, Singapore
[3]Saw Swee Hock School of Public Health, National University of Singapore, Singapore
[4]Office of Clinical Sciences, Duke-NUS Graduate Medical School, Singapore
[5]Department of Bioengineering, Faculty of Engineering, National University of Singapore, Singapore
[6]Department of Medical Physics and Bioengineering, Faculty of Engineering Science, University College London, London, UK
[7]Department of Ophthalmology, Tan Tock Seng Hospital, Singapore
[8]DSO National Laboratories, Defense Medical and Environmental Research Institute, Singapore
[9]Vision Performance Centre, Military Medical Institute, Singapore Armed Forces, Singapore

ABSTRACT.

Purpose: **To determine the distribution of choroidal thickness (CT) and ocular factors associated with CT in high myopic eyes in comparison with emmetropic eyes of young healthy adults.**

Methods: **A case–control study of 648 young, male subjects, including 520 high myopes and 128 emmetropes. Choroidal imaging was performed using enhanced depth imaging spectral domain optical coherence tomography. Images were postprocessed using adaptive compensation for quality enhancement. CT was measured at nine locations, including subfovea and 1.5 and 3 mm nasal, temporal, superior and inferior to fovea.**

Results: **The CT at the subfovea was significantly thinner (mean ± standard error: 225.87 ± 5.51 μm) for high myopes compared to emmetropes (375.15 ± 6.58 μm, $p < 0.001$). Likewise, CT in high myopic group was significantly thinner than emmetropic control group at all locations (p for trend <0.001 for all locations). Distribution of CT showed a markedly different pattern in high myopic eyes (thickest superiorly at 3 mm, 265.97 ± 5.97 μm) and emmetropic eyes (thickest subfoveally, 375.15 ± 6.58 μm). Choroid was thinnest at nasal 3 mm location in both the myopic (108.85 ± 3.97 μm) and emmetropic (238.25 ± 6.72 μm) groups. Among the ocular factors studied, axial length, posterior staphyloma and chorio-retinal atrophy were the significant predictors of CT.**

Conclusions: **Highly myopic eyes have significantly thinner choroid and showed different distribution pattern, compared to emmetropes. Axial length, posterior staphyloma and chorio-retinal atrophy are the strongest determinants of CT.**

Key words: case-control study – choroidal thickness – EDI SD-OCT – high myopia

Acta Ophthalmol. 2015: 93: e585–e592

doi: 10.1111/aos.12631

Introduction

Pathological myopia or high myopia is one of the leading causes of visual impairment in the world (Fredrick 2002; Hayashi et al. 2010). Although the prevalence of high myopia (defined as −6.0 dioptres or more) varies with ethnic groups and countries, high myopia is more common in Asian populations with rates of 9–21%, (Wong et al. 2000; Lin et al. 2004) compared with 2–4% in white people (Hofman et al. 1991; Wang et al. 1994; Attebo et al. 1999).

In pathological myopia, excessive axial elongation of globe can cause biomechanical stretching and thinning of choroid and retinal pigmented epithelium layers, leading to increased risk of chorioretinal complications such as choroidal neovascularization, posterior staphyloma, lacquer cracks in Bruch's membrane and myopic foveoschisis, which may lead to visual loss (Curtin & Karlin 1971; Curtin 1982; Noble & Carr 1982; Avila et al. 1984; Ohno-Matsui & Tokoro 1996; Wu et al. 2001; Vongphanit et al. 2002; Hsiang et al. 2008; Cheung et al. 2013; Jonas et al. 2014).

As some of the earliest changes in pathological myopia begin in the

choroid, choroidal thickness (CT) could be an important parameter to study the pathogenesis of macular vision loss in high myopia. The thickness of the choroid can be measured by enhanced depth imaging (EDI) spectral domain optical coherence tomography (SD-OCT) (Spaide et al. 2008) in a variety of ocular diseases (Kim et al. 2013; Hashizume et al. 2014; Tan et al. 2014; Zhou et al. 2014). Using this method, studies have now shown that myopic eyes have thinner CT (ranging from: 93.2 ± 62.5 to 156.07 ± 86.39 μm) (Fujiwara et al. 2009; Ikuno & Tano 2009; Flores-Moreno et al. 2013; Ho et al. 2013) compared to emmetropes (normal range of subfoveal CT: 191 ± 74.2 to 354 ± 111 μm) (Margolis & Spaide 2009; Ikuno et al. 2010; Fujiwara et al. 2012; Wei et al. 2013). However, these studies were either conducted on small sample populations (Fujiwara et al. 2009; Ikuno & Tano 2009) or were mainly limited in their assessment of CT to horizontal locations only (Flores-Moreno et al. 2013; Ho et al. 2013). To the best of our knowledge, there are no studies which investigated CT by severity of myopia and the distribution of CT and assessed ocular factors associated with CT in Asian eyes. Knowledge of such factors is crucial before drawing inferences on how CT influences the development of pathological myopia.

The aim of our study was to compare the distribution of CT in different myopic groups based on the degree of myopia and to assess ocular determinants of macular CT measured by EDI SD-OCT. We used a case–control study approach of young, highly myopic and emmetropic healthy male adults in Singapore.

Materials and Methods

Study population

A total of 28 908 male adults were screened for myopia (mean age ± SD: 19.8 ± 1.2 years; range: 17–29 years) from 2009 to 2010 as part of a mandatory medical eye review for employment purposes. Measured using non-cycloplegic autorefraction (Huvitz MRK-3100P), 2584 persons were identified to have myopia with spherical equivalent (SE) of −6.0 dioptres (D) or worse. Of these 2584 persons, 719 were selected on the basis of a refractive error-stratified random sampling strategy and underwent a further comprehensive ophthalmologic examination at Singapore Eye Research Institute from December 2011 to June 2012. Their SE was further confirmed by subjective refraction, and those with SE >−6.0 D (n = 96) were excluded, leaving 623 subjects with high myopia (251 with SE between −6.0 and −8.0 D; 207 with SE between −8.0 and −10.0 D; 165 with SE −10.0 D or worse). In addition, 151 emmetropes who had SE < 0.5 D in both eyes measured using autorefraction were recruited as controls and went through a similar ophthalmologic examination. Subjects were further excluded if they did not give consent to take part in this medical review, had any previous ocular trauma or surgery, and those with other clinically significant ocular comorbidity.

Written informed consent was taken from the subjects and their parents/guardians (if they were 21 years old and below). Ethics approval was obtained from the Institutional Review Board of DSO National Laboratories, Singapore. The study was conducted in accordance with the tenets of the World Medical Association's Declaration of Helsinki.

Ophthalmic examination and measurements

Each subject underwent a standardized questionnaire and a complete ophthalmologic examination. The subjects were asked a series of questions, such as previous ocular trauma or surgery, history of ocular diseases.

Their refractive error screened with autorefraction (Canon Autorefractor RK-F1; Canon Inc. Ltd., Tochigiken, Japan) and confirmed with manifest refraction in which the best corrected visual acuity, which was measured monocularly using a logarithm of the minimum angle of resolution (LogMAR) chart (Lighthouse International, New York, NY, USA) at a distance of 4 m, was performed. Contrast sensitivity (CS) was measured using the Rabin super vision test (Davies et al. 2004), with and without a night vision goggle filter (SVT-NVG) and low and high luminance log CS were taken for this test. The NVG filter used was a dark green, low-luminance filter which slides in place in front of the illuminated chart, reducing chart luminance (from 100 to 4 cd/m^2) to simulate the low luminance (i.e. wearing NVG). To minimize memorization of optotypes, two different sequences were displayed for right and left eyes and measurement of CS was recorded by counting the number of letters correctly read by the subjects using the Conversion Table.

Biometry measurements, that is axial length (AL), anterior chamber depth, and K-readings, were obtained from the non-contact Zeiss IOL Master (V3.01; Carl Zeiss Meditec AG, Jena, Germany). Intraocular pressure (IOP) was measured using non-contact tonometry (Auto Non-Contact Tonometer, NT-3000; Nidek, Gamagori, Aichi, Japan), and if IOP was found to be 21 mmHg or more, a further IOP measurement using Goldmann applanation tonometry (Haag-Streit, Bern, Switzerland) was performed by study ophthalmologists.

Subjects underwent slit-lamp examination. Binocular indirect ophthalmoscopy was performed approximately 30 min after topical instillation of three drops of tropicamide and 2.5% phenylephrine, given 5 min apart. Dilated fundus examination was carried out by ophthalmologists. The presence and type of peripheral retinal degenerations and vitreous degenerations were systematically documented. Fundus photography was performed using non-mydriatic retinal camera (Canon CR-DGi with a 10-DSLR back, Tokyo, Japan).

OCT imaging

The retina, optic disc and choroidal architectural parameters were determined using SD-OCT (Spectralis, Wavelength: 870 nm; Heidelberg Engineering, Heidelberg, Germany). Choroid was imaged with EDI modality after pupil dilation. EDI is a method that improves resolution of choroidal detail by automatically setting the choroid closer to the zero-delay line and thus theoretically provides better visualization of the choroid scleral interface (CSI) than in standard retinal SD-OCT images. Radial scan consisting of six sections, each comprising 100 averaged scans (using the automatic averaging and eye tracking features of the proprietary device), was obtained in an angle of 30° centred onto the fovea (30° angles between the lines).

The horizontal and vertical sections passing through the centre of the fovea were selected for analysis. Following Spectralis user manual guidelines, subjects' keratometry readings and refraction were entered into the Spectralis' software before imaging choroid to estimate optical magnification, thus allowing for more accurate comparisons across individuals. However, Spectralis OCT does not allow AL to be input; our methods may still have residual errors (2–7%) (Garway-Heath et al. 1998) due to ocular magnification from methods that additionally uses AL. For each subject, only right eye was chosen for subsequent analysis.

Measurement of choroidal thickness

As an accurate evaluation of the CT with EDI-OCT relies mainly on the visibility of CSI, which anatomically represents the junction between the choroid and the sclera and is a principal landmark for quantitative measurements of choroid. Therefore, in our study, To accurately determine CT, CSI was enhanced using our novel technique of adaptive compensation described in detail elsewhere (Girard et al. 2011; Mari et al. 2013; Gupta et al. 2014). Our method has shown higher intra- and intergrader reliability of CT measurements compared to conventional method (Gupta et al. 2014).

The CT in the enhanced images was measured as the perpendicular distance between the outer portion of the hyperreflective line corresponding to the RPE (automatically detected by the instrument) to the now clear hyporeflective line or margin corresponding to the CSI (manually drawn by an experienced grader, who was masked to subject characteristics and clinical diagnosis) at the following locations: subfovea and 1.5 and 3 mm nasal, temporal, superior and inferior to fovea. As there was no significant difference between the horizontal and vertical subfoveal CT (horizontal SFCT = 225.87 μm, vertical SFCT = 232.09 μm, p = 0.399), only horizontal CT was used for analysis. In addition, we evaluated the intra-observer reliability of CT measurements in both the myopic and emmetropic group. Forty randomly selected Spectralis images (20 from each group) were assessed again by the same grader (grader 1 versus grader 1) after an interval of 1 week.

Statistical analysis

Subjects were excluded from analysis if they had any history of anterior ocular diseases, previous ocular trauma, evidence of macular or vitreoretinal diseases or any form of refractive surgery performed in their eyes. However, conditions such as peripapillary atrophy, lacquer crack, posterior staphyloma or chorio-retinal atrophy were not excluded, as they are commonly seen in high myopic eyes. Statistical analysis was performed using SPSS version 17.0 (SPSS, Inc., Chicago, IL, USA) and MedCalc version 12.3 (MedCalc Software, Ostend, Belgium).

The demographics and ocular parameters between myopic and control eyes were compared using independent *t*-tests. The intrasession repeatability of the CT was measured by the absolute agreement model of the intraclass correlation coefficient (ICC) (Fleiss & Cohen 1973). For the purpose of analyses, myopic eyes were divided into three groups based on SE: <−6 to −8 D, <−8 to −10 D and <−10 D. Generalized linear model was used to assess the mean CT across different locations in eyes with varying degree of myopia, and conditions such as posterior staphyloma and chorio-retinal atrophy were included to adjust for potential residual confounding. Repeated-measures analysis of variance (ANOVA) with Bonferroni post-test was used to compare mean thickness at various locations within each group. Univariate and multiple linear regression analyses were performed to determine the association of ocular factors (independent variables) with CT measurements (dependent variables). For multiple linear regression, age and factors which showed significant association in univariate analysis ($p < 0.05$) were included.

Results

Of the 623 eligible high myopes (SE ≤ −6.0 D), we further excluded 103 subjects because either their choroidal images were not successfully attained ($n = 69$) or the available images were not of optimal quality to perform accurate measurements ($n = 31$) or they did not meet the inclusion criteria ($n = 3$), leaving 648 subjects (520 high myopes and 128 emmetropes) with complete data on CT for analysis.

The mean age of included myopic and emmetropic subjects was 21.59 ± 1.15 years and 22.06 ± 0.97 years, respectively. The mean SE was −8.68 ± 2.05 dioptres (range, −6 to −23 D) for myopic group and 0.12 ± 0.24 dioptres for emmetropic group. Among the myopic group, all our subjects had peripapillary atrophy, 35.6% had posterior staphyloma, 6.5% had chorio-retinal atrophy and 2% had lacquer cracks. The demographics and ocular characteristics of the study population are shown in Table 1. In terms of reliability of CT measurements, the intra-observer reliability for myopic (ICC: 0.95–0.98) and emmetropic group (ICC: 0.95–0.97) was excellent for all locations of CT (Table 2).

CT varied significantly across the myopic subgroups and the emmetropic control group at all the locations (p for trend <0.001 for all locations, Table 3). It was significantly thinner in the more myopic eyes over a range of eccentricities, and the pattern of distribution was different from emmetropes (Fig. 1A,B). Across the three myopic subgroups, CT was found to be thickest at the superior location, followed by the temporal, subfoveal, inferior and the nasal locations ($p < 0.001$ by repeated-measures ANOVA). In comparison, the choroid in emmetropic eyes was thickest at the fovea, followed by the superior, inferior, temporal and the nasal locations ($p < 0.001$ by repeated-measures ANOVA). However, in both the myopia and emmetropic groups, choroid was thinnest at the nasal location being 108.85 μm and 238.25 μm in myopic and emmetropic group, respectively (Fig. 1A,B).

In the univariate analysis, SE, AL, corneal curvature, presence of posterior staphyloma and chorio-retinal atrophy were significantly associated with SFCT (all $p < 0.05$, Table 4 and Fig. 2). For each mm increase in AL and corneal curvature, SFCT on average decreased by 32.31 μm ($p < 0.001$) and 84.31 μm ($p < 0.001$), respectively. A decrease in mean SFCT by 13.10 μm was observed for each myopic dioptre increase ($p < 0.001$). Presence of posterior staphyloma and chorio-retinal atrophy decreased the mean SFCT by 22.69 μm and 26.91 μm respectively.

Both AL and SE influenced CT but a larger extent from AL. The results remained similar after adjusting for age (data not shown).

Because of collinearity between AL and SE (correlation coefficient = −0.65), only AL was selected and retained in the multivariate analysis as it had a greater explanatory power on CT change than did SE (standardized β, −0.489 versus 0.348). In the multiple linear regression analysis, AL, presence of posterior staphyloma and chorio-retinal atrophy remained significantly associated with CT (all $p < 0.05$), whereas the association with corneal curvature was abolished ($p = 0.975$). However, there was no change in results after adjusting for age.

In addition, SFCT correlated negatively with the logMAR visual acuity ($r = -0.085$, $p = 0.054$) and log low luminance CS ($r = -0.115$, $p = 0.009$) although the association was not statistically significant in multivariate analysis (Fig. 3).

Table 1. Baseline characteristics of study subjects.

	Myopes (n = 520)	Emmetropes (n = 128)	p-value
Age, years	21.59 (1.15)	22.06 (0.97)	<0.001
Axial length, mm	27.32 (1.16)	23.69 (0.62)	<0.001
Anterior chamber depth, mm	3.74 (0.25)	3.46 (0.27)	<0.001
Corneal curvature, mm	7.76 (0.25)	7.85 (0.41)	0.137
Spherical equivalent, D	−8.68 (2.05)	0.12 (0.24)	<0.001
Best corrected visual acuity Log MAR	0.01 (0.08)	−0.09 (0.06)	<0.001
Log low luminance contrast sensitivity	0.36 (0.28)	0.50 (0.20)	<0.001
Log high luminance contrast sensitivity	0.66 (0.33)	0.88 (0.21)	<0.001
Intraocular pressure, mmHg	16.12 (2.94)	15.26 (2.74)	0.002

Data are mean (SD).

Table 2. Intragrader reliability of choroidal thickness measurements in myopic and emmetropic group at different locations.

	Myopes		Emmetropes	
Locations of measurement	ICC (95% CI)	Mean difference (μm)* (SD)	ICC (95% CI)	Mean difference (μm)* (SD)
Choroidal thickness				
Subfoveal	0.98 (0.96–0.99)	9.9 (11.3)	0.97 (0.95–0.99)	11.5 (17.7)
Nasal, 1.5 mm	0.96 (0.93–0.98)	9.6 (14.8)	0.96 (0.93–0.98)	10.1 (20.6)
Nasal, 3 mm	0.94 (0.87–0.97)	8.0 (14.4)	0.96 (0.93–0.98)	−15.0 (20.8)
Temporal, 1.5 mm	0.97 (0.93–0.98)	9.1 (14.8)	0.97 (0.94–0.98)	14.3 (19.4)
Temporal, 3 mm	0.97 (0.94–0.98)	10.8 (13.0)	0.96 (0.91–0.98)	11.1 (18.5)
Superior, 1.5 mm	0.96 (0.93–0.98)	−7.5 (16.2)	0.95 (0.90–0.98)	13.2 (20.4)
Superior, 3 mm	0.95 (0.90–0.98)	9.2 (17.8)	0.97 (0.94–0.99)	−14.9 (17.2)
Inferior, 1.5 mm	0.97 (0.95–0.99)	11.0 (13.5)	0.96 (0.92–0.98)	14.7 (18.0)
Inferior, 3 mm	0.96 (0.93–0.98)	−8.6 (17.0)	0.97 (0.94–0.99)	13.1 (18.5)

ICC = intraclass correlation coefficient; CI = confidence interval; SD = standard deviation.
* Mean difference was determined from the 1st measurement minus 2nd measurement.

Discussion

Although the understanding of the characteristics of the *in vivo* choroid has increased substantially in recent years, to date, only a few studies have examined CT in high myopia. To our best knowledge, this study measured CT directly with EDI SD-OCT in the largest group of young, high myopic Asian subjects. CT in the myopic group was significantly lower than that of the emmetropic control group at any locations. We demonstrated further decrease in CT with increase in degree of myopic refractive error. CT distribution follows a different profile in

Table 3. Distribution of mean adjusted choroidal thickness at nine different locations across the myopic and control groups using generalized linear model.

						Changes in choroidal thickness across 3 myopic groups	
Location	Emmetropes (N = 128)	Myopia, 6−8 (D) (N = 233)	Myopia, <−8–10 (D) (N = 169)	Myopia > 10 (D) (N = 118)	All myopes (N = 520)	Beta†	p for trend†
Subfoveal	375.15 (6.58)	241.54 (6.63)	223.90 (7.14)	210.60 (7.13)	225.87 (5.51)	−15.74	<0.001
Nasal, 1.5 mm	324.01 (6.59)	187.01 (6.17)	165.27 (6.66)	150.70 (6.64)	168.35 (5.18)	−18.60	<0.001
Nasal, 3 mm	238.25 (6.72)	121.19 (4.76)	106.90 (5.13)	97.13 (5.12)	108.85 (3.97)	−12.30	<0.001
Temporal, 1.5 mm	359.27 (6.51)	249.52 (6.38)	235.82 (6.87)	223.47 (6.85)	236.64 (5.27)	−13.10	<0.001
Temporal, 3 mm	328.41 (6.04)	251.51 (6.02)	243.83 (6.49)	235.77 (6.47)	243.88 (4.94)	−07.84	<0.001
Superior, 1.5 mm	365.01 (5.66)	263.84 (7.05)	250.70 (7.59)	238.81 (7.57)	251.47 (5.81)	−12.59	<0.001
Superior, 3 mm	358.03 (5.74)	278.23 (7.25)	263.61 (7.81)	254.64 (7.79)	265.97 (5.97)	−12.14	<0.001
Inferior, 1.5 mm	358.93 (6.14)	243.27 (6.32)	219.94 (6.81)	202.87 (6.79)	222.74 (5.32)	−20.59	<0.001
Inferior, 3 mm	339.41 (6.30)	232.76 (6.25)	214.86 (6.74)	199.84 (6.72)	216.32 (5.21)	−16.63	<0.001
	p < 0.001*	p < 0.001*	p < 0.001*	p < 0.001*	p < 0.001*		

Data are mean (standard error) in μm, adjusted for presence of posterior staphyloma and chorio-retinal atrophy.
† Adjusted for presence of posterior staphyloma and chorio-retinal atrophy.
* Repeated-measures ANOVA, comparing the distribution of choroidal thickness across fovea, nasal (3 mm), temporal (3 mm), superior (3 mm) and inferior (3 mm) locations.

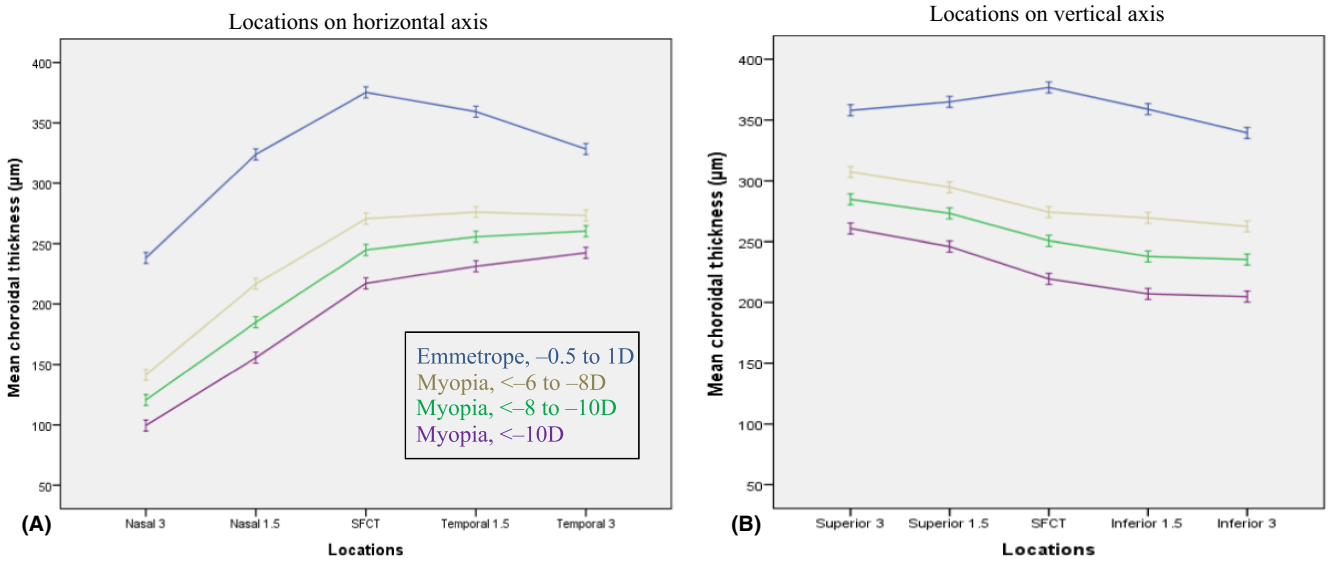

Fig. 1. Graph showing the differences in macular choroidal thickness (CT) in the high myopic groups and emmetropic group along the horizontal axis (A) and vertical axis (B). Mean thickness at each of the nasal, temporal, superior and inferior locations measured at 1.5 and 3 mm intervals eccentric to the subfoveal area. Error bars indicate standard error. SFCT is subfoveal CT.

Table 4. Association of ocular factors with subfoveal choroidal thickness in all myopes (n = 520).

	Univariate analysis			Multivariate analysis		
	Unstandardized beta coefficient	Standardized beta coefficient	p-value	Unstandardized beta coefficient	Standardized beta coefficient	p-value
Ocular factors						
Spherical equivalent, D	13.109	0.348	<0.001	–	–	–
Axial length, mm	−32.319	−0.489	<0.001	−24.232	−0.370	<0.001
Corneal curvature, mm	−84.318	−0.279	<0.001	0.397	0.001	0.975
Anterior chamber depth, mm	−8.200	−0.027	0.541	–	–	–
Intraocular pressure, mmHg	0.714	0.027	0.535	–	–	–
Posterior Staphyloma	−22.698	−0.443	<0.001	−15.642	−0.306	<0.001
Chorio-retinal atrophy	−26.910	−0.289	<0.001	−10.585	−0.114	0.003

high myopia (thickest CT superiorly), compared to emmetropia (thickest CT subfoveally). Among the range of ocular factors studied, AL, presence of posterior staphyloma and chorio-retinal atrophy were the significant predictors of CT.

Our study provided new data on CT and severity of myopia. There were significant differences in the mean CT among myopic subgroups and the emmetropic group at various eccentricities (p for trend <0.001 for all locations). Myopes had significantly thinner choroid compared to emmetropes at all eccentricities. Our findings are consistent with previous experimental animal studies (Wallman et al. 1995; Shaikh et al. 1999; Troilo et al. 2000) which have shown that chicks developing experimentally induced myopia show profound thinning of choroid (Troilo et al. 2000). The mean SFCT in myopic group was 225.87 ± 5.51 μm, which is much thicker than those reported in previous studies that showed a mean CT of 93.2 (Fujiwara et al. 2009) to 115.5 (Flores-Moreno et al. 2013) μm (Table 5). In Table 5, on performing a metaregression on various studies to quantify the change in mean CT with SE adjusting for age, we found no significant association between SE and mean CT (β = 0.429, p = 0.952) indicating AL to be a more important predictor of CT than SE. The mean SFCT in emmetropes was 375.15 μm which is also thicker than previous studies that reported a mean thickness of 272–354 μm (Spaide et al. 2008; Margolis & Spaide 2009; Esmaeelpour et al. 2010; Manjunath et al. 2010).

The differences in CT in our study compared to other studies could be because of differences in participants' characteristics, such as age, refractive error and ethnicity. Our study participants are twice as young, mean age 21.63 years compared to other studies (Fujiwara et al. 2009; Ikuno & Tano 2009; Margolis & Spaide 2009; Esmaeelpour et al. 2010; Manjunath et al. 2010; Flores-Moreno et al. 2013). In addition, there were variations in OCT device characteristics such as wavelength, eye tracking method and averaging software among studies. In our results, CT decreased with increase in severity of myopic refractive error. The findings suggest that thinning or abnormalities of choroid play a role in the pathogenesis of myopic degeneration and thus visual impairment.

We found that CT in highly myopic eyes was thickest superiorly and thinnest nasally. In comparison, the choroid in normal eyes was thickest at the fovea and thinnest nasally. The observed pattern of CT distribution in our study is similar to the previous studies, in both myopes (Ikuno & Tano

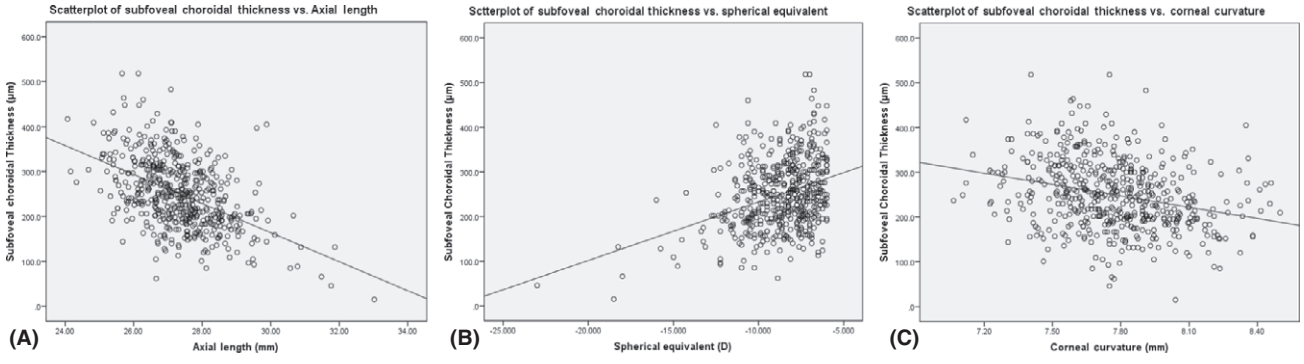

Fig. 2. (A) Scatterplot showing negative correlation between subfoveal choroidal thickness (CT) and axial length in all myopes. (B) Scatterplot showing positive correlation between subfoveal CT and spherical equivalent in all myopes. (C) Scatterplot showing negative correlation between subfoveal CT and corneal curvature in all myopes.

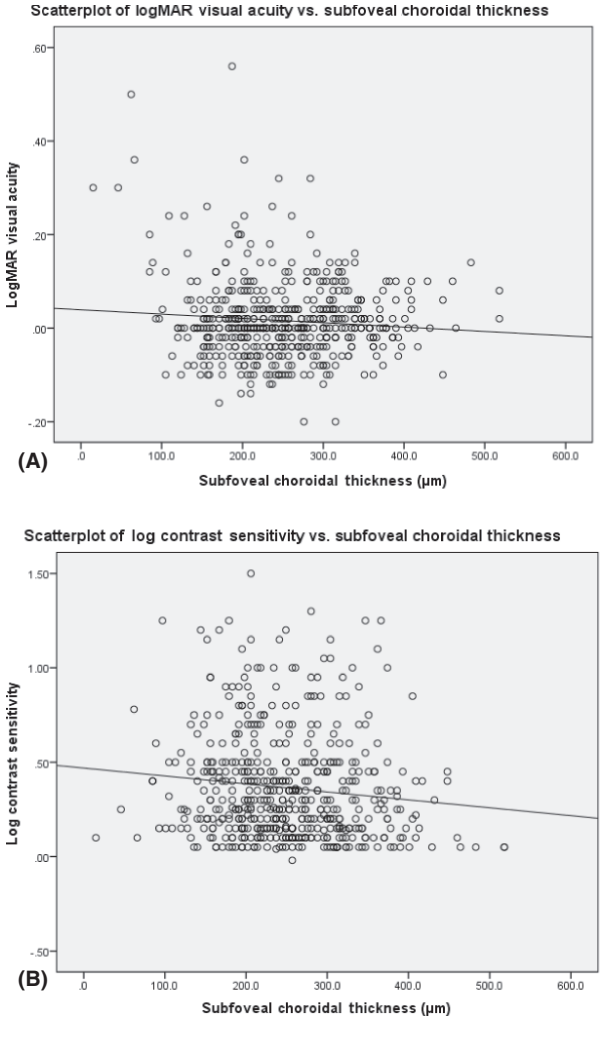

Fig. 3. (A) Scatterplot showing negative correlation between LogMAR visual acuity and subfoveal choroidal thickness (CT) in all myopes. (B) Scatterplot showing negative correlation between Log contrast sensitivity and subfoveal CT in all myopes.

2009; Goldenberg et al. 2012) and emmetropes (Margolis & Spaide 2009). Fujiwara et al. (2009) measured CT in high myopes only in the horizontal meridian and reported CT to be thickest temporal to the fovea (Hsiang et al. 2008). Two possible reasons for the relative choroidal thinning nasally and inferiorly in normal eyes are the choroidal watershed and the fetal choroidal fissure, which closes inferiorly at 7 weeks (Sadler 2006). In summary, the current thickness data agreed with the previous studies.

We found a significant negative association of SFCT with AL. In high myopia because of axial elongation, both the retina and choroid are stretched (Yanoff & Fine 1989; Lim et al. 2005; Lam et al. 2007) leading to thinning (Fujiwara et al. 2009; Ikuno & Tano 2009; Margolis & Spaide 2009). However, thinner choroid is still adequate to nourish proportionally thin retina which is consistent with fairly normal visual functions in adolescents and young adults with high myopia than their aged counterparts which undergoes further age-related reduction in choroid (Fujiwara et al. 2009). In contrast, in non-myopic elderly eyes, thinner choroid may not be adequate to supply the relatively thick retina which might in turn influence visual function. We therefore speculate that the relatively thin choroid in young myopes may be physiologically sufficient, although the same CT may be considered pathologic in older eyes without myopia.

In contrast to Nishida's study (Nishida et al. 2012) that demonstrated CT to be an important predictor of visual acuity in high myopes, we did not find a significant correlation between SFCT and visual acuity. They speculated that a thin choroid may deliver decreased amounts of oxygen and nutrients to the retina, thus potentially affecting signal generation from the photoreceptors or cause loss of the overlying photoreceptors as a consequence (Nishida et al. 2012). The discrepancy may be due to differences in age groups and CT between our study and Nishida's study. The mean age of the participants in Nishida et al. study was 57 years, and with the advancing age, the choroid may undergo further age-related attenuation (Fujiwara et al. 2009; Margolis

Table 5. Summary of CT and other variables in various studies in high myopia.

Study	No of eyes	Mean Age, years	AL, mm	SE, dioptres	OCT Machine	EDI (yes/no)	Mean CT,* μm
Current study	520	21.59	27.32	−8.68	Spectralis SD-OCT	Yes	225.87 (5.51)
Flores-Moreno et al. (2013)	120	54.4	29.17	−14.34	Topcon 3D-2000 OCT	No	115.5 (85.3)
Fujiwara et al. (2009)	55	59.7	–	−11.9	Spectralis SD-OCT	Yes	93.2 (62.5)
Ikuno & Tano (2009)	31	51.7	29.6	−15.5	Cirrus SD-OCT	No	99.3 (58.8)
Takahashi et al. 2012;	20	63.4	28.37	−10.8	Cirrus SD-OCT	No	68.1 (10.5)
Chen et al. (2012)	20	28.8	–	−9.29	Spectralis SD-OCT	Yes	156.07 (86.3)

EDI = enhanced depth imaging; SD-OCT = spectral domain optical coherence tomography; AL = axial length; CT = choroidal thickness; SE = spherical equivalent; "–"not available.
* Data are mean (SD) except current study which is mean (standard error).

& Spaide 2009). A substantially thinner choroid (113.3 μm) observed in Nishida's study suggests that the magnitude of thinning is likely the reason for the observed relationship with visual acuity, that is there is a threshold level of choroidal thinning, beyond which retinal function becomes compromised. Thus, available supply from choroid may not be sufficient to support outer retina, the RPE and even the choroid itself, which may explain why vision was affected. In contrast, our young participants with thicker choroid (225.87 μm) retained their retinal function and therefore enjoyed better vision. In addition, their results may be confounded by other ocular comorbidities due to ageing, while our study involved younger subjects with few ocular comorbidities, and thus, the results are less complicated by confounding factors.

Presence of posterior staphyloma, a hallmark of high myopia, was significantly associated with choroidal thinning. Similar results were reported in the previous studies which demonstrated posterior staphyloma formation as a key factor in choroidal thinning in highly myopic eyes (Fujiwara et al. 2009; Ikuno & Tano 2009). This association is probably because in myopic eyes with posterior staphyloma, choroidal circulation is altered with marked attenuation and reduction in number of large choroidal vessels (Quaranta et al. 1996). In addition, there is a shift in the entry site of the posterior ciliary arteries towards the staphyloma's border leading to scarce choroidal arterial network in the area occupied by staphyloma (Moriyama et al. 2007). Thus, all these changes lead to choroidal thinning in eyes with staphyloma.

The study has several strengths. Our study has a relatively large sample size, and EDI SD-OCT images were enhanced using adaptive compensation (Wang et al. 1994) to improve CSI visibility. Therefore, the CT measurements obtained in our study are likely more reliable and accurate. Unlike other studies, our study included an emmetropic group, and therefore, we could examine the differences between highly myopic eyes and non-myopic eyes in our case–control study. The study also has some limitations. First, due to our cross-sectional study design, we were unable to determine the causal relationships between the various risk factors and CT. Second, all of our study subjects were males, and thus, some of our findings may not be generalized to females. Previous studies have shown higher CT in men than in women adjusting for age and AL (Li et al. 2011). Third, by not taking into account AL to correct for ocular magnification, there may still be some residual error. Lastly, only horizontal and vertical scan lines were used to determine the CT profile. A denser scanning protocol is likely to provide further insights regarding the thickness profile across the posterior pole. While denser scanning protocols may not be feasible with manual segmentation and large subject numbers, the development of automated choroidal segmentation methods opens the door for potential future studies to use denser scanning protocols to determine the topographical thickness profile of the choroid, which will likely provide additional insights into the changes in the choroid associated with myopia.

Conclusion

Our study shows that CT is significantly lower in high myopic eyes. Macular CT distribution follows a different profile in high myopia compared to emmetropes. AL, presence of posterior staphyloma and chorio-retinal atrophy are the significant predictors of CT in high myopia and must be taken into account when interpreting the data on CT. Given the large number of people with myopia in the world, these findings seem to have widespread implications.

References

Attebo K, Ivers RQ & Mitchell P (1999): Refractive errors in an older population: the Blue Mountains Eye Study. Ophthalmology **106**: 1066–1072.

Avila MP, Weiter JJ, Jalkh AE, Trempe CL, Pruett RC & Schepens CL (1984): Natural history of choroidal neovascularization in degenerative myopia. Ophthalmology **91**: 1573–1581.

Chen W, Wang Z, Zhou X, Li B & Zhang H (2012): Choroidal and photoreceptor layer thickness in myopic population. Eur J Ophthalmol **22**: 590–597.

Cheung CM, Loh BK, Li X, Mathur R, Wong E, Lee SY, Wong D & Wong TY (2013): Choroidal thickness and risk characteristics of eyes with myopic choroidal neovascularization. Acta Ophthalmol **91**: e580–e581.

Curtin BJ (1982): Posterior staphyloma development in pathologic myopia. Ann Ophthalmol **14**: 655–658.

Curtin BJ & Karlin DB (1971): Axial length measurements and fundus changes of the myopic eye. Am J Ophthalmol **71**: 42–53.

Davies BW, Rabin J, Gooch J et al. (2004): Quantification of visual resolution in the contrast domain. Invest Ophthalmol Vis Sci, e-abstract 4351.

Esmaeelpour M, Povazay B, Hermann B et al. (2010): Three-dimensional 1060-nm OCT: choroidal thickness maps in normal subjects and improved posterior segment visualization in cataract patients. Invest Ophthalmol Vis Sci **51**: 5260–5266.

Fleiss JL & Cohen J (1973): The equivalence of weighted kappa and the intraclass correlation coefficient as measures of reliability. Educ Psychol Measur **33**: 613–619.

Flores-Moreno I, Lugo F, Duker JS & Ruiz-Moreno JM (2013): The relationship between axial length and choroidal thickness in eyes with high myopia. Am J Ophthalmol **155**: 314–319 e311.

Fredrick DR (2002): Myopia. BMJ (Clinical Research ed.) **324**: 1195–1199.

Fujiwara T, Imamura Y, Margolis R, Slakter JS & Spaide RF (2009): Enhanced depth imaging optical coherence tomography of the choroid in highly myopic eyes. Am J Ophthalmol **148**: 445–450.

Fujiwara A, Shiragami C, Shirakata Y, Manabe S, Izumibata S & Shiraga F (2012): Enhanced depth imaging spectral-domain optical coherence tomography of subfoveal choroidal thickness in normal Japanese eyes. Jpn J Ophthalmol **56**: 230–235.

Garway-Heath DF, Rudnicka AR, Lowe T, Foster PJ, Fitzke FW & Hitchings RA (1998): Measurement of optic disc size: equivalence of methods to correct for ocular magnification. Br J Ophthalmol **82**: 643–649.

Girard MJ, Strouthidis NG, Ethier CR & Mari JM (2011): Shadow removal and contrast enhancement in optical coherence tomography images of the human optic nerve head. Invest Ophthalmol Vis Sci **52**: 7738–7748.

Goldenberg D, Moisseiev E, Goldstein M, Loewenstein A & Barak A (2012): Enhanced depth imaging optical coherence tomography: choroidal thickness and correlations with age, refractive error, and axial length. Ophthalmic Surg Lasers Imaging **43**: 296–301.

Gupta P, Sidhartha E, Girard MJ, Mari JM, Wong TY & Cheng CY (2014): A simplified method to measure choroidal thickness using adaptive compensation in enhanced depth imaging optical coherence tomography. PLoS ONE **9**: e96661.

Hashizume K, Imamura Y, Fujiwara T, Machida S, Ishida M & Kurosaka D (2014): Choroidal thickness in eyes with posterior recurrence of Vogt-Koyanagi-Harada disease after high-dose steroid therapy. Acta Ophthalmol **92**: e490–e491.

Hayashi K, Ohno-Matsui K, Shimada N et al. (2010): Long-term pattern of progression of myopic maculopathy: a natural history study. Ophthalmology **117**: 1595–1611, 1611 e1591–1594.

Ho M, Liu DT, Chan VC & Lam DS (2013): Choroidal thickness measurement in myopic eyes by enhanced depth optical coherence tomography. Ophthalmology **120**: 1909–1914.

Hofman A, Grobbee DE, de Jong PT & van den Ouweland FA (1991): Determinants of disease and disability in the elderly: the Rotterdam Elderly Study. Eur J Epidemiol **7**: 403–422.

Hsiang HW, Ohno-Matsui K, Shimada N, Hayashi K, Moriyama M, Yoshida T, Tokoro T & Mochizuki M (2008): Clinical characteristics of posterior staphyloma in eyes with pathologic myopia. Am J Ophthalmol **146**: 102–110.

Ikuno Y & Tano Y (2009): Retinal and choroidal biometry in highly myopic eyes with spectral-domain optical coherence tomography. Invest Ophthalmol Vis Sci **50**: 3876–3880.

Ikuno Y, Kawaguchi K, Nouchi T & Yasuno Y (2010): Choroidal thickness in healthy Japanese subjects. Invest Ophthalmol Vis Sci **51**: 2173–2176.

Jonas JB, Holbach L & Panda-Jonas S (2014): Bruch's membrane thickness in high myopia. Acta Ophthalmol **92**: 470–474.

Kim DY, Silverman RH, Chan RV, Khanifar AA, Rondeau M, Lloyd H, Schlegel P & Coleman DJ (2013): Measurement of choroidal perfusion and thickness following systemic sildenafil (Viagra((R))). Acta Ophthalmol **91**: 183–188.

Lam DS, Leung KS, Mohamed S et al. (2007): Regional variations in the relationship between macular thickness measurements and myopia. Invest Ophthalmol Vis Sci **48**: 376–382.

Li XQ, Larsen M & Munch IC (2011): Subfoveal choroidal thickness in relation to sex and axial length in 93 Danish university students. Invest Ophthalmol Vis Sci **52**: 8438–8441.

Lim MC, Hoh ST, Foster PJ, Lim TH, Chew SJ, Seah SK & Aung T (2005): Use of optical coherence tomography to assess variations in macular retinal thickness in myopia. Invest Ophthalmol Vis Sci **46**: 974–978.

Lin LL, Shih YF, Hsiao CK & Chen CJ (2004): Prevalence of myopia in Taiwanese schoolchildren: 1983 to 2000. Ann Acad Med Singapore **33**: 27–33.

Manjunath V, Taha M, Fujimoto JG & Duker JS (2010): Choroidal thickness in normal eyes measured using Cirrus HD optical coherence tomography. Am J Ophthalmol **150**: 325–329 e321.

Margolis R & Spaide RF (2009): A pilot study of enhanced depth imaging optical coherence tomography of the choroid in normal eyes. Am J Ophthalmol **147**: 811–815.

Mari JM, Strouthidis NG, Park SC & Girard MJ (2013): Enhancement of lamina cribrosa visibility in optical coherence tomography images using adaptive compensation. Invest Ophthalmol Vis Sci **54**: 2238–2247.

Moriyama M, Ohno-Matsui K, Futagami S et al. (2007): Morphology and long-term changes of choroidal vascular structure in highly myopic eyes with and without posterior staphyloma. Ophthalmology **114**: 1755–1762.

Nishida Y, Fujiwara T, Imamura Y, Lima LH, Kurosaka D & Spaide RF (2012): Choroidal thickness and visual acuity in highly myopic eyes. Retina **32**: 1229–1236.

Noble KG & Carr RE (1982): Pathologic myopia. Ophthalmology **89**: 1099–1100.

Ohno-Matsui K & Tokoro T (1996): The progression of lacquer cracks in pathologic myopia. Retina **16**: 29–37.

Quaranta M, Arnold J, Coscas G, Francais C, Quentel G, Kuhn D & Soubrane G (1996): Indocyanine green angiographic features of pathologic myopia. Am J Ophthalmol **122**: 663–671.

Sadler TW (2006): Langman's medical embryology. Baltimore, MD: Lippincott Williams and Wilkins.

Shaikh AW, Siegwart JT Jr & Norton TT (1999): Effect of interrupted lens wear on compensation for a minus lens in tree shrews. Optom Vis Sci **76**: 308–315.

Spaide RF, Koizumi H & Pozzoni MC (2008): Enhanced depth imaging spectral-domain optical coherence tomography. Am J Ophthalmol **146**: 496–500.

Takahashi A, Ito Y, Iguchi Y, Yasuma TR, Ishikawa K & Terasaki H (2012): Axial length increases and related changes in highly myopic normal eyes with myopic complications in fellow eyes. Retina **32**: 127–133.

Tan CS, Cheong KX & Sadda SR (2014): Changes in choroidal thickness after photodynamic therapy in patients with central serous chorioretinopathy. Acta Ophthalmol **92**: e79.

Troilo D, Nickla DL & Wildsoet CF (2000): Choroidal thickness changes during altered eye growth and refractive state in a primate. Invest Ophthalmol Vis Sci **41**: 1249–1258.

Vongphanit J, Mitchell P & Wang JJ (2002): Prevalence and progression of myopic retinopathy in an older population. Ophthalmology **109**: 704–711.

Wallman J, Wildsoet C, Xu A, Gottlieb MD, Nickla DL, Marran L, Krebs W & Christensen AM (1995): Moving the retina: choroidal modulation of refractive state. Vision Res **35**: 37–50.

Wang Q, Klein BE, Klein R & Moss SE (1994): Refractive status in the Beaver Dam Eye Study. Invest Ophthalmol Vis Sci **35**: 4344–4347.

Wei WB, Xu L, Jonas JB et al. (2013): Subfoveal choroidal thickness: the Beijing Eye Study. Ophthalmology **120**: 175–180.

Wong TY, Foster PJ, Hee J, Ng TP, Tielsch JM, Chew SJ, Johnson GJ & Seah SK (2000): Prevalence and risk factors for refractive errors in adult Chinese in Singapore. Invest Ophthalmol Vis Sci **41**: 2486–2494.

Wu HM, Seet B, Yap EP, Saw SM, Lim TH & Chia KS (2001): Does education explain ethnic differences in myopia prevalence? A population-based study of young adult males in Singapore. Optom Vis Sci **78**: 234–239.

Yanoff M & Fine BS (1989): Ocular pathology: a text and atlas. Philadelphia, PA: JB Lippincott.

Zhou M, Wang W, Huang W, Gao X, Li Z, Li X & Zhang X (2014): Is increased choroidal thickness association with primary angle closure? Acta Ophthalmol **92**: 514–520.

Received on June 15th, 2014.
Accepted on November 14th, 2014.

Correspondence:
Dr Ching-Yu Cheng, MD, PhD
Singapore Eye Research Institute
20 College Road, The Academia, Level 6,
Discovery Tower, Singapore 169856
Tel: +65 6576 7277
Fax: +65 6225 2568
Email: ching-yu_cheng@nuhs.edu.sg

This study was funded by Ministry of Defence (MINDEF), Singapore and Singapore Ministry of Education, Academic Research Fund, Tier 1. The funding organization had no role in the design or conduct of this research. No conflicting relationship exists for any author.

Peripapillary Choroidal Thickness in Young Asians With High Myopia

Preeti Gupta,[1,2] Carol Y. Cheung,[1–3] Seang-Mei Saw,[1–4] Mayuri Bhargava,[1,2] Colin S. Tan,[5,6] Mellisa Tan,[7] Adeline Yang,[7] Frederick Tey,[7] Gerard Nah,[2,8] Paul Zhao,[2,8] Tien Yin Wong,[1–4] and Ching-Yu Cheng[1–4]

[1]Singapore Eye Research Institute and Singapore National Eye Centre, Singapore
[2]Department of Ophthalmology, Yong Loo Lin School of Medicine, National University of Singapore and National University Health System, Singapore
[3]Duke-NUS Graduate Medical School, Singapore
[4]Saw Swee Hock School of Public Health, National University of Singapore, Singapore
[5]National Healthcare Group Eye Institute, Tan Tock Seng Hospital, Singapore
[6]Fundus Image Reading Center, National Healthcare Group Eye Institute, Singapore
[7]DSO National Laboratories, Defence Medical and Environmental Research Institute, Singapore
[8]Vision Performance Centre, Military Medical Institute, Singapore Armed Forces, Singapore

Correspondence: Ching-Yu Cheng, Ocular Epidemiology Research Group and Statistics Unit, Singapore Eye Research Institute, 20 College Road, The Academia, Level 6, Discovery Tower, Singapore 169856; ching-yu_cheng@nuhs.edu.sg.

Submitted: September 25, 2014
Accepted: January 27, 2015

Citation: Gupta P, Cheung CY, Saw S-M, et al. Peripapillary choroidal thickness in young Asians with high myopia. *Invest Ophthalmol Vis Sci*. 2015;56:1475–1481. DOI:10.1167/iovs.14-15742

Purpose. To describe the topography and predictors of peripapillary choroidal thickness (PPCT) in highly myopic eyes of young, healthy, Asian subjects.

Methods. A total of 870 young male subjects aged 21.63 ± 1.15 years were recruited from the Singapore military. Choroidal imaging was performed using enhanced depth imaging (EDI) spectral-domain optical coherence tomography (SD-OCT). Peripapillary choroidal thickness was manually measured at eight locations around the optic disc.

Results. We analyzed 448 subjects with high myopia (defined as spherical equivalent [SE] worse than −6.0 diopters [D]) and 116 with emmetropia (SE > −0.5 and < 0.5 D). The mean SE was −8.52 ± 1.20 D for the high-myopic group, and 0.11 ± 0.24 D for the emmetropic group. The mean peripapillary choroid was significantly thinner (142.62 ± 43.84 μm) in high myopes compared with emmetropes (181.90 ± 46.43 μm, $P < 0.001$). Likewise, PPCT showed further decrease with increase in degree of myopic refractive error. Distribution of PPCT showed a markedly different pattern in high-myopic eyes (thickest superiorly) and emmetropic eyes (thickest temporally). However, peripapillary choroid in both the groups was thinnest at the inferior location. Among the ocular factors studied, axial length, IOP, presence of posterior staphyloma, and chorioretinal atrophy were the factors significantly associated with PPCT.

Conclusions. Highly myopic eyes have significantly thinner peripapillary choroid and showed different distribution of thickness, compared with emmetropes. Axial length, IOP, and presence of posterior staphyloma and chorioretinal atrophy significantly influence PPCT and should be taken into consideration during clinical interpretation of PPCT measurement.

Keywords: myopia, peripapillary choroidal thickness, spectral-domain optical coherence tomography

The choroid contributes blood supply not only to the outer retina[1] including retinal pigmented epithelium (RPE) and photoreceptors, but also to the prelaminar portion of the optic nerve.[2] Given the role of the choroidal vasculature in the blood supply of the anterior optic nerve head, a variety of ocular pathologies including glaucoma[3,4] and high myopia[5] occur in the peripapillary choroidal region. High myopia itself is also associated with a high prevalence of retinal complications such as posterior staphyloma,[6,7] lacquer cracks,[8] chorioretinal atrophy as well as optic disc changes, such as oval configuration, larger area of peripapillary atrophy, and disc tilt and rotation,[9] which may potentially affect the thickness and distribution profile of peripapillary choroid. Quantitative analysis of peripapillary choroidal thickness (PPCT) may help elucidate the mechanisms through which the peripapillary choroid affects these diseases. With the advancement in imaging technology, optical coherence tomography–based enhanced depth imaging (EDI-OCT)[10] provides an easy and noninvasive way to measure PPCT.

Several studies have previously compared choroidal thickness in the macula area between myopes versus healthy eyes.[11–15] However, none of the studies have explored the distribution of choroidal thickness around the optic disc in high myopes. Although a few studies have also reported on the characteristics of PPCT in healthy eyes,[16–19] most were performed retrospectively in relatively small clinic-based samples, and thus generalization of findings may be limited. The aim of our study was to quantify and compare the pattern of distribution of PPCT based on the degree of myopia and to determine the ocular determinants of PPCT measured by EDI

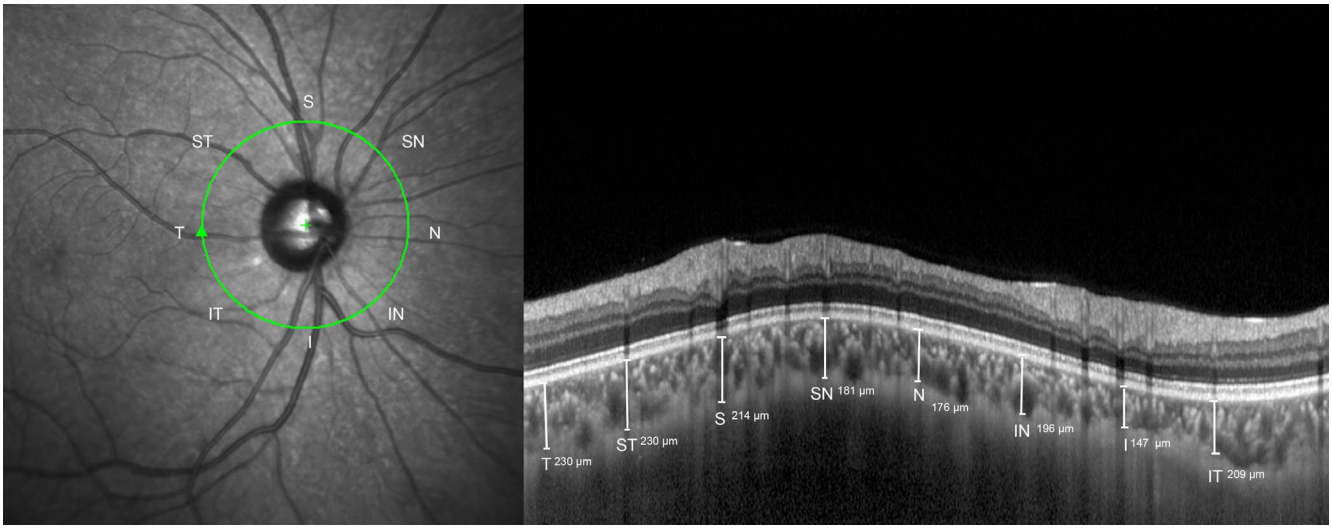

Figure 1. Enhanced-depth imaging OCT image demonstrating peripapillary region scanned using a 360°, 3.5-mm diameter circle centered on the optic disc. The peripapillary choroidal thickness was measured as the perpendicular distance between Bruch's membrane and the choroid–scleral interface at the following locations: T, temporal; ST, superotemporal; S, superior; SN, superonasal; N, nasal; IN, inferonasal; I, inferior; IT, inferotemporal.

spectral-domain (SD)-OCT in an Asian sample. We used a case-control study approach of young, highly myopic, and emmetropic healthy male adults selected from a large population from the Singapore military. Accurate and reliable measurements of PPCT and knowledge of its normal distribution is of clinical importance in the diagnosis and management of diseases where choroid is implicated in the pathophysiology.

Materials and Methods

Study Population and Design

A total of 28,908 male adults were screened for myopia (mean age ± SD: 19.8 ± 1.2 years; range, 17–29 years) from 2009 to 2010 as part of a mandatory medical eye review for employment purposes. Measured using noncycloplegic autorefraction (Huvitz MRK-3100P; Huvitz Co., Ltd., Geumjeong-dong, Gunpo-si Gyeonggi-do, South Korea), 2584 persons were identified to have myopia with spherical equivalent (SE) of –6.0 diopters (D) or worse. Of these 2584 persons, 719 were selected on the basis of a refractive error–stratified random sampling strategy and underwent a further comprehensive ophthalmologic examination at Singapore Eye Research Institute from December 2011 to June 2012. Their SE was further confirmed by subjective refraction, and those with SE less than –6.0 D ($n = 96$) were excluded, leaving 623 subjects with high myopia (251 with SE between –6.0 D and –8.0 D; 207 with SE between –8.0 D and –10.0 D; 165 with SE –10.0 D or worse). In addition, 151 emmetropes who had SE between ±0.5 D in both eyes measured using autorefraction were recruited as controls and went through a similar ophthalmologic examination. Subjects were further excluded if they did not give consent to take part in this medical review, had any previous ocular trauma or surgery, and those with other clinically significant ocular comorbidity.

Written informed consent were taken from the subjects and their parents/guardians (if they were 21 years old and younger). Ethics approval was obtained from the institutional review board of Singapore Eye Research Institute, Singapore. The study was conducted in accordance with the tenets of the World Medical Association's Declaration of Helsinki.

Ophthalmic Examination and Measurements

Objective refraction was measured using Canon Autorefractor RK-F1 (Tokyo, Japan). Spherical equivalent was calculated as the sum of the spherical power and one-half of the cylinder power. Best-corrected visual acuity (BCVA), in which refraction was corrected, was measured monocularly using a logarithm of the minimum angle of resolution (logMAR) chart (Lighthouse International, New York, NY, USA) at a distance of 4 m. Biometry measurements (i.e., axial length [AL], anterior chamber depth [ACD], and keratometry readings) were obtained from the noncontact Zeiss IOL Master (V3.01; Carl Zeiss Meditec AG, Jena, Germany). Intraocular pressure was measured using Nidek noncontact tonometry (Auto Non-Contact Tonometer, NT-3000; Nidek, Gamagori, Aichi, Japan) and if IOP was found to be 21 mm Hg or more, Goldmann applanation tonometry (Haag-Streit, Bern, Switzerland) was performed by study ophthalmologists.

Subjects underwent slit-lamp examination. Binocular indirect ophthalmoscopy was performed approximately 30 minutes after topical instillation of three drops of tropicamide and 2.5% phenylephrine, given 5 minutes apart. Dilated fundus examination was carried out by the study ophthalmologist. The presence and type of peripheral retinal degenerations and vitreous degenerations were systematically documented. Fundus photography was performed using nonmydriatic retinal camera (Canon CR-DGi with a 10D/20D/40D SLR back; Canon, Tokyo, Japan).

OCT Imaging

The peripapillary choroidal parameters were determined using SD-OCT (Spectralis, Wavelength: 870 nm; Heidelberg Engineering, Heidelberg, Germany). Peripapillary choroid was imaged with EDI modality after pupil dilation. Enhanced-depth imaging is a method that improves resolution of choroidal detail by automatically setting the choroid closer to the zero-delay line, and thus provides better visualization of the choroid scleral interface than in standard retinal SD-OCT images. The peripapillary region was scanned using a 360°, 3.5-mm diameter circle centered on the optic disc (Fig. 1), each comprising 100 averaged scans (using the proprietary automatic averaging and eye tracking features of the SD-OCT

Table 1. Clinical Characteristics of the Study Subjects

	Myopes, $n = 448$	Emmetropes, $n = 116$	P Value*
Age, y	21.63 (1.15)	22.03 (0.96)	<0.001
AL, mm	27.23 (1.07)	23.70 (0.61)	<0.001
ACD, mm	3.74 (0.25)	3.46 (0.27)	<0.001
Corneal curvature, mm	7.76 (0.25)	7.81 (0.41)	0.123
SE, D	−8.52 (1.80)	0.11 (0.24)	<0.001
BCVA, logMAR	0.01 (0.07)	−0.09 (0.06)	<0.001
IOP, mm Hg	16.11 (2.95)	15.22 (2.64)	0.003
RNFL thickness, μm	87.21 (8.94)	103.76 (9.99)	<0.001

Data presented are means (SD).
* Based on independent sample *t*-test.

Table 2. Intragrader Reliability of Peripapillary Choroidal Thickness Measurements in Myopic and Emmetropic Group at Different Locations

Locations of Measurement	Myopes ICC (95% CI)	Emmetropes ICC (95% CI)
PPCT		
Temporal, 360°	0.97 (0.92–0.98)	0.96 (0.90–0.98)
Superotemporal, 45°	0.97 (0.94–0.99)	0.98 (0.95–0.99)
Superior, 90°	0.98 (0.96–0.99)	0.96 (0.90–0.98)
Superionasal, 135°	0.98 (0.96–0.99)	0.97 (0.92–0.98)
Nasal, 180°	0.97 (0.93–0.99)	0.96 (0.90–0.98)
Inferonasal, 225°	0.96 (0.92–0.98)	0.96 (0.91–0.98)
Inferior, 270°	0.96 (0.91–0.98)	0.95 (0.88–0.98)
Inferotemporal, 315°	0.96 (0.90–0.98)	0.96 (0.90–0.98)

device). Following Spectralis user manual guidelines, subjects' keratometry readings and refraction were entered into the Spectralis' software before the choroid was imaged to estimate optical magnification, thus allowing for more accurate comparisons across individuals. However, Spectralis OCT does not allow AL to be input, our methods may still have residual errors (2%–7%)[20] due to ocular magnification from methods that additionally uses AL. Only the right eye of each study participant was included for analysis.

Measurement of Peripapillary Choroidal Thickness

The PPCT was measured manually using the Heidelberg Eye Explorer software (version 1.5.12.0; Heidelberg Engineering) as the perpendicular distance between the outer portion of the hyperreflective line corresponding to the RPE (automatically detected by the instrument) to the hyporeflective line or margin corresponding to the sclerochoroidal interface (manually drawn by an experienced grader, who was masked to subject characteristics and clinical diagnosis) at the following locations around the optic disc: temporal, superotemporal, superior, superonasal, nasal, inferonasal, inferior, and inferotemporal. In addition, the intraobserver reliability of PPCT measurements was evaluated in both the myopic and emmetropic group. Forty randomly selected Spectralis images (20 from each group) were assessed again by the same grader after an interval of 1 week.

Statistical Analysis

Subjects were excluded from analysis if they had any history of anterior ocular diseases, previous ocular trauma, evidence of macular or vitreoretinal diseases or any form of refractive surgery done in their eyes. However, conditions such as, peripapillary atrophy, lacquer crack, posterior staphyloma, chorioretinal atrophy, or tilted discs were not excluded, as they are commonly seen in high-myopic eyes. Statistical analysis was performed using SPSS version 17.0 (SPSS, Inc., Chicago, IL, USA) and MedCalc version 12.3 (Medcalc Software, Ostend, Belgium). The intrasession repeatability of the PPCT was measured by the absolute agreement model of the intraclass correlation coefficient (ICC).[21]

The demographics and ocular parameters between myopic and control eyes were compared using independent *t*-tests. For the purpose of analyses, myopic eyes were divided into three groups based on SE: less than –6.0 to –8.0 D, less than –8.0 to –10.0 D, and worse than –10.0 D. Subgroup analysis of choroidal thickness across different locations in eyes with varying degree of myopia was performed. Repeated measures ANOVA with Bonferroni posttest was used to compare mean thicknesses at various locations within each group. Univariate and multiple linear regression analyses were performed to determine the association of ocular factors (independent variables) with PPCT measurements (dependent variables). For multiple linear regression, age, and factors, which showed significant association in univariate analysis ($P < 0.05$) were included.

Results

Of the 623 eligible high myopes (SE ≤ –6.0 D), we further excluded 175 subjects because their choroidal images were not successfully attained due to unstable fixation ($n = 62$), the available images were not of optimal quality (a quality index of < 25 dB as suggested by the manufacturer for the image quality assurance, $n = 39$), those where the choroid–scleral interface was not clearly delineated ($n = 21$) to perform accurate measurements, subjects whose peripapillary atrophy involved the OCT scanning ring ($n = 30$), or they did not meet the inclusion criteria ($n = 23$), leaving 448 high myopes with complete data on PPCT for analysis. Of the 151 emmetropes recruited, 35 were found to have SE greater than ± 0.5 D on subjective refraction and were excluded, leaving 116 emmetropes for analysis.

The mean age of included myopic and emmetropic subjects was 21.63 ± 1.15 years and 22.03 ± 0.96 years ($P < 0.001$), respectively. The mean SE was –8.52 ± 1.80 D (range, –6 to –18.25 D) for myopic group, and 0.11 ± 0.24 D for emmetropic group. Among the myopic group, nearly all our subjects (97.3%) had peripapillary atrophy, 41.3% had posterior staphyloma, 6.3% had chorioretinal atrophy, 0.4% had lacquer cracks, and 22.5% had tilted disc. The demographics and ocular characteristics of the study population are shown in Table 1. In terms of reliability of PPCT measurements, the intraobserver reliability for myopic (ICC: 0.96–0.98) and emmetropic (ICC: 0.95–0.98) group was excellent for all locations of PPCT (Table 2).

Peripapillary choroidal thickness varied significantly across the myopic subgroups and the emmetropic group at all the locations (P for trend < 0.001 for all locations, Table 3). Peripapillary choroidal thickness was significantly thinner in the more myopic eyes over a range of eccentricities and their pattern of distribution was different from emmetropes (Fig. 2). Across the three myopic subgroups, peripapillary choroid was thickest (163.41 ± 50.43 μm) at the superior location, whereas in emmetropes it was thickest (207 ± 58.01 μm) at the temporal location. Peripapillary choroid was thinnest in both myopes (109.98 ± 37.30 μm) and control eyes (137.90 ± 44.53 μm) at the inferior location.

In the univariate analysis, SE, AL, corneal curvature, IOP, average retinal nerve fiber layer (RNFL) thickness, and

Table 3. Distribution of Mean Peripapillary Choroidal Thickness at Different Locations Across the Three Myopic and Control Groups

Locations	Emmetropes, $n = 116$	High Myopia: All, $n = 448$	High Myopia: SE < -6 to -8 D, $n = 211$	High Myopia: SE < -8 to -10 D, $n = 143$	High Myopia: SE < -10 D, $n = 94$	*P* for Trend*
Temporal, 360°	207.00 (58.01)	138.47 (58.57)	151.30 (62.21)	132.45 (51.00)	118.85 (54.41)	<0.001
Superotemporal, 45°	201.89 (53.13)	150.32 (54.10)	160.10 (57.14)	144.51 (49.02)	137.23 (50.82)	<0.001
Superior, 90°	188.18 (50.17)	163.41 (50.43)	170.60 (52.08)	160.88 (47.30)	151.14 (49.03)	<0.001
Superionasal, 135°	189.15 (52.85)	162.21 (50.50)	169.58 (52.26)	159.19 (47.63)	150.24 (48.45)	<0.001
Nasal, 180°	189.24 (53.17)	161.97 (51.82)	170.66 (55.30)	157.36 (47.22)	149.51 (47.30)	<0.001
Inferonasal, 225°	168.68 (50.38)	137.82 (46.16)	146.83 (50.15)	132.62 (41.11)	125.53 (40.04)	<0.001
Inferior, 270°	137.90 (44.53)	109.98 (37.30)	117.01 (39.41)	106.91 (33.54)	98.88 (34.80)	<0.001
Inferotemporal, 315°	173.17 (52.10)	116.81 (49.12)	128.19 (54.12)	110.73 (41.25)	100.52 (42.05)	<0.001
Average	181.90 (46.43)	142.62 (43.84)	151.78 (46.79)	138.08 (38.53)	128.99 (40.20)	<0.001
	$P < 0.001$†	$P < 0.001$†	$P < 0.001$†	$P < 0.001$†	$P < 0.001$†	

Data presented are mean (SD) in micrometers.

* Peripapillary choroidal thickness varied significantly across the myopic subgroups and the emmetropic group at all the locations (*P* for trend < 0.001 for all locations).

† Repeated measures ANOVA, comparing the distribution of peripapillary choroidal thickness at various locations within each group.

presence of posterior staphyloma and chorioretinal atrophy were significantly associated with PPCT (all $P < 0.05$, Table 4). For each millimeter increase in AL and corneal curvature, PPCT on average decreased by 13.02 ($P < 0.001$) and 36.72 μm ($P < 0.001$), respectively. A decrease in mean PPCT by 5.39 μm was observed for each myopic diopter increase ($P < 0.001$). Each millimeter of mercury increase in IOP increased the PPCT by 1.40 μm, whereas for each micrometer increase in average

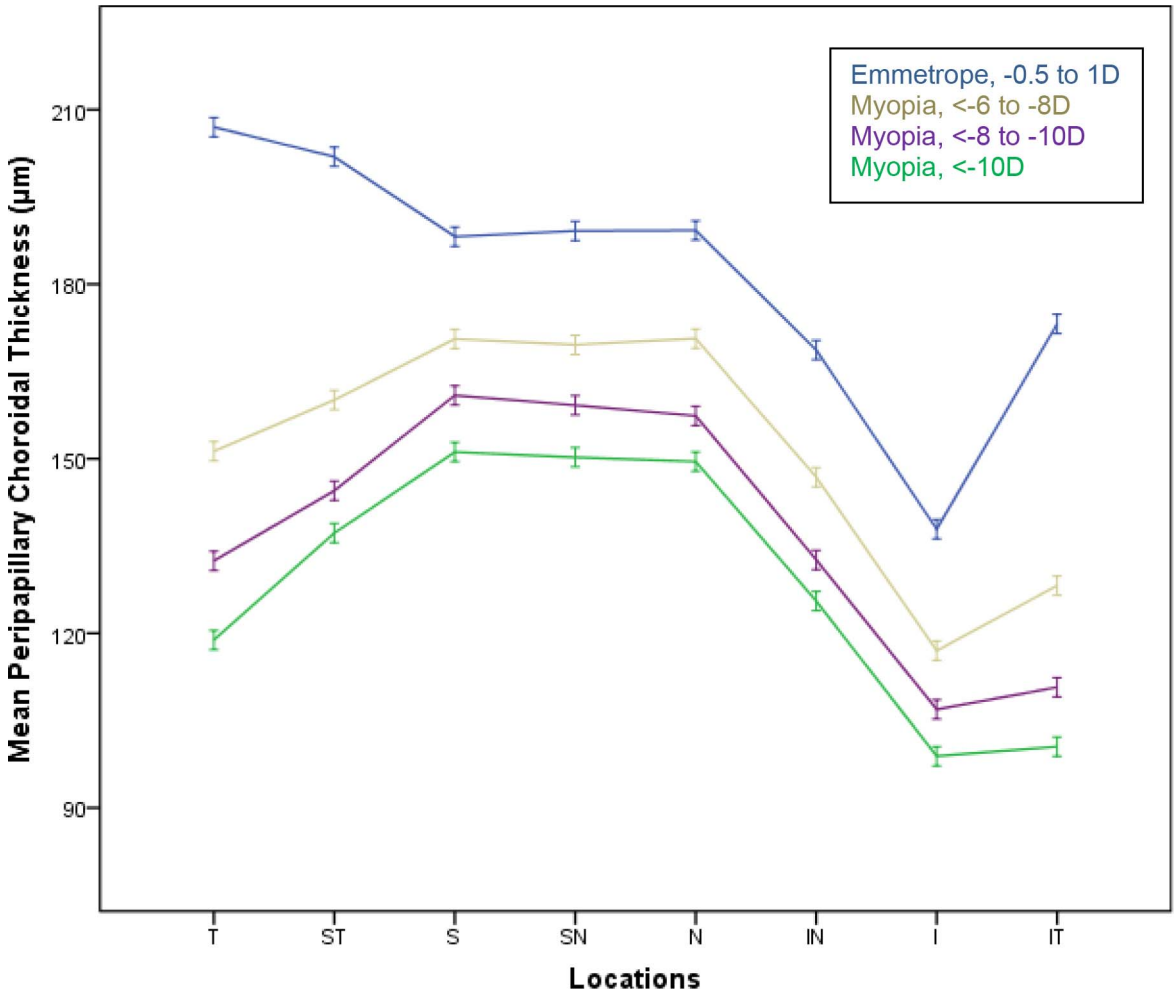

Figure 2. Graph showing the distribution of mean peripapillary choroidal thickness (μm) in high-myopic and emmetropic groups at different locations around the optic disc. The *x*-axis represents the locations of the measurements of peripapillary choroidal thickness around the optic disc. *Error bars* indicate standard error.

Table 4. Association of Ocular Factors With Average Peripapillary Choroidal Thickness in All Myopes ($n = 448$)

	Univariate Analysis			Multivariate Analysis		
	Unstandardized β Coefficient	Standardized β Coefficient	*P* Value	Unstandardized β Coefficient	Standardized β Coefficient	*P* Value
Ocular factors						
Age, y	−0.412	−0.011	0.818	-	-	-
SE, D	5.396	0.222	<0.001	-	-	-
AL, mm	−13.029	−0.319	<0.001	−7.090	−0.175	**0.001**
Corneal curvature, mm	−36.720	−0.216	<0.001	−4.456	−0.026	0.602
ACD, mm	−3.989	−0.023	0.631	-	-	-
IOP, mm Hg	1.407	0.095	0.045	1.628	0.111	**0.006**
Average RNFL thickness, μm	0.745	0.152	0.001	0.287	0.059	0.156
Posterior staphyloma	−15.296	−0.519	<0.001	−12.160	−0.433	**<0.001**
Chorioretinal atrophy	−14.768	−0.247	<0.001	−0.533	−0.089	**0.032**
Tilted disc	−2.814	−0.081	0.088	-	-	-

For multivariate analysis after adjusting for age there was no change in the result. Bold values indicate statistical significance.

RNFL thickness, PPCT increased by 0.74 μm. Presence of posterior staphyloma and chorioretinal atrophy decreased the PPCT by 15.29 and 14.76 μm, respectively (both $P < 0.001$). The results remained similar after adjusting for age (data not shown).

Because of collinearity between AL and SE (correlation coefficient = –0.574), only AL was selected and retained in the multivariate analysis as it had a greater explanatory power on PPCT change than did SE (standardized β, –0.319 vs. 0.222). There was no collinearity between posterior staphyloma and chorioretinal atrophy as variance inflation factor (VIF) was close to 1. In the multiple linear regression analysis, AL ($P = 0.001$), IOP ($P = 0.006$), presence of posterior staphyloma ($P < 0.001$), and chorioretinal atrophy ($P = 0.032$), remained significantly associated with PPCT, whereas the association with corneal curvature ($P = 0.062$) and RNFL thickness was abolished ($P = 0.156$). The results remained similar after adjusting for age. However, on performing a linear regression analysis between IOP and average PPCT in the emmetropic group we found no significant association ($P = 0.964$; regression coefficient = –0.075; 95% confidence interval [CI], –3.334 to 3.183).

Discussion

To our knowledge, this is the first study to measure PPCT directly with EDI SD-OCT in a large group of young, highly myopic Asian subjects. Peripapillary choroid in myopic group was significantly thinner than emmetropic control group at any locations. We demonstrated further decrease in PPCT with increase in degree of myopic refractive error. Peripapillary choroidal thickness distribution follows a different profile in high myopia (thickest superiorly), compared with emmetropia (thickest temporally). However in both the groups peripapillary choroid was thinnest at inferior location. Among the range of ocular factors studied, AL, IOP, and presence of posterior staphyloma and chorioretinal atrophy were the significant factors associated with PPCT.

None of previous studies so far have explored the profile of peripapillary choroid in high myopia and only a limited number of studies have reported the distribution of peripapillary choroid in emmetropic eyes. The mean PPCT in emmetropes was 181.90 ± 46.43 μm, which is in concurrence with former studies showing a mean thickness of 165.03[18] to 191.62[19] μm (Table 5).

In terms of distribution of PPCT, in both myopic and emmetropic eyes, peripapillary choroid was thinnest inferiorly. Studies done so far have consistently shown inferior region to be the thinnest among other regions of the posterior pole.[16–19] As optic fissure is located in the inferior aspect of the optic cup and is the last part of the globe to close,[22] this regional difference in ocular development may contribute to the thinner choroid found in inferior region. Thinner choroid would lead to decreased blood flow in choriocapillaris, which nourishes the prelaminar portion of the optic disk, making it more susceptible to hypoxia or to elevated IOP. This is supported by a very common observation that glaucoma typically affects the inferior optic disc region first.[16,23] The possible role of thinner choroid in glaucoma development is further supported by the findings of Usui et al.[24] and Hirooka et al.[23] who reported significant choroidal thinning in myopic normal-tension glaucoma–damage eyes as compared with myopic controls. Likewise, a substantial reduction in PPCT in patients with glaucoma who have sclerotic optic disc was demonstrated by Robert et al.[4] Tanabe et al.[16] showed thinner choroid in the inferior region of optic disks of healthy eyes. While some investigations[25–27] have reported finding that the PPCT did not seem to differ between healthy and glaucoma patients.

Table 5. Summary of Peripapillary Choroidal Thickness and Other Variables in Various Studies in Healthy Eyes

Study	No. of Eyes	Mean Age, y	AL, mm	SE, D	OCT Machine	EDI (Yes/No)	Mean PPCT,* μm
Current study (myopes)	448	21.63 (1.15)	27.23 (1.07)	−8.52 (1.80)	Spectralis SD-OCT	Yes	142.62 (43.84)
Current study (emmetropes)	116	22.03 (0.96)	23.70 (0.61)	0.11 (0.24)	Spectralis SD-OCT	Yes	181.90 (46.43)
Huang et al.[13]	76	56.95 (12.99)	23.20	0.31 (1.12)	Spectralis SD-OCT	Yes	165.03 (40.37)
Oh et al.[14]	40	41.2 (20.6)	-	−0.4 (1.1)	Topcon 3D-OCT	No	191.2 (62)
Tanabe et al.[11]	28	54.1 (20.0)	-	−3.6 (4.1)	Spectralis SD-OCT	Yes	-
Ho et al.[12]	36	48 (16)	-	-	Cirrus SD-OCT	No	-

* Data presented are means (SD).

We found peripapillary choroid in highly myopic eyes was thickest superiorly, whereas in emmetropic eyes was thickest temporally. This variation in the refractive error differences in choroidal thickness profile could be attributed to the presence of posterior staphyloma in highly myopic eyes. Although staphylomas may have various morphologic features, the most common types involve the macular and optic nerve regions.[28] Similar to our observation in emmetropes, Oh et al.[19] also reported peripapillary choroid to be thickest temporally. However, the observed pattern of PPCT distribution in emmetropes in our study differs from most of the previous studies in healthy eyes, which reported choroid to be thickest superiorly.[4,16–18,23,26] Although, the magnitude of the difference in thickness of the thickest point is not clinically significant (range, 15–20 μm). The differences in PPCT profile in our study compared with other studies could be because of the differences in age of our study participants. Our study participants are twice as young, mean age 22 years compared with other studies.[4,16–18,23,26] Thus, the exact reason for the variations in topographic profile of PPCT is not clear and further studies on a wide range of age group are needed.

Peripapillary choroidal thickness was significantly thinner in eyes with longer AL. The possible reason might be the anatomic differences in eyes of different refractive status with more stretched and therefore thinner peripapillary choroid in longer eyes. Therefore, AL deserves consideration in a normative database of PPCT measurement and should be taken into account while interpreting the results.

Interestingly, we found a positive association between PPCT and IOP in high myopes. Our results are in concordance with previous studies,[29] which using the pressure–volume relationship of the eye,[30] estimated that to produce an IOP increase of 5 mm Hg from the average IOP of 15 mm Hg, the choroid would need to expand uniformly by approximately 10 μm. Our subjects had a mean choroidal thickness increase of 2.38 μm for every millimeter of mercury increase in IOP supporting the conclusion that the IOP increase resulted from choroidal thickness increase.

In addition, we found that presence of posterior staphyloma was significantly associated with choroidal thinning in high myopes. Similar results were observed in the previous studies, which reported posterior staphyloma formation as a key factor in choroidal thinning in highly myopic eyes.[5,31] This association is probably because in myopic eyes with posterior staphyloma, choroidal circulation is altered with marked attenuation and reduction in number of large choroidal vessels.[32] In addition, there is a shift in the entry site of the posterior ciliary arteries toward the staphyloma's border leading to scarce choroidal arterial network in the area occupied by staphyloma.[33] Thus, all these changes contribute to choroidal thinning in eyes with staphyloma.

Strength and Limitations

The present study is one of the most large-scale, prospective studies conducted to investigate the topography and predictors of PPCT in myopic subjects. Unlike other studies, our study included a control group and therefore we could examine the differences between highly myopic eyes and nonmyopic eyes in our cohort. It involved a group of young, healthy, male, Asian subjects of uniform age and was thus free of confounding factors. However, these features may limit the application of these data to females and subjects of other groups or ethnicities. Further studies in other ethnic populations are warranted to confirm the results. Another limitation is that the cause–effect relationship cannot be ascertained due to the cross-sectional nature of our study. Recently, diurnal fluctuation of choroidal thickness was reported[34] and this could have impacted our results, though any impact of diurnal variation should be randomly distributed among myopic and emmetropic eyes.

Conclusions

There are regional differences in terms of distribution of PPCT. Peripapillary choroid was significantly thinner in the more myopic eyes over a range of eccentricities and follows a different profile compared with emmetropes. Axial length, IOP, presence of posterior staphyloma, and chorioretinal atrophy are the significant factors associated with PPCT in high-myopia eyes and must be taken into consideration when interpreting these data. Knowledge of normal PPCT and its profile in young, high myopes and emmetropes may aid in the understanding of physiological and pathological changes of peripapillary chorioretinal conditions.

Acknowledgments

Supported by grants from the Ministry of Defence (MINDEF), Singapore and Singapore Ministry of Education, Academic Research Fund, Tier 1.

Disclosure: **P. Gupta**, None; **C.Y. Cheung**, None; **S.-M. Saw**, None; **M. Bhargava**, None; **C.S. Tan**, None; **M. Tan**, None; **A. Yang**, None; **F. Tey**, None; **G. Nah**, None; **P. Zhao**, None; **T.Y. Wong**, None; **C.-Y. Cheng**, None

References

1. Linsenmeier RA, Padnick-Silver L. Metabolic dependence of photoreceptors on the choroid in the normal and detached retina. *Invest Ophthalmol Vis Sci*. 2000;41:3117–3123.
2. Hayreh SS. Blood supply of the optic nerve head and its role in optic atrophy, glaucoma, and oedema of the optic disc. *Br J Ophthalmol*. 1969;53:721–748.
3. Yin ZQ, Vaegan, Millar TJ, Beaumont P, Sarks S. Widespread choroidal insufficiency in primary open-angle glaucoma. *J Glaucoma*. 1997;6:23–32.
4. Roberts KF, Artes PH, O'Leary N, et al. Peripapillary choroidal thickness in healthy controls and patients with focal, diffuse, and sclerotic glaucomatous optic disc damage. *Arch Ophthalmol*. 2012;130:980–986.
5. Fujiwara T, Imamura Y, Margolis R, Slakter JS, Spaide RF. Enhanced depth imaging optical coherence tomography of the choroid in highly myopic eyes. *Am J Ophthalmol*. 2009;148:445–450.
6. Curtin BJ. Posterior staphyloma development in pathologic myopia. *Ann Ophthalmol*. 1982;14:655–658.
7. Curtin BJ, Karlin DB. Axial length measurements and fundus changes of the myopic eye. *Am J Ophthalmol*. 1971;71:42–53.
8. Jonas JB, Holbach L, Panda-Jonas S. Bruch's membrane thickness in high myopia. *Acta Ophthalmol*. 2014;92:e470–e474.
9. Jonas JB, Gusek GC, Naumann GO. Optic disk morphometry in high myopia. *Graefes Arch Clin Exp Ophthalmol*. 1988;226:587–590.
10. Spaide RF, Koizumi H, Pozzoni MC. Enhanced depth imaging spectral-domain optical coherence tomography. *Am J Ophthalmol*. 2008;146:496–500.
11. Margolis R, Spaide RF. A pilot study of enhanced depth imaging optical coherence tomography of the choroid in normal eyes. *Am J Ophthalmol*. 2009;147:811–815.
12. Rahman W, Chen FK, Yeoh J, Patel P, Tufail A, Da Cruz L. Repeatability of manual subfoveal choroidal thickness measurements in healthy subjects using the technique of

enhanced depth imaging optical coherence tomography. *Invest Ophthalmol Vis Sci*. 2011;52:2267–2271.

13. Ikuno Y, Maruko I, Yasuno Y, et al. Reproducibility of retinal and choroidal thickness measurements in enhanced depth imaging and high-penetration optical coherence tomography. *Invest Ophthalmol Vis Sci*. 2011;52:5536–5540.
14. Ikuno Y, Kawaguchi K, Nouchi T, Yasuno Y. Choroidal thickness in healthy Japanese subjects. *Invest Ophthalmol Vis Sci*. 2010;51:2173–2176.
15. Koizumi H, Yamagishi T, Yamazaki T, Kawasaki R, Kinoshita S. Subfoveal choroidal thickness in typical age-related macular degeneration and polypoidal choroidal vasculopathy. *Graefes Arch Clin Exp Ophthalmol*. 2011;249:1123–1128.
16. Tanabe H, Ito Y, Terasaki H. Choroid is thinner in inferior region of optic disks of normal eyes. *Retina*. 2012;32:134–139.
17. Ho J, Branchini L, Regatieri C, Krishnan C, Fujimoto JG, Duker JS. Analysis of normal peripapillary choroidal thickness via spectral domain optical coherence tomography. *Ophthalmology*. 2011;118:2001–2007.
18. Huang W, Wang W, Zhou M, et al. Peripapillary choroidal thickness in healthy Chinese subjects. *BMC Ophthalmol*. 2013;13:23.
19. Oh J, Yoo C, Yun CM, Yang KS, Kim SW, Huh K. Simplified method to measure the peripapillary choroidal thickness using three-dimensional optical coherence tomography. *Korean J Ophthalmol*. 2013;27:172–177.
20. Garway-Heath DF, Rudnicka AR, Lowe T, Foster PJ, Fitzke FW, Hitchings RA. Measurement of optic disc size: equivalence of methods to correct for ocular magnification. *Br J Ophthalmol*. 1998;82:643–649.
21. Fleiss JL, Cohen J. The equivalence of weighted kappa and the intraclass correlation coefficient as measures of reliability. *Educ Psychol Meas*. 1973;33:613–619.
22. Schoenwolf GC, Bleyl SB, Brauer PR, Francis-West PH. *Larsen's Human Embrology*. Philadelphia: Elsevier; 2009.
23. Hirooka K, Tenkumo K, Fujiwara A, Baba T, Sato S, Shiraga F. Evaluation of peripapillary choroidal thickness in patients with normal-tension glaucoma. *BMC Ophthalmol*. 2012;12:29.
24. Usui S, Ikuno Y, Miki A, Matsushita K, Yasuno Y, Nishida K. Evaluation of the choroidal thickness using high-penetration optical coherence tomography with long wavelength in highly myopic normal-tension glaucoma. *Am J Ophthalmol*. 2012;153:10–16, e11.
25. Ehrlich JR, Peterson J, Parlitsis G, Kay KY, Kiss S, Radcliffe NM. Peripapillary choroidal thickness in glaucoma measured with optical coherence tomography. *Exp Eye Res*. 2011;92:189–194.
26. Li L, Bian A, Zhou Q, Mao J. Peripapillary choroidal thickness in both eyes of glaucoma patients with unilateral visual field loss. *Am J Ophthalmol*. 2013;156:1277–1284, e1271.
27. Mwanza JC, Hochberg JT, Banitt MR, Feuer WJ, Budenz DL. Lack of association between glaucoma and macular choroidal thickness measured with enhanced depth-imaging optical coherence tomography. *Invest Ophthalmol Vis Sci*. 2011;52:3430–3435.
28. Hsiang HW, Ohno-Matsui K, Shimada N, et al. Clinical characteristics of posterior staphyloma in eyes with pathologic myopia. *Am J Ophthalmol*. 2008;146:102–110.
29. Arora KS, Jefferys JL, Maul EA, Quigley HA. Choroidal thickness change after water drinking is greater in angle closure than in open angle eyes. *Invest Ophthalmol Vis Sci*. 2012;53:6393–6402.
30. Silver DM, Geyer O. Pressure-volume relation for the living human eye. *Curr Eye Res*. 2000;20:115–120.
31. Ikuno Y, Tano Y. Retinal and choroidal biometry in highly myopic eyes with spectral-domain optical coherence tomography. *Invest Ophthalmol Vis Sci*. 2009;50:3876–3880.
32. Quaranta M, Arnold J, Coscas G, et al. Indocyanine green angiographic features of pathologic myopia. *Am J Ophthalmol*. 1996;122:663–671.
33. Moriyama M, Ohno-Matsui K, Futagami S, et al. Morphology and long-term changes of choroidal vascular structure in highly myopic eyes with and without posterior staphyloma. *Ophthalmology*. 2007;114:1755–1762.
34. Tan CS, Ouyang Y, Ruiz H, Sadda SR. Diurnal variation of choroidal thickness in normal, healthy subjects measured by spectral domain optical coherence tomography. *Invest Ophthalmol Vis Sci*. 2012;53:261–266.

Investigative Ophthalmology & Visual Science

Acta Ophthalmologica

Choroidal thickness does not predict visual acuity in young high myopes

Preeti Gupta,[1,2] Carol Y. Cheung,[1,2,3] Seang-Mei Saw,[1,2,3] Victor Koh,[2] Mellisa Tan,[5] Adeline Yang,[5] Paul Zhao,[6] Chui Ming Gemmy Cheung,[1,2,4] Tien Yin Wong[1,2,3,4] and Ching-Yu Cheng[1,2,4]

[1]Singapore Eye Research Institute and Singapore National Eye Centre, Singapore, Singapore
[2]Department of Ophthalmology, Yong Loo Lin School of Medicine, National University of Singapore and National University Health System, Singapore, Singapore
[3]Saw Swee Hock School of Public Health, National University of Singapore, Singapore, Singapore
[4]Duke-NUS Medical School, Singapore, Singapore
[5]DSO National Laboratories, Defence Medical and Environmental Research Institute, Singapore, Singapore
[6]Vision Performance Centre, Military Medical Institute, Singapore Armed Forces, Singapore, Singapore

ABSTRACT.

Purpose: **To investigate the influence of choroidal thickness (CT) on visual acuity (VA) in young persons with extremely high myopia.**

Methods: **We conducted a case–control study of young men with extremely high myopia and controls with emmetropia recruited from a mandatory medical eye review for employment purposes. Retinal and choroidal imaging was performed using enhanced depth imaging (EDI) spectral-domain optical coherence tomography (SD-OCT).**

Results: **We included 105 extremely high myopic subjects with spherical equivalent (SE) -10 dioptre (D) or worse and 50 emmetropic subjects with SE less than 0.5 D. The mean SE was −11.56 ± 2.04 D (range, −10 to −23 D) for myopic group and 0.14 ± 0.25 D for emmetropic group. The mean age of included myopic and emmetropic subjects was 21.51 ± 1.22 years and 21.96 ± 0.89 years, respectively. In the univariate analysis, subfoveal CT was significantly associated with best-corrected visual acuity (BCVA) (β = −0.039, p = 0.015). However, in the multiple linear regression analysis, after adjusting for SE and presence of any pathological myopia lesions such as posterior staphyloma, lacquer cracks or chorioretinal atrophy, subfoveal CT was not independently associated with BCVA (p = 0.937).**

Conclusion: **Extremely high myopic eyes had thinner choroid, but CT was not an independent predictor of VA. Other factors related to myopia are likely responsible for the diminished VA in young extremely high myopic eyes.**

Key words: choroidal thickness – enhanced depth imaging optical coherence tomography – high myopes – visual acuity

Acta Ophthalmol.

doi: 10.1111/aos.13084

Introduction

Although myopia is one of the major causes of visual impairment in the world (Klaver et al. 1998; Liu et al. 2001; Iwano et al. 2004), it is more common in Asian populations (Wong et al. 2000, 2014; Wu et al. 2001; Morgan et al. 2012). In young Asian adults (age range between 18 and 24 years), the prevalence of myopia [spherical equivalent refraction (SE) less than -0.50 dioptres (D)] and high myopia (SE less than −6.00 D) are 81.6–96.5% and 6.8–21.6%, respectively (Lee et al. 2011, 2013a,b; Koh et al. 2014). High myopia is characterized by excessive and progressive elongation of the globe, causing biomechanical stretching and thinning of not only the retina (Lim et al. 2005; Lam et al. 2007) but also the choroid (Fujiwara et al. 2009; Ikuno & Tano 2009; Spaide 2009). This excessive elongation of the globe results in a variety of pathological changes known as myopic macular degeneration (Neelam et al. 2012; Wong et al. 2014; Ohno-Matsui et al. 2015) and include lacquer cracks in the Bruch's membrane (Jonas et al. 2014), choroidal neovascularization (Cheung et al. 2013) and chorioretinal atrophy leading to vision loss.

The changes in the choroid are significant but not well studied. Histological studies showed both vessel density and diameters to be reduced in choriocapillaris of highly myopic eyes (Grossniklaus & Green 1992; Hirata & Negi 1998). In a recent study by Zaben et al. (2015), significant correlation between retinal sensitivity and choroidal thickness (CT) in highly myopic eyes was presented. As the choroid provides the major blood supply to the outer retina and supports the metabolic demands of the retinal pigment epithelium (RPE) and photoreceptors (Nickla & Wallman

2010), compromised choroidal circulation and morphology may account, in part, for outer retinal dysfunction and vision loss in high myopia. Thus, some researchers have hypothesized a relationship between CT in high myopes and visual acuity (VA) (Nishida et al. 2012; Flores-Moreno et al. 2013b; Ho et al. 2013).

Enhanced depth imaging spectral-domain optical coherence tomography (EDI SD-OCT) (Spaide et al. 2008) has now allowed investigators to measure CT in high myopes. Using this method, studies have shown that myopic eyes have thinner CT ranging from 90 to 160 μm (Fujiwara et al. 2009; Ikuno & Tano 2009; Flores-Moreno et al. 2013a; Ho et al. 2013; Wang et al. 2015). There is now evidence from recent studies that suggest CT to be a predictor of VA and thinner choroid to be associated with poorer VA (Nishida et al. 2012; Flores-Moreno et al. 2013b; Ho et al. 2013; Shao et al. 2014). However, these studies included only older participants mostly above 40 years, and their results may be confounded by other ocular comorbidities due to ageing. In addition, in some studies (Flores-Moreno et al. 2013b; Ho et al. 2013), the association was tested using univariate analysis only; thus, it remained unclear whether the observed association between VA and CT was a primary relationship or was due to confounding effects from other myopia-related changes, such as elongated axial length (AL). Finally, these studies were performed in myopic eyes free of myopic macular degeneration. It is unclear whether CT influences VA in the presence of myopic macular degeneration.

The purpose of this study was to examine the potential influence of CT on VA in young, extremely high myopic persons with and without myopic macular degeneration changes. We conceived that if there exists an association between CT and VA, it would be more apparent in this group of subjects. We therefore conducted a case–control study of young, extremely high myopic and emmetropic healthy male adults in Singapore.

Subjects and Methods

Study population

A total of 28 908 young male subjects (mean age ± SD: 19.8 ± 1.2 years; range: 17–9 years) were screened for myopia from 2009 to 2010 as part of a mandatory medical eye review for employment purposes. Measured using non-cycloplegic autorefraction (Huvitz MRK-3100P), 2584 persons were identified to have myopia with SE of −6.0 D or worse. Of these 2584 persons, 719 were selected on the basis of a refractive error-stratified random sampling strategy and underwent a further comprehensive ophthalmologic examination at Singapore Eye Research Institute from December 2011 to June 2012. Their SE was further confirmed by subjective refraction, leaving 520 subjects with high myopia (SE greater than −6D).

Of these 520 subjects, we selected 118 subjects with SE −10.0 D or worse in both eyes (mean SE in the right and left eyes was −11.56 ± 2.04 D and −11.26 ± 2.30 D, respectively) as cases for the current analysis. We also selected 55 emmetropic male subjects with SE less than ±0.5 D in both eyes (mean SE in the right and left eyes was 0.14 ± 0.25 D and 0.16 ± 0.26 D, respectively) as controls who underwent a similar ophthalmologic examination. Subjects were further excluded if they did not give consent to take part in this medical review, had any previous ocular trauma or surgery and those with other clinically significant ocular co-morbidity.

Written informed consent was taken from the subjects and their parents/guardians (if they were 21 years old and below). Ethics approval was obtained from the Institutional Review Board of DSO National Laboratories, Singapore. The study was conducted in accordance with the tenets of the World Medical Association's Declaration of Helsinki.

Ophthalmic examination and measurements

Each subject underwent a standardized questionnaire and a complete ophthalmologic examination. The subjects were asked a series of questions, such as previous ocular trauma or surgery, history of ocular diseases. Their refractive error screened with autorefraction (Canon Autorefractor RK-F1; Canon Inc. Ltd., Tochigiken, Japan) and confirmed with manifest refraction in which the best-corrected visual acuity (BCVA) was measured monocularly using a logarithm of the minimum angle of resolution (LogMAR) chart (Lighthouse International, New York, USA) at a distance of 4 m was performed. Biometry measurements, that is AL, anterior chamber depth (ACD), and keratometry readings were obtained from the non-contact Zeiss IOL Master (V3.01, Carl Zeiss Meditec AG, Jena, Germany). Intra-ocular pressure (IOP) was measured using non-contact tonometry (Auto Non-Contact Tonometer, NT-3000, Nidek, Gamagori, Aichi, Japan), and if IOP was found to be 21 mmHg or more, a further IOP measurement using Goldmann applanation tonometry (Haag-Streit, Bern, Switzerland) was performed by study ophthalmologists.

Subjects underwent slit-lamp examination. Binocular indirect ophthalmoscopy was performed approximately 30 min after topical instillation of three drops of tropicamide and 2.5% phenylephrine, given 5 min apart. Dilated fundus examination was carried out by ophthalmologists. The presence and type of peripheral retinal degenerations and vitreous degenerations were systematically documented. Fundus photography was performed using retinal camera (Canon CR-DGi with a 10-DSLR back, Tokyo, Japan).

OCT imaging

The retina, optic disc and choroidal architectural parameters were determined using SD-OCT (Spectralis, Wavelength: 870 nm; Heidelberg Engineering, Heidelberg, Germany) after pupil dilation. Retinal thickness was obtained using non-EDI mode, whereas choroid was imaged with EDI modality after pupil dilation. EDI is a method that improves resolution of choroidal detail by automatically setting the choroid closer to the zero-delay line and thus theoretically provides better visualization of the choroid scleral interface (CSI) than in standard retinal SD-OCT images.

Radial scan consisting of six sections, each comprising 100 averaged scans (using the automatic averaging and eye tracking features of the proprietary device), were obtained in an angle of 30° centred onto the fovea (30° angles between the lines). The horizontal and vertical section passing through the centre of the fovea was selected for analysis. Following Spectralis user manual guidelines, subjects' keratometry readings and refraction were

entered into the Spectralis' software before imaging choroid to estimate optical magnification, thus allowing for more accurate comparisons across individuals. However, Spectralis OCT does not allow AL to be input, and our methods may still have residual errors (2–7%) (Garway-Heath et al. 1998) due to ocular magnification from methods that additionally uses AL. For each subject, only right eye was chosen for subsequent analysis.

Measurement of choroidal and retinal thicknesses

The CT in the enhanced images was measured as the perpendicular distance between the outer portion of the hyperreflective line corresponding to the RPE (automatically detected by the instrument) to hyporeflective line or margin corresponding to the CSI (manually drawn by an experienced grader, who was masked to subject characteristics and clinical diagnosis) at the following locations: subfovea and 1.5 and 3 mm nasal, temporal, superior and inferior to fovea. We found significant correlation ($r = 0.95$, $p < 0.001$) in the horizontal and vertical subfoveal CT (mean horizontal subfoveal CT = 194.8 ± 57.7 μm and mean vertical subfoveal CT = 198.4 ± 61.7 μm); thus, only horizontal subfoveal CT was used in the analysis. Figure 1 shows an EDI-OCT scan comparing CT between a young emmetrope and a young myope. Retinal thickness was measured as the perpendicular distance between internal limiting membrane and RPE (both detected automatically by the instrument), at subfovea and 1.5 and 3 mm nasal, temporal, superior and inferior to fovea. We have previously demonstrated excellent intra-observer reliability of CT measurement in emmetropes and myopes (ICC ranging from 0.94 to 0.98) at various locations in posterior pole (Gupta et al. 2015).

Assessment of myopic macular degeneration

The colour fundus photographs were graded similar to previously established grading techniques by a single trained grader masked to the participant characteristics (Vongphanit et al. 2002). Adjudication was performed by an experienced medical retina specialist from an accredited fundus photograph grading centre. The main findings which were graded included myopia-related macular pathology, including staphyloma, lacquer crack and peripapillary atrophy (PPA). The presence of lacquer crack, its location and number were evaluated. Curtin and Karlin classification was used to determine the subtype and position of PPA (Curtin & Karlin 1970). Staphyloma was determined by visualizing the border of the ectasia; then, its location and type were documented based on the Curtin classification (Curtin 1977).

Intergrader reliability in grading for the aforementioned features was assessed with additional grading of 100 randomly selected eyes by trained graders, and reliability was found to be good (all intraclass correlation coefficient above 0.75). To confirm the presence of posterior staphyloma, the cross-sectional images from SD-OCT were graded by a medical retinal specialist. Figure 2 shows the presence of posterior staphyloma on horizontal scan of the macular central on the fovea (20°) obtained using SD-OCT. The presence of posterior staphyloma was defined as curvature of the RPE layer, with a foveal depth of ≥ 500 μm relative to the 3 mm periphery of the OCT B-scan. This allows posterior staphyloma with more gentle and subtle sloping edges to be detected.

Statistical analysis

For this analysis, we did not exclude subjects with presence of PPA, lacquer crack, posterior staphyloma or chorioretinal atrophy, as such changes are commonly seen in high myopic eyes.

The differences between high myopic and control eyes were compared using independent t-tests. Repeated-measures analysis of variance (ANOVA) with Bonferroni posttest was used to compare mean CT at various locations within each group. Multiple linear regression analyses were performed to determine the independent association of subfoveal CT (independent variable) with logMAR BCVA (dependent variable), adjusting for factors which showed association in univariate analysis ($p < 0.05$). The data were analysed with SPSS version 20.0 (SPSS, Inc., Chicago, IL, USA).

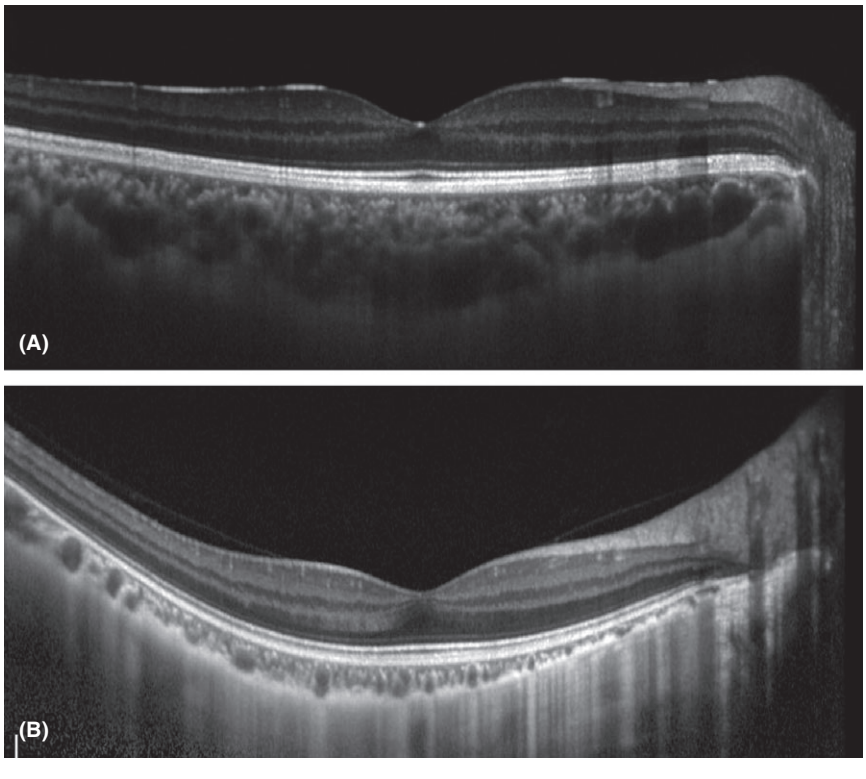

Fig. 1. Comparison of spectral-domain optical coherence tomography (EDI-OCT) scans of choroidal thickness between emmetrope and myope. (A) A 22-year-old male with no refractive error axial length (AL = 23.61 mm) and an average choroidal thickness of 325 μm. (B) A 23-year-old male with spherical equivalent (SE) of −12.25D (AL = 29.35 mm) and an average choroidal thickness of 117 μm.

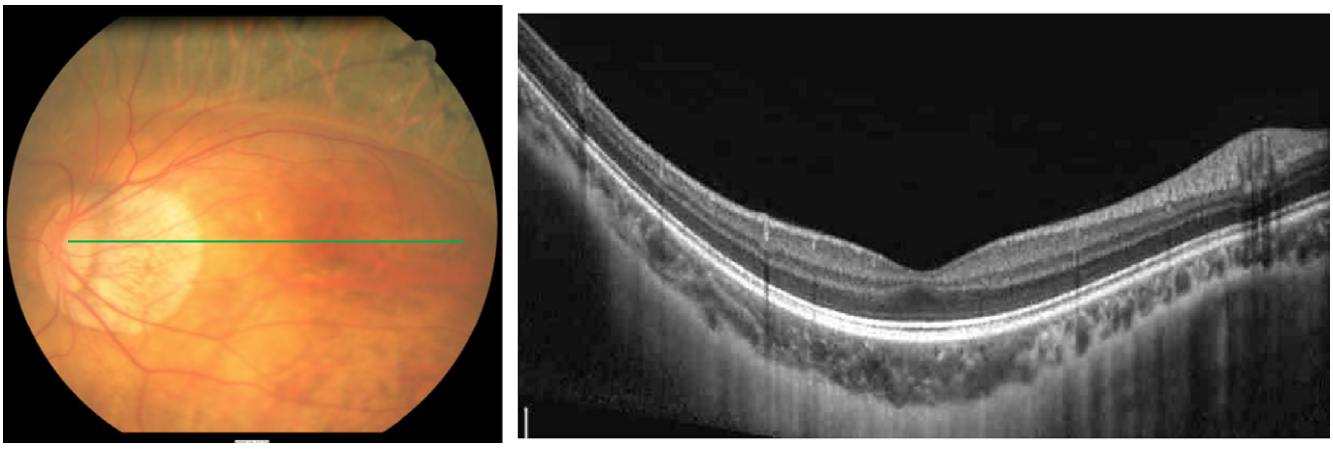

Fig. 2. shows the presence of posterior staphyloma on horizontal scan of the macular central on the fovea (20°) obtained using spectral-domain optical coherence tomography (SD-OCT).

Results

Of the 118 subjects who had SE −10.0 D or worse, 13 subjects were excluded as their choroidal images were not successfully attained ($n = 8$) due to unstable fixation, those where the CSI was not clearly delineated ($n = 4$) to perform accurate measurements or they did not meet the study inclusion criteria ($n = 1$), leaving 105 highly myopic subjects with complete data on CT for analysis.

The mean age of included myopic and emmetropic subjects was 21.51 ± 1.22 years and 21.96 ± 0.89 years, respectively. The mean SE was −11.56 ± 2.04 D (range, −10 to −23 D) for myopic group and 0.14 ± 0.25 D for emmetropic group (Table 1). Among the high myopic group, nearly all the subjects (99%) had PPA, 66.7% had posterior staphyloma, 22.9% had chorioretinal atrophy, and 4.8% had lacquer cracks.

Table 2 shows the distribution profile of choroidal and retinal thicknesses at different locations in both high myopic and emmetropic groups. In the highly myopic group, the mean CT was 194.81 ± 57.78 μm and the mean retinal thickness was 287.39 ± 31.75 μm. Choroid was significantly thinner in the highly myopic eyes over a range of eccentricities, and the pattern of distribution was different from emmetropes (Fig. 3A). Among the high myopes, choroid was found to be thickest at the superior location, followed by the temporal, subfoveal, inferior and the nasal locations ($p < 0.001$ by repeated-measures ANOVA). In comparison, the choroid in emmetropic eyes was thickest at the fovea, followed by the superior, inferior, temporal and the nasal locations ($p < 0.001$ by repeated-measures ANOVA). However, in both the highly myopic and emmetropic groups, choroid was thinnest at the 3 mm nasal location being 87.34 and 237.10 μm, respectively (Fig. 3A). Retinal thickness in both myopes and emmetropes showed similar distribution pattern, being thickest in the nasal location and thinnest subfoveally (Fig. 3B).

Both AL and SE influenced BCVA but a larger extent from SE (standardized β, −0.505 versus 0.214), and thus, only SE was selected and retained in the multivariate analysis due to collinearity between AL and SE ($r = -0.638$).

Table 3 shows the linear regression analyses of the associations of subfoveal CT (exposure variable of interest) evaluated against BCVA (dependent variable) to calculate regression coefficients (β). In model 1 (univariate analysis), subfoveal CT was significantly associated with BCVA ($\beta = -0.039$, $p = 0.015$). However, after adjusting for SE (model 2), subfoveal CT was no more significantly associated with BCVA ($p = 0.761$). In model 3, including both SE and presence of any pathological myopia lesions such as posterior staphyloma, lacquer cracks or chorioretinal atrophy, we found that subfoveal CT was not independently associated with BCVA ($p = 0.937$). There was no significant interactions between subfoveal CT and SE or subfoveal CT and pathological myopia lesions on BCVA (*both p interaction > 0.05*).

Furthermore, the association between BCVA and subfoveal CT in a group of 33 highly myopic subjects without any pathological myopic lesions (except PPA) was found to be insignificant ($\beta = 0.012$, $p = 0.776$).

It is speculated that if there exist any association between CT and VA, it would most likely be subfoveal CT due to maximum number of photoreceptors at subfovea. To confirm whether the distribution pattern of CT has influence on BCVA, we analysed the association of CT at different locations (nasal, temporal, superior

Table 1. Baseline characteristics of study subjects.

	Myopes ($n = 105$)	Emmetropes ($n = 55$)	p-value*
Age, years	21.51 (1.22)	21.96 (0.89)	0.033
Axial length, mm	28.46 (1.23)	23.65 (0.58)	<0.001
Anterior chamber depth, mm	3.74 (0.22)	3.47 (0.29)	<0.001
Corneal curvature, mm	7.76 (0.24)	7.79 (0.44)	0.686
Spherical equivalent, Dioptre	−11.56 (2.04)	0.14 (0.25)	<0.001
Best-corrected visual acuity, LogMAR	0.07 (0.09)	−0.10 (0.05)	<0.001
Intra-ocular pressure, mmHg	16.42 (3.04)	15.28 (2.78)	0.035

Data presented are means (standard deviations).
LogMAR, logarithm of the minimum angle of resolution.
*p-value was obtained with independent sample *t*-test.

Table 2. Distribution of choroidal and retinal thicknesses at different locations across the myopic and control groups.

Locations	Choroidal thickness Myopes (n = 105)	Emmetropes (n = 55)	p-value*	Retinal thickness Myopes (n = 105)	Emmetropes (n = 55)	p-value*
Subfoveal	194.81 (57.78)	377.98 (77.61)	<0.001	237.19 (22.24)	224.36 (19.31)	<0.001
Nasal, 1.5 mm	136.69 (54.650	325.67 (71.93)	<0.001	338.51 (24.22)	361.70 (21.19)	<0.001
Nasal, 3 mm	87.34 (39.39)	237.10 (69.49)	<0.001	291.00 (31.56)	312.90 (22.05)	<0.001
Temporal, 1.5 mm	210.48 (60.17)	358.60 (73.62)	<0.001	315.84 (19.11)	337.94 (13.72)	<0.001
Temporal, 3 mm	225.30 (62.57)	316.69 (68.28)	<0.001	250.47 (27.89)	273.67 (14.73)	<0.001
Superior, 1.5 mm	225.67 (76.06)	370.58 (67.58)	<0.001	327.36 (19.89)	349.70 (23.92)	<0.001
Superior, 3 mm	242.82 (84.77)	355.63 (72.81)	<0.001	273.15 (20.14)	288.10 (13.14)	<0.001
Inferior, 1.5 mm	188.21 (60.68)	362.23 (67.49)	<0.001	316.29 (19.13)	344.52 (16.90)	<0.001
Inferior, 3 mm	188.50 (69.05)	338.50 (81.60)	<0.001	259.16 (18.46)	274.43 (13.99)	<0.001
Average	188.85 (55.78)	338.11 (59.69)	<0.001	287.39 (31.75)	307.48 (18.87)	<0.001

Data presented are means (standard deviations) in μm. For both choroidal and retinal thicknesses repeated-measures ANOVA showed significant difference between the mean location measures within myopes and emmetropes.
*p-value was obtained from independent sample T-test.

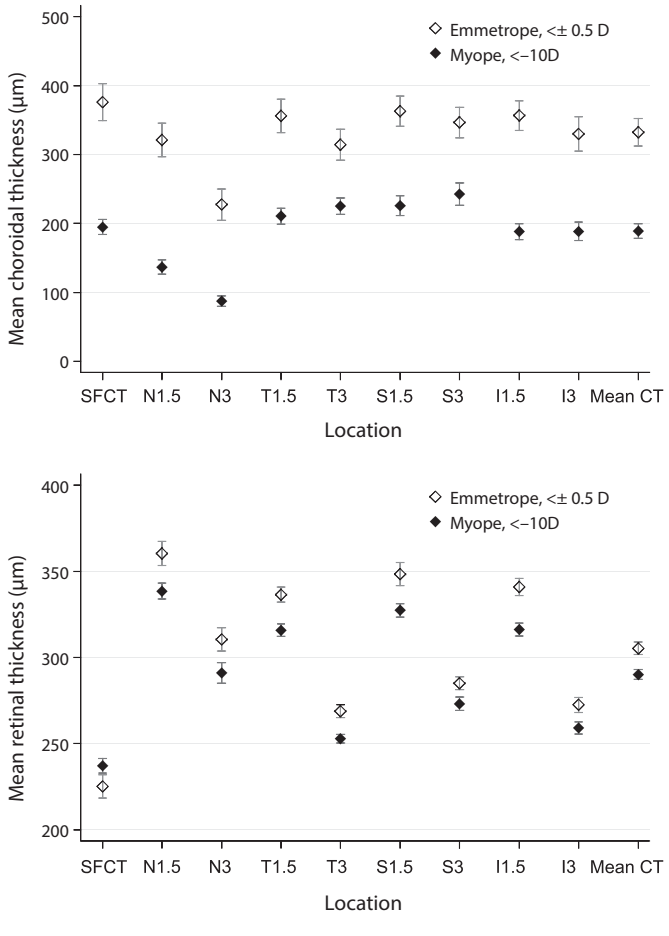

Fig. 3. Distribution profile of choroidal and retinal thicknesses at different locations in high myopic and emmetropic groups. Mean thickness at each of the nasal, temporal, superior and inferior locations was measured at 1.5 and 3 mm intervals eccentric to the subfoveal area. Error bars indicate standard error. SFCT, subfoveal choroidal thickness; SFRT, subfoveal retinal thickness; N, nasal; T, temporal; S, superior; I, inferior.

and inferior) with BCVA. However, we found no significant associations (all $p > 0.05$) between CT at different locations and BCVA (data not shown).

Discussion

Our results suggest that CT alone is not an independent indicator of VA in these young, highly myopic eyes, and factors such as SE still remains to be more important predictors of BCVA. Choroid was significantly thinner in the highly myopic eyes (mean CT 188.85 ± 55.78 μm verus 388.11 ± 59.69 μm in emmetropes) over a range of eccentricities, and the pattern of distribution was different from emmetropes. However, in terms of retinal thickness, both myopes and emmetropes showed similar distribution pattern.

Our finding of no independent association between subfoveal CT and VA is in contrast to most of the previous hospital-based investigations (Nishida et al. 2012; Flores-Moreno et al. 2013b; Ho et al. 2013). Nishida and colleagues in 145 myopic eyes (≥−6 D) with no other retinal or optic nerve pathology demonstrated CT to be an important predictor of VA. The discrepancy may be due to differences in age groups between our study and Nishida's study. Our study participants are much younger with mean age of 22 years compared to Nishida's study (mean age 57 years). With the advancing age, the choroid may undergo further age-related attenuation (Fujiwara et al. 2009; Spaide 2009). Therefore, in Nishida's study, choroidal thinning is attributed to dual factors: myopic refractive error and older age. In addition, with advancing age, other myopic maculopathy and severity develop progressively (Chang et al. 2013), which may lead to reduced VA. In contrast, our young subjects with relatively thicker choroid retained their visual function and therefore enjoyed better vision.

In the Beijing Eye Study (Shao et al. 2014), better BCVA was found to be

Table 3. Association of subfoveal choroidal thickness with best-corrected visual acuity in young, high myopic eyes (n = 105).

	Best-corrected visual acuity (LogMAR)		
	β	95% CI	p-value
Model 1			
SFCT	−0.039	−0.070 to −0.008	0.015
Model 2			
SFCT + SE	0.005	−0.027 to 0.037	0.761
Model 3			
SFCT + SE + presence of any pathological myopia lesions*	−0.001	-0.036 to 0.033	0.937

Model 1: univariate.
Model 2: adjusted for SE.
Model 3: adjusted for SE and presence of any pathological myopia lesions* (posterior staphyloma, lacquer cracks or chorioretinal atrophy).
SFCT was analysed per 100 μm.
SFCT, subfoveal choroidal thickness (μm); SE, spherical equivalent (dioptre); LogMAR, logarithm of minimal angle of resolution.

associated with thicker subfoveal CT after adjusting for age, AL and other parameters. However, Beijing Eye Study is a population-based study with a mean age of participant's being 64.3 years and a mean refractive error (SE) of −0.18 D. The observed association between subfoveal CT and VA could be due to residual confounding effects of AL which was taken as a binary variable (>26 mm versus ≤26 mm).

Flores-Moreno and colleagues (2013b) examined 60 eyes of 46 highly myopic subjects (SE ≥−6 D; mean age 45.9 years) without macular diseases and found that in univariate analysis, BCVA (logMAR) was significantly correlated with thinner subfoveal CT (r = −0.36; p = 0.004). Similarly, Ho and co-workers (2013) evaluated 56 myopic subjects (SE ≥−6 D; mean age 50.4 years) and found that in univariate analysis subfoveal CT was correlated with logMAR VA (r^2 = 0.295, p = 0.008). In both studies, the association between BCVA and subfoveal CT was tested in univariate analysis only, without taking into account other potential confounders, such as SE, AL and other ocular comorbidities due to ageing. By contrast, our study involved younger subjects with few ocular comorbidities, and thus, the results are less complicated by confounding factors.

The results of our study are in concordance with the results of a recent study by Pang et al. (2015) who reported no significant reduction in VA (mean VA = 20/30) in highly myopic eyes (mean AL = 30.7 mm) with extreme choroidal thinning (mean subfoveal CT = 14 ± 6 μm), suggesting CT alone is not a reliable indicator of visual function. However, their study involved relatively small sample size (36 eyes of 20 myopic subjects) and older subjects (mean age of 71 years) with ocular comorbidities, and thus, their results may be complicated by confounding factors. In addition, use of manual callipers to measure very small CT might have introduced some measurement errors.

It is interesting that although previous studies (Nishida et al. 2012; Flores-Moreno et al. 2013b; Ho et al. 2013; Shao et al. 2014) have concluded subfoveal CT to be inversely correlated to VA, this study has shown that there are clear exceptions to these observations. We did not find any significant association between decreased VA and thinner choroid in our young, extremely high myopic subjects with or without myopic maculopathy. Although retinal thickness was reduced in myopic eyes (average thickness 287 μm) than in a comparable group of control eyes (average thickness 307 μm), thinning of 20 μm may not be clinically meaningful and photoreceptor layer might not have been disrupted maintaining a fairly normal visual functions in adolescents and young adults with high myopia than their aged counterparts in which both severity of myopia and other myopic maculopathy increases with advancing age leading to reduced VA.

To satisfy the normal metabolic demands of the outer retina, choroidal blood flow is highest of any tissue in the body. It has been shown to be decreased in myopia (Akyol et al. 1996) although a recent study by Sogawa et al. (2012) demonstrated no significant correlation between subfoveal CT and total choroidal blood flow or subfoveal choroidal blood flow, and therefore, the relationship between choroidal perfusion and CT remains unclear. In myopic eyes with choroidal thinning, the good VA in face of thinner choroid may be explained by intact choroidal perfusion from larger patent choroidal vessels, which are typically in Haller's layer and located eccentric to the subfoveal area (Nickla & Wallman 2010). However, this study lacks choroidal blood flow measurements, and future studies of choroidal circulation will be useful to correlate CT with perfusion in normal eyes and in high myopes with choroidal thinning.

The strength of this study includes a relatively large sample size of highly myopic young Asian adults who prospectively underwent standardized examinations and highly detailed colour fundus photographs grading. Unlike other studies, our study included an emmetropic group and therefore we could examine the differences between highly myopic eyes and non-myopic eyes in our case–control study. The limitations of our study include the following: First, due to our cross-sectional study design, we were unable to determine the causal relationships between the various risk factors and BCVA. Second, all of our study subjects were males, and thus, some of our findings may not be generalized to females. Third, by not taking into account axial length to correct for ocular magnification, there may still be some residual error.

In conclusion, we report that high myopic eyes had thinner choroid, but CT was not an independent predictor of VA. Other factors related to myopia are likely responsible for the diminished VA in young highly myopic eyes.

References

Akyol N, Kukner AS, Ozdemir T & Esmerligil S (1996): Choroidal and retinal blood flow changes in degenerative myopia. Can J Ophthalmol **31**: 113–119.

Chang L, Pan CW, Ohno-Matsui K et al. (2013): Myopia-related fundus changes in

Singapore adults with high myopia. Am J Ophthalmol 155: 991-999 **99**: 1.
Cheung CM, Loh BK, Li X, Mathur R, Wong E, Lee SY, Wong D & Wong TY (2013): Choroidal thickness and risk characteristics of eyes with myopic choroidal neovascularization. Acta Ophthalmol **91**: e580–e581.
Curtin BJ (1977): The posterior staphyloma of pathologic myopia. Trans Am Ophthalmol Soc **75**: 67–86.
Curtin BJ & Karlin DB (1970): Axial length measurements and fundus changes of the myopic eye. I. The posterior fundus. Trans Am Ophthalmol Soc **68**: 312–334.
Flores-Moreno I, Lugo F, Duker JS & Ruiz-Moreno JM (2013a): The relationship between axial length and choroidal thickness in eyes with high myopia. Am J Ophthalmol **155**: 314–319 e311.
Flores-Moreno I, Ruiz-Medrano J, Duker JS & Ruiz-Moreno JM (2013b): The relationship between retinal and choroidal thickness and visual acuity in highly myopic eyes. Br J Ophthalmol **97**: 1010–1013.
Fujiwara T, Imamura Y, Margolis R, Slakter JS & Spaide RF (2009): Enhanced depth imaging optical coherence tomography of the choroid in highly myopic eyes. Am J Ophthalmol **148**: 445–450.
Garway-Heath DF, Rudnicka AR, Lowe T, Foster PJ, Fitzke FW & Hitchings RA (1998): Measurement of optic disc size: equivalence of methods to correct for ocular magnification. Br J Ophthalmol **82**: 643–649.
Grossniklaus HE & Green WR (1992): Pathologic findings in pathologic myopia. Retina **12**: 127–133.
Gupta P, Saw S, Cheung CY et al. (2015): Choroidal thickness and high myopia: a case-control study of young Chinese men in Singapore. Acta Ophthalmol **93**: e585–592.
Hirata A & Negi A (1998): Morphological changes of choriocapillaris in experimentally induced chick myopia. Graefes Arch Clin Exp Ophthalmol **236**: 132–137.
Ho M, Liu DT, Chan VC & Lam DS (2013): Choroidal thickness measurement in myopic eyes by enhanced depth optical coherence tomography. Ophthalmology **120**: 1909–1914.
Ikuno Y & Tano Y (2009): Retinal and choroidal biometry in highly myopic eyes with spectral-domain optical coherence tomography. Invest Ophthalmol Vis Sci **50**: 3876–3880.
Iwano M, Nomura H, Ando F, Niino N, Miyake Y & Shimokata H (2004): Visual acuity in a community-dwelling Japanese population and factors associated with visual impairment. Jpn J Ophthalmol **48**: 37–43.
Jonas JB, Holbach L & Panda-Jonas S (2014): Bruch's membrane thickness in high myopia. Acta Ophthalmol **92**: e470–474.
Klaver CC, Wolfs RC, Vingerling JR, Hofman A & de Jong PT (1998): Age-specific prevalence and causes of blindness and visual impairment in an older population: the Rotterdam Study. Arch Ophthalmol **116**: 653–658.
Koh V, Yang A, Saw SM et al. (2014): Differences in prevalence of refractive errors in young Asian males in Singapore between 1996-1997 and 2009–2010. Ophthalmic Epidemiol **21**: 247–255.
Lam DS, Leung KS, Mohamed S et al. (2007): Regional variations in the relationship between macular thickness measurements and myopia. Invest Ophthalmol Vis Sci **48**: 376–382.
Lee SJ, Urm SH, Yu BC, Sohn HS, Hong YS, Noh MS & Lee YH (2011): [The prevalence of high myopia in 19 year-old men in Busan, Ulsan and Gyeongsangnam-do]. J Prev Med Public Health **44**: 56–64.
Lee JH, Jee D, Kwon JW & Lee WK (2013a): Prevalence and risk factors for myopia in a rural Korean population. Invest Ophthalmol Vis Sci **54**: 5466–5471.
Lee YY, Lo CT, Sheu SJ & Lin JL (2013b): What factors are associated with myopia in young adults? A survey study in Taiwan Military Conscripts Invest Ophthalmol Vis Sci **54**: 1026–1033.
Lim MC, Hoh ST, Foster PJ, Lim TH, Chew SJ, Seah SK & Aung T (2005): Use of optical coherence tomography to assess variations in macular retinal thickness in myopia. Invest Ophthalmol Vis Sci **46**: 974–978.
Liu JH, Cheng CY, Chen SJ & Lee FL (2001): Visual impairment in a Taiwanese population: prevalence, causes, and socioeconomic factors. Ophthalmic Epidemiol **8**: 339–350.
Morgan IG, Ohno-Matsui K & Saw SM (2012): Myopia. Lancet **379**: 1739–1748.
Neelam K, Cheung CM, Ohno-Matsui K, Lai TY & Wong TY (2012): Choroidal neovascularization in pathological myopia. Prog Retin Eye Res **31**: 495–525.
Nickla DL & Wallman J (2010): The multifunctional choroid. Prog Retin Eye Res **29**: 144–168.
Nishida Y, Fujiwara T, Imamura Y, Lima LH, Kurosaka D & Spaide RF (2012): Choroidal thickness and visual acuity in highly myopic eyes. Retina **32**: 1229–1236.
Ohno-Matsui K, Kawasaki R, Jonas JB et al. (2015): International photographic classification and grading system for myopic maculopathy. Am J Ophthalmol **159**: 877–883 e877.
Pang CE, Sarraf D & Freund KB (2015): Extreme choroidal thinning in high myopia. Retina. **35**: 407–415.
Shao L, Xu L, Wei WB et al. (2014): Visual acuity and subfoveal choroidal thickness: the Beijing Eye Study. Am J Ophthalmol **158**: 702–709 e701.
Sogawa K, Nagaoka T, Takahashi A, Tanano I, Tani T, Ishibazawa A & Yoshida A (2012): Relationship between choroidal thickness and choroidal circulation in healthy young subjects. Am J Ophthalmol **153**: 11291132 e1121.
Spaide RF (2009): Enhanced depth imaging optical coherence tomography of retinal pigment epithelial detachment in age-related macular degeneration. Am J Ophthalmol **147**: 644–652.
Spaide RF, Koizumi H & Pozzoni MC (2008): Enhanced depth imaging spectral-domain optical coherence tomography. Am J Ophthalmol **146**: 496–500.
Vongphanit J, Mitchell P & Wang JJ (2002): Prevalence and progression of myopic retinopathy in an older population. Ophthalmology **109**: 704–711.
Wang S, Wang Y, Gao X, Qian N & Zhuo Y (2015): Choroidal thickness and high myopia: a cross-sectional study and meta-analysis. BMC Ophthalmol **15**: [Epub ahead of print].
Wong TY, Foster PJ, Hee J, Ng TP, Tielsch JM, Chew SJ, Johnson GJ & Seah SK (2000): Prevalence and risk factors for refractive errors in adult Chinese in Singapore. Invest Ophthalmol Vis Sci **41**: 2486–2494.
Wong TY, Ferreira A, Hughes R, Carter G & Mitchell P (2014): Epidemiology and disease burden of pathologic myopia and myopic choroidal neovascularization: an evidence-based systematic review. Am J Ophthalmol **157**: 925 e12.
Wu HM, Seet B, Yap EP, Saw SM, Lim TH & Chia KS (2001): Does education explain ethnic differences in myopia prevalence? A population-based study of young adult males in Singapore. Optom Vis Sci **78**: 234–239.
Zaben A, Zapata MA & Garcia-Arumi J (2015): Retinal sensitivity and choroidal thickness in high myopia. Retina **35**: 398–406.

Received on June 26th, 2015.
Accepted on March 7th, 2016.

Correspondence:
Dr. Ching-Yu Cheng, 20 College Road, The Academia, Level 6, Discovery Tower, Singapore 169856, Singapore
Tel: + 65 6576 7277
Fax: + 65 6225 2568
Email: ching-yu_cheng@nuhs.edu.sg

This study was funded by Ministry of Defence MINDEF, Singapore, and Singapore Ministry of Education, Academic Research Fund, Tier 1. The funding organization had no role in the design or conduct of this research.